UNIVERSITY OF Southampton

A Tissue Engineered Approach to the Modelling of Alveolar Epithelium and Application to Idiopathic Pulmonary Fibrosis

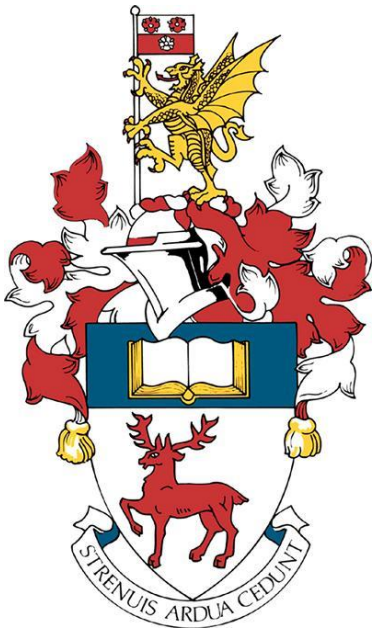

University of Southampton

James Ross Cooper

Thesis for the Degree of Doctor of Philosophy

January 2021

University of Southampton

Faculty of Medicine

Clinical and Experimental Sciences Division

A Tissue Engineered Approach to the Modelling of Alveolar Epithelium and Application to Idiopathic Pulmonary Fibrosis

by

James Ross Cooper BSc (Hons)

Thesis for the degree of Doctor of Philosophy

January 2021

University of Southampton

Abstract

Faculty of Medicine

Clinical and Experimental Sciences Division

Doctor of Philosophy

A Tissue Engineered Approach to the Modelling of Alveolar Epithelium and Application to Idiopathic Pulmonary Fibrosis

by

James Ross Cooper

Alveolar epithelial cells comprise type I (ATI) cells which facilitate gas exchange and type II (ATII) cells which play a critical role in alveolar homeostasis, innate immunity and self-renewal to replace ATI cells. Idiopathic Pulmonary Fibrosis (IPF) is a fatal fibrotic interstitial lung disease of unknown cause, however current theories implicate recurrent microinjuries to alveolar epithelium in association with activation of aberrant repair pathways. Thus, IPF research requires effective *in vitro* ATII cell models. Challenges of primary and stem cell culture and animal models have resulted in widespread use of the immortal A549 lung adenocarcinoma cell line, however its suitability remains unproven. It was hypothesised that modifying the culture conditions of A549 cells through three-dimensional (3D) or long term culture can enable *in vitro* tissue-like differentiation evidenced by expression of ATII marker genes and multilamellar body (MLB) production. Initially prolonged spheroid culture of A549 cells was tested for induction of ATII-like differentiation. RNA Microarray analysis demonstrated gene expression differences between spheroids and log phase two-dimensional (2D) cultures, suggesting the spheroids adopted a muco-secretory phenotype evidenced by markers of host defence and goblet cells. These properties were confirmed by QRT-PCR, histochemistry and transmission electron microscopy (TEM) but there was no evidence of ATII differentiation in spheroids. Next, ATII related gene expression in long term 2D cultures of A549 cells in Ham's F12 medium was compared to freshly isolated human ATII cells using RNA microarray. Long term 2D culture cultures had patterns of gene expression similar to primary ATII cells but not of the same magnitude. MLB expression was confirmed by histology and TEM. As A549 cells may be ultimately limited by their cancerous origin, an investigation into the novel lung progenitor cell line 'E-Cad/LGr6+' was initiated but genotyping raised concerns about the cell line's validity leading to the necessity to continue with A549 cells. Dexamethasone upregulated surfactant protein (SFTP) gene expression in the long term 2D A549 model, but had the undesirable side effect of downregulating genes involved in epithelial/mesenchymal communication. Finally, the ability of fibroblasts to support an ATII-like phenotype was tested using (i) conditioned medium from MRC-5 lung fibroblasts, (ii) A549 and MRC-5 co-cultures on Transwell™ and (iii) Alvetex™ 3D scaffold supports. Histochemical, gene expression and TEM analyses demonstrated that MRC-5 fibroblasts expressed factors for epithelial support driving subsequent SFTP gene expression in A549 cells. Alvetex™ scaffold co-culture initiated tissue-like organisation, ECM secretion and MLB expression. With optimisation and demonstration of reproducibility it is expected this approach will deliver a reproducible and accessible ATII model for airways research.

Table of Contents

Table of Tables

Table of Tables

Table of Figures

Table of Figures

Table of Figures

Research Thesis: Declaration of Authorship

Print name: James Ross Cooper

Title of thesis: **A Tissue Engineered Approach to the Modelling of Alveolar Epithelium and Application to Idiopathic Pulmonary Fibrosis**

I declare that this thesis and the work presented in it are my own and has been generated by me as the result of my own original research.

I confirm that:

1. This work was done wholly or mainly while in candidature for a research degree at this University;
2. Where any part of this thesis has previously been submitted for a degree or any other qualification at this University or any other institution, this has been clearly stated;
3. Where I have consulted the published work of others, this is always clearly attributed;
4. Where I have quoted from the work of others, the source is always given. With the exception of such quotations, this thesis is entirely my own work;
5. I have acknowledged all main sources of help;
6. Where the thesis is based on work done by myself jointly with others, I have made clear exactly what was done by others and what I have contributed myself;
7. Parts of this work have been published as:-
   'Long Term Culture of the A549 Cancer Cell Line Promotes Multilamellar Body Formation and Differentiation towards an Alveolar Type II Pneumocyte Phenotype'
   James Ross Cooper, Muhammad Bilal Abdullatif, Edward C. Burnett, Karen E. Kempsell, Franco Conforti, Howard Tolley, Jane E. Collins, Donna E. Davies
   PLOS ONE 11, e0164438 (2016).
   https://journals.plos.org/plosone/article?id=10.1371/journal.pone.0164438

Signature:

Date: 16th June 2021

Acknowledgements

- Sincerest thanks to my supervisors: Professor Donna Davies, Dr Jane Collins of the University of Southampton (UoS) and Dr Edward Burnett of Public Health England (PHE) for their scientific guidance, mentorship, calm lead and pastoral support.

- I am grateful to the all the students and staff of the Brooke Laboratories, UoS, past and present, for their help, guidance and friendship, in particular: Dr David Smart, Dr Natalie Smithers, Dr Robert Ridley, Dr Matt Loxham and Dr Joanne Kelly. Thanks to Dr Franco Conforti for providing primary ATII cultures and RNA.

- Thanks to John Ward, Jenny Norman and the Staff of the Biomedical Imaging Unit, University of Southampton for their guidance in histological methods, paraffin embedding and to Dr Anton Page for training me in TEM methods.

- Thanks to all in the Culture Collections of PHE and the PHE staff at Porton Down. Special thanks go to:

    - Julie Russell for giving me the time and space to undertake the study.

    - Dr Karen Kempsell for guidance and training in the use of Agilent® Genespring™ software.

    - Dr Muhammad Abdulatif who prepared the cRNA and executed RNA microarray hybridisations for Chapters 3 and 4.

    - Howard Tolley and Katherine Davies for professionally repeating my amateurly executed TEM work and findings (Chapter 4), for preparing TEM for Chapter 7 and for the SEM work.

- Eternal thanks to my long-suffering wife, Nicki Cooper who provided tea, sympathy, assistance with compiling the list of abbreviations and with proof reading. (She says she *never* wants to see or hear the words "Surfactant Protein" ever again in her life).

- Thanks to my daughters for their endless love, inspiration and support.

- And to my Mum and the memory of my Dad, to whom this thesis is dedicated.

- If it wasn't for the mental and physical health benefits of cycling I could never have achieved this.

Definitions and Abbreviations

Abbreviation	Definition
2D	Two-dimensional
3D	Three-dimensional
AA	Ascorbic Acid
ABCA3	ATP-binding Cassette Class A3
ABCG2	ATP Binding Cassette Subfamily G Member 2
ACE	Angiotensin Converting Enzyme
ACTA2	Gene symbol for αSMA
ACTB	β-Actin
ADRP (PLIN2)	Adipose Differentiation-Related Protein (see PLIN2)
AKPA13	A-Kinase Anchor Protein 13
ALI	Air-Liquid Interface
ALK5	Activin receptor-like kinase 5. Also known as TGF-β receptor 1. Gene symbols: *ALK5* or *TGRBR1*
ANOVA	Analysis of variance
AQP5	Aquaporin 5
ARDS	Acute Respiratory Distress Syndrome
αSMA	α-Smooth Muscle Actin (see ACTA2)
ATCC	American Type Culture Collection
ATI	Alveolar Type 1 Cell
ATII	Alveolar Type 2 Cell
ATP5B	ATP synthase F1 subunit beta, mitochondrial
ATS	American Thoracic Society
B2M	Beta 2-Microglobulin
BASC	Bronchioalveolar Stem Cell
BH FDR	Benjamini-Hochberg False Discovery Rate

Abbreviation	Definition
BMP	Bone Morphogenic Protein
BSC	Basal Stem Cells
C57BL/6	C57 black 6 (mouse)
CAMP	Cathelicidin Antimicrobial Peptide
cAMP	Cyclic Adenosine Monophosphate.
CAV-1	Caveolin - 1
CCL2	Chemokine (C-C motif) Ligand 2
CCL21	Chemokine (C-C motif) Ligand 21
CCSP	Club Cell Secretory Protein
CD63	Cluster of Differentiation Marker 63
CDH1	E-Cadherin
CDKN1A	Cyclin Dependent Kinase Inhibitor 1A
cDNA	Complementary DNA
CEACAM6	Carcinoembryonic antigen cell adhesion molecule 6
CF	Cystic Fibrosis
CK	Cytokeratin
CL2-MSC	Class II Microbiological Safety Cabinet
CMV	Cytomegalovirus
COL1A	Collagen
COPD	Chronic Obstructive Pulmonary Disease
COVID 19	Coronavirus Infectious Disease 2019
cRNA	Fluorescent Complimentary RNA
CRUK	Cancer Research UK
CTGF	Connective Tissue Growth Factor
CYC1	Cytochrome c1, Heme Protein, Mitochondrial
DAO	Diamine Oxidase

Abbreviation	Definition
DAPI	4′,6-diamidino-2-phenylindole
DCCM -1	Undisclosed proprietary acronym
Dex	Dexamethasone
DMEM	Dulbecco's Modified Eagle's Medium
DPPC	Dipalmitoylphosphatidyl Choline
DSMZ	Deutsche Sammlung von Mikroorganismen und Zellkulturen (German Collection of Microorganisms and Cell Cultures)
EBV	Epstein-Barr Virus
ECACC	European Collection of Authenticated Cell Cultures
ECM	Extra Cellular Matrix
EDTA	Ethylenediaminetetraacetic acid
ELISA	Enzyme Linked Immunosorbent Assay
EMT	Epithelial-to-mesenchymal Transition
EPN3	Epsin-3
ER	Endoplasmic Reticulum
ERBB	Epidermal growth factor (EGF) family of receptor tyrosine kinases (also known as HER receptors)
EV	Extracellular Vesicles
FA	Fatty Acid
FABP	Fatty Acid Binding Proteins
FAM	Fluorescein Amidite
FBS	Foetal Bovine Serum
FCM	Fibroblast Conditioned Medium
FGF	Fibroblast Growth Factor
FGF7	Keratinocyte Growth Factor
FITC	Fluorescent Isothiocyanate

Abbreviation	Definition
FPF	Fibroblast Pneumocyte Factor (Also known as Fibroblast Pneumonocyte Factor)
FVC	Forced Vital Capacity
Fxa	Coagulation Factor 10 ('Factor X')
GAG	Glycosaminoglycan
GAPDH	Glyceraldehyde 3-phosphate dehydrogenase
GFP	Green Fluorescent Protein
GMA	Glycol Methacrylate
GM-CSF	Granulocyte-Macrophage Colony-stimulating Factor
GO	Gene Ontology
GOLD	Global Initiative for Chronic Obstructive Lung Disease
GPCR	G Protein Coupled Receptor
GPR172B	G protein-coupled receptor 172B
GR	Glucocorticoid Receptor
Gro	Growth-related Oncogenes
HA	Hyaluronic Acid
hAEpC	Human Alveolar Type-1 like Cells
HAS1-hi cells	Hyaluronic Acid Synthetase
HCI	Hydrochloric Acid
HCV	Hepatitis C Virus
HEK-293	Human Embryonic Kidney Cell
hESC	Human Embryonic Stem Cells
HGF	Hepatocyte Growth Factor
HH	Hedgehog
hiPSC	Induced Pluripotent Stem Cells
HPAEpiC-II	Human Type-II Pulmonary Alveolar Epithelial Cells

Abbreviation	Definition
HRCT	High Resolution Computerised Tomography
hTERT	Human Telomerase
ICG-001	Small Molecule Wnt Inhibitor
ICLAC	International Cell Line Authentication Committee
IF	Intermediate Filament Protein
IFNγ	Interferon Gamma
IgA	Immunoglobulin A
IGFBP	Insulin-like Growth Factor
IILDS	Idiopathic Interstitial Lung Disease
IL-	Interleukin-
ILD	Interstitial Lung Diseases
IILD	Idiopathic Interstitial Lung Diseases
IPF	Idiopathic Pulmonary Fibrosis
iPSC	Induced Pluripotent Stem Cells
JAK STAT	Janus Kinase Signal Transducer and Activation Transcription
JNK	c-Jun N-terminal kinases
KB	KB – a misidentified cell line
KL-6	Alias for Mucin-1
KRT-17	Keratin-17
LAMP	Lysosomal Associated Membrane Protein
Lck	lymphocyte-specific protein tyrosine kinase
Let-7d	A non-coding micro-RNA (miRNA) regulator of cell cycle
LEV	Low Elution Volume
LOXL	Lysyl Oxidase
LOXL2	Lysyl Oxidase-Like Enzyme 2
LPA	Lysophosphatidic Acid

Abbreviation	Definition
LREC	Local Research Ethics Committee
LRP5/6	Lipoprotein Receptor Related Protein
LSC	Lung Stem Cells
LY6D	Lymphocyte antigen 6D
MCP-1	Monocyte Chemoattractant Protein-1
MDCK	Madin-Darby Canine Kidney
MG	Mucin Granules
Micro-CT	Micro Computerised Tomography
miR-21	MicroRNA 21 associated with fibrogenesis
MLB	Multilamellar body
MMP7	Metalloproteinase
MMP-7	Matrix Metalloproteinase
MMP	Matrix Metalloproteinase
mtDNA	Mitochondrial DNA
MUC5AC	Mucin 5AC
MUC5B	Mucin 5B
NCS	Newborn Calf Serum
NCX1	Sodium/calcium exchanger
NE	Neutrophil Elastase
NOD/SCID	Non-obese Diabetic / Severe Combined Immuno-deficiency
NRG	Neuregulin-1β (shorthand: when used in experiments)
NRG-1β	Neuregulin-1β
NRTK	Nonreceptor tyrosine kinase
NS	Not Significant
OCT	Organic Cation Transporter
OIS	Oncogene Induced Senescence

Abbreviation	Definition
PAS	Periodic Acid-Schiff
PBS	Phosphate Buffered Saline
PD	Population Doubling
PDGF	Platelet Derived Growth Factor
PDGFR	Platelet Derived Growth Factor Receptor
PGC1α	Peroxisome proliferator-activated receptor gamma coactivator 1-alpha (protein)
PGE_2	Prostaglandin E2
PLIN2	Perilipin 2 (see ADRP)
PLL	Poly-L-Lysine
PMCA1	Plasma membrane calcium ATPase
PolyHIPE	Porous Polymers from High Internal Phase Emulsions
PPARγ	Peroxisome proliferator-activated receptor gamma
PPARGC1A	Proliferator Activated Receptor Gamma Co-activator 1-alpha (gene)
PRODH	Proline dehydrogenase
PTHrP	Parathyroid-like hormone
PVRL4	Poliovirus Receptor-Like 4 (also known as Nectin 4)
QRT-PCR	Quantitative Real-Time Polymerase Chain Reaction (also known as Quantitative Reverse Transcription Polymerase Chain Reaction)
REVIGO	Reduce+Visualize Gene Ontology Tool
RGZ	Rosiglitazone
RIN	RNA Integrity Number
RNA	Ribonucleic Acid
RO	Reverse Osmosis
RTK	Receptor Tyrosine Kinase
SARS	Severe Acute Respiratory Syndrome
SASP	Senescent Associated Secretory Phenotype

Abbreviation	Definition
Scgb 1a1	Secretoglobin Family 1A Member 1
SDO	Standards Development Organisation
SEM	Scanning Electron Microscopy
SFTP	Surfactant Protein
SNA1	Human equivalent of Drosophila Snail gene
SNA2	Human equivalent of Drosophila Slug gene
SNAI1	See SNAI1
SNP	Single-nucleotide Polymorphism
SOX2	SRY (sex determining region Y)-box 2
SP-D	Surfactant Factor Protein D
SPDEF	SAM pointed domain-containing Ets transcription facto
Src	Proto-oncogene tyrosine-protein kinase Src (also known as proto-oncogene c-Src)
STR	Short Tandem Repeat
SV40	Simian Virus 40
T1α	A specific marker of AT1 cells
TBS	Tris Buffered Saline
TEER	Trans-Epithelial Electrical Resistance
TEM	Transmission Electron Microscopy
TERT	Telomerase Reverse Transcriptase
TF	Tissue Factor
TGF-β	Transforming Growth Factor Beta
TGF-β1	Transforming Growth Factor Beta -1
TGF-β3	Transforming Growth Factor Beta -3
Th2	T Helper Cell Type 2
TIMPs	Tissue Inhibitors of Metalloproteinases

Abbreviation	Definition
TNF	Tumour Necrosis Family
TOLLIP	Toll Interacting Protein
TOP1	DNA Topoisomerase 1
TRPV6	Transient receptor potential vanilloid subfamily member 6
TWIST	Twist transcription factor
UIP	Usual Interstitial Pneumonia
ULA	Ultra-Low Attachment
UPR	Unfolded Protein Response
VEGF	Vascular Endothelial Growth Factor
VEGFR	Vascular Endothelial Growth Factor Receptor
VIM	Vimentin
Wnt	Wingless-related integration site
ZEB-1	Zinc finger E-box-binding homeobox 1

Note: where an abbreviation is written in *italics* it generally refers to an expressed gene.

1. Introduction

1.1 The Respiratory Tract: an overview

The primary function of the lungs is gas exchange; providing oxygen to blood and the tissues and the liberation of carbon dioxide removed by the blood supply from the tissues, from blood to air. In order for this to happen air must be transported through the conducting airways of upper and lower respiratory tract to the distal lung and the alveolar sacs where gas exchange can take place[1].

The respiratory tract is comprised of the upper and lower airways. The upper tract or 'airways' include the nose and nasal passages, paranasal sinuses, the pharynx, and the section of the larynx above the vocal cords. The lower airways include the larynx below the vocal folds, trachea, bronchi and bronchioles. The lungs are generally included as a part of the lower respiratory tract however they can also be considered as a separate entity. The lungs are comprised of respiratory bronchioles, alveolar ducts, alveolar sacs, and alveoli[2 3].

The respiratory airways are further categorised into the conducting zone and the respiratory zone. The distinction is based on whether the zones are involved with the transport of gases or their exchange to and from the blood stream.

The conducting zone includes anatomical structures outside the lungs (nose, pharynx, larynx, and trachea) and some structures inside the lungs (bronchi, bronchioles, and terminal bronchioles). In the conduction zone inhaled air is filtered, warmed, and moistened[2 3].

The respiratory zone consists of respiratory bronchioles, alveolar ducts and alveoli, and is the site of oxygen and carbon dioxide exchange with the blood. Respiratory bronchioles and the alveolar ducts are responsible for approximately 10% of the gas exchange whereas the alveoli are responsible for the remaining 90%[3].

A further categorisation of the airways makes the distinction between proximal and distal airways. There is broad overlap between the proximal airways and the upper respiratory tract and the distal airways and the lower respiratory tract, however 'proximal versus distal' concept distinguishes the airways on their diameter, function and the way in which air passes through them rather than their anatomical location. Proximal airways are greater than 2 mm in diameter, they provide 80 to 90% of the physical resistance in inspiration, the airflow within them is turbulent and they do not contribute to gaseous exchange. In contrast, distal airways are less than 2 mm in diameter, they contribute 10-20% of the physical resistance in breathing, they display laminar airflow and contribute to gaseous exchange[4].

Inhaled air carries with it chemicals, particulates and pathogens from the external environment and the airway epithelium is the first point of contact for these materials therefore its integrity is essential for tissue protection and stable equilibrium between the various cellular components of the lung. Junctional complexes (tight and adherens junctions) between the cells of the respiratory epithelium not only physically maintain this barrier but result in an internal compartmentalisation that aids immunity and helps maintain internal homeostasis[5]. The junctional complexes also regulate in a controlled manner the traffic of chemicals, salts and water into and across the epithelial barrier[1].

The characteristics and functions of the cellular epithelium change throughout the length of the airway from proximal to distal regions. The upper respiratory tract consists of the trachea and large bronchi which are typified by pseudostratified epithelium and basal cells supporting predominantly columnar ciliated epithelium and mucous secreting goblet cells[6]. A viscous covering of mucus, water, ions and protective molecules is found in the upper airway and is rich in protective antioxidants, IgA, and lysozyme[7]. This mucilaginous lining protects the epithelium, traps inhaled particles and microbes which are then trafficked back up to the pharynx by the beating action of the cilia expressed on the surface of the bronchial epithelial cells[8].

Further down the airway are the bronchioles. These small airways are less than 1mm in diameter and typified by the presence of ciliated columnar epithelium and fewer goblet cells than the upper airways and therefore there is less mucus. The epithelium of the bronchioles includes Club cells[9]. These non-ciliated epithelial cells may have several roles including a protective role against airway obstruction (removal of Club cells in transgenic mice results in fibrosis that resembles chronic obstructive pulmonary disease (COPD)[10]). The major secreted products of the Club cells are: uteroglobin (secretoglobin family 1A member 1, also called Club cell secretory protein (CCSP)), surfactant proteins A, B and D, proteases, antimicrobial compounds, cytokines and chemokines and mucins[8].

After further branching of the bronchioles, the airway finally splits into the alveolar ducts before terminating in the pulmonary alveoli[8]. Each alveolar duct connects to two or three alveoli, the structural units of gaseous exchange[8 11]. There are in the order of 300 million alveoli in a normal human lung[12] representing a total internal surface area of around 40 square metres[13]. The thin alveolar walls are comprised of alveolar type one (ATI) and alveolar type two (ATII) epithelial pneumocytes[14] which in turn are surrounded by a network of pulmonary capillaries[11]. Figure 1.1 shows a diagrammatic representation of the conducting airways together with their epithelia.

The ATI pneumocytes are responsible for gas exchange, they are comparatively large in surface area, thin, flat and membranous covering around 95% of the alveolar surface. ATI cells form an immunological barrier with the ability to sense microbial products and to generate inflammatory responses[15] [16]. It is generally considered that ATI cells are terminally differentiated.

ATII cells, in contrast, are granular cuboidal cells that secrete and recycle all components of surfactant, the regulator of surface tension in the alveolus, preventing respiratory collapse of the lungs at the end of expiration by reducing surface tension. In addition to surfactant, ATII cells also secrete antimicrobial substances such as lysozyme and complement. In the event of loss of ATI cells and to enable wound healing, it is generally believed that ATII cells can undergo mitosis to produce two daughter cells, one of which will trans-differentiate into an ATI cell, whilst the other retains the type II phenotype[14]. Although little is known about the molecular regulation of this process it seems to be critical to lung repair. Recent work using rat ATI cells suggests they may have the potential to divide and participate in wound healing, challenging the belief that they are terminally differentiated[17] but despite this new evidence it is clear that ATII cells have a key role in lung homeostasis; regulating lung defence, immune regulation, epithelial repair and ion transport[14].

Microbial defence and innate immunity is reinforced by the pulmonary macrophage cells that reside within the alveolus. These alveolar macrophages phagocytose and remove pathogens, toxic and allergic particles that have evaded the muco-ciliary clearance and physical defences of the upper respiratory tract[18].

The ultrastructural hallmark of ATII cells is the expression of multilamellar bodies (MLB)[19] containing dipalmitoylphosphatidyl choline (DPPC), the major lipid component of pulmonary surfactant. ATII cells play an important role in innate immune responses within the lung and there is evidence that lung surfactant proteins, especially SFTPA and D (also known as "collectins") have anti-microbial effects and reduce inflammation caused by the inhalation of irritants[20]. ATII cells also help clear alveolar fluid through active sodium transport and it is believed their potential trans-differentiation function is to act as self-renewing progenitors to replace ATI cells that have been damaged, therefore maintaining normal lung architecture[14].

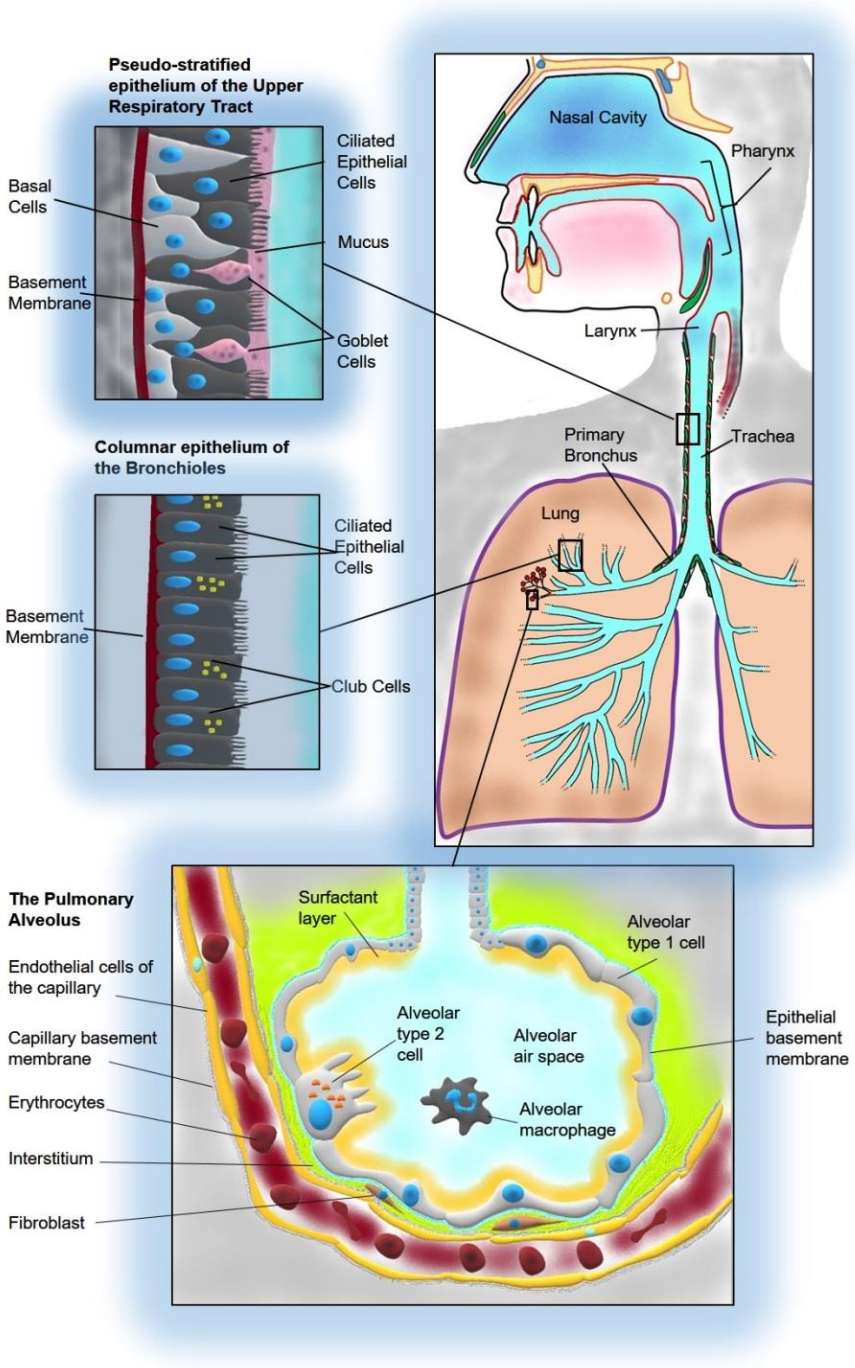

Figure 1.1. An overview of the conducting and respiratory zones of the upper and lower airways of the human respiratory tract.

Air enters through the mouth and nose, via the pharynx, larynx and trachea to the subdividing bronchi and bronchioles until termination at the alveoli, comprised of ATI and ATII epithelial cells, where gas exchange to the blood capillaries takes place. The epithelial linings of the trachea, bronchi, bronchioles and the alveoli are distinctly different. (Diagram by the author after Marchin[21]).

1.1.1 Respiratory Diseases

Diseases of the respiratory tract, particularly those that affect the homeostasis of the tissues of the distal lung pose a significant health threat as they can interfere with normal gas exchange and metabolism. According to the European Respiratory Society's "White Book"[22], in the European Union alone, lung disease contributes to two thirds of all deaths and approximately 6 million hospital admissions each year. These diseases range vary from the target site within the respiratory tract, whether they are chronic or acute in their causes.

Significant diseases affecting the lungs are: childhood and adult asthma, chronic obstructive pulmonary disease (COPD), cystic fibrosis, tuberculosis, acute lower respiratory infections, lung cancer, acute respiratory distress syndrome (ARDS) pulmonary vascular disease and interstitial lung diseases (ILD). These diseases have a variety of causes and contributing risk factors and patients may have a genetic susceptibility towards developing a disease. The simplest form of genetic susceptibility is when there is a clear single gene association (a monogenic disease) such as cystic fibrosis (CF). More commonly however, in the cases of diseases such as asthma, COPD and pulmonary fibrosis, genetic susceptibility is far more complex and disease progression can involve a combination of genotype and environmental factors such as diet, nutrition, the indoor and outdoor environment, occupational risk factors (such as exposure to particulates and chemicals), smoking and passive smoking. The most enigmatic and perplexing of the lung diseases are the ILDs, a diverse collection of more than 200 lung disorders which are classified together because they share a common feature of affecting the tissue and space around the alveoli. Some of the ILDs have clear environmental and occupational associations with the inhalation of air contaminated with coal and silica dust (pneumoconiosis and silicosis[23 24 25]) , farm dust[26], asbestos dust[27] and welding fumes[28] along with emerging diseases such as indium lung disease, nylon flock worker's lung, World Trade Centre –related lung disease, popcorn worker's lung and diseases associated with the inhalation of nanoparticles[29]. These conditions are often complicated by genetic predisposition[30], other environmental and lifestyle factors such as smoking[24 31], and microbial infections (e.g. Epstein-Barr virus (EBV), cytomegalovirus (CMV), adenovirus, hepatitis C virus (HCV), fungi and bacteria[32]. It is also worth mentioning concerns about the long-term effects of the novel severe acute respiratory syndrome (SARS) coronavirus, SARS-CoV-2, the causative agent of COVID-19. Persistent, long term respiratory complications of COVID-19 may cause substantial population morbidity including fibrotic lung disease with unclear clinical management strategies[33]. The demographics of COVID-19 morbidity and mortality are similar to idiopathic pulmonary fibrosis (IPF)[33], which will be discussed in the next section. Generally, environmentally associated diseases, the inhaled particles cause inflammation and eventual fibrosis. There is however a subgroup of ILDs where the cause is

so far, unknown, the so called "idiopathic" ILDs (IILDs). The most common of these is Idiopathic Pulmonary Fibrosis (IPF).

1.2 Idiopathic Pulmonary Fibrosis

IPF is the most common and lethal form of the IILDs, affecting in the order of 20 in 10,000 people in Europe and the United States[34] with a worldwide total of around 5 million patients[35]. It is a devastating disease of unknown origin. Its causes are difficult to determine as most patients present at an advanced stage. A diagnosis of IPF has poor prognosis[36] with a mean survival of just two to three years[37].

Diagnosis is defined by precise clinical, radiological and histopathological features together with the patient's clinical history. A surgical lung biopsy may be required for confident diagnosis, however this is not always appropriate in elderly or weakened patients[38]. Two thirds of patients are confidently diagnosed using clinical history and high resolution computerised tomography (HRCT) or surgical lung biopsy[39].and the observation of a typical pattern of "usual interstitial pneumonia" (UIP) described as gross honeycombing[40] at the macroscopic level and the appearance of so called fibroblast foci at a microscopic level. The histological pattern of UIP is thought to be the result of repeated epithelial injury together with unregulated fibroproliferation[41] with groups of proliferating fibroblasts and myofibroblasts known as fibroblastic foci. These foci are a key histological diagnostic feature of UIP and thought to signify areas of active fibrosis[42]. When histological sections are visualised using standard two-dimensional (2D) examination, the foci are considered small, distinct lesions, and their extent may be of prognostic significance. They have, however, been proposed to be linked in a complex interconnected reticulum that extends from the pleura into the underlying parenchyma[43]. However, using three dimensional (3D) micro-computerised tomography (micro-CT) imaging, Jones *et al* (2016) demonstrated that foci in proximity with shared areas of fibrosis form complex structures but are discrete in nature[44].

There is heterogeneity in the radiological and histological appearances of IPF patents, the rate of progression of the disease and the treatment response of the patients. This may indicate the involvement of a complex series of pathogenic pathways[38] and it is not obvious if IPF is a single disease or an umbrella condition to other subgroups of disease[40]. It is clear, however, that the pathology of the disease involves excessive, unresolved fibrosis[36].

1.2.1 The Need for Early Diagnosis

Despite the research into treatment of IPF there may be benefit in early diagnosis leading to earlier interventions and treatments known to slow the disease progression. Although not officially classified as a disease of smoking, and IPF is not solely associated with smokers, there is a clear correlation between smoking, age and genetics[45]. In a study of 566 IPF patients earlier diagnosis and treatment was correlated with increased survival[46]. Early diagnostic markers such as distinctive "Velcro crackles" and associations of localised sounds detected by electronic stethoscopes, together with observed HCRT abnormalities and mass screenings may help as an early diagnostic tools[45]. Several biomarkers have been proposed as predictors of disease progression in IPF patients. These include gene expression profiles, serum levels of proteins associated with lung epithelial injury and tissue remodelling (e.g. KL-6, matrix metalloproteinase (MMP-7), surfactant protein D (SFTPD)), type III procollagen peptide in bronchoalveolar lavage fluid and bacterial load[47]. However, as of yet no biomarkers have been identified predict disease progression nor to guide treatment and management in individuals[48]. There may be ways forward through genetic profiling, identification of specific microRNAs and identification of epigenetic markers, however such approaches would be costly, involve lung biopsy and unlikely to be suitable for mass screening[49].

1.2.2 Fibroblasts and their Interactions with the Epithelium

Cell to cell and tissue to tissue interactions initiate, regulate and maintain of cell differentiation and tissue morphogenesis in most vertebrate organ systems. They act as the major signalling system between the extracellular microenvironment, cells, and tissues. Signalling can be direct, through of intimate cell-to-cell contact or indirect, through the release and recognition of signalling molecules. Alternatively signalling can be mediated through extracellular matrices[50].

In all multicellular animals, cells are organized either into sheets of connected, polarized cells (epithelia) that typically rest on an extracellular basement membrane that is deposited from their basal surfaces, or as loose networks of fibroblastic cells (mesenchyme) that are connected through the extracellular matrix they secrete[50]. Cell-to-cell signalling typically occurs between epithelial and mesenchymal cells. This interaction or 'crosstalk' can be one-way or bi-directional. Epithelial to mesenchymal crosstalk is a key regulator in both lung development and normal wound healing processes and may be critical in the development of *in vitro* models of lung epithelia to recapitulate normal tissue architecture or the diseased state[51]. Evidence suggests that disruptions to the paracrine signalling between alveolar epithelium and interstitial fibroblasts may lead to disease progression in multiple

pathologies[52] including cancer[53] and IPF [54]. Generally, to investigate epithelial-mesenchymal interactions *in vitro* the mesenchyme and epithelium are separated with each component is maintained either in isolation or in recombination[52].

The epithelial to mesenchymal crosstalk involved in the development and maintenance of the ATII cell is not fully understood, however potential ATII epithelial derived molecules acting on the mesenchyme may include prostaglandin E2 (PGE2) and parathyroid hormone related peptide (PTHrP). Historically, the partially defined fibroblast derived components that support ATII cells have been grouped under the umbrella of 'fibroblast pneumonocyte factor' (FPF)[55]. The putative molecules in FPF have been variously suggested as including leptin, neuregulin-1β (NRG-1 β) and Perilipin-2 (PLIN2) [56 57 58 59].
Furthermore, in normal development and tissue repair, the process of epithelial to mesenchymal transition (EMT), whereby epithelial cells reversibly acquire mesenchymal features and enhanced capacity for mesenchymal cross-talk, plays a crucial role in the differentiation of multiple tissues and organs. Lung epithelial cells are a frequent target of injury and EMT is a key element in the pathobiology of cancer and fibrotic lung diseases often in response to TGFβ-1[60].

1.2.3 Dysfunctional Wound-Healing and Fibrosis in IPF

In humans, the adult lung is largely quiescent, yet is capable of limited regenerating in response to injury. Basal stem cells (BSCs) can regenerate both secretory and ciliated epithelium of the trachea and bronchi through partial control by Notch signalling[61]. There is some evidence that BSCs can also generate alveolar epithelium after extreme injury[62]. Secretory and ciliated cells of the bronchi largely regenerate themselves[63], however it also seems possible they may be regenerated from neuroendocrine cells[64]. SFTPC and Secretoglobin Family 1A Member 1 (Scgb1a1) positive bronchioalveolar stem cells (BASCs) are found at the border between the bronchiolar and alveolar regions and are thought to contribute to repair of both bronchiolar and alveolar regions[65]. ATII cells have been shown to self-renew and differentiate to replace ATI cells lost to injury in order to maintain homeostasis[66 67]. It also seems that ATII cells are capable of migrating considerable distances to effect repairs within the lung and may not just act locally[67].

In general, response to injury in humans is via fibrogenesis, rather than regeneration observed in amphibians and some reptiles. Fibrogenesis aids wound closure, prevents blood loss and invasion from microbial pathogens[36]. Historically IPF was thought of as a state of chronic inflammation leading to fibrosis however it is now generally thought to be the result of an abnormal wound healing fibrotic response[37] driven by persistent or recurring micro-injuries caused by factors such as cigarette smoke, micro-aspiration (aspiration of small

volumes of oropharyngeal secretions or gastric fluid into the lungs), other particulates, autoimmunity or possibly viral infection[38]. Some experiments have shown that certain infections will worsen fibrosis, suggesting a role of pathogens in IPF progression[68 69] and interestingly, there is a distinct IPF microbiome[70]. However, there is a lack of ongoing inflammation in IPF patients and anti-inflammatory therapies are ineffective in treatment suggesting that infection may not be a causative agent, yet inflammatory cytokines and immune cell invasion have been observed in IPF patients[71 72].

The most significant factor associated with IPF is inhalation of environmental agents, in particular cigarette smoke or occupational dusts, which may lead to a sustained response after an initial injury[73] and to epigenetic modifications in the genes that regulate tissue repair, through DNA methylation and other changes impacting on chromosomes[74].

In the pathological development of IPF it is believed an initial injury initiates the wound healing process but impaired wound healing mechanisms allow the progression of uncontrolled fibrosis, possibly via a combination of genetic predisposition through genetic polymorphisms. Gene mutations have been identified in IPF patients[74] including mutations in Mucin 5B (*MUC5B*), Surfactant Protein C (*SFTPC*), Telomerase (*TERT*) and Toll interacting Protein (*TOLLIP*)[38] but it is not known if these are causes, predispositions or simply associations. For example, *SFTP* and mucin mutations can lead to epithelial injury and death and telomerase gene mutations can lead to abnormal growth repair of damaged epithelia. However, IPF patients that have these kinds of mutations only account for 40% of those diagnosed[36].

In normal, unaffected individuals, lung injury is overcome through a wound healing response that repairs and restores normal tissue homeostasis in the damaged area. This process is mediated by fibroblasts, blood vessel formation and inflammatory cells. In normal wound healing, mesenchymal cells differentiate and migrate to the wound site. The epithelium becomes re-established and there is local and correctly aligned synthesis of collagen to provide strength and scaffold for the new tissue[37]. Blood vessels constrict and a fibrin blood clot is formed. Pro-inflammatory cytokines and the growth factors transforming growth factor beta (TGF-β), fibroblast growth factor (FGF) and platelet derived growth factor (PDGF) are released. The activation of the coagulation cascade is associated with excessive deposition of extra cellular matrix (ECM) is a feature of IPF and dysregulated coagulation eventually leads to fibrosis. The extrinsic system of coagulation is activated by tissue factor (TF) which is highly upregulated in ATII cells and alveolar macrophages and associated with fibrin deposits in IPF patients[37]. The extrinsic system appears to be the coagulation cascade that is activated in IPF patients. Protein C (also known as autoprothrombin IIA or blood coagulation factor XIV), an important regulator of anticoagulation, inflammation and cell death, appears

to be inhibited in the IPF lung. This causes decreased intrinsic blood clotting pathway activity which is associated with abnormal collagen deposition in patients with ILDs[75]. In the normal lung parenchyma collagen and other ECM factors form a stabilising scaffold to maintain functional lung architecture. In IPF the collagen, produced by myofibroblasts, is not only deposited in excess, it is qualitatively dissimilar to collagen from normal lungs. Tissue from IPF lungs has been shown to express significantly higher levels of the genes for collagen cross-linking enzymes lysyl oxidase like (*LOXL*) enzymes *LOXL 2*, *3* and *4* in association with an increase in 'bone-type' pyridonoline cross links and overall tissue stiffness with individual collagen fibrils from IPF tissue being smaller in diameter, yet structurally stiffer than in the normal lung. In an *in vitro* model of the fibroblastic focus, inhibition of LOXL using a selective small molecule inhibitor prevented pryidinoline crosslinking and reduced tissue stiffness[76] giving deeper insight into disease mechanisms and suggesting strategies for clinical treatment. Although the anti-LOXL2 monoclonal antibody 'Simtuzumab', failed to show efficacy in the clinic[77], its ability to inhibit crosslinking is limited[78].

After the activation of coagulation cascades there is subsequent activation of antioxidant pathways, fibroblasts and circulating immune cells. In IPF there appears to be a homeostatic imbalance of pro–fibrotic factors such as connective tissue growth factor (CTGF), Transforming TGF-β, PDGF, Coagulation Factor 10 (FXa), Vascular Endothelial Growth Factor (VEGF) and anti-fibrotic mediators such as Prostaglandin E2 (PGE_2), Interferon Gamma (IFNγ) and Hepatocyte Growth Factor (HGF)[38]. Interleukin-1β may induces an early inflammation response to trigger the activation of profibrotic pathways through transforming growth factor beta-1 (TGF-β1)[36].

Normally, inflammatory cells migrate to the wound, neutrophils clear cellular debris and macrophages then remove apoptotic neutrophils that release cytokines to recruit other immune cells and to stimulate fibroblasts, keratinocytes and local angiogenesis to re-establish normal tissue architecture[37]. This normal response can be prevented by a prolonged inflammatory phase that might be caused by infection, which may upset the homeostasis of wound healing[37].

In IPF, patients the histopathology typically shows localised epithelial damage, hyperplasia of ATII cells, fibrosis[37], abnormal cellular trans-differentiation, proliferation, apoptosis and ECM turnover leading to eventual fibrosis[38] through excessive deposition of collagen and other ECM proteins[37]. Vascular complications then lead to reduced blood blow to the areas and ischemia (oxygen deprivation) compromising tissue repair and ultimately in IPF, the tissue of the lung becomes remodelled. Much of this remodelling involves aberrant expression of ECM and may involve imbalanced expression of two families of proteins: matrix

metalloproteinases (MMPs) and their inhibitors: tissue inhibitors of metalloproteinases (TIMPs) [37].

In IPF, fibroblasts in the appear to have a distinct invasive and apoptosis resistant phenotype that contributes to the development of lung[40]. Myofibroblasts produce excessive amounts of fibrotic extracellular matrix (ECM) increasing lung stiffness, decreasing lung volume, in turn leading to shortness of breath. There is evidence that this accumulation of ECM and increasing stiffness may initiate a positive feedback loop driven by TGF-β1 further driving myofibroblast activity[79] with latent TGF-β1 becoming trapped in the ECM[36] manifesting in the typical pattern of fibroblastic foci seen in the micro-CT analyses of IPF patient biopsies[80 81 44].

The source of the mesenchymal cells in the fibroblast foci and that appear to drive the ongoing fibrosis is a conundrum. Fibroblasts accumulate via four possible mechanisms: firstly through uncontrolled proliferation and differentiation of resident lung fibroblasts; secondly epithelial-to-mesenchymal transition (EMT) of ATII cells and trans-differentiation to fibroblast like cells under the influence of TGF-β1 signalling[82] and *SNA1* and *2* (the human homologues of Drosophila 'snail' and 'slug' genes[83]). Evidence of EMT in the IPF lung has been demonstrated by the co-expression of epithelial and mesenchymal markers in human lung samples[84 85]. Thirdly, bone marrow derived fibrocytes are recruited from the blood and trans-differentiation into fibroblasts [86 87]. Finally, in the mouse, pericytes (the mesenchymal cells that wrap around capillaries) can become fibrotic and express collagen in response to injury. There are many sub-populations of pericytes, and it may be that a sub-population, expressing the ATP binding cassette ABCG2, are capable of transdifferentiating to myofibroblasts[88].

Using perilipin-2 (PLIN2) (also known as adipose differentiation-related protein (ADRP) as a lineage tracer in mice, resident interstitial fibroblasts and lipofibroblast populations expressing PDGFRα seem to be capable of trans-differentiation to myofibroblasts following partial pneumonectomy, repair and remodelling.[89]. The expression of αSMA and myofibroblastic differentiation induced by TGFβ can be halted and reversed *in vitro* by the addition of Rosiglitazone (PPARγ agonist)[90]. Lipofibroblast cells seem essential for ATII support in the mouse, however, evidence of lipid droplet containing fibroblast cells in the human lung is debatable, with conflicting reports of their presence[91 92].

Senescent fibroblasts have been implicated in IPF. Lung fibroblasts from IPF patients were found to be growth limited. They expressed senescence markers and reduced mitochondrial function[93]. An investigation into fibroblasts derived from IPF lungs and from bleomycin treated mice showed that the proliferator activated receptor gamma co-activator 1-alpha (*PPARGC1A*, encoding PGC1α) are repressed in human IPF fibroblasts and in the bleomycin

injured rodents[94]. This effect could be reversed in juvenile rodents but not in mature adults. PGC1α is linked transcriptionally to PPARγ expression, a driver of lipofibroblast differentiation. It may be that senescence in the fibroblast and any lipofibroblast-like cells in the IPF lung might contribute to the development of, and failure to resolve fibrosis. This evidence is further supported by single cell RNA sequencing of cell populations from the lungs of patients with various pulmonary fibroses[95]. There was a specific enrichment in fibrotic lungs of αSMA positive myofibroblasts, a PLIN2+ lipofibroblast-like group, and a fibroblast population positive for hyaluronic acid synthetase 'HAS1-hi cells' specific to only IPF patients. There was a collection of dysregulated genes shared across the fibroblast subpopulations. HAS1hi cells indicated enrichment for pathways associated with cellular stress, interleukin-4 (IL-4)/IL-13 signalling and previously implicated in EMT in other systems (TWIST and SNAI1). Evidence of a growth arrested potentially senescent epithelial population of cells expressing KRT17, collagen and other ECM components was also described[95].

1.2.4 The ATII Cell in IPF

Cellular homeostasis of the alveolar structure is dependent on signalling between ATII, ATI cells and mesenchymal cells[96]. Loss of homeostasis and ineffective re-epithelialization following injury result in loss of cell to cell adhesion, impaired ATII migration, senescence and apoptosis. Injury can also cause integrin-mediated activation of TGF-β1[97], altered biomechanics, and release of proteases, cytokines, and growth factors from the epithelium that activate mesenchymal cells. Activated fibroblasts and myofibroblasts can subsequently acquire an apoptosis-resistant phenotype, increased TGF-β1 expression, and subsequent induction of apoptosis or senescence in ATII cells leading to a cycle of extracellular matrix modification and accumulation with tissue remodelling[98] (Figure 1.2).

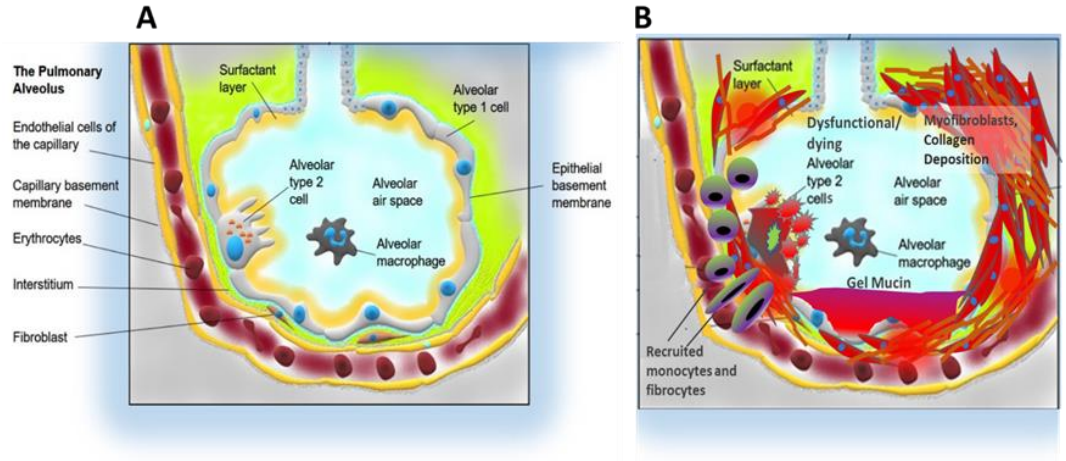

Figure 1.2. Overview of ATII functions in the normal and fibrotic lung.
In normal homeostasis ATII cells secrete surfactant and act as stem cells to replace lost or defective ATI cells (A). In IPF ATII cells become dysfunctional and are unable to maintain ATI populations. The lung parenchyma becomes remodelled through recruitment of fibroblasts, fibroblast to myofibroblast differentiation, and excessive deposition of ECM leading to the destruction of normal lung architecture and substantial reduction in gaseous exchange capability (B). Diagram by the author after Marchin[21].

As previously discussed, ATII cells are generally considered to be stem cells for ATI cells[67] and in normal homeostatic conditions the ATII cell expresses hyaluronic acid (HA) which promotes stem cell renewal in a Toll-like receptor 4-dependent manner through the release of IL-6. In a mouse model of fibrosis this IL-6 mediation appears to be lost, contributing to the loss of ATII innate restorative capability[99].

Defects in genes associated with telomerase, the enzyme responsible for the telomeres of chromosomes therefore maintaining stem cell longevity, are associated with IPF. These defects include mutations in telomerase reverse transcriptase (*TERT*) and the telomerase RNA component (*TERC*)[100]. Other genetic faults include those involved with protein expression and secretory functions of MUC5B, (specifically rs35705950 SNP), possible

pathogenic variants in *SFTP* genes[101] and mutations in ATP Binding Cassette A3 (*ABCA3*) and A-kinase anchor protein 13 (*AKPA13*)[100]. Smoking, environmental influences and viral infections, when combined with age and the genetic risk factors above, initiate ATII damage at an early stage of the disease. ATII loss through apoptosis reduces capability for repair and ATII dysfunction can drive fibrosis[102].

Apoptosis is a distinct form of cell death often referred to as "programmed cell death" and normally occurs during development or during defence and wound repair to remove damaged cells. It can occur through two linked pathways: the extrinsic or death receptor pathway and through the intrinsic or mitochondrial pathway. Extrinsic apoptosis involves transmembrane death receptor members of the tumour necrosis factor (TNF) family. Intrinsic apoptosis is triggered via non-receptor mediated intracellular events and signals that culminate in loss of mitochondrial membrane potential[103].

In the bleomycin mouse model, extrinsic apoptosis can be induced by TGF-β1. Subsequent Inhibition of apoptosis by the angiotensin converting enzyme (ACE) inhibitor, catropil, can lessen fibrosis [104] whereas stimulation of Fas mediated apoptosis in bleomycin challenged mice augments fibrosis[105]. Age, viral infection and genetics drive intrinsic apoptosis and is associated with endoplasmic reticulum (ER) stress. ER stress activated via the accumulation of misfolded proteins has been linked to IPF[106]. Misfolded proteins activate the unfolded protein response (UPR) in an attempt to retain homeostasis, however, if that is not achievable, the cell will enter apoptosis[106]. Due to their high metabolic activity, ATII cells are rich in mitochondria, particularly when responding to injury[107] and therefore it is possible that in IPF, ER stress and mitochondrial dysfunction act as profibrotic signals[108] which may in turn activate cell death via apoptosis[109]. Myofibroblasts in areas of fibrosis are thought to evolve hydrogen peroxide as an additional paracrine inducer of apoptosis in the alveolar epithelium[110].

Not only do ATII cells become apoptotic and depleted in IPF but they can become phenotypically altered. Normal ATII cells are depleted in the IPF patient, however hypertrophic and hyperplastic "ATII-like" cells can be found overlying the fibroblastic foci[111]. These hyperplastic cells appear to be one of the major sources of TGF-β1 expression in lung fibrosis[112]. TGF-β1 transcriptionally activates expression of connective tissue growth factor (CTGF) by ATII cells and by interstitial fibroblasts which in turn acts as a growth and chemotactic factor along with other chemo-attractants and activators such as CCL21[113] to recruit fibrocytes, exacerbating the cascade of fibrosis that typifies IPF[114 115]. Altered ATII cells have impaired capacity to renew[98] and it is thought that under the influence of telomere shortening, there is reactivation of developmental pathways. These include Wnt, Hedgehog, Hippo and Notch signalling, that in the aged lung, force the adoption of senescent associated

secretory phenotype (SASP) ATII cells[116] [96], rather than maintaining ATII self-renewal. Wnt is a glycosylated signalling protein and operates via its 'frizzled' seven-transmembrane receptor and associated low-density lipoprotein receptor related protein (LRP5/6) with subsequent β-catenin mediated effects on gene expression[117] in canonical Wnt signalling whereas non-canonical signalling is independent of β-catenin. Wnt signalling is prominent in the fibrotic lung[118]. It is necessary for ATII self-renewal during development[119] and to drive ATII to ATI trans-differentiation in alveolar repair[120]. The prevalence of Wnt signalling in IPF could be due to constant and continuing attempts to repair damaged alveoli[117] or, as more generally accepted[96], due to pathological alteration of homeostatic signals, leading to ATII senescence[121]. The resulting aberrant, senescent ATII phenotype has been suggested to drive fibrosis through decreased prostaglandin E_2 (PGE_2), decreased bone morphogenic protein (BMP), increased connective tissue growth factors (CTGF) and the recruitment of circulating immune cells and fibrocytes[96]. The stem cell potential of ATII to replenish ATI cells through differentiation becomes limited under the paracrine influence of SASP factors. Recent work has demonstrated that senescent ATII cells alone may be sufficient to initiate lung fibrosis[122]. ATII 'SASP' cells may also induce a secondary "bystander" senescence in neighbouring populations of cells[123] through direct contact (Notch signalling) or through secreted lipid bound extracellular vesicles (EV) with various senescence inducing cargoes such as DNA and RNA sequences and peptides[124].

Epithelial cells with senescent associated secretory phenotype (SASP), potentially as the result of mitochondrial dysfunction induced by factors such as aging[125], may persist in the lung without clearance and contribute to fibrotic disease by secreting factors such as IL-6, IL-8, MMPs and TGF-β1[126] and through Nanog mediated fibroblast activation[127].

Hedgehog (HH) signalling is a key factor in the regulation of epithelial-mesenchymal interactions in lung development and during fibrosis. In alveogenesis, cancer, and wound healing, paracrine action of HH is regulated by 'patched' receptor to release the activity of the 'smoothened' transmembrane G protein coupled receptor (GPCR) which binds to an unknown ligand and activates Gli-family transcription factors[128]. In the adult lung, however, HH signalling controls epithelial-mesenchymal cross-talk to maintain fibroblast quiescence[128]. In IPF there appears to be pathological re-activation of HH signalling[129].

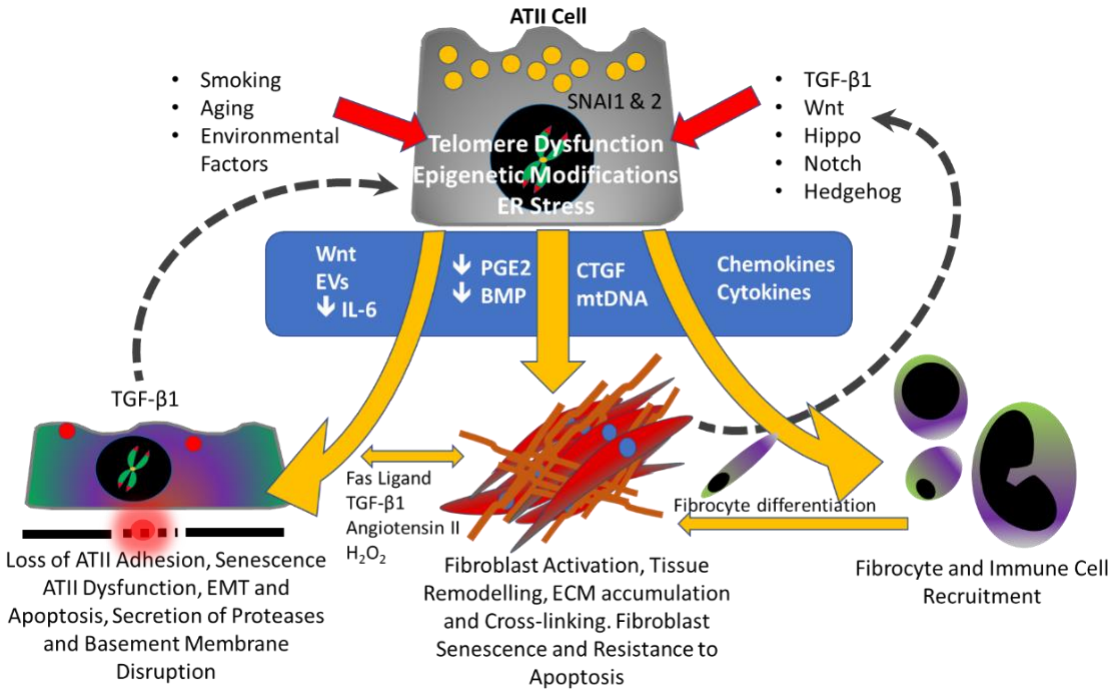

Figure 1.3 Regulatory signalling and ATII dysfunction in IPF.

Under the influence of aging, environmental and genetic factors, developmental regulatory pathways (Hippo, Wnt, Hedgehog and Notch) are pathologically re-activated as part of an aberrant wound healing response Defects in telomere maintenance, pathological expression of TGF-β1 induce: SNAI1 and 2 expression, EMT, senescence and apoptosis in ATII cells, an inability to replace ATI cells and development of an ATII SASP phenotype. ATII SASP cells and apoptotic loss of normal ATII, Wnt signalling, release of mitochondrial DNA (mtDNA), CTGF, extracellular vesicles (EVs) containing senescence inducing cargoes, reduced expression of PGE2, IL-6 and BMP lead to fibroblast activation, ECM accumulation, unresolved fibrosis and bystander senescence in adjacent cells. Chemokines cytokines recruit immune cells and circulating fibrocytes to exacerbate fibrosis. (Modified from Parimon (2020)[96])

1.2.5 Epithelial to Mesenchymal Transition

The epithelial to mesenchymal transition (EMT) is a process by which epithelial cells (with apical-basal polarity) transform into migratory and invasive mesenchymal cells (with front end–back end polarity). Epithelial cells form strong junctions such as adherens junctions with other cells whereas mesenchymal cells only form transient contacts with their neighbours[130]. EMT It is a fundamental event in embryonic development. It is crucial for the generation of the tissues and organs of both vertebrates and invertebrates[60]. The majority of adult tissues form as the result of one or more rounds of EMT and the reverse mechanism of mesenchymal to epithelial transition (MET). EMT has been established as an important step in pathologies the metastasis of epithelial tumours and in the development of fibrosis. Three different types of EMT have been defined developmental and wound healing (type 1), cancer progression (type 2) and fibrosis (type 3). It seems that in the pathological states, the molecular and cellular mechanisms involved in type 1 EMT (including Snail, Twist and other factors (see Figure 1.4)) become 'hijacked'. Loss of cell polarity and adherens junctions, such as

transcriptional downregulation of the epithelial marker E-cadherin and upregulation of N-cadherin and the mesenchymal marker vimentin, are characteristic of EMT[131].

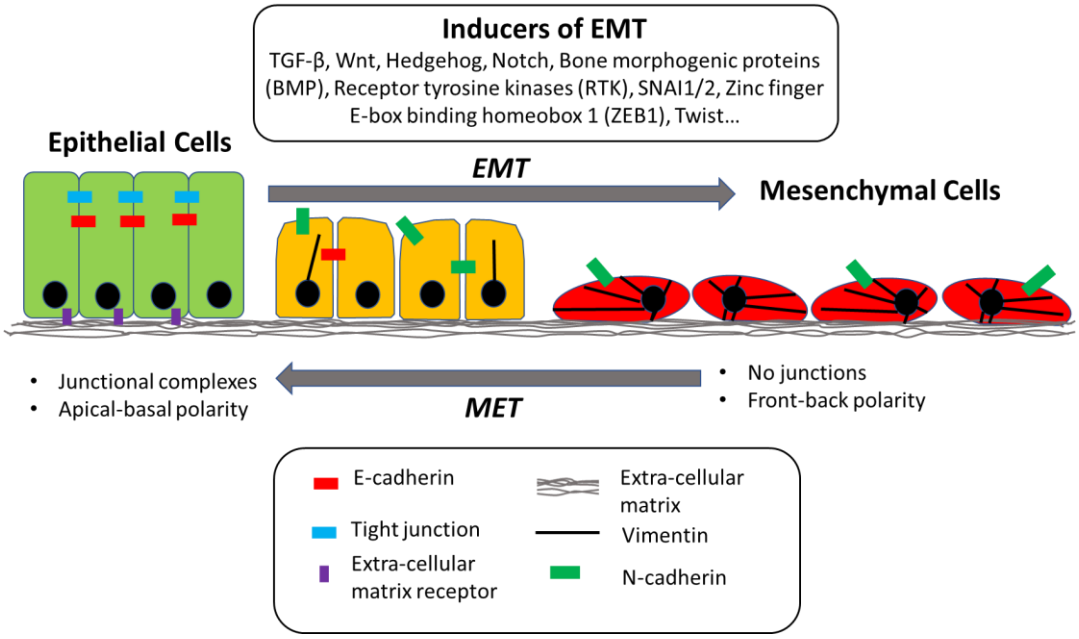

Figure 1.4 The Inducers and Effects of Epithelial to Mesenchymal Transition (EMT).
Under the influence of a variety of factors, epithelial cells can lose their apical-basal polarisation, downregulate epithelial markers such as E-cadherin and upregulate mesenchymal markers such as N-cadherin and vimentin and transform to a migratory mesenchymal phenotype with front-back polarisation. The transition may be temporary and may be reversed through the process of mesenchymal to epithelial transition (MET). Diagram by the author after Hill and Wang[132].

EMT may play role in IPF but it seems unlikely that ATII cells differentiate to contribute to the myofibroblastic population typical of the disease[133]. Using bleomycin treated rodents and lineage tracing of specific stromal markers, Rock *et al* (2011) demonstrated that many fibrotic cell populations could be obtained without any apparent ATII EMT[133]. Primary ATII cultures from bleomycin treated rodents have been used *in vitro* to study EMT (as demonstrated by reduced E-cadherin, increased expression of the fibroblast specific marker S100A4 and type 1 pro-collagen) and similarly *in vivo* using lineage tracing of SFTPC positive cells and the same EMT markers[134]. Using single cell RNA sequencing Xu *et al* investigated possible EMT in samples from fibroblastic foci in IPF lung[102]. Their data implies that some epithelial cells were partially transitioned to a mesenchymal phenotype with transcriptome analysis indicating activation of basal cells to "indeterminate" cells with upregulation of many EMT related transcriptional factors and markers. Data indicated that ATII cells might have transdifferentiated to a mesenchymal phenotype, expressing vimentin and collagen but not the αSMA hallmark of the myofibroblast. It is likely that these cells undergo EMT to facilitate epithelial repair, rather than contributing to the mesenchymal cell population.

In early stages of IPF it is thought that TGF-β1 acts on ATII cells to initiate EMT through the induction of *SNAI1*, *SNAI2* genes[82]. *SNAI1* (also referred to as "Snail") and *SNAI2* are transcriptional repressors, the human homologs of *Drosophila* snail (sna) and slug genes. *SNAI1* represses transcription of *CDH1* (E-cadherin) gene. *SNAI2* induces the first phase of EMT to induce desmosome dissociation, cell spreading, and initiation of cell separation[83]. The increasing stiffness of the cellular micro-environment caused by the increase of ECM in fibrosis may be a further driver of phenotypic change in the ATII through Hippo signalling, a highly conserved mechano-sensing developmental pathway that is dysregulated in the ATII of the IPF lung[135]. Myofibroblasts do not only play a role fibrosis, they are required for normal alveolar development where cross-talk with ATII cells occurs through optimal Notch signalling in alveogenesis. This process appears to be very finely balanced as over-persistent Notch signalling in mice can lead to a developmental outcome very similar to the honeycombed lung in IPF[136].

There may be a role for β-catenin in the development of EMT, showing that β-catenin and TGFβ signalling are involved in lung EMT in conjunction with the involvement of the TGF-β intracellular signalling and transcription factor proteins Smad2, Smad3 and other co-activators at the alpha smooth muscle actin (α-SMA) promoter[137 138 139 140 141 142 143 144 145]. EMT and fibrosis may also be initiated via the epidermal growth factor receptor (EGFR)[146]. Experimentally, the downregulation of specific epithelial cell adhesion markers such as E-cadherin (CDH1) and upregulation of the mesenchymal counterpart, N-Cadherin indicate an EMT response[147]. Several potential candidates for IPF therapy have arisen through research into EMT, including galectin-3 inhibitor[148], IL-17A neutralizing antibody[149], tankyrase inhibitor[142], and the small molecule inhibitor ICG-001[140].

The significance of EMT within the fibrogenic process may go beyond direct generation of fibroblasts and might include an attempt to escape apoptosis in response to injury and the subsequent release of cytokines to promote a pathological fibrogenic microenvironment.

Epigenetic changes in ATII cells accumulated through environmental factors, cigarette smoke and age and distinctly different patterns of DNA methylation are found in IPF patients with multiple histone modifications that have been associated with alterations in key pro-fibrotic pathways[74].

1.2.6 Current IPF Treatments

In 2016 a systematic review by Rogliani *et al* of published clinical trials of three potential IPF treatments (pirfenidone, nintedanib and N-acetylcysteine) showed that the only two approved anti-fibrotic treatments that appear to slow the disease progression in IPF were pirfenidone and nintedanib[150]. Pirfenidone is a well-established antifibrotic drug with both anti-inflammatory and antifibrotic properties. It appears to reduce fibroblast proliferation in *in vitro* and *in vivo* studies[151 152] and inhibits collagen production stimulated by TGF-β1. Nintedanib is an orally administered small molecule tyrosine kinase inhibitor originally developed as a cancer therapy. The drug inhibits both nonreceptor tyrosine kinases (nRTKs) and receptor tyrosine kinsases (RTKs) by binding competitively to their ATP- binding pockets[153]. This mechanism is exploited in the treatment of IPF by targeting three specific RTKs which are important drivers of fibrosis: α and β platelet derived growth factor receptors (α and β PDGFRs), fibroblast growth factor receptors (FGFRs)[153] and the vascular endothelial growth factor receptor (VEGFR)[154]. In fibrosis, binding of PDGF, VEGF and FGF to their corresponding receptors on fibroblasts stimulates the proliferation of these cells and the secretion of ECM. Nintedanib inhibition results in the blockage of the autophosphorylation of the receptors and their downstream signalling cascades[153]. Nintedanib may exert additional activity by blocking nRTKs such as Src and Lck. Treatment with nintedanib has been shown improve the quality of life of IPF patients[155] and to slow down the rate of decline of the forced vital capacity (FVC)[156 157] as recorded in spirometric analysis used in the diagnosis and monitoring of disease progression.

It is worth noting that IPF is not the only form of ILD resulting in fibrosis, it is therefore vitally important for clinicians to make a correct diagnosis as treatments that are effective in other fibrotic disorders may increase mortality in IPF[158] and although pirfenidone and nintedanib have some limited usefulness, they are not effective in all cases and simply manage to slow the rate of progression of the disease[159 160]. In the search for new therapies and potential cures for IPF it is believed that treatments that reduce myofibroblast expansion or reduce alveolar apoptosis should be beneficial[161 162]. To develop these putative new treatments it is important to understand the signals and pathways involved in disease progression[36]. Current studies into lung repair and wound healing in the lung are hampered by a lack of relevant models[37] therefore effective and physiologically relevant *in vitro* and *in vivo* models are required.

1.2.7 The Need for Mechanistic Models for Pre-clinical Drug Discovery and Efficacy Testing for IPF Research

Model systems are important tools for drug discovery and research into diseases such as IPF. It is important that they can display processes involved in fibrosis such as fibrotic changes

associated with epithelial tissues (e.g. EMT) and in mesenchymal cells (e.g. expression of collagen and α SMA)[110]. It is important the models are reproducible and deliver experimental results with acceptable throughput in a reasonable time-frame and cost[163].

(1) Animal Models

Mammalian animal models are anatomically and physiologically similar to humans and under appropriate ethical control can be treated with agents and conditions to induce fibrosis and with potential therapies. Animals can be assessed for the impact on their biology, through invasive and non-invasive analytical techniques, post-mortem histological investigation and comparison to the known disease state[164].

Animal models for lung fibrosis have been reviewed by Tashiro *et al*[164]. These include: Fluorescent isothiocyanate (FITC) and radiation induced fibrosis, familial animal models with targeted and naturally occurring deletions and mutations associated with IPF, humanised models where human IPF lung fibroblasts are injected into immunodeficient non-obese diabetic (NOD/SCID) mice. Recombinant models such as an *in vivo* animal model of lung fibrosis in the rat through a replication deficient adenovirus vector to deliver TGF-β1 cDNA directly to the animals' lungs[165]. Silica induced fibrosis, asbestos induced fibrosis and age related models[164]. Domestic animals such as West Highland terriers and horses are alternative lung fibrosis models, however ethical and animal husbandry requirements render them impractical for most experimental use[164].

The most commonly used model in IPF research is the bleomycin challenged rodent. Bleomycin is an antibiotic derived from *Streptomyces verticillus*, a species of Gram-positive bacteria[166]. Bleomycin is conventionally used as a cancer chemotherapeutic[167 168], causing single and double-strand DNA breaks in tumour cells[169 170], interrupting the cell cycle, leading to apoptosis[171]and cell death[172 173]. In most tissues, bleomycin is inactivated by bleomycin hydrolase, an intracellular DNA-protecting protease[174]. In many cancer cells and lung tissues there are lower levels of the enzyme, leading to successful cancer cell destruction with the side-effect of increased risk of lung injury[175 176]. Low levels of bleomycin hydrolase in rodent lungs allow the development of fibrosis. Typically, bleomycin is administered to the animals via the intra-tracheal route[177 178 179] .

The rodent bleomycin model of lung fibrosis is cost effective, relatively simple and rapid and reproducible and most extensively used experimental model of IPF[164]. It has provided invaluable insights into IPF pathogenesis, prognosis, and treatment[164]. Pirfenidone and nintedanib were selected based on their efficacy in the inflammatory or early-fibrotic phase of the bleomycin model[180 181].

Despite its widespread use, the bleomycin rodent model has several shortcomings when compared to human IPF. The similarities and differences between the human disease and the model are summarised in Table 1.1.1.

Where the model seems to recapitulate the IPF successfully is in the increase in the numbers of collagen synthesising myofibroblasts in the distal lung[182 183 184] which typifies the clinical disease[185 186]. In all other respects, however, the bleomycin model does not represent the disease well. Most significantly, human IPF is a slowly developing, non-reversible, incurable fibrotic disease with little obvious inflammatory involvement, IPF pathology is entirely located in the distal lung. Fibrosis in the bleomycin induced rodent model initiates in the bronchi, it involves inflammation, develops rapidly and is reversible[187].

Human idiopathic pulmonary fibrosis (IPF)	**Pulmonary fibrosis induced by the intra-tracheal delivery of bleomycin**
Human IPF is a slowly developing disease; it develops over years and is characterized by irreversible progression punctuated with periods of acute exacerbation[188]	Bleomycin induced fibrosis develops rapidly over days to weeks. It progresses at a stable rate and critically, fibrosis is reversible[189]
Alveolar epithelial cell death is a rarely observed in IPF and a poorly understood feature of the disease[190] .	Alveolar epithelial cell death is widely described and observed in bleomycin induced fibrosis[191 192]
The role of inflammation in IPF progression is not well understood and although it may have a role in disease progression it is not a prominent hallmark[188 193 194].	Inflammation, the infiltration of the lung by a variety of cell types, and the expression of pro-inflammatory cytokines is a generally accepted feature of bleomycin induced fibrosis[195 196].
Increased numbers of collagen synthesizing myofibroblasts and fibrotic cytokines are observed[186 197]	Increased numbers of fibrotic cytokines and collagen synthesizing myofibroblasts are seen in rodent. In this particular case the bleomycin model is very similar to clinical IPF[198]
The development of IPF fibrosis is characterized by basal, sub-pleural distribution with the appearance of fibroblastic foci[80 81 44]	bleomycin induced fibrosis shows a more bronchiolocentric distribution[179]
In IPF the patient displays Dyspnea (shortness of breath) and there is evidence of airway restriction, leading to decreased forced vital capacity and lung compliance[199 200].	Lung compliance seems unchanged in the rodent model[179]. Any changes in forced vital capacity are unknown due to the challenges of measuring lung function in the rodent[201 202 203].

Table 1.1.1 Comparison of the features of clinical IPF and the bleomycin induced rodent model of fibrosis
(Adapted and updated from Williamson *et al* (2015)[189]).

An example of this limitation includes the potential targeting of Interleukin-13 (IL-13). The lung of an IPF patient is rich in T helper cell type 2 (Th2) cells which express Interleukin-13 (IL-13) which in turn, through the expression of the chemokine CCL2, increases the expression of TGF-β1 leading to fibrosis. In the bleomycin model, inhibition of CCL2 by antibody therapy reduces fibrosis. However, a clinical trial of Tralokinumab, an anti-IL13 monoclonal antibody, in subjects with IPF was terminated due to lack of efficacy in the patients[204].

In 2017 The American Thoracic Society (ATS) convened a workshop to review and recommend considerations for the pre-clinical assessment of potential therapies for pulmonary fibrosis[205]. The panel considered not only the choice of animal in terms of species, age and gender but also emphasized the need for practical considerations of fibrosis modelling and which fibrotic endpoints should be used for results evaluation to balance reproducible data and physiological relevance with ease of use within the time and cost constraints.

The conclusion of the workshop was that the most appropriate protocol involves the intra-tracheal bleomycin treatment of both male and female C57Bl/6 mice with bleomycin, with restrictions: the compound under investigation should be administered after the acute inflammatory response induced by bleomycin has subsided, generally at least 7–10 days after bleomycin exposure. Hydroxyproline measurements for collagen accumulation and histologic assessments are recommended as the most appropriate end point measurements and the outcomes of all animals used in a study should be reported[205].

(2) Alternative "Omics" Strategies

At this point it is worth discussing an alternative strategy to aid the understanding of complex diseases such as IPF; the application of "omics" technologies. Genomic, proteomic and lipidomic studies have enhanced the understanding of how genes, epigenetics and gene expressed products contribute to the pathogenesis of the disease. These techniques have been used in the genomic profiling of patients to identify biomarkers, molecular phenotypes and exon sequencing to identify and confirm of multiple novel molecules that are mechanistically involved in IPF pathology including MMP-7, TWIST, IGFBP5, osteopontin, Wnt5a, Let-7d, miR-21, LOXL2, TGF-β3, Collagen V, TGF-β1, angiotensin II, JNK, CTGF, and CCL2[206]. They have also provided insight into the aberrant activation of developmental pathways and distinctive gene signatures in IPF that may aid disease prediction and progression[206]. Proteomic analysis of bronchoalveolar lavage and blood using techniques

such as two dimensional (2D) electrophoresis[207] and hybridisation chips[208] have shown that epithelial endoplasmic reticulum and oxidative stress[207] are key in IPF and lipidomics have been applied to IPF research using the mouse model[209].

Although "omics" approaches are useful, they are costly, time consuming and require access to patient cohorts and specialist computing resources. Results analyses from such studies can be time consuming and rather than focussing on and answering specific biological questions, they are more appropriate to generating new hypotheses. Consequently, there is still a requirement for mechanistic functional *in vitro* cell biology models that can be controlled and measured in a reductionist way to test hypotheses[210].

After animal models and "omics" approaches there are the options of *in vitro* model systems. These do not offer the benefit of working with a whole organism, however, they offer certain advantages over *in vivo* models in that they allow the scaling down of experiments, increase in throughput at early stages of research and drug discovery and negate the need for establishing colonies of animals and the associated ethical and time constraints[8 211 212].

(3) *In vitro* Models

In IPF research there is a need for *in vitro* models that are able to recapitulate ATII epithelial biology, disease relevant fibrosis and lung remodelling in line with current opinions on disease pathogenesis[213 38 40 37]. Such models also have a wider application in other lung diseases such as asthma[214], infection biology[215 216] and the effect of environmental particulates on lung epithelia[217 218 219].

(a) Lung Slices

The most physiologically relevant *in vitro* model available for IPF research comes in the form of *ex vivo* precision-cut human lung slices. These can be obtained from lung cadaver, surgical resections or from explanted lungs from normal unaffected donors or from the lungs of patients with IPF. These lung slices have the key advantage of being very close to the *in vivo* state and therefore offer physiological relevance[220 221 222] and they can be maintained viable in culture for 5–7 days whilst still preserving their complex three-dimensional architecture. Their usefulness is limited to a week in culture as such slices generally soon display extensive apoptosis[223]. Another drawback is that not all laboratories in the field will have access to primary lung material due to limited supply and the ethical and consent constraints that might prove to be insurmountable for many researchers. In addition, there will also be basic issues of standardisation due to genotypic and phenotypic (in terms of age, gender and life

style) differences from donor to donor that may have a confounding effect on results[224], There will be additional issues regarding variation in the method and time of necropsy, the time and method taken to transfer specimens to the laboratory and issues with environmental and patient derived microbial contamination together with laboratory safety issues surrounding potential virus infection and subsequent testing of donor derived tissues[225]. This variability will be impact on results from different labs and within labs as it unlikely to be possible to return to the same donor material for repeat experiments.

The use of lung slices, therefore, may neither be possible nor desirable for many laboratories, calling for the adoption of alternative approaches and most researchers will have to fall back to alternative *in vitro* cell culture techniques. Complex co-culture airway systems with three dimensional (3D) tissue like interactions can be generated in the laboratory through the isolation of primary cell cultures from patient biopsy or cadaver derived tissues[226 227]. Examples include work by Lehmann *et al* (2011) in the generation of their triple cell co-culture model involving primary human alveolar type-1 like cells (hAEpC) with human blood monocyte derived macrophages and dendritic cells[228].

(b) Primary Cells

Primary cell isolates are close to *in vivo* tissues in lineage, they present the potential of physiological relevance, however, they also offer technical challenges. They are limited by tissue availability, ethical approval and patient consent for access to regions of resected lung tissue surplus to requirement [229 230]. There will be the issues of donor to donor variability and the limitation of not being able to return to the same donor for repeat experiments, impacting on experimental reproducibility. Primary cell types must be identified and selectively isolated and maintained in culture. In the isolation of ATII cells from surgical biopsy, sections of tissue must be perfused to remove blood cells, digested with trypsin and the ATII cells enriched by removing more adherent contaminating fibroblast cells. ATII cell enriched populations will stain positive for alkaline phosphatase to help confirm their isolation, however the populations will not be pure and will retain residual contaminating cell types of other lineages and may also be subject to microbial contaminations acquired during preparation or from patient pathologies. Other characterisation techniques such as cell morphology and expression of surfactant protein *mRNA* can be used to help increase confidence that the isolated cells are ATII[229]. The cell culture media used have to be selected for their compatibility to maintain the cells in a healthy proliferating state and to maintain active selection for the desired cell types[231]. The usefulness of primary cultures is restricted. Cell division is limited to a few passages before the cells become senescent and this capacity becomes reduced with increasing donor age [232]. Primary ATII cell cultures are useful in short

term culture however they can spontaneously differentiate to the ATI cells over 1-2 weeks[233]. *In vivo*, a proportion of ATII cells are thought to transdifferentiate to ATI [234 235]. Thus, from characterisation and functionality standpoints, the ability for the ATII cells to differentiate further and demonstrate self-renewal to express markers of ATI cells might be desirable[236 237]. Recapitulating the level of complexity homeostasis within the alveolus may require advanced three dimensional cell culture models such as scaffolds and hydrogels[238 217 239].

(c) Tissue Engineering and Advanced Techniques

Tissue engineering approaches offer the potential to generate lung tissue *in vitro* but the field is challenging as the lung is a complex organ comprised of around 40 different cell types, all of which are required for optimal function[240]. Current approaches include the culture of lung cells or lung progenitor cells on biologically derived or synthetic scaffolds[241].

Biologically derived scaffolds generally rely on decellularisation of lung tissue from human donors or animals through the use of detergents and nucleases to provide a biologically typical extracellular matrix (ECM) to act as a scaffold to provide structure and help direct correct cellular differentiation[242]. The aim of decellularisation is to remove the cells without affecting the acellular scaffold structure and ECM composition[243]. The acellular scaffold is then repopulated with cells from another source. For example, scaffolds from animal sources could be re-cellularised with human derived cells. A major advantage of acellular lung scaffolds is that they retain the complex structure of native lung tissue, which cannot be artificially generated using current techniques. Human scaffolds from aged patients or those with pre-existing lung diseases are not suitable however, as they lead to less than optimal tissue orientation[241].

Synthetic biomimetic lung scaffolds may be generated using casting, electrospinning, cryogelation (where gel formation occurs under semi-frozen condition) or micro-fabrication techniques. Synthetic or naturally occurring polymers can be used in these approaches, a variety of materials have already been explored for tracheal, bronchial and parenchymal lung tissue engineering[241]. Artificial scaffolds for tracheas have been intensively investigated for the field of human transplantation with some success due to the trachea's simple, tubular structure[244]. Engineering of the lung parenchyma is more challenging due to the more complex three-dimensional (3D) structure. It requires thin boundaries and interconnected pores for efficient gas exchange. Potential scaffolds for parenchymal tissue engineering have been made using foaming[245], porogen-solvent techniques, cryogelation[246], photodegradation[247] and self-assembly of microspheres[248]. Although these techniques have generated alveolar-like structures, they lack the vasculature and airways required to

generate a complete functional model for gas exchange. Recent manufacturing processes, however, have been developed that offer the promise of generating perfusable vascular channels in tissue-engineered constructs[249].

Electrospinning of synthetic and natural polymers is an effective method of producing nanoscale fibres for use in tissue engineering of the trachea[241]. Electrospinning can also create porous scaffolds similar to the ECM capable of supporting cell attachment, proliferation and differentiation. Growth factors or pharmaceuticals may then be included in the scaffold to influence and direct regeneration. Electrospinning has already been used as an *in vitro* platform for studying the IPF lung micro-environment[250].

3D printing has potential as a strategy for bioengineering[251] but current 3D printing approaches rely on solvents or heating to generate polymer solutions that can flow as liquids nozzles and are currently incompatible for the printing of living cells.

Ultimately neither decellularized or completely artificial scaffolds may be the optimal for the *in vitro* modelling of lung tissue. Hybrid, composites of two or more materials may provide a solution as sites for cell adhesion and organisational and differentiation cues. These hybrid biological and synthetic materials together with advanced manufacturing approaches may produce more reproducible products[241].

Organoid technology is another promising advanced technique for *in vitro* modelling of many biological systems[252]. Mimicking developmental processes, lung organoids have been generated from monolayer cultures of induced pluripotent stem cells (iPSCs) directed to endoderm and then anterior foregut endoderm over the course of nine to ten days. The resulting spheroids were cultured in a 3D Matrigel™ droplets and subsequently directed to become airway-like human lung organoids forming airway-like structures and cell types. These include mesenchymal populations and epithelial cells that expressed ATI and ATII markers. Foregut spheroids embedded in Matrigel and grown in serum-free medium containing FGF7 and all trans retinoic acid (ATRA) give rise to lung progenitor organoids with a transcriptome similar to that of bud tip progenitors found in the human foetal lung during branching morphogenesis[253].

(d) Stem Cells

The recent development of human embryonic stem cell alveolar models from human embryonic stem cells[254] (hESC), induced pluripotent stem cells (iPSC)[255 256 257], mesenchymal stem cells[258] and lung cell progenitor populations[259] combined with tissue engineering and

3D cell culture offers the potential of the development of advanced cultures to provide differentiated lung epithelial cultures into more relevant models[260] [261] suitable for pre-clinical IPF research. However, these techniques are technically challenging and their widespread uptake has been limited.

(e) Characterisation of *in vitro* ATII models

To aid researchers to evaluate and characterise *in vitro* ATII models, many of their critical phenotypic properties were outlined in a review paper by Beers and Moodley (2017)[262] which provides a useful checklist for ATII functionality.

The key function of ATII cells is to produce surfactant[263]. *In vitro* ATII models should have evidence of a mature surfactant production system including the expression and maintenance of *mRNA* for surfactant proteins B and C (*SFTPB* and *SFTPC*)[264]. Expression of *SFTPC* is particularly important as it is widely agreed that it as exclusively expressed in ATII epithelial cells[265]. The expression of Surfactant Protein A (*SFTPA*) which has innate immune properties *in vivo* [266] [267] is desirable together with expression of the gene for the ATP-binding cassette class A3 (*ABCA3*)[268] [269]. Cells should demonstrate biosynthesis pro SFTB and C proteins and their intermediates[262]. There should be evidence that the cells can biosynthesize and store surfactant phospholipids, especially Dipalmitoylphosphatidylcholine (DPPC), the major lipid constituent of pulmonary surfactant[270]. Multilamellar bodies (MLB) should be present in the cytoplasm of the cells at a distribution similar to primary ATII cells[271] [272] [14]. In addition, the cells should express the markers CD63, ABCA3 and the lysosomal associated membrane protein (LAMP)3[262]. Surfactant phospholipids and SFTPB and C Proteins should be secreted together via regulated exocytosis[273]. MLBs are lysosome-related organelles, thus presence of acidic, lipid-rich organelles would also be a desirable feature[274].

Other key *mRNAs* and proteins associated with ATII include progastricin C which is downregulated in ATII to ATI differentiation[275] and napsin[276]. As ATII cells are thought to trans-differentiate to ATI[234], the exclusion of ATI markers such as aquaporin 5 (*AQP5*)[277] and *T1α*[278] would be desirable. ATII cell models should establish an epithelial barrier in *in vitro* Transwell™ growth conditions, establish tight junctions[279] , transport sodium[280] and therefore generate high trans-epithelial resistance (TEER)[281].

Beers and Moodley suggest that any novel model should be compared at a proteomic and lipidomic level with primary ATII isolates. Although these technologies are not, accessible to most researchers, comparison of any results with primary ATII isolates and with results other models, such as conventional cancer derived cell lines would provide insights into how physiologically relevant a putative model may be.

Primary cell monoculture of ATII isolates from IPF patients samples and normal individuals can be a useful strategy[282], however, the use of primary cells as ATII models in monoculture presents the same ethical, reproducibility, trans-differentiation to ATI and longevity issues as seen in lung slices and complex co-culture systems.

(f) Immortalisation

The availability of novel immortalised primary alveolar epithelial cells would be useful to the field of ATII research. Attempts have been made to increase the longevity of primary cells using combination of simian virus 40 (SV40) large T antigen and telomerase. Recent attempts at generating transformed ATII cell lines from ATII primary cells have had mixed results. Kemp *et al* immortalised AT2 cells from normal tissue through viral transfection of the catalytic subunit of telomerase (hTERT) and the temperature-sensitive mutant of simian virus 40 large-tumour antigen (SV40)[283], however, the resulting cell line exhibited an AT1-like cell phenotype[283]. More recently, in 2020, a series of cell lines designated 'HAEL' (human alveolar epithelial lung) were generated using a non-viral vector to transfect hTERT and the SV40 large T antigen to immortalise primary epithelial lung cells with promising results[284]. These HAEL cell lines, however are not universally available, neither have they been authenticated nor curated into the Cellosaurus database of cell lines[285].

An alternative strategy for increasing primary cell longevity involves the use of Rho kinase inhibitors. These have been used to prolong ATII phenotype in *in vitro* foetal tissue derived primary lung epithelial cultures[286]. .

(g) Conventional Cancer Derived and Immortalised Cell Lines

Despite recent advances, there is still considerable reliance and widespread use of authentic[287] continuous cancer or other immortalized cell lines. Sometimes these cell lines are derived by retroviral transduction[288], but more commonly they are derived from tumours or through viral transformation of primary cells, often many decades previously. Continuous cell lines are often used as an alternative to primary cells. They offer several practical and financial advantages. In comparison to primary cells they are cost effective. Primary cells must be replenished from a new source once the cells have reached replicative senescence after a limited number of population doublings[232]. Whereas, if properly managed, a single seed vial of a continuous cell line can provide a near inexhaustible supply for an entire institute and culture can be scaled-up to generate the quantities of cells required for high-throughput experiments. Continuous cell lines are considered easy to use as they can be

grown in standard tissue culture flasks from frozen vials using standardised and reproducible protocols and relatively simple media formulations as compared to primary cells. Generally, they exhibit an adherent phenotype which allows easy microscopic observation and allows the seeding of cells into multi-well tissue culture plates to provide practically useful cell numbers per replicate, to provide adequate amounts of *mRNA* for QRT PCR analysis for example. The cells can be easily treated with compounds or conditions expected to cause an observable change in the cells. Cell lines circumvent ethical concerns associated with the use of animal and human tissues. They also provide a pure population of cells with the potential of consistent samples and reproducible results to allow standardisation within and between laboratories and research groups[289].

Continuous cell lines have revolutionized scientific research through use in vaccine production, testing drug efficacy, metabolism and cytotoxicity. They are used in antibody production, genetics studies and the generation of artificial tissues such as artificial skin[290]. Cell lines can be predictably genetically engineered to enable the synthesis of biological compounds such as therapeutic proteins[291]. The popularity of cell lines can be estimated from the numerous publications using cell lines. Suppliers such as The American Type Culture Collection (ATCC, Manassas, Virginia, USA) and the European Collection of Authenticated Cell Cultures (ECACC, Salisbury, Wiltshire, UK) provide thousands of standardised continuous cell lines representing hundreds of tissues and dozens of species[289].

Despite their major advantages, researchers must be aware of the significant drawbacks of using cell lines in place of primary cells. Cell line models should display and maintain functional features as close to primary cells as possible. However, these features may be difficult to determine. Often the functions of the tissues of interest or primary cells derived from them are not entirely understood. Cell lines are genetically manipulated, either deliberately through immortalisation techniques or pathologically through carcinogenesis. This may alter their phenotype, functions and their responsiveness to stimuli. Serial subculture of cell lines can further cause genotypic and phenotypic variation over extended periods. Although continuous cell lines can maintain a stable phenotype through many subcultures [292], they differ from original tissue, compromising their ability to fully reproduce *in vivo* physiological state, often displaying uncontrolled proliferative growth and a de-differentation[293]. Cell lines may not, therefore, adequately represent primary cells and may provide different results[289].

Other major problems associated with continuous cell lines are cryptic contaminations with other cell lines or even complete misidentification and mycoplasma contamination. Cross-contamination of cell lines was exposed by Walter Nelson-Rees in the early 1970s. He showed that the majority of cell lines being used worldwide and distributed by cell banks were

contaminated with the cervical cancer cell line HeLa[294]. This still remains a substantial problem even after several decades[295]. If a rapidly proliferating cell line contaminates another, it only takes a few passages until the culture is entirely taken over. Mycoplasmas can persist undetected in cell cultures to cause extensive alterations in gene expression and cell behaviour. It is estimated that laboratories 15–35% of cell lines were estimated to be contaminated with mycoplasma[296] . Care should be taken when using cell lines and experiments and if possible validated by primary cultures[289].

Continuous cell lines derived from pulmonary tissue offer simple human based models for the study of airways responses. These have been established from cancers or through viral transformation of cells from normal lung tissue to generate bronchial epithelial cells, smooth muscle cells and fibroblast cell lines[297]. Cell lines based are widely used for the analysis of cell signalling pathways and basic cellular airway responses. The BEAS-2B bronchial epithelial cell line has been used to demonstrate IL-1β as a potential therapeutic target in rhinovirus-induced inflammatory responses in asthma[298]. 16HBE14o-, an SV-40 transformed cell line and the adenocarcinoma cell line CaLu-3 have both retained their ability to form an electrically resistant tight barrier through expression of epithelial tight junction proteins. Hence, these cell lines are widely used for toxicology and drug transport studies and studies of barrier function in response to allergens[299], particulates[300], cigarette smoke[301] or viral infections[302]. Despite retaining epithelial features, BEAS-2B, 16HBE14o- and CaLu-3 are considered as models of the bronchial epithelium[303] [297]. To investigate the role of the ATII cell in fibrosis, a suitable ATII cell line is required. The options available to researchers for *in vitro* ATII research are limited and there are very few alveolar epithelial cell lines derived from human lung tissue[284]. The NCI-H441 cell line was isolated in 1982[304] from the pericardial fluid of a patient with papillary pulmonary adenocarcinoma but the cell line shows mixed characteristics of both ATII and Club cell-like bronchiolar epithelial cells[305] [12]. Novel hTERT/SV40 large T antigen transformed alveolar cell lines are limited in terms of functionality and supply as discussed in the previous section. This leaves the majority of researchers left with the options of using primary ATII cells, the generation of ATII from iPSC[306] [256], with associated complications, or use of the A549 cell line. Established in 1972 by Giard et al[307] from a human pulmonary adenocarcinoma A549 is the most frequently used human alveolar cell model for biopharmaceutical research. A549 cells have over 19,000 citations in the PubMed database since their inception. The cell line has been characterised as being representative of ATII cells[19] [308] [309] [310]. However, while work with early passage A549 cells provided evidence of their ability to exhibit features of an ATII epithelial cell phenotype[308] [309] [310] more recent studies have presented conflicting findings[311] [312]. Due to its widespread use and accessibility, it would be of benefit to determine if the ATII cellular phenotype of the A549 cell line could be improved. The objectives of this study focus on

determining cell culture growth conditions and media formulations that might result in more representative ATII characteristics in the A549 model.

1.3 Hypothesis

1.3.1 Overarching Hypothesis:

Reproducible, easy to access, cost effective pulmonary epithelial models can be developed from readily and widely available cell lines such as A549 to facilitate the study of ATII cells in lung pathology and fibrosis with particular focus on IPF.

(1) Sub-hypothesis 1:

Enhancement of the cell microenvironment through the use of different medium formulations and three-dimensional (3D) cell culture strategies will result in changes in A549 alveolar epithelial cell line behaviour to recapitulate the phenotype of ATII cells of the pulmonary alveolus. Furthermore, the developed model(s) will have the potential to be modulated under experimental conditions to reproduce aspects of ATII dysfunction specific to the fibrosis observed in progression of IPF.

(2) Sub-hypothesis 2:

The models will be quantifiably enhanced through the combination of the A549 epithelial component with the corticosteroid dexamethasone and signalling factors derived from a fibroblastic component. This will include signalling by the ERRB ligand neuregulin-1β and factors derived from foetal lung fibroblasts leading to the A549 cells adopting a more physiologically relevant alveolar epithelial phenotype and responses.

1.3.2 Aims

- To contrast and compare epithelial and ATII specific gene and protein expression in A549 cells cultured as 3D spheroids and as 2D conventional cell culture in simple cell culture medium (DMEM) and more complex physiological medium (Ham's F12). To evaluate the ATII differentiation potential of a novel lung progenitor cell line.
- To develop the most appropriate ATII epithelial models using various factors and compare gene expression with primary human ATII isolates.
- Develop the model further through the use of the corticosteroid dexamethasone and the ERRB receptor ligand neuregulin-1β or with factors derived from human lung

fibroblast (MRC-5) cultures to attempt to further recapitulate the epithelial to mesenchymal cross-talk of the lung parenchyma. This will be achieved through the use of conditioned medium derived from MRC-5 cells cultured in the presence and absence of the PPARγ agonist rosiglitazone and subsequent co-culture of the epithelial and fibroblast cells in Transwell™ and a 3D scaffold system (Alvetex™ Scaffold).

- To determine the aspects of normal alveolar ATII biology and of IPF pathology that are recapitulated in these systems. To evaluate their appropriateness for IPF research and identify further work that could be carried out.

1.3.3 Objectives

- To grow A549 cells for short term and extended culture periods in ultra-low attachment (ULA™) multi-well plates as three-dimensional (3D) spheroids and evaluate the effect of simple (DMEM) and complex cell culture (Ham's F12) media on expression of ATII properties.
- To grow A549 cells for short term and extended culture periods in ultra-low attachment (ULA™) multi-well plates as three-dimensional (3D) spheroids and evaluate the effect of simple (DMEM) and complex cell culture (Ham's F12) media on expression of ATII properties.
- To employ phase contrast microscopy and cell counting techniques to assess possible adoption of epithelial and ATII cellular morphology and to assess cellular viabilities and rates of cellular proliferation in the 3D and 2D cultures.
- To carry out extensive gene expression analysis of the long and short term 2D and 3D spheroid cultures using *RNA* microarray analysis followed by gene ontology and pathway analysis with the aim of determining patterns of gene regulation consistent with epithelial and ATII differentiation. To validate and further investigate gene expression with quantitative real time polymerase chain reaction (QRT PCR).
- To further validate findings in the 2D cultures and 3D spheroid cultures using immunohistochemistry and transmission electron microscopy (TEM) to evaluate ATII differentiated features including multilamellar bodies.
- To validate and characterise the authenticity and ATII differentiation potential of a novel lung progenitor cell line.
- To determine the effect of the corticosteroid dexamethasone and the potential mesenchymal to epithelial signalling molecule neuregulin-1β (NRG-1β) on ATII-like differentiation in A549 cells and using morphology assessments by phase contrast microscopy, gene expression analysis for specific epithelial and ATII and ATI markers by

gene expression using QRT-PCR and expression of characteristic ATII markers (e.g. surfactant proteins) using immunofluorescent microscopy.

- To compare gene and protein expression of epithelial and ATII and ATI markers in the NRG-1β and dexamethasone treated A549 cells the with that of human primary ATII cells.
- To attempt to further differentiate A549 cells closer to an ATII phenotype by recapitulating mechanisms of mesenchymal to epithelial cross talk through co-culture with foetal lung fibroblasts (MRC-5) using conditioned medium derived from MRC-5 cells cultured in the presence and absence of the PPARγ agonist rosiglitazone and subsequent co-culture of the epithelial and fibroblast cells in Transwells™.
- Using QRT-PCR determine the gene expression of characteristic epithelial ATI and ATII markers in the conditioned media and co-culture systems and compare them to the dexamethasone and NRG-1β cultures and to primary ATII cells.
- Combine co-culture conditions that present the most potential for ATII differentiation in A549 cells into 3D Alvetex™ Scaffold in the presence of ascorbic acid to encourage collagen deposition. Carry out histochemical and TEM analysis to determine the histotypic distribution and morphology of the epithelial and mesenchymal cells in the scaffold, the presence and distribution of multilamellar bodies and the distribution and nature of any extracellular matrix secreted by the cells.

2. Materials and Methods

2.1 Maintenance of Cell Stocks and General Cell Culture

All cell culture was performed in a class II Microbiological Safety Cabinet (CL2-MSC).
A549 cells were obtained from the European Collection of Authenticated Cell Cultures (ECACC) (catalogue number 86012804) and cultured in Ham's F12 Nutrient Medium (Sigma Aldrich product N4888) containing 2 mM L-Glutamine and 10% v/v Foetal Bovine Serum (FBS) (Sigma Aldrich, Gillingham, Dorset). Hereinafter referred to as 'Ham's F12/10%FBS' or Dulbecco's Modified Eagle's Medium (DMEM) (Sigma Aldrich Product D5796) containing 2mM L-Glutamine and 10% v/v Foetal Bovine Serum (FBS) (Hereinafter referred to as 'DMEM/10%FBS'.
MRC-5 Human Lung Foetal Fibroblasts were obtained from the European Collection of Authenticated Cell Cultures (ECACC) (catalogue number 05081101) at a population doubling number of 25. Cells were initially maintained in Eagle's Minimal Essential Medium (MEM) supplemented with 1x (v/v) Non-Essential Amino acids (NEAA) from a 100x stock, 2mM L-Glutamine and 10% v/v Foetal Bovine Serum (FBS) (All from Sigma Aldrich, Gillingham, Dorset), herein referred to as 'MEM/10%FBS'.
Cultures were incubated at 37°C in a humidified 5% CO_2 incubator and subculture was carried out on sub-confluent monolayers (as determined by phase contrast microscopy) by washing the cell monolayers twice with physiological calcium and magnesium free phosphate buffered saline (PBS) (Life Technologies, Paisley, UK) followed by addition of 1x Trypsin/EDTA solution (0.05% Trypsin, 0.02% EDTA v/v in Hank's balanced salt solution (HBSS) (Sigma Aldrich, Gillingham, Dorset) to wash over the monolayer before immediate aspiration of excess trypsin/EDTA Solution. Subsequent incubation at 37°C for 2-5 minutes until the cells detached ("trypsinization"), trypsin was inactivated by the addition of growth medium before seeding into fresh flasks at densities of 1.5-2 x 10^4 cells/cm^2.

COMPONENTS:	F12 (Sigma Aldrich Product No. N4888)[313 314] Components in g/L	DMEM (Sigma Aldrich Product No. D5796) [315 316] Components in g/L
INORGANIC SALTS		
$CaCl_2 \cdot 2H_2O$	0.0441	0.2
$CuSO_4 \cdot 5H_2O$	0.0000025	
$FeSO_4 \cdot 7H_2O$	0.000834	0.0001
$MgCl \cdot 6H_2O$	0.123	
$MgSO_4$		0.09767
KCl	0.224	0.4

COMPONENTS:	F12 (Sigma Aldrich Product No. N4888)[313 314] Components in g/L	DMEM (Sigma Aldrich Product No. D5796) [315 316] Components in g/L
$NaHCO_3$	1.176	3.7
NaCl	7.5	6.4
Na_2HPO_4	0.14204	0.109
$ZnSO_4 \bullet 7H_2O$	0.000863	
AMINO ACIDS		
L-Alanine	0.009	
L-Arginine•HCl	0.211	0.084
L-Asparagine•H_2O	0.01501	
L-Aspartic Acid	0.133	
L-Cysteine•HCl•H_2O	0.035	0.0626
L-Glutamine	(Added to 2mM)	0.584
L-Glutamic Acid	0.147	
Glycine	0.00751	0.03
L-Histidine•3HCl•H_2O	0.02096	0.042
L-Isoleucine	0.00394	0.105
L-Leucine	0.0131	0.105
L-Lysine•HCl	0.0365	0.146
L-Methionine	0.00448	0.03
L-Phenylalanine	0.00496	0.066
L-Proline	0.0345	
L-Serine	0.0105	0.042
L-Threonine	0.0119	0.095
L-Tryptophan	0.00204	0.016
L-Tyrosine 2Na•2H_2O	0.0078	0.10379
L-Valine	0.0117	0.094
VITAMINS		
D-Biotin	0.0000073	
Choline Chloride	0.01396	0.004
Folic Acid	0.00132	0.004
myo-Inositol	0.018	0.0072
Niacinamide	0.000037	0.004
D-Pantothenic Acid •½Ca	0.00048	0.004
Pyridoxine•HCl	0.000062	0.00404
Riboflavin	0.000038	0.0004
Thiamine•HCl	0.00034	0.004
Vitamin B-12	0.00136	
OTHER		
D-Glucose	1.802	4.5
Hypoxanthine	0.00408	
Linoleic Acid	0.000084	
Phenol Red (sodium)	0.0013	0.0159
Putrescine•HCl	0.000161	

COMPONENTS:	F12 (Sigma Aldrich Product No. N4888)[313 314] Components in g/L	DMEM (Sigma Aldrich Product No. D5796) [315 316] Components in g/L
Pyruvic Acid (sodium)	0.11	
Thioctic Acid	0.00021	
Thymidine	0.00073	

Table 2.1 Formulations of Cell Culture Media used with A549 Cells in this Study.

2.1.1 Culture of 2D Cultures of A549 on Coverslips.

Round 15 mm coverslips Bellco RD German, SciQuip Ltd, Shrewsbury UK) were sterilised by heating in an oven to 110°C for 20 minutes. Once cooled the coverslips were transferred under sterile laminar flow using sterile forceps to 12 well tissue culture plates (Corning, New York, USA). A549 cells were cultivated in 2D monolayer as described above and after trypsinisation and cell counting the cell concentration was adjusted to inoculate 1 mL of cell suspension to each well, providing 1.5 x 10^4 cells/cm^2. The cells were maintained by careful medium exchange every 2-3 days.

2.1.2 Cell Counting and Viability Assessment.

Cell Counting throughout and viability assessment was carried out throughout the study using Trypan Blue staining (Neubauer Haemocytometer) and Acridine Orange / DAPI dye exclusion viability counting using the Nucleocounter 3000™ viability assays (Chemometec, Allerod, Denmark).

2.1.3 Calculation of Population Doublings.

Population doublings (also known as generation number) were calculated using the following formula[317]:

$$\boldsymbol{Population\ Doubling} = \frac{(\boldsymbol{ln\ Total\ Cells\ Harvested} - \boldsymbol{ln\ Viable\ Cells\ Seeded})}{\boldsymbol{ln\ 2}}$$

Where ln = the natural logarithm.

2.1.4 Induced Pluripotent Stem Cell Culture for Positive Expression of Stem Cell Marker.

The human induced pluripotent stem cell line (hiPSC) UKi2007A was obtained from ECACC, Salisbury, UK. Colonies of the were cultivated on coverslips in E8 medium (Thermo Fisher

Scientific, Gloucester, UK) and used as a positive control for immunofluorescent staining (Appendix C).

2.2 Generation of 3D Spheroid Cultures

Three dimensional (3D) spheroids (or aggregates) of A549 cells were generated using a modification of the method published by Wong *et al*[318]. Corning Ultra Low Attachment (ULA) surface was used in preference to other surface coatings due to its ease of use, proven reproducibility and advantages over agar coating as demonstrated by Vinci *et al*[319].

To generate uniform spheroids; monolayer cultures of cultures of log phase A549 cells were cultivated in either DMEM/10% FBS or Ham's F12/10% FBS. Cells were trypsinised using two PBS washes and removal from the substrate by the addition of trypsin/EDTA and incubation at 37°C in a humidified 5% CO_2 incubator for 5 minutes or until the cells were suspended. An excess volume (more than double the volume of trypsin/EDTA cell suspension) of the relevant FBS containing culture medium was then added to inactivate the trypsin and the resulting cell suspension triturated using a 5 mL stripette to produce a single cell suspension. The cell suspension was then passed through a 70 μm sterile cell strainer (Falcon® Corning Inc. Reference 352350) and the cells counted using either an improved Neubauer hemocytometer or automated cell counter (Nucleocounter™ Chemometec, Allerod, Denmark) and subsequently adjusted with the addition of cell culture medium to 5,000 viable cells/mL. taking care to keep the cell suspension gently agitated to maintain a homogenous cell suspension, using a micropipettor and sterile aerosol resistant tips, 200 μL of the cell suspension was then dispensed into each well of a 24 well Ultra Low Attachment (ULA) multi-well cell culture plate (Costar®, Product 3473) (Corning, New York, USA). Plates were then agitated at 40 rpm on an orbital shaker in a humidified 5% CO_2 / 37°C incubator for 12 hours (overnight incubation). After inspecting the cultures the following day to ensure that cells had started to aggregate a further 200 μL of the relevant cell culture medium was added in the CL2-MSC and the cultures transferred to a static shelf in the humidified 5% CO2 / 37°C incubator. Cultures were inspected and imaged daily and medium exchanged every 2-3 days by gently pipetting 400 μL of medium from and then to the side of the wells so as not to disturb the developing colonies of cells. Spheroids developed within 5-10 days and could be maintained for 20 or more day[320]. This method generated 1 spheroid per well.

To compare growth in DMEM/10% FBS and F12/10% FBS cells were seeded into replicate T25 flasks and medium changed every 2-3 days. Phase contrast images were captured of the monolayers and at the end of a 25 days continuous culture the flasks were harvested by trypsinisation and cells were counted and assessed for viability and cell size by both Trypan

Blue staining and viability counting using the Nucleocounter™ 3000 Viacount™ assay (Chemometec, Allerod, Denmark).

To harvest 25cm^2 flasks containing approximately 2 x 10^6 A549 cells for RNA extraction, culture medium was decanted to waste and the monolayer washed with PBS, 2 mL trypsin/EDTA (Sigma Aldrich, Gillingham UK) was added to each flask. Chilled homogenisation solution (Promega) supplemented with thioglycerol was then added directly to the cell monolayer and the tube and pellet immediately snap frozen in dry ice before transfer to a -80°C Freezer for storage prior to RNA extraction. One single 25cm^2 flask represented each biological replicate for the Two Dimensional (2D) cultures.

A set of triplicate pellets of log phase P+95 A549 cells were prepared in a similar manner to the 2D time-course pellets on "Day 0" and designated "T0" to act as a base-line control.

3D Spheroids were harvested by aspiration and transfer to centrifuge tubes, centrifugation at 150 x *g* for 5 minutes, aspiration of supernatant and addition of ice-cold PBS, further centrifugation at 150 x *g* for 5 minutes, aspiration of supernatant to waste and immediately snap frozen in dry ice before transfer to a -80°C Freezer for storage prior to RNA extraction.

2.3 Cell Culture of the TRiP WT/E-cad/LGR6+ Cells

Frozen vials of the cells were stored in liquid nitrogen vapour phase (below -150°C) in an insulated cryogenic storage vessel (Custom Biogenic Systems, Michigan, USA) and transferred on solid carbon dioxide pellets in an insulated box to the tissue culture laboratory where they were thawed in a 37°C in a waterbath whilst wearing eye protection. Once the final crystal of ice had disappeared in the vial its was wiped with 70% Isopropyl Alcohol Spray/30% water (v/v) and the vial contents added to a sterile conical 15 mL centrifuge tube. Pre-warmed (37°C) RHB-A Medium (Takara, Saint-Germain-en-Laye, France) was added drop-wise to a total volume of 5 mL and the tube capped and inverted to mix and centrifuged for 5 minutes at 150 x *g* to remove the cryoprotectant. Following centrifugation, the supernatant was aspirated to waste and the cell pellet resuspended into 5 mL of fresh prewarmed medium. The cell suspension was assessed for cell numbers and viability (Nucleocounter® 3000, Allerod, Denmark) a volume containing 1 x 10^5 viable cells was dispensed onto an FTA (FTA is a proprietary tradename) cards (Whatman PLC, Buckingham, UK)[321] using a micropipette and submitted to Northgene (Newcastle UK) for STR profiling using Powerplex 16 (Promega 16 locus STR kit that includes the gender marker amelogenin. The remainder of the cells were then further diluted with the RBH-A medium and seeded into cell a cell culture flask at 3 x 10^4 viable cells/cm^2 and incubated in a 37°C humidified 5% CO_2 incubator. Cells were observed daily and once confluent, sub-cultured washing the cell monolayer twice with physiological

calcium and magnesium free phosphate buffered saline (PBS) (Life Technologies, Paisley, UK) followed by addition of 1x Trypsin/EDTA solution (0.05% Trypsin, 0.02% EDTA v/v in Hank's balanced salt solution (HBSS) (Sigma Aldrich, Gillingham, Dorset) to wash over the monolayer before immediate aspiration of excess trypsin/EDTA Solution. Subsequent incubation at 37°C for 2-5 minutes until the cells detached. Trypsin was inactivated by the addition of soya bean trypsin inhibitor solution and cell suspension aspirated into a conical centrifuge tube which was capped, inverted to mix and centrifuged for 5 minutes at 150 x *g* after which the supernatant was aspirated to waste and the cell pellet resuspended into fresh prewarmed medium. The resulting cell suspension was assessed for cell numbers and viability and then further diluted with the RBH-A medium and seeded into cell a cell culture flask at 3 x 10^4 viable cells/cm^2.

2.4 Dexamethasone and Neuregulin Treatment of A549 Cells

A549 cells were seeded into triplicate six-well culture plates at 2 x 10^4 cells/cm^2 in Ham's F12/10% FBS and incubated overnight in a 37°C humidified CO_2 incubator. The following day the cultures were exchanged into medium supplemented with 50 ng/mL Neuregulin-1β (NRG), Dexamethasone100 nM (Dex) and Dex+NRG together with untreated medium and an ethanol vehicle control for the Dex treatment. Concentrations were selected based on those used in published literature[322] [323] [324]. Cultures were subsequently maintained for 21-day time-course. Medium exchange with the relevant treatments every 2-3 days ensured chronic exposure with fresh Dex and NRG.

Cultures were examined by microscopy daily and phase contrast images were recorded throughout the time-course.

2.4.1 Preparation of Neuregulin Solutions

100 µg Lyophilised Recombinant Neuregulin-1β (part no 100-03) (Peprotech, London UK) was initially reconstituted by adding 1 mL sterile water to give a concentration of 100 µg/mL. Sterile phosphate buffered saline (PBS) (Life Technologies, Paisley, UK) solution was supplemented with 0.1% BSA (Sigma Aldrich, Gillinlgham, Dorset, UK) and gently mixed without vortexing. This was used to further dilute the 1 mL of 100 µg/mL to a final volume of 10 mL and a final concentration of 10 µg/mL. 0.5 mL aliquots of this solution were stored in sterile cryovials and stored frozen at -20°C. A single 0.5 mL aliquots added to 100 mL of culture medium (a 1:200 dilution) to give a working concentration of 50 ng/mL of Neuregulin-1β.

2.4.2 Preparation of Dexamethasone solutions

To prepare 20 µM stock solution of dexamethasone, an initial 1 mg/mL (2.55 mM) stock solution was prepared by adding 100 mL of absolute ethanol to 100 mg dexamethasone

(D4902, Sigma Aldrich, Gillingham, UK) and gently swirled to dissolve. This was then further diluted by adding 64 mL sterile PBS (Gibco, Paisley, UK) for every 0.5 mL 2.55 mM ethanolic dexamethasone, to achieve final concentration of 20 μM. This stock solution was dispensed into 0.5 mL aliquots and stored frozen at -20°C. One 0.5 mL vial was then thawed and added to 100 mL of culture medium to give a final 100 nM. Stock solutions of an ethanol 'vehicle control' was prepared similarly by adding 0.5 mL ethanol to 64 mL PBS for further dilution (1:200) into culture medium.

2.5 MRC-5 Generation of Fibroblast Conditioned Medium

2.5.1 Growth Profile Assessment of MRC-5 Cells to Ham's F12 10% FBS

Flasks of MRC-5 cells were seeded at 2 x 10^4 cells/cm^2 in Ham's/10% FBS and MEM/10% FBS in duplicate. Flasks were placed into the Incucyte Zoom® automated microscope (Essen Bioscience, Ann Arbor, Michigan, USA) at 37°C in a humidified 5% CO_2 incubator for four days. The automatic microscope captured phase contrast images from 63 sectors from each flask every two hours (126 replicates for each medium). Representative images from different stages of growth were manually analysed using the Incucyte® software to "teach" the difference between cells and unpopulated substrate in order to calculate accurate assessments of 'confluence' (area covered by cells/total area x 100). The software then generated accurate growth profile. Images overlaid with a mask representing the software's assessment of what constituted cellular coverage were manually checked to manually quality control the data. Once it had been established that transfer of MRC-5 cells to Ham's F12/10% did not significantly affect their growth characteristics, these cells were cultivated in Ham's F12/10% FBS for the generation of conditioned medium.

2.5.2 MRC-5 Conditioned Media Assessment and Production (With and Without Rosiglitazone)

(1) MRC-5 Gene Expression Time-course

Log phase cultures.MRC-5 (Pd25) cultures were seeded 2 x 10^4 cells /cm^2 into tissue culture treated 6 well plates (Corning, New York, USA) in Ham's F12/10% FBS and incubated overnight in a humidified CO_2 incubator at 37°C.

10mg/mL (28 mM) stock Rosiglitazone (RGZ) (Sigma Aldrich, Gillingham, Dorset, UK) was prepared in Dimethyl Sulphoxide (DMSO) (Sigma Aldrich, Gillingham, Dorset, UK). Bottles of Ham's F12/10% FBS medium at 1, 10, 20 and 30 μM RGZ were prepared using the 28 mM RGZ stock. In addition, a vehicle control was prepared with the equivalent amount of DMSO as the 30 μM RGZ dilution. Ham's F12/10% FBS was used as a negative control. All media were supplemented with 100 Units penicillin and 100 μg streptomycin/mL (Sigma Aldrich, Gillingham, Dorset, UK).

After overnight incubation, MRC-5 cultures were medium exchanged into their respective media and incubated a humidified CO_2 incubator at 37°C. Every 2-3 days, plates were medium exchanged, phase contrast imaged and three replicates harvested for RNA extraction. After 12 days remaining plates were fixed and stained with Oil-Red-O.

(2) Preparation of MRC-5 Fibroblast Conditioned Medium

MRC-5 cultures were seeded at 2 x 10^4 cells/cm^2 into T175 flasks in Ham's F12 /10% FBS. For RGZ treated cells, bottles of Ham's F12 10% FBS were supplemented with 10 μM Rosiglitazone (RGZ). From stock 28 mM RGZ in DMSO (178 μL per 500 mL bottle of medium). Cells were incubated overnight in a 37°C, 5% CO_2, humidified incubator then medium exchanged into 10 μM Rosiglitazone medium or untreated Ham's F12 /10% FBS. Medium was exchanged after two days and on the 5th day of culture medium was decanted and the cell monolayers washed with PBS, 5 minutes each wash and then both sets of cultures medium exchanged into RGZ-Free Ham's F12 /10% FBS and left to condition for five days in the incubator before harvesting by decanting the conditioned media (control and RGZ treated cells) into sterile bottles, chilling on ice and filtering using low protein binding 0.22 μm filters into sterile bottles before aliquoting into labelled 50 mL Falcon tubes and stored at -80°C. To determine the effects of any RGZ carry-over into the conditioned medium an "Absorption control" was prepared. 10 μM Rosiglitazone medium was added to a confluent monolayer of cells in a T175 flask and incubated at before decanting the medium to waste. Cells were washed twice with PBS and replenished with Ham's F12/10% FBS and incubated for a further hour at 37°C before harvest, filtering and freezing as per the conditioned media.

2.5.3 Treatment of A549 cells with MRC-5 Fibroblast Conditioned Media

Six-well plates were seeded with A549 cells at 2 x 10^4 cells/cm^2 and incubated overnight at 37°C / 5% CO_2 (humidified). Previously prepared conditioned media were rapidly thawed in a 37°C in a water bath and fresh Ham's F12/10% FBS and used to prepare 25%, 50% and 75% v/v dilutions of the RGZ and RGZ-free conditioned media in sterile 100 mL bottles (Corning, New York, USA). The A549 cells were medium exchanged into their respective media and medium exchanged every 2-3 days to maintain chronic exposure to the conditioned medium for 21 days' incubation (37°C / 5% CO_2 (humidified)) before harvest for RNA extraction. Cultures were observed daily by phase contrast microscopy

2.6 Transwell™ A549/MRC-5 Co-Culture

Six-well Transwell™ Supports (collagen coated (COL), product number 3491 and 'Clear' Polyester (product number 3450) 0.4 μm pore size, 24 mm diameter (Corning, New York, USA)) were seeded with A549 cells in the apical chambers at 2 x 10^4 cells / cm^2 and MRC-5 cells at 2 x 10^4 cells / cm^2 in the basal chambers in Ham's F12/10% FBS for 'conventional'

Transwell™ culture. Membranes were 'pre-wet' by submerging them in medium and incubating at 37°C for one hour. For 'Sandwich' culture, MRC-5 cells were trypsinised from culture, counted and resuspended in 600 µL medium and dispensed onto inverted supports in a meniscus. MRC-5 Cells were allowed to attach to the membranes through one hour's incubation at 37°C in a humidified 5% CO_2 incubator before re-inverting and seeding the apical side with A549 cells. Apical chambers were maintained with 1.5 mL medium and the basal chambers with medium exchange every 2.4 days. Samples for RNA extraction were harvested by direct addition of RNA homogenisation buffer (Promega-maxwell, Maddison, Wisonsin, USA) (conventional culture) or by gentle scraping with an inverted sterile 1000 µL pipette tip into the homogenisation buffer.

2.7 3D Cell Culture in Alvetex™ Scaffold

2.7.1 General Procedure for Alvetex™ Scaffold

Alvetex™AVP005 12 well inserts (Reprocell Europe Ltd, Glasgow, UK) were used with 6- well plates. Alvetex was first rendered hydrophylic by filling wells with 70% ethanol, ensuring the inserts were submerged. 70% ethanol was aspirated and the inserts immediately washed twice with warmed culture medium and the second wash discarded. Culture medium was added to the outer well so that the medium rose through the insert but not over its sides. 500 µL of cell suspension was added dropwise to the surface of the Alvetex disc. The following day further growth medium was added to fully submerge the Alvetex disc Cultures were completely medium exchanged the on a daily basis.

2.7.2 A549 Monoculture in Alvetex™

A549 cells were trypsinised from flasks and counted to prepare 5 x 10^4 cells per 500 µL in Ham's F12/10% FBS. Cells were directly pipetted to the centre of the pre-wetted Alvetex™ discs. The following day further growth medium was added to fully submerge the Alvetex disc, before two weeks' culture with daily medium exchange and then fixing and paraffin embedding.

2.7.3 Determination of Optimal MRC-5 Seeding Densities in Alvetex

Log phase cultures of MRC-5 cells were trypsinised from flasks and counted to prepare 1 x 10^6, 0.5 x 10^6 and 0.25 x 10^6 cells per 500 µL in both MEM/10% FBS and Ham's F12/10% FBS to seed per scaffold inserts by pipetting directly to the centre of the pre-wetted Alvetex™ discs. The following day further growth medium was added to fully submerge the Alvetex disc, before two weeks' culture with daily medium exchange prior to fixing and paraffin embedding.

2.7.4 Short Term MRC-5 / A549 Culture in Alvetex™

Cells were seeded at 0.5 x 10^6 cells per 500 µL in Ham's F12/10% FBS to pre-wetted Alvetex™ discs and cultured for two weeks with daily medium exchange. An inoculum of 5 x 10^4 A549 cells was added as per the initial MRC-5 seeding. The following day further growth medium was added to fully submerge the Alvetex disc. Cultures were maintained for a further two weeks with daily medium exchange prior to fixing and paraffin embedding.

2.7.5 Long term MRC-5 / A549 Culture and Ascorbic Acid Treatment in Alvetex™

Long term culture of MRC-5 cells has not been confirmed in Ham's F12/10% FBS therefore MRC-5 cells were seeded at 0.5 x 10^6 cells per 500 µL in MEM/10% FBS with or without supplementation with ascorbic acid (AA). Ascorbic acid 2-phosphate (Sigma Aldrich, Gillingham, Dorset, UK, Product A8960) stock solution was prepared at 10mg/mL (34.5mM) in sterile de-ionised water and sterile filtered. Stock solution was then diluted 1:1000 in culture medium give a working concentration of 34.5 µM AA. MRC-5 cells were maintained in in MEM/10% FBS with or without AA for one month before medium was switched to Ham's F12/10% FBS, the medium volume was lowered and as with the initial inoculum and 5 x 10^4 A549 cells was pipetted onto the disc. The following day further growth medium was added to fully submerge the Alvetex™ disc. Cultures were maintained in Ham's F12/10% for a further two weeks with daily medium exchange prior to fixing and paraffin embedding.

The working concentration of ascorbic acid was selected based on work on *in vitro* fibrillar collagen induction in IPF fibroblasts by Jones *et al* (2008)[76]. It was also recognised that the lysysl oxidase (LOX) mediated cross-linking of fibrillar collagen requires copper ions as a co-factor[325]. Adequate physiological levels of copper were expected to be provided by the 10% v/v FBS supplementation[326] and by Ham's F12 medium that contains copper sulphate in its formulation[314].

2.8 Primary ATII Cells Cultures and RNA from Primary ATII Cells

Primary ATII cells and RNA samples from seven donors were kindly provided by Dr Franco Conforti, Roger Brooke Lab, University of Southampton, UK. Cells were isolated from a macroscopically normal tissue from ex-smokers undergoing lung resection. RNA samples from Donors 1, 2 and 3 were used in Chapter 4 and for gene expression analysis in Chapters 6 and 7. 1 Donor 1 (female aged 57), Donor 2 (female aged 69) (Tissue was from a wedge lobectomy and Donor 3 (male, aged 69). RNA from Donor 2 was used for RNA microarray analysis in Chapter 4. RNA from additional two donors (Donors 4 and 5) (reference numbers TL1230 (female, aged 61), and TL1276 (male, aged 63)) were used alongside Donors 1-3 for gene expression analysis in Chapters 6 and 7 and growing cells ATII cells from more additional donors (Donors 6 and 7) (TL1631 (female, aged 73) and TL1642 (female aged 59)) were provided by Dr Conforti for use as positive controls for immunofluorescence microscopy in Chapter 6. Written consent from the donors of the primary lung tissue was given under the governance of the National Health Service (NHS) England Southampton and South West Hampshire 'A' Research Ethics Committee; Local Research Ethics Committee (LREC) Reference Number 08/H0502/32.

Primary cultures were generated using established methods[229]. In short, the lung tissues were perfused with 0.9 % saline solution and instilled with Trypsin 0.25% (Sigma Aldrich T8003) 37°C for 45 min. After Trypsin digestion, the tissues were finely sliced in presence of newborn calf serum (NCS) and DNase 250 μg/mL, then cells were filtered by sequential filtration through a 400 μm metal mesh and 40 μm nylon filter. The cells were re-suspended in DCCM-1 medium (Biological Industries. Kibbutz Beit-Haemek, Isreal) supplemented with 1% penicillin, 1%streptomycin and 1% L-glutamine, and incubated at 37°C in a humidified incubator for two hours in tissue culture flasks to allow differential adherence and removal of contaminating mononuclear cells. The Alveolar cells were re-suspended in fresh DCCM-1 supplemented with 10% NCS, 1% penicillin, 1%streptomycin and 1% L-glutamine and plated on collagen 1 (PureCol 5005-b) (Advanced Biomatrix, San Diego, California, USA) coated 24 well plates at 60% confluence and after 72h cell purity, tested by alkaline phosphatase stain (marker of Alveolar type 2 cells). RNA was isolated from one well of a 24 well plate using Trizol reagent in accordance with manufacture's protocol (Life technologies, Paisley, UK).

2.9 RNA Extraction

In Chapters 3 and 4 Pellets of cells from 2D and 3D spheroid cultures were processed in batches for RNA extraction using the Promega Maxwell Low Elution Volume (LEV) Simply RNA Cell kit to the manufacturer's instructions (Promega, Maddison, Wisconsin, USA).

Pellets of cells from Spheroid cultures (approximately 2 x 10^6 cells in 15 mL Falcon tubes) were removed from -80°C storage and transferred to the laboratory on dry-ice. Batches of 16 (maximum) pellets were thawed rapidly and as briefly as possible in a 37°C water-bath. As soon as the samples were thawed they were transferred to wet ice and 200 µL of homogenisation solution supplemented with thioglycerol added as per manufacturer's instructions (Promega, Maddison, Wisconsin, USA) and the samples vortexed to mix.

In later experiments (Chapters 6 and 7), cultures grown in multi-well plates were treated with homogenisation buffer supplemented with thioglycerol and snap frozen into solid CO_2 at -79°C to enable longer term storage of RNA samples.

200 µL of lysis solution was then added to each tube, vortexed again and the sample loaded into the Maxwell cassettes. DNAse was added to the reactions as per the manufacturer's instructions to ensure the eluted RNA was free from and contaminating co-purified DNA. The extracted RNA was eluted into 50 µL of nuclease free water supplemented with 2µL (40 Units) of RNAse inhibitor ("Superase ™, Life Technologies, Paisley, UK)".

The RNA was quantified and quality controlled by assessing the absorption spectrum of the eluted nucleic acid, the absorbance $(A)_{260}$ (representative of the amount of nucleic acid), A_{260}/A_{280} (the ratio that typifies the nature of the nucleic acid "pure" DNA having an A_{260}/A_{280} ratio near 1.8, and RNA having an A_{260}/A_{280} ratio near 2. A_{230} represents the resultant contamination absorbance. A_{260}/A_{230} ratios for RNA were in the order of 2.0-2.2 using a spectrophotometer (Nanodrop, Thermo Scientific, Paisley, UK) or Denovix (Wilmington, Delaware, USA). In early experiments 5 µL of each eluted RNA sample was qualified by electrophoresis in a 1.4% agarose (Sigma Aldrich, Gillingham, Dorset) gel and visualised using Ethidium Bromide and UV illumination to ensure there were intact 18S and 28S bands, indicating that the RNA was intact). In Chapters 3 and 4, extracted RNA was stored at -80°C before analysis by RNA Micro array and repeat assessment of RNA integrity was carried out to determine RNA Integrity Number (RIN) using a bio-analyzer (BioAnalyzer 2100, Agilent Technologies).

In later experiments (Chapters 6 and 7), 1 µL RNA was qualified for integrity using the Tapestation™ Bioanalyser (Agilent, Santa Clara, California, United States) to generate RIN scores.

2.10 RNA MicroArray Analysis

Fluorescent complimentary RNA (cRNA) labelled with Cyanine 3 was generated from the extracted RNA samples using the Agilent Single Colour Low Input Quick Amp Labelling kit as per the manufacturers' instructions. The RNA was reverse transcribed to complimentary DNA

(cDNA) from which cRNA was transcribed, amplified and purified prior to hybridisation to the Agilent Human Single Colour 39494 array slides. Following hybridisation the slides were scanned using the microarray scanner and the scanned images extracted into text files containing the probe intensity data. The text files were subsequently uploaded into Genespring version 13 (Agilent Technologies, Santa Clara, CA, US) for statistical and comparative analysis at the probe and gene level. Data was quality controlled by excluding any compromised entities and only entities where all replicates were either detected or not detected. Samples were normalised by shift to the 75th percentile and the baseline transformation on the median of all samples. The A549 time course samples were analysed by One way analysis of variance (ANOVA) p-value computation was asymptotic with a p cut-off: of 0.05 and Benjamini-Hochberg multiple testing correction. The primary ATII cell cultures were statistically compared to the triplicate slides of log phase A549 cells from the time course by unpaired *t*-test, p-value computation was asymptotic with a p cut-off: of 0.05 and Benjamini-Hochberg multiple testing correction.

Euclidian hierarchical clustering analysis using Ward's linkage rules of the normalized intensity values of the entities generated by the One-way ANOVA was performed.

Lists of entities up and down regulated as compared to log phase A549 cells in both the A549 2D and 3D time courses and the ATII primary cells were generated at fold change cut offs of 2.0.

Venn diagram analysis was carried out in Genespring to determine the level of similarity of gene expression of sequential samples from the 2D A549 timecourse and the primary ATII cells (note: this analysis generated lists of overlapping genes. It did not generate a Venn diagram).

Gene ontology analysis was performed on the fold change analysis of the clusters identified in the Genespring ANOVA analysis of the 3D vs log phase A549 cultures (Chapter 3): significantly up and down regulated genes were ranked by their fold change in expression and uploaded to "GOrilla" a tool for discovery and visualization of enriched GO terms in ranked gene lists[327]. Further simplification was achieved by applying , the outputs of the GOrilla analyses were run through the 'REVIGO' (REduce+VIsualize Gene Ontology tool[328] to allow focus on data with the lowest p values.

2.11 Preparation of cDNA by Reverse Transcription

First strand cDNA synthesis (reverse transcription (RT)) was carried out on normalised RNA samples in thin-walled PCR tubes using Oligo dt primers using the Omniscript™ cDNA synthesis kit (Qiagen, Hilden, Germany) or the Superscript ® II Reverse Transcriptase Kit

(Life Technologies, Paisley, UK) to the manufacturer's instructions. cDNA samples were diluted 1:10 before amplification and analysis by QRT PCR.

2.12 Quantitative Real-Time* Polymerase Chain Reaction (QRT-PCR)

*Sometimes referred to as Quantitative Reverse Transcription PCR

2.12.1 Selection of Reference Genes For QRT-PCR

(1) Genorm Analysis using SYBR Green

A set of 12 primer pairs specifically designed as potential reference or "housekeeping" genes were obtained from Primer Design (Southampton, UK) (*UBC, YWHAZ, EIF4A2, 18s, RPL13A, SDHA, ACTB, TOP1, CYC1, GAPDH, B2M* and *ATP5B* and their stability of expression was evaluated using 15 normalised (300ng input into the RT reaction) cDNA samples from the 25 day time-course of A549 Culture in Spheroid and 2D culture. Potential confounding amplification from carry over of genomic DNA in the extracted RNA was evaluated by running PCR reactions on the RNA samples against primer pairs specific for *GAPDH, CYC1, B2M, ATP5B, ACTB* and *TOP1.* Genorm analysis QRT PCR Reactions were set up as per Table 2.2, Table 2.3 and Table 2.4 below in 96 well 'FAST' plates in a laminar flow PCR hood, the plates were sealed with adhesive film (Bio-Rad, Deeside, UK) and centrifuged in plate carriers in a swing out rotor centrifuge (Sorval, Thermo Fisher, Paisley, UK) and then run on a QRT-PCR Cycler (Bio-Rad, Deeside, UK).

Reagent	**Volume per reaction**
Primer pair 1:1 mix of primers reconstituted to the manufacturer's instructions	1 µL
Water	4 µL
2 x Sybr Green Mastermix (Primer design)	10 µL
cDNA template	5 µL

Table 2.2 PCR set up for Sybr Green reactions.

All 15 samples were run in duplicate on the same plate, evaluating three reference genes on each plate; plates were set up as follows:

	1	2	3		4	5	6	7	8	9	10	11	12
		Reference Gene 1				Reference Gene 2				Reference Gene 3			
A	1	1	9		9	1	1	9	9	1	1	9	9
B	2	2	10		10	2	2	10	10	2	2	10	10
C	3	3	11		11	3	3	11	11	3	3	11	11
D	4	4	12		12	4	4	12	12	4	4	12	12
E	5	5	13		13	5	5	13	13	5	5	13	13
F	6	6	14		14	6	6	14	14	6	6	14	14
G	7	7	15		15	7	7	15	15	7	7	15	15
H	8	8	Water		Water	8	8	Water	Water	8	8	Water	Water

Table 2.3 Typical plate layout for QRT PCR Genorm analysis.

Temperature	**Time**	**Number of Cycles**
95ºC	10 minutes	1
95ºC	15 seconds	45
60ºC	1 minute	
	Capture (fluorescence)	
95ºC	Hold	1

Table 2.4.Reaction conditions for QRT PCR Genorm analysis (Sybr Green™).

Once the PCR reactions had been run the CT values determined and input into the QBASE software package Primer Design (Southampton, UK) that determined the geNorm M value and advised the least variable reference genes.

Results of the analysis are described in Appendix E.

For cDNA generated in Chapters 3 and 4, Genorm (Appendix E) analysis showed *TOP1* and *ATP5B* to be the most appropriate genes. In Chapter 6, it was found that *TOP1* expression was perturbed by Dex treatment, hence the adoption of *GAPDH* and *TOP1* as reference genes in Chapters 6 and 7. A separate study (data not included) found most stable reference gene for MRC-5 gene expression to be *B2M.*

2.12.2 QRT PCR for *MUC5AC* using PerfectProbe™

Primer and Probes were obtained from Primer Design, Southampton, UK (Table 2.5) QRT PCR was carried out as per Table 2.6 and Table 2.7 below.

Predicted: Homo sapiens mucin 5, subtypes A and C, tracheobronchial / gastric (MUC5AC), mRNA					
Accession Number	Official Gene Symbol		Sequence Length		
XM_4955860	MUC5ac		3681		
Amplicon Details					
Product Length (bp)	Melting Temperature (Tm)	Distance from 3' end of sequence	Single exon	Structure	
113	92.8ºC	2943	Not Tested	None	
Primer Details					
Sense Primer	Position	Tm	GC Content (%)	3'dG	Dimer
CAGAGGGGTTGACAGTGAC	738	55.1	57.9	-4	0
Sense Primer	Position	Tm	GC Content (%)	3'dG	Dimer
GAACCGCATTTGGGCATC	850	54.7	55.6	-4.6	0
Perfect Probe Sequence					
CGTCCACCACGCTGCCTCCTGCCCtggacg					

Table 2.5 Gene sequences and design of *MUC5AC* primer.

Reagent	**Volume per reaction**
Primer mix	1 µL
Water	4 µL
2 x Perfect Probe Master Mix	10 µL
cDNA template	5 µL

Table 2.6. Volumes used for *MUC5AC* PerfectProbe™QRT-PCR.

Temperature	**Time**	**Number of Cycles**
95ºC Enzyme Activation	10 minutes	1
95ºC Denaturation	15 seconds	50
50ºC Data Collection	30 seconds	
72ºC Extension	15 seconds	

Table 2.7. Reaction Conditions used for *MUC5AC* QRT-PCR (PerfectProbe™).

Reactions were set up in a laminar flow PCR hood in 96 well FAST plates with reagents on wet ice. Once reagents and samples were added the plates were sealed with adhesive film (Thermo Fisher Scientific, Waltham, MA, USA) and briefly centrifuged in a microplate centrifuge (fixed speed, relative centrifugal force not specified) (Thermo Fisher Scientific, Waltham, MA, USA) on the ABI Systems Quant Studio 7 (Thermo Fisher Scientific, Waltham, MA, USA). Reference genes for these assays were *TOP1* and ATP synthase subunit beta,

mitochondrial (*ATP5B*) (Primers and Probes obtained from Primer Design, Southampton, UK). Following amplification delta-delta Ct analysis was carried out to determine relative gene expression[329] (see Section 2.94).

2.12.3 QRT-PCR using TaqMan™ Assays

QRT PCR was performed on the cDNA using a Quant-Studio 7 thermocycler (Life Technologies, Paisley, UK), and curated TaqMan™ assays with fluorescein amidite (FAM) fluorophore were obtained from Life Technologies Paisley, UK as described per Table 2.8.

Gene of Interest	Gene Symbol	TaqMan Assay ID	Primers Span Exons	Probe Spans Exons
SFTPA1	*SFTPA1*	Hs00831305_s1	Yes	Yes
SFTPA2	*SFTPA2*	Hs00359837_m1	No	Yes
SFTPB	*SFTPB*	Hs01090667_m1	No	Yes
SFTPC	*SFTPC*	Hs00161628_m1	No	Yes
SFTPD	*SFTPD*	Hs01108490_m1	No	Yes
PTH1R	*PTH1R*	Hs00896826_g1	No	Yes
PLIN2	*PLIN2*	Hs00605340_m1	No	Yes
ABCA3	*ABCA3*	Hs00387048_m1	No	Yes
ABCB4	*ABCB4*	Hs00983945_m1	No	Yes
ERBB3	*ERBB3*	Hs00176538_m1	No	Yes
PTHrP	*PTHLH*	Hs00174969_m1	No	Yes
NRG-1β	*NRG1*	Hs00247620_m1	No	Yes
PPARγ	*PPARG*	Hs01115513_m1	No	Yes
CDH1	*CDH1*	Hs01023895_m1	No	Yes
VIM	*VIM*	Hs00958111_m1	No	Yes
ZEB1	*ZEB1*	Hs01566408_m1	No	Yes

Reference Gene		Assay ID	Primers Span Exons	Probe Spans Exons
TOP1	*TOP1*	Hs00243257_m1	No	Yes
ATP5B	*ATP5B*	Hs 00969569_m1	No	Yes
BT2M	*BT2M*	Hs00187842_m1	No	Yes
GAPDH	*GAPDH*	Hs02786624_g1	No*	No*

*Used as reference gene and tool to detect carried over DNA in RT-Free Controls

Component	Catalogue Number	Comments
Gene Expression Mastermix	ABI 4369016	

Table 2.8. TaqMan™ QRT-PCR expression assays used in the study.
Proprietary sequence data for TaqMan™ assays is not available. Details of amplicon size and genomic mapping can be found by following this URL:
https://www.thermofisher.com/taqman-gene-expression.

(1) TaqMan QRT PCR Set-up and Reaction Conditions

PCR reactions were prepared in a dedicated laminar-flow PCR isolation hood with reagents kept on wet ice. cDNA (previously diluted 1:10 in sterile RNAse-free water) was mixed with the TaqMan™ primer/probe gene expression assay mix and the Gene expression Mastermix (providing Taq polymerase and appropriate ionic balance) (ABI 4369016, Life Technologies, Paisley, UK) in the proportions as per Table 2.9 in TaqMan™ 10 µL Fast 96-well assay plates (Life Technologies, Paisley, UK). Plates were sealed, shaken and briefly centrifuged to collect liquids into the bottom of the wells prior to amplification and analysis using the QuantStudio 7'QRT-PCR amplifier (Life Technologies, Paisley, UK).

Each cDNA sample was assessed for the gene of interest (in duplicate). Reverse-Transcription-Free (RT-Free) controls were amplified in parallel to assess any genomic DNA carry over into the source RNA. "Water" controls were also prepared for each gene to counter any non-specific amplification. TaqMan™ primer/probe sets used (apart from *GAPDH*) were selected for sequences that spanned intron-exon boundaries, thus, ensuring that any amplification was specific to expressed mRNA gene sequences. The GAPDH primer/probe did not span exons, thus added an extra level of quality control as it should be more sensitive at identifying any unwanted genomic carry over in RT-Free controls.

Component	**Volume (µL)**
Gene Expression Mastermix	5 µL
Primer/Probe Mix (TaqMan Assay)	0.5 µL
1:10 diluted cDNA (or water control or RT-Free control)	4.5 µL
Total reaction volume	10 µL

Table 2.9 Volumes of components used in each TaqMan™ QRT-PCR reaction.

Step	**PCR Stage**	
1	Ramp-up temperature from room temperature to 50°C at 1.6°C/second	Initiation
2.	Hold at 50°C for 2 minutes	
3	Ramp-up temperature from room temperature to 95°C at 1.6°C/second	
4	Hold at 95°C for 10 minutes	
5	Hold at 95°C for 15 seconds	Repeat Steps 5 to 7 for 40 cycles.
6	Ramp-down temperature to 60°C at 1.6°C/second	
7	Hold at 60°C for 1 minute. Measure Fluorescence.	

Table 2.10. Reaction conditions for TaqMan™ QRT-PCR.

2.12.4 Interpretation of QRT-PCR Results and Calculation of Relative Gene Expression

Results from QT-PCR assays were accepted the following basis:

- Water and RT-Free control samples returned Ct values of 35 or greater (in most cases no amplification was observed).
- Evidence of gene expression was recognised as Ct values less than 35. In most cases these were 30 or less.

The "Delta-Delta Ct" method was used to calculate relative gene expression[330]. In short, the mean Ct values of biological and technical replicates of the reference genes were calculated and the geometric mean deduced for each sample. This value was then subtracted from the mean values of the gene of interest to provide the first "delta" value. The mean delta value of the control samples was then subtracted from the delta value of each of the samples to provide the "delta-delta Ct" (ΔΔCt) value for each sample (if calculated correctly the delta-delta for the control should be zero). To convert the ΔΔCt to a meaningful "relative expression" value and to reflect the exponential doubling of amplified product in the PCR reaction, relative expression was calculated by raising two to the power of the negative ΔΔCt value ($2^{-\Delta\Delta Ct}$) giving the control a value of "one" and all other samples a value of expression relative to the control.

Throughout this study "Housekeeping Genes" are referred as "Reference Genes" as per the terminology advised by MIQE *Minimum Information for Publication of QRT_PCR Experiments" Guidelines[331]
Calculations were performed using Microsoft Excel.

2.13 Preparation of A549 Cultures for Electron Microscopy

13 days after seeding, coverslips of A549 cells in12 well plates had their medium removed by aspiration, washed in PBS once (Severn Biotech, Swindon, UK, Product No. 20-74-01) and then fixed by the addition of 1 mL of 2.5 % glutaraldehyde to each well and incubation at room temperature for 1.5 hours, before aspirating the glutaraldehyde solution waste, washing the cells twice in PBS and then finally adding 1 mL of PBS or Sorenson's buffer before parafilm™ wrapping and storing the plates at 4° C prior to processing for SEM.

2D A549 Monolayers, 3D Spheroids and Alvetex™ Scaffold cultures were washed twice with Sorensen's Buffer (0.1 M phosphate buffer, pH 7.2 (prepared from 0.2 M disodium hydrogen phosphate and 0.2 M monosodium dihydrogen phosphate plus de-ionised water). 2D cells were removed by gentle scraping (sterile disposable cell scrapers, Becton Dickenson).

Scraped cell monolayers, spheroids and Alvetex™ inserts were fixed by a 2-hour incubation in 3 mL (a volume more than 20 times the volume of the sample) of 2.5% glutaraldehyde solution. 2D scraped cells and spheroids were centrifuged (100 x *g* for 3 minutes). Supernatant aspirated to waste and the cells, spheroids or Alvetex inserts were washed twice with Sorenson's buffer before re-suspending them in a 0.5 mL skirted conical microtube in 100 µL of Sorenson's Buffer.

2.14 Transmission Electron Microscopy (TEM)

Glutaraldehyde fixed cellular material (2D A549 Monolayers, 3D Spheroids and Alvetex™ Scaffold cultures) were further fixed and stained with osmium tetroxide before embedding in resin (Aradlite™). The resulting blocks were sectioned 80-120 nm thickness using a glass knife and placed onto grids (copper side) before being stained with 2 % uranyl acetate for 30 minutes, washed four times with deionised water and further stained with 0.1 % lead citrate before a final four washes in deionised water. Sections were imaged by transmission electron microscopy using Philips CM100 (Philips Electron Optics, Cambridge, UK) and Hitachi H7000 instruments (Hitachi Group, Maidenhead, Berkshire, UK) electron microscopes.

2.15 Scanning Electron Microscopy

Glutaraldehyde fixed cellular material (2D A549 Monolayers, 3D Spheroids and Alvetex™ Scaffold cultures) were secondarily fixed in osmium tetroxide for 1-2 hours at room temperature before being dehydrated sample through graded ethanol series at room temperature (25% ethanol for 15 minutes, 50% ethanol for 15 minutes, 75% ethanol for 15 minutes, 100% ethanol for 15 minutes, 100% ethanol for 15 minutes and finally two transfers to 100% Hexamethyldisilazane for 15 minutes each. The samples were then air-dried, mounted on SEM stubs and conductive coated with gold in the AtomTech Z705 ultra-fine grain ion beam coater prior to examination in the FEI XL30 FEG scanning electron microscope (Philips Electron Optics, Cambridge, UK).

2.16 Histology.

2.16.1 Preparation of 3D Spheroids and Alvetex™ Scaffold Co-Cultures for Paraffin Embedding

(1) Spheroids

5 plates (120 wells of A549 spheroids at 13 days from set up) were harvested by gentle aspiration using a 5 mL stripette into two 50 mL Falcon centrifuge tubes (60 spheroids per tube). The spheroids settled by gravity in two minutes. The medium was aspirated and replaced with 5 mL of PBS and the resulting suspension transferred to 15 mL Falcon tubes

which were again, allowed to settle for two minutes. 4 mL of the medium was aspirated and the resulting 1 mL suspension transferred to 10 % Formalin. before three washes in PBS (three minutes each), before finally being suspended in 70 % ethanol solution.

(2) Alvetex™ Scaffold Cultures

Medium was aspirated from the cultures before fixation in 4 % paraformaldehyde (w/v) in phosphate buffered saline (PBS). Scaffold inserts were removed from their holders before two washes in PBS (three minutes each), before finally being suspended in 70 % ethanol solution.

2.16.2 Paraffin Embedding and Cutting of Paraffin Sections

Samples were processed through increasing concentrations of ethanol: 70% Ethanol, two changes 1 hour each; 80% Ethanol, one change, 1 hour; 95% Ethanol, one change, 1 hour; 100% Ethanol, three changes, 1.5 hour each. Then into paraffin wax at 60°C, two changes, 2 hours each.

Paraffin blocks were cooled on ice, then placed into the manual rotary microtome (Leica Microsystems Ltd, Milton Keynes, UK) with the blade angle set to 5°. 4.5 µm thick sections were cut and then 'floated out' in a 45°C water bath allowing 1 minute for the wax to stretch. Sections were then picked up onto pre-labelled coated slides before drying overnight at 37°C (or on a hotplate for one hour at 60°C for tinctorial staining).

2.16.3 Processing of Tissue and Cell Culture Samples into Glycol Methacrylate (GMA) Blocks for PAS Staining and Immunohistochemistry

The control tissue samples, A549 Spheroids or scraped cell monolayer were immediately placed into fixative comprised of ice cold acetone with 2mM phenyl methyl sulphonyl fluoride (35 mg/100 mL) and 20 mM iodoacetamide (370 mg/100 mL). The samples were fixed overnight at -20°C. The following day the fixative was removed and replaced with acetone at room temperature and incubated at room temperature for 15 minutes. The acetone was then replaced with Methyl Benzoate at room temperature for 15 minutes, followed by three, two hour incubations at with "processing solution" (5 % v/v mix of methyl benzoate with glycol methacrylate ('GMA Solution A')). GMA 'embedding solution' (resin) was prepared by dissolving 70 mg benzoyl peroxide in 10 mL of ('GMA Solution A') by gentle shaking. Once dissolved 250 µL of "GMA Solution B" was added the fixed spheroids, cells or tissue samples were them placed into the bottom of flat bottomed capsules (Taab Laboratories, Berkshire, United Kingdom) into which the resin was added, filling them to the brim and closing the lid

to exclude the air. The resin was left to polymerise for at least 48 hours at 4°C before sectioning.

2.16.4 Preparation of Poly-L-Lysine (PLL) Coated Microscope Slides

Microscope slides (CellPath, Newtown, Powys, Wales, UK) were immersed in a 0.01% (w/v) solution of poly-L-lysine (Sigma Aldrich, Gillingham, United Kingdom) for five minutes and allowed to air dry overnight at room temperature before use.

2.16.5 Periodic Acid-Schiff (PAS) Staining of Mucins from GMA Embedded Slide Material

The slides were flooded with Periodic Acid (1 g/100 mL) for 10 minutes followed by two washes with reverse osmosis (RO) water, a flooding with Schiff's reagent (Feulgen stain, prepared in distilled water, pararosaniline (0.5 % w/v), sodium metabisulphite (1 % w/v) concentrated hydrochloric acid (91 % v/v) and decolourising charcoal 0.1% (w/v) for 25 minutes followed by a 10-minute wash in running tap water before counterstaining in Haematoxylin and Eosin for 30 seconds and a wash in running tap water. Slides were then washed in 70 % v/v ethanol very briefly, transferred to absolute ethanol for one minute before three two minute washes in Clearene for two minutes each. Slides were blotted dry before mounting with coverslips using Pertex™ (CellPath, Newtown, Powys, Wales, UK).

2.16.6 Preparation of Sections for Histology from GMA Prepared Blocks

Once the GMA resin had hardened, the plastic capsule was scored with a blade and removed to free the GMA block. The block was then trimmed by filing to remove excess resin to readily present the spheroids or tissue samples at the cutting surface.

2 µm sections were then prepared using a freshly prepared glass blade in a microtome and floated into dilute ammonia solution (0.2% v/v ammonia in distilled water) and then transferred to PLL coated microscope slides and allowed to air dry.

Sections could then be immediately processed for histochemical staining or wrapped in foil and stored at -20ºC.

2.16.7 Inspection of GMA Prepared Slides using Toluene Blue Stain

To ensure the sections were properly presented and ready for staining, one slide was removed from each set prepared and stained with toluene blue before inspecting by light microscopy.

2.16.8 Haematoxylin and Eosin Staining (Paraffin Embedded Sections)

Slides were placed into a staining rack and de-waxed: 2 x 10minutes in Tissue-Clear (CellPath, Newtown, Powys, Wales, UK); 2 x 5 minutes in 100% ethanol; 5 minutes in 70% ethanol; and 5 minutes in distilled water. 5 minutes in Mayer's haematoxylin; 5 minutes running tap water; 5 minutes in eosin; dipped briefly in distilled water three times before transfer to 100% ethanol (three times) and Tissue Clear (three times). Slides were mounted in XTF mountant (CellPath, Newtown, Powys, Wales, UK).

2.16.9 Periodic Acid-Schiff (PAS) Staining of Mucins from Paraffin Wax Embedded Slide Material

Slides were de-waxed through two, five-minute wash solutions of Clearene™ solvent (Leica Microsystems GmbH, Wetzlar, Germany), two five minute washes of absolute alcohol, one five-minute wash in 70% v/v ethanol and a five-minute wash in reverse osmosis (RO) water. The slides were flooded with Periodic Acid (1g/100 mL) for 5 minutes followed by two washes with RO water, a flooding with Schiff's reagent (Feulgen stain, prepared in distilled water: pararosaniline (0.5%w/v), sodium metabisulphite (1%w/v) concentrated hydrochloric acid 91% v/v) and decolourising charcoal 0.1% w/v) for 15 minutes followed by a 10-minute wash in running tap water before counterstaining in Haematoxylin and Eosin for 30 seconds and a wash in running tap water. Slides were then washed in 70% v/v ethanol very briefly, transferred to absolute ethanol for one minute before three two minute washes in Clearene™ for two minutes each. Slides were blotted dry before mounting with coverslips using Pertex ™ (CellPath, Newtown, Powys, UK).

2.16.10 Sirius Red Collagen Staining (Paraffin Embedded Samples)

Slides were de-waxed through two, five-minute wash solutions of Clearene™ solvent (Leica Microsystems GmbH, Wetzlar, Germany), two five minute washes of absolute alcohol, one five minute wash in 70 % v/v ethanol and a two five minute washes in reverse osmosis (RO) water. 5 minutes in 0.2 %phosphomolybdic acid; two hours Pico-Sirius Red; washed briefly in 0.01 % Hydrochloric Acid (HCl); Rinsed in distilled water; stained in Mayer's haematoxylin for 2 minutes followed by two minutes in running tap water before transfer to 70 % v/v ethanol very briefly, transferred to absolute ethanol for one minute before three two minute washes in Clearene™ for two minutes each. Slides were blotted dry before mounting with coverslips using Pertex ™ (CellPath, Newtown, Powys, UK).

2.16.11 Masson's Trichrome Connective Tissue Staining (Paraffin Embedded Samples)

Slides were de-waxed through two, five-minute wash solutions of Clearene™ solvent (Leica Biosystems), two five minute washes of absolute alcohol, one five-minute wash in 70 % v/v ethanol and a two five minute washes in reverse osmosis (RO) water. Weigert's haematoxylin for 5 minutes; running tap water for 5 minutes; Ponceau-acid Fuchsin Solution, 3 minutes before washing in water and counterstaining in aniline blue solution for 5 minutes. Then transferred to 100% ethanol (three times) and Tissue Clear (three times). Slides were mounted in XTF mountant (CellPath, Newtown, Powys, Wales, UK).

2.16.12 Immunohistochemical Staining of Cells Grown as Monolayers on Coverslips or Slides

Cells were fixed by flooding the slides with methanol for 10 minutes in a staining dish and then washed three times, two minutes each time, in Tris Buffered Saline (TBS). Slides were drained and any endogenous peroxidase activity was blocked by the addition of 0. 3% (v/v) hydrogen peroxide solution in 1 % (w/v) sodium azide solution prepared in distilled water and incubated for 30 minutes at room temperature. Following this the slides were washed a further three times using TBS as above.

The blocking of non-specific avidin and biotin binding was effected by using the proprietary "Avidin and Biotin Block Solutions" provided in the staining kits (Vector Laboratories Ltd, Peterborough, United Kingdom). Slides were incubated for 20 minutes in each blocking solution, with a TBS washes as above before and after each treatment.

Non-specific antibody binding was blocked by the addition of Dulbecco's Modified Eagle's Medium (DMEM) supplemented with 10% (v/v) Foetal Bovine Serum (FBS) for 30 minutes room temperature incubation. An appropriate dilution of the primary antibodies (Mouse Anti-Human Pan-cytokeratin Antibody (as a positive control) at 1:4000 v/v (Dako, Agilent, Santa Clara, CA, US), Mouse anti-Human MUC5AC (MAB2011, Merck-Millipore, Billerica, MA, US), (dilution was determined by a prior titration exercise and used at 1:1000) was applied to the slides and incubated for 60 minutes at room temperature. After which the slides were further washed three times with TBS followed by an appropriate dilution of a biotinylated secondary antibody specific to the primary antibody (1:1000) (Rabbit anti-Mouse, E0413 (Dako, Agilent, Santa Clara, CA, US), for a further 60 minutes room temperature incubation followed by three washes in TBS. Streptavidin / Biotin Peroxidase Enzyme Complex (Vector Laboratories, Peterborough, UK) prepared in TBS was then added for a further 60 minute incubation, the slides given another three washes in TBS and after draining the substrate and

chromagen solution (Hydrogen Peroxide and 3,3'-Diaminobenzidine (DAB) (Vector Laboratories, Peterborough, UK) was applied and incubated for 5 minutes before a final rinse in TBS and wash in running tap water for five minutes. The slides were counterstained in Mayer's haematoxylin for 90 seconds and washed in tap water for 5 minutes before applying aqueous mounting medium, baking in an oven at 80° C for 15 minutes and mounting in Pertex™ (CellPath, Newtown, Powys, Wales, UK) under a coverslip.

2.16.13 Immunohistochemical Staining of GMA Embedded Sections

Endogenous peroxidase activity was blocked by the addition of 0.3% (v/v) hydrogen peroxide solution in 1% (w/v) sodium azide solution prepared in distilled water and incubated for 30 minutes at room temperature. Following this the slides were washed a further three times using TBS as above.

Non-specific antibody binding was blocked by the addition of Dulbecco's Modified Eagle's Medium (DMEM) supplemented with 10% (v/v) Foetal Bovine Serum (FBS) for 30 minutes room temperature incubation. An appropriate dilution of the primary antibodies (Mouse Anti-Human Pan-cytokeratin Antibody (as a positive control) at 1:4000 v/v (Dako, Agilent, Santa Clara, CA, US), Mouse anti-Human MUC5AC (MAB2011, Merck-Millipore, Billerica, MA, US), (dilution was determined by a prior titration exercise, a dilution of 1:1000 was determined) was applied to the slides and the sections covered with coverslips before incubation overnight at room temperature. The following day the slides were further washed three times with TBS followed by an appropriate dilution (1:1000) of an biotinylated secondary antibody specific to the primary antibody (Rabbit anti-Mouse, E0413 (Dako, Agilent, Santa Clara, CA, US), for a further two hour room temperature incubation followed by three washes in TBS. Streptavidin / Biotin Complex (Vector Laboratories, Peterborough, UK) prepared in TBS was then added for a further 60 minute incubation, the slides given another three washes in TBS and after draining the substrate and chromagen solution (Hydrogen Peroxide and 3,3'-Diaminobenzidine (DAB) (Vector Laboratories, Peterborough, UK) was applied and incubated for 10 minutes before a final rinse in TBS and wash in running tap water for five minutes. The slides were counterstained in Mayer's haematoxylin for 90 seconds and washed in tap water for 5 minutes before applying aqueous mounting medium, baking in an oven at 80° C for 15 minutes and mounting in Pertex™ under a coverslip.

2.16.14 Oil-Red-O Staining

Cell monolayers were rinsed with phosphate buffered saline (PBS), fixed with two applications of 10% formalin before rinsing with purified water followed by addition of 60 % isopropanol and air drying. The cells were stained using Oil red-O (Sigma Aldrich, Dorset, UK) (0.21 g/mL

in iso-propanol, filtered), rinsed four times in purified water before imaging by light microscopy.

2.16.15 Immunofluorescent Microscopy

All incubations were carried out at room temperature. Cell cultures were prepared in multi-well plates or coverslips and fixed using 4 % paraformaldehyde in PBS (Thermo Scientific, Alfa Aesar, Heysham, UK) for 15 minutes before PBS washes (x3). Cell membranes were permeabilised with 1% v/v saponin (Thermo Scientific, Alfa Aesar, Heysham, UK) in a 15-minute incubation before aspiration to waste. Blocking solution (3 % Bovine Serum Albumin v/v (Sigma Aldrich, Gillingham, Dorset) in PBS) was added and incubated for 30 minutes. Blocking solution was removed to waste. Primary antibody, prepared in the blocking solution at the recommended concentration was then added for a three-hour incubation before washing three times with PBS, the final wash aspirated to waste Fluorescent labelled secondary antibody was prepared at the manufacturer's recommended concentration in PBS and incubated for one hour, aspirated to waste and the cells washed three times in PBS and cells left in their final wash. Nuclear counterstain at the manufacturer's recommended concentration (e.g. three drops/ mL Nuc-Blue, ThermoScientific, Life Technlogies, Paisley, UK) was added as a nuclear counterstain and incubated for a further 10 minutes before a final three washes with PBS. Cells in multi-well plates were left in their final wash before imaging. Coverslips were rinsed briefly in de-ionised water and mounted on slides in Moviol mounting medium (Sigma Aldrich, Gillingham, Dorset, UK). Antibodies used are detailed in Table 2.11.

Fluorescence Imaging was captured using the EVOS fluorescence microscope (Life Technologies, Paisley, UK) or the Leica Cytogenic Workstation (Leica Microsystems GmbH, Wetzlar, Germany). Antibodies used are described in Table 2.11.

Target	Primary Antibody	Dilution	Secondary Antibody	Dilution
Human SFTPB	Mouse IgG2a Fisher Scientific 15688018	1:50	Goat anti-mouse Alexafluor 488 Fisher Scientific 15626746	1:200
Human SFTPD	Mouse IgG1 Abcam Ab17781	1:100	Goat anti-mouse Alexafluor 488 Fisher Scientific 15626746	1:200
HT1-56 (Human ATI)	Mouse IgG1 Terrace Bioscience	1:150	Goat anti-mouse Alexafluor 488 Fisher Scientific 15626746	1:200
HT2-280 (Human ATII)	Mouse IgM Terrace Bioscience	1:150	Rat Anti-Mouse IgM Efluor 660 Fisher Scientific 15373058	1:100
Human OCT4	Rabbit. Invitrogen A24867	1:200	Donkey anti-rabbit Alexafluor 594. Invitrogen A24870	1:250
Human SSEA4	Mouse IgG3 Invitrogen A24866	1:100	Goat anti-mouse Alexafluor 488. Invitrogen A24877	1:250
SOX2	Rat. Invitrogen A24759	1:100	Goat ant-mouse Alexafluor 488. Invitrogen A24877	1:250
TRA-1-60	Mouse IgM Invitrogen A24868	1:100	Goat anti-mouse IgM Alexafluor 594. Invitrogen A24872	1:250

Table 2.11. Antibodies used for Immunofluorescence.

Antibody Suppliers (refer to Table 2.11): Abcam PLC, Cambridge, UK. Fisher Scientific, Loughborough, UK. Invitrogen, Paisley, UK. Terrace Biotech, San Francisco, California, USA.

2.17 Mycoplasma and STR Profiling of TRiP WT / E-Cad/LGR6+ Cells

TRiP WT / E-Cad/LGR6+ cells were resuscitated into Serum-Free RHB medium (Takara Bio Inc, Shiga, Japan) as prescribed and cultivated for submission to human STR profiling and mycoplasma testing by PCR analysis, and Mycoplasma DNA Hoechst Staining.

2.17.1 Short Tandem Repeat (STR) Profiling

Short tandem repeat (STR) profiling techniques were originally developed for forensic applications. Using this approach, a number of polymorphic short repeated sequences believed to be involved in the structural sequences within DNA (STR loci) are amplified by using commercially available sets of primers. The PCR products are analysed simultaneously using a capillary based sequencer with size standards (an 'allelic ladder') using automated fluorescent detection techniques to produce an electropherogram which is subsequently analysed using proprietary software (Genemapper™, Thermo Fisher, Waltham, MA USA). The result is a numerical code corresponding to the lengths of the PCR products amplified at each locus accurate to less than one base pair, each score at specific locus refers to the number of times the STR is repeated and represents an allele. As each individual inherits a chromosome set form each parent, the allelic scores will be a single number for each locus (homozygous)

or there will be two scores (heterozygous). Through application of this method to cell lines, any laboratory could either check the authenticity of its cell lines if it has the appropriate technologies or have them checked commercially[332 333].

1 x 10^5 TRiP WT/ECad/LGR6+ or 293 cells were dispensed onto an FTA® card (Whatman PLC, Buckingham, UK) and air dried before testing by multiplex PCR by a subcontractor (Northgene Ltd, Newcastle, UK). In short: the dried cell 'spot' was punched from the card and solubilised in proprietary resuspension reagent (Promega, Madison, Wisconsin, USA) before DNA quantification and multiplex PCR amplification of the polymorphic Single Tandem Repeat (STR) sequences using the fluorescently labelled primers from the forensic human Powerplex™ STR profiling kit (Promega, Madison, Wisconsin, USA) to the manufacturer's instructions whilst also observing the ASN-0002 Standard for STR Profiling[333]. The capillary based genetic analyser (ABI Prism®, Life Technologies, Paisley, UK) was then used to electrophorese the PCR products and the sizes and identity of the amplicons were determined using the instrument's laser detection system. Using an allelic ladder and internal size standard (ISS) and Genemapper™ software (Promega, Madison, Wisconsin, USA) the repeat allele scores for each of the STRs was generated, providing the STR profile for the cell line. The resultant profile was then compared to known reference profiles stored in a publicly accessible database (Cellosaurus (Swiss Institute of Bioinformatics)[285].

TOTAL ALLELES in the Test Sample	
TOTAL ALLELES in the Reference Sample	
SHARED ALLELES, Test and Reference Samples	
Percent Match for Test and Reference Samples	

$$\text{Match Algorithm} = \frac{\text{SHARED ALLELES} \times 2}{\text{TOTAL ALLELES in the Test Sample} + \text{TOTAL ALLELES in the Reference Sample}}$$

Percent Match = Match Algorithm result x 100

Interpretation of Results

Are there multiple peaks that would be consistent with a mixture?	YES/NO
Is the percent match result in the range 0-55 %? This result is consistent with the two samples being unrelated (different donors)	YES/NO
Is the percent match result in the range 56-79 %? This result is indeterminant and may need further testing	YES/NO
Is the percent match result in the range 80-100 %? This result is consistent with the two samples being related (same donor)	YES/NO

Figure 2.1. Match Algorithm for STR Analysis.

Percentage match scores were calculated using the algorithm outlined in the ASN-0002 Standard[333] (Figure 2.1).

2.17.2 Mycoplasma Testing

Mycoplasma testing was carried out by the European Collection of Cell Cultures (ECACC) (Salisbury, UK) by proprietary PCR, Hoechst Staining and Culture Isolation methods. In short, DNA was extracted from the cells and amplified by standard PCR using mycoplasma specific primers (5' GGG AGC AAA CAG GAT TAG ATA CCC T 3' and 5' TGC ACC ATC TGT CAC TCT GTT AAC CTC 3')[334]. After PCR cycling the product was assessed using capillary electrophoresis in the Tapestation™ bioanalyser (Agilent, Santa Clara, California, USA). Positive results were indicated by a 255-285bp product. A positive assay control to generate a synthetic 392bp product was included (Thermo Scientific, Paisley, UK).

Supernatant from growing cell culture was inoculated onto coverslips of Vero cells(ECACC, Salisbury, UK) in multi-well plates and incubated for 3 and 5 days in a humidified CO_2 incubator at 37°C. Coverslips were then fixed (Carnoy's fixative) and stained with the DNA specific stain Hoechst 33258™ (Thermofisher Scientific Waltham, Massachusetts, US), mounted on microscope slides and visualised using fluorescent microscopy and assessed to presence of +typical mycoplasma punctate staining as visualised against the Vero cell cytoplasm.

2.18 Statistical Analysis and Graphical Data Presentation

Statistical analysis of RNA micro-array data was performed as per Section 2.5.

Other analyses utilised parametric or non-parametric statistical tests as appropriate. These were: Student's *t*-test for normally distributed data and for data that were not normally distributed: Mann-Whitney for comparison of two conditions or Kruskal-Wallis for multiple comparisons. Data were tested for normality using the Kolmogorov-Smirnov test.

Statistical analyses and plotting of graphs were performed using Graphpad® Prism™ (San Diego, California, USA).

3. 3D Spheroid Growth of A549 Cells

3.1 Introduction

Continuous cancer derived cell lines such as A549 have been shown to be limited in terms of their ability to fully recapitulate physiologically function. Many cellular processes, such as cell cycle regulation and differentiation, are deregulated[212]. They do, however, have major advantages as discussed in Chapter 1. Above all their supply is practically inexhaustible, they are readily accessible from suppliers as 'ready to use' reagents with full traceability and confirmation of origin and certificates of analysis confirming absence of microbial contamination[212 292].

Environmental factors such as choice of substratum, medium and continuous culture can have a substantial impact on the phenotype and gene expression of cell lines. For example epithelial differentiation can be induced in continuous cell lines such as CaCo2[335] and MDCK[336] through long term cell culture conditions demonstrating that under the influence of optimised culture conditions, cancer derived continuous cell lines can be driven to a more physiologically relevant state.

Recently there has been development and adoption of technologies that enable cultured cells to acquire their natural morphology and structure that have been under the umbrella term 'Three-dimensional' (3D) cell culture. These techniques enhance cellular organisation and the physiological relevance of experiments performed *in vitro*. 3D culture allows greater cell-to-cell contact and increased intercellular signalling to facilitate developmental processes thereby allowing cells to differentiate into more complex structures. The 3D environment enables cells to organize into tissue-like structures through uniform expression of adhesion molecules distributed across the cell surface[337]. In 2D culture cells become flattened and polarized leading to the tendency for binding proteins to accumulate on the ventral surface where they attach to the tissue culture plastic rather than other cells[338].

3D cell culture may be achieved using three distinct strategies, the first of which involves cultivation of cells in solid scaffolds. Such scaffolds can be broadly divided into fibrous or porous matrices manufactured using a range of different techniques and alternative materials[339]. The second strategy involved encapsulation of cells in hydrogels comprised of a loose scaffold framework of a cross-linked materials such as agarose, fibrin, collagen or hyaluronic acid with high water content[340]. Finally, there is the formation of multi-cellular aggregates or "spheroids".

in 3D spheroid culture, cells form their own extracellular matrix components. Spheroid culture can be achieved using the hanging drop technique[341], where cells are cultured in a drop of media suspended on the lid of a cell culture dish or alternatively by the use of low adherence substrates such as agarose coated plastic or commercially supplied materials such as Ultra-Low Attachment (ULA™) plastic (Corning, New York, USA). In both cases, cells are unable to adhere to a surface and subsequently form aggregates in suspension[339]. Spheroid culture appears to sustain tissue function better than 2D monolayer cultures[342] but here are also limitations in spheroid culture, as nutrient and gaseous diffusion may become limiting, leading to necrosis in the centre of the spheroid[339].

The literature suggests that three dimensional 3D spheroid cultures of A549 may be better models than conventional two dimensional 2D cultures grown on flat glass or plastic tissue culture surfaces, in inflammation studies[77] and infection studies[343] and that they may better represent the distal lung. Barkauskas *et al* (2013)[344], working with 3D spheroid cultures of cells from mouse lungs, developed self-renewing ATII derived lung organoids or "alveolospheres," which contained both ATII cells and cells expressing multiple ATI markers, including the novel *Hopx*, marker for ATI cells[345]. Recreating the 3D architecture of the alveolar epithelium is challenging and previous attempts to create this environment have presented complex technical challenges[247].

Historically, researchers have not been consistent in the formulation of cell culture medium used in their experiments with A549 cells nor with the phase of growth from which the A549 cells were used[19 346 347 348]. This is despite the fact that early work with A549 cells reported that extended culture resulted in cellular 'differentiation', as evidenced by high numbers of MLB[19 349].

It is therefore proposed that an approach that combines cell culture medium optimisation, long term culture and 3D spheroid culture might drive A549 cells closer to an ATII phenotype.

3.2 Hypothesis

Long term three-dimensional spheroid cultivation of the A549 cells in physiologically formulated cell culture medium (Ham's F12) will produce a phenotype more representative of ATII cells than equivalent cells in 2D log phase culture.

3.2.1 Aims

- To grow A549 cells as long term cultured self-assembling spheroids on Ultra Low Attachment (ULA™) plastic or in 2D log phase culture in conventional tissue culture plastic.
- To assess the effect of two different media formulations, Ham's F12 nutrient medium and Dulbecco's modified minimal essential medium (DMEM), both supplemented with 10% (v/v) foetal bovine serum (FBS) and 2 mM L-Glutamine.
- Through analysis of morphology, viability, proliferation, gene expression (using RNA microarray analysis, quantitative real time polymerase chain reaction (QRT PCR), immunohistochemistry and electron microscopy) determine if the conditions chosen drove an ATII phenotype and if they did not, what phenotype was expressed.

3.2.2 Objectives

- To establish 3D spheroid cultures in ULA plastic in both Ham's F12 nutrient medium and Dulbecco's modified minimal essential medium (DMEM), both supplemented with 10% (v/v) foetal bovine serum (FBS) and 2 mM L-Glutamine and establish a protocol for spheroid maintenance over a three to four-week period.
- To employ phase contrast microscopy and cell counting techniques to assess evidence of cellular differentiation and possible adoption of epithelial and ATII cellular morphology. Assess cellular viabilities and rates of cellular proliferation in the 3D spheroid cultures.
- To carry out extensive gene expression analysis of the long and short term 2D and 3D spheroid cultures using *RNA* microarray analysis followed by gene ontology and pathway analysis with the aim of determining patterns of gene regulation consistent with epithelial and ATII differentiation. To validate and further investigate gene expression with quantitative real time polymerase chain reaction (QRT PCR).
- Use immunohistochemistry and transmission electron microscopy (TEM) to analyse the nature of secreted and expressed proteins and cellular ultrastructure in the spheroid cultures to validate the nature of the cellular differentiation as suggested by the gene expression results.

3.3 Results

3.3.1 Selection of Growth Medium

Initial experiments examined the growth of A549 spheroids on Ultra Low Attachment (ULA™) plastic using DMEM or Ham's F12 media, both supplemented with 10% FBS and 2mM L-Glutamine and cultivated for up to 25 days. (DMEM/10%FBS and Ham's F12/10% FBS).

Phase contrast images of the developing spheroids over a 25-day time-course in the two different media are shown in Figure 3.1. Spheroids cultivated in F12/10% FBS gave consistently more compact spheroid colonies than those in DMEM/10% FBS as illustrated in Figure 3.2. DMEM/10%FBS cultured spheroids developed into larger, apparently looser bound colonies and were often disrupted by what appeared to be a mucilaginous secretion (data are not included).

DMEM/10% FBS cultivated spheroids appeared, overall, larger than those generated in Ham's F12/10% (Figure 3.2) , however both media supported growth of spheroid colonies of equivalent cell numbers and viabilities as measured by automated cell counting (Figure 3.3A) but there was a higher degree of variability in the numbers of cells derived from DMEM/10%FBS cultured spheroids compared to those grown in F12/10% FBS is indicated by the wide error bars (Figure 3.3A). The significantly larger cells in DMEM 10% FBS spheroids (Figure 3.3C) and the apparently looser cellular associations might explain their larger appearance In comparison with standard 2D cultures, growth as spheroids reduced the number of population doublings regardless of which medium was used (Figure 3.3D).

Based on the morphological appearance of the spheroids and the cell metrics, cells cultivated in Ham's F12/10% FBS seemed to generate spheroids of more consistency and less variability than those grown in DMEM/10% FBS.

To determine what genes might be being differentially regulated between conventional 2D log phase cultured A549 cells and cells grown using the 3D spheroid methodology, cultures grown in Ham's F12/10% FBS medium were progressed to RNA microarray analysis.

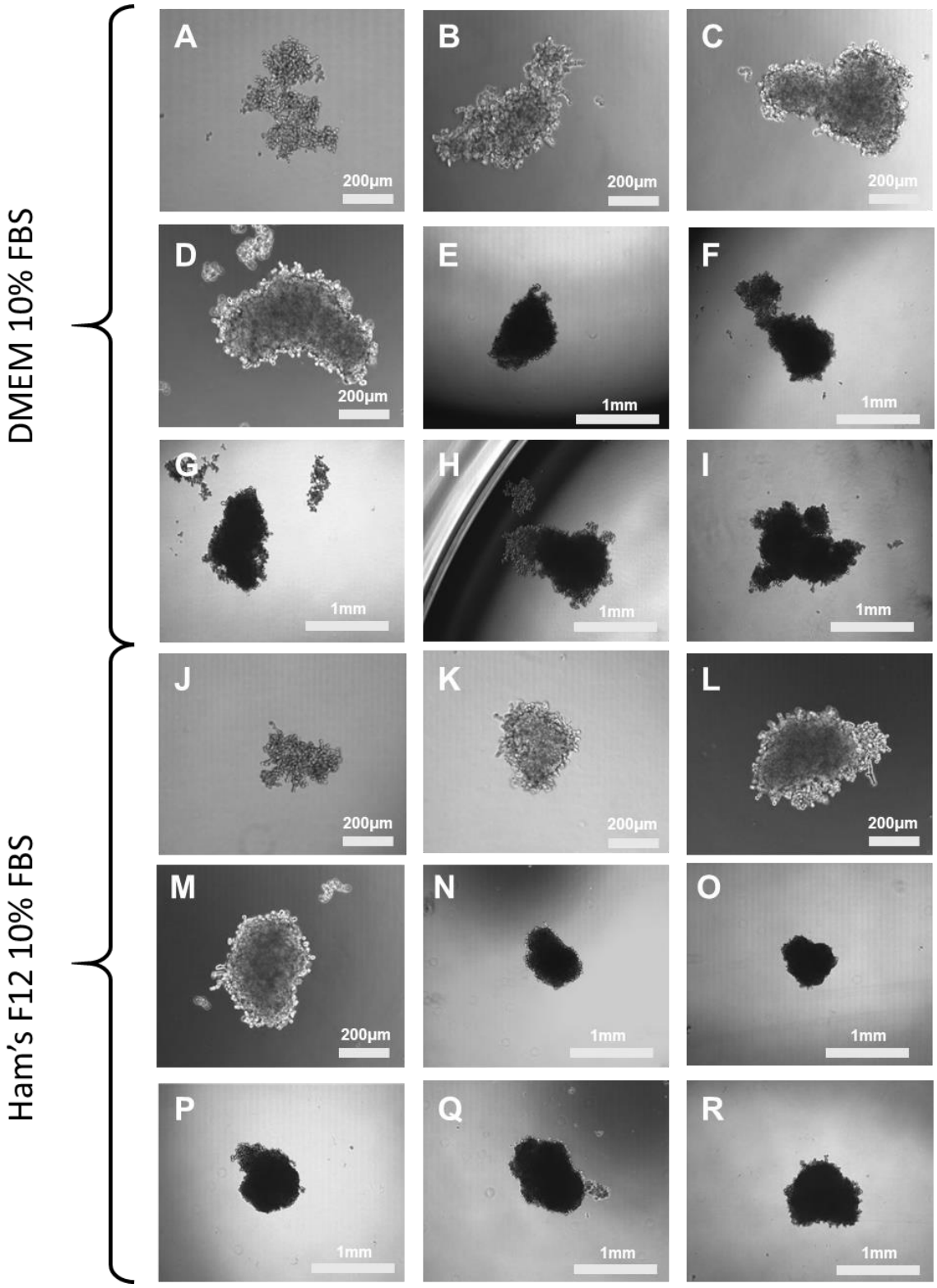

Figure 3.1. A549 spheroids in different medium formulations over a 25-day time-course.

A549 spheroids were generated in either DMEM/10%FBS (A to I) or Ham's F12/10% FBS (J to R) in ULA plates and maintained for 25 days with regular medium exchange. Phase contrast images were recorded throughout the time-course. 1 day (A and J), 3 days (B and K), 5 days (C and L), 8 days (D and M), 12 days (E and N), 14 days (F and O), 18 days (G and P),19 days (H and Q) and 25 days (I and R). The figure shows representative images from two independent experiments.

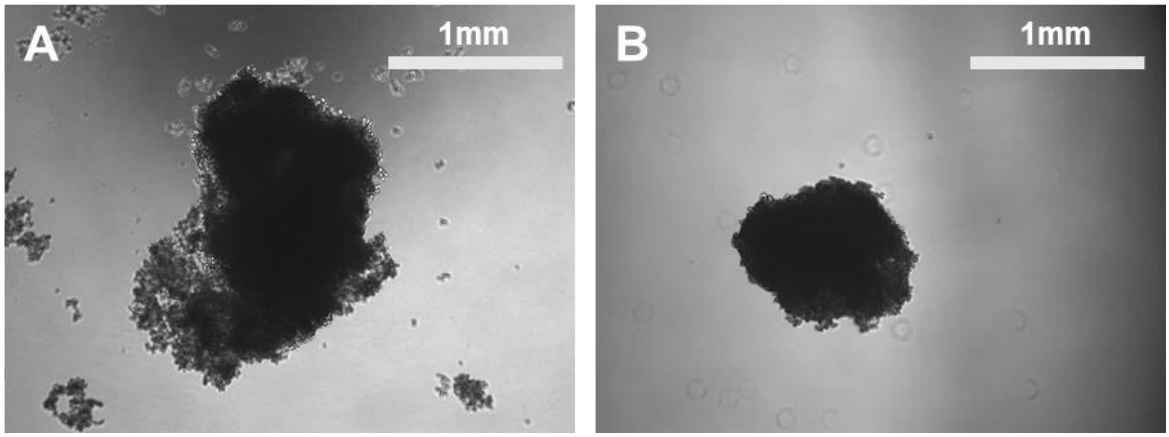

Figure 3.2. Spheroids in different medium formulations at day 25 of culture.
A549 cells were generated in either DMEM/10%FBS or Ham'sF12/10% in 24 ULA plates and maintained for 25 days with regular medium exchange. Phase contrast image images of spheroids generated DMEM/10% FBS (A) and Ham's F12/10% FBS (B). The figure shows representative images from two independent experiments.

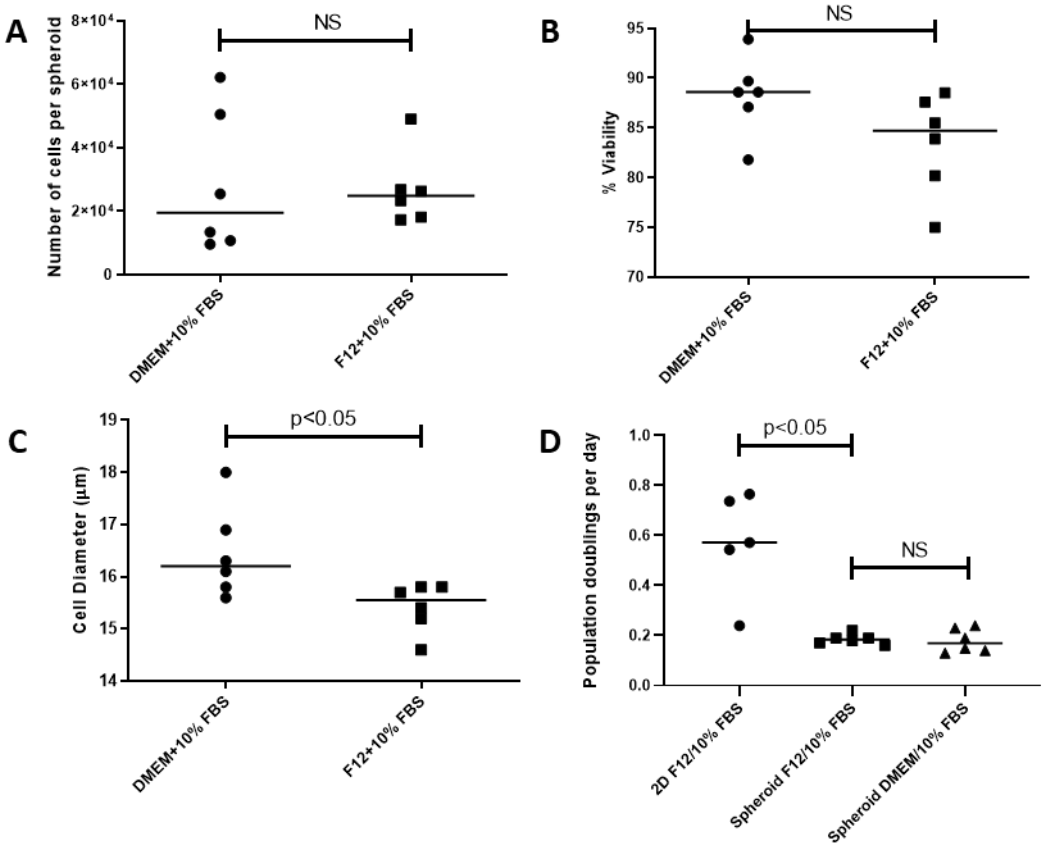

Figure 3.3. Metrics of cells from 25-day old A549 spheroids generated in different culture media.

A549 spheroids were cultivated in DMEM/10% FBS and Ham's F12/10% FBS. Spheroids were individually harvested, digested with 0.05% trypsin/0.02%EDTA PBS washed and analysed for total cell numbers (A), percentage viability (B) and average cell diameter (C) using the Chemometec Nucleocounter® 3000. A to C represents six technical replicates from a single experiment. Graph D shows the calculated number of population doublings of A549 cells per day in 2D log phase (five technical replicates of 2D cultures and six technical replicates of spheroid culture from a single experiment). Statistics = Mann Whitney non-parametric test.

3.3.2 RNA Microarray Analysis.

3D spheroid and 2D log phase A549 cultures were grown in Ham's F12/10% FBS medium, RNA was extracted from the log phase cells and from the spheroids at days 7, 11, 18, and 25. The RNA was used as a template to generate fluorescently labelled complementary RNA (cRNA) for analysis using Agilent® Genespring™ analysis software package with Benjamini-Hochberg false discovery rate (BH FDR) corrected ANOVA analysis. Analysis compared the gene expression of the spheroid time-course to log phase 2D cultured A549 cells. Cluster analysis showed significant regulation genes over the 25-day time course as shown in the clustered heat map (Figure 3.4; upregulated genes are in green and those downregulated in red).

To further explore patterns in changes of gene expression, fold changes were determined using Genespring™ and gene ontology (GO) analysis was carried out on ranked lists of significantly up- and down-regulated genes that had a fold-change of two or more. GO analysis was enabled in 'GOrilla': a tool for discovery and visualization of enriched GO terms in ranked gene lists[327]. The detailed results of the gene ontology analysis that had a level of significance less than p=0.0001 are graphically presented in Figure 3.5, 3.5, 3.6, 3.8, 3.9, 3.11, 3.13 and 3.15. To clarify the gene ontology, the outputs of the GOrilla analyses were run through the 'REVIGO' (REduce+VIsualize Gene Ontology tool[328] that allows focus on data with the lowest p values. The resulting simplified gene ontology overview is presented in Figure 3.7, 3.10, 3.12, 3.14, and 3.16.

Compared to 2D log phase A549 cultures the 25-day spheroids displayed a pattern of gene up-regulation that suggested differentiation toward a secretory phenotype involved with host-defence. Upregulated genes include those associated with detection of stimuli, response to bacteria, immune system process, antibacterial innate immune response., water transport and regulated exocytosis (Figure 3.5, Figure 3.6 and Figure 3.7). The ontology of genes associated with "cellular component" also indicated the adoption of secretory cellular differentiation with gene associations, alluding to the development of intracellular structures with organelle membrane enclosed lumens and secretion of extracellular vesicles (Figure 3.9 and Figure 3.10).

Genes involved with adhesion to cells in other tissues (heterotypic cell to cell adhesion) were also up regulated as were genes that have a negative impact on apoptotic signalling Figure 3.6 and Figure 3.7 .

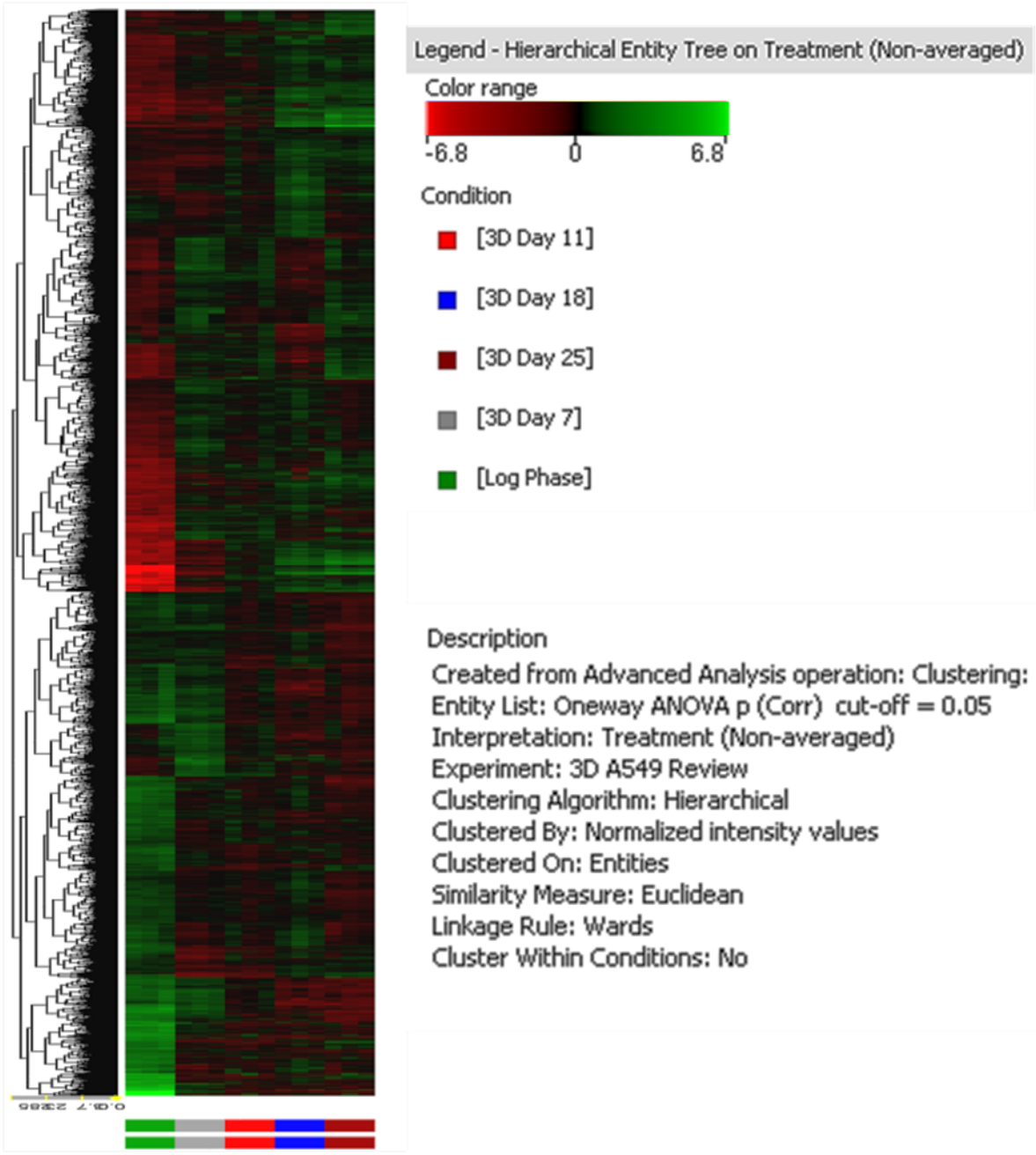

Figure 3.4. RNA Microarray heat map of the ANOVA analysis of A549 cells comparing a 25-day time-course of changes in spheroid gene expression compared to 2D log phase cultures.

RNA was extracted from 2D log phase cultures from tissue culture flasks and over a 25-day time-course of spheroids grown in Ham's F12/10% FBS with medium exchange every two to three days. RNA was extracted and analysed using Agilent® Human Single Colour 39494 micro-array slides then Benjamini-Hochberg false discovery rate (BH FDR) corrected ANOVA analysis in Genespring™ prior to Hierarchical clustering (Euclidian similarity measure, clustered using Ward's linkage rule). Three technical replicates, single experiment.

Retinoids are important factors in proliferation and differentiation in epithelia and have been shown as having a key role in ATII differentiation[350]. Interestingly the principal "molecular

function" upregulated in the 25-day spheroids appeared to be upregulation if retinol dehydrogenase activity which may indicate evidence of cellular differentiation in the spheroids.

(1) Gene Ontology

Focussing on the most significant regulation of genes from ontological analysis of the RNA microarray revealed that cells in the 3D spheroids were significantly expressing genes related to humoral, anti-bacterial response indicating cellular differentiation towards a host defence phenotype. Processes involved with sensory perception and interaction with the extracellular environment and the detection of chemical stimuli and in terms of function increased fluid transport and secretion by regulated exocytosis were also regulated (Figure 3.5). These findings were further reinforced by highly significant regulation of genes associated with interactions with extracellular interactions and the development of organelle, vesicle and secretory granule lumens (Figure 3.9).

Evidence of increased extracellular interaction was seen by the significant regulation of genes involved with the secretion and organisation of extracellular matrix, in particular, collagen fibril organisation (Figure 3.11) and secretion of extracellular matrix components with high tensile strength (Figure 3.13 and 3.15).

Regulation of processes involved with cell division (cell cycle process, chromosome segregation, mitosis, mitotic spindle organisation, nuclear division and metaphase to anaphase transition) together with the negative regulation of apoptosis and upregulation of developmental pathways and processes point towards development of cancerous properties within the spheroids. There was an increased expression of genes involved with heterotypic cell to cell adhesion but negative regulation of apoptotic signalling, indicating cells were becoming more resistant to apoptotic signalling cues, further indicating possible adoption of a more cancerous phenotype (Figure 3.6).

Upregulation of retinol dehydrogenase activity (Figure 3.8) indicates the possibility of adoption of a phenotype responsive to differentiation factors such as retinol.

Simplified diagrams of the ontology data are also included (Figure 3.7, 3.10, 3.12, 3.14 and 3.16).

Thus, the gene ontology analysis paints a picture of a confused cell population within the spheroids that on the one hand appears to be adopting a differentiated, secretory host defence phenotype but on the other, there appears to be increasing regulation of genes

associated with organised cell division, developmental processes and avoidance of apoptosis; the hallmarks of cancer[351 352].

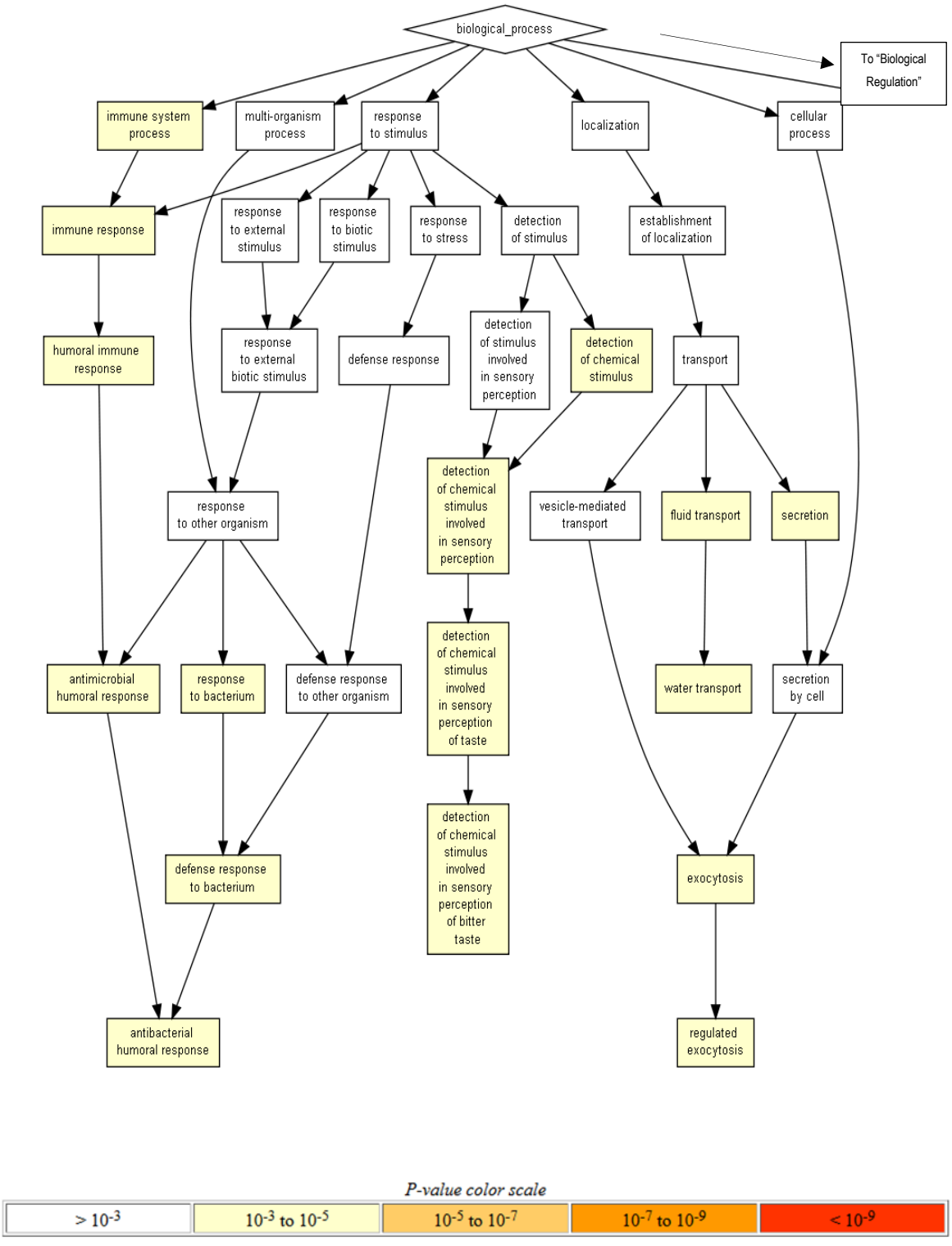

Figure 3.5. Gene ontology analysis of upregulated genes associated with "biological process" from 25-day 3D spheroids compared to log phase 2D A549 cultures (Part 1). Fold change (cut-off >2) comparing A549 spheroids and 2D log phase cultures was detemined using Genespring™ on clustered genes generated by the ANOVA analysis. The list of upregulated genes was further analysed for gene ontology using the 'GOrilla' online analysis tool. P cut off <0.0001.

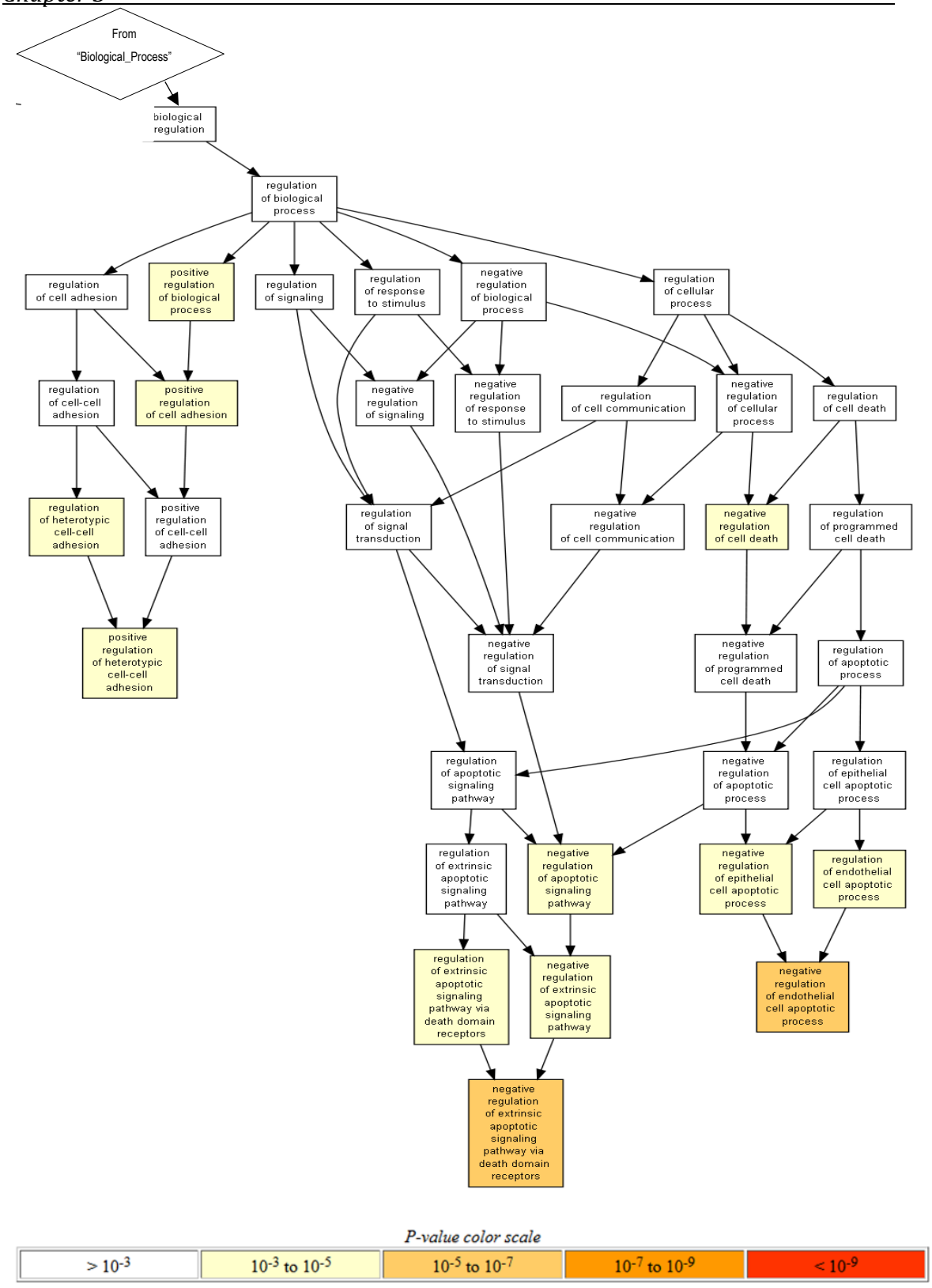

Figure 3.6. Gene ontology analysis of upregulated genes associated with "biological process" from 25-day 3D spheroids compared to log phase 2D A549 cultures (Part 2).
Fold change (cut-off >2) comparing A549 spheroids and 2D log phase cultures was detemined using Genespring™ on clustered genes generated by the ANOVA analysis. The list of upregulated genes was further analysed for gene ontology using the 'GOrilla' online analysis tool. P cut off <0.0001.

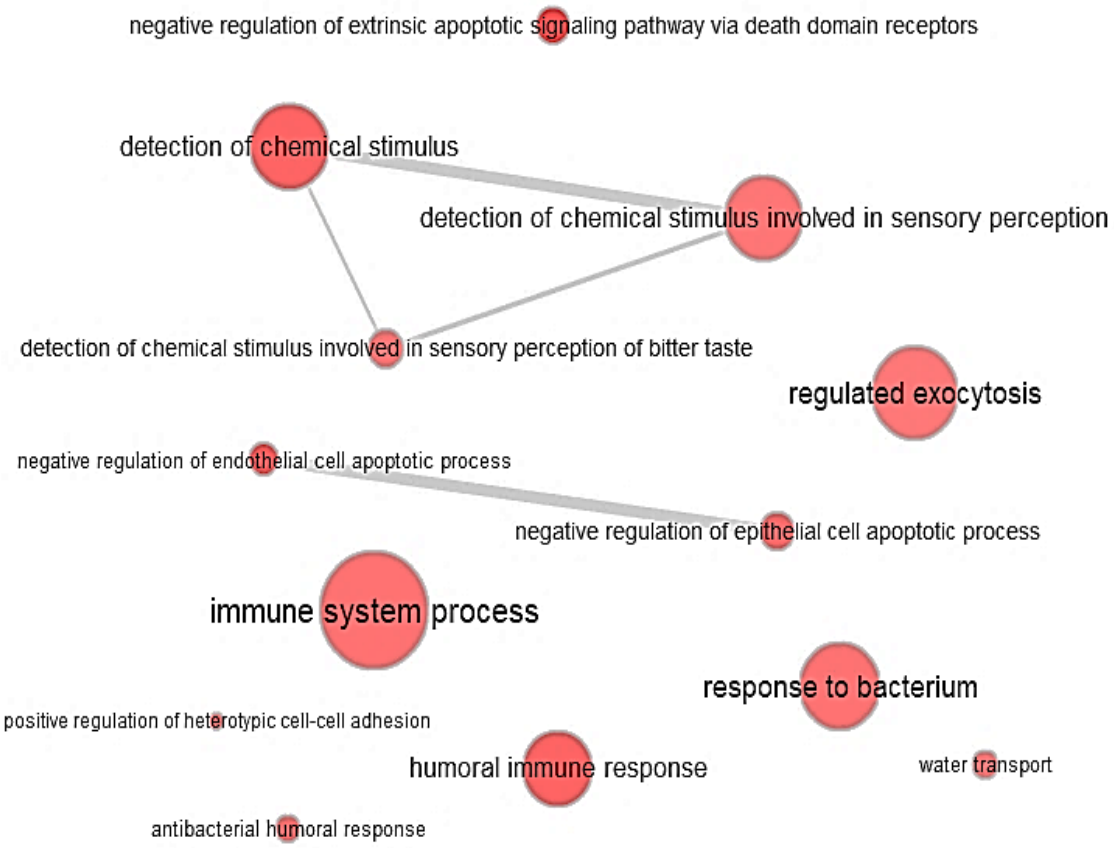

Figure 3.7. Simplified gene ontology analysis of upregulated genes associated with "biological process" from 25-day 3D spheroids compared to log phase 2D A549.
Fold change (cut-off >2) comparing A549 spheroids and 2D log phase cultures was detemined using Genespring™ on clustered genes generated by the ANOVA analysis. The list of upregulated genes was further analysed for gene ontology using the 'GOrilla' online analysis tool. P cut off <0.0001. The GOrilla analysis output was subsequently simplified and streamlined using the 'REVIGO' visualisation tool[328].

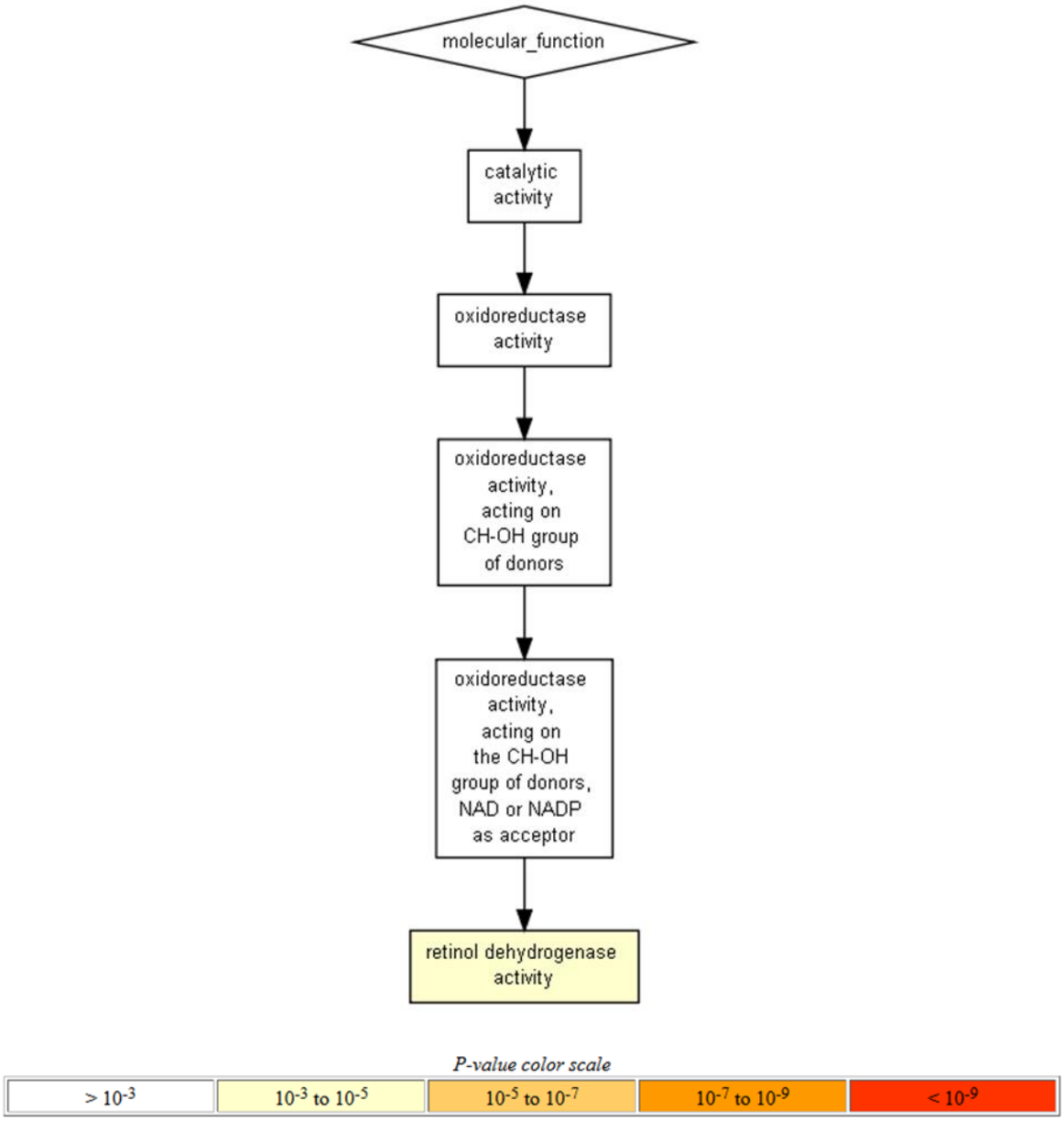

Figure 3.8. Gene ontology analysis of upregulated genes associated with "molecular function" from 25-day 3D spheroids compared to log phase 2D A549.
Fold change (cut-off >2) comparing A549 spheroids and 2D log phase cultures was detemined using Genespring™ on clustered genes generated by the ANOVA analysis. The list of upregulated genes was further analysed for gene ontology using the 'GOrilla' online analysis tool. P cut off <0.0001.

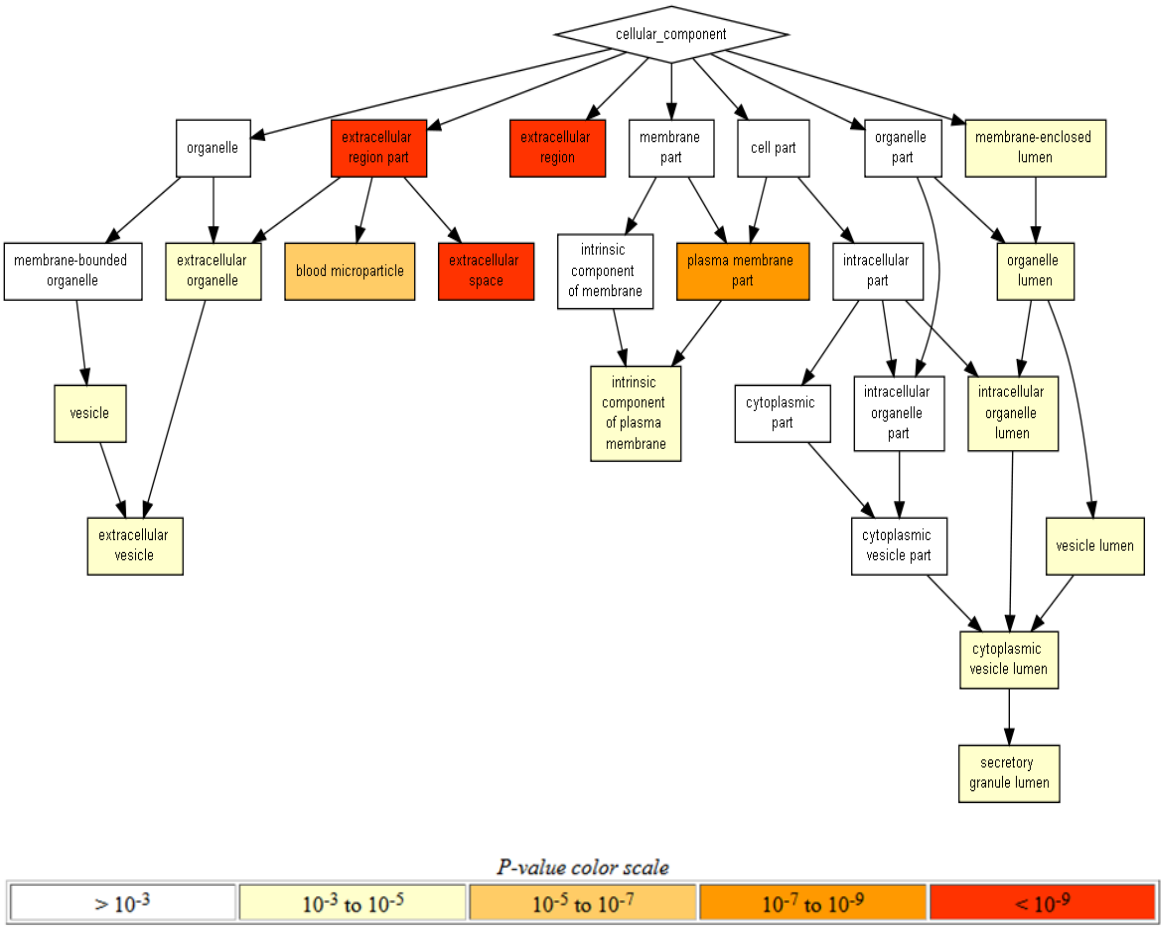

Figure 3.9. Gene ontology analysis of upregulated genes associated with "cellular component" from 25-day 3D spheroids compared to log phase 2D A549.

Fold change (cut-off >2) comparing A549 spheroids and 2D log phase cultures was detemined using Genespring™ on clustered genes generated by the ANOVA analysis. The list of upregulated genes was further analysed for gene ontology using the 'GOrilla' online analysis tool. P cut off <0.0001.

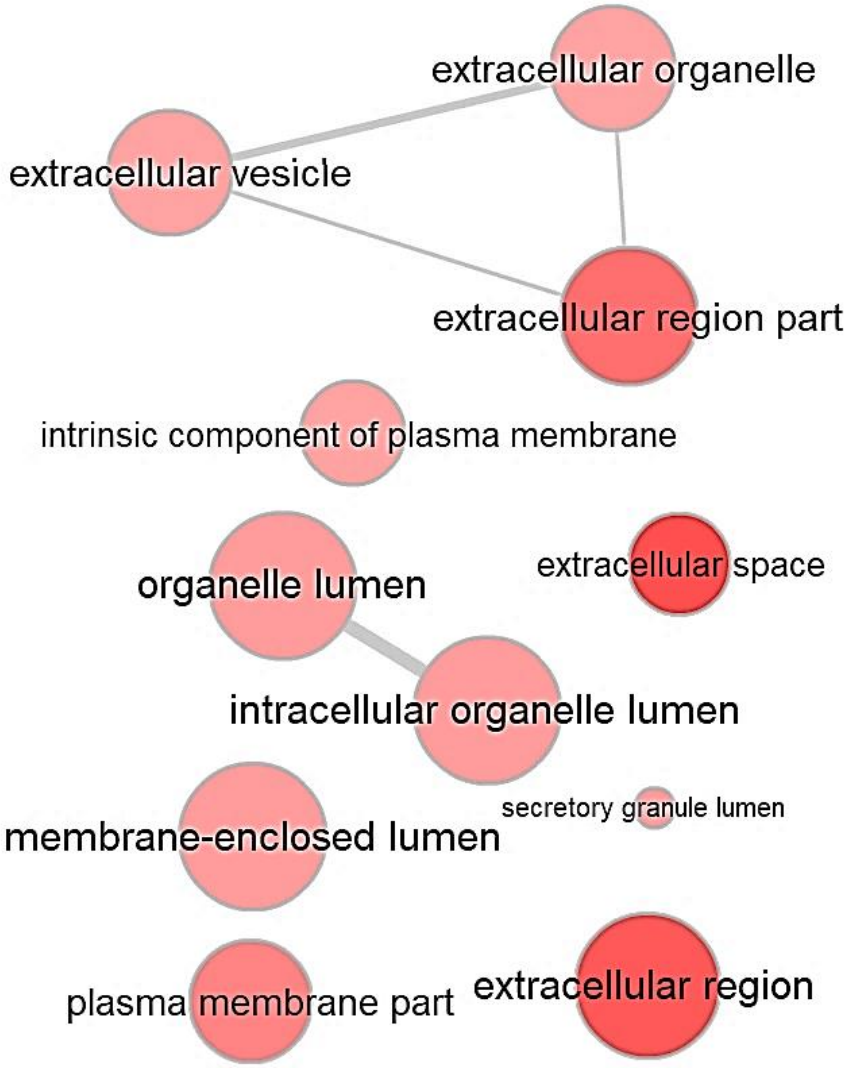

Figure 3.10. Simplified gene ontology analysis of upregulated genes associated with "cellular component" from 25-day 3D spheroids compared to log phase 2D A549.

Fold change (cut-off >2) comparing A549 spheroids and 2D log phase cultures was detemined using Genespring™ on clustered genes generated by the ANOVA analysis. The list of upregulated genes was further analysed for gene ontology using the 'GOrilla' online analysis tool. P cut off <0.0001. The GOrilla analysis output was subsequently simplified and streamlined using the 'REVIGO' visualisation tool[328].

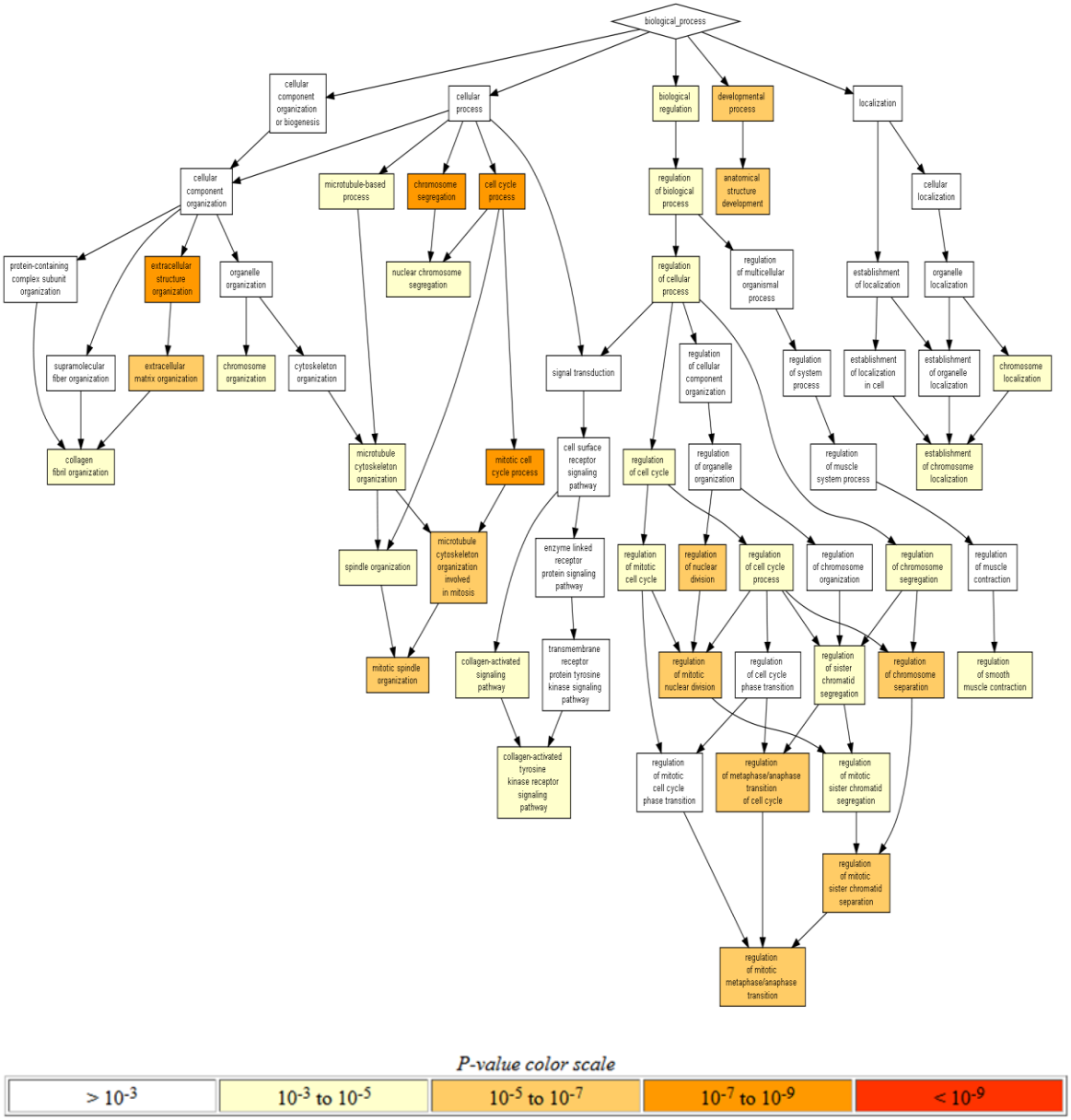

Figure 3.11. Gene ontology analysis of down-regulated genes associated with "biological process" from 25-day 3D spheroids compared to log phase 2D A549.

Fold change (cut-off >2) comparing A549 spheroids and 2D log phase cultures was detemined using Genespring™ on clustered genes generated by the ANOVA analysis. The list of upregulated genes was further analysed for gene ontology using the 'GOrilla' online analysis tool. P cut off <0.0001.

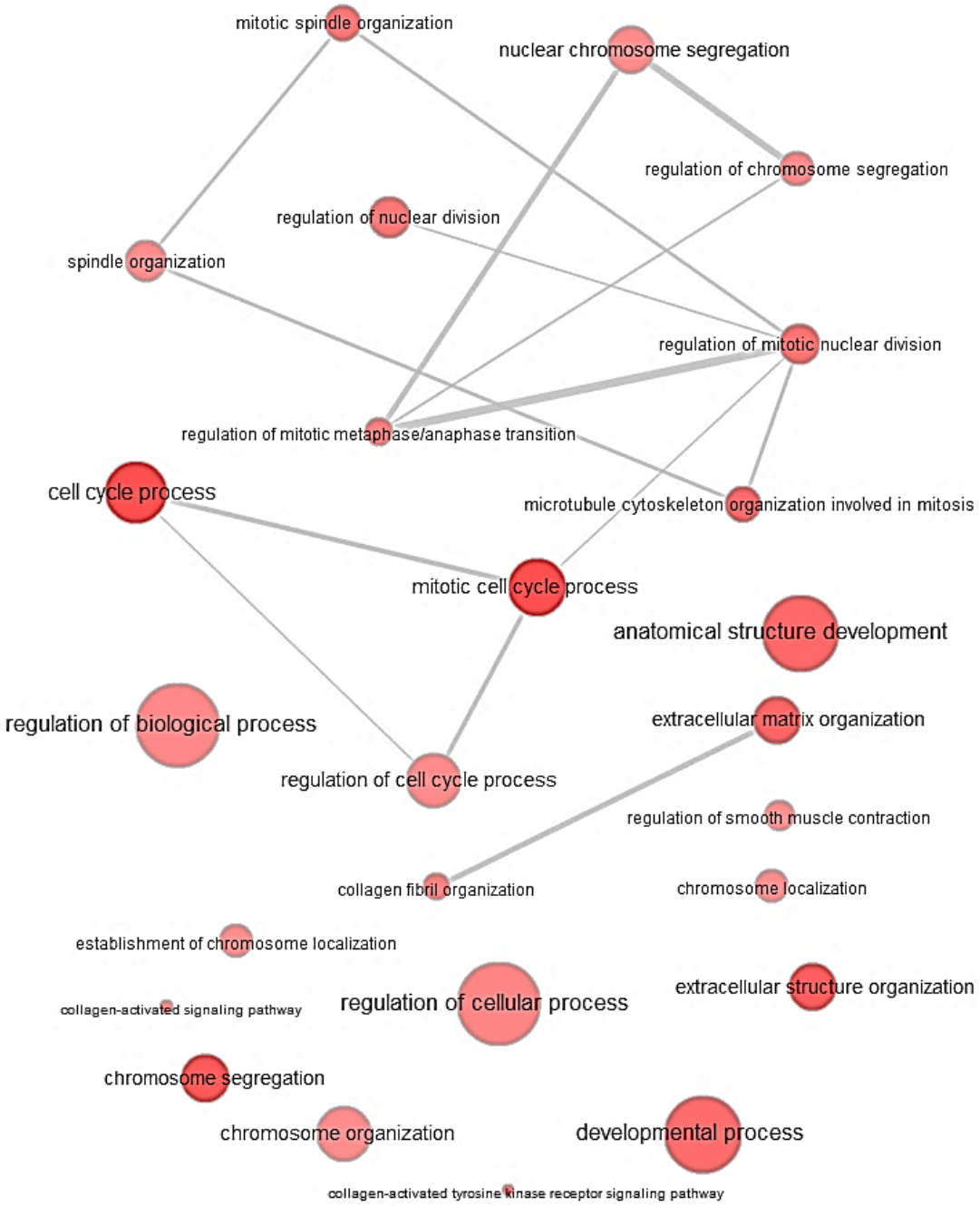

Figure 3.12. Simplified gene ontology analysis of down-regulated genes associated with "biological process" from 25-day 3D spheroids compared to log phase 2D A549.
Fold change (cut-off >2) comparing A549 spheroids and 2D log phase cultures was detemined using Genespring™ on clustered genes generated by the ANOVA analysis. The list of upregulated genes was further analysed for gene ontology using the 'GOrilla' online analysis tool. P cut off <0.0001. The GOrilla analysis output was subsequently simplified and streamlined using the 'REVIGO' visualisation tool[328].

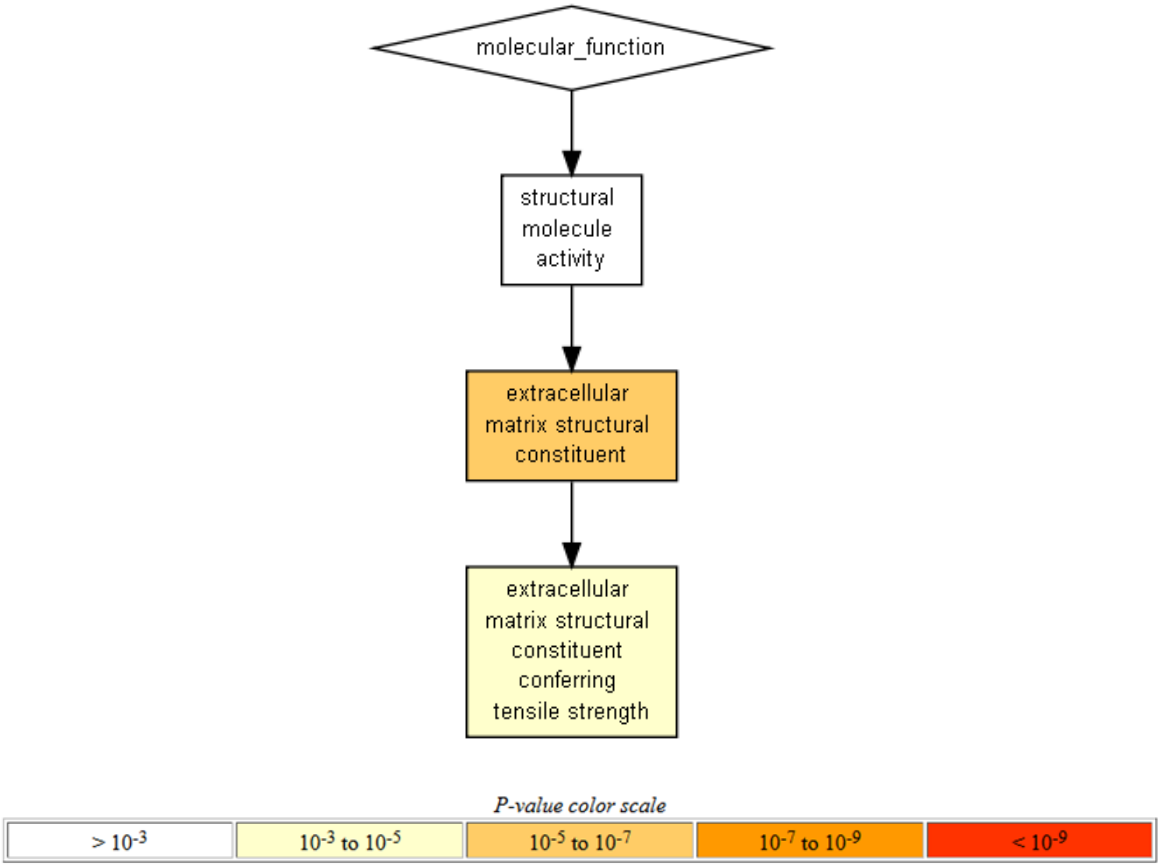

Figure 3.13. Gene ontology analysis of down-regulated genes associated with "molecular function" from 25-day 3D spheroids compared to log phase 2D A549.
The "fold change" (cut off of a fold change of 2) between A549 spheroids and 2D log phase cultures was calculated using Genespring™ on the clustered genes generated by the ANOVA analysis presented previously. The list of upregulated genes was further analysed for gene ontology using the 'GOrilla' online analysis tool. P cut off <0.0001.

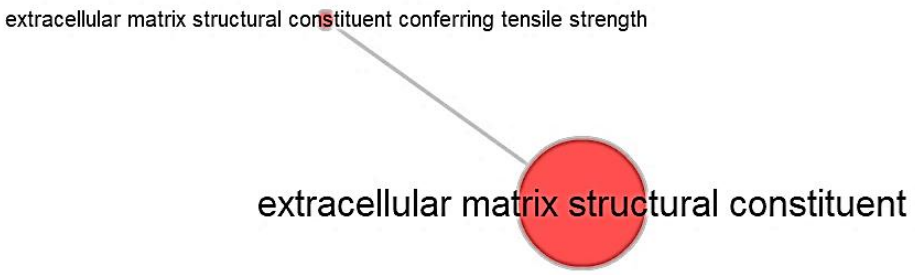

Figure 3.14. Simplified gene ontology analysis of down-regulated genes associated with "molecular function" from 25-day 3D spheroids compared to log phase 2D A549.
Fold change (cut-off >2) comparing A549 spheroids and 2D log phase cultures was detemined using Genespring™ on clustered genes generated by the ANOVA analysis. The list of upregulated genes was further analysed for gene ontology using the 'GOrilla' online analysis tool. P cut off <0.0001. The GOrilla analysis output was subsequently simplified and streamlined using the 'REVIGO' visualisation tool[328]

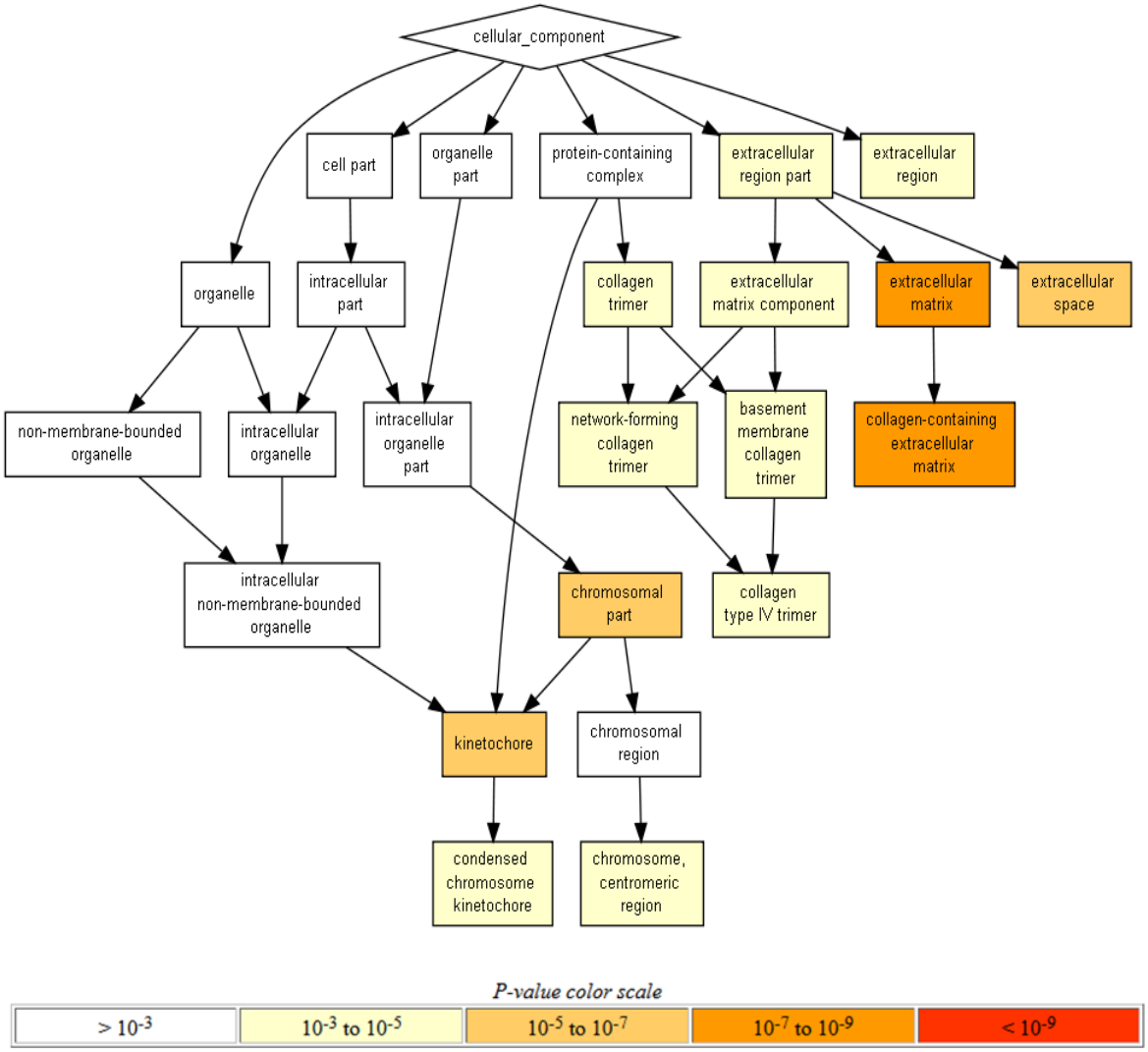

Figure 3.15. Gene ontology analysis of down-regulated genes associated with "cellular component" from 25-day 3D spheroids compared to log phase 2D A549.
Fold change (cut-off >2) comparing A549 spheroids and 2D log phase cultures was detemined using Genespring™ on clustered genes generated by the ANOVA analysis. The list of upregulated genes was further analysed for gene ontology using the 'GOrilla' online analysis tool. P cut off <0.0001.

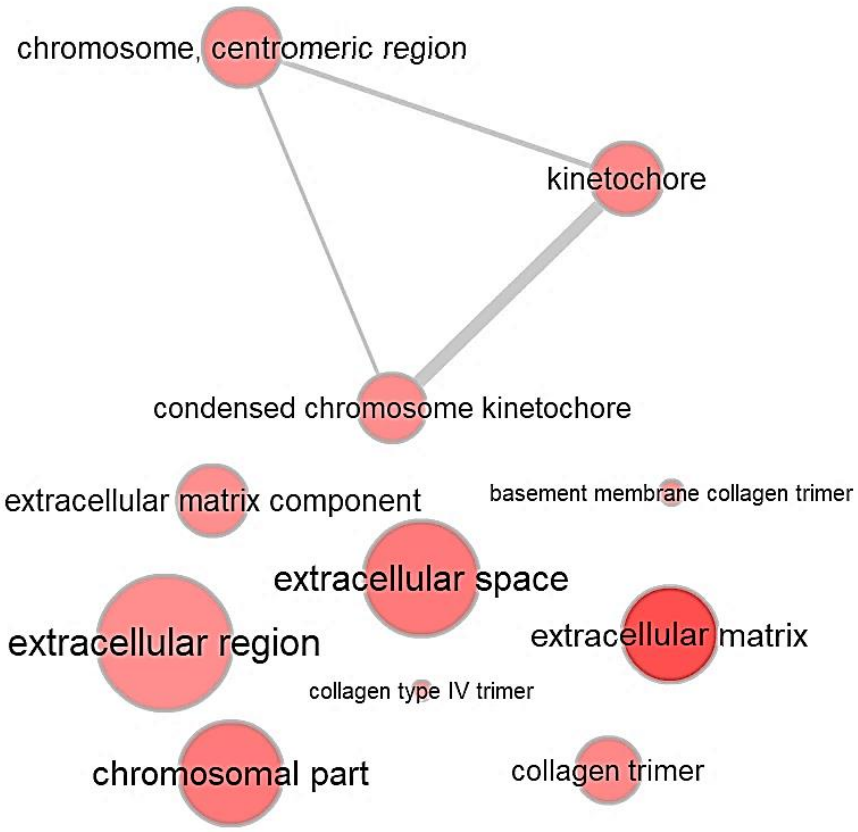

Figure 3.16. Simplified gene ontology analysis of down-regulated genes associated with "cellular component" from 25-day 3D spheroids compared to log phase 2D A549.

Fold change (cut-off >2) comparing A549 spheroids and 2D log phase cultures was detemined using Genespring™ on clustered genes generated by the ANOVA analysis. The list of upregulated genes was further analysed for gene ontology using the 'GOrilla' online analysis tool. P cut off <0.0001. The GOrilla analysis output was further simplified and streamlined using the 'REVIGO' visualisation tool[328].

(2) Regulation of Specific Genes Involved with Differentiation and Host Defence

To further explore the possibility that the cells in the spheroid cultures had adopted a secretory, host cell defence differentiated phenotype the clusters of up and down regulated genes were investigated to determine their biological relevance. Figure 3.17 shows the upregulation of the genes displaying the some of the highest fold changes from Genespring™ analysis. These genes encoded the cellular adhesion molecules *CECAM 6* and *7*, the Cathelicidin antimicrobial peptide (*CAMP*) and *ERBB3*, a member of the epidermal growth factor receptor tyrosine kinases which plays a role in the maintenance and repair of epithelial tissues[353].

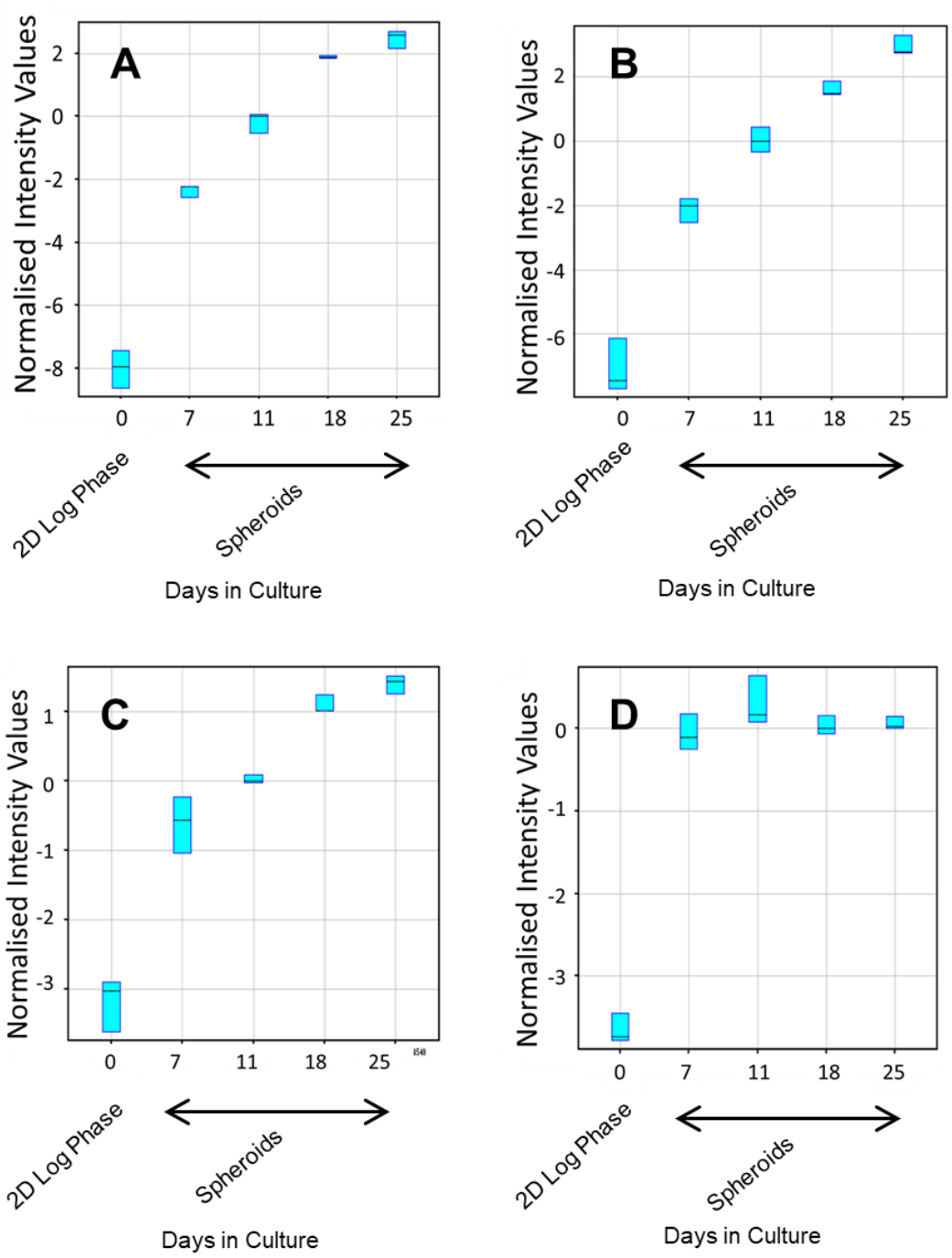

Figure 3.17 . Regulation of the expression of genes for tumour marker cellular adhesion molecules *CEACAM6* and *7*, the antimicrobial peptide *CAMP* and *ERBB3* in 3D spheroids.

Using Genespring™ the variation in gene expression using the normalised intensity values from the RNA microarray analysis over the 25-day time course was plotted. *CEACAM6* (A), *CEACAM7* (B), cathelicidin (*CAMP*) (C) and *ERBB3* (D). "Day 0" represents log phase, Three replicates from a single experiment. The FDR adjusted mean intensity value from all genes was used as the normalisation baseline.

Mucins play a major role in host defence in the lung[354], to determine the direction of differentiation the cells might be undergoing, the expression of the gel forming mucins *MUC5AC* and *MUC5B* was investigated together with a known regulator of mucin production, SAM-pointed domain–containing Ets-like factor (*SPDEF*), which controls goblet cell differentiation[355]. Figure 3.18 shows that these genes were all regulated at mRNA level throughout the time-course.

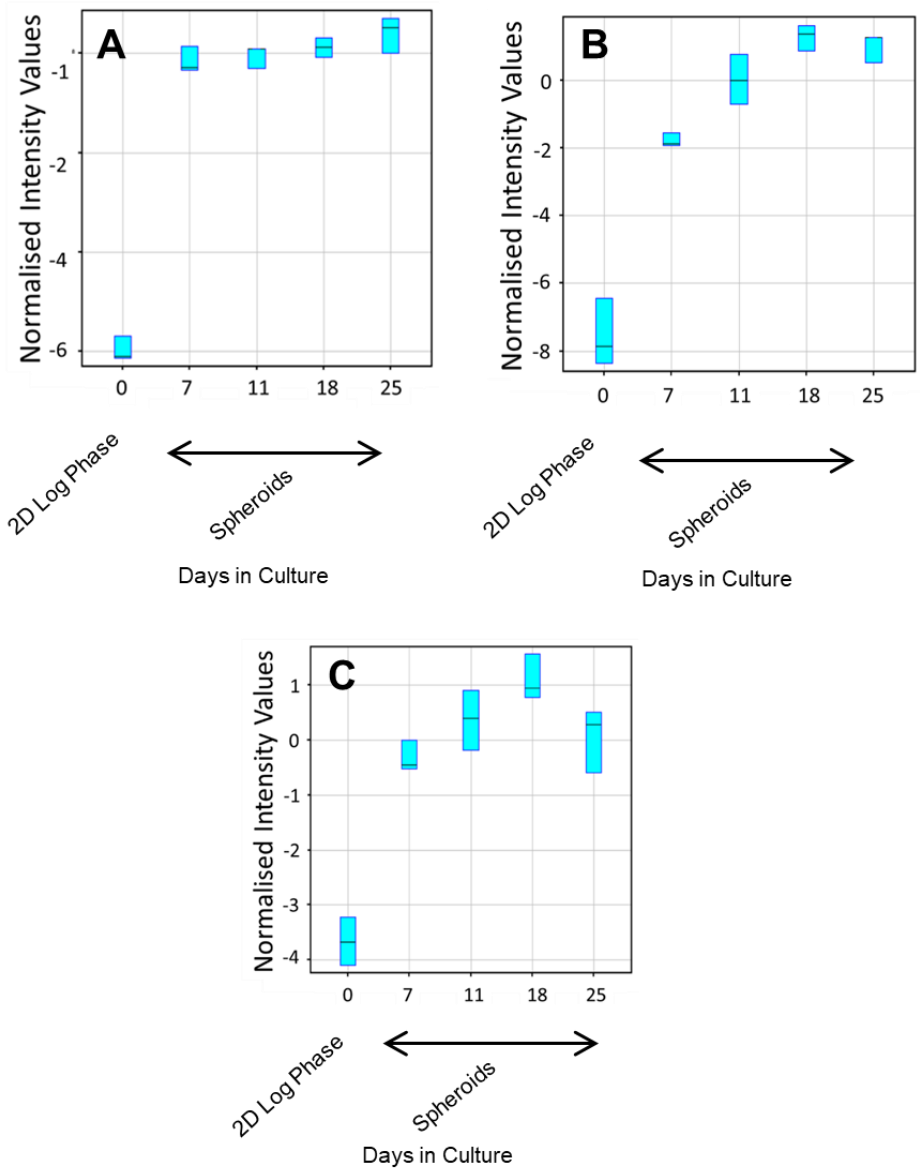

Figure 3.18. Regulation of Mucin genes MUC5AC and MUC5B and their regulator SPDEF.
Using Genespring™ the variation in gene expression using the normalised intensity values from the RNA microarray analysis over the 25-day time course was plotted. MUC5AC (A), MUC5B (B), SPDEF (C) "Day 0" represents log phase, Three replicates from a single experiment. The FDR adjusted mean intensity value from all genes was used as the normalisation baseline.

3.3.3 QRT PCR of MUC5AC Expression

QRT PCR using probe based primers and relative gene expression analysis (delta delta ct method)[330] was performed initially to confirm the upregulation of gene expression of the gel forming mucin MUC5AC using an independent measure of gene expression (Figure 3.19).

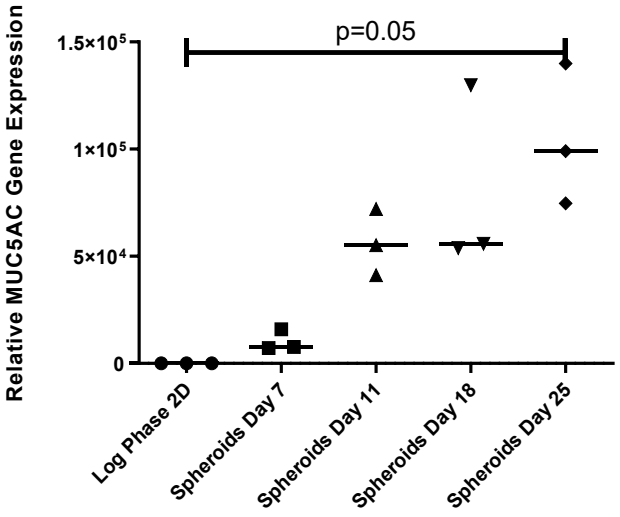

Figure 3.19. MUC5AC gene expression in A549 spheroids.
RNA from A549 spheroids at days 7, 11, 18 and 25. was prepared for reverse transcription to cDNA, QRT PCR analysis of human MUC5AC. Expression was normalised to the geometric mean of Ct values obtained using TaqMan™ primers and probes specific for *TOP1* and *ATP5B* as reference (or housekeeping) genes (selected from the results of prior 'Genorm' analysis[330] using unlabelled primers and SYBR Green). Expression is relative to Log Phase 2D A549 cells. Three technical replicates (wells) from a single experiment. Statistical testing (Mann-Whitney non-parametric test).

Note: QRT-PCR MUC5AC gene expression data in Figure 3.19 were generated using probe-based primers for MUC5AC with TOP1 and ATP5B as reference genes. TOP1 and ATP5B were selected beforehand using Genorm analysis[330] with twelve potential reference gene primer pairs and Sybr Green based QRT PCR. cDNA from log phase A549 and samples time-course of spheroid provided samples for the Genorm analysis (see Appendix E).

These data indicate that the fold change of mRNA expression of the MUC5AC gene steadily increased over the 25-day time-course and was upregulated over 100,000 times above the 2D log phase cultures by day 25, supporting the observation of the RNA microarray analysis.

3.3.4 Analysis of Spheroids using Histochemistry and Electron Microscopy

To further characterise the spheroids, they were fixed and processed for histological analysis. Figure 3.20 shows that by day 13 the spheroids had formed into what appeared to be solid cellular regular masses with clearly defined margins indicating some degree of cellular, tissue like organisation[356]. By day 18, however, the organisation of the spheroids was less regular with rather more irregular cellular organisation with less sharply defined margins indicating loss of organisation and possible adoption of tumour-like growth[356] (Figure 3.21). To further explore the nature of cellular differentiation in the spheroids and to confirm findings of previous gene expression analyses, immunohistological analyses of the spheroids was undertaken.

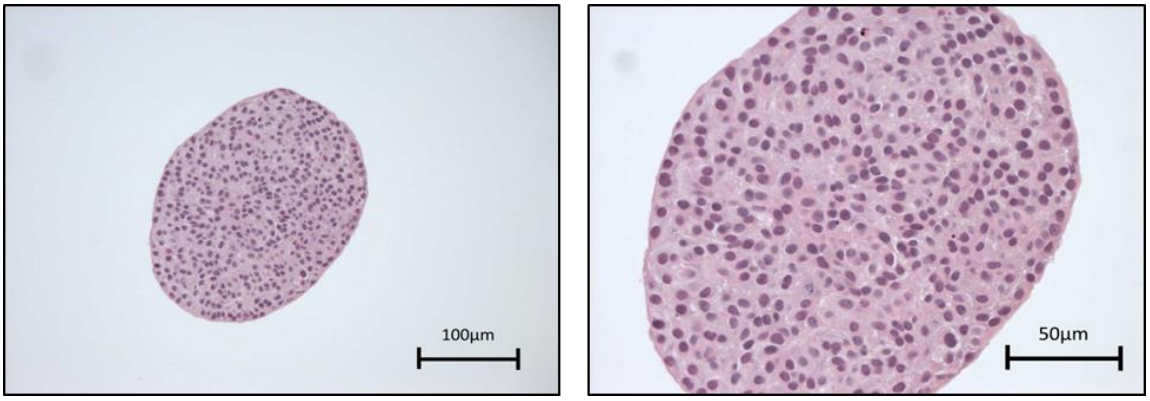

Figure 3.20. Cross section of an A549 3D spheroid cultivated in Ham's F12/10% FBS for 13 days.
Spheroids were 4% paraformaldehyde fixed, embedded in paraffin, sectioned and stained with Haematoxylin and Eosin. Images are representative of a single experiment.

At day 18 the cells in spheroid culture expressed cytokeratin, a marker of epithelia. A proportion of the spheroids at day 18 had developed lumens (Figure 3.21) which on the one hand was encouraging, however on the other the walls of these developing cysts were several cells thick and showed little evidence of epithelial organisation supporting the gene expression data that showed down regulation of developmental processes associated with anatomical structure morphogenesis, cellular organisation and extracellular matrix structure organization and gene ontology analysis indicated that markers of cellular proliferation were being down-regulated in the later spheroid cultures as compared to log phase cultures. These data were supported by the significant reduction in population doubling rates observed in spheroid cultures compared to 2D cultures (Figure 3.3D).

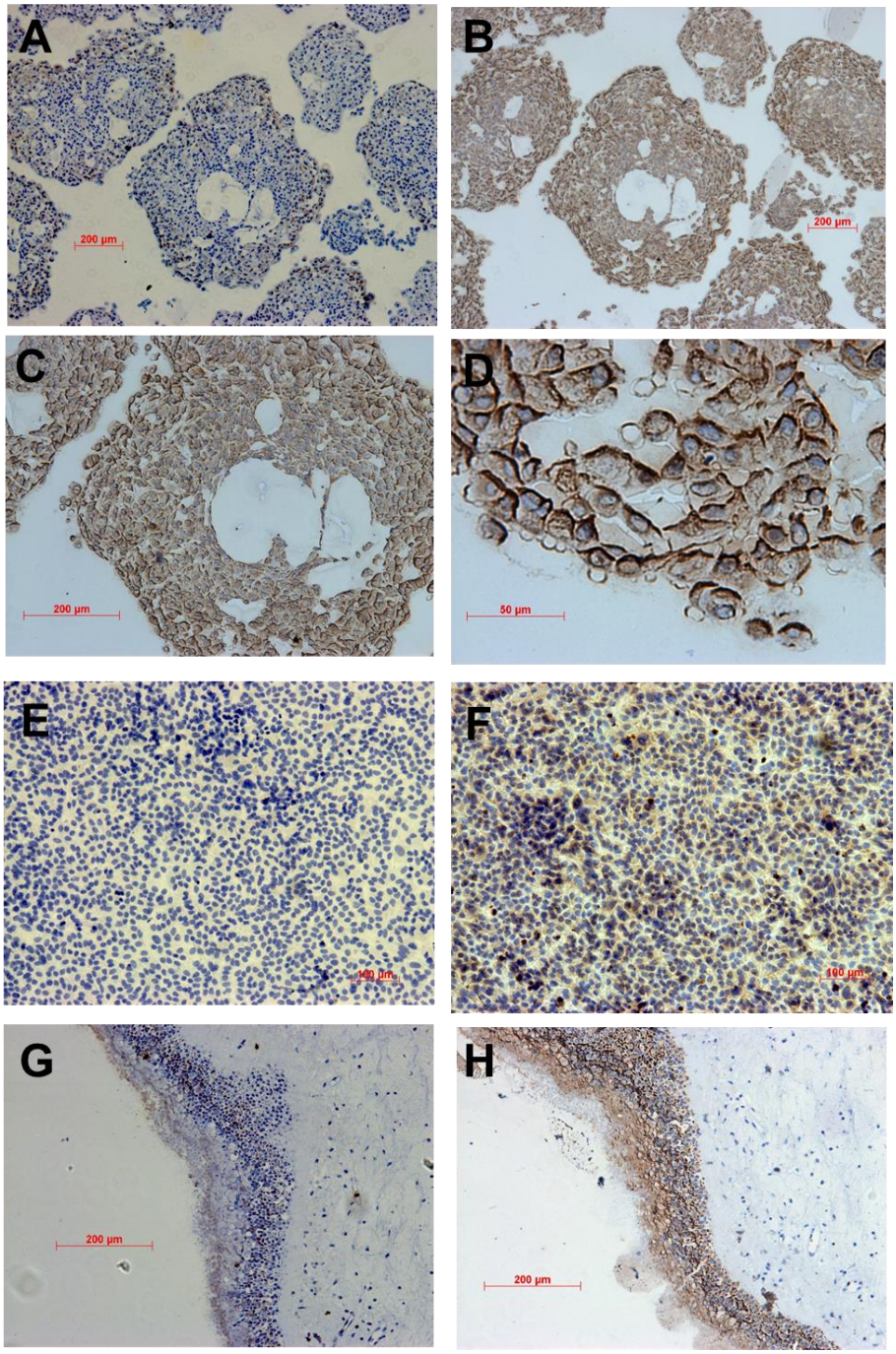

Figure 3.21. Cytokeratin expression and morphology in A549 spheroids.
A549 spheroids were maintained for 18 days before fixation and GMA embedding. Sections were then immunostained for the epithelial marker cytokeratin (CK) using mouse anti-human pan-cytokeratin primary antibody. A (Control), spheroids immune stained for Neutrophil Elastase (NE) to assess non-specific staining. B, C and D: Spheroids stained for CK with increasing magnification (D from the periphery of a spheroid). Control (Log phase 2D A549 monolayer (methanol fixed)) stained for NE with Haematoxylin counterstain (E) and for CK(F). Positive Control (human nasal polyp) stained for NE (G) and CK (H). Images are representative of a single experiment.

Further histochemical analysis of the spheroid cultures and log phase monolayers of A549 cells by PAS staining of mucins and specific immune-histochemical staining for the mucin MUC5AC supported the gene expression analyses by RNA microarray and QRT PCR. The pattern of mucin staining indicated that a large proportion of the cells in the 18 day spheroids were secreting mucins in a disorganised manner; both between the cells in the solid tissue like mass of the spheroids and into the lumens of the spheroids, whereas there was no evidence of mucin production or secretion in the log phase 2D cultured cells, again supportive of the microarray analysis data that indicated a down regulation of markers of cellular organisation in the 3D spheroid cultures (Figure 3.22).

Scanning Electron Microscopy (SEM) was carried out on day 13 and day 18 spheroid cultures to provide further characterisation data (Figure 3.23) EM supported the light microscopy data that the spheroids were forming into tissue like aggregates with the cells apparently more deeply integrated into the spheroids at day 13 as compared to day 18 where the cells were more rounded at the surface of the spheroid indicating less strong attachment to the cellular mass, in accordance with the GO data that showed downregulation of genes involved with extracellular matrix synthesis and cell to cell adhesion. Mucin granules are typically electron lucent, i.e. they appear as white voids on electron micrographs in transmission electron microscopy (TEM). Figure 3.24 A and B clearly show characteristic electron lucent mucin granules filling a large proportion of the cytoplasm of the cells from 21-day spheroid cultures whereas these mucin granules are noticeably absent from the cytoplasm of 2D cultured A549 cells. These data confirmed the adoption of a muco-secretory phenotype in the cells of the 3D spheroid cultures but not in the 2D cultures

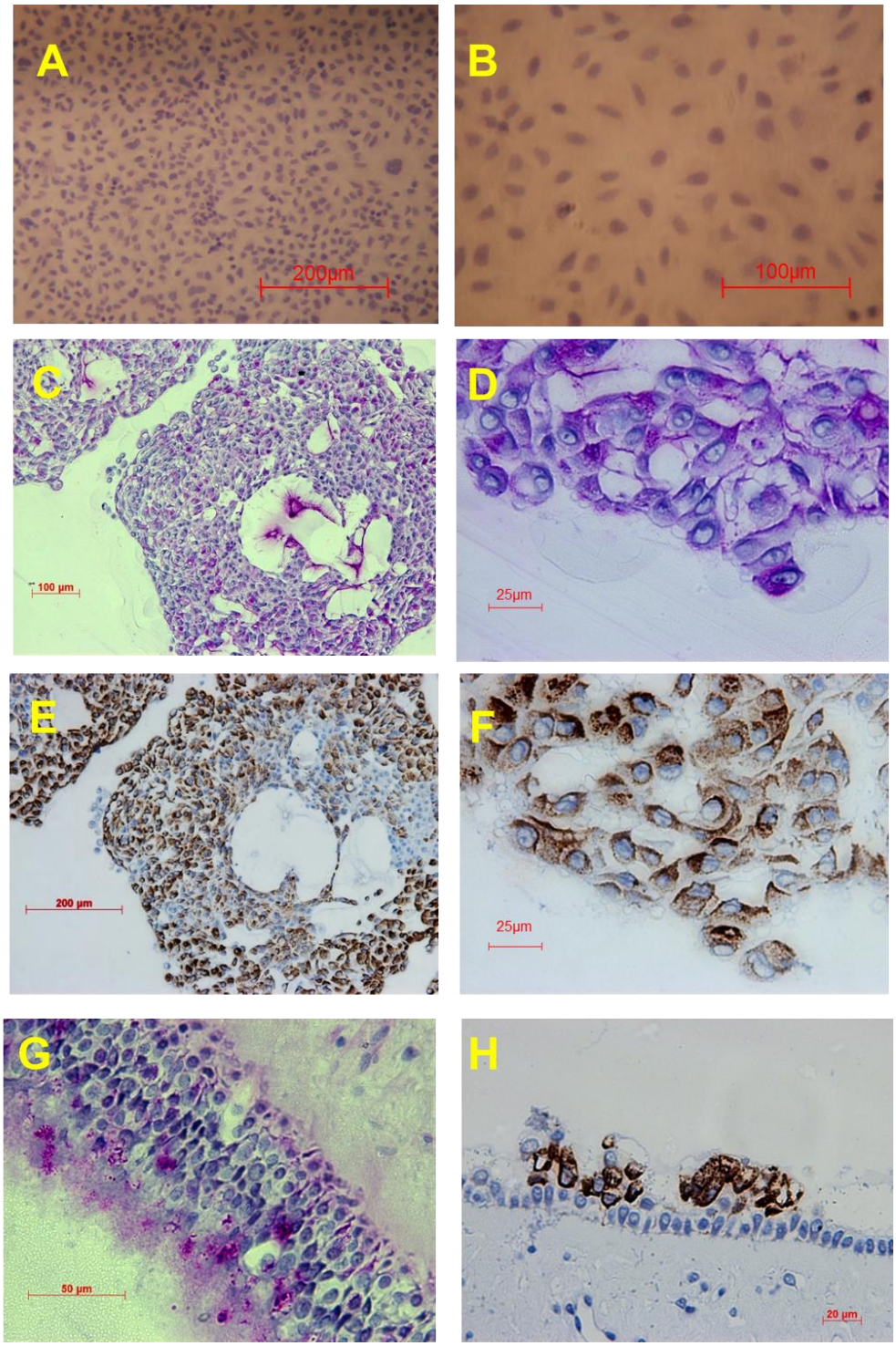

Figure 3.22. Mucin expression in A549 spheroids.
A549 spheroids were cultivated in Ham's F12/10% FBS for 18 days. Spheroids were 4% paraformaldehyde (PF) fixed, GMA embedded, sectioned and stained for evidence of gel mucin using PAS (C and D) and immunostaining using mouse anti-human MUC5AC (Dako) and a biotinylated secondary Rabbit anti mouse with DAB Chromagen (Vector) and Meyer's Haematoxylin counterstain (E and F). Methanol fixed log phase A549 2D cultures were fixed and stained with PAS as a negative control (A and B). Positive Control (human nasal polyp) was stained for mucin (PAS) (G) and the MUC5AC immune-stain (H). Images are representative of a single experiment.

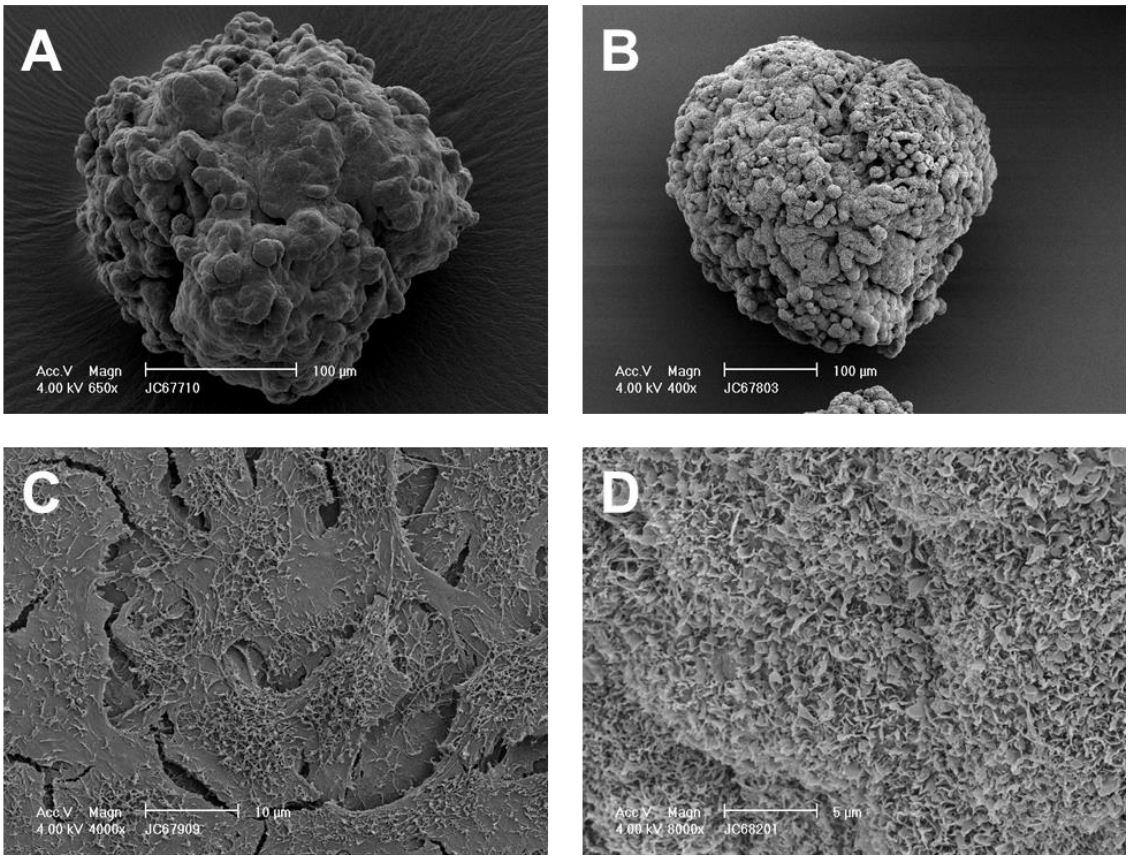

Figure 3.23. Scanning electron micrographs of A549 spheroids.
A549 spheroids were cultivated in Ham's F12/10% FBS and maintained for 13 days (A) and 18 days (B) Spheroids were fixed in glutaraldehyde, dehydrated and cold coated prior to examination by scanning electron microscopy. (C) shows the surface of 2D cultured A549 cells at 13 days at high magnification and (D) the surface of cells in an 18-day spheroid. Images are representative of two independent experiments.

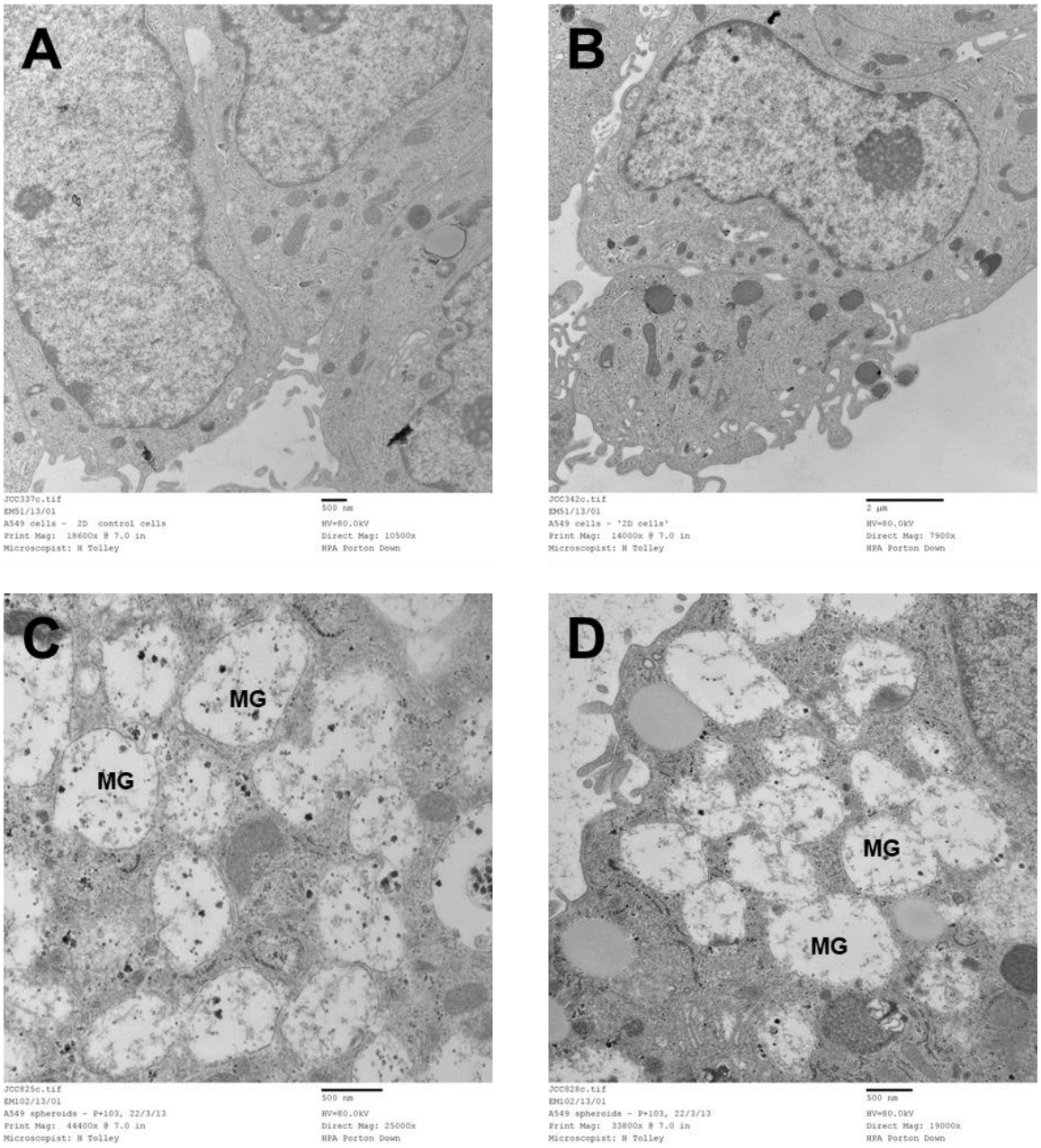

Figure 3.24. Transmission electron micrographs showing mucin granules in A549 spheroids.

A549 cells were maintained for11-days in 2D culture (A and B) or for 21 days as 3D spheroids in Ham's F12/10% FBS (C and D). Cells were fixed in glutaraldehyde, embedded in resin (Araldite™), sectioned and stained with osmium tetroxide and uranyl acetate prior to transmission electron microscopy (TEM). Mucin Granules (MG). Images are representative of two independent experiments.

.

3.4 Discussion

Three-dimensional (3D) spheroid cell cultures are easily accessible 3D culture systems. They provide simple models for cell migration, differentiation, survival, and growth. Spheroids form *in vitro* due to the tendency of adherent cells to aggregate and the technique is commonly employed in the field of cancer research[356]. Spheroids of the A549 cell line have been usefully employed to screen potential new therapeutic anti-cancer drugs[357 358]. In this study, it was hypothesised that allowing cultures of A549 cells to differentiate into 3D aggregate spheroid cultures in ultra-low adherence (ULA™) culture plates might drive the cells into a more ATII-like epithelial phenotype and that some degree of epithelial differentiation could be demonstrated.

It is generally accepted that cellular differentiation in *in vitro* models require several weeks of culture to provide cells of the required phenotype. For example, primary differentiated human airway epithelia generally require 14 days minimum before use[359] and the CaCo2 model of intestinal absorption requires the cells to undergo a 21 day differentiation period before the cells achieve epithelial differentiated state[360]. For most applications and experimental requirements longer periods than this would be undesirable from a practical point of view and longer term culture increases the risk of microbial or cross contamination of the cell cultures[292]. For these reasons the experiments here were conducted over a 25-day time-course.

The first factor evaluated was the cell culture medium formulation. Some researchers had used DMEM for A549 culture[358 361] whereas others had used RPMI 1640[362]. To determine a standard medium formulation that would produce consistent and uniform spheroids, growth of the cells in DMEM and Ham's F12 (both supplemented with 2mM L Glutamine and 10%v/v FBS) was evaluated. DMEM was selected because of its widespread use throughout the literature and Ham's F12 because of its more complex, physiologically relevant formulation (see Table 2.1Chapter 2, Materials and Methods). Both Ham's F12 medium and DMEM supplemented with 10%v/v FBS and 2mM L-glutamine supported the growth of the spheroids, however, results indicated that Ham's F12/10% FBS cultured spheroids were consistently more uniform and less likely to break apart into loose non-uniform aggregates as was the case with DMEM/10% FBS. Ham's F12/10% FBS generated more rounded colonies of cells, whereas the spheroids produced in DMEM/10% FBS tended to be more loosely aggregated and less uniform in shape.

3D Spheroid culture is used in cancer research as it enables quick discovery of morphological changes in transformed cells; a near perfect sphere will form if the cells are of normal phenotype whereas a distorted structure indicates malignancy. It may therefore be that the

DMEM/10% FBS cultured cells were adopting a more tumour like, malignant phenotype than those cultured in Ham's F12/10% FBS[356].

Although the cell numbers per spheroid at day 25 were not significantly different between the two media, neither were the observed population doubling rates however there was greater variability in cell numbers and it was observed that the looser bound DMEM 10% FBS spheroids appeared to be shedding more free cells into the growth medium indicating a possible increased rate of proliferation in DMEM 10%FBS and different cellular behaviour as these shed cells did not form part of the cell count calculations.. DMEM medium contains high a concentration of glucose (4.5 g/L) as compared to normal a human blood glucose level of 0.7-1 g/L[363] and Ham's F12 which has a nearer to physiological glucose concentration of 1.8 g/L. It has been shown that increased levels of glucose in culture medium may induce Warburg and Crabtree effects in cell cultures driving them into non physiologically relevant over proliferative states and aberrantly affecting their cell metabolism[364 365 366]. In addition (data not shown) it was observed that DMEM cultivated A549 spheroids tended to produce a mucilaginous secretion that disrupted the spheroids.

This suggested that Ham's F12 was a more suitable cell culture medium for further work and generating colonies of cells with a potential lower proliferative rates, more physiological metabolism and possible epithelial phenotype, hence F12 was used for cultures progressed to RNA microarray analysis.

Gene expression analysis of the RNA microarray data from 3D spheroids cultivated in Ham's F12 over a 25-day time-course compared to conventional 2D log phase cultivated A549 cells showed that there was a differential up and down regulation of many genes indicating the adoption of gross phenotypic differences between spheroid cultures and 2D cultured cells. Regulation of genes associated with cell cycle progression and cell division along with reduced population doubling rates and the fact that the cells in the spheroids remained viable after 25 days in culture indicated the possibility of cellular differentiation. The work of Mehta *et al* (2012)[367] and others[368] has previously shown that cells in the centre of tumour cell line spheroids can become quiescent due to anoxia which may ultimately lead to necrosis[367], whilst cells at the periphery remain proliferative. This may go in part to explain the ambiguity of the observation of regulation of genes associated with proliferation with the simultaneous apparent slowing of cellular proliferation in the A549 spheroids.

The pattern of gene regulation suggested a potential multifaceted nature to differentiation. In the A549 spheroids. Down regulation of genes involved with collagen metabolism, cell-cell adhesion, regulation of cell differentiation and ECM organisation indicated that factors such

as the establishment of the basement membrane (where collagen deposition is essential[369]) and differentiation towards an organised alveolar epithelial phenotype were unlikely.

Upregulation of genes involved in antibacterial humoral immune response, secretory cellular components and the lumens of secretory granules indicated the possible adoption of a host defence, secretory cell phenotype, whereas upregulation of genes involved with tissue regeneration, wound healing[370], substrate adhesion dependent cell spreading and establishment of circulatory system[351 352] suggested the possibility of the development of tumour-like characteristics.

Within the many genes analysed there was upregulation of the expression of genes for tumour marker cellular adhesion molecules *CEACAM6* and *7* indicating adoption of a more tumour-like population of cells in the spheroid colonies. *CEACAM 6* and *7* are normally expressed on the surface of myeloid and epithelial cells. However, over-expression of these markers can be associated with malignancy and CECAM6 is associated with disruption of the normal cell death process of anoikis (the programmed cell death of epithelial cells if they become detached from their basement membrane) and an invasive tumour phenotype. *CEACAM 6* upregulation appears to be mediated by excessive TGFβ, AKT, FAK and SRC signalling and is a putative target for anticancer therapies[371]. This finding, supported by upregulation of genes involved in the negative regulation of apoptotic processes implies one of two possibilities, that the cells in the A549 spheroids may have adopted a tumour-like population and perhaps less epithelial than desired for this programme of work, suggesting that A549 spheroid culture using the techniques established here may have use in the field of cancer biology.

The second possibility is that although it was the intent of the work to derive an alveolar epithelial ATII phenotype of the distal airway, the conditions of long term spheroid culture in Ham's F12 medium have driven the A549 cells to differentiate to a muco-secretory phenotype similar to the goblet cells of the upper airway epithelium. As well as being cancer markers, CEACAM molecules also have a role in host defence immunity[372 373]. CEACAMs allow the binding of bacteria and other pathogens to epithelial cells, which although allows targeting and tissue invasion by the pathogens[374] also effects a cell signalling response of the innate immune system in mucosal epithelia. Binding of fungal pathogen to CEACAM6 has been shown to elicit an CXCL8 (interleukin-8) inflammatory response in C2BBe1 intestinal cells [375] and the increased level of expression *CEACAM 7* has been used as a marker to demonstrate response to bacterial challenge in colon cell lines[376]. This potential development of a host defence phenotype in the spheroids was further demonstrated through the upregulation of the antimicrobial peptide cathelicidin[377] in the 3D spheroids. Cathelicidins (CAMP) are cationic and usually amphipathic molecules with a functional sequence that is conserved

throughout the animal kingdom[378]. They have a direct effect on bacterial, viral and fungal infections and can trigger specific defence responses in the host[379] such as chemotactic factors for immune cells. Cathelicidins are important factors in the defence of the airways against pathogens and are found in the mucin rich airway surface fluid of the proximal airways[380]. RNA microarray analysis of the spheroid cultures also demonstrated upregulation of ERBB3, a member of the epidermal growth factor receptor tyrosine kinases. ERBB3 plays a role in the maintenance and repair of epithelial tissues[353] and is found in the bronchial epithelium. Previous work by Carterson *et al* (2005)[343] demonstrated that growth of 14 day differentiated A549 cells on microcarrier beads in rotating wall bioreactors, although not 3D spheroid culture, displayed higher levels of innate immunity pulmonary to *Pseudomonas aeruginosa* infection compared with conventional monolayer cultivated cells. Liu *et al* (2011)[361] demonstrated that A549 cells in spheroid culture exhibited epithelial innate immune responses. The development of a host defence phenotype through the expression of CEACAM molecules, ERBB3 and cathelicidin in the A549 spheroids generated in this work might help explain the observations seen by other researchers and supports a second potential application, the use of the A549 spheroid as an epithelial model in infection studies. The gel forming mucins MUC5B and MUC5AC alongside cathelicidins are critical part of the primary immune response of the airways to chronic bacterial infections, *in vivo* they are secreted by and work in conjunction with ciliated cells of the upper airway to form the glycocalyx[381] and there is a need for models that recapitulate this function[382]. MUC5B is also associated with IPF through a relationship of a of a MUC5B promoter single-nucleotide polymorphism (SNP) (rs35705950) with mucus production in the disease. Hypersecretion of MUC5B is observed in IPF patients with advanced disease, where gel mucins accumulate in the honeycomb cysts and terminal bronchioles[383].

Mucins have been identified as key effectors in cell growth and tissue remodelling processes observed in IPF. Mucins are classified two groups: those that are secreted (secreted mucins) or those that remain tethered to cell membranes (transmembrane mucins). Secreted mucins (MUC2, MUC5AC, MUC5B, MUC6-8 and MUC19) are released to the extracellular space and recent evidence has shown that a promoter polymorphism in secreted MUC5B is associated with IPF. The transmembrane mucins (MUC1, MUC3, MUC4, MUC12-17 and MUC20) have a receptor-like structure. They sense the external environment and activate intracellular signal transduction pathways essential for mucosal maintenance and wound repair. In these cases, the extracellular domain can be released to the external environment by action of metalloproteinase which is increased in IPF. Thus, this process could contribute to the activation of fibrosis. Indeed, there is increased serum extracellular secreted KL6/MUC1 during IPF acute exacerbation. Moreover, MUC1 and MUC4 overexpression in IPF cells has been observed. Therefore, mucins hold some promise as druggable targets for IPF[384].

This muco-secretory A549 phenotype may therefore also have application in *in vitro* modelling of IPF.

To confirm and validate the gene expression data that indicated the 3D spheroids of A549 had differentiated to a mucus-secreting, possibly goblet cell phenotype, histological and TEM microscopy was carried out. Histological sectioning of the A549 spheroids showed that at the early stages of development (day 13) the colonies of cells were indeed spheroid and comprised of a regular, solid mass of cells, with a clear boundary, whereas by day 18 the spheroids had developed an internal cavity or lumen, become more irregular and the boundaries of the spheroids were less clearly defined. The exact mechanism of the lumen development is unknown, however it is postulated that the lumens were potentially voids left by necrotic cells as has been demonstrated in spheroids from tumours from other tissues[385]. PAS staining for mucin production showed most of the cells in the spheroids were secreting mucin, possibly into the media, between the cells and into the lumens of the spheroids. Immunostaining demonstrated that one component of this mucin secretion was MUC5AC, whose expression is increased in the bronchial tissues of patients suffering from chronic obstructive pulmonary disease (COPD)[386]. QRT PCR and subsequent transmission electron microscopy (TEM) confirmed the presence of a high proportion of mucin secreting cells in the spheroid colonies. This observation alongside upregulation of the *ERBB3* gene and the SAM-pointed domain–containing Ets-like factor (*SPDEF*) may suggest a third potential use for A549 cells grown in this manner for *in vitro* research into diseases such as COPD and asthma where, in the patient, submucosal glands increase in size and the number of goblet cells increase, contributing to the pathologies of the condition[387]. SPDEF controls the transcriptional programme for goblet cell differentiation[355] and may be important factor in the control of the goblet cell hyperplasia[388], a common feature of COPD.

A549 cells grown as solid spheroids did not attain the desired ATII phenotype. There was no evidence from TEM that the cells expressed the hallmarks of ATII differentiation, multilamellar bodies (MLB), at any point in the time-course. At later stages in the time-course the A549 spheroids grown in this study had developed internal voids, the surrounding tissue was several cells thick, unlike the alveolus, which has a lining of a polarised monolayer of continuous epithelium lining the cyst wall on an epithelial basement membrane platform[389].

It was appreciated that the 3D spheroid approach would have its limitations as the cells did not have any *in vivo*-like supporting mesenchymal or parenchymal cells, nor an epithelial basement membrane on which an epithelium of polarised cells might establish[390 391 392]. Indeed, the histological data presented here show that the cellular structure of the spheroids is not organised into the simple epithelial monolayer of polarised cells that is found in the pulmonary alveolus[14], rather, a more disorganised pseudo-stratified structure is obtained

(Figure 3.21and 3.22). Data and observations on the continual increase and eventual disintegration of the spheroids over the 25 day time-course also indicate that the cells within the spheroids were still in a background proliferative state and not becoming quiescent and fully differentiated as one would expect in functional pulmonary epithelium[234]. In 2012 Zschenker *et al* published gene expression data on A549 cells grown in 3D culture for 8 days in matrigel, a basement membrane analogue[393] where it was demonstrated that 3D growth conditions had a profound impact on the cell phenotype. Independent analysis of their curated data suggested that the expression of Mucin Genes *MUC5AC* and *MUC5B* was elevated in these cultures. Mucin is not an expected expression product of ATII cells[14] indicating that this source of the cell line may have drifted from its original reported phenotype suggesting that the augmentation of spheroid culture of A549 cells with basement membrane may not be adequate to drive the cells to an ATII-like state.

The physical modelling of the alveolus is challenging. Lewis *et al* attempted to model alveoli using photodegradable microsphere templates[247] and although they used this method to generate hollow cysts of A549 monolayers no data on their functionality was presented and they concluded that the A549 cell line proliferated too rapidly for effective use in their model. However, they used DMEM for their cell culture which, as shown here, may not be suitable for generating more quiescent, differentiated cultures.

The results here demonstrate that rather than driving A549 cells to an ATII phenotype, 3D Spheroid culture generated a mucus secretory phenotype more akin to a goblet cell of the bronchial epithelium[387] with a background of proliferating cells. Although this was not the intent of the study, this finding may be of use in other fields of cancer biology, infection biology and airway research where *in vitro* models of mucus secreting epithelium might be required.

Considering the data presented here and the evidence from the literature spheroid cultures of A549 cells, an investigation is required into the long-term culture of the cell line in a physiologically relevant culture in a system that generates a simple epithelial monolayer culture of similar architecture to the alveolus that might allow a non-proliferative, quiescent, differentiated population of cells to develop more akin to ATII cells.

3.4.1 Summary

- A549 cells were grown as 3D spheroids on ULA plastic in DMEM and Ham's F12 medium for 25 days and their morphologies, behaviour and gene expression were compared to conventional 2D cultured A549 cells in an attempt to drive ATII-like differentiation.
- F12 was identified as being the optimal medium for spheroid growth. The use of DMEM resulted in irregular, loosely bonded spheroids with highly variable numbers of cells per spheroid whereas F12 generated regular, closely packed spheroid cultures.
- RNA Microarray analysis of 3D A549 spheroids cultured over a 25-day time course in F12/10% medium compared to conventional 2D culture A549 cells suggested multifaceted cellular differentiation with two potential explanations: (1) The adoption of an epithelial muco-secretory phenotype similar to the goblet cells of the upper airway, characterised by the expression of markers of host defence and mucus secretion and (2) the adoption of a tumour like phenotype.
- The further characterisation and confirmation of the potential muco-secretory phenotype of the A549 cells in the 3D spheroid cultures was carried out using QRT PCR, histochemical methods and electron microscopy.
- Although no evidence of the characteristics of ATII differentiation was observed in cultures in this chapter and it was concluded that 3D spheroid culture of A549 cells may not appropriate to recapitulate the pulmonary alveolar epithelium. There is, however, a suggestion that the 3D spheroid A549 model a developed may have application in three distinct areas of biological research:

  - The use of A549 spheroids in drug discovery in cancer research
  - Use in infection biology, as a model of the host defence of the upper respiratory tract.
  - As a model in the study of goblet cell hyperplasia, a complication of COPD.

4. Long Term 2D Growth of A549 Cells

4.1 Introduction

The data in Chapter 3 indicated that spheroid culture with A549 cells may not be an appropriate strategy to attempt to recapitulate the pulmonary alveolar environment. It was found that long term culture in Ham's F12 in spheroid culture generated cultures of cells that showed some evidence of epithelial differentiation but there was no evidence that the cells grown in 3D expressed the ultrastructural characteristic of ATII cells: multilamellar bodies (MLB)[19]. MLBs play a key role in the synthesis storage and secretion of dipalmitoylphosphatidyl choline (DPPC), the major lipid component of pulmonary surfactant essential for respiration. Surfactant reduces surface tension to retain the integrity of the alveolus and allow efficient gaseous exchange[394]. Cellular division in the supposed differentiated spheroid cultures from Chapter 3 was not arrested indicating that the cells may not have been fully differentiated. The next step was to identify conditions that might slow or arrest cellular division and allow differentiation to a point where the cells attained a differentiated phenotype more akin to the ATII cells of the distal lung.

In vivo the alveolus forms a hollow cavity with a lining of a polarised monolayer of continuous alveolar epithelial cells on an epithelial basement membrane platform[389]. Previous attempts by others to cultivate A549 cells in 3D culture in suspension in a basement membrane analogue (Matrigel™) seemed to have also resulted in a mucin secreting phenotype[393] suggesting that using Matrigel to attempt to refine the A549 spheroid culture system by introducing basement membrane may not improve the progression to an ATII phenotype. It was therefore decided to explore cell monolayer growth on conventional tissue culture treated plastic to attempt to recapitulate the structure of the alveolar wall.

Many continuous cell lines, such as A549, are derived from malignant tumours. However, a hallmark of many tumours is that the cells derived from them bear little resemblance to the normal cells from the tissues in which the cancer originated. This process is referred to as 'dedifferentation'[395]. Dedifferentiation is the transition of a cell to a state characteristic of an earlier stage of development[396]. It has been implicated as a contributing to cancer progression[397] and involves a reversal of developmental processes, yet dedifferentiation is also a normal, essential response to tissue damage[398] to effect repair. Artificially triggered dedifferentiation and subsequent targeted differentiation, over several weeks, are central approaches to generate induced pluripotent stem cells (IPSCs) and further differentiate them for tissue repair strategies[399].

A549 cells in normal log phase growth appear to be dedifferentiated but it has been shown that they can be driven to other multi-lineage differentiated states, such as adipocyte-like cells, through long term culture and the use of specific differentiation media and optimised culture conditions[400]. Indeed, soon after the A549 cell line was generated in the 1970s[307], the cells were reported to have morphological and ultrastructural similarities to ATII cells. In 1978, Shapiro *et al* demonstrated ATII-like differentiation in A549 cells confirmed by the expression of high numbers of MLB but only after three weeks in continuous culture[19]. This protocol, however does not seem to have become common place in the general growth of the cell line. Epithelial differentiation can be induced in other continuous cell lines such as the intestinal epithelial cell line CaCo2[335] and the canine kidney cell line MDCK[336]. These differentiation processes, however, are time dependent, in most cases, taking four or more weeks[400].

The apparent plasticity and differentiation potential of A549 cells as seen from historical[19] and more recent insights[400] into the cultivation of the cell line, suggest that long term culture may be a relatively easy-to-implement strategy to achieve an ATII-like phenotype.

The alveolar epithelial cells of the distal lung consist of a thin monolayer of cells that form a quiescent, tightly bound barrier[401]. A clear objective of this work therefore, was to recapitulate the quiescent cellular organisation of the alveolar epithelium and to identify evidence of lipid synthesis and MLB expression. Phenotypic characterisation of the putative differentiated A549 cultures over a 25-day time course was to be determined by morphological, cytometric, gene expression and histological and histochemical analysis. To determine how similar the differentiated cells were to the *in vivo* state the data were compared to that of primary ATII cells obtained from biopsy wherever possible.

4.2 Hypothesis

Long term two-dimensional (2D) cultivation of the A549 human lung cancer cell line on a on a conventional plastic substratum in an optimised nutrient medium will produce a differentiated population cells with a phenotype more like Alveolar Type 2 (ATII) cells than conventional log phase cultivated cells.

4.2.1 Aims

To determine if long term culture of A549 cells results in a quiescent monolayer culture with a gene expression profile that is more similar to primary ATII cells. To demonstrate that this expression profile bears more similarity to ATII cells than that of log phase A549 cells and of A549 cells grown in 3D spheroids.

To demonstrate the expression of MLBs together with ATII specific genes and genes involved in surfactant synthesis in the 2D long term A549 cells. Demonstrate the absence of expression of mucin granules.

4.2.2 Objectives

- To cultivate A549 cells in 2D culture in Ham's F12 and DMEM medium in tissue culture coated plastic and allow them to differentiate over a 21 (or more) day period
- To harvest cells at regular time-points in the differentiation period and extract RNA for RNA microarray analysis, to determine the gene expression of pathways and markers of ATII differentiation and where relevant validate results using Quantitative Real Time Polymerase Chain Reaction (QRT PCR).
- Use bioinformatic software resources, such as pathway analysis, to compare the gene expression of log phase and long term differentiated A549 cells with primary ATII cells.
- Using phase contrast microscopy and automated cell counting techniques to observe the morphology and determine cell numbers and viabilities to assess the effect of different media formulations on cellular growth and differentiation. Identify the development of a thin quiescent monolayer over the time-course.
- To determine if A549 cells differentiated in an optimised medium formulation and cultivated for long periods in 2D culture express Multilamellar Bodies (MLB) using histochemical techniques and transmission electron microscopy.
- Using these data, determine if the cells had adopted features and markers of differentiation that typify ATII cells, or if not, what phenotype these conditions would generate.

4.3 Results

4.3.1 Selection of Culture Medium

Initial experiments in Chapter 3 demonstrated that Ham's F12 supplemented with 10% FBS(v/v) was more suitable than DMEM with 10% FBS for the growth of A549 cells in spheroids. Therefore, the effect of these two different culture media was further explored on A549 cells grown as monolayers. After 24 hours of plating, the cells cultured in either medium appeared morphologically similar with mitotic cells evident in both conditions. Cells continued to divide as the cultures progressed, however there appeared to be more cell division, crowding and piling up of cells in DMEM/10% FBS (Figure 4.1A) In contrast, in Ham's F12/10%FBS, the cells displayed a more flattened contact-inhibited quiescent appearance that was maintained until the cultures were terminated at day 25 (Figure 4.1B). At this point, cell counts determined using two independent methods demonstrated that culture of cells in DMEM/10%FBS yielded significantly more cells than Ham's F12/10% FBS (Figure 4.3A and B). Although there was no difference in cell viability between the two culture conditions, cells grown in DMEM/10%FBS had a significantly smaller diameter (Figure 4.3 C and D). A series of photomicrographs comparing the growth and morphology over the time course is included in Figure 4.2 . Closer examination of the cells cultured in Ham's F12 showed the presence of organized vesicles of uniform size within the cells Figure 4.2H(i) suggesting the possibility of cellular differentiation.

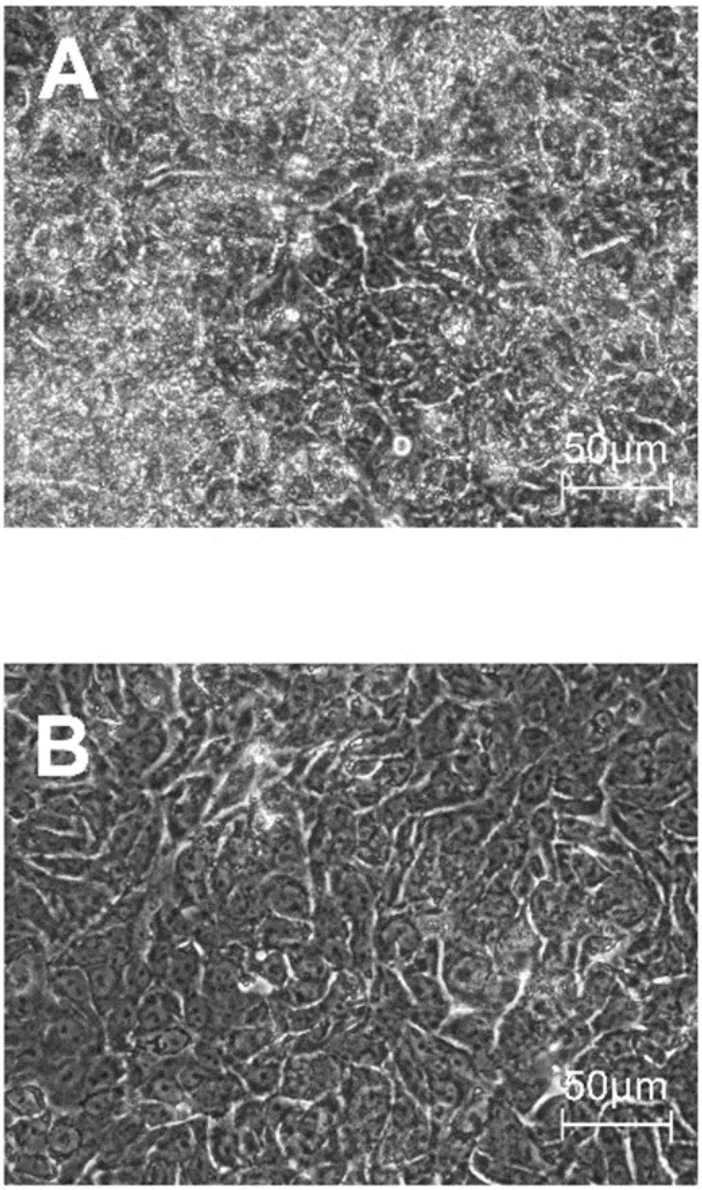

Figure 4.1. Morphlogy of A549 monolayers cultivated in DMEM/10% FBS or Ham's F12/10%FBS.
Phase contrast images of A549 cells monolayers maintained for 25 days with regular medium exchanges in DMEM/10% FBS (A) and Ham's F12/10% FBS (B). at day 25. Images are representative of two independent experiments.

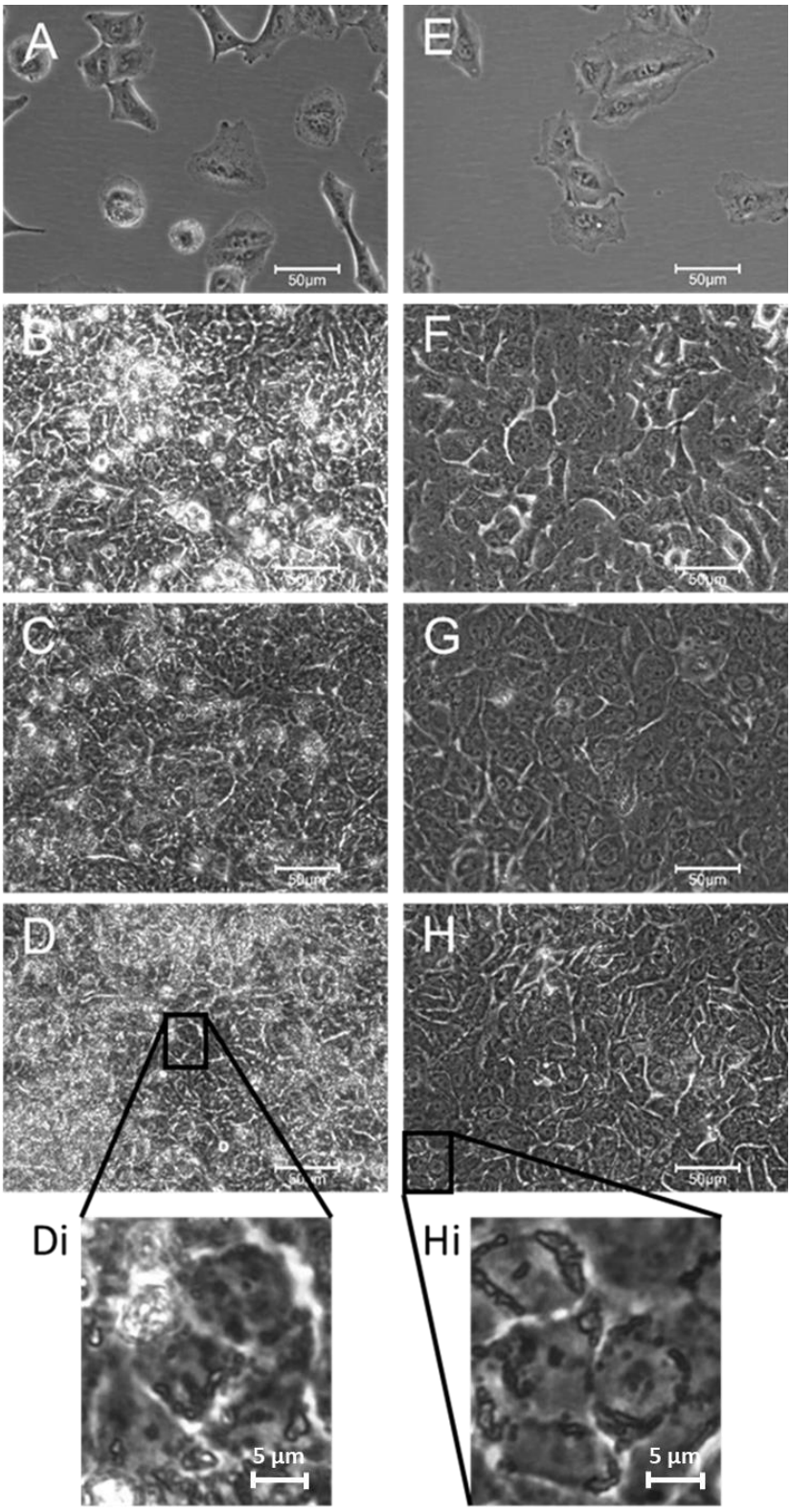

Figure 4.2. 25-day time-course of A549 monolayers cultivated in DMEM/10% FBS or Ham's F12/10%FBS.

Phase contrast images of A549 cells monolayers maintained for 25 days with regular medium exchanges in DMEM/10% FBS (A-D) or Ham's F12/10% FBS (E-F). Day 1 (A and E), day 8 (B and F) day14 (C and G) and day 25 (D and H). Insets H(i) and D(i), show higher magnification of the monolayers at day 25**.** Images are representative of two independent experiments.

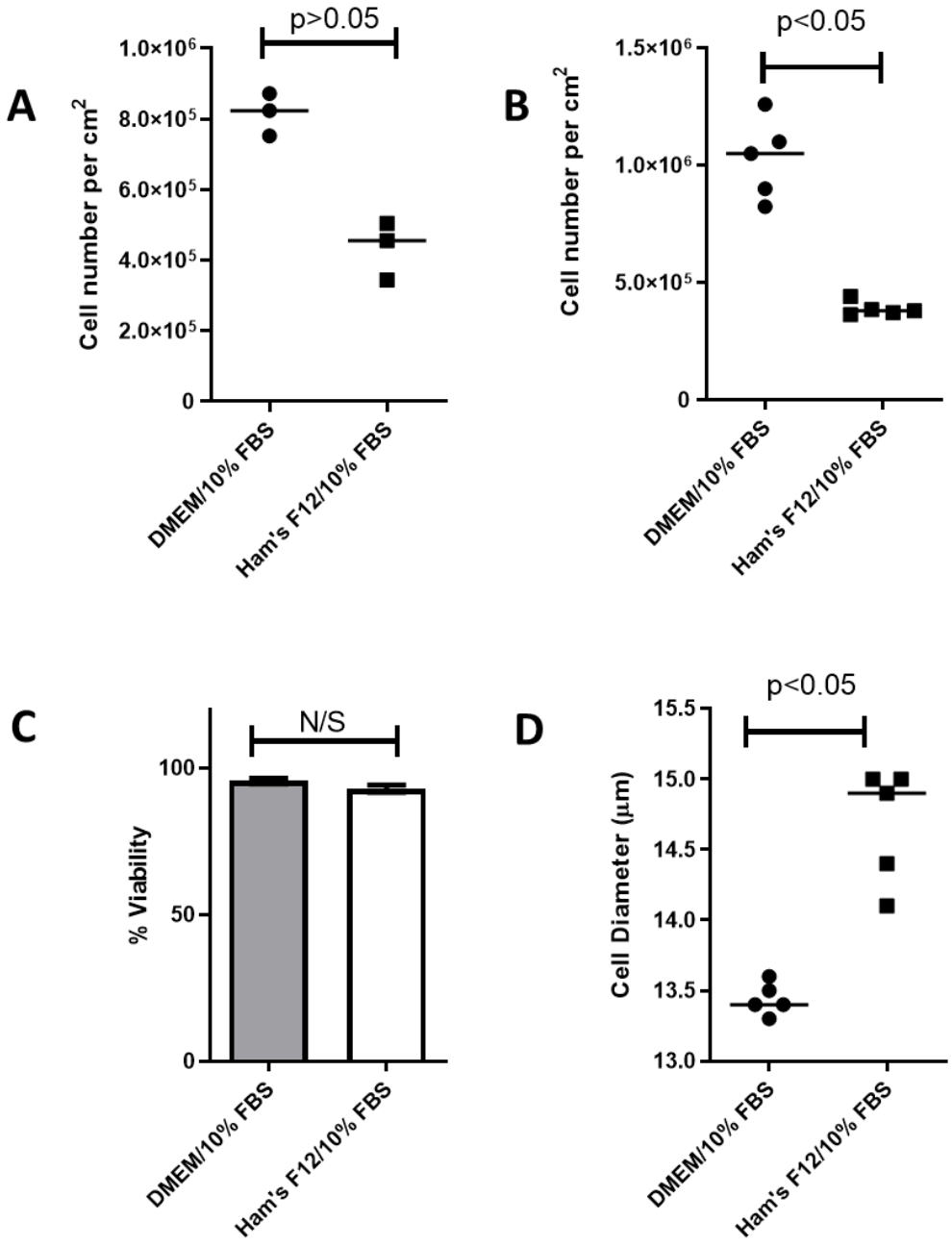

Figure 4.3 Cell counts, viability and cell diameters from 25 day old 2D A549 cell cultures grown in DMEM/10% FBS or Ham's F12/10% FBS.
A549 cells were maintained for 25 days with regular medium exchanges in DMEM/10% FBS (A-D) or Ham's F12/10% FBS (E-F). A: cell yield per unit area based on cell counting using Trypan blue dye exclusion (3 technical replicates from a single experiment) and B: cell numbers as measured by automated cell counting. C: Cell viability based on DAPI dye exclusion. D: cell diameter of trypsinised cells using automated image analysis (Nucleocounter® NC3000). B-D; 5 technical replicates from a single experiment. Statistics: A, B and D Mann Whitney non-parametric test. C passed the Kolmogorov-Smirnov test for normality hence *t*-test. Error bars (D) represent standard deviation.

4.3.2 RNA Microarray Analysis

To obtain deeper insight into the changes occurring in A549 cells during long term culture in Hams F12/10% FBs, RNA microarray analysis was used to compare the gene expression of long-term cultures at seven, eleven, eighteen and twenty-five days from seeding compared to samples from log phase cultured A549 cells using Benjamini-Hochberg false discovery rate (BH FDR) corrected ANOVA analysis of microarray data. The ANOVA demonstrated that of the 39,013 genes examined, 5,346 were significantly up or down regulated ($p<0.05$) during the 25-day time course and, of these, 3,926 were up or down regulated with a fold change of two or greater (see Figure 4.4). Pathway analysis of the genes regulated at a fold change of two or more highlighted nineteen pathways with significant p values involved with aspects of cell cycle regulation (Table 4.1). Within these pathways, the markers of proliferation KI-67, PCNA and TCF7L1 were down regulated and the inhibitor of cell cycle progression CDKN1B was upregulated during the 25-day time-course (see Figure 4.5).

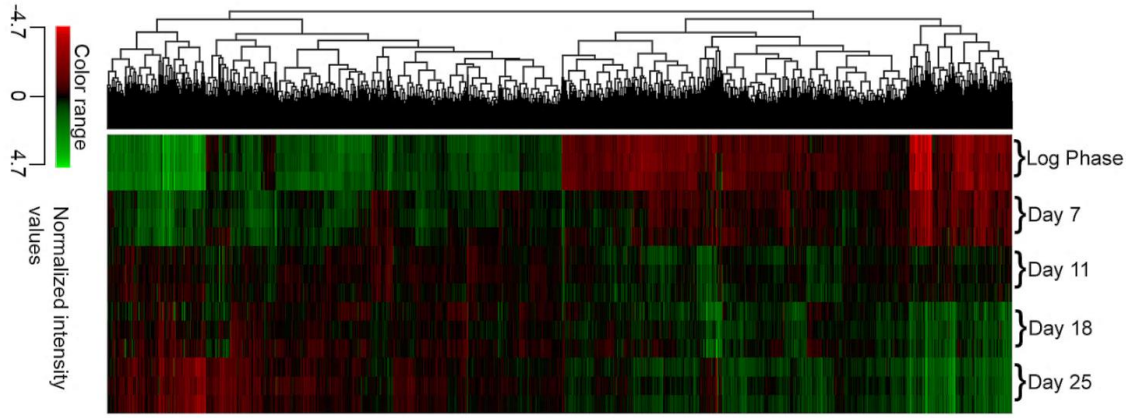

Figure 4.4. RNA Microarray Heatmap of Gene Expression in 2D Ham's F12/10% FBS cultured A549 cells over a 25-day time-course.
A549 were cultured for 25 days as monolayers in Ham's F12/10% FBS with regular medium exchange. RNA was extracted at log phase, days 7, 11, 18 and 25 and converted to fluorescently labelled cRNA for hybridisation and analysis using Agilent® Human Single Colour 39494 micro-array slides then Benjamini-Hochberg false discovery rate (BH FDR) corrected ANOVA analysis in Genespring™ prior to Hierarchical clustering (Euclidian similarity measure, clustered using Ward's linkage rule). Three technical replicates from a single experiment.

Pathway	**Wiki-Pathway Reference**	**P Value**	**Number of regulated genes**	**Number of genes in pathway**
Cell Cycle	WP179 70629	<0.001	51	103
S Phase	WP2772 77049	<0.001	46	116
Mitotic G1-G1-S phases	WP1858 76928	<0.001	46	120
Mitotic Metaphase and Anaphase	WP2757 77009	<0.001	57	153
Synthesis of DNA	WP1925 76968	<0.001	39	94
Nuclear Receptors Meta-Pathway	WP2882 78569	<0.001	80	318
RB in Cancer	WP2446 78573	<0.001	55	87
Mitotic Prometaphase	WP2652 76819	<0.001	54	98
DNA Replication	WP466 76196	<0.001	31	42
G1 to S cell cycle control	WP45 71377	<0.001	34	68
Telomere Maintenance	WP1928 76893	<0.001	24	37
Cell Cycle Checkpoints	WP1775 76816	<0.001	38	115
Nucleosome assembly	WP1874 76826	<0.001	15	22
miRNA Regulation of DNA Damage Response	WP1530 78503	<0.001	28	98
DNA Damage Response	WP707 78527	<0.001	27	68
Mitotic G2-G2-M phases	WP1859 77022	<0.001	31	89
M-G1 Transition	WP2785 77074	<0.001	27	79
Regulation of DNA replication	WP1898 76824	<0.001	18	70
Mitotic Prophase	WP2654 76823	0.002	12	44

Table 4.1. Pathways Associated with Cell Cycle Control in long term 2D cultured A549 cells.

Statistically significant pathways associated with cell cycle control for differentially expressed genes expressed over the 25-day time-course of A549 differentiation in Ham's F12 medium. Pathways were identified by Genespring™ pathway analysis after one way ANOVA of all of time points compared to log-phase A549 cells (P cut off = 0.05, Fold change ≥ 2.0).

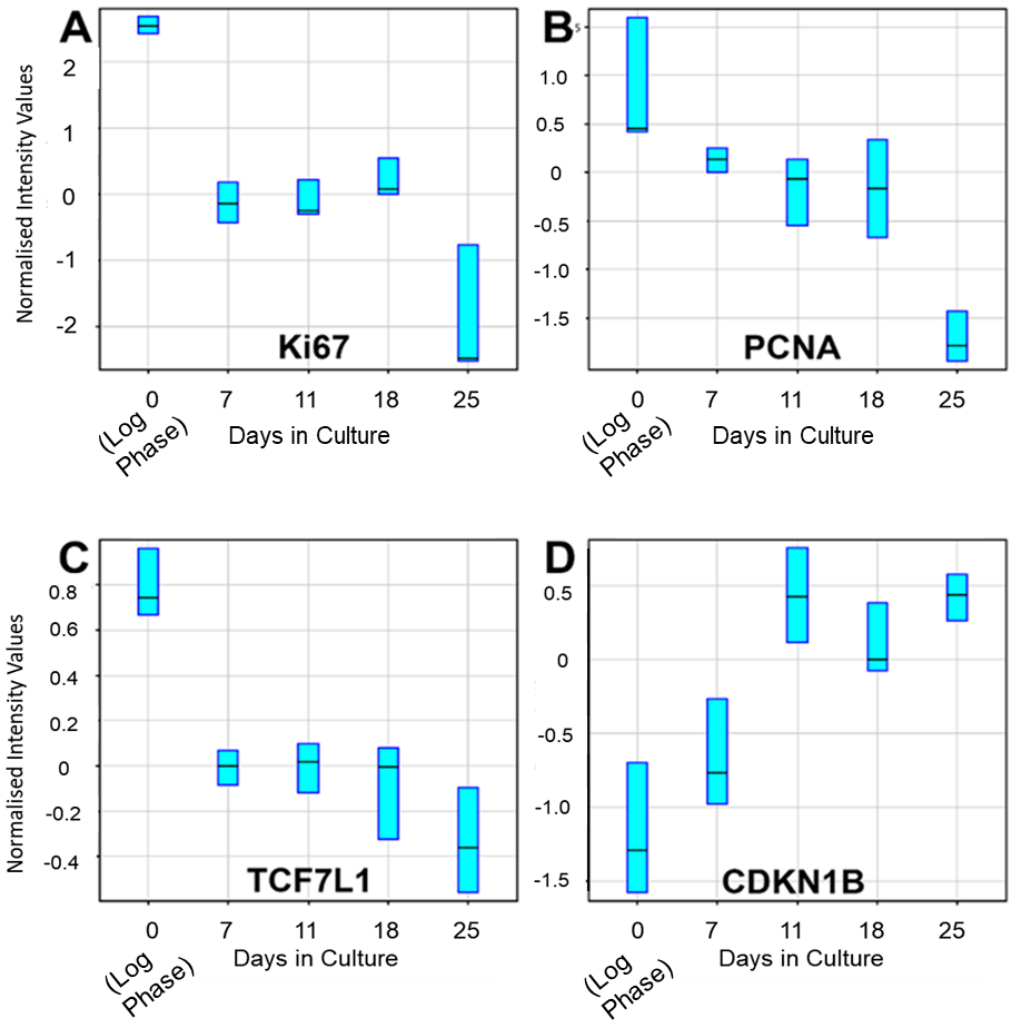

Figure 4.5. Changes in expression of genes associated with proliferation and cell cycle control in A549 monolayers over a 25-day time-course.
A549 cells were cultured for 25 days as 2D monolayers in Ham's F12/10% FBS with regular medium exchange. RNA was extracted at log phase, days 7, 11, 18 and 25 and converted to fluorescently labelled cRNA for hybridisation and analysis using Agilent® Human Single Colour 39494 micro-array slides. Intensity values for proliferation markers *Ki-67* (A), *PCNA* (B) and *TCF7L1* (C) and cell cycle inhibitor *CDKN1B* (D) were normalised to the mean intensity value of all genes on the microarray slides. Three replicates from a single experiment.

In addition to a reduction in expression of genes involved in cell proliferation, a small number of pathways involved in cellular autophagy, senescence and apoptosis were modulated during long term culture (Table 4.2 and Table 4.3). In contrast, there were 28 pathways related to differentiation of epithelial and endodermal tissues (Table 4.4). For example, *WNT4*, which has been implicated in lung development and repair, was upregulated as were the pluripotency markers *Nanog* and *SOX2*. Parallel up-regulation of SOX9 was also observed along with the Wnt target Metalloproteinase 7 (*MMP7*) (see Figure 4.6).

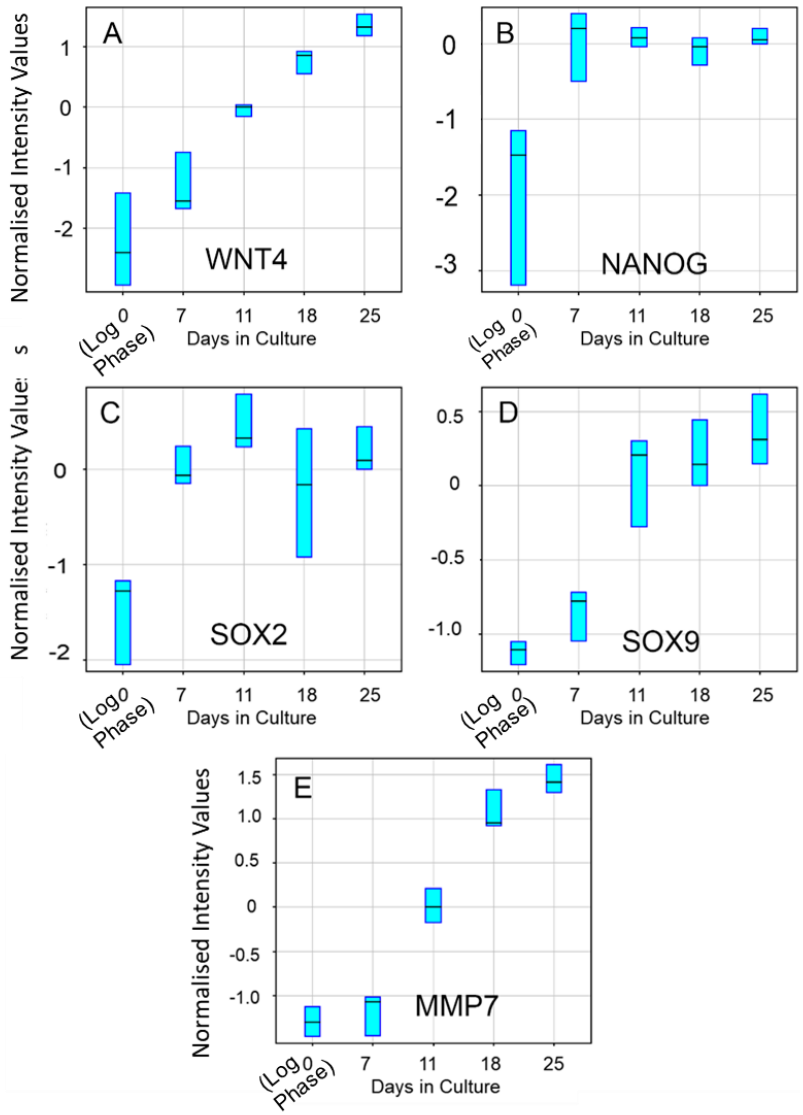

Figure 4.6. Changes in expression of genes associated with pluripotency, development and tissue modelling in A549 monolayers over a 25-day time-course.

A549 cells were cultured for 25 days as 2D monolayers in Ham's F12/10% FBS with regular medium exchange. RNA was extracted at log phase, days 7, 11, 18 and 25 and converted to fluorescently labelled cRNA for hybridisation and analysis using Agilent® Human Single Colour 39494 micro-array slides. Intensity values for *WNT4* (A), *Nanog* (B), *SOX2* (C), *SOX9* (D) and *MMP7* (E) were normalised to the mean intensity value of all genes on the microarray slides. Three replicates from a single experiment.

A feature suggestive of ATII cell differentiation was significant expression of complement component pathways with, for example, increased expression of C3, C4b and C5 (Figure 4.7).

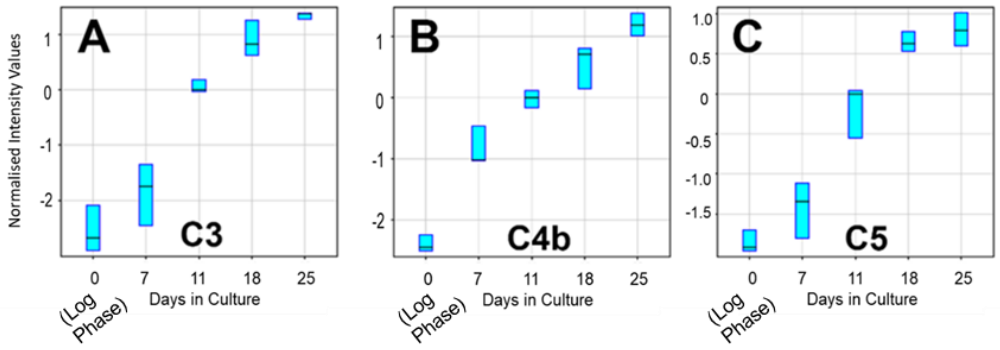

Figure 4.7. Changes in gene expression of complement component genes in A549 monolayers over a 25-day time-course.
A549 cells were cultured for 25 days as 2D monolayers in Ham's F12/10% FBS with regular medium exchange. RNA was extracted at log phase, days 7, 11, 18 and 25 and converted to fluorescently labelled cRNA for hybridisation and analysis using Agilent® Human Single Colour 39494 micro-array slides. Intensity values for *C3* (A), *C4b* (B) and *C5* (C) were normalised to the mean intensity value of all genes on the microarray slides. Three replicates from a single experiment.

In addition to induction of differentiation pathways, Table 4.5 shows 10 pathways involved in lipid metabolism that achieved statistical significance over the 25-day time course.

Pathway	Wiki-Pathway Reference	P Value	Number of regulated genes	Number of genes in pathway
Apoptosis	WP254 78808	0.021	17	84
FAS pathway and Stress induction of HSP regulation	WP314 71366	0.033	9	38
Apoptotic execution phase	WP1784 76813	0.033	10	46

Table 4.2. Pathways Associated with Apoptosis.
Statistically significant pathways associated with apoptosis for genes expressed over the 25-day time-course of A549 differentiation in Ham's F12 medium. Pathways were identified using Genespring™ pathway analysis after one way ANOVA of all time points compared to log-phase A549 cells (P cut off = 0.05, Fold change ≥ 2.0).

Pathway	**Wiki-Pathway Reference**	**P Value**	**Number of regulated genes**	**Number of genes in pathway**
Senescence and Autophagy	WP615 71375	<0.001	32	106
AMPK Signaling	WP1403 78804	0.006	16	68
Folate Metabolism	WP176 74202	0.020	14	67

Table 4.3 Pathways Associated with Senescence and Autophagy.
Statistically significant pathways associated with senescence and autophagy for genes expressed over the 25-day time-course of A549 differentiation in Ham's F12 medium. Pathways were identified using Genespring pathway analysis after one way ANOVA of all of the time points compared to log-phase A549 cells (P cut off = 0.05, Fold change ≥ 2.0).

Pathway	Wiki-Pathway Reference	P Value	Number of regulated genes	Number of genes in pathway
miR-targeted genes in epithelium - TarBase	WP2002 78530	<0.001	69	345
Complement and Coagulation Cascades	WP558 67786	<0.001	21	64
TGF Beta Signalling Pathway	WP366 69026	<0.001	21	55
TGF Beta Signalling Pathway	WP560 68944	<0.001	21	55
Cell junction organization	WP1793 77057	<0.001	20	61
Human Complement System	WP2806 78589	<0.001	28	136
Signaling by TGF-beta Receptor Complex	WP2742 76980	<0.001	13	36
Focal Adhesion	WP306 78800	<0.001	41	188
Integrin cell surface interactions	WP1833 77019	<0.001	19	64
Oncostatin M Signaling Pathway	WP2374 73668	<0.001	19	65
Integrin-mediated Cell Adhesion	WP185 71391	<0.001	24	99
Complement cascade	WP1798 77042	<0.001	13	192
Assembly of collagen fibrils and other multimeric structures	WP2798 77089	8.62E-04	11	33
Endoderm Differentiation	WP2853 78496	<0.001	18	146
Differentiation Pathway	WP2848 78558	0.001	14	50
Wnt Signalling Pathway and Pluripotency	WP399 74897	0.003	22	100
Cell Differentiation - meta	WP2023 68892	0.005	7	67
ID signaling pathway	WP53 67360	0.006	6	16
Prostaglandin Synthesis and Regulation	WP98 72088	0.008	9	31
Cell surface interactions at the vascular wall	WP1794 77039	0.008	19	91
Constitutive Androstane Receptor Pathway	WP2875 78537	0.009	8	32
EGF-EGFR Signalling Pathway	WP437 78502	0.010	30	162
Complement Activation, Classical Pathway	WP545 72062	0.011	6	17
Angiogenesis	WP1539 78807	0.015	7	24
Mitotic Telophase-Cytokinesis	WP2765 77030	0.020	5	14
Activation of Matrix Metalloproteinases	WP2769 77041	0.035	5	16
Gap junction trafficking and regulation	WP1820 76886	0.042	3	8
Wnt Signalling Pathway	WP428 78532	0.046	12	61

Table 4.4. Pathways Associated with Epithelial and Endodermal Differentiation.
Statistically significant pathways associated with epithelial and endodermal differentiation for genes expressed over the 25-day time-course of A549 differentiation in Ham's F12 medium. Pathways were identified by Genespring™ pathway analysis after one way ANOVA of all of the time points compared to log-phase A549 cells (P cut off = 0.05, Fold change ≥2.0).

Pathway	Wiki-Pathway Reference	P Value	Number of regulated genes	Number of genes in pathway
Adipogenesis	WP236 78584	<0.001	38	131
SREBF and miR33 in cholesterol and lipid homeostasis	WP2011 75253	<0.001	9	18
Nuclear Receptors in Lipid Metabolism and Toxicity	WP299 78587	<0.001	12	35
Ganglio Sphingolipid Metabolism	WP1423 76323	0.002	7	18
Signal Transduction of S1P Receptor	WP26 78492	0.005	8	25
Cholesterol biosynthesis	WP1795 77044	0.020	6	21
Regulation of Lipid Metabolism by Peroxisome proliferator-activated receptor alpha (PPARalpha)	WP2797 77088	0.025	21	118
Globo Sphingolipid Metabolism	WP1424 71392	0.026	6	24
Cholesterol Biosynthesis	WP197 78758	0.027	5	15
Fatty Acid Biosynthesis	WP357 70641	0.041	6	22

Table 4.5. Pathways Associated with Lipid Synthesis and Metabolism.
Statistically significant pathways associated with lipid synthesis and metabolism for genes expressed over the 25- day time-course of A549 differentiation in Ham's F12 medium. Pathways were identified using Genespring pathway analysis after one way ANOVA of all of the time points compared to log-phase A549 cells (P cut off = 0.05, Fold change ≥ 2.0).

To determine whether modulation of A549 cell growth and differentiation resulted in their transition towards an ATII cell phenotype, gene expression of the long term cultured A549 cells was compared to that of freshly isolated human primary ATII cultures. Comparison of relative gene expression using primary ATII cells from three donors showed a similar pattern of expression of five surfactant proteins (*SFTPD, A2, A1*, *B* and *C*) (Figure 4.8); therefore Donor 2 was selected for RNA microarray studies to represent normal ATII cells. In this analysis, each of the time-points of A549 differentiation and the primary ATII cells was compared to log phase A549 cells as the point at which it is assumed that most researchers would use their A549 cells in experiments.

The RNA microarray comparison of primary ATII cells with long term cultured A549 showed that for a minimum of fold change of two, the number of shared up regulated genes increased from 280 at day 7 of the differentiation time-course to 591 at day 25. Similarly, the number shared down regulated genes increased from 458 at day 7 to 796 at day 25 (Figure 4.9). Analysis of the shared up regulated genes indicated pathways involved with the Complement System (*C3* and *C4b*), senescence and autophagy, lipid metabolism (including fatty acid biosynthesis, adipogenesis, sphingolipid metabolism, cholesterol and lipid homeostasis, peroxisome proliferator activated receptor alpha (*PPARα)*), endodermal and cellular differentiation and TGF-β signalling.

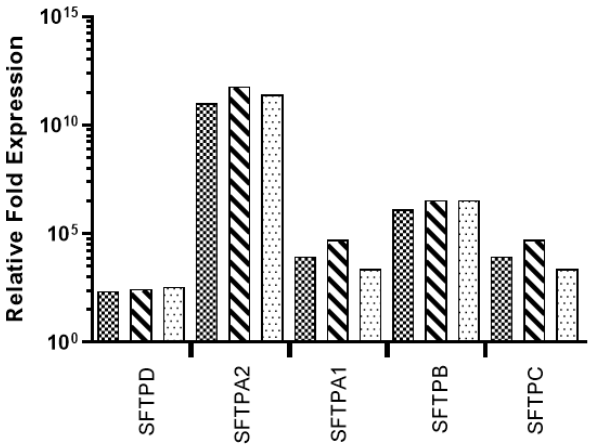

Figure 4.8. The pattern of expression of surfactant protein genes in human primary ATII isolated from three separate donors.
RNA was prepared from ATII cells isolated from three donors for QRT-PCR for *SFTPD*, *A2*, *A1*, *B* and *C* with *ATP5B* and *TOP1* as reference genes. Donor 1 (chequered bars), Donor 2 (hatched bars) and donor 3 (speckled bars). RNA from Donor 2 ATII was used for RNA micro array analysis. *SFTPD*, *A1*, *B* and *C* expression was normalised to log phase A549 cells. *SFTPA2* expression was relative to 25 day differentiated A549 cells. A549 data are not presented on the graph.

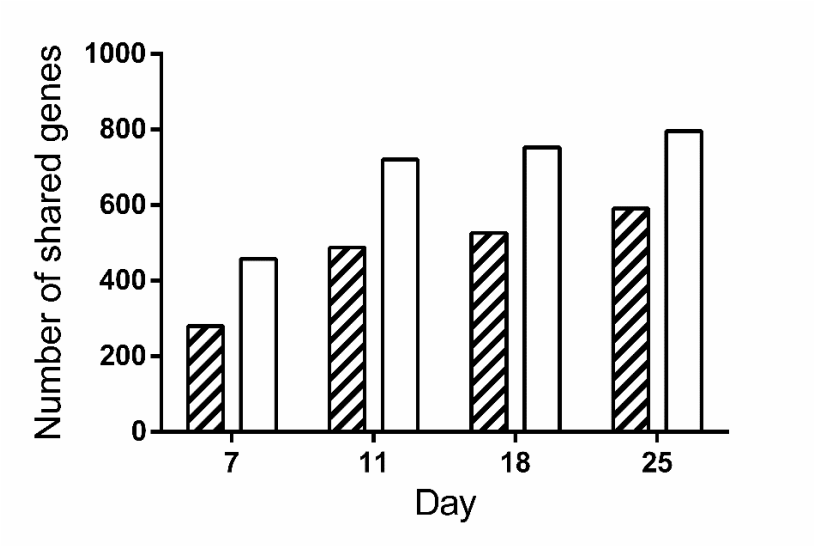

Figure 4.9. Shared regulated (≥ 2-fold) gene expression of differentiated A549 with freshly isolated human primary ATII cultures.

Gene expression in 2D A549 cells cultured for 7, 11, 18 or 25 days or primary ATII cells were compared to log phase A549 cells. The figure shows the number of shared up- (hatched bars) or down- (clear bars) regulated genes between the A549 cells and ATII cells over the 25 day A549 time course. Gene lists were extracted from Genespring™ analysis of shared up and down regulated genes. Results from a single experiment, one donor for ATII cells and three technical replicates for A549 cells.

Pathway	Wiki Pathways Reference	Most significant timepoint (Day)	P Value	Number regulated genes	Number genes in pathway
Complement cascade	WP1798 77042	25	<0.001	9	192
Human Complement System	WP2806 78589	18	<0.001	12	136
Senescence and Autophagy	WP615 71375	25	<0.001	9	106
Complement Activation, Classical Pathway	WP545 72062	25	<0.001	4	17
Complement and Coagulation Cascades	WP558 67786	18	<0.001	6	64
Adipogenesis	WP236 78584	11	<0.001	10	131
Differentiation Pathway	WP2848 78558	11	0.001	5	50
Globo Sphingolipid Metabolism	WP1424 71392	18	0.005	3	24
Sphingolipid Metabolism	WP1422 78591	25	0.006	3	21
Sphingolipid metabolism	WP2788 77079	25	0.010	4	46
SREBF and miR33 in cholesterol and lipid homeostasis	WP2011 75253	11	0.026	2	18
Ganglio Sphingolipid Metabolism	WP1423 76323	7	0.010	2	18
Regulation of Lipid Metabolism by Peroxisome proliferator-activated receptor alpha (PPARalpha)	WP2797 77088	11	0.009	6	118
TGF Beta Signalling Pathway	WP366 69026	7	0.013	3	55
TGF Beta Signalling Pathway	WP560 68944	7	0.013	3	55

Table 4.6. Statistically significant pathways considered to be associated with ATII phenotype.
Two-fold (or greater) upregulated genes shared with primary ATII cells and differentiated A549 cells over the 25-day time-course were identified by Genespring™. The table represents Genespring™ shared pathway analysis of the two cell populations.

Table 4.6 summarizes the 'shared pathway analysis' (note, in the Genespring software interface this is referred to as a "Venn Diagram" analysis, however the outputs are lists of genes, not a presentable Venn Diagram) conducted in Genespring™ of significantly regulated pathways involved in ATII differentiation shared by 25-day differentiated A549 cells and primary ATII cells as compared to a baseline of log phase A549 cells. ATP lipid transporters have been associated with the organized transport of lipids into developing MLB and are considered a key marker of ATII cells. ABCA3 was expressed in abundance in the primary ATII cells but not

significantly upregulated in the differentiated A549 cells. However, other lipid transporters were significantly upregulated in differentiated A549 cells (Figure 4.10).

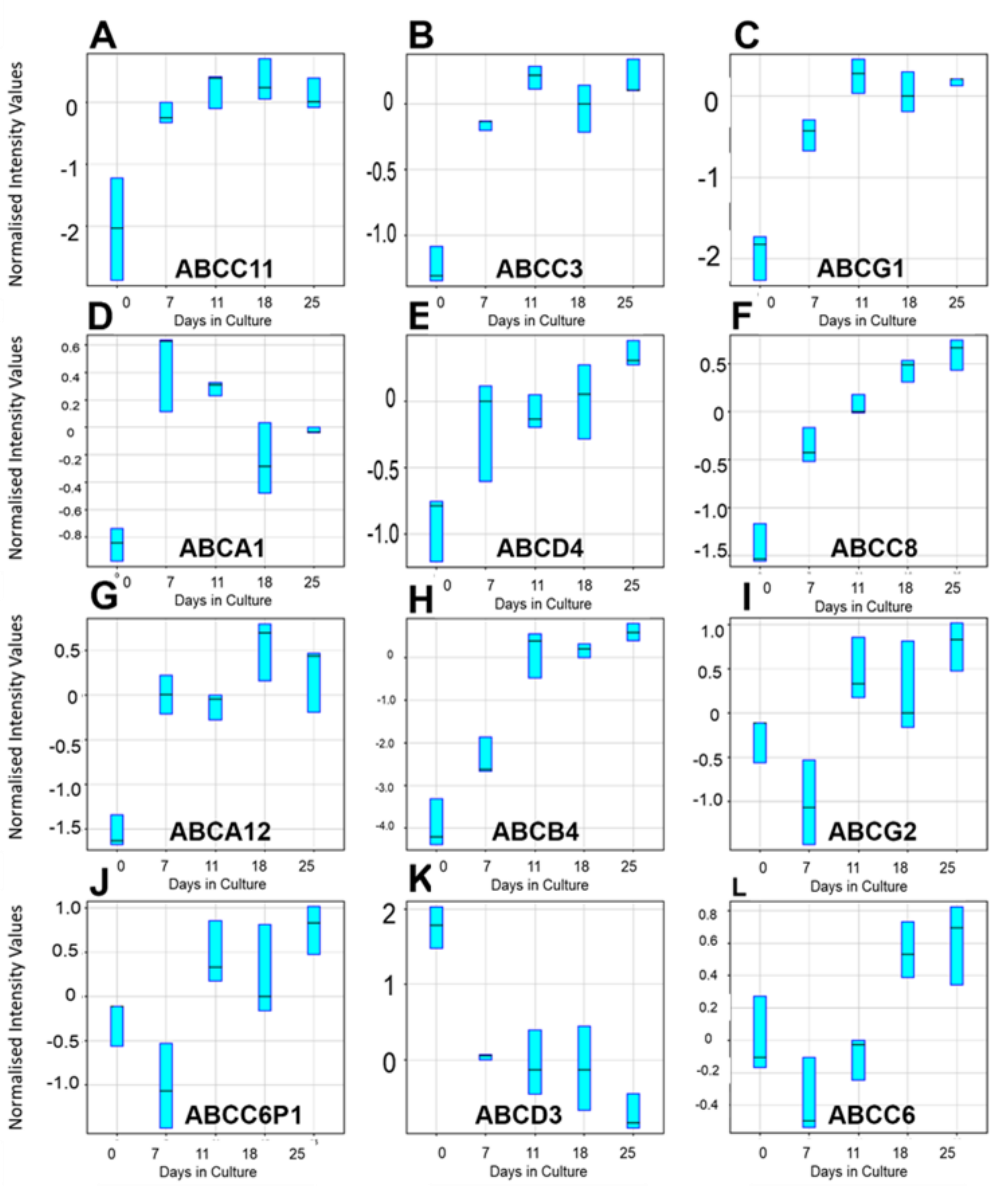

Figure 4.10. Changes in gene expression of ATP-binding cassette lipid transporters in long term A549 culture.
A549 cells were cultured for 25 days as 2D monolayers in Ham's F12/10% FBS with regular medium exchange. RNA was extracted at log phase, days 7, 11, 18 and 25 and converted to fluorescently labelled cRNA for hybridisation and analysis using Agilent® Genespring™. Intensity values for *ABCC11* (A), *ABCC3* (B), *ABCG1* (C), *ABCA1* (D), *ABCD4* (E), *ABCC8* (F), *ABCA12* (G), *ABCB4* (H), *ABCG2* (I), *ABCC6P1* (J), *ABCD3* (K) and *ABCC6* (L) were normalised to the mean intensity value of all genes on the microarray slides. Three technical replicates from a single experiment.

Gene Symbol	Up or Down Regulation in A549 Cells throughout time-course	Fold Change at Day 25 in A549 Cells	Up or Down Regulation in ATII primaries compared to log phase A549	Fold Change (ATII vs log Phase A549)
Proliferation Markers				
Ki67	Down	-5.08	Down	-15.83
PCNA	Down	-2.19	Down	-6.17
TCF7L1	Down	-5.85	N/S	
Cell Cycle Inhibitor				
CDKN1B	Up	3.05	N/S	
Lipid Metabolism				
PPAPDC1B	Up	2.45	N/S	
PPAPDC1A	N/S		Up	15.19
PPAP2A	Up	2.62	Up	7.03
PPAP2B	Up	2.90	N/S	
DGAT2	Up	3.21	N/S	
FABP5	Down	-5.96	Down	-3.6
ACSL5	Up	16.00	Up	16.00
Autophagy and Lysosomal				
ULK4	Up	3.64	Down	-3.53
LAMP2	Up	2.08	Up	3.23
LAMP3	Up	2.65	Up	16.00
PLD1	Up	2.0	N/S	
PLD2	N/S		Up	2.83
PLD5	Up	4.97	N/S	
WNT Associated Differentiation				
CASP1	Up	16.00	Up	16.00
CASP4	Up	6.28	Up	16.00
BIRC5	Down	-16.00	Down	-16.00
WNT4	Up	12.10	Up	6.12
Stem Cell Markers and Differentiation				
NANOG	Up	4.06	Up	N/S
SOX2	Up	3.19	Up	4.75
SOX9	Up	2.79	N/S	
Complement Components				
C3	Up	14.92	Up	16.00
C4B	Up	12.00	Up	9.06

Gene Symbol	Up or Down Regulation in A549 Cells throughout time-course	Fold Change at Day 25 in A549 Cells	Up or Down Regulation in ATII primaries compared to log phase A549	Fold Change (ATII vs log Phase A549)
C4BPA	Up	16.00	Up	16.00
C5	Up	6.31	Down	-3.25
Cellular Differentiation				
IL1B	Up	16.00	Up	15.56
AGT	Up	16.00	Up	9.92
PPARA	Up	3.71	Up	4.16
FST	Up	8.81	Up	7.75
BMP4	Up	13.65	Up	7.98
TGFBR2	Up	2.93	Up	2.81
ATP Lipid Transporters				
ABCA3	N/S		Up	4.26
ABCC6P1	Up	5.07	Up	16.00
ABCC3	Up	2.7	Down	-8.11
ABCG1	Up	4.35	Down	-3.44
ABCA1	Up	2.48 (Day 7)	N/S	
ABCA8	Up	4.09	N/S	
ABCA12	Up	3.45	Up	5.06
ABCB4	Up	16.00	N/S	
ABCG2	Up	2.05	Down	-16.00
ABCD3	Down	-3.30	Down	-2.67
ABCC11	Up	4.45	N/S	
Matrix Metalloproteinases				
MMP1	Up	5.76	Up	16.00
MMP15	Down	-3.45	N/S	
MMP7	Up	6.65	Up	2.98
MMP9	Down	2.41	N/S	

Table 4.7. Genes Related to ATII Differentiation.
Comparison of genes related to ATII differentiation in 25 day differentiated A549 cells grown in F12 compared to ATII Primary Cells using the gene expression of log phase proliferating A549 cells as a baseline.

Finally, Table 4.7 provides a summary of the regulation of at the gene level of shared genes associated with ATII differentiation over the 25-day differentiation in A549 cells and primary ATII cells as compared to a baseline of log phase A549 cells.

4.3.3 Histochemistry and Electron Microscopy

To confirm the presence of lipidogenesis and possible MLB formation, differentiated A549 monolayers were stained with Oil-red-O. This showed that lipid production increased over the time course of differentiation (Figure 4.11 A-D) and was manifested by an increase in number and size of lipid inclusions, with more than half of the cells in the monolayer at day 18 showing evidence of lipid containing bodies. However, from this staining it was not possible to discriminate MLB from oil droplets within the cells. Therefore, TEM microscopy was performed to assess the ultrastructure of the lipid droplets. At day 11, lipid droplets appeared as uniform structures with no evidence of MLB formation (Figure 4.12 A and C). However, by day 21 of differentiation, the lipid containing structures showed clear evidence of MLB formation (Figure 4.12 B and D) with a distribution similar to that identified by the oil red-O staining.

A differential count of 164 cells in TEM micrographs of long term differentiated A549 cells showed that 90 (54.9%) of the cells examined contained MLBs.

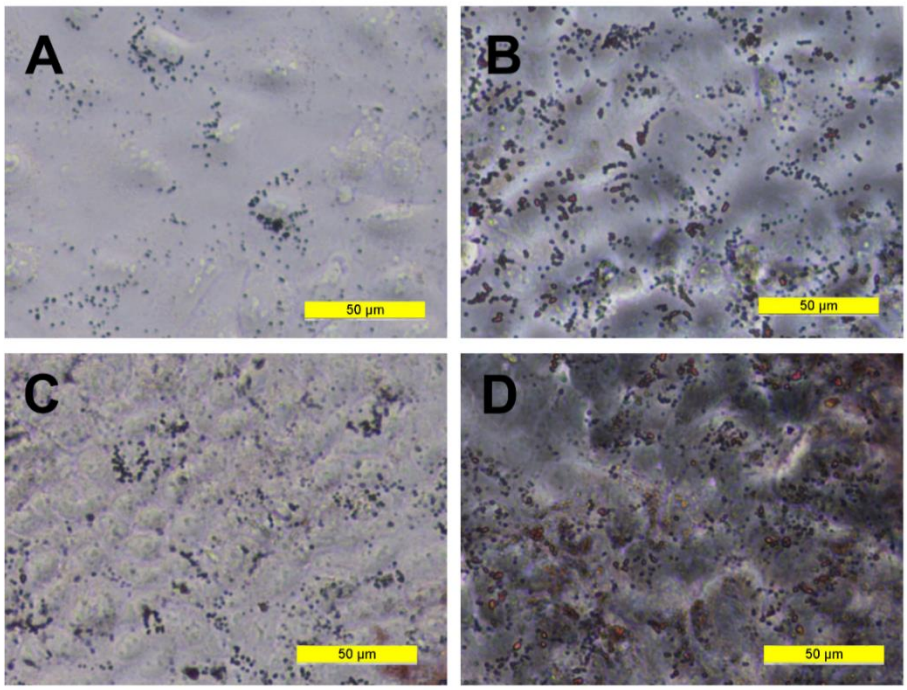

Figure 4.11. Oil-Red-O Staining of a time-course A549 monolayers cultures.
A549 cells were cultured in Ham's F12/10% FBS in flasks for 18 days. Monolayer cultures were fixed and stained with Oil-Red-O for lipid droplets in log phase (A), day 7 (B), day 11 (C) and day 18 (D). Data from a single experiment.

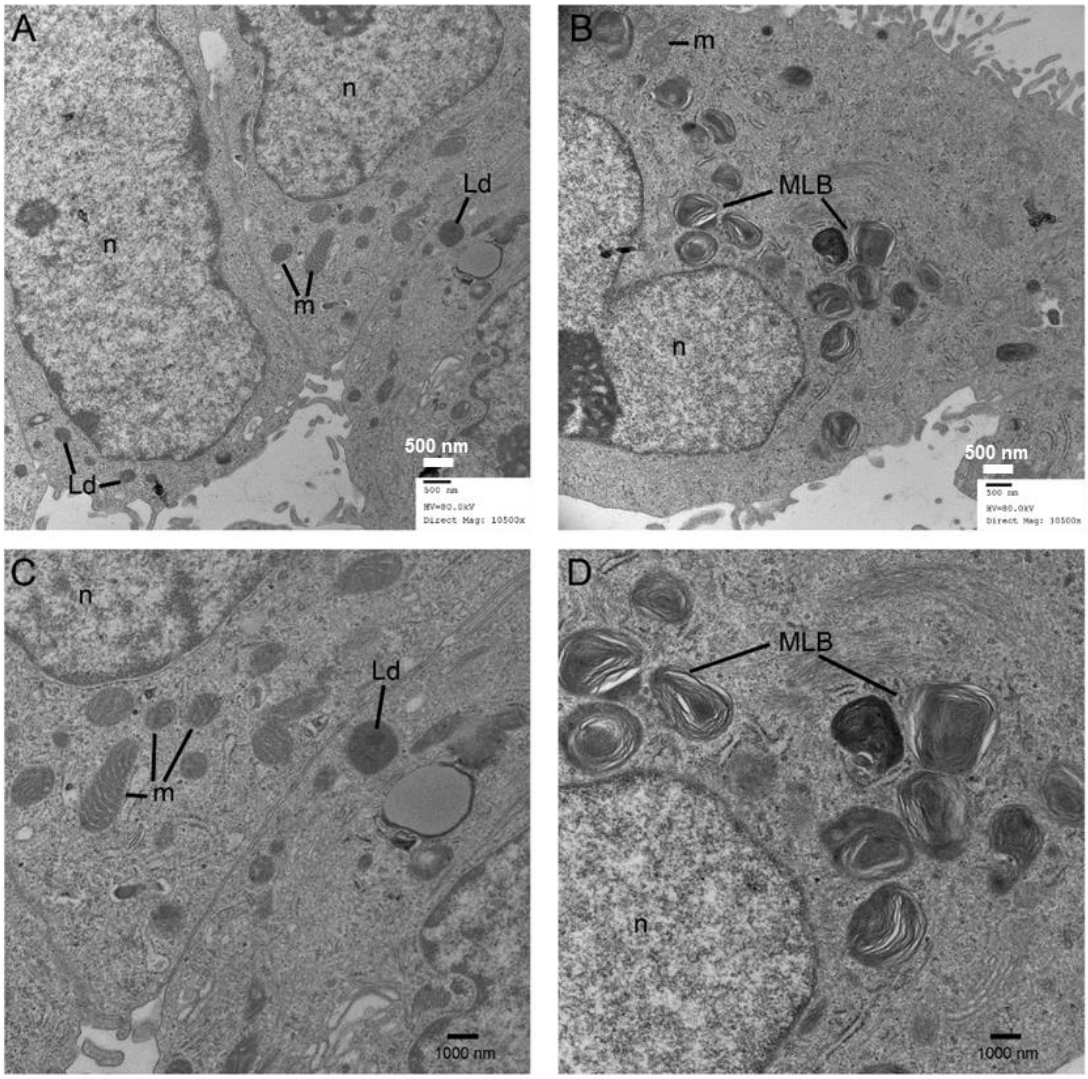

Figure 4.12. Electron Micrographs Showing Multilamellar Body Expression in A549 Cells.

A549 cells were cultured as 2D monolayers in Ham's F12/10% FBS for 21 days with regular medium exchange. Cells were scraped from the flasks, fixed (glutaraldehyde), embedded in resin (Araldite™), sectioned and stained with osmium tetroxide and uranyl acetate prior to transmission electron microscopy (TEM). Images show typical ultrastructural features at 11-days (A and B) and 21 days (C and D). 'MLB': multilamellar body; 'm': mitochondrion; 'n': nucleus; 'Ld' lipid droplet. Data from a single experiment.

4.3.4 QRT-PCR Evaluation of *MUC5AC* Gene Expression

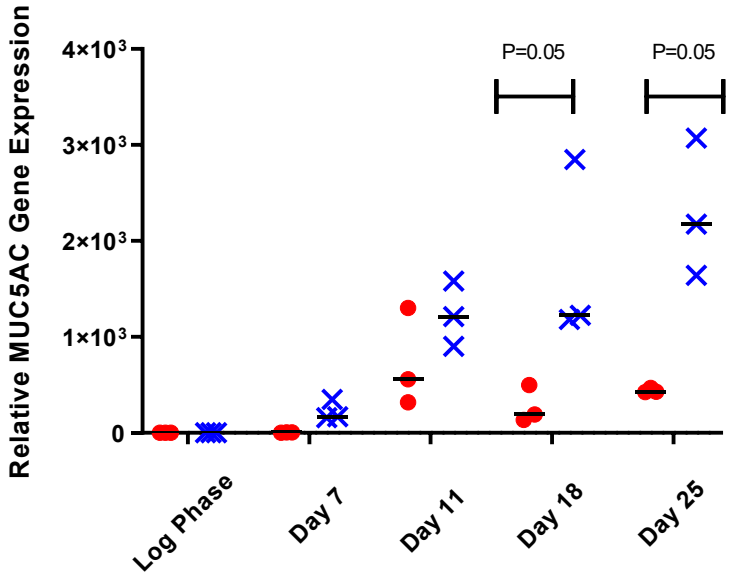

Figure 4.13. *MUC5AC* expression QRT-PCR by in A549 cells cultivated as 3D Spheroids and 2D Monolayers over a 25-day time-course.
A549 cells were grown in Ham'sF12/10% as spheroids (blue crosses) or as 2D monolayers (red dots) for 25 days with regular medium exchange. At days 7, 11, 18 and 25 spheroids RNA extraction and QRT PCR analysis was carried out using TaqMan™ primer/probe sets specific to human *MUC5AC*. Expression was normalised *TOP1* and *ATP5B* reference genes and further normalised to Log Phase 2D A549 cells. Data from single experiment. Statistical testing (Mann-Whitney test).

As was demonstrated in Chapter 1, cultivation of A549 cells in 3D spheroid culture resulted in a mucin secreting phenotype. Gene expression analysis by QRT PCR comparing 3D and 2D long-term cultivated A549 cells demonstrated that there was significantly greater *MUC5AC* gene expression in the 3D spheroid cultures than 2D (Figure 4.13) supporting the inference that long term 2D culture was driving the cells to a different phenotype.

The expression of a panel of genes considered to be of interest in their association with an ATII differentiated state, host defence, cell cycle arrest and tumour phenotype from the 3D cultivated cells was compared between the 3D cultivated cell in chapter 1 and the 2D cultivated cells from chapter 2. A table comparing the fold induction of these genes is included in Appendix 1 where it can be seen that that although the general pattern of gene regulation follows a similar pattern in the 2D and 3D cultivated cells there are large differences in the 3D spheroid cultures' expression *CEACAM 6* and *7* indication potential increased host resistance or tumour phenotype in the 3D cells and the less pronounced down regulation of the *Ki67* proliferation marker in 3D cultivated cells.

4.4 Discussion

This study reports that long term culture of A549 cells in Ham's F12 medium resulted in substantial suppression of genes involved in cell division in association with significant up-regulation of genes involved in autophagic, differentiation and lipidogenic pathways. There were also increased numbers of up- and down-regulated genes shared with primary ATII cells isolated using conventional methodology[312] suggesting adoption of some ATII characteristics including multilamellar body (MLB) development, a feature which was confirmed by electron microscopy. This work defines a set of conditions for promoting ATII differentiation characteristics in A549 cells that may be advantageous for functional studies with these cells. Novel alternative methods for ATII preparation have been defined from which future studies may benefit[402].

The evidence for the A549 cell line's suitability as an ATII model is conflicting and is not fully explored in contemporary literature. The cell line was originally reported to have morphological and ultrastructural similarities to ATII cells. As long ago as 1978[19], Shapiro *et al* showed that by three weeks in continuous culture, cell division in A549 cells, as measured by DNA content, was low and the authors considered the cells as 'differentiated' as confirmed by the expression of high numbers of MLB similar in phospholipid content to those found in primary lung tissue. These findings were later supported by Nardone and Andrews[310].

It is now well established that environmental factors such as choice of substratum, medium and continuous culture can have a substantial impact on the phenotype and gene expression. For example epithelial differentiation can be induced in continuous cell lines such as CaCo2[335] and MDCK[336] through the application of well-defined long term cell culture conditions. From the literature, it is evident that pulmonary researchers have not been consistent in the formulation of cell culture medium used in their experiments nor with the phase of growth from which the A549 cells are used. The cell line was originally isolated using RPMI medium[19] yet subsequent researchers have used a number of different media with little or no justification for their choice. By way of example, concerns for the cell line's suitability were raised in 1980[346] with A549 cells cultivated in DMEM and subjected to a 10 day differentiation period. In this case, the MLB content of the cells could be increased with 2 days of serum starvation, however, the lipid content of these A549 cells differed significantly from freshly isolated rat primary ATII cells and the authors advised that the cell line should be considered as a model of ATII dysfunction. More recently, using Raman spectroscopy to investigate the biochemical characteristics of A549 cells, Swain *et al*[347] cast further doubt on the A549 cell line's performance as an ATII model but used cells grown in DMEM. Heijink *et al*[348] also reported functional deficiencies of the cell line using cells grown in RPMI 1640

medium. Based on the observations that DMEM supports a proliferative phenotype even in long term culture, it is possible that inconsistency in the choice of medium and/or culture duration used for A549 experiments may contribute to variability in phenotypic properties. This highlights the need for standardization in the use of A549 cells, and speaks to a larger problem that has been identified in life science research[403].

One of the key roles of ATII cells *in vivo* is to secrete surfactant, thus surfactant lipid production and evidence of MLB biogenesis in A549 cells, as originally reported[308] is supportive of their suitability as an ATII model. Lung surfactant has a role in immune protectiveness and the production of complement[404] and the finding of up-regulated gene expression of *C3*, *C4b* and *C5* suggest the synthesis of components of the classical and alternate complement pathways by the long term A549 cell cultures consistent with their differentiation into a more ATII-like phenotype.

It is generally accepted that MLB biogenesis can be achieved by *de novo* synthesis of DPPC or alternatively through cellular autophagy[394 274]. Since MLB are thought to be lysosomal in origin, the expression of the Lysosomal Associated Membrane Proteins (*LAMP*) *2*, and *3*[274 405] and the lytic phospholipase enzymes *PLD1* and *5*[394] observed in the present study suggest that the long-term A549 cultures are developing lysosomes. These data and pathway analyses further support the involvement of autophagy in MLB biogenesis with upregulation of autophagic pathways including the autophagy gene *ULK4*[406] in the long term A549 cultures. Autophagy seems to be an important process in the early development of the lung in particularly in the intervening period of starvation between birth and nutrient supply from maternal lactation. Autophagy provides a nutritional bridge at this critical stage at which point the lung has to adapt from an environment of amniotic fluid to breathing air and the immediate secretion of surfactant from MLBs[407]. Failure to respond in this manner can lead to infant respiratory distress syndrome[408] and mice with targeted deletions of individual autophagy genes such as *ATG16L1*[409 410] have high mortality rates in their offspring.

Lipid and fatty acid (FA) precursors for DPPC are not only derived from autophagy in the development of MLB, they can also be synthesized *de novo*. In adults it is thought that FAs are sequestered from the circulation via Fatty Acid Binding Proteins (FABP)[263], however these data show that *FAB5* is down regulated throughout the A549 time course and in primary ATII cells, perhaps indicating that there are insufficient FAs provided in the culture medium or that the cells have switched to autophagic and biosynthetic generation of FAs. The significant upregulation of genes involved in lipid biosynthesis and metabolism support this hypothesis.

Membrane bound ATP lipid transporters, for example *ABCA3*[269], have been associated with the organized transport of lipids into developing MLB and are considered a key marker of

ATII cells. Although *ABCA3* was not significantly upregulated in the differentiated A549 cells, other ATP lipid transporters are involved MLB formation and surfactant production. For example *ABCA1*, *2*, *3*, and *5*, have been implicated[411] and *ABCA2* has been shown to be associated with the limiting membranes of MLB while other work has demonstrated that ABCA1 is enriched in the lung[412]. The results presented here from long-term cultures of A549 cells show the upregulation of several candidate ATP Lipid transporters that could play a part in MLB assembly.

Analysis of up-regulated genes that are shared between primary ATII cells and differentiated A549 confirmed that over the 25-day time-course of differentiation the A549 cell line became more similar in terms of gene expression to the ATII cells than log phase A549 cells. However, while the 25-day differentiated A549 cultures are more similar to primary ATII cells there are still many differences. This may be because A549 cells retain an abnormal phenotype as a consequence of their malignant background, or because they consist of a phenotypically heterogeneous population possibly due to the presence of cancer stem cells with the potential to differentiate to ATII or non-ciliated bronchial cell types[349]. Increases in expression of the progenitor cell markers *SOX2*, *SOX9* and *NANOG* in A549 cells seen in the present study could be indicative of the presence of a stem cell or cancer stem cell population[413]. This supposition is further supported by the upregulation of two key genes as shown in Figure 26. The G Protein Coupled Receptor *LGR6*, a receptor for R-spondins, potentiates Wnt/β-Catenin signalling and has been associated with stem cells and lineages[414]. E Cadherin (*CDH1*) expression is also upregulated throughout the time-course in both 2D and 3D cultivated A549 cells. Ruiz *et al* (2014) identified a subset of human lung cells that express elevated levels of LGR6 and CDH1. These cells were categorised as potential lung stem cells (LSC) and subsequently demonstrated the ability to differentiate into airway epithelia[415]. The expression of these stem cell markers suggests a certain plasticity in the A549 and the potential to further differentiate to an ATII like state under the influence of appropriate stimuli.

To further demonstrate the potential advantage of the 2D cell culture system over the 3D spheroid system as presented in Chapter 1, QRT-PCR data for *MUC5AC* expression and RNA microarray analysis data were compared. These data are shown (Figure 4.13) where it can be seen that *MUC5AC* gene expression was significantly lower in 2D cultured A549 cells, further demonstrating that the mucin producing property of the spheroid cultures is less dominant in the 2D cultures. Data in Appendix A showing fold changes of gene expression in 25 day differentiated 2D and 3D cultures clearly demonstrates that both *CEACAM 6* and *7* genes are upregulated by two orders of magnitude in 3D cultures as opposed to 2D and downregulation of markers of proliferation is greater in 2D cultures. Upregulation of other genes in the 2D

cultures and the cell count and viability data presented in Figure 4.3 indicated that although the 2D cultures had reduced expression of markers of proliferation, they were still viable and metabolically active and not simply non-viable.

As with all models, recapitulation of the *in vivo* state is imperfect but the aim is to reproduce, as faithfully as possible those aspects of the physiology (or pathology) that are being investigated. The gene expression data of the A549 time-course, the upregulated pathways and genes shared with primary ATII cells together with the confirmatory TEM data demonstrates the definition of a reproducible and standard set of conditions for promoting ATII differentiation characteristics in A549 cells. In conclusion, it is suggested that whereas proliferating log-phase A549 cells are most suitable for cancer biology studies, the new long term culture system might be more suitable for studies requiring a more representative and continuous source of ATII-like cells.

Data in Appendix C shows differences in gene regulation between long term 2D A549 cultures and 25-day A549 3D spheroid culture.

4.4.1 Summary

- An attempt to better model alveolar epithelium using A549 cells was explored through the use on long term 2D cell culture.
- The effects of DMEM and F12 were investigated in the long-term culture of A549 cells in 2D.
- Over a 25-day time-course F12 medium was found to generate quiescent, growth arrested, viable, confluent monolayers that appeared contact inhibited and exhibited evidence of cellular differentiation, whereas use of DMEM resulted in non-contact inhibited, overgrown cultures with significantly higher cell densities that were not growth arrested.
- RNA Microarray analysis of long term F12 cultured monolayers compared to log phase A549 cells showed a down regulation of cellular proliferation markers and up regulation of cell cycle inhibitors. Markers of epithelial and ATII differentiation were upregulated and there was increasing significant overlap of gene expression between the long term cultured A549 cells and primary ATII cells compared to log phase A549 cells. This included gene involved in the biosynthesis of multilamellar bodies (MLB), the hallmarks of ATII cells.
- The expression of MLB in the long term, 2D, Ham's F12 cultured A549 cells and therefore confirmation of the adoption of an ATII-like phenotype, was corroborated by histological and transmission electron microscopic analysis.

- Comparison of gene expression profiles and QRT PCR for mucin expression of the long-term 3D A549 spheroid cultures from Chapter 1 and the long term 2D A549 cultures from Chapter 2 confirmed the adoption of two distinct cellular phenotypes from the 2D and 3D methodologies.

5. The Suitability of a Novel E-Cadherin/LGR6 Expressing Lung Progenitor Cell Line 'TRiP WT' in Alveolar Type 2 Research

5.1 Introduction

As has been discussed previously human stem cell derived models offer huge potential for the development of differentiated cell models[416 417] and human induced pluripotent stem cells[306] offer the possibility of the generation of both disease and patient specific *in vitro* models. However, the specialised expertise and timelines required to differentiate cultures from pluripotent progenitors through the required developmental intermediaries and then to qualify the final cellular models[306 418] render them unsuitable for shorter-term projects such as this one.

An alternative approach proposed here to develop alveolar epithelial cells is to use pre-developed lung progenitor cell lines that are already committed to an airway lineage.

Cadherin-1 (also known as CAM 120/80, epithelial cadherin (E-cadherin) or uvomorulin) and Leucine Rich Repeat Containing G Protein-Coupled Receptor 6 (LGR6) are markers for epithelial stem cells[147 419]. A novel E-Cadherin and LGR6 expressing lung progenitor cell line isolated from a healthy human lung tissue biopsy was reported by Oeztuerk-Winder *et al*[420] and Ruiz *et al*[415]. The authors demonstrated these cells could be grown in culture in the form of loosely adherent suspension aggregates for over 50 passages. These *in vitro* cultures expressed both stem cell markers (LGR5 and 6, Sox9 and Integrin a6) together with the airway epithelial markers: surfactant protein C (SFTPC), Club Cell Protein (CC10) also called uteroglobin, urinary protein 1 or (historically) Clara Cell Secretory Protein) and Aquaporin-5 (AQP5). When cultured on laminin and fibronectin the cells adopted a monolayer phenotype and tended to express SFTPC suggesting the adoption of an alveolar-like phenotype. The authors explored the regenerative potential of the cells by injecting green fluorescent protein (GFP) labelled cells into human lung explants with pre-induced bleomycin injury and into bleomycin treated mice. The labelled cells replenished damaged cells at the site of injury in the alveoli and also appeared to migrate to the bronchial tissues, adopting ATII and Club cell morphologies and expression of SP-C and CC-10 respectively. Preliminary results were presented where "ATII–like" cells were generated *in vitro* by culturing the cells on laminin and fibronectin[420].

It was postulated that culturing the E-Cad/LGR6 cells on adherent matrices together with the long-term cell culture approach previously employed for A549 cells with treatment with

factors used for stem cell differentiation such as EGF, FGF, KGF and WNT might drive an ATII phenotype with more physiologically relevant properties than the A549 derived model. The major advantage being that the E-Cad/LGR6+ cells have over iPSC cells is that they are already committed to a bronchio-alvleolar lineage.

The work by Oeztuerk-Winder *et al* creating and characterising the E-Cad/LGR6+ cell line was funded by grants from the Medical Research Council (MRC) and Cancer Research UK (CRUK). In accordance with this funding the cell line was made available by the originating authors through Ximbio (London UK), a non-profit organisation established by CRUK to enable researchers to share research reagents, including cell lines. https://ximbio.com/reagent/152715/human-lung-stem-cell-line The cell line and its derivatives are also listed on the Cellosaurus[285] database: https://web.expasy.org/cellosaurus/CVCL_AS77

When novel cell lines are developed, and reported in the literature, other researchers will desire access to these cells for their own work and it is important that any laboratory receiving cells from another properly characterises and tests the cell lines for authenticity. The objective of organisations such as Ximbio and culture collections such as ECACC is to ensure that cellular reagents can be transferred from laboratory to laboratory and fidelity is preserved. The principles described here should be followed as basic good cell culture practice[292].

Acquisition of a cell line from another laboratory presents challenges as the cells acquired may have lost their reported phenotypic properties or simply not be what they are claimed to be[421]. The need for validation of cell lines is often overlooked by the scientific community[421]. Key issues of cell-line misidentification, contamination with microorganisms (principally mycoplasma) and genetic and phenotypic instability continue to affect cell culture based research with significant financial, scientific and reputational impact. These issues are believed to contribute to irreproducibility of biomedical research and can drive the initiation of further questionable studies[292] .

Problems with cell line misidentification have been known for decades[294]. They arise through the simple fact it is relatively easy to accidentally mix up two different cell lines by sub-optimal laboratory technique or even through mislabelling; a rapidly multiplying cell line will soon outgrow a slower growing cell and it not easy to distinguish one cell line from another using basic microscopy[422]. The issue was first unearthed through discoveries of HeLa cell contaminations in the 1960s[423] but even in contemporary times, misidentification continues to severely damage biomedical research, with recent revelations of cross-contaminations and use of misidentified cell lines[295] [424]. As an example, KB cells, originally described as oral or

squamous epithelioid carcinoma cells, were conclusively discovered to be HeLa in the 1960s[423] yet in 574 recent articles they were only correctly described as HeLa in 57[425]. The extent of cell line misidentification is estimated between one fifth and one third of all cell cultures used in labs globally[426]. To add to the problem, misidentified cell lines are continually used under their original, false, identities, long after they have been revealed[427], whilst other researchers, oblivious to the issue, continue to cite results to unwittingly perpetuate the problem. The consequences of false findings based on misidentified cells are severe and costly[428] with grants, patents and erroneous drug trials based on misidentified cells. For example, the frequently used oesophageal adenocarcinoma cell lines SEG-1 and BIC-1 and the SK-GT-5 are, in reality, cell lines derived from other tumour types. Results based on these contaminated cell lines have led to flawed clinical trials, more than 100 potentially invalid scientific publications, National Institutes of Health (NIH) cancer research grants and 11 US patents[429]. Recently the extent of the problem has been more widely acknowledged, with several calls for immediate action by the editorial boards of journals [425] [430] yet, despite calls to action, the issue remains unresolved.

The commonly used technique for the authentication of human cell lines is short tandem repeat (STR) profiling originally developed for forensic applications. For more details, see Chapter 2, Materials and Methods. In short: repeated sequences in human DNA (STR loci) are amplified using PCR. The PCR products using a capillary based sequencer with size standards to produce an electropherogram which is subsequently analysed using proprietary software. The result is a numerical code corresponding to the lengths of the PCR products amplified at each locus accurate to less than one base pair, each score at specific locus refers to the number of times the STR is repeated and represents an allele. As each individual inherits a chromosome set form each parent, the allelic scores will be a single number for each locus (homozygous) or there will be two scores (heterozygous). The advantage of this technique is that there are dozens of potential allele scores for up to 32 loci meaning that the chances of any two different people or human cell lines having the same or very similar STR profiles are billions to one. The only people who have identical STR profiles are homozygotic twins[332] [333].

There are many advisory texts on the validation of cell lines, such as the Guidelines for the Use of Cell Lines in Biomedical Research[292] and there are some clear checks that should be observed when deriving and acquiring cell lines:

- Cell Line designation: the cell line should have a unique and unambiguous cell line name
- Confirmation of origin of human cell lines: samples of tissue or DNA should be taken from the donor and a Short Tandem Repeat (STR) profile generated. This provides a baseline for checking subsequent cell line authenticity. The identification of cell lines

should be regularly checked, for example when being transferred to another lab, at the beginning, during and at the end of studies Screening for cryptic contamination (mycoplasmas and viruses): Mycoplasmas are small bacteria that associate with animal cells. Individual mycoplasma bacteria can outnumber those of the cell culture by several orders of magnitude and can alter the metabolic and phenotypic responses of cell cultures whilst going unnoticed thus invalidating results. Mycoplasmas can only be detected using metabolic, PCR or specialised growth techniques.

It was expected that following initial validation of the E-Cadherin/LGR6 'TRiP WT' cell line through authentication mycoplasma testing, the cell line would have advantaged over A549 cells. It was intended to treat the cells with the corticosteroid dexamethasone and the signalling molecule neuregulin-1β (NRG-1β) and determine their effects on AT-II like differentiation. Then, attempt to further differentiate A549 cells closer to an ATII phenotype by through co-culture with foetal lung fibroblasts (MRC-5) and ultimately,

combine co-culture conditions that present the most potential for ATII differentiation in A549 cells into 3D Alvetex™ Scaffold.

5.2 Hypothesis

It was hypothesised that the E-Cad/LGR6+ lung progenitor cells, a potential *in vitro* model for human ATII cells, were an authentic, unique human cell line and free from mycoplasma contamination.

5.2.1 Aims

- To validate the E-Cad/LGR6+ cell line by determining the uniqueness of the cells by STR profiling and to determine the mycoplasma status of the cells.
- Once validated take the cell line forward for ATII differentiation assessment.

5.2.2 Objectives

- Resuscitate and cultivate the cell line and determine if the cell line is contaminated with mycoplasma by testing using the indirect Hoechst DNA staining method and by PCR using specific mycoplasma specific PCR primers.
- Submit samples of cells for short tandem repeat (STR) analysis using proprietary multiplex PCR kit(s). Determine the STR profile of the cells using a capillary analyser (sequencer) and use Genemapper™ software to interpret the resulting electropherogram(s).
- Compare the obtained STR profile and with on-line bioinformatics databases of known cell line STR profiles to determine the authenticity of the cells.

5.3 Results

Two vials of the cells were received from Ximbio labelled: "TRiP WT" (not E-Cad/LGR6+). The vials were also labelled "Post MycoP Treatment". In order to clarify this discrepancy, the first author of the paper and the Professor leading the laboratory (Professor Juan-Jose Ventura) were contacted. Email communication clarified the cells were those referenced in their 2012 paper[420]. The cell line name was derived for internal control in the lab reflecting the capacity of the cells to grow and differentiate under the kidney capsule as "a trip to another location". The authors also confirmed that the cell line had previously been tested positive for mycoplasma contamination (test unknown) however an attempt had been made to eradicate the contamination using Plasmocin (Invivogen, Toulouse, France).

The cell line was resuscitated in the specialised RHB medium (see materials and methods) as prescribed and cultivated for submission to human STR profiling and mycoplasma testing by PCR analysis, Hoechst staining and culture isolation.

5.3.1 Mycoplasma Testing

Testing cell cultures for the presence of mycoplasma is an important aspect of good cell culture practice[317]. As mycoplasmas can alter cell line gene and protein expression, alter cellular metabolism, induce chromosomal damage and change cell surface receptor expression amongst many other detrimental effects. As mycoplasma infections are difficult, if not impossible, to eradicate, infection is generally considered to invalidate a cell culture[431]:

Samples of the cultures were submitted for Mycoplasma testing by the European Collection of Cell Cultures (ECACC) (Salisbury UK) by PCR with mycoplasma specific primers (5' GGG AGC AAA CAG GAT TAG ATA CCC T 3' and 5' TGC ACC ATC TGT CAC TCT GTT AAC CTC 3')[334] (see materials and methods) demonstrated that the TRIP WT cells were infected with mycoplasma (Figure 5.1).

Mycoplasma contamination in TRiP WT cells was confirmed by ECACC by a secondary confirmatory test by inoculating supernatant from the cell line onto coverslips of Vero Monkey Kidney cells in multi-well plates and incubating them for 3 and 5 days in a humidified CO_2 incubator at 37°C. Subsequent staining with the DNA specific stain Hoechst AG 33258™ and fluorescent microscopy demonstrated the presence of typical mycoplasma staining as visualised against the Vero cell cytoplasm (data not shown).

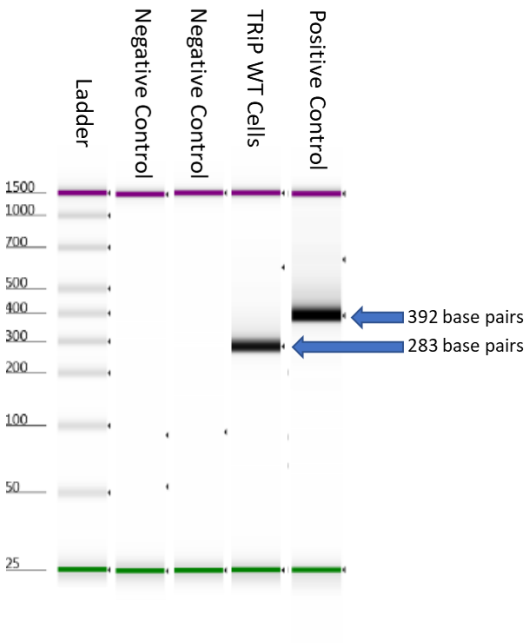

Sample ID	Expected Amplicon Size	Estimated Amplicon Size (Bio-Analyser)	Conclusion
Negative Control 1	N/A	N/A	Negative - Pass
Negative Control 2	N/A	N/A	Negative - Pass
TRiP WT Cells	255-285 bp	283 bp	Positive for mycoplasma; no positive control carry-over - Pass
Synthetic Positive Control	392 bp	392 bp	Positive - Pass

Figure 5.1. Mycoplasma PCR testing of TRiP WT.
Left-hand panel is a visualisation of the Agilent® Tapestation™ Bio-analyser electropherogram data showing no amplification in the two negative control lanes where water was added in place of DNA template. The positive assay control was a synthetic 506bp double stranded DNA construct (Life Technologies) with target sequences for the mycoplasma PCR primers designed to generate a 392bp product. Due to the genetic variability between different mycoplasma spp the expected amplicon size for positive results is in the region of 255-285bp. The positive assay control amplicon is a different size to that of a positive sample to identify any "false positive" results caused by carry-over of the positive assay control. The right-hand panel summarises the testing.

5.3.2 STR Profiling

Two vials of TRiP WT cells were resuscitated on two independent occasions and immediately after resuscitation samples of the cultures were dispensed onto FTA cards (Whatman)[321] and submitted to Northgene (Newcastle UK) for STR profiling using Powerplex 16 (Promega 16 locus STR kit that includes the gender marker amelogenin. The electropherograms were initially electronically analysed using GeneMapper software (ThermoFisher) and then manually verified. To screen the profiles of the TRIP WT cells the STR profiles were electronically uploaded to a database of 6,790 known STR profiles (Cellosaurus CLASTR STR Similarity Search Tool)[432] for comparison to determine if there were potential matches with other cell lines. An immediate potential match was identified with the cell line 293. The results are represented in Table 5.1.

Marker	293 reference profile (ECACC)			TRiP WT Vial 1			TRiP WT Vial 2			A549 reference Profile (ECACC)	
	Allele 1	Allele 2	Allele 3	Allele 1	Allele 2	Allele 3	Allele 1	Allele 2	Allele 3	Allele 1	Allele 2
AMEL	**X**			**X**			**X**			**X**	Y
CSF1PO	11	**12**		**12**			**11**	**12**		10	**12**
D13S317	**12**	14		**12**			**12**			11	
D18S51	**17**			**17**			16	**17**		11	12
D5S818	**8**	**9**		**8**	**9**		**8**	**9**		11	
D7S820	**10**	**11**	**12**	**10**	**11**	**12**	**10**	**11**	**12**	8	**11**
TH01	7	**9.3**		**9.3**			**9.3**			8	**9.3**
TPOX	**11**			**11**			**11**			8	**11**
vWA	**16**	19		**16**	18	17	**16**	18			14
D16S539	**9**	13		**9**			**9**			NT	NT
D21S11	**28**	30.2		**28**			**28**			NT	NT
D3S1358	15	**17**		16	**17**	18	16	**17**	18	NT	NT
D8S1179	**12**	**14**		**12**	**14**		**12**	**14**		NT	NT
FGA	**23**			**23**			**23**			NT	NT
Penta D	9	**10**		**10**			**10**			NT	NT
Penta E	**7**	**15**		**7**	**15**		**7**	**15**		NT	NT

Table 5.1. STR Locus Alleles of 293 cells and samples of DNA taken from two independent resuscitations of vials of TRiP WT cells.
The reference core loci STR profile of A549 cells is included to demonstrate the dissimilarity of another human cell line to both TRiP WT and 293 cells Matching alleles in red. (NT=Not Tested).

Superficial observation of the STR profiles of the two vials of TRiP WT and the reference profile of 293 cells in Table 5.1 show a striking similarity where matching alleles are shown in bold and red immediately indicating the possibility of a cross contamination event. The "Core" alleles (believed to be the minimum for cell line authentication[433]) are highlighted in the blue area in the top half of the table. There are, however some differences. Using the match algorithm percentage matches of the samples within 'core loci' were calculated as described in Table 5.2, Table 5.3, Table 5.4 and Table 5.5.

293 vs TRiP WT Vial 1 (Core Loci)	
Total Number of alleles in test sample	14
Total Number of alleles in Reference Sample	16
Number of Shared Alleles	12
Percentage match	**80**

Table 5.2. Match score calculation for 293 vs TRiP WT Vial 1 (Core Loci).

293 vs TRiP WT Vial 2 (Core Loci)	
Total Number of alleles in test sample	15
Total Number of alleles in Reference Sample	16
Number of Shared Alleles	13
Percentage match	**84**

Table 5.3. Match score calculation for 293 vs TRiP WT Vial 2 (Core Loci).

TRiP WT Vial 1 vs TRiP WT Vial 2 (Core Loci)	
Total Number of alleles in test sample	14
Total Number of alleles in Reference Sample	15
Number of Shared Alleles	13
Percentage match	**90**

Table 5.4. Match score calculation for TRiP WT Vial 1 vs TRiP WT Vial 2 (Core Loci)

293 vs A549 (Core Loci)	
Total Number of alleles in test sample	15
Total Number of alleles in Reference Sample	16
Number of Shared Alleles	5
Percentage match	**32**

Table 5.5. Match score calculation for 293 vs A549 (Core Loci).

Using Core Loci the match algorithm for both vials of TRiP WT cells matched the 293 cells by 80 and 84% indicating that they are a consistent match from the same donor, i.e. both same lines have either come from the same donor, or there has been a cross contamination event.

The two vials of TRiP WT matched each other by 90% confirming them as genotypically from the same donor. This higher percentage indicated that the cells from the vials were likely to be genotypically more similar to each other than they were to the reference 293 cells.

As the match was at the lowest range of the percentage score the match algorithm was widened out to include all 16 of the STR loci analysed as in Table 5.6, Table 5.7 and Table 5.8.

293 vs TRiP WT Vial 1 (16 Loci)	
Total Number of alleles in test sample	25
Total Number of alleles in Reference Sample	29
Number of Shared Alleles	21
Percentage match	**78**

Table 5.6. Match score calculation for 293 vs TRiP WT Vial 1 (16 Loci)

293 vs TRiP WT Vial 2 (16 Loci)	
Total Number of alleles in test sample	26
Total Number of alleles in Reference Sample	29
Number of Shared Alleles	22
Percentage match	**80**

Table 5.7. Match score calculation for 293 vs TRiP WT Vial 1 (16 Loci).

TriP WT Vial 1 vs TRiP WT Vial 2 (16 loci)	
Total Number of alleles in test sample	25
Total Number of alleles in Reference Sample	26
Number of Shared Alleles	24
Percentage match	**94**

Table 5.8. Match score calculation for TriP WT Vial 1 vs TRiP WT Vial 2 (16 loci).

Analysis of the full 16 loci demonstrated a lower percentage match between the TRiP WT vials and 293 cells, although still at a 78 and 80% match indicating an indeterminate result and the requirement of further testing.

A growing culture generated from 'vial 2' of TRiP WT cells was submitted for 24 loci analysis along with 293 cells. The results of this analysis are shown in Table 5.9 and the match algorithm analysis shown in Table 5.10.

Marker	293		TRiP WT – Passaged from Vial 2			
	Allele 1	Allele 2	Allele 1	Allele 2	Allele 3	Allele 4
AMEL	**X**		**X**			
CSF1PO	**11**	**12**	**11**	**12**	13*	
D13S317	**12**		**12**			
D18S51	**17**		**17**	16		
D5S818	**8**	**9**	**8**	**9**		
D7S820	**11**	12	**11**	10		
TH01	7	**9.3**	**9.3**			
TPOX	**11**		**11**			
vWA	**16**	19	**16**	17	18	
D16S539	**9**	13	**9**			
D21S11	**28**	30.2	**28**			
D3S1358	**15**		**15**	16	18	
D8S1179	**12**	**14**	**12**	**14**		
FGA	**23**		**23**			
Penta D	9	**10**	**10**			
Penta E	**7**	**15**	**7**	**15**		
D10S1248	**14**		**14**	15	16	
D12S391	**19**	**21**	**19**	**21**	20	
D19S433	15	**18**	**18**	17		
D1S1656	**15**	**17.3**	**15**	**17.3**	14	16
D22S1045	**16**		**16**	15		
D2S1338	**19**		**19**	18		
D2S441	**11**	**15**	**11**	**15**		

Table 5.9. STR Profile Allelic scores of Passaged TRiP WT Cells from Second Resuscitation as Compared to 293 cells using a 24 Loci STR Assay. Core loci in blue. Matching alleles are in red.

293 vs Passaged TRiP WT (24 Loci)	
Total Number of alleles in test sample	45
Total Number of alleles in Reference Sample	37
Number of Shared Alleles	30
Percentage match	**73**

Table 5.10. Match score calculation for 293 vs Passaged TRiP WT (24 Loci).

The percentage match between TRiP WT and 293 cells using the allelic scores returned by the 24 loci kit are somewhat lower than those returned by the 8 core loci comparison and by the 16 loci comparison, however the results still show a striking similarity between the 293 cells TRiP WT cells indicating a potentially indeterminate result however there are several factors that need to be taken into account:

- There may have been assay to assay variability in the running of the 24 locus and 16 locus kit and a certain amount of subjectivity in the calling of the allele scores.
- CSF1PO Allele 13 had not previously been observed in TriP WT using the 16 locus kit, although review of electropherogram showed a small peak at 13 that had not been called previously.
- D7S820 Allele 10, 11 and 12 were previously shared in both 293 and TRIP WT. In this analysis 10 missing from the 293 profile and 12 from TRiP WT. D7S820 allele12 can be seen as a small uncalled peak in electropherogram,
- D3S1358 Allele 17 missing from 293 and TRiP WT whereas previously observed in both profiles.

5.3.3 Morphology of TRiP WT

Microscopic analysis of the monolayers of TRiP WT cells revealed the cells grew in tightly packed colonies with little resemblance to 293 or 293T, with their suggesting adoption of a de-differentiated phenotype. Others have reported a high degree of plasticity in the morphology of 293 cells[434]. There is also evidence that the 293 cell can express neuronal chatacterisitcs. Neurite-like structures can be seen in in 293 and 293T cells in Figure 5.2.

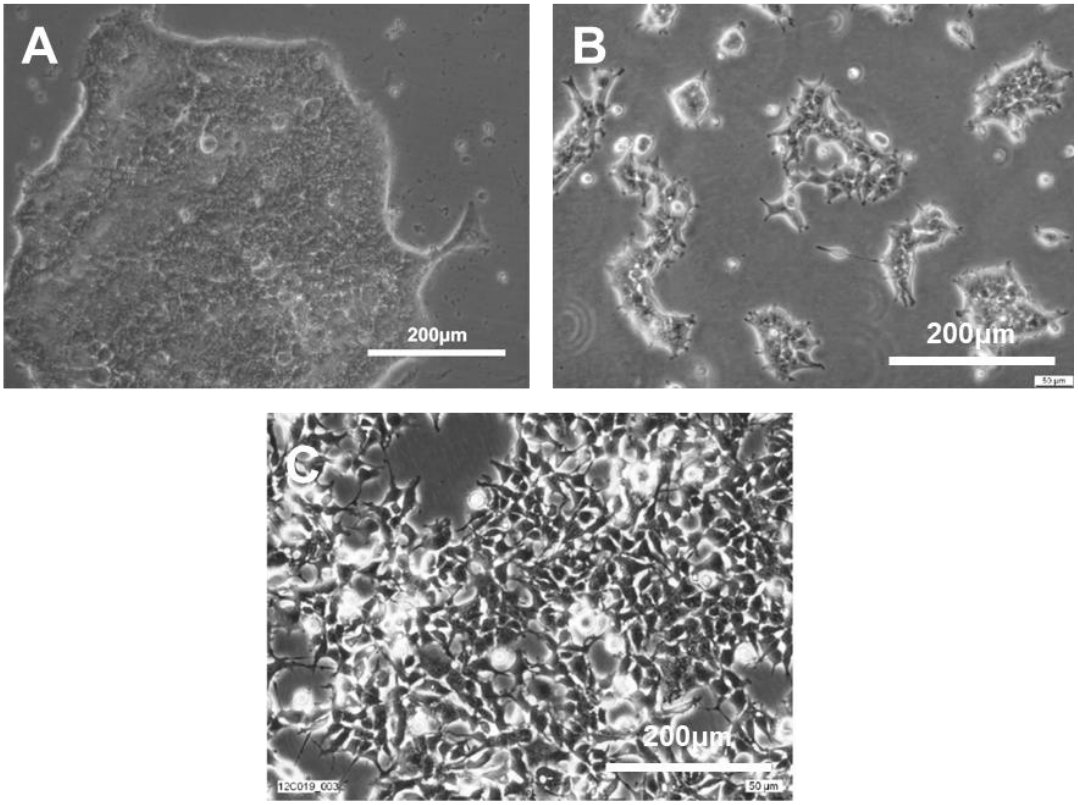

Figure 5.2. Morphology of TRiP WT, 293T and 293 cells.
Phase contrast micrographs of monolayers of TRiP WT (A), 293-T (B) and 293 (C).

5.4 Discussion

5.4.1 Authentication and STR Profiling

Many journals are beginning to adopt guidelines for authentication prior to publication[435] however these are not always policies that are insisted upon, often they are encouraged rather than demanded.

Ian Freshney and Amada Capes-Davis together with a world-wide team of scientists endeavoured to tackle the problem of the continued use of misidentified cell lines by establishing the International Cell Line Authentication Committee (ICLAC)[292,436] to help steer, advise and lobby scientific opinion on the subject and to compile and maintain a contemporary database of all known misidentified cell lines[295]. Currently there are over 480 misidentified cell lines in the ICLAC database. This register, however, does not include all instances where an 'identified' legitimate cell line has been accidentally mixed or confused with another.

A study by the German DSMZ Cell collection estimated that 18% of the cell lines that had been submitted to them were misidentified[437]. Vaughan *et al* recently appraised the academic and financial cost of a single misidentified cell line to the scientific community (KB). Its inappropriate use constituted 574 articles over a 14 year period, that affected thousands of subsequent citations and potentially millions of US dollars in follow-up research[425].

Cell line misidentification can arise through the contamination of one cell line with another during routine non-segregated cell culture (through droplet contamination, sharing of media, reagents or pipettes) or by mislabelling or labelling corruption. Due to its basis in the forensic science and maternity testing field STR profiling is currently only predominantly applicable to human cell lines. Species identification by the sequencing of the cyctochrome c oxidase subunit 1 (CO1) gene is also required to screen for contamination from cells of other species[438].

Cell line misidentification was first reported as an issue in life science research in 1966, when Stanley Gartler, after employing iso-enzyme analysis, reported at a conference on cell, tissue, and organ culture[439] that 18 human cell lines of independent origin had probably been mixed or replaced with HeLa cells[423]. Since then the techniques for screening misidentified cell lines have been developed and refined, yet the issue remains. The current and widely adopted PCR based technique of STR profiling involves the scoring of the copy numbers of specific short tandem repeats (STRs). STRs are non-coding regions of repeated DNA that are found throughout eukaryotic genomes and are amongst the most polymorphic loci in humans. Typically, STRs are two to six base pairs in length and the frequency of their repeats differs between different people. The frequency each STR can occur is specific to a specific allele,

thus each STR locus will have a frequency score determined from the number of base pairs in the repeat (allele)[333]. The STRs themselves are named after the chromosome on which they are located with a unique numerical identifier. For example: in 'D3S1266' D represents DNA, 3 means chromosome 3 on which the STR locus is found, S stands for STR, and 1266 is the unique identifying number[440]. As most people carry two copies of genetic information (put simply: one set of chromosomes from each parent) then each person will have two allelic scores for each STR locus. If the allelic score for a single STR locus is the same on both chromosomes then the score is said to be homozygous and if it is different; heterozygous. As there are dozens of STR loci, several available allelic scores for each STR locus and there are potentially two different allelic scores for each locus for any person: if many STR loci are profiled then the discriminatory power of STR profiling becomes extremely powerful.

STR profiling is carried out on DNA extracted from the cell line through a multiplex PCR reaction using a mixture of primers specific to regions of DNA containing each of the STR sequences these regions are amplified. Generally, the STR primer cocktail will include the gender marker amelogenin. This dental enamel gene has two allelic forms specific to the X and Y chromosomes hence the amplified products of this locus can be used to discriminate gender of the DNA sample[441]. The PCR Products are then electrophoresed in capillary sequencer to generate an electropherogram. PCR products are compared in size to a synthetic allelic ladder using software and the allele scores for each locus is determined. The process is subject to artefactual problems such as stutter peaks arising from strand slippage during PCR amplification. Stutter peaks will in general be 1 repeat unit lower than the true allele and may appear as an extra peak on the electropherogram leading to a spurious triploid allele score (see below). It is therefore essential that an experienced operator checks and quality controls the automated software 'calls' making any corrections as required. In forensic STR profiling a triploid score of uneven peak height would automatically be discounted as stutter, whereas in cell line identification, where cells can become genetically unstable or be missed populations, multiple peaks could indicate a real result and must be manually checked[332 333].

A conservative estimate of the discriminatory power of a 16 locus STR assay is in the region of 1×10^{17}, meaning that the chances of two people sharing the exact STR profile are over 10^{17} to one against even if they are closely related. As this chance exceeds the living human population of the planet; in reality, the only people who could share STR profiles are monozygotic twins. Due to the inheritance of one set of STR alleles from each parent, the chances of two individuals having very similar STR profiles are also small, unless they come from an extremely isolated and in-bred population.

Once an STR profile is obtained for a cell line it should be compared to databases of the STR profiles of known cell lines and/or a reference sample. In the case of a putative novel cell line this will help confirm (or deny) its uniqueness or for known cell lines the data will give researchers the confidence that their cells match those used by other researchers at a genotypic level.

Forensic STR profiling was developed to aid criminal investigations and for paternity testing. DNA samples from people reflect the genetic stability of an individual where their cells are subject to the cellular checks and balances (mismatch repair mechanisms[442]) that secure a stable genotype. As alluded to above, cell lines, particularly those derived from cancers, have a far more plastic genome than individuals, hence are subject to genetic variability and the adoption of polyploid and aneuploid karyotypes[295]. Cell lines can easily lose part or entire chromosomes through long term continuous passaging and still retain acceptable growth characteristics. It is quite common for cell lines derived from male subjects to lose part or all of their Y chromosome, leading them to subsequently lose some STR loci and return a female STR profile[443].

This genetic variability issue in cell lines drove the International Standards Development Organisation (SDO) and the International Cell Line Authentication Committee (ICLAC) to develop a scoring and comparison algorithm using a forensic 16 loci assay to determine the 'uniqueness' of cell lines[333]. Initially the assay concentrates on what are known as the eight core loci[433] but the algorithm can be expanded to include as many loci as required.

Both organisations recognise that the innate genetic variability in cell lines does not lend itself to a simple binary result and in the event of complex assay results and ambiguity a pragmatic peer reviewed approach is required, accounting for treatments the cell lines may have undergone in culture and events such as re-cloning and number of passages in culture.

The accepted algorithm for calculating the percentage match between the test sample and the reference sample is taken as two times the number of matching alleles divided by the total number of alleles observed, expressed as a percentage.

The data generated in this study show that it is highly likely that the Lung Stem Cell Line designated 'TRiP WT' is in fact a variant of the transformed immortal human embryonic kidney cell line designated '293' (also known as HEK-293). The 293 cell line was developed in 1977 by transformation of human embryonic kidney tissue with DNA from adenovirus 5[444]. The cell line is inherently genetically unstable with a reported unstable hypotriploid karyotype[445].

Since inception 293 cells have become the second most commonly used cell line in laboratories world-wide[446] where they are used in the drug discovery field for efficacy testing, as a transfection host and in virology amongst other applications. A search of the Cellosaurus[285] on-line cell line knowledge resource that attempts to describe all cell lines used in biomedical research[285] shows that there are currently over 90 different variant cell lines based on 293 including 293T (sometimes referred to as 'HEK 293T' (human embryonic kidney (HEK)) (often mistakenly used synonymously with 293). This commonly used cell line was derived from parental 293 cells through transfection with the temperature sensitive neomycin / G418 resistant tsA1609 allele of SV40 large T antigen[447]. According to PubMed there are thousands of publications that reference the cell line in their abstracts. It can therefore be safely assumed that 293 cells are commonly found and grown in a sizeable majority of tissue culture facilities. Despite being originally derived from normal human embryonic kidney tissue, 293T cells display some the features of cancer stem cells and may have the capacity to differentiate into other tissue-like states[448] [449].

The genotypic similarity between TRiP WT cells and 293 cells as determined by STR profiling in this study varied between 73 and 84% depending on the number of the loci used in the analysis. Guidelines developed by the American Standards Development Organisation (SDO) and The International Cell Line Authentication Committee state that this level of similarity constitutes evidence that the two cell lines are likely to be from the same donor but with an indication that there is a degree of genetic instability involved[433] [333]. This raises the question of whether the difference between TRIP WT and the 'reference' STR profile of 293 could be attributable to the degree of variability seen between other strains of 293.

Lin *et al* (2014) conducted a study to evaluate the genome dynamics of six cell lines cells of the 293 lineage[446]. Their results showed that 293 cells have lost control over chromosomal structure and that a high degree of variability in genetic variability within a single culture of 293 cells. In all six strains the telomeric end of chromosome 1q was rearranged through deletions and inversions. There were many other deletions and inversions on the q arm of chromosome 8 and that almost all polymorphisms were heterozygous and that genetic changes may be driven by selective pressures of specific media and culture conditions.

There are several pieces of evidence in the STR profiling data of TRiP WT that indicate an increased likelihood they are a genetically unstable version of 293.

At the 16 locus comparison level the major differences between 293 and TRiP WT that constitute most of the 20% or so difference between the two cell lines are contributable to the fact that the 293 cell line is generally heterozygotic in its STR locus alleles, whereas TRiP WT appears to be homozygotic at six out of 16 loci that are heterozygotic in 293 (STR Loci

CSF1PO (Chromosome 5), D13S317 (Chromosome 13), THO1 (chromosome 11), D16S539 (chromosome 16), D21S11 (chromosome 21) and Penta D (Chromosome 21)).. Acquired homozygosity or "null alleles" can be due to two reasons. Firstly the allele may actually have been present in the DNA sample from the cell line but it failed to be amplified due to a nucleotide mutation in the PCR primer binding site[450] during the PCR step of the STR profiling assay. It is not unreasonable to hypothesise that during the creation and characterisation of the TRiP WT cell line an accidental contamination of the experiments with the 293 cells that were used to generate lentiviral vectors and their subsequent extensive sub-culture and transfer and recovery from mouse kidney capsules[420] could have resulted in a highly passaged population of 293 cells subject to the acquisition of mutations compounded by the 293 cell line itself having defective DNA mismatch repair mechanisms[451 452 453]. Such acquired mutations could lead to corruption of the primer binding sites that flank the specific loci.

Loss of chromosomal material, genetic drift and change in genotype through extended cell culture has been known for many years and is one of the drivers for adopting good cell culture banking practices to minimise passaging of cells and maintain cell line integrity[332]. Binz *et al* (2019) studied the karyotype of the 293 cells obtained from the ATCC (the STR profile of which matches with the ECACC 293 cells used in this study as compared by the Cellosaurus dataset). Their findings confirmed that the 293 cell line was overall near-triploid, there was partial tetraploidy and loss of the q arm in chromosome 5, addition of a fragment of unknown origin to chromosome 13, triploid chromosome 11 with a large fragment of unidentifiable banding pattern, triploid Chromosome 16 and tetraploid chromosome 21. They found substantial translocations in the chromosomes indicating a potentially unstable karyotype. It is interesting to note a large degree of overlap in the more unstable chromosomes and those that appear to have become homozygous for STR alleles in TRiP WT cells. *In vitro* studies have shown that polyploid cultures, such as 293 are more likely to tolerate the loss of a chromosome as the cells re-configure themselves to uni-cellularity and this actually may of benefit to the cells[454 455] Thus a second possibility for the acquisition of null alleles in TRiP WT could be the loss of part or entire chromosomes. Huang *et al* compared the STR profiles of 293 cells from the ATCC (USA) and the CCTCC (People's Republic of China) which had been grown and banked separately from each other for many years. They found that that the CCTCC stocks of the 293 cell line had lost D16S539 allele 13, THO1 allele 7[456]; two of the same losses acquired by TRiP WT. Loss of chromosomes would have to be confirmed through the karyotyping of the TRiP WT Cells, however due to the mycoplasma status of the cells and the risk of contaminating cell culture facilities this is not something that could be carried out readily.

The remaining differences in the STR profiles were attributable to gains in alleles at certain loci. Before addressing these, it is worth discussing the phenomenon of strand slippage. See Figure 5.3 .

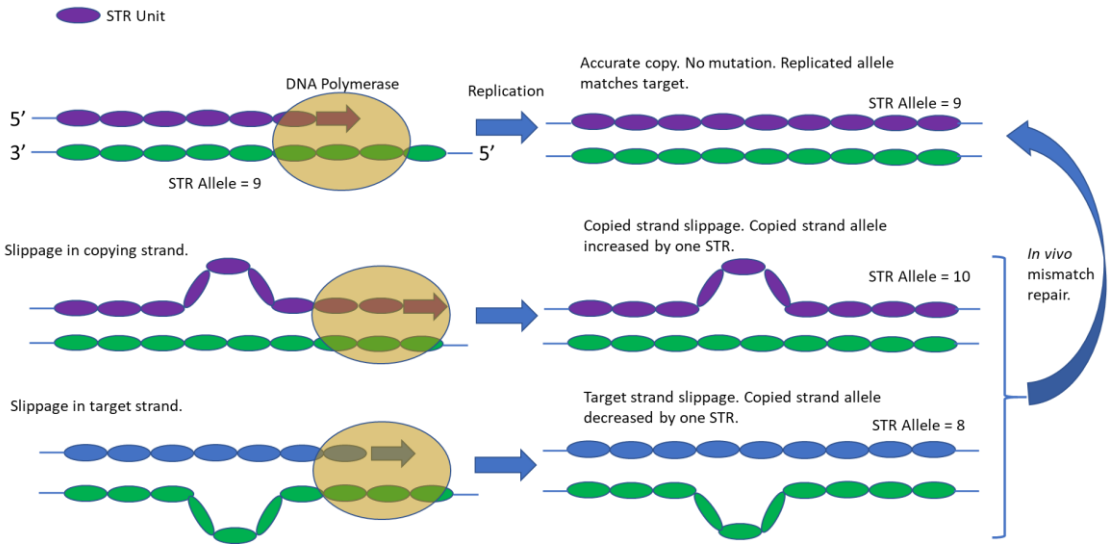

Figure 5.3. The phenomenon of STR strand slippage.
In vivo strand slippage without mismatch repair results in a mutated STR allele. *In vitro* (in the STR assay) strand slippage can occur at the PCR stage leading to so-called "stutter" where a small peak is observed on the electropherogram one STR repeat away from the expected allele (after Fan and Chu)2007)[440].

As cells divide *in vivo* the DNA is copied by DNA polymerase to give the daughter cells a full complement of genetic material. In the process of copying the STR sequences the STR repeats can "loop out" causing strand slippage as shown in Figure 5.3. Usually these copying errors are detected and rectified by the cells' mismatch repair mechanisms[442]. 293 cells are compromised in their ability to repair STR allelic mutations due to defective repair mechanisms[451 453 452]. The STR profiling assay generates allelic peaks in a multiplex PCR reaction to allow allele scoring. The phenomenon of slippage can also occur during the PCR reaction itself resulting in small artefactual stutter peaks either side of the true allele peak (Figure 5.4). Generally stutter peaks can be discounted if they are less than 10% of the height of the allelic peaks[433 333].

At locus D3S1358, TRiP WT has gained extra alleles at 16 and 18 which could indicate *in vitro* strand slippage mutation in cell line or presence of another cell line or genome. (Electropherograms are appended (Appendix B)). The signal for allele 18 is very strong and unlikely to be an assay artefact such as stutter.

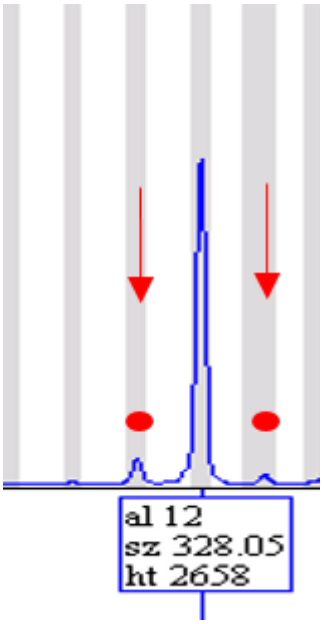

Figure 5.4. Example of stutter in a STR electrogram.
The true allele (here at the D13S317 locus) is 12 but there are stutter peaks at 11 and 13 (red dots).

The differences between the allelic pattern between 293 cells and TRiP WT cells can be seen more clearly in the 16 locus result (insert, Appendix). However, the absence of similar strong peaks at other loci suggests something subtler than a single contaminating genome or simple slippage mutation. Binz *et al*[457] demonstrated that chromosome 3 is corrupt in the 293 cell line with a breakpoint located at 3p21 which is coincidentally the same location as the D3S1358 locus (3p21.31). If the breakpoint were to have occurred in the STR sequence, disrupting the STR, as series of recombinations could have potentially occurred between the STR fragments leading to multiple new STR alleles. For example, if STR allele 15 was to be broken into 8 and 7, and allele 17 into 10 and 7; 7 and 7 could recombine to give 14, 8 and 7 to 15, 8 and 8 to 16, 7 and 10 to 17, 8 and 10 to 18 and finally 10 and 10 to give 20 which is very similar to the STR allelic pattern at D3S1358 observed in TRiP WT. Similar re-arrangement could possibly have occurred at D1S1656 which shows a similar complex mutli-allelic pattern. Again 293 displays a breakpoint on the q arm of chromosome 1 near the location of the STR locus. The remaining allele gains by TRiP WT are one allele away from expected allelic scores for 293 cells suggesting the possibility of un-corrected slippage mutations gained by the cell line during culture.

Another unusual STR feature shared by 293 and TRiP WT cells increasing the likelihood they are one in the same cell line are the presence of rare markers (according to the Promega forensic probability data for the STR loci from a mixed-race sample of 1036 people[458]). The

Penta E 15 allele has a population frequency of just 0.0656 (6.6%), the D5S818 locus allele 8 has a probability of 0.0198 (2%) and the D19S433 locus allele 18 is unreported in the Promega dataset. These three alleles are conserved and found in 293, its derivative 293T (Cellosaurus[285]) and in TRIP WT.

Theorising about the differences between 293 and TRiP WT however is conjecture and It remains unknown as to whether TRiP WT cells represent a pure population of a genetically corrupted version of 293 cells or whether they embody a mixed population that might still harbour cells from the original donor of the intended progenitor cell line. This could only be resolved by further analysis (by cell sorting for example). It may be technically feasible to determine if there is a second cell population and attempt to salvage it by cloning, however it is likely that any background second population of cells would be extremely low in number and the difficulties surrounding dealing with mycoplasma infected cultures and the low likelihood of success make any salvage attempt impractical.

5.4.2 Mycoplasma Status

It should also be remembered that the TRiP WT cells harboured a mycoplasma contamination and it has been shown that mycoplasmas can affect the karyotype and therefore potentially the STR profile of cell cultures as shown by Namiki *et al* in their study of persistent exposure of human prostate cells to mycoplasmas[459].

Mycoplasma contaminations in cell cultures can be devastating to *in vitro* research. Any microbial contamination will waste time, effort, cause frustration and have a financial impact. Most microbiological infections are immediately identifiable due to increased turbidity of the cell culture medium together with the observation of fungal filaments, yeasts or bacteria by standard phase contrast microscopic investigation. Contaminations of this type can be addressed and resolved by discarding of contaminated cultures and adoption of good aseptic technique and good laboratory practices[292]. Mycoplasmas, however, present a far more insidious problem[431 460]. Mycoplasmas are a large group of microorganisms within the class *Mollicutes* characterised by having no cell wall. The organisms associate themselves and can reach titres of 10^6 to 10^8 colony-forming units (cfu) per mL within five days of infecting a culture and typically an infected culture will have 100 to 1000 mycoplasma organisms per cell. Because of their size even the highest titres of infection in cell cultures cannot be seen by the naked eye nor by conventional phase contrast microscopy. More than 20 species of mycoplasma have been isolated from cell lines and there are three main sources of infection[431]:

- Poor hygiene and aseptic technique of laboratory personnel who may have commensal mycoplasmas on their skin, mouths and respiratory tracts; the majority of cell culture mycoplasma contaminations are of human species.
- From an innate infection of the donor (human or animal) from which the cell line was derived.
- Transfer from other contaminated cultures or reagents in the laboratory.

Observed effects of mycoplasmas on cell cultures include[431]:

- Altered levels of protein, RNA and DNA synthesis
- Alteration of cellular metabolism
- Induction of chromosomal aberrations (numerical and structural alterations)
- Change in cell membrane composition (surface antigen and receptor expression)
- Alteration of cellular morphology
- Induction (or inhibition) of lymphocyte activation
- Induction (or suppression) of cytokine expression
- Increase (or decrease) of virus propagation
- Interference with various biochemical and biological assays
- Influence on signal transduction
- Promotion of cellular transformation
- Alteration of proliferation characteristics (growth, viability)
- Total culture degeneration and loss.

There are several techniques available for mycoplasma detection but due to the wide genetic range and phenotypic differences within the group of organisms it is generally advised that two or more complementary techniques with different specificities and sensitivities are employed to counter issues presented by false positive and negative results[292].

These techniques include culture of cell culture supernatants in specific mycoplasma indicating broths and on agar plates prepared with mycoplasma broths where colonies of mycoplasmas can be observed[431]. PCR detection using mycoplasma specific primers[460 334] and the use of fluorescent DNA stains (such as DAPI or Hoechst DNA stains) to visualise mycoplasmas on the cytoplasm of cells fixed on coverslips, using fluorescence microscopy[431]

The remaining paradox regarding this misidentification event is answering the question of how or why 293, a cell line derived from human embryonic kidney, could display the properties of a lung progenitor and subsequently express key markers as reported by Oeztuerk-Winder *et al*[420] and Ruiz[415].

293 cells themselves are epithelial in origin and have been shown to express both E-and N-cadherin[461]. The 293T derivative of the cell line[447] has been shown to adopt a cancer stem cell phenotype when grown in suspension or spheres expressing the stem cell markers of Oct4, Nanog, Sox2 and Klf4[448] and the cell line therefore may have a certain amount of plasticity and potential to differentiate. Although the presence of SOX9 was not reported by Debeb *et al*[448], Sox9 is reported as a marker of cancer cell lines[462]. Further work would be required to test the hypothesis that mycoplasma free 293 cells could be driven to a differentiated state where they might express LGR5, 6 and the airway epithelial markers SFTPC, CCSP and AQP5 although it is noted that studies have generated recombinant versions of 293 cells that express these markers [463] [464] [465] [466] [467].

5.4.3 Summary

- The E-Cad/LGR6+ cell line designated TRiP WT tested positive for Mycoplasma invalidating its use for further work.
- STR profiling and subsequent analysis demonstrated the extremely strong likelihood that the TRiP WT cell line is derived from a genetically unstable population of 293 cells possibly caused by a cross-contamination event in the originating laboratory.
- Following sensitive dialogue and investigations with originating laboratory to determine if earlier, non-corrupted TRiP WT cell stocks exist, these data may be ultimately submitted to the International Cell Line Authentication Committee for consideration and potential inclusion in the database of misidentified cells.
- Communications with Ximbio based on the results of this chapter have resulted in the cell line being removed from the Ximbio catalogue and website.
- The identification of TRiP WT (E-Cad/LGR6+) as being a derivative of 293, an immortalised human embryonic kidney cell line and the confirmation of mycoplasma contamination in the cell line made any further work with the cells impossible.

6. Effect of Dexamethasone and Neuregulin-1β on ATII Specific Gene and Protein Expression A549 Cells

6.1 Introduction

An E-Cadherin/LGR6 Expressing Lung Progenitor Cell Line had been identified to provide the focus for the final stage of this study, however the cell line was deemed unsuitable for further endeavours due to cross contamination and mycoplasma infection (Chapter 5). It was therefore decided to continue to work with A549 cells.

Differentiated *in vitro* ATII models should have evidence of the expression of mRNA and protein for surfactant proteins (*SFTP) A, B, C* and *D*. *SFTPB* and *C* are hallmarks of ATII cells[265] with *SFTPC* apparently exclusive to ATII[262]. Expression of SFTPA[266 267] is desirable together with that of *SFTPD*, as these proteins help regulate host immune defence and modulate inflammatory responses. SFTPD however, is not exclusively expressed *in vivo* in ATII cells but also in other airway cells such as basal cells, glandular cells and Club cells[468]. Another key ATII attribute is the expression of the gene for the ATP-binding cassette class A3 *(ABCA3*)[268 269].

Prematurely born infants are at risk of a respiratory distress syndrome (RDS) which is a result of developmental deficiency of pulmonary surfactant. For many years, early postnatal treatment with the glucocorticoid dexamethasone (Dex) has been used to boost pulmonary surfactant production in the infant lung therefore preventing RDS. The precise mechanisms by which dexamethasone induces surfactant production are unknown.

Surfactant protein production in primary rodent and human epithelial cells, A549 or NCI-H441cells, primary ATII cultures and *in vivo* has been shown to be modulated by treatment with glucocorticoids such as Dex or hydrocortisone. This has been demonstrated either by direct treatment of rat primary ATII cells with Dex[469 470] or indirectly, through the stimulation of fibroblasts with Dex to produce factors thought to regulate and maintain ATII differentiation[471]. The latter can be brought about through the generation of fibroblast conditioned medium[471 472] or through epithelial/mesenchymal co-culture systems[473 474].

Direct induction of rat primary ATII cells with Dex seems to augment both phosphatidylcholine secretion and cyclic AMP formation in the cells whilst also upregulating β-adrenoceptor gene and protein expression in the rat ATII cells. This indicates that Dex induced pulmonary surfactant secretion may act through an enhancement of β_2-adrenoceptor gene expression[475].

Using A549 cells, Jeon *et al*[476] showed that Dex increased the level of intracellular calcium. The gene expression of the epithelial calcium transport channel transient receptor potential vanilloid subfamily member 6 (*TRPV6*) significantly increased, whereas the expressions of the calcium outflow genes *NCX1* (sodium/calcium exchanger) and *PMCA1* (plasma membrane calcium ATPase) significantly decreased with Dex treatment.

The mechanism that is believed to operate in the foetal lung involves interactions between ATII cells and foetal lung fibroblasts. Glucocorticoids seem to stimulate fibroblasts to produce a putative compound, unknown protein or cocktail of proteins designated 'fibroblast pneumocyte factor' (FPF)[472] which can drive ATII differentiation, surfactant protein production and lung maturation. The ATII differentiation effects of FPF have been inhibited using monoclonal antibodies raised against FPF produced from fibroblast culture conditioned medium[55]. Glucocorticoids are believed to enhance surfactant associated phosphatidylcholine production and that this effect is mediated by an activation of choline-phosphate cytidylyltransferase. In response to Dex, foetal lung fibroblasts are thought to produce FPF which in turn stimulates the formation of saturated phosphatidylcholine The mechanism by which fibroblast-pneumonocyte factor stimulates the cytidylyltransferase activity remains unknown[477].

Despite years of research, the true composition of FPF has remained elusive with various candidate molecules including keratinocyte growth factor (KGF), leptin and neuregulin-1β (NRG-1β)[59]. Considering the complexity of epithelial to mesenchymal interactions in the development of lung[58] and the non-specific and potent *in vivo* and *in vitro* effects that Dex has on the gene expression of hundreds of glucocorticoid responsive genes [478] [479] ,the reality of Dex and FPF interactions with ATII cells and A549 cells are likely to be very complex and difficult to de-lineate.

ERBB receptors and their stimulation by neuregulin-1β (NRG-1β) play a critical role in surfactant protein synthesis by ATII cells[480]. The possibility has been raised that in rodent models at least, NRG-1β may control foetal lung maturation via mesenchymal to epithelial interaction[323] [481]. Evidence for this has been demonstrated through the observation that antibodies raised against NRG-1β inhibit FPF activity[323]. In addition, a synergistic effect of Dex and NRG-1β has been suggested in the development of rat lungs[322] [482] [324]. Evidence a significant component of FPF may be NRG-1β[59].

Based on this evidence it is postulated that NRG-1β and Dex are two of the key factors that could be employed to treat A549 cells to achieve elevated SFTP and ATII marker expression without the need for mesenchymal co-culture.

6.2 Hypothesis

It was hypothesised that a combination of the long-term A549 culture technique developed in Chapter 4, together with combinations of NRG-1β and Dex and NRG-1β alone will drive A549 cells closer to an ATII phenotype.

6.2.1 Aims

- Attempt to further develop the long-term A549 culture technique developed in Chapter 4 with the chronic treatment of the long-term cultures with combinations of dexaththasone (Dex), a known known inducer of surfactant protein production in A549 and ATII cells, and with the ERBB receptor ligand neuregulin-1β (NRG-1β), a potential component of fibrocyte pneumocyte factor (FPF). The latter will reiterate work carried out on *in vitro* rat ATII cell differentiation to determine if a similar response can be achieved in human A549 cells.
- To determine if combinatorial treatment with Dex and NRG-1β results in an additive or synergistic effect on the adoption of ATII characteristics in A549 cells.
- To compare and contrast data with that obtained from the non-treated long term cultures and from primary human ATII cell isolates.

6.2.2 Objectives

- To cultivate 2D cell cultures of A549 over a 3 to 4 week period in the presence of NRG-1β and determine effects on expression of epithelial marker genes, AT1 marker genes and *SFTPA1* and *2*, *B*, *C* and *D mRNA* as determined by relative QRT PCR gene expression. Compare these data with that obtained from untreated long-term A549 cells and from untreated human ATII primary cell isolates.
- Dex is known to have wide-ranging and potent effects on many glucocorticoid sensitive genes. Using phase contrast microscopy determine any gross effects that the treatments have on the A549 cells' morphology that might indicate off-target effects of Dex treatment.
- To determine, by indirect immunofluorescence, if the combinations of treatments increase the expression of surfactant proteins and other specific ATI and ATII markers as compared to ATII primary cells and untreated long -term A549controls.

6.3 Results

6.3.1 Effect of Dex and NRG on A549 cell morphology

Cultures of A549 cells were placed in long term culture for 3 weeks in the absence or presence of Dex and/or NRG-1β and the morphology of control or treated cultures was monitored by phase contrast microscopy. After the culture period, it was observed that the untreated control cells adopted the quiescent epithelial-like morphology that had been observed previously (Chapter 4)[483]. (Figure 6.1 (A)). Similar morphology was observed in the NRG-1β treated cells (Figure 6.1(B)). However, markedly different morphologies were observed in both the Dex treated cells (Figure 6.1(C)) and with the Dex+NRG-1β combination (Figure 6.1(D)).

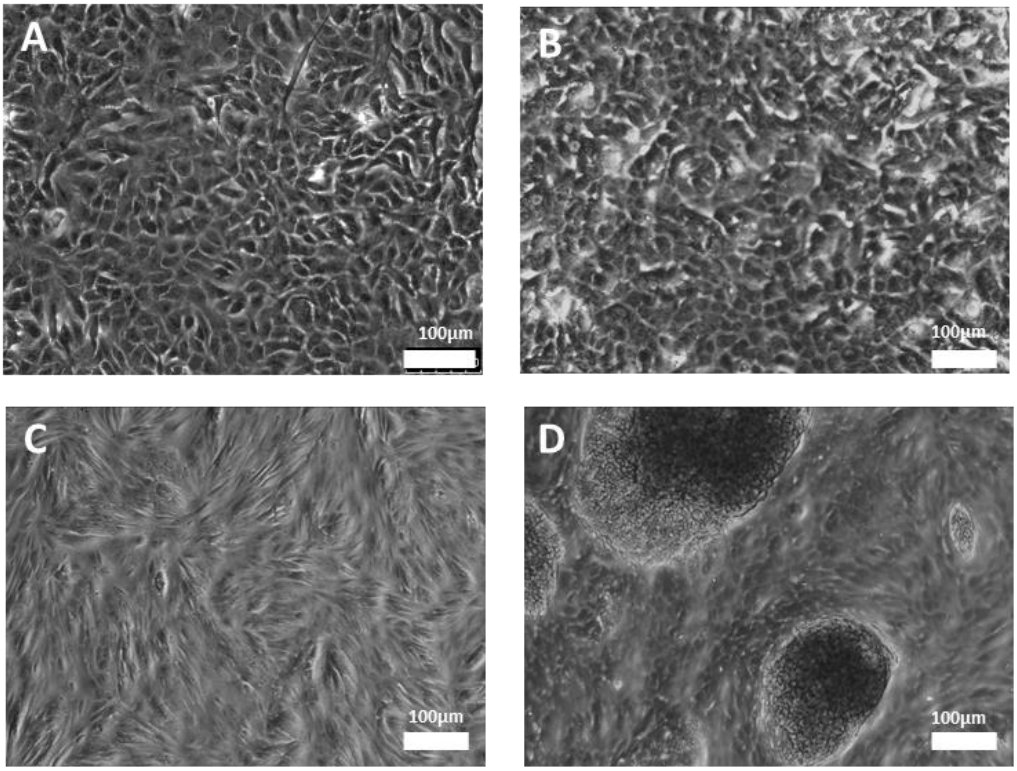

Figure 6.1. Cell morphology in long term A549 cultures is influenced by chronic treatment with Dexamethasone (Dex) and neuregulin-1β (NRG-1β).
A549 cells were cultured in Ham's F12/10 % FBS for three weeks with no treatment ("Long Term"), with NRG-1β at 50 ng/mL ("NRG"), Dex at 100 nM ("Dex") and a combination NRG-1β at 50 ng/mL and Dex at 100 nM (Dex+NRG). Cultures were medium exchanged regularly. Representative phase contrast images were captured at 21 days. Medium alone (Long term) = A, NRG=B, +Dex=C and +Dex+NRG=D. The four conditions were set up at the same time and pictures represent the morphologies at the end of the chronic treatments. Images were representative of three independent experiments with two different batches of A549 cells.

Dex caused the cells to adopt a flattened and elongated "fibroblastic" morphology whereas the combination of Dex and NRG-1β resulted in a similar background of the fibroblast-like cells as seen in the Dex culture but with regularly spaced rounded colonies of small closely packed cells (Figure 6.1(D)). To discount any possibility that these differences in morphology were down to a cross-contamination event with another cell line, the experiment was repeated independently on multiple occasions, always with the same result. Samples of all treated cultures were submitted for human STR profiling[333]. In all occasions, human STR profiling returned scores with 100% match with A549 cells (data not shown).

Investigations into the gene and protein expression to determine possible mechanisms driving these unusual morphologies were carried out however these data were considered to be a digression from the main study and are not included in this chapter. They are presented in Appendix C but discussed below. It was postulated that EMT or dedifferentiation to a stem cell like phenotype might explain the phenomenon.

(1) Epithelial markers and EMT

As the morphology of Dex treated cells tended to be fibroblastic, some initial QPRT-PCR analyses were performed to determine whether Dex could be driving epithelial to mesenchymal transition (EMT). EMT is a phenomenon observed in developmental and cancer biology and has been suggested as a potential mechanism for the lung remodelling involved in the progression of IPF. Vimentin (VIM) is a type III intermediate filament (IF) protein that is expressed in mesenchymal cells while ZEB1 is a transcription factor that induces EMT in association with a reduction in E-cadherin expression. E-cadherin is a calcium dependent adhesion molecule (also known as CDH1) involved in the establishment of adherens junctions in the establishment of epithelia and can be used as a marker for epithelial cells. Therefore, as markers of potential EMT, the levels of gene expression of ZEB-1, VIM and CDH1 were assessed in the A549 cultures using QRT-PCR (Appendix C Figure 1 and Appendix C Figure 2). While there was some evidence that VIM was upregulated by Dex treatment ($p=0.05$), this effect was negated by the addition of NRG-1β. Furthermore, there was no significant change in ZEB1 expression in response to Dex and CDH1 expression was increased in the presence of Dex suggesting that while Dex affected cell morphology, it was not driving EMT.

Nether VIM or ZEB1 mRNA were significantly up-regulated above levels observed in primary cells with Dex or Dex and NRG treatment (Appendix C Figure 2A and B) but the level of expression of CDH1 was significantly lower than that observed in primary cells.

To investigate the possibility that the "stem-cell like" colonies observed in Dex+NRG-1β treated A549 cells were actually stem cell in nature, the level of expression of the stem cell specific markers TRA-1-60, SOX2, Oct4 and SSEA4 were assessed by indirect immunofluorescence.

(2) Expression of Stem Cell Markers

Clusters of Dex+NRG treated A549 cells bore a superficial resemblance to the typical morphology of stem cell colonies (Appendix C Figure 3). Results of indirect immunofluorescence suggested the presence of stem cell markers in some cells in and around the colonies of small cells seen in Dex and NRG-1β treated A549 cells. Appendix C Figure 4. (A) and (C) show positive control cultures of induced pluripotent stem cell colonies demonstrating the typical cytoplasmic and nuclear expression of the stem cell markers OCT4, SSEA4, Tra-160 and SOX2. In Dex and NRG-1β treated A549 cells bright nuclear expression of OCT4 was observed in a proportion of cells in the cluster and specific cytoplasmic SSEA4 expression in some cells in and around the clustered colonies (Appendix C Figure 4B). Cytoplasmic TRA-1-60 expression was observed in a proportion of cells in the A549 clusters (Appendix C Figure 4(D) however SOX2 expression was not observed in A549 cells.

6.3.2 Effect of Dex and NRG on SFTP expression

Using QRT PCR it was found that Dex significantly upregulated expression of *SFPTA1*, *SFPTB*, *SFPTC* and *SFPTD* mRNAs in long term cultures of A549 cells compared to log phase culture and/or long term untreated cultures (Figure 6.2). The effect of Dex was most pronounced for expression of *SFTPB* (Figure 6.2A) and *SFTPD* (Figure 6.2B) both of which were markedly increased compared with untreated long-term cultures. NRG-1β alone was without effect and it had little additional effect in combination with Dex. *SFTPA2* gene expression was not detected in any of the A549 cultures.

Note: Genorm analysis (Appendix E) demonstrated that *TOP1* and *ATP5B* were the most appropriate reference genes for use in QRT-PCR for untreated time-course studies of A549 cells. However, it was found that treatment with Dex perturbed *TOP1* expression (data not included). This warranted substitution with *GAPDH* as a reference gene which was proved to be more stably expressed in conjunction with *ATP5B*, hence the use of *GAPDH* for QRT-PCR analysis of A549 cells in this and further chapters.

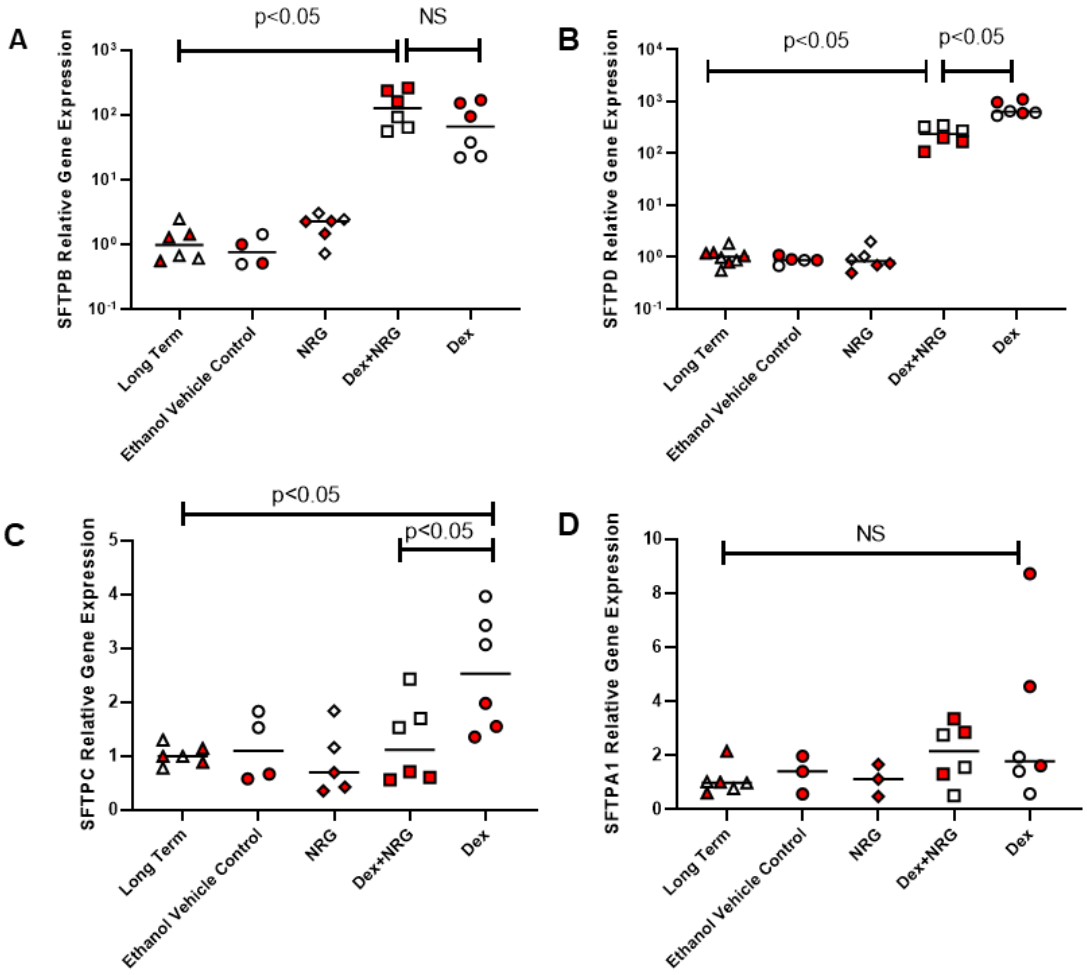

Figure 6.2. Surfactant protein gene expression in long term A549 cultures is influenced by chronic treatment with Dexamethasone (Dex) but not neuregulin-1β (NRG-1β).
A549 cells were cultured in F12/10% FBS for three weeks with: no treatment ("Long Term"), with NRG-1β at 50 ng/mL ("NRG"), Dex at 100 nM ("Dex") and a combination NRG-1β at 50 ng/mL and Dex at 100 nM (Dex+NRG). Cultures were medium exchanged regularly. At day 21 RNA was extracted for QRT-PCR analysis with TaqMan™ primer/probe sets for surfactant protein gene expression. *SFTPB* (A), *SFTPD* (B), *SFTPC* (C) and *SFTPA1* (D). *GAPDH* and *ATP5B* were used as reference genes and gene expression normalised to "Long Term" cultures. Mann-Whitney Non-Parametric Test. Data from two independent experiments. Data points from each experiment presented in a different colour.

Comparison of *SFTPA- SFPTD* gene expression with primary ATII cells and long term cultured A549 treated with Dex without or with NRG-1β showed that the primary cells expressed *SFPTA1, SFPTB* and *SFPTC* mRNAs at levels several orders of magnitude higher than the levels observed in the treated A549 cells (Figure 6.3 A, C and D). In contrast, the level of *SFTPD* gene expression in Dex treated A549 cells (with or without NRG-1β) was significantly higher than in the ATII primary cultures (Figure 6.3B).

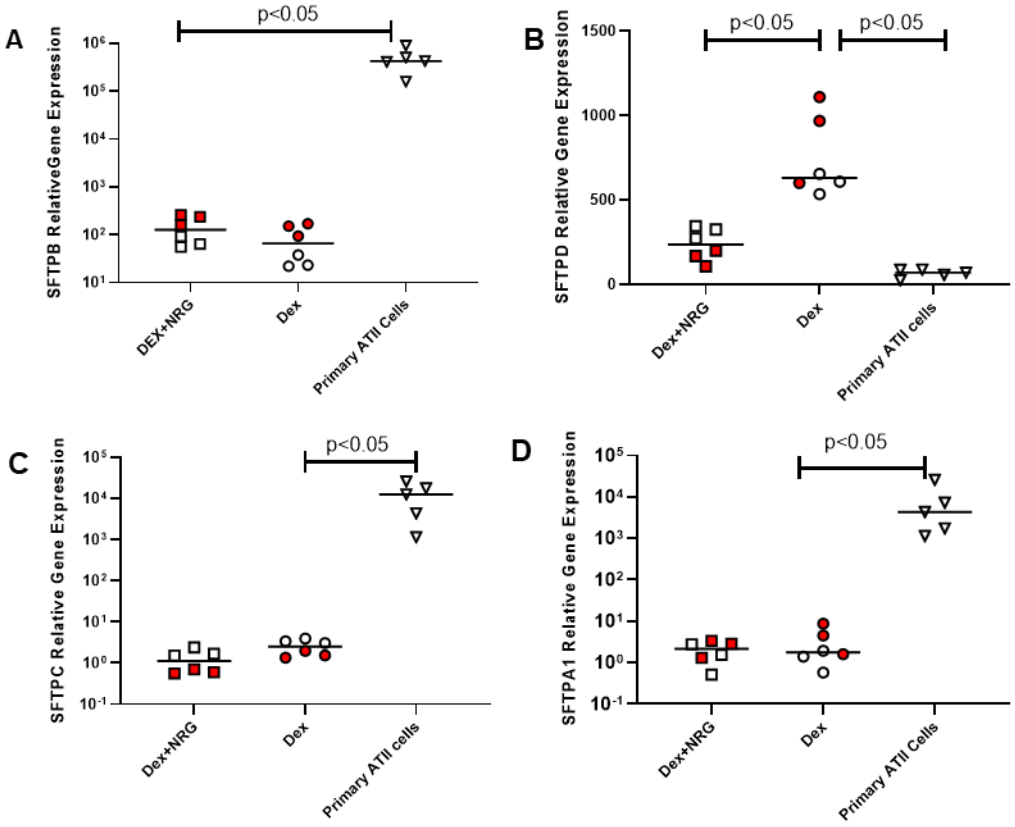

Figure 6.3. Surfactant protein gene expression in long term A549 cultures treated with Dexamethasone (Dex) and neuregulin-1β (NRG-1β) compared to primary human ATII cells.

A549 cells were cultured in F12/10 % FBS for three weeks with: no treatment ("Long Term"), with NRG-1β at 50 ng/mL ("NRG"), Dex at 100 nM ("Dex") and a combination NRG-1β at 50 ng mL and Dex at 100 nM (Dex+NRG). Cultures were medium exchanged regularly. At day 21 RNA was extracted for QRT-PCR TaqMan™ primer/probe sets for surfactant protein gene expression analysis in parallel with *RNA* freshly isolated human primary ATII cells from lung biopsies from five donors. *SFTPB A*, (B), *SFTPC* (C) and *SFTPA1* (D). *GAPDH* and *ATP5B* (or *ATP5B* and *TOP1* genes for primary cells) were used as reference. Expression data in all cases were normalised to "Long Term" cells (data not shown). Mann-Whitney Non-Parametric Test. Data from two independent experiments. Data points from each experiment presented in a different colour.

To further assess the effects of Dex and NRG-1β on surfactant protein expression, a preliminary experiment was carried out where cultures were stained for *SFTPB* and *D* using indirect immunofluorescence (Figure 6.4).

The difference in *SFPTB* expression seen in the gene expression experiments was confirmed at the protein level by bright and localised *SFTPB* expression in many of the primary ATII cells. (Figure 6.4E). However, whilst treated cultures appeared to be expressing surfactant proteins at higher levels than the control long term treated cells, results were not entirely consistent with the mRNA expression data. Expression of SFPTD mirrored the mRNA gene expression data showing an effect with Dex alone or in combination with NRG-1β (Figure 6.4H2 and I2). SFPTB appeared to be increased by NRG-1β treatment (Figure 6.4B2), an effect not observed in the gene expression experiments, however, with this preliminary experiment the specificity of the antibody, was not validated here. Expression of SFTPB appeared to be strongly localised to cells in the colony-like clusters in the cultures treated with a combination of Dex+NRG-1β Figure 6.4C2) reflecting either localised expression in the clusters or an effect related to greater cell density such as non-specific binding.

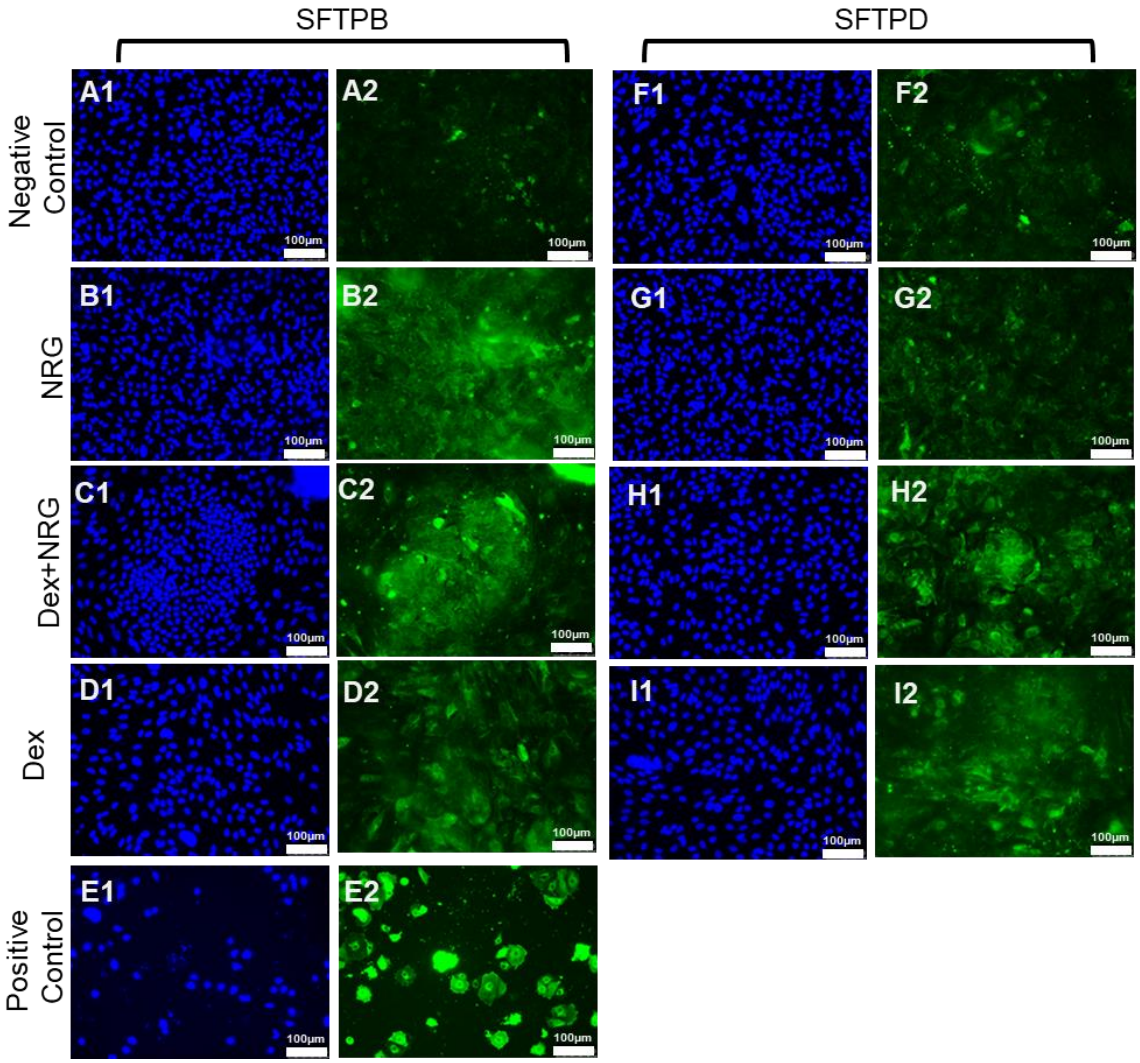

Figure 6.4. Surfactant protein secretion in long term A549 cultures is influenced by chronic treatment with Dexamethasone (Dex) and neuregulin-1β (NRG-1β). A549 cells were cultured in F12/10 % FBS for three weeks with: no treatment ("Long Term"), with NRG-1β at 50 ng/mL ("NRG"), Dex at 100 nM ("Dex") and a combination NRG-1β at 50 ng mL and Dex at 100 nM (Dex+NRG). Cultures were medium exchanged regularly. At day 21 cells were formaldehyde fixed and indirect immunofluorescent stained with a nuclear counterstain (NucBlue™). Human primary ATII cells from a single donor were cultured for 48 hours and processed similarly to the A549 cells ('Positive Control'). Staining for SFTPB: mouse IgG2a anti-human SFTPB primary antibody with Alexafluor®488 conjugated goat anti-mouse IgG secondary antibody. Staining for SFTPD: mouse IgG1 anti-human SFTPD primary antibody with Alexafluor®488 conjugated goat anti-mouse IgG secondary antibody. A to E: SFTPB staining; F to I: SFTPD staining. A and F = Long Term, B and G = NRG, C and H = Dex+NRG, D and I = Dex ; Images "E1 and 2": primary human ATII cells. For each pair of images, the first "1" is of the nuclear counterstain to show cellular distribution. "2" is of the fluorescent staining. Scale bar = 100 µm. Preliminary data from a single experiment.

6.3.3 Effect of Dex and NRG on Other Characteristics of A549 cells

While surfactant proteins are characteristic of ATII cells, the morphological changes seen with Dex and particularly Dex and NRG-1β treatment, led to assessment of the gene expression analysis of other ATII and ATI markers, as well as markers of epithelial cells, EMT and stem cells.

(1) ATII markers

The Adenosine Triphosphate–Binding Cassette Member ABCA3 is a transmembrane protein that is highly expressed in ATII cells, where it is found at limiting membrane of multi-lamellar bodies (MLBs). ABCA3 it is thought to have a transport role; importing the lipids required for surfactant function into lamellar bodies. Levels of expression of ABCA3 were significantly and undesirably down regulated in A549 treated with Dex compared to untreated and NRG-1β treated long term A549 (Figure 6.5A). At the gene transcript level primary ATII cells expression expressed significantly greater ABCA3 than Dex or Dex/NRG-1β treated long term A549 cells (Figure 6.6).

Previously (Chapter 4) it was suggested that other ATP binding cassettes associated with lipid transport may have a role in MLB assembly in A549 cancer cells. No significant up or down regulation was observed in ABCB4 gene expression in control or treated A549 cultures, (Figure 6.5B). ABCB4 gene expression was negligible in all the primary ATII cultures.

Gonzales *et al* recently identified novel marker named HT2-280[484]. In short, BALB/C mice were immunised with crude extractions of human ATII isolates to produce a monoclonal antibody specific to a yet unidentified antigen expressed on the apical plasma membrane of human ATII cells[484].

In an attempt to determine if the treated A549 cells had truly adopted an ATII phenotype, indirect immunofluorescence using anti-HT2-280 antibodies was carried out on 48 hour cultured primary cells (from donor TL1631) and compared to non-treated and Dex and NRG-1β treated A549 cells. The results are shown in Figure 6.7. HT2-280 specific fluorescence was detected in the primary ATII cells but not in the other cultures.

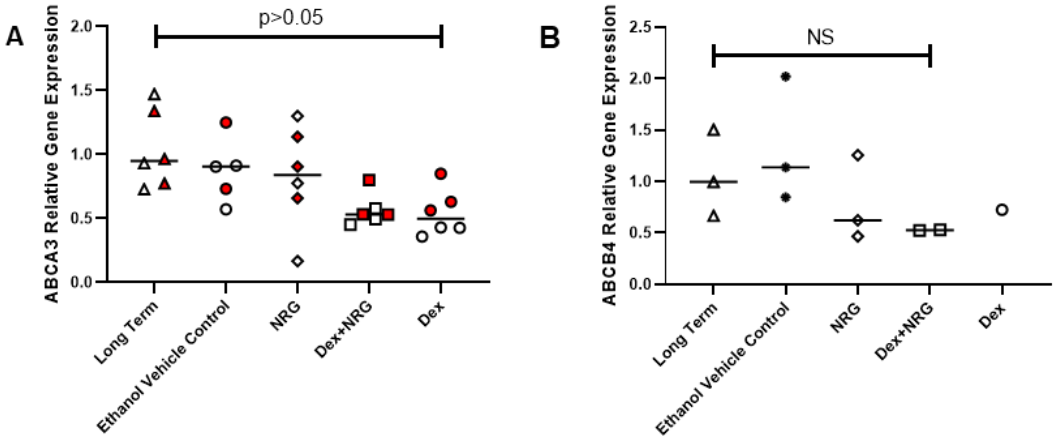

Figure 6.5. Response of the gene expression of lipid transporters ABCA3 and ABCB4 in long term A549 cultures following chronic treatment with Dexamethasone (Dex) and neuregulin-1β (NRG-1β).

A549 cells were cultured in F12/10% FBS for three weeks with: no treatment ("Long Term"), with NRG-1β at 50 ng/mL ("NRG"), Dex at 100 nM ("Dex") and a combination NRG-1β at 50 ng mL and Dex at 100 nM (Dex+NRG). Cultures were medium exchanged regularly. At day 21 RNA was extracted for QRT-PCR analysis with TaqMan™ primer/probe sets for *ABCA3* and *ABCB4* gene expression. *ABCA3* (A) (two experiments), and *ABCB4* (B) (a single experiment). *GAPDH* and *ATP5B* were used as reference genes and expression was normalised to non-treated "Long Term" cells. Mann-Whitney Non-Parametric Test.

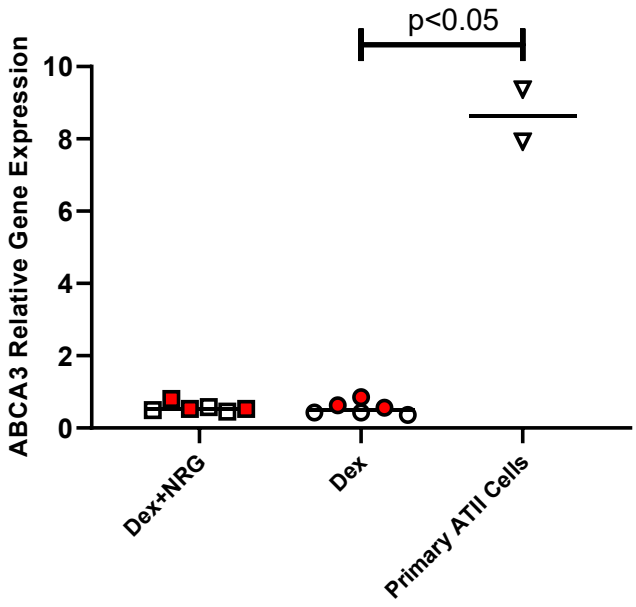

Figure 6.6. *ABCA3* gene expression in long term A549 cultures treated with Dexamethasone (Dex) and neuregulin-1β (NRG-1β) compared to primary human ATII cells.

A549 cells were cultured in F12/10% FBS for three weeks with: no treatment ("Long Term"), with NRG-1β at 50 ng/mL ("NRG"), Dex at 100 nM ("Dex") and a combination NRG-1β at 50 ng mL and Dex at 100 nM (Dex+NRG). Cultures were medium exchanged regularly. At day 21 RNA was extracted for QRT-PCR analysis in parallel with RNA from freshly isolated human primary ATII cells two different donors with TaqMan™ primer/probe sets for *ABCA3* gene expression. *GAPDH* and *ATP5B* genes were used as reference genes. And gene expression was normalised to non-treated "Long Term" A549 cells (data not shown). Data for Dex and Dex+NRG from two experiments. Mann-Whitney Non-Parametric Test. Similar analyses for *ABCB4* in A549 and primary cells was conducted, however *ABCB4* expression could not be detected in primary ATII cells.

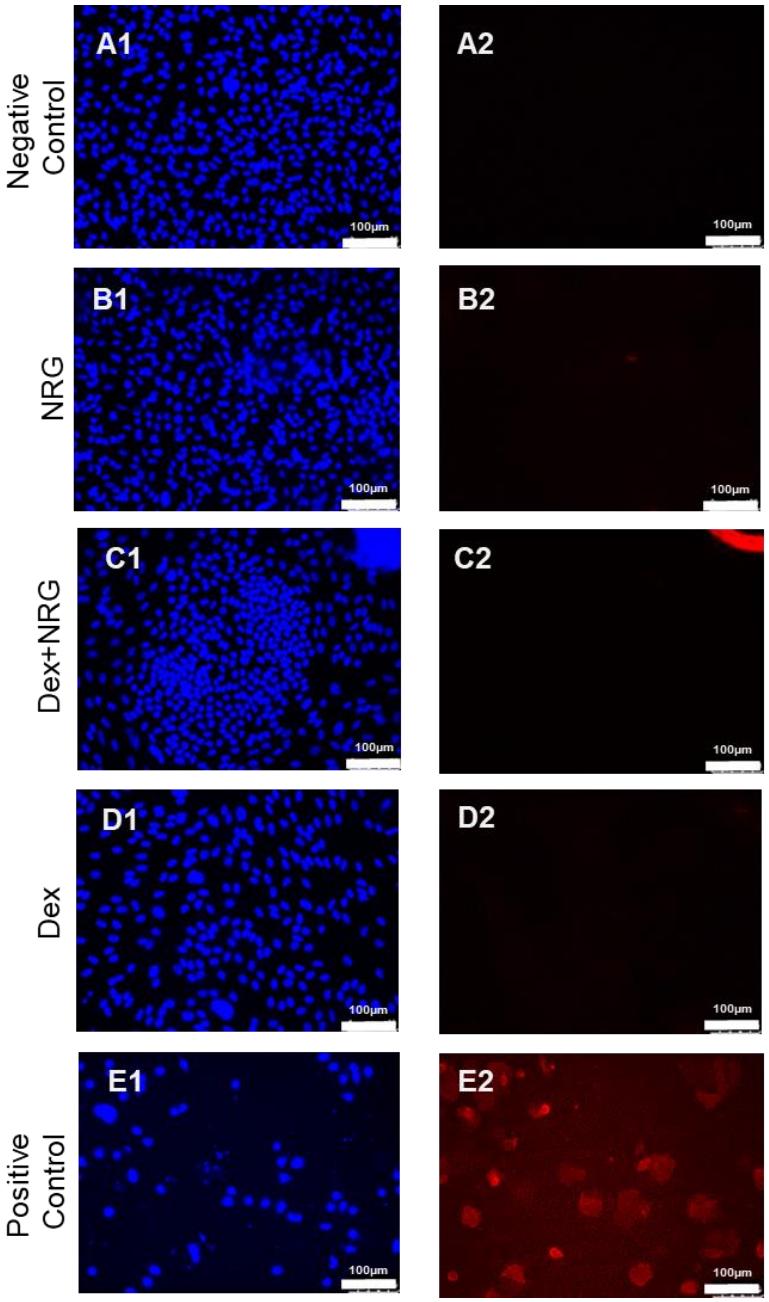

Figure 6.7. Expression of the specific ATII marker HT-280 in A549 cells exposed to chronic treatment with Dexamethasone (Dex) and neuregulin-1β (NRG-1β) compared to primary ATII cells.

A549 cells were cultured in F12/10% FBS for three weeks with: no treatment ("Long Term"), NRG-1β at 50 ng/mL ("NRG"), Dex at 100 nM ("Dex") and a combination NRG-1β at 50 ng mL and Dex at 100 nM (Dex+NRG). Cultures were medium exchanged regularly. At day 21 cells were formaldehyde fixed and indirect immunofluorescent stainined with a nuclear counterstain (NucBlue™) Human primary ATII cells were cultured for 48 hours before similar processing to the A549 cells. Staining for HT-280: mouse IgM anti-human HT-280 primary antibody with Alexafluor®660 conjugated rat anti-mouse IgM secondary antibody. Images from a preliminary single experiment are shown: A and F = Long Term; B and G = NRG; C and H = Dex+NRG; D and I = Dex ; E1 and 2 = primary human ATII cells. For each pair of images, "1" is of the nuclear counterstain to show cellular distribution and "2" is of the fluorescent staining. Scale bar = 100 µm. Data from a single preliminary experiment.

(ii) ATI markers:

ATII cells are thought to differentiate into alveolar type 1 (ATI) cells; over time *in vitro* and to replace damaged ATI cells *in vivo*. Thus, in attempting to establish *in vitro* ATII-like models it is important to assess the level of expression of ATI associated markers. Caveolin-1 (CAV-1) is a scaffolding protein and a component of the caveolae plasma membranes and is highly expressed in ATI cells. Figure 6.8 shows a significant upregulation of *CAV-1* in Dex treated A549 cells, but interestingly not in cells treated with both Dex and neuregulin. Dex induced *CAV-1* to levels above those detected in primary ATII cells; an unwanted feature.

Aquaporin 5 (AQP5) is a water channel protein and is associated with ATI cells where it is thought to play a role in aqueous secretions in the lung. *AQP5* gene expression was assessed in the treated A549 cells and primary ATII cells using QRT PCR however the Ct values returned for the *AQP5* gene were either very high or there was no detectable amplification in samples. It was concluded that there was no appreciable gene expression of AQP5 in primary ATII cells or in any of the A549 cultures assessed hence data are not presented.

When compared to the *CAV-1* gene expression in ATII primary cultures (Figure 6.9) it can be seen that expression was substantially higher in Dex treated A549 than in the primary cells.

Indirect Immunofluorescent staining for the ATI specific marker HT1-56 was undertaken on the treated A549 cultures. The strongest signal for this marker was seen in Dex+NRG-1β treated cultures and particularly localised to the clusters of cells (Figure 6.10).

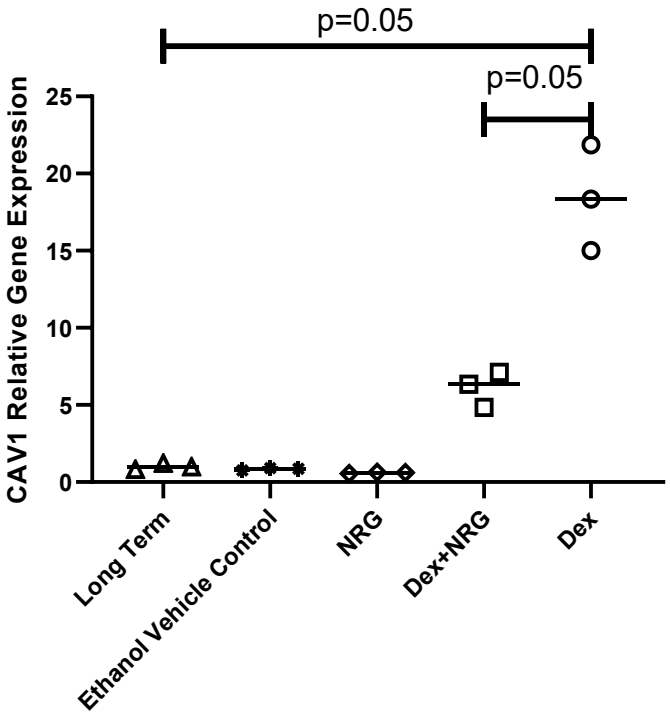

Figure 6.8. The gene expression of the ATI marker *CAV-1* in long term A549 cultures is influenced by chronic treatment with Dexamethasone (Dex) and neuregulin-1β (NRG-1β).

A549 cells were cultured in F12/10% FBS for three weeks with no treatment ("Long Term"), with NRG-1β at 50 ng/mL ("NRG"), Dex at 100 nM ("Dex") and a combination NRG-1β at 50 ng/mL and Dex at 100 nM (Dex+NRG). Cultures were regularly medium exchanged. At day 21 RNA was extracted for QRT-PCR analysis with a TaqMan™ primer/probe set for *CAV-1* gene expression. *GAPDH* and *ATP5B* genes were used as reference. Gene expression was normalised to "Long Term" A549 cells. Mann-Whitney Non-Parametric Test. Data from a single experiment. Similar analysis was carried out for the ATI marker *AQP5*, however there was little or no detectable amplification.

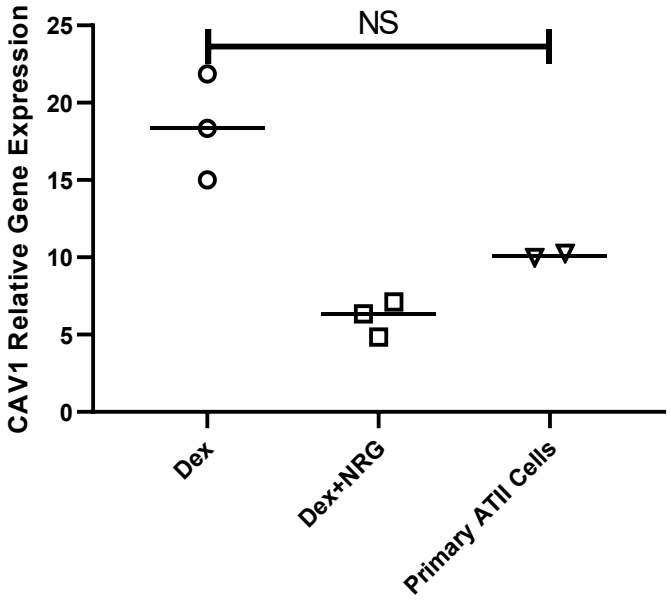

Figure 6.9. CAV1 gene expression in long term A549 cultures treated with Dexamethasone (Dex) and neuregulin-1β (NRG-1β) compared to primary human ATII cells.
A549 cells were cultured in F12/10% FBS for three weeks with: no treatment ("Long Term"), with NRG-1β at 50 ng/mL ("NRG"), Dex at 100 nM ("Dex") and a combination NRG-1β at 50 ng/mL and Dex at 100 nM (Dex+NRG). Cultures were medium exchanged regularly. At day 21 RNA was extracted for QRT-PCR TaqMan™ primer/probe sets for *CAV-1* gene expression analysis in parallel with RNA freshly isolated human primary ATII cells from lung biopsies from two donors. *GAPDH* and *ATP5B* were used as reference. Expression data were normalised to "Long Term" cells (data not shown). Mann-Whitney Non-Parametric Test. Data from a single experiment.

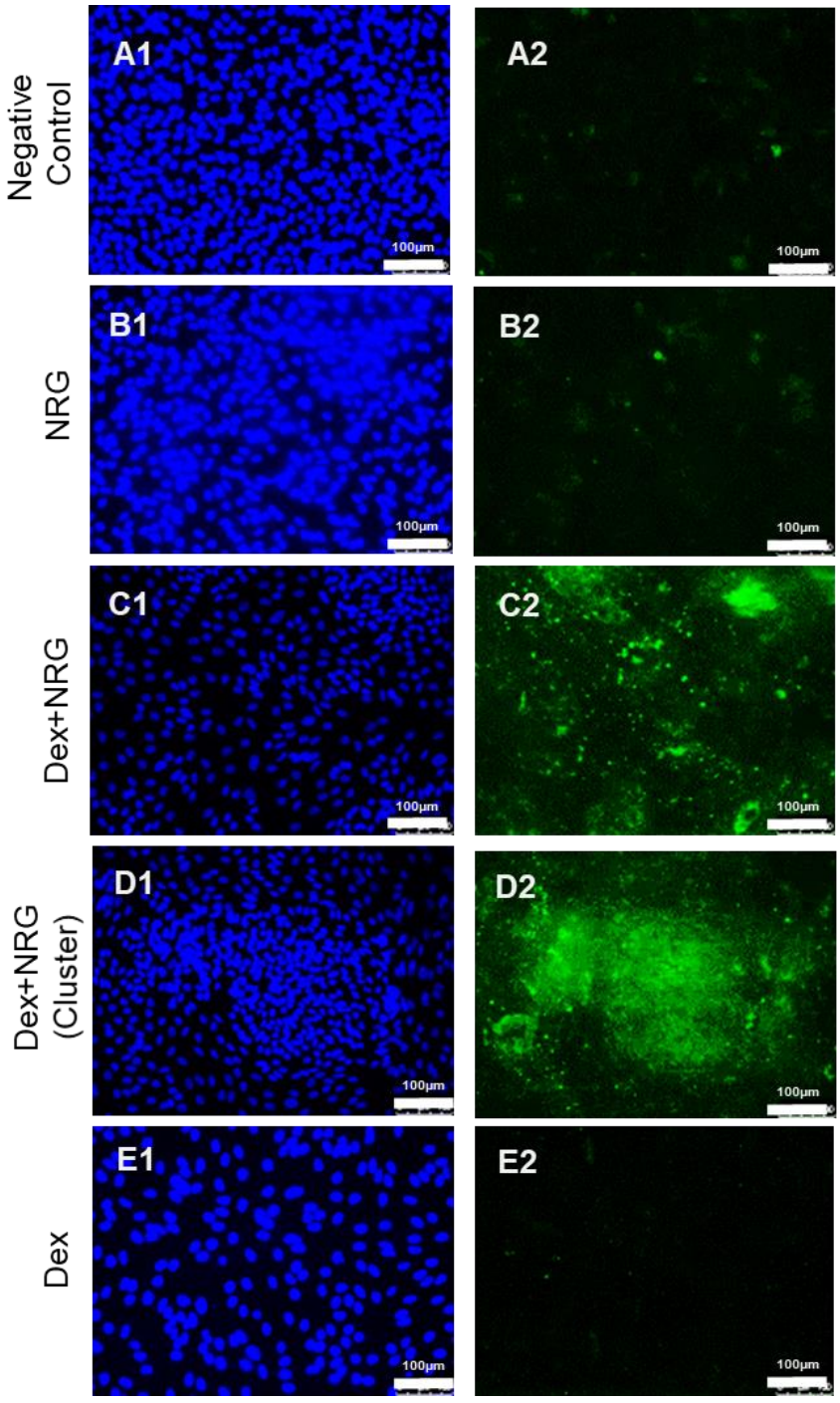

Figure 6.10. Expression of the specific ATI marker HT1-56 in long term cultured A549 cells exposed to chronic treatment with Dexamethasone (Dex) and neuregulin-1β (NRG-1β).
A549 cells were cultured in F12/10% FBS for three weeks with: no treatment ("Long Term"), NRG-1β at 50 ng/mL ("NRG"), Dex at 100 nM ("Dex") and a combination NRG-1β at 50 ng/mL and Dex at 100 nM (Dex+NRG). Cultures were medium exchanged regularly. At day 21 cells were formaldehyde fixed and indirect immunofluorescent stained with a nuclear counterstain (NucBlue™).™). Staining for HT1-56: mouse IgG anti-human HT1-56 primary antibody with Alexafluor™ 488 conjugated goat anti-mouse IgG secondary antibody. Representative images from a preliminary single experiment are shown: A = Long Term, B = NRG, C = Dex+NRG, D = Dex+NRG but centred on a cellular cluster, E = Dex. For each pair of "1" is of the nuclear counterstain to show cellular distribution and "2" is of the fluorescent staining. Scale bar = 100 µm. Data from a single preliminary experiment.

6.3.4 Effect of Dex on ERBB3 Expression

Neuregulins (also known as heregulins), particularly neuregulin-1β (NRG-1β), play a critical role in the developing lung. It is generally accepted that they are produced by lung fibroblasts and act as ligands for the epidermal growth factor (EGF) family of receptor tyrosine kinases (ErbB or HER)[323]. ErbB (ErbB1-4) receptors are found on the lung epithelia and, in the rat, and ErbB3 and 4 appear to play a pivotal role in the epithelial to mesenchymal cross-talk required for the development and maintenance of the alveolar epithelium[323] and are therefore a desirable requirement for *in vitro* ATII models.

Previously conducted microarray analysis (Chapter 4) indicated that *ERBB4* expression in long term A549 cells was not significantly up or down regulated (fold change two or more) between log phase cultured A549 cells and long term cultured cells.

The microarray data did however indicate that gene expression of the alternative *ERBB3* receptor was significantly upregulated by long term culture. This result was validated by QRT PCR gene expression (Figure 1.1) where it can also be seen that the expression of the receptor was significantly down regulated in the presence of Dex.

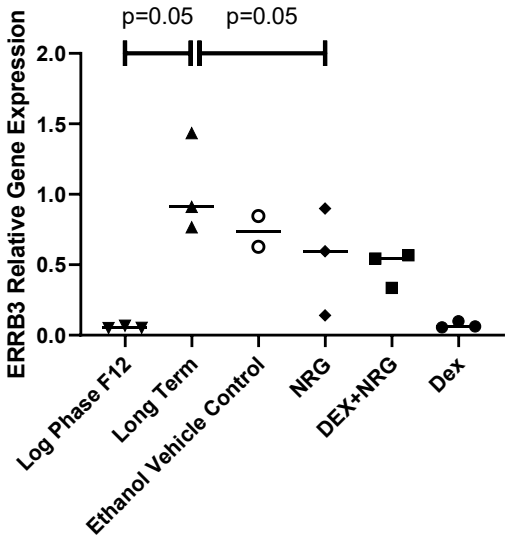

Figure 6.11. The gene expression of ERBB3 in long term A549 cultures is influenced by chronic treatment with Dexamethasone (Dex) and neuregulin-1β (NRG-1β).
A549 cells were cultured in F12/10% FBS in short term log phase culture (Log Phase), for three weeks with no treatment ("Long Term"), with NRG-1β at 50 ng/mL ("NRG"), Dex at 100 nM ("Dex") and a combination NRG-1β at 50 ng/mL and Dex at 100 nM (Dex+NRG). Cultures were regularly medium exchanged. At day 21 RNA was extracted for QRT-PCR analysis with a TaqMan™ primer/probe set for *ERBB3*. *GAPDH* and *ATP5B* were used as reference genes and gene expression data were normalised to non-treated "Long Term" A549 cells. Mann-Whitney Non-Parametric Test. Data from a single experiment.

6.4 Discussion

Two factors have been identified that might drive A549 cells to an ATII like state: Dexamethasone (Dex) and the ERBB ligand NRG-1β. This assertion was based on the evidence that fibroblast conditioned medium or co-culture with fibroblasts together with glucocorticoids such as Dex can drive mouse ATII cells to surfactant protein (*SFTP*) production through the release of a putative factor or combination of factors known as Fibroblast Pneumocyte Factor (FPF) of which NRG-1β has been suggested as an active component[481 323 485]. It was hypothesised that a combination of the long-term three-week differentiation ('Long Term') protocol developed in Chapter 2, together with Dex and NRG-1β treatment would drive an ATII like phenotype in A549 cells manifested by the expression of *SFTP*s, ATII markers and absence of ATI markers.

In agreement with the published literature[470 486], significant and promising induction of *SFTPB, C* and *D* genes was induced by Dex in A549 cells as compared to the non- long-term cultures. However, the levels of *SFTPB* and *C* expression did not approach those seen in primary ATII cells. In contrast, *SFTPD* mRNA was up-regulated above that observed in primary ATII.

It was expected that a combination of NRG-1β and Dex would have an additive or synergistic effect on A549 cells bringing them closer to a true ATII phenotype. The Dex+NRG-1β results obtained, however, were disappointing with no significant advantages seen in any of the ATII markers evaluated and in the case of *SFTPC* and D NRG-1β may have inhibited the positive effects of Dex.

NRG-1β ERBB4 mediated induction of *SFTPB* gene and protein expression requires the ERBB4 receptor to be expressed on the membrane of the target cell. ERBB4 is believed to dimerise with ERBB1 and once bound to the NRG-1β ligand the complex acts as a transcription factor for the *SFTPB* gene[487]. Protein expression of ERBB4 in A549 cells, however, may be very low or negligible[488]. This was alluded to in earlier experiments (RNA micro-array data (Chapter 4)) where no significant upregulation of *ERBB4* gene expression was detected in long term A549 cells. It is possible that NRG-1β stimulated *SFTP* response in A549 cells may be absent simply because there are no receptors to which the ligand could bind. The data here indicated that ERBB3 gene expression was suppressed by Dex. It is possible that any residual ERBB4 expression was repressed by Dex also.

There is a close relation between ERBB receptor and glucocortoid receptor signalling, ERBB signalling is considered to be mediated via the receptor tyrosine kinase (RTK) pathway which in itself is inhibited by glucocorticoids such as Dex [489] indicating potential intrinsic conflict between NRG-1β and Dex stimulation.

Dex operates through interaction with the glucocorticoid receptor (GR) and has multiple inhibitory and stimulatory effects on most cells with a multi-facetted effect on gene regulation[490] [491] and at least 71 glucocorticoid responsive genes are regulated by Dex treatment of A549 cells[479] . GR binding can also affect many other cell signalling events as described in an in a recent review[492].

A substantial increase in Dex induced *SFTPB* was observed whereas although *SFTPC* regulation was significant it was not in the same order of magnitude. Others have shown that Dex induced gene expressions of *SFTPB* and *C* are regulated by different mechanisms. Induction of *SFTPB* seems to be a primary response with increases in transcription rate and mRNA stability, whereas induction of *SFTPC* is a secondary process, requiring ongoing protein synthesis, increased transcription rate without a change in mRNA stability[493]. The increased SFTPB mRNA stability, which can increase the half-life (by two fold), induced by Dex[494] may have contributed to observed mRNA levels in QRT PCR experiments presented here.

There was no significant effect of Dex or Dex+NRG-1β on induction of *SFTPA1* or *A2* gene expression in long term A549 cells and it may be that Dex inhibited *SFTPA* gene transcription (as shown through the glucocorticoid inhibition of cAMP and IL-1 to stimulate *SFTPA* gene expression in human foetal ATII cells[495]). Surfactant A production in response to IL-1 treatment of A549 would be an interesting study for future work although cancer research studies have demonstrated that A549 cells display an EMT-like response to IL-1 treatment, alluding to the inherent cancerous phenotype of the cell line[496].

Several factors could explain the substantial gene induction of *SFTPB* and *SFTPD* in Dex treated A549 cells. The pro-inflammatory cytokine IL-6 has been identified as a an alternative stimulator of *SFTP* expression, in particular *SFTPD*[497]. Both IL-6 and SFTPD are upregulated lung injuries in cases of acute respiratory disease (ARDS) where lung function is dysfunctional due to alveolar damage[498] and in ARDS associated with Covid-19 where they have been identified as markers associated with mortality[499]. A positive additive effect of IL-6 and Dex on *SFTPB* expression in A549 and H441 cell lines has been reported suggesting a role for IL-6 in ATII-like differentiation of the cell lines[471] [500]. The signalling for this Dex / IL-6 induction appears to be transduced via the Janus Kinase Signal Transducer and Activation of Transcription (JAK STAT) pathway[501] which is independent to the Dex inhibited RTK mediated pathway for *SFTP* transcription[500]. Treatment of lymphocytes with Dex led to upregulation of IL-6 receptor [502] and it would be of interest to determine if Dex has similar effect on A549 cells. Lee *et al* (2016) have reported that A549 cells secrete high levels of endogenous IL-6 in culture suggesting that endogenous IL-6 secretion by A549 cells together with Dex mediated upregulation of IL-6 receptors could explain, in part, the induction of

SFTPB and *D* genes via an autocrine IL-6 response. This would be mediated by the JAK STAT pathway and explain the shift from RTK mediated *SFTP* regulation to the GR stimulated JAK STAT pathway. *SFTPD* has a role in maintaining pulmonary homeostasis and high concentrations of secreted *SFTPD* as seen with Dex treatment may exhibit a negative feedback effect on *SFTP* induction[503].

Dex induced a morphological change in the cultures leading to the adoption of a more flattened morphology. The adoption of this property might explain the observed modest increase in vimentin mRNA expression in the Dex treated cells (Appendix C). This does not, however appear to be evidence of EMT as there is an opposing increase in the gene expression of the epithelial marker CDH1(Appendix C).

The changes in morphology may have an impact on the expression of surfactant proteins. The maintenance of *SFTP* gene expression in ATII cells is dependent on signals provided by cell-cell interactions, extracellular matrix, and growth factor stimulation in the alveolar microenvironment. Primary ATII in 2D cell culture lose expression of SP-A, SP-B and SP-C. Culture under conditions that maintain ATII morphology prolongs surfactant protein gene expression and ATII differentiation *in vitro*. ATII cells cultured on a 3D substrate of foetal lung fibroblasts embedded in a collagen matrix retained ATII phenotype with sustained expression of *SFTPA*, *B* and *C mRNA*[504] suggest that organization of the ATII cytoskeleton may influence *SFTP* gene expression[505].

NRG-1β alone had little effect on cell morphology but Dex+NRG-1β induced an unusual morphology with regularly spaced colonies of apparently proliferative small cells amongst a background of flattened and elongated cells. This morphology was unlike that observed in Dex treated cells. These cellular clusters of cells bore a resemblance to colonies of embryonic stem cells (Appendix C). Initial experiments with immunofluorescent staining suggested that the expression of surfactant proteins B and C were associated with these clusters, however, it could also be that this is simply a result of non-specific antibody binding to the higher cell densities in these colonies. It should be noted that the QRT PCR *mRNA* results for the Dex+NRG-1β cultures included all cells in the treated wells. It may be of interest in future work to attempt to physically separate the two different morphologies and compare their gene expression. This possible masking of the responses of one population with another may account for the lack of meaningful results from the Dex+NRG-1β cultures.

Investigation of the Dex+NRG-1β induced 'stem cell-like' A549 colonies by immunofluorescent staining for stem cell specific markers in the colonies showed sporadic staining for Oct-4, and SSEA4 and extensive Tra-1-60 expression was observed clusters.

(Appendix C). The results suggested expansion of cancer stem cell-like sub-populations within the colonies supporting findings of other researchers[506].

Dex treatment did not increase the expression of the key ATII marker ABCA3 above that seen with three week non-treated cultures**.** ABCA3 expression was downregulated significantly by Dex, however the Ct values in the PCR reactions were relatively low in all samples indicating that there was substantial expression in all samples but not at the levels seen in Primary ATII cells.

It is important that ATII cellular models do not exhibit properties of ATI cells. The gene expression of the ATI marker AQP5 could not be detected at significant levels in any of the treatments not the ATII primary cells. Caveolin (*CAV*), which is considered to be a marker of ATI cells was expressed at significantly higher levels in Dex treated A549 cells, this was, however, not significantly higher than the levels observed in primary ATII Cells.

Dex+NRG-1β also appeared to drive the apparent expression of the ATI marker HT1-56 indicating potential differentiation to an ATI like-state rather than ATII indicating that the effects of Dex may not only be non-beneficial, they might be inducing de-differentiation and the adoption of undesirable characteristics of other cell types.

The objective was to drive the A549 cells to a ATII-like differentiated state, these data show potential de-differentiation which is an undesirable retrograde step suggesting that the supplementation of cultures with Neuregulin 1-β may not be a suitable strategy in the quest to derive an ATII phenotype from A549 cells.

As well as having beneficial roles in cellular differentiation, Neuregulins may have a role in the development/progression of certain types of human cancers. Neuregulins can be strong mitogenic factors in cells that express ERBB receptors[507]. Although it seems unlikely that A549 cells substantially express ERBB4, other studies and data presented here suggest that A549 cells might express ERBB3 and ERBB2 (also known as HER2) receptors[508] and it is known that NRG-1β will activate malignant progression of tumours on interaction with ERBB3[509]. This evidence suggests that the Dex+NRG-1β treatment may be inducing a tumour-like phenotype in the A549 cells, potentially activating a cancer stem cell side population[506].

Some further work is required to further evaluate the effect of Dex treatment of A549. at this point it is unknown if Dexamethasone treated A549 cultures derived in expressed multilamellar bodies, therefore this should be repeated and samples analysed by TEM. Immunofluorescent work examining SFTP expression needs to be repeated with a full set of positive and negative control to provide more robust results. The use of Western Blotting to evaluate SFTP protein, expression should be considered and a more extensive investigation of

EMT markers and stem cell markers on Dex/NRG treated cultures would be of interest. However, considering the wide-ranging effect of Dex on A549 cells, these studies would not be high priority.

In summary Dex treatment confers modest advances over the non-treated long term A549 cultures in the form of increased STPC, B and D expression and increased CDH1 however the phenotype of the Dex treated "differentiated" A549 cells is limited and functionally distant from that of primary human ATII cells. NRG-1β alone had little or no effect on cellular differentiation and when used in combination with Dex it seemed to drive a cancer stem cell phenotype.

Supplementation of long term A549 cultures with just one or two purified factors is not enough to bring about a true ATII phenotype in A549 cells, a more complex co-culture approach employing lung fibroblasts may be required. It is also evident that Dex treatment may not be entirely beneficial with negative effects that might negate the *SFTP* expression advantages.

7. Development of an *in vitro* Co-Culture Model of the Alveolar Epithelium

7.1 Introduction

In developing a more complex and physiologically relevant co-culture model it is worth considering the way in which ATII and fibroblasts interact in lung development. Rehan and Torday and others[510 31 32] have proposed a mesenchymal–epithelial cross talk model of lung development in the rodent focussing on the key paracrine factors and cell types required. (Figure 7.1) In this model, the mesenchymal support is provided by PLIN-2 positive differentiated lipofibroblasts. Following stimulation of PPARγ receptors, lung fibroblasts differentiate into lipofibroblasts which are believed to be the supporting mesenchyme required for proper ATII development. Under the influence of parathyroid hormone related peptide (PTHrP) (also known as parathyroid -like hormone) the lipofibroblasts are thought to secrete leptin and PLIN2 which together with triglycerides from the blood (*in vivo*) or cell culture medium (*in vitro*) and retinoids drive ATII differentiation and provide the raw materials for MLB formation (Figure 7.1).

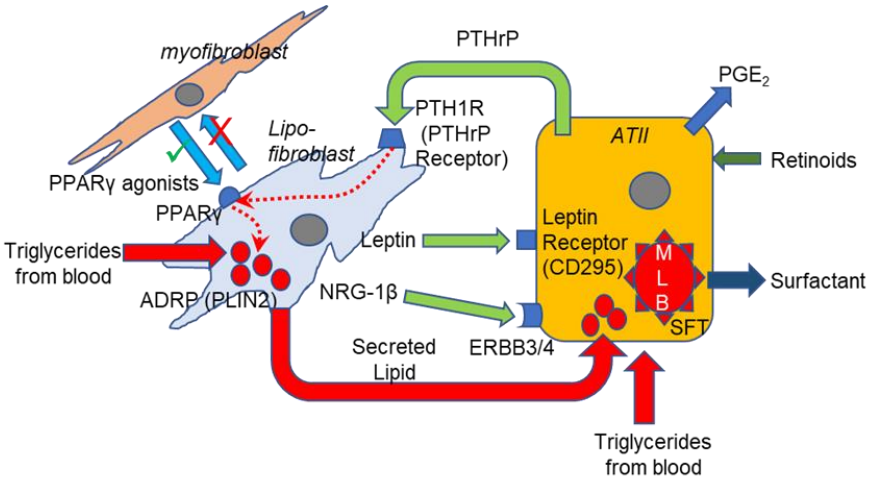

Figure 7.1. Lipofibroblast mediated ATII development, differentiation and support in rodent.
In rodents ATII cells express parathyroid hormone related protein (PTHrP) and prostaglandin E_2 (PGE_2). PTHrP acts on its receptor on the lipofibroblast via protein kinase A activation to positively regulate PPARγ along with PGE_2. This has a downstream effect of upregulating and activating adipose differentiation-related protein (ADRP), also known as perilipin 2 (PLIN2, ADRP) surrounds lipid droplets and mediates triglyceride uptake by fibroblasts and the ATII cell. Leptin expression by the fibroblast stimulates surfactant phospholipid production by ATII cells leading to MLB formation and the maintenance of both ATII and lipofibroblast phenotypes. PPARγ agonism is thought to prevent transdifferentiation[510] of the lipofibroblasts to myofibroblasts[90]. Retinoids have a role in ATII support[511] and Neuregulin (NRG-1β) and its associated ERBB receptors have a role in the developing alveolus[323] (After Torday and Rehan)[58].

It is probable that the cross-talk between fibroblasts and ATII cells in humans is far more complex than the model proposed here. The presence of lipid droplet containing lipofibroblast cells in the human lung is controversial [91] [92] [512] and there is emerging evidence that fibroblast Wnt signalling and other developmental pathways may also be important in maintaining homeostasis in the alveolar epithelium[513], particularly in providing ATII stem cells with capacity to differentiate into ATI cells to effect epithelial repair[514] [515].

It was proposed that the next tranche of experimental work should employ co-culture of A549 cells with human lung fibroblasts. A candidate fibroblast cell line is the normal human foetal fibroblast cell line MRC-5[516] which might have the capacity to be differentiated to a PLIN-2 expressing adipogenic lipofibroblast-like fibroblast under the influence of a PPARγ agonist such as Rosiglitazone™ (RGZ)[90].

A step wise constructive approach was proposed. In Chapter 6 it was seen that Dex had some positive benefits in the induction of *SFTP* genes and potentially SFTP expression, however detrimental effects were also seen on ERBB3 gene expression and A549 cell morphology. It is also known that Dex has a wide ranging and significant effect on gene expression in A549 cells[479]. The first step would therefore be to determine if Dex treatment A549 cells impacts on the expression of key autocrine factors thought to be expressed by ATII cells (Figure 7.1). Indirect co-culture with conditioned medium from MRC-5 fibroblasts, both untreated and treated with RGZ would then show the benefits of any paracrine factors produced by the MRC-5 cells. The two cell lines could then be brought together in co-culture, firstly in a proven Transwell™ system[517] and finally a novel 3D scaffold system. Alvetex™ Scaffold (an emulsion-templated porous polystyrene based polymer (PolyHIPE))[338] which offers the potential of providing a tissue-like micro-environment that might encourage physiological cross-talk between ATII-like A549 cells and MRC-5 fibroblasts. This scaffold has been used to provide an *in vitro* model of human skin using human dermal fibroblasts and keratinocytes[518]. It is hypothesised that a similar approach might be effective *in vitro* modelling of the alveolar epithelium to provide appropriate physical cues to increase the efficiency of the paracrine factors involved epithelial- mesenchymal cross talk[519] as outlined in Figure 7.1.

7.2 Hypotheses

It was hypothesised that A549 co-culture with lung fibroblast cells both indirectly through the use of medium conditioned by the foetal lung fibroblast cell line MRC-5 in 2D culture and through direct co-culture in Transwells™ or an advanced 3D scaffold will recapitulate elements of *in vivo* alveolar epithelial to mesenchymal cross-talk. This cross-talk will drive the A549 into a more physiological ATII state, as compared to primary ATII isolates, than seen previously with long term culture and treatment with dexamethasone and neuregulin-1β. Furthermore, directed differentiation of the lung fibroblast cells to a lipofibroblast-like phenotype will be advantageous to ATII-like differentiation in A549 cells.

7.2.1 Aims

- Evaluate the suitability of the human lung fibroblast cell line MRC-5 though its gene expression of factors implicated in cellular cross talk between epithelium and mesenchyme.
- Determine suitability of dexamethasone incorporation into a co-culture model though gene expression analysis.
- Evaluate the effect of fibroblast conditioned medium on A549 cells grown in 2D and Co-culture in Transwells™ through the use of gene expression analysis of surfactant proteins, ATII and epithelial markers and factors implicated in the cellular cross talk between epithelium and mesenchyme.
- Generate 3-D co-culture models in Alvetex™ Scaffold with and without the addition of ascorbic acid to stimulate collagen production by the fibroblast cells. Evaluate the tissue-like organisation in the potential models through the use of histology and electron microscopy.

7.2.2 Objectives

- Adapt MRC-5 cells to the media requirements of the co-culture models to avoid confounding media formulation effects and confirm the cells can be cultivated in the medium.
- Define an optimal timeframe for conditioned medium production and generate FCM from MRC-5 cells
- Determine an optimal ratio of FCM to growth medium to elicit SFTP regulation in A549 cells.
- Determine an optimum concentration and time-frame for lipofibroblast differentiation in MRC-5 cells.

- Identify, establish and evaluate methods for producing A549/MRC-5 co-cultures in Transwell™ and Alvetex™.
- Quantify and qualify the level of ATII-like differentiation in A549 cells in these systems through assessment of gene expression of epithelial marker genes and ATII specific genes such as surfactant genes. Compare these data with those obtained from Dex and NRG-1β treated cells and primary cultures.
- Use histological techniques and transmission electron microscopy to assess development of features of the lung parenchyma in the 3D co-culture model namely signs of histo-typical cell growth and morphology and quiescence in the fibroblastic and epithelial compartments, ECM deposition by the fibroblast cells and monolayer growth and MLB expression in the A549cells.

7.3 Results

7.3.1 Dexamethasone Down Regulates PTHrP Gene Expression

It was postulated that parathyroid hormone related protein (PTHrP) might play a role in epithelial/mesenchymal crosstalk in any A549 based co-culture model. The previous chapter showed that dexamethasone (Dex) had a positive impact on SFTP regulation in A549 cells, however It is known from the literature that Dex has a significant impact on expression of glucocorticoid responsive genes in A549 cells[479] and previous work has implied at its overall incompatibility with physiologically relevant cellular behaviour. It was therefore important to determine if Dex treatment affected *PTHrP* regulation before considering its incorporation into a co-culture model. Long term A549 cultures were chronically treated in a similar manner to Chapter 6 with Dex and NRG-1β singularly and in combination, and *PTHrP* expression compared with that found in untreated 'long term' and log phase A549 cells (Figure 7.2).

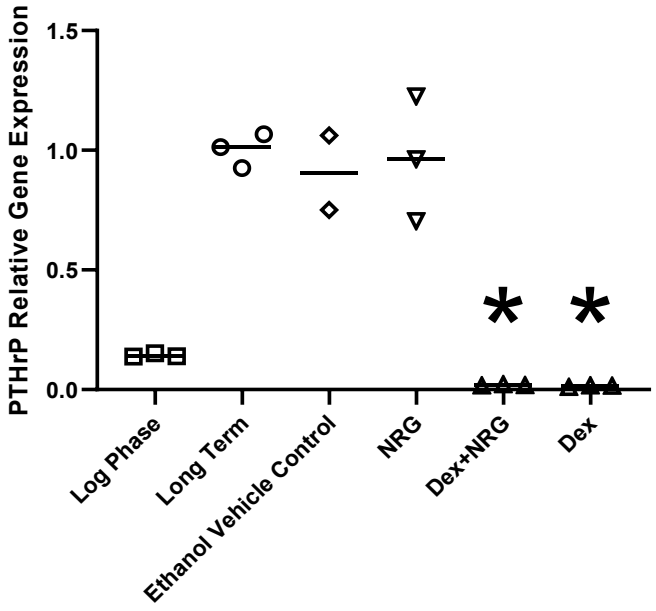

Figure 7.2. PTHrP gene expression in long term A549 cultures is influenced by chronic treatment with Dexamethasone (Dex).
A549 cells were cultured in F12/10% FBS for three weeks with no treatment ("Long Term"), with NRG-1β at 50 ng/mL ("NRG"), Dex at 100 nM ("Dex") and a combination NRG-1β at 50 ng/mL and Dex at 100 nM (Dex+NRG). At day 21 RNA was extracted, quantified, for QRT-PCR analysis with TaqMan™ primer/probe sets for *PTHrP* gene expression. *GAPDH* and *ATP5B* were used as reference genes. Relative expression was normalised to "Long Term" A549 cells. RNA from log phase cultured A549 cells was also included as an additional low-expressing control. Non-parametric Kruskal-Wallis test with comparison to Long Term (Control). Data from a single experiment. *=$p<0.05$.

It was found that Dex treatment significantly down regulated *PTHrP* gene expression in A549 cells to level even less that that found in log phase cultures. This, together with other negative aspects of Dex treatment that have previously been discussed lead to the decision to cease the incorporation of Dex in experiments. Addition of NRG-1β was not shown to have significant impact on A549 ATII gene or protein expression in the previous chapter, however it still may be required in the milieu of factors involved in putative co-culture model. It is suggested that appropriate fibroblast cells line such as the human foetal lung fibroblast MRC-5 might provide naturally secreted NRG-1β avoiding any need to add the factor exogenously.

It should be noted that NRG-1β is not specifically produced by lung fibroblasts it is a key signalling molecule secreted by fibroblasts in many other tissues and is important in the development of the heart, nervous system and mammary tissue[323]. It is not produced in all fibroblasts, as some (for example cardiac fibroblasts) also express ErbB receptors[520]. It seems absence of ErbB receptors is a pre-requisite for NRG-1β expression[323].

7.3.2 Adaptation of MRC-5 Cells to Ham's F12 Medium.

Previous work showed that Ham's F12 culture medium supplemented with 10% v/v Foetal Bovine Serum and 2mM L-glutamine (Ham's F12/10% FBS) is an appropriate medium for steering A549 cells to an ATII-like phenotype through long term culture. It has also been demonstrated that other cell culture media may have a detrimental effect ATII features in the cell lines. The recommended culture medium for MRC-5 fibroblasts, however, is MEM/10% FBS. Prior to combining A549 and MRC-5 cells together it was necessary to ensure that MRC-5 cells grew favourably in Ham's F12/10% FBS. Cultures of MRC-5 fibroblasts were set up in both media and their growth profiles determined by automated microscopy (Incucyte Zoom). No significant difference could be discerned in the growth profiles in either culture medium formulation (Figure 7.3A). The cells were cultivated for four passages in the different media and the cell yields at subculture compared. No diminishment in cell viabilities was observed (Figure 7.3C) however there was a small but significant reduction in cell yields (Figure 7.3B).

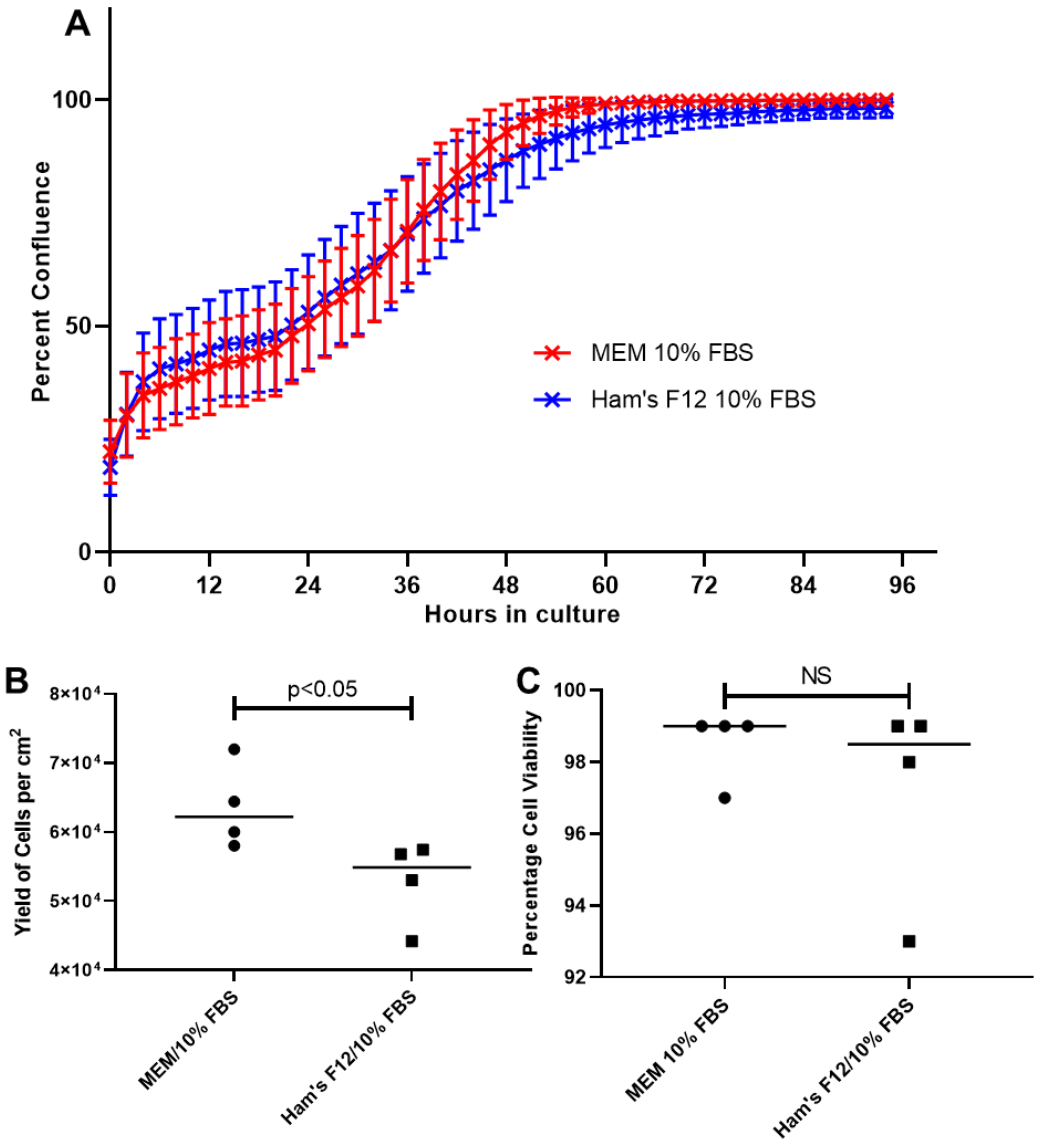

Figure 7.3. Growth comparison of MRC-5 cells cultured in MEM/10%FBS or in Ham's/F12 10% FBS.

MRC-5 fibroblasts were grown in tissue culture flasks in MEM 10% FBS or Ham's F12/10% FBS (126 sectors analysed in two independent flasks per condition) and cultured for 96 hours. Confluence data was acquired using the Incucyte Zoom™ automated microscope from 63 sectors within each flask every two hours to generate growth profiles (A). Growth profile differences between the media were found to not be significantly different by statistical test (*t*-test). The cells were then sub-cultured for four passages in the two media and the cell yields (cells/cm^2) (B) and viabilities (C) determined using a proprietary acridine orange/propidium iodide viability assay (Chemometec NC3000 ViaCount™). Statistical analysis: Mann Whitney non-parametric test. Data from a single experiment.

Microscopic examination of the cultures showed there was a slight increase in cell spreading and a slightly flatter morphology in the Ham's F12/10% FBS cultured cells that might explain the reduction in cell yield however this impact was not considered to be disadvantageous (Figure 7.4).

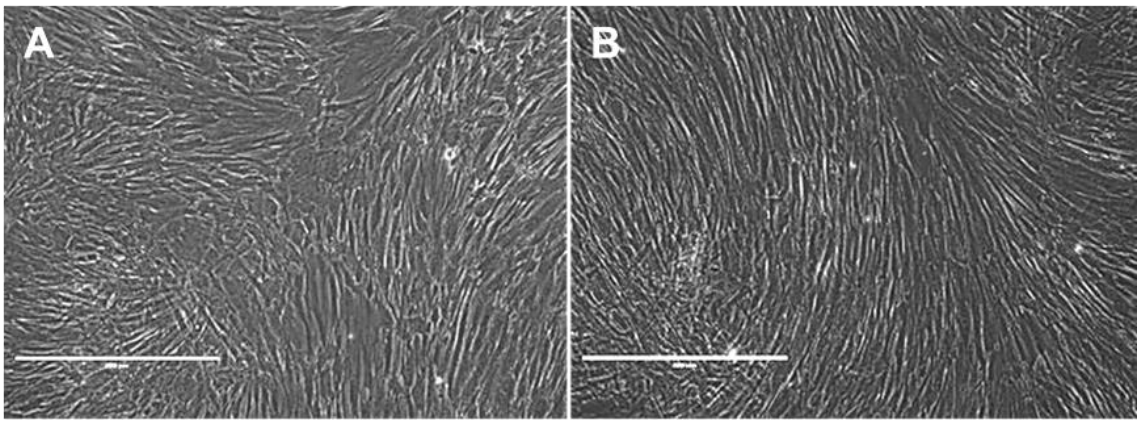

Figure 7.4. Morphological comparison of MRC-5 cells cultured in MEM/10%FBS or Ham's/F12 10% FBS.
Representative images of MRC-5 fibroblasts after culture in Ham's F12/10% FBS (A) or MEM/10% FBS (B) and imaging by phase contrast microscopy 3 days after seeding. Scale bar = 200 μm. Data from a single experiment.

7.3.3 Generation of Fibroblast Conditioned Medium

Before embarking on establishing a co-culture model using A549 and MRC-5 cells it was important to characterise the key factors expressed by MRC-5 cells that might be involved in epithelial/mesenchymal cross talk and to explore the effect of MRC-5 fibroblast conditioned medium (FCM) on A549 cells. On the premise that the expression of these factors might be optimal at specific time point in the growth of the MRC-5 cells a time-course was set up according to the schematic (Figure 7.5). Six well tissue culture plates and flasks were seeded with MRC-5 and cultured for nine days with regular medium exchange and sampling of cells for RNA extraction and gene expression analysis.

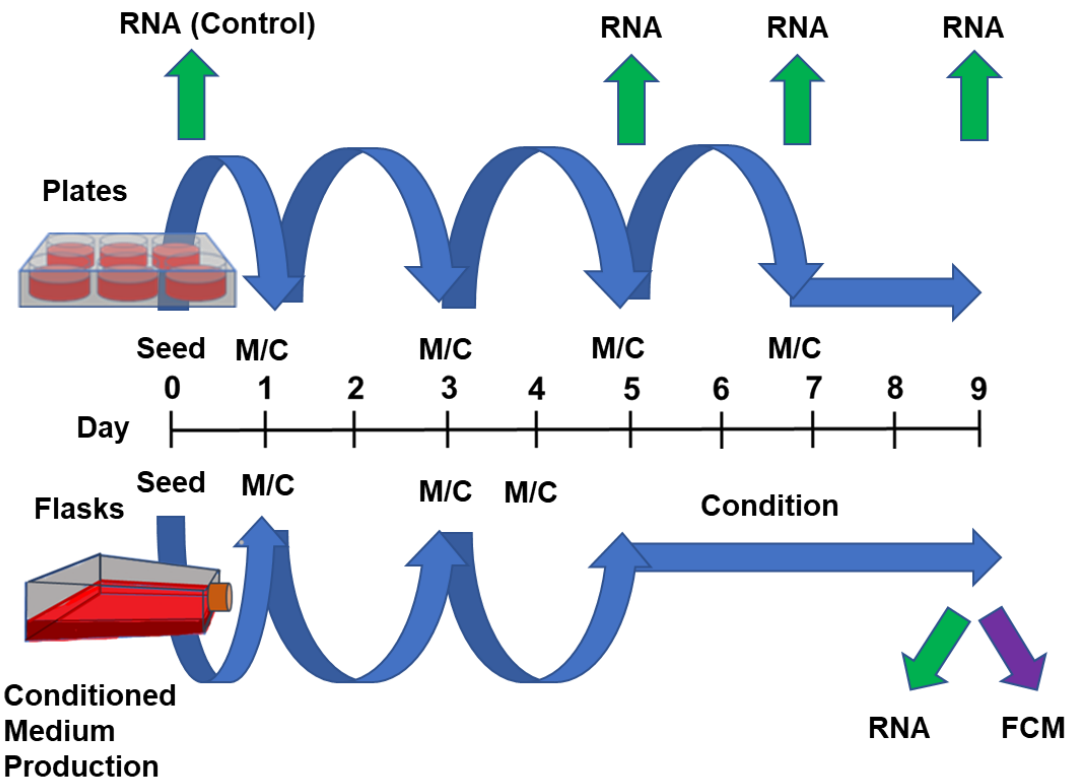

Figure 7.5. Schematic to describe the time course of RNA samples generated for the gene expression analysis of MRC-5 fibroblasts and the production of fibroblast conditioned medium (FCM).
Six-well plates were seeded with MRC-5 cells in Ham's F12 and medium exchanged ("M/C") the day after seeding and every two days until day 7. Cells were harvested on days 5,7 and 9. Flasks were set up in a similar manner, however at day 5 the flask cultures were medium changed but left without further replenishment until day 9 to generate conditioned medium.

As it has been demonstrated that A549 cells can express *PTHrP* at the gene transcription level it is desirable that MRC-5 cells express its receptor: PTH1R. It was also suggested that endogenous expression of NRG-1β would be desirable. Gene expression data (Figure 7.6A and Figure 7.6B) showed that *PTH1R* was at its highest expression level at Day 5, the beginning of the media conditioning period in the flask cultures, and that NRG-1β was highly expressed at the end of the conditioning period.

Although *GAPDH* and *ATP5B* had been identified as being suitable refence genes for use in QRT-PCR for A549 cells it was found that neither of these genes was stably expressed by MRC-5 cells over the time-course of conditioned medium culture. Results of a subsequent investigation (data not shown) demonstrated *B2M* as an appropriate reference gene for normalisation of PCR data from MRC-5 cells.

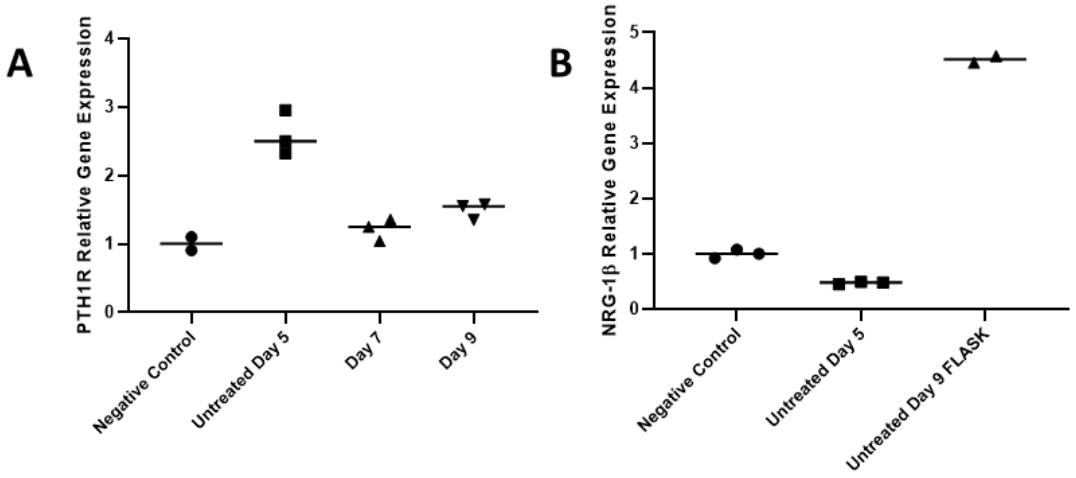

Figure 7.6. Expression of *PTH1R* and *NRG-1β* genes in MRC-5 foetal fibroblasts cultured for nine days.

MRC-5 cells were cultured for nine days in F12/10% FBS according to the schematic (Figure 7.5). On days 5, 7, 9 and day 9 'FLASK' (the point of harvest of the conditioned medium), RNA was extracted, for QRT-PCR analysis with TaqMan™ primer/probe sets for *PTH1R* (A) and *NRG-1β* (B). *B2M* gene was used as a reference. Relative expression was normalised to log phase cultured MRC-5 cells ("Negative Control"). Data from a single experiment. Plate samples from day 7 and 9 were not assessed for NRG-1β. Statistical analysis was not performed due to low sample number. Results from a single experiment.

Throughout the-time course, bright, light refracting inclusions resembling lipid droplets were observed during microscopic examination of the MRC-5 cells suggesting the adoption of an adipogenic or lipofibroblast-like phenotype. These inclusions appeared to be most prevalent at day 5 (the point at which medium conditioning commenced) (Figure 7.7). Lipofibroblasts have been identified as important in the support of ATII cells in rodents It has been suggested that this differentiated fibroblast sub-population may also play a role in the support of human ATII cells, but the evidence for these cells *in vivo* is controversial[91 521]. With this in mind, the gene expression of the lipofibroblast markers *PLIN2* and *PPARγ* in the MRC-5 time-course was investigated.

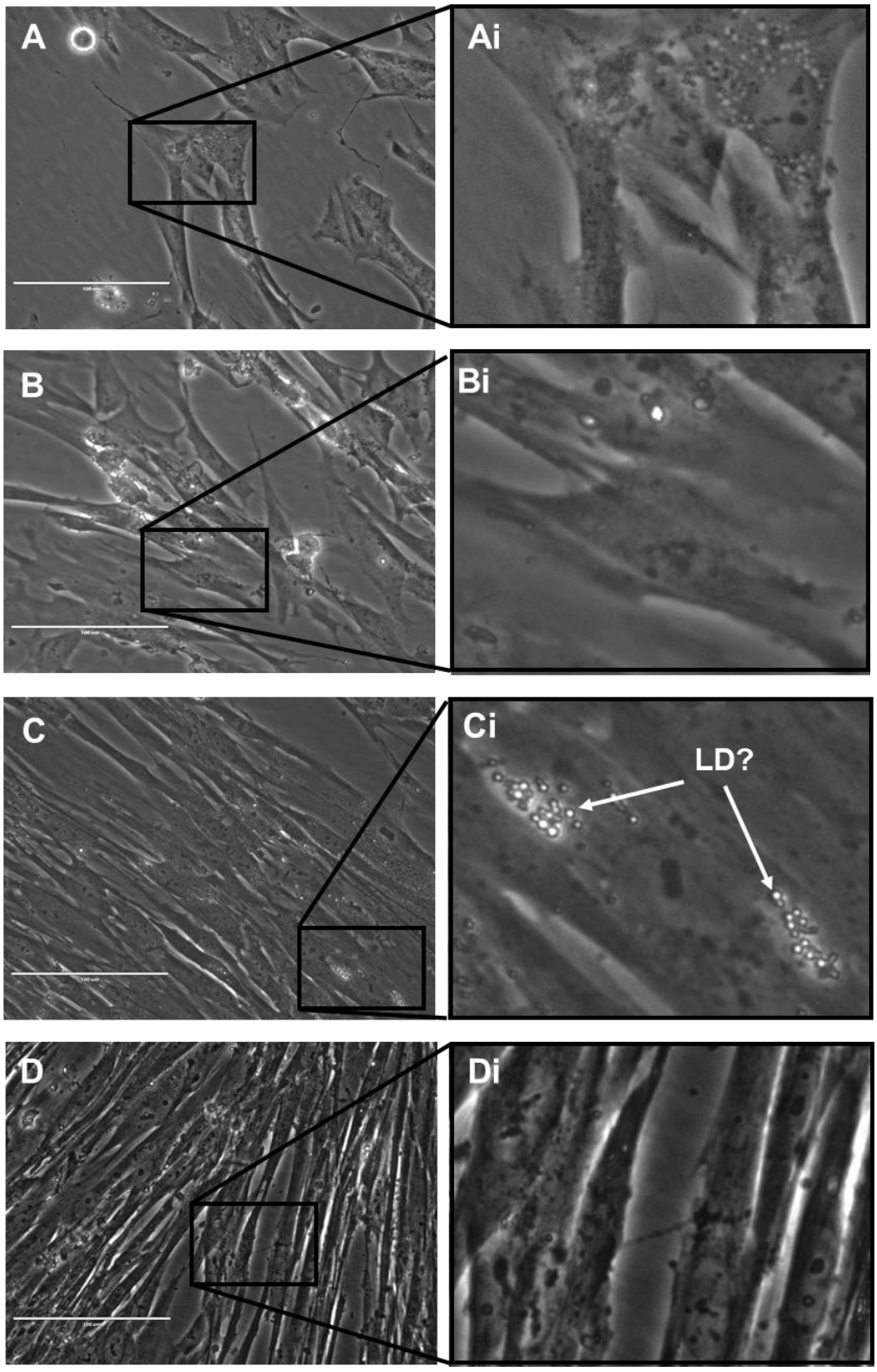

Figure 7.7. Expression of possible lipid droplets in time-course of MRC-5 fibroblast cultures.

MRC-5 cells were cultured for seven days with regular medium exchange. Phase contrast microscopy showed the presence of bright, refractive vesicles within some of the cells that resembled lipid droplets (LD?). A and Ai: day 1, B and Bi: day 2, C and Ci day 5 and D and Di: day 7 after seeding. Scale bar = 100 μm. Data from a single experiment.

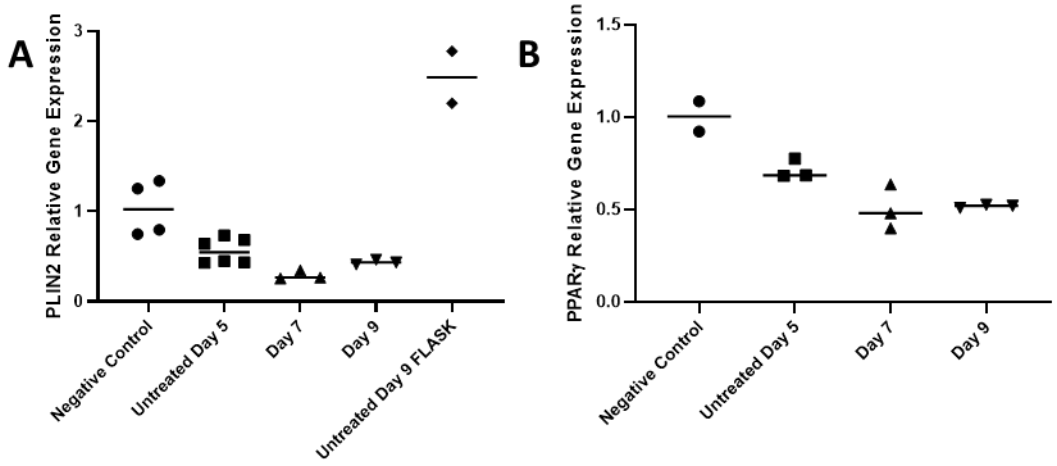

Figure 7.8. Expression of *PLIN2* and *PPARγ* genes in MRC-5 foetal fibroblasts cultured for nine days.
MRC-5 cells were cultured in in six well plates tissue culture flasks in F12/10% FBS for 9 days with regular medium exchange (refer to schematic, Figure 7.5). On days 5, 7, 9 and day 9 FLASK (the point of harvest of the conditioned medium), RNA was extracted, for QRT-PCR analysis with TaqMan™ primer/probe sets for *PLIN2* (A) and *PPARγ* (B) gene expression. *B2M* was used as reference gene. Relative expression was normalised to log phase cultured MRC-5 cells ("Negative Control"). Data from a single experiment.

There was no appreciable regulation of the *PPARγ* receptor gene over the time-course however cells at the end of the medium conditioning period (Day 9 "Flask") appeared to be expressing the *PLIN2* gene at a substantial level (Figure 7.8) suggesting the adoption of a desirable cellular phenotype.

7.3.4 Treatment of A549 Cells with Fibroblast Conditioned Medium (FCM)

(1) Surfactant Protein and ATII Associated Genes

MRC-5 conditioned medium was prepared according to the schematic (Figure 7.5). In order to determine an appropriate balance of conditioned medium with nutrient medium with fresh growth medium, three percentage mixtures were prepared: 25%, 50% and 75% v/v FCM in Ham's F12/10% FBS.

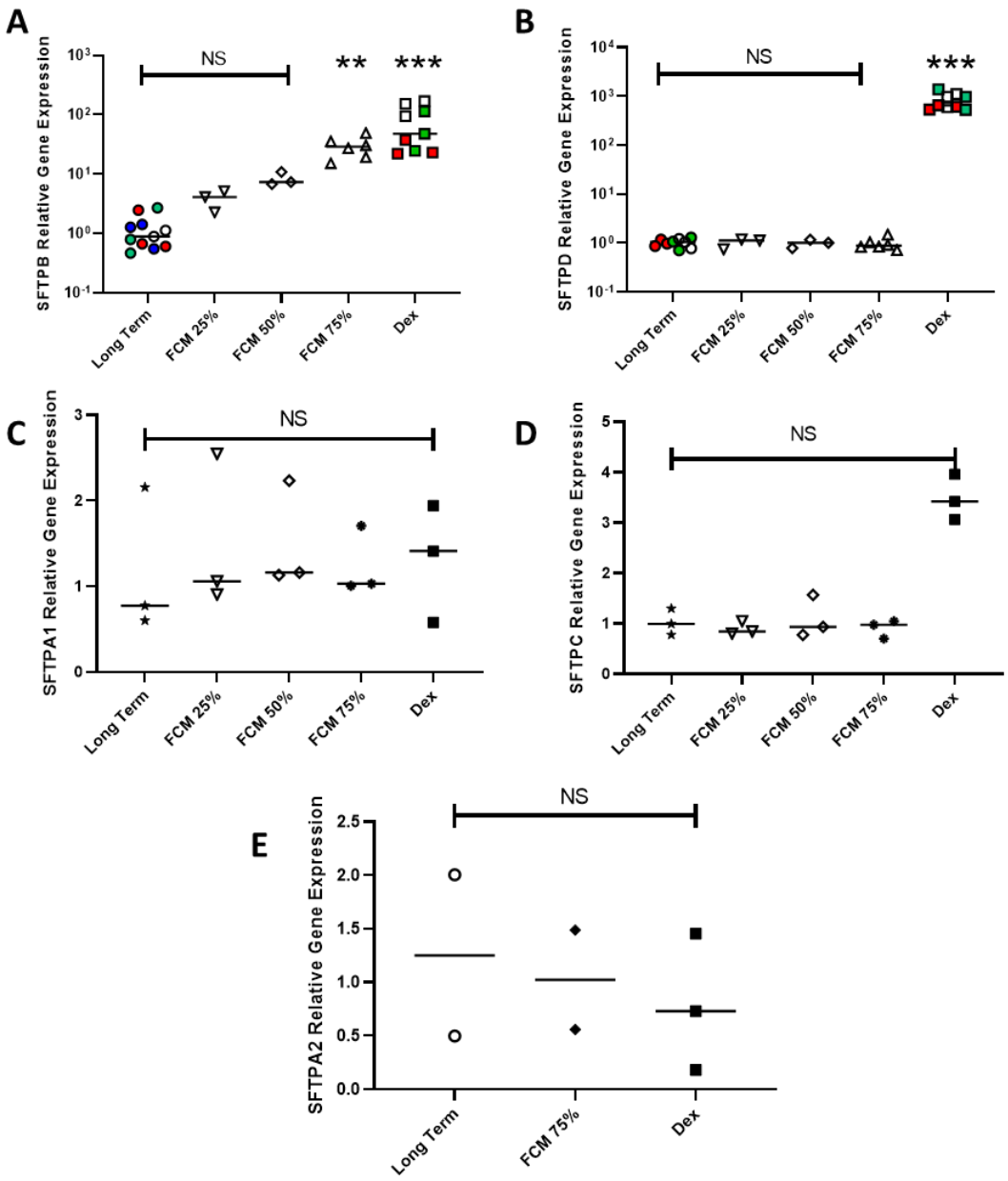

Figure 7.9. Surfactant protein gene expression in long term A549 cultures is influenced by chronic treatment with fibroblast conditioned medium (FCM). A549 cells were cultured for three weeks with: no treatment ("Long Term") and with 25%, 50% and 75% (v/v) fibroblast conditioned medium (FCM) from "Day 9" MRC-5 cultures (refer to schematic, Figure 7.5). On day 21 RNA was extracted for QRT-PCR analysis with TaqMan™ primer/probe sets for surfactant protein gene expression. *SFTPB*, (B) *SFTPD* (B), *SFTPA1* (C) and *SFTPC* (D) and *SFTPA2* (E). Data from 100 nM Dexamethasone (Dex) treated A549 cells are included as a control; this treatment has been previously demonstrated as effective for SFTP gene induction in A549 cells. *GAPDH* and *ATP5B* were used as reference genes. Relative expression was normalised to "Long Term" A549 cells. Non-parametric Kruskal-Wallis test with comparison to Long Term (Control). 25% and 50% FCM samples were not assessed for SFTPA2 gene expression. Data from 'long term' and 'Dex' treatment from 2-4 experiments, the remainder from a single experiment as shown by coloured data points. *=p<0.05, **=p<0.005, ***=P<0.001. NS=Not significant.

Long term A549 cultures were set up in these media with a negative control consisting of the standard long term conditions and dexamethasone as the previously identified best treatment. None of the conditioned formulations influenced the expression of *SFTPC*, *D*, *A1* or *A2* (Figure 7.9B, C, D and E), however there was a positive effect dependent of the percentage mixture of conditioned medium on the gene expression of *SFTPB* that at 75% v/v FCM was equivalent to that seen with dexamethasone (Figure 7.9A).

With regard to expression of genes associated with ATII phenotype, 75% FCM did not appear to regulate the expression of *ABCA3* compared with standard long term A549 cultures (Figure 7.10A). Similarly, there was no effect on *PTHrP,* unlike the previously demonstrated severe down-regulation observed with dexamethasone (Figure 7.10B).

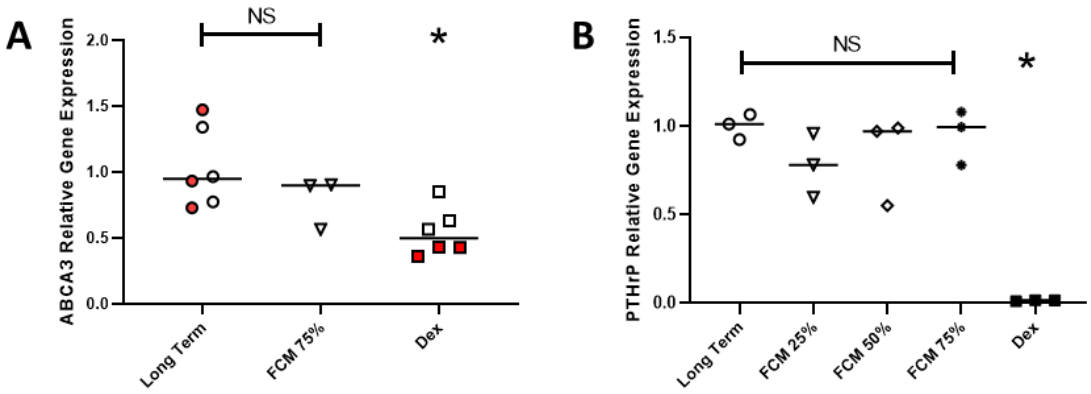

Figure 7.10. The effect of chronic treatment with fibroblast conditioned medium (FCM) on ATII related gene expression in long term A549 cultures. A549 cells were cultured in F12/10% FBS for three weeks with: no treatment ("Long Term") and with 25%, 50% and 75% (v/v) fibroblast conditioned medium (FCM) from "Day 9" MRC-5 cultures. Cultures were regularly medium exchanged. On day 21 RNA was extracted for QRT-PCR analysis with TaqMan™ primer/probe sets for (A) *ABCA3* and (B) *PTHrP*. Data from 100 nM Dexamethasone (Dex) treated A549 cells are included for comparison as this treatment has been previously demonstrated as effective for ATII specific SFTP gene induction in A549 cells *GAPDH* and *ATP5B* were used as reference genes and relative expression was normalised to "Long Term" A549 cells. Non-parametric Kruskal-Wallis test with comparison to Long Term (Control). 25% and 50% FCM treated samples were not assessed for *ABCA3* expression. Data from ABCA3 treatment from two independent experiments; PTHrP a single experiment as shown by coloured data points. *=$p<0.05$. NS=Not significant.

(2) Epithelial Markers

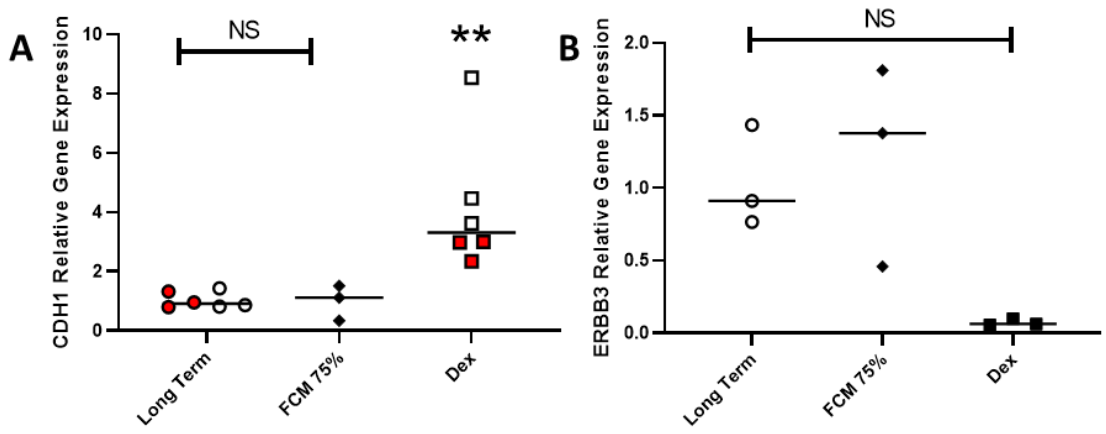

Figure 7.11. The effect of chronic treatment with fibroblast conditioned medium (FCM) on epithelial gene expression in long term A549 cultures.
A549 cells were cultured in F12/10% FBS for three weeks with: no treatment ("Long Term") and with 25%, 50% and 75% (v/v) fibroblast conditioned medium (FCM) from "Day 9" MRC-5 cultures. Cultures were regularly medium exchange. On day 21 RNA was extracted, for QRT-PCR analysis with TaqMan™ primer/probe sets for (A) *CDH1* and (B) *ERBB3*. Data from 100 nM Dexamethasone (Dex) treated A549 cells are included as this treatment has been previously demonstrated as effective *SFTP* gene induction in A549 cells. *GAPDH* and *ATP5B* were used as reference genes. Relative expression was normalised to "Long Term" A549 cells. Non-parametric Kruskal-Wallis test with comparison to Long Term (Control). Error bars represent standard deviation. CDH1 data from two independent experiments; ERBB3 from a single experiment as shown by coloured data points. **=p<0.005. NS=Not significant.

Dexamethasone had previously been shown to upregulate the epithelial market CDH1 in long term A549 cultures. This effect was not observed with 75% FCM treatment (Figure 7.11A), however as can be seen in Figure 7.11B the downward trend in *ERBB3* regulation induced by Dex (p=0.07) treatment was not replicated with 75% FCM treatment.

7.3.5 Transwell™ Co-Culture

As MRC-5 FCM looked to be a promising treatment for inducing ATII phenotype in A549 cells and MRC-5 fibroblasts appeared to be a suitable mesenchymal cell line, a preliminary experiment was conducted to explore the feasibility of several Transwell™ co-culture strategies:

- Collagen treated Transwell inserts with 0.4 µm pore size
- Non-treated "Clear" Transwell inserts with 0.4 µm pore size
- Conventional Co-Culture with A549 cells on the insert surface and MRC-5 cells in the basal chamber.
- "Sandwich" Co-Culture with A549 cells cultured on the apical surface of the Transwell™ insert and MRC-5 cells on the underside of the membrane.

The establishment of these co-cultures is described in Figure 7.12 and Figure 7.13.

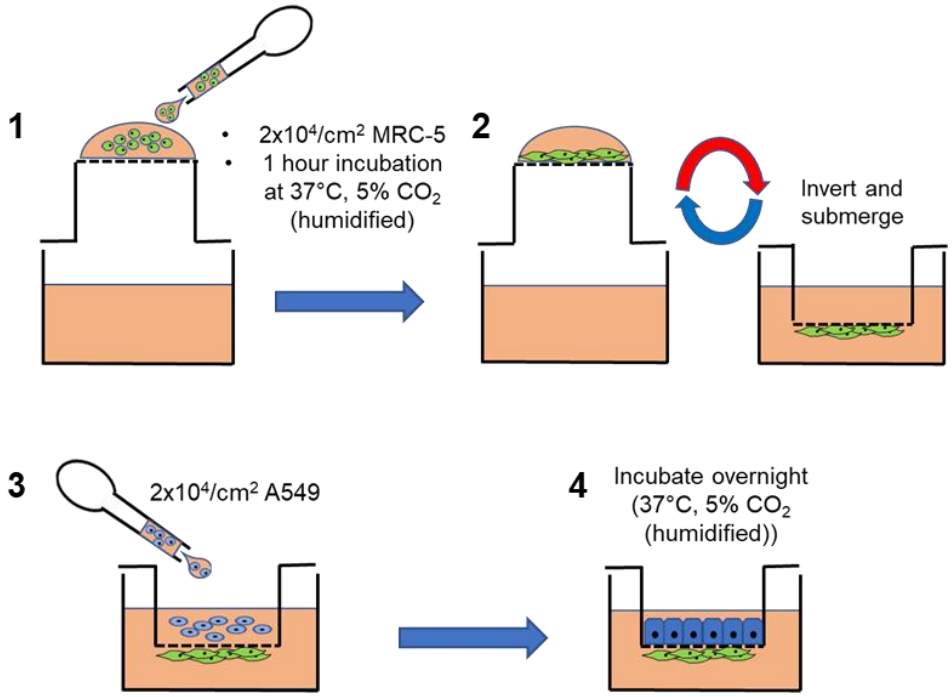

Figure 7.12. Diagram to demonstrate the set-up of "Sandwich" co-cultures of A549 and MRC-5 cells on six-well Transwells ™
(1) 0.4 µm pore size Transwell™ inserts (untreated and collagen treated) were pre-wet in culture medium (Ham's F12/10% FBS) and inverted. MRC-5 cells (green) suspended in the growth medium were pipetted to give $2x10^4$ cells/cm^2 in a domed meniscus on the inverted underside of the insert. The cells were allowed to attach for 1 hour in a humidified incubator before inverting and submerging (2). A549 cells (blue) suspended in the growth medium were pipetted to give $2x10^4$ cells/cm^2 to the inside of the Transwell™ insert and the resulting co-culture incubated overnight.

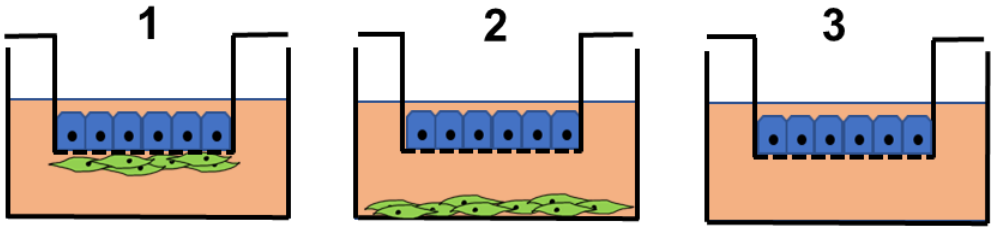

Figure 7.13. Diagram demonstrating the configuration of the Transwell™ co-cultures for data presented in Figure 7.14.
"Sandwich" (1), "Co-culture" (2) and "Long-term" (A549 monoculture) (3). MRC-5 cells green, and A549 blue.

In this preliminary feasibility experiment, RNA was extracted from A549 cells after a period of long term culture and assessed for the gene expression of *SFTPB* (Figure 7.14). As can be seen in the figure the optimal conditions of co-culture for the expression of *SFTPB* appeared to be the use of conventional co-culture on untreated or collagen-coated inserts. As there was no significant advantage to using the technically difficult sandwich technique, it was decided to proceed with conventional co-culture for further Transwell™ experiments (Figure 7.13(2)).

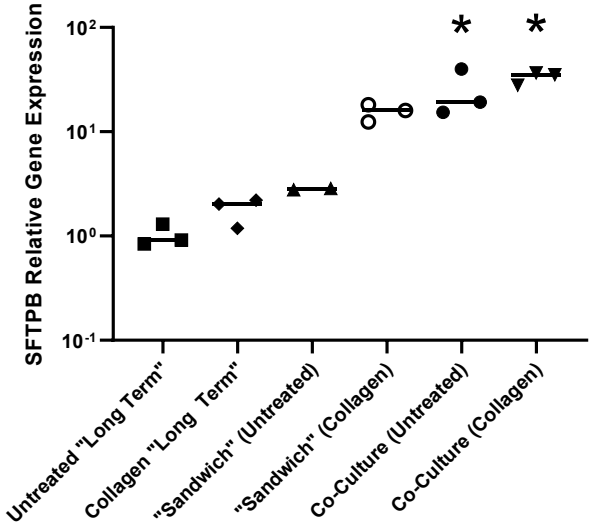

Figure 7.14. Surfactant protein B (*SFTPB*) gene expression in A549 cultures is influenced by Transwell™ co-culture with MRC-5 foetal fibroblasts.
A549 cells were grown in non-treated and collagen coated Transwell™ inserts (upper compartment): in monoculture ("Untreated "Long Term" and Collagen "Long Term)"; with MRC-5 cells on the underside of the Transwell™ membrane ("Sandwich") and in co-culture with MRC-5 cells cultured on the base of the lower compartment (refer to Figure 7.12 and Figure 7.13). Cultures were grown submerged in Ham's F12/10% FBS and regularly medium exchanged before A549 cells were removed by scraping after two weeks. RNA was extracted for QRT-PCR analysis with a TaqMan™ primer/probe set for *SFTPB* gene expression with *GAPDH* and *ATP5B* as reference genes. Relative expression was normalised to "Untreated "Long Term"" A549 (Figure 7.13(3), as an equivalent to "Long Term" control cultures used in previous experiments. Non-parametric Kruskal-Wallis test with comparison to Long Term (Control). Data from a single experiment. *=$p<0.05$.

(1) Surfactant Protein Gene Expression in Transwell™ Cultures

Transwell A549/MRC-5 cultures were established as per (Figure 7.13(2) on collagen coated and untreated Transwells™ and assessed for *SFTP* gene expression and compared to 75% FCM treatment in long term 2D culture (Figure 7.15). As can be seen any evidence for regulation of SFTPA1, A2, C and D was inconclusive (Figure 7.15B-E), however SFTPB induction in the co-cultures grown on collagen coated Transwells was comparable to that seen in 75% FCM.

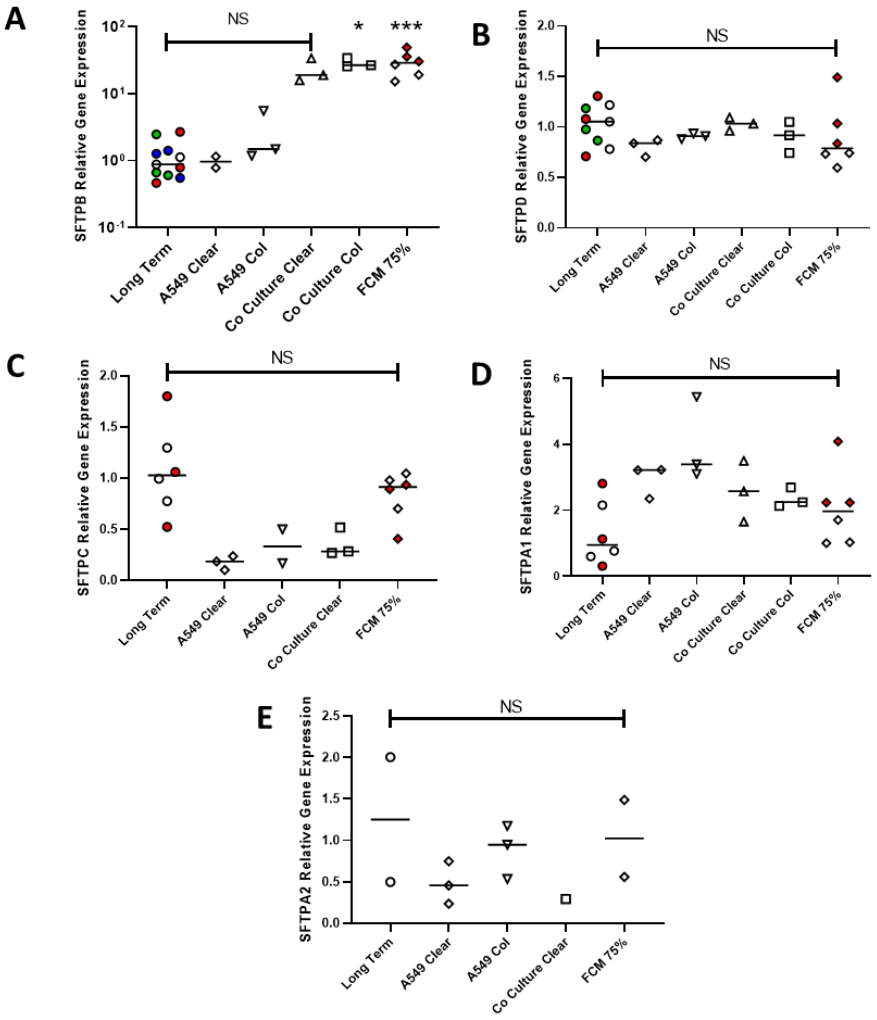

Figure 7.15. Surfactant protein gene expression in A549 cultures is influenced by Transwell™ co-culture with MRC-5 foetal fibroblasts.
A549 grown in untreated ("Clear") and collagen coated ("Col") Transwell™ inserts (upper compartment): in monoculture ("A549 Clear" and "A549 Col") and in co-culture with MRC-5 cells cultured on the base of the lower compartment ("Co Culture Clear" and "Co Culture Col"). Cultures were grown submerged in Ham's F12/10% FBS. A549 cells were removed by scraping. RNA was extracted for QRT-PCR analysis with TaqMan™ primer/probe sets for *SFTPB* (A), *SFTPD* (B), *SFTPC* (C), *SFTPA1* (D) and *SFTPA2* (E) gene expression. *GAPDH* and *ATP5B* were used as reference genes and relative expression was normalised to control A549 cells grown in "Long Term" culture. Non-parametric Kruskal-Wallis test with comparison to Long Term (Control). Different coloured data points represent independent experiments. *=p<0.05, ***=P<0.001.

(2) ATII and Epithelial Associated Gene Expression in Transwell™ Cultures

No significant regulation of *ABCA3*, *CDH1* or *ERBB3* Regulation was seen in Transwell™ Cultures (Figure 7.16).

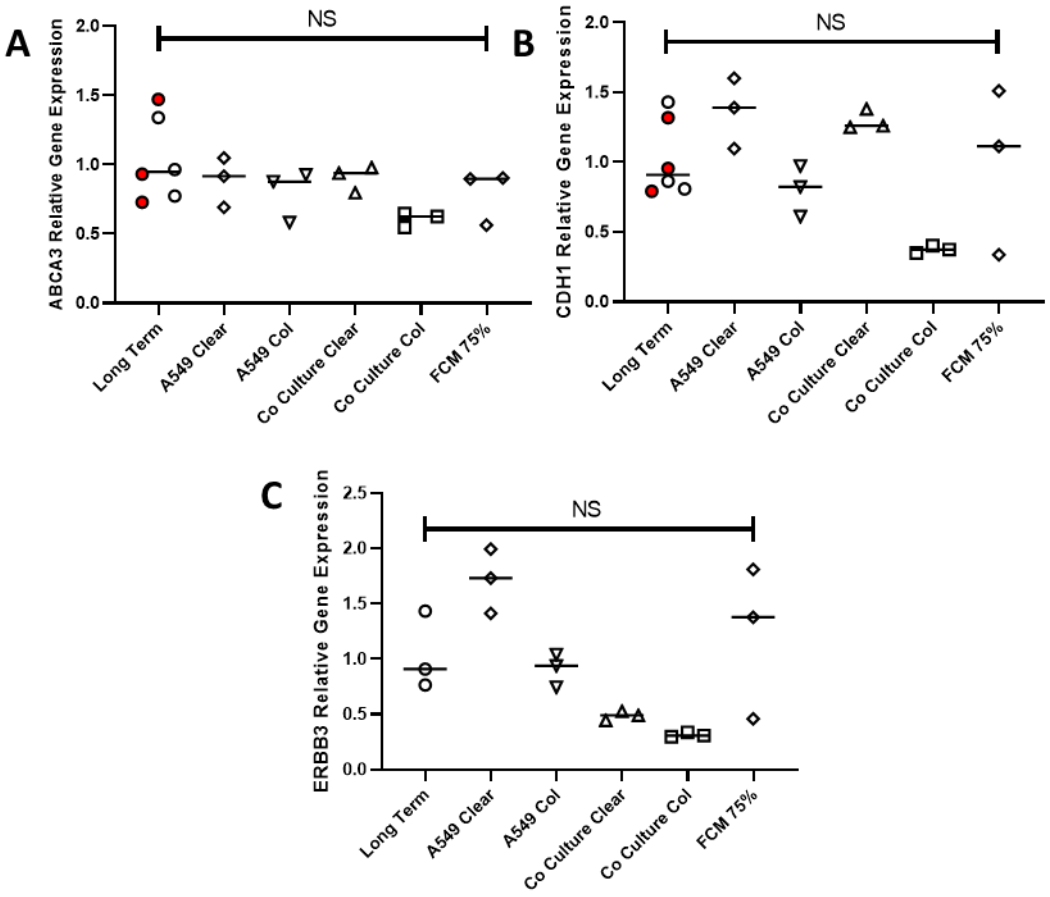

Figure 7.16. Effect of Transwell Co-Culture on gene expression on the ATII marker ABCA3 and the epithelial markers *CDH1* and *ERBB3*.

A549 cells were grown in non-treated ("Clear") and collagen coated ("Col") Transwell™ inserts (upper compartment): in monoculture ("A549 Clear" and "A549 Col") and in co-culture with MRC-5 cells cultured on the base of the lower compartment ("Co Culture Clear" and "Co Culture Col"). Cultures were grown submerged in Ham's F12/10% FBS and regularly medium exchanged before the A549 cells from the Transwell™ support were removed by scraping. RNA was extracted for QRT-PCR analysis with a TaqMan™ primer/probe sets for *ABCA3* (A), *CDH1* (B), and *ERBB3* (C). *GAPDH* and *ATP5B* were used as reference genes. Relative expression was normalised to A549 cells grown in three week "Long Term" culture. Non-parametric Kruskal-Wallis test with comparison to Long Term (Control). "NS" denotes no significant difference. Different coloured data points represent independent experiments.

7.3.6 Treatment of MRC-5 with the PPARGγ Agonist Rosiglitazone (RGZ) and Generation of FCM from RGZ Treated MRC-5 Cells

Results for MRC-5 cells used previously suggested that the cells might have adopted a lipofibroblast phenotype in the generation of FCM that had a positive impact on the expression of SFTPB in A549 cells. In rodent models, it appears that lipofibroblast-differentiated fibroblasts and PPARγ signalling support the development and maintenance of ATII cells[510]. *In vitro* studies have shown that in mouse and in lung fibroblasts from IPF patients, functional intervention with the PPARγ agonist rosiglitazone reinforced the lipogenic phenotype to antagonise the TGFβ1-mediated fibrogenic response[90]. To explore the hypothesis that a lipofibroblast phenotype is required to support ATII differentiation in A549 cells, it was postulated that treatment of MRC-5 cells with RGZ might drive more robust lipofibroblast phenotype which in turn might induce ATII-like differentiation in A549 cells.

The first step was to determine a non-toxic and effective concentration of RGZ with which to treat MRC-5 cells and would have utility in a pragmatic timeframe.

The literature suggests a range of RGZ between 1 and 30 μM[90 94]. MRC-5 cells were treated with 0, 1, 10, 20 and 30 μM RGZ over an initial 12-day time-course and the effect on the expression of lipid droplets and cell morphology and potential toxicity observed.

Putative lipid droplets were observed at day 5 of the time-course with tentative indications that this response might be dose dependent (Figure 7.17) and that day 5 might be the optimum time point for the establishment of FCM.

Presence of lipid droplets was confirmed after 12 days in culture as shown by Oil-Red-O staining (Figure 7.18) however the higher concentrations of RGZ appeared to have a toxic effect on the cells as shown by the disruption of the cell monolayer and shrivelled appearance of cells in Figure 7.19. These data indicated that 20 and 30 μM RGZ may have an undesirable toxic effect on the MRC-5 cells.

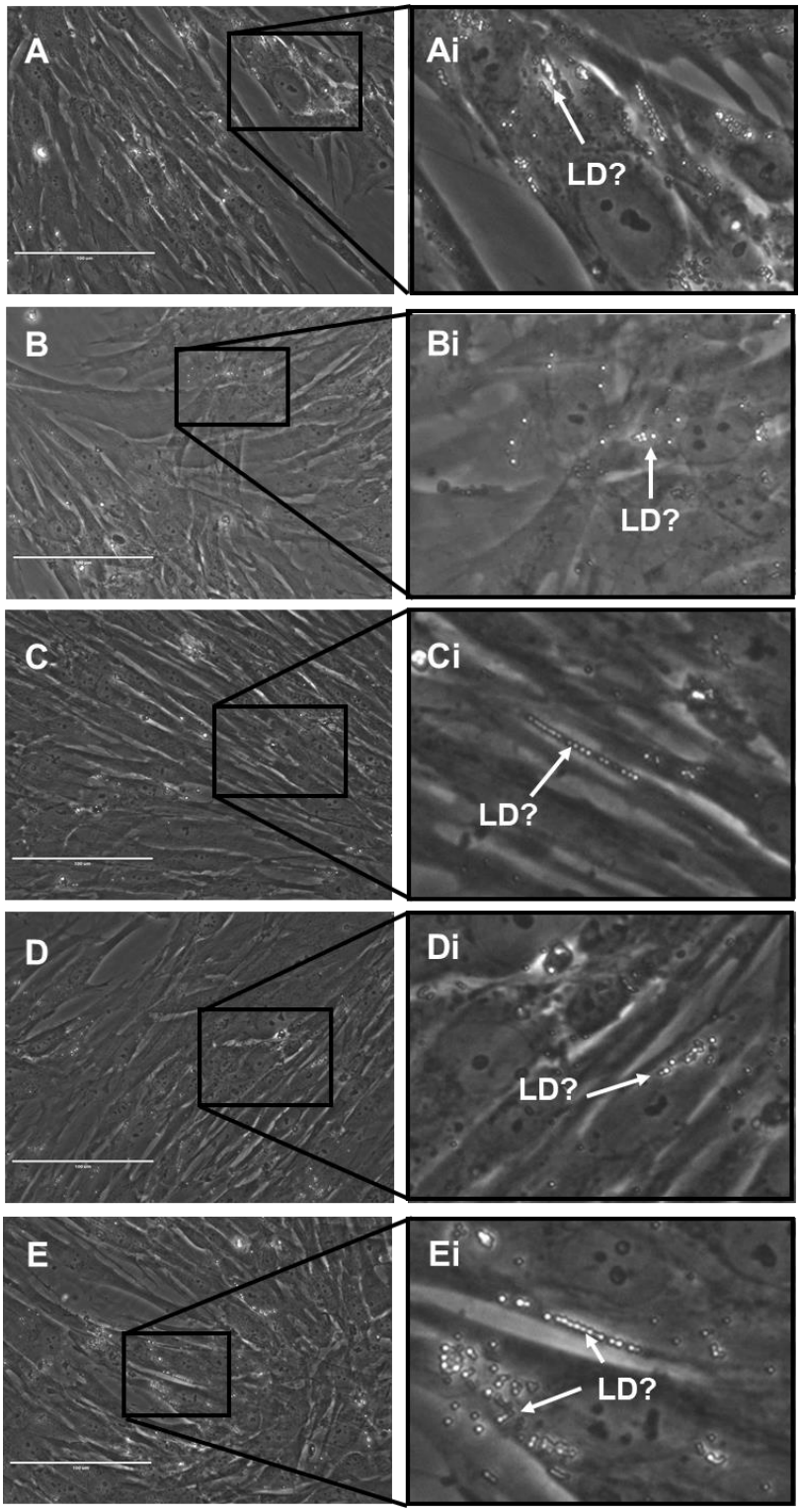

Figure 7.17. Expression of possible lipid droplets in MRC-5 fibroblast cultures five days after treatment with increasing concentrations of Rosiglitazone (RGZ) at early stage of treatment (5 days).

MRC-5 cells were cultured in the presence of increasing concentrations of RGZ. Phase contrast microscopy at day 5 showed the presence of bright, 'refractive' vesicles within some of the cells that resembled lipid droplets (LD?). RGZ at 0 μM (A and Ai), 1 μM (B and Bi), 10 μM (C and Ci), 20 μM (D and Di), and 30 μM (E and Ei). Scale bar = 100 μm. Results represent a single experiment.

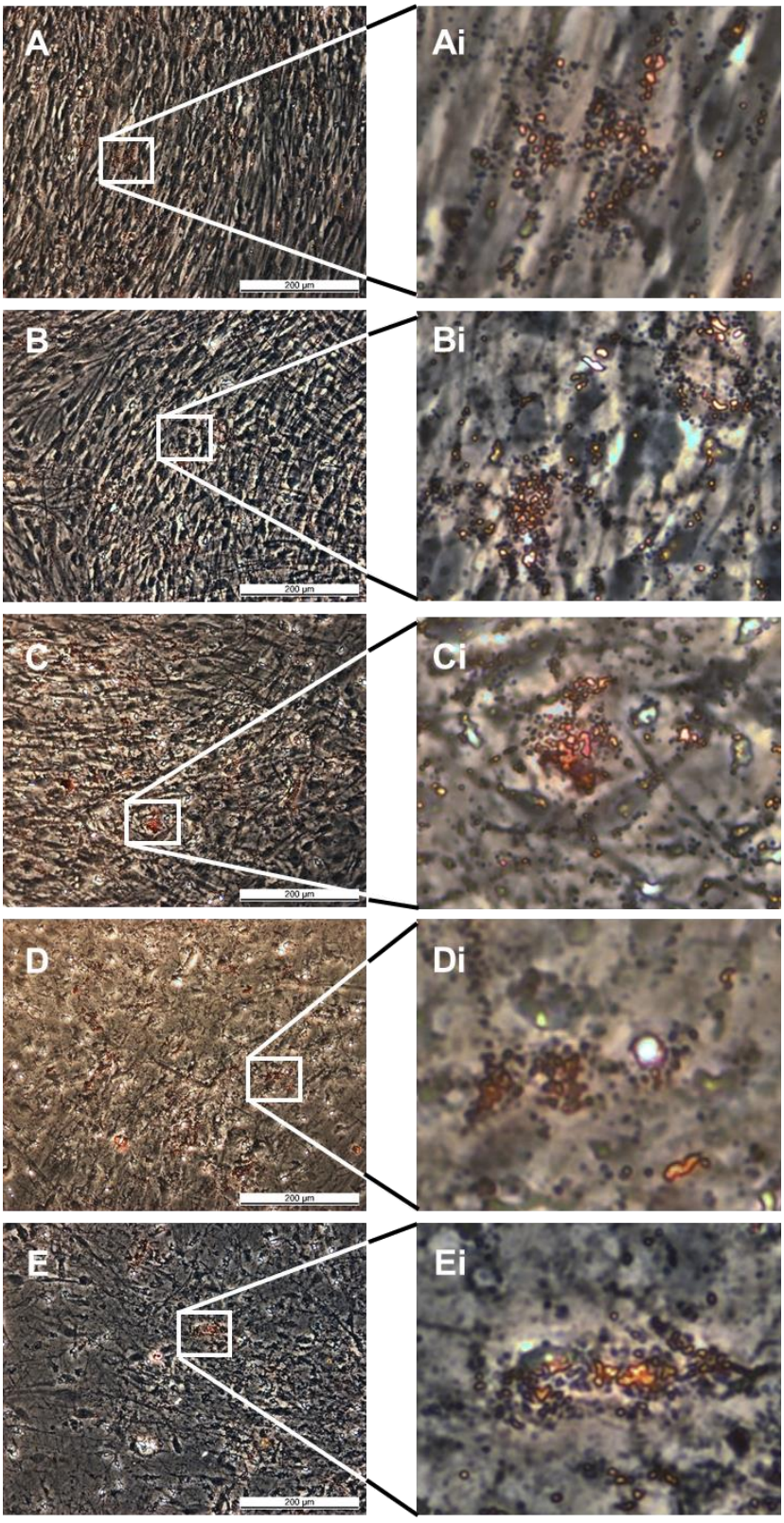

Figure 7.18. Lipid droplet expression in MRC-5 fibroblasts cultured in increasing concentrations of Rosiglitazone (RGZ) at later stage of treatment (12 days).
MRC-5 cells were cultured in the presence of RGZ at 0 μM (A and Ai), 1 μM (B and Bi), 10 μM (C and Ci), 20 μM (D and Di), and 30 μM (E and Ei). Cultures were regularly medium exchanged until day 12 when they were paraformaldehyde fixed prior to Oil-Red-O staining for lipid and imaged by phase contract microscopy. Scale bar = 200 μm. Data from a single experiment.

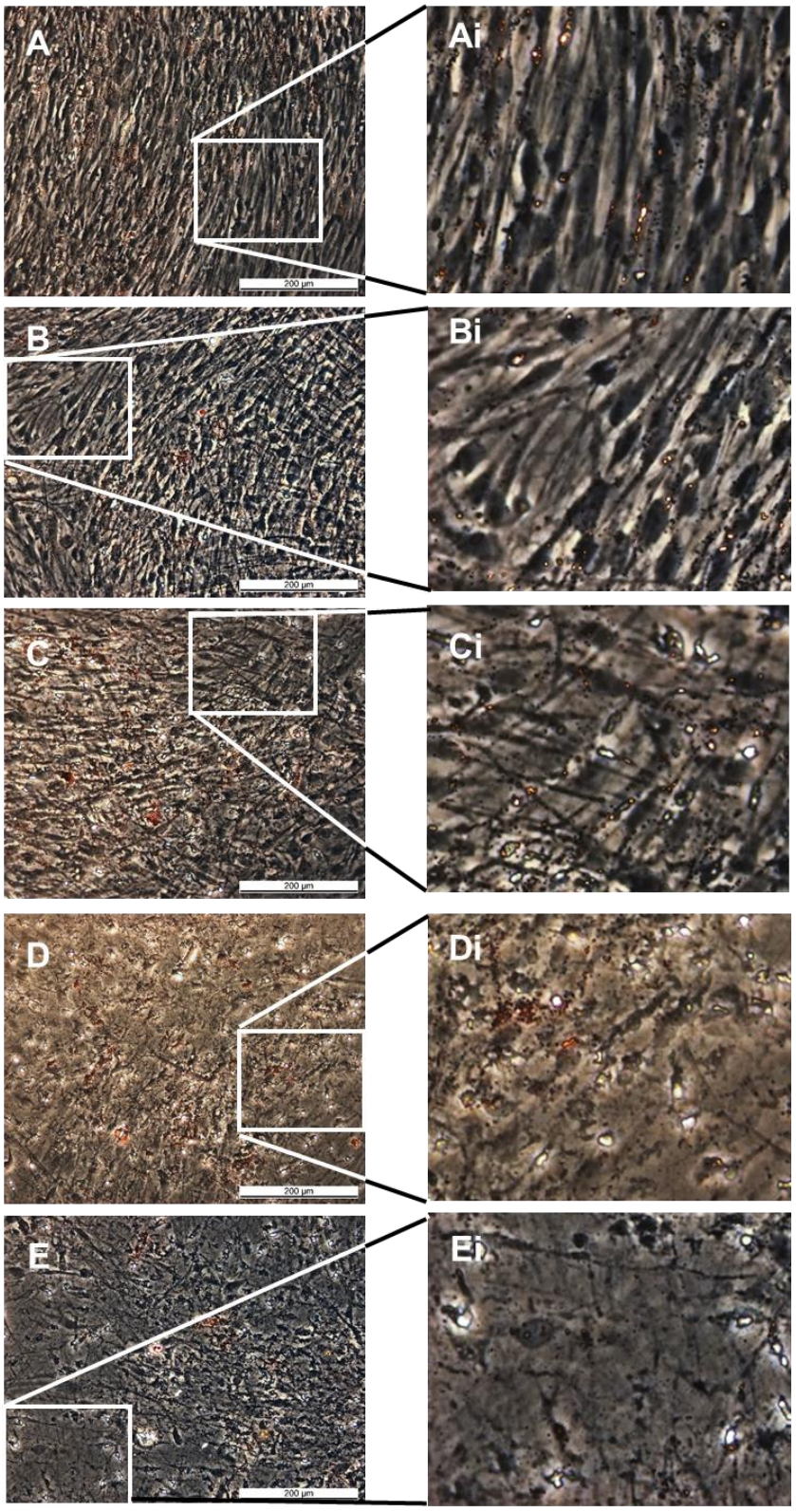

Figure 7.19. Deterioration of MRC-5 fibroblast monolayers cultured in increasing concentrations of Rosiglitazone (RGZ) after 12 days treatment.
MRC-5 cells were cultured in the presence of RGZ at 0 μM (A and Ai), 1 μM (B and Bi), 10 μM (C and Ci), 20 μM (D and Di), and 30 μM (E and Ei). Cultures were regularly medium exchanged until day 12 when they were paraformaldehyde fixed prior to Oil-Red-O staining for lipid and imaged by phase contract microscopy. Scale bar = 200 μm. Results represent a single experiment.

In a similar manner to the previous generation of FCM a time-course of cultures was set up with increasing concentrations of RGZ in plates, and a batch of conditioned medium prepared with 10 µM RGZ (schematic, Figure 7.20).

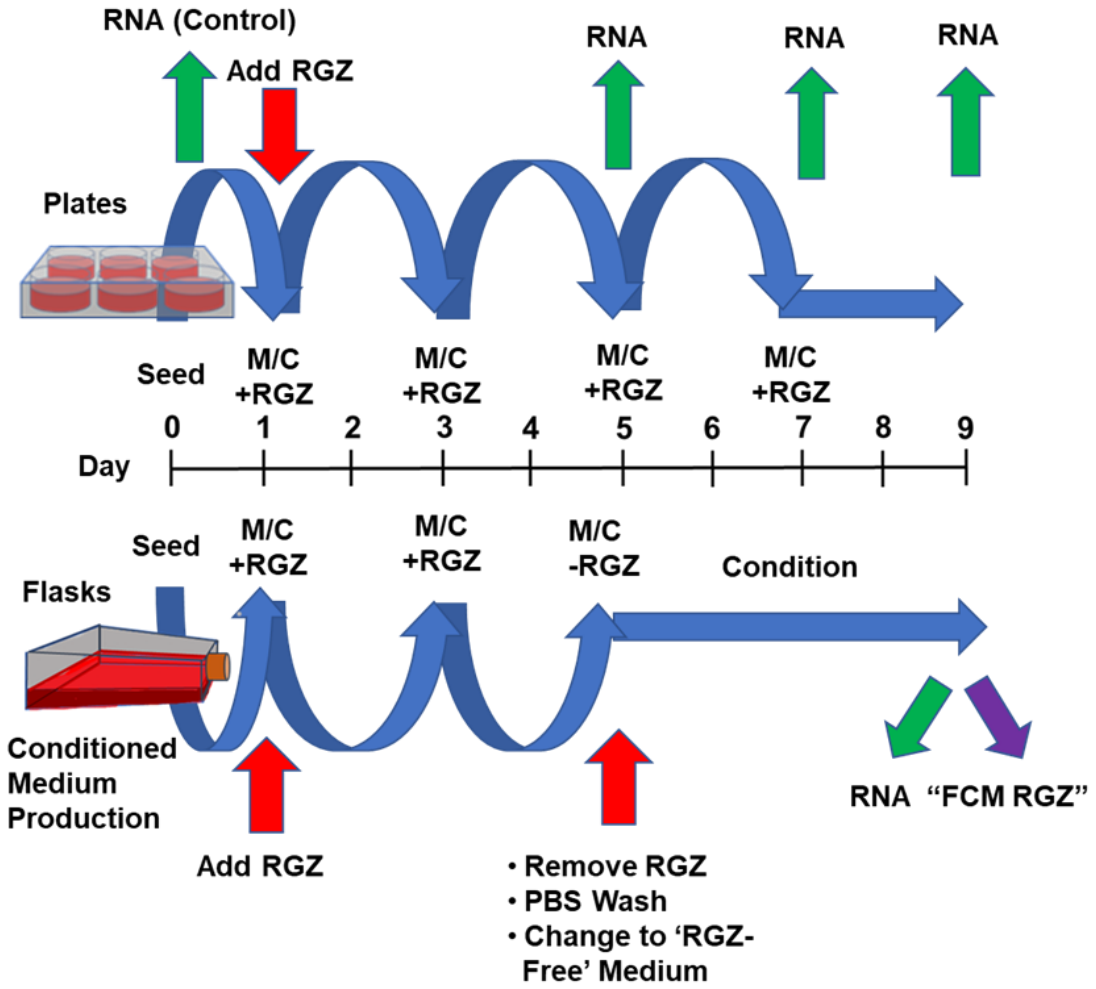

Figure 7.20. Schematic to describe the time course of RNA samples generated for the gene expression analysis of MRC-5 fibroblasts and the production of fibroblast conditioned medium (FCM).
Six-well plates were seeded with MRC-5 cells in Ham's F12/10% FBS at $2x10^4$ cells/cm^2, medium exchanged ('M/C') the day after seeding into medium containing 10 µM Rosiglitazone (RGZ) and every two days until day 7. Cells were harvested on days 5,7 and 9. Flasks were set up in a similar manner, however at day 5 the RGZ containing medium was removed, the monolayers were washed twice with PBS and replenished with RGZ-free Ham's F12 10% FBS. Flask cultures were left without subsequent medium change until 'day 9' to generate conditioned medium.

Optimal gene expression of the lipofibroblast marker *PLIN2* appeared be at day 5 of culture and in the cells at the point of harvest of the conditioned medium flasks at day 9 (Figure 7.21)

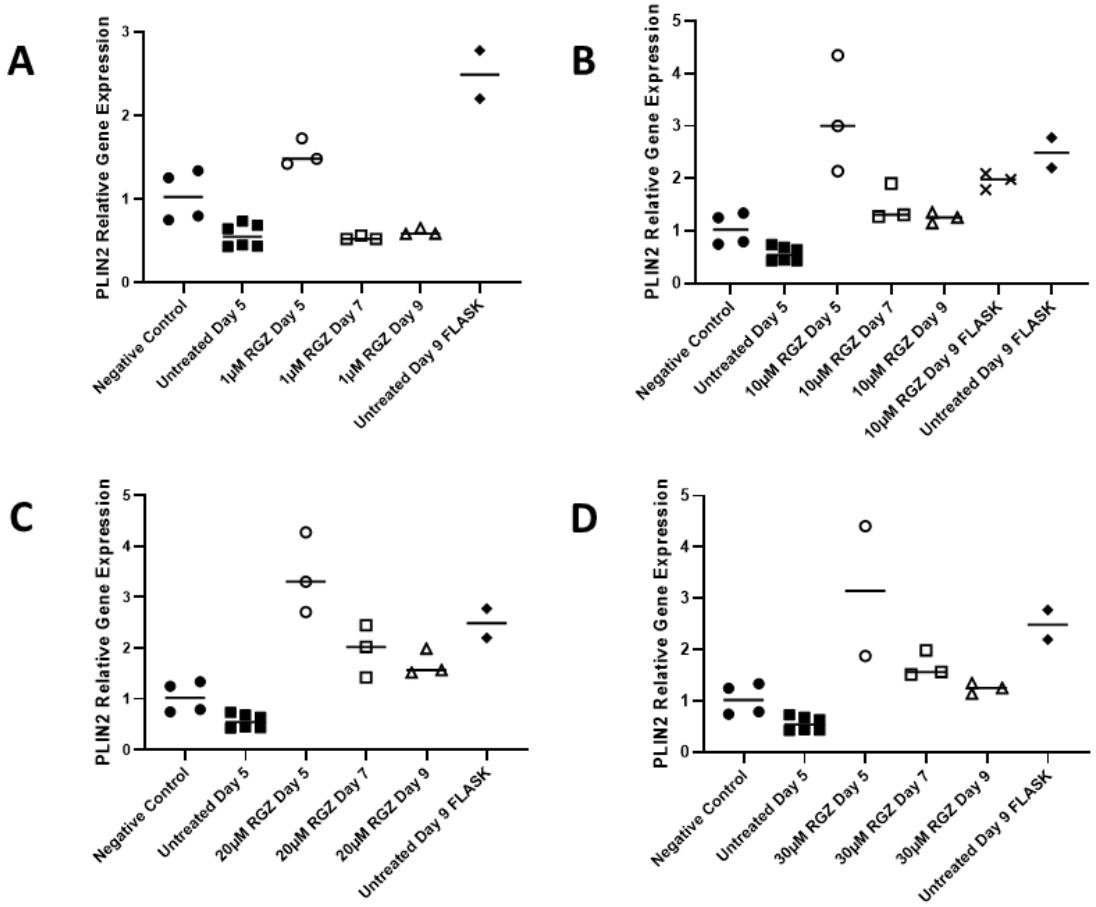

Figure 7.21. The time-course of *PLIN2* gene expression of in MRC-5 foetal fibroblasts cultured with increasing concentrations of Rosiglitazone.
MRC-5 cells were cultured in F12/10% FBS with 1 μM (A), 10 μM (B), 20 μM (C) and 30 μM (D) RGZ with regular medium exchange (refer to the schematic, Figure 7.20). The flask cultures (untreated 'Day 9 FLASK' and 10 μM 'RGZ Day 9 FLASK') were left without medium exchange for the final 5 days of culture to allow medium conditioning. On days 5, 7, and 9 RNA was extracted for QRT-PCR analysis with TaqMan™ primer/probe set for *PLIN2* gene expression with *B2M* as a reference gene. Relative expression was normalised to log phase cultured MRC-5 cells ("Negative Control"). Data from Day 5 and Day 9 'flask' untreated MRC-5 cells are also included (hatched and chequered bars) for comparison. Data represent a single experiment. Samples from day 9 FLASK RGZ treated cells were only available for the 10 μM treatment. Statistical analysis was not performed due to low sample number.

Conversely there appeared to be no upregulation of the *PPARγ* receptor during the time-course (Figure 7.22).

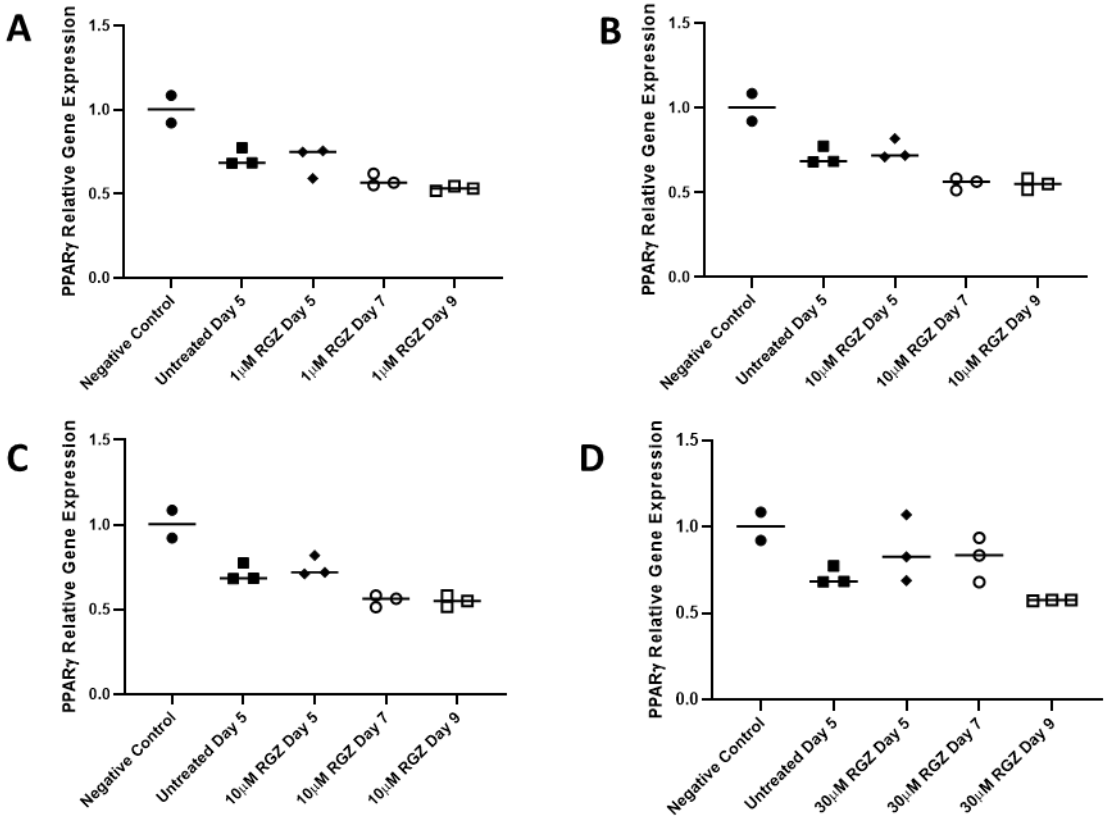

Figure 7.22. The time-course of *PPARγ* gene expression in MRC-5 foetal fibroblasts cultured with increasing concentrations of rosiglitazone (RGZ).
MRC-5 cells were cultured for nine in F12/10% FBS supplemented with 1 μM (A), 10 μM (B), 20 μM (C) and 30 μM (D) RGZ according the schematic (Figure 7.20). On days 5, 7 and 9 RNA was extracted for QRT-PCR analysis with TaqMan™ primer/probe set for *PPARγ* gene expression with *B2M* as a reference gene. Relative expression was normalised to log phase MRC-5 cells ("Negative Control"). Data from Day 5 untreated MRC-5 cells are also included (hatched bars) for comparison. Data represent a single experiment. Error bars represent standard deviation. Statistical analysis was not performed due to low sample number.

Encouragingly the optimal expression *of PTHR1* appeared to be at day 5 (the commencement of the medium conditioning period in the flasks) (Figure 7.23) and as with the non-treated FCM, *NRG1-β* appeared to be highly expressed at day 9 in the flasks (Figure 7.24).

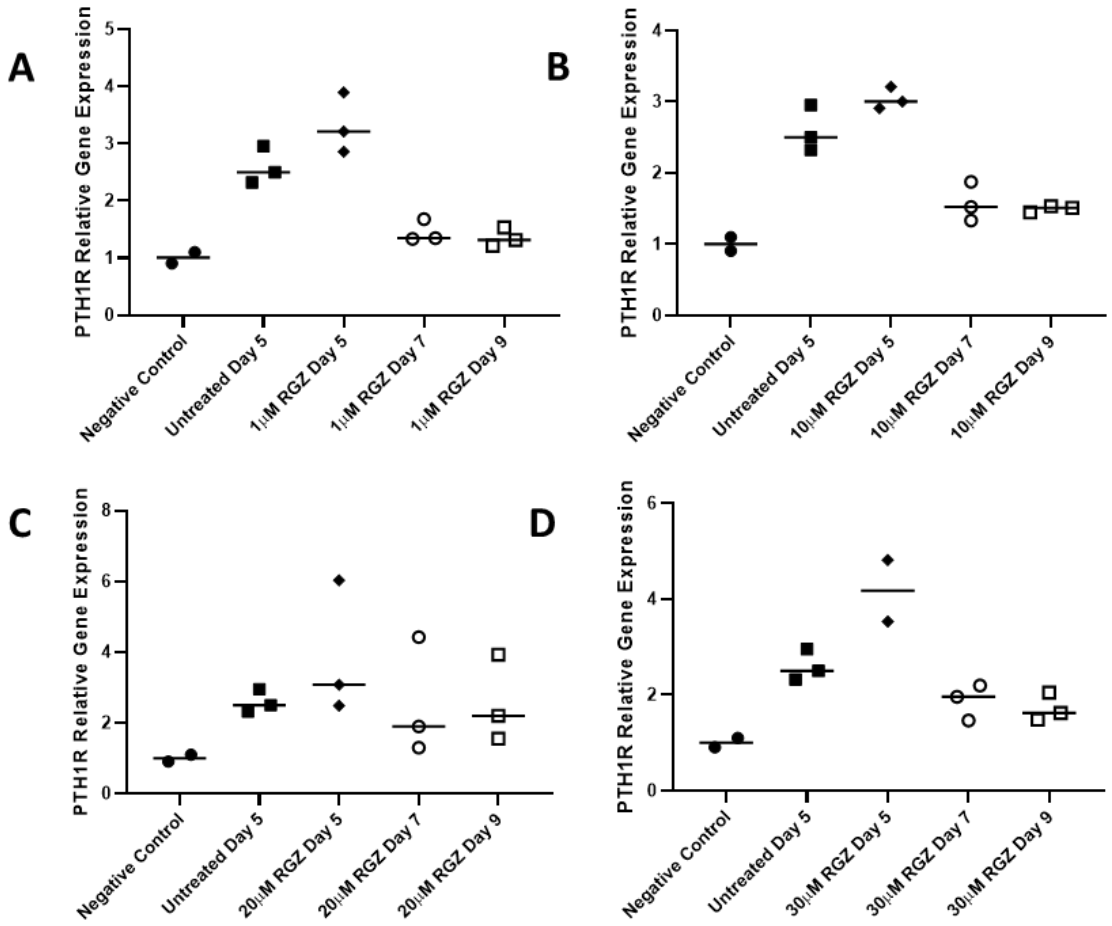

Figure 7.23. The time-course of *PTHR1* gene expression in MRC-5 foetal fibroblasts cultured with increasing concentrations of Rosiglitazone (RGZ).

MRC-5 cells were cultured for nine days in F12/10% FBS supplemented with 1 μM (A), 10 μM (B), 20 μM (C) and 30 μM (D) RGZ with regular medium exchange (refer to the schematic, Figure 7.20). On days 5, 7, 9 RNA was extracted for QRT-PCR analysis with TaqMan™ primer/probe set for *PTHR1* gene expression. with *B2M* as a reference gene. Relative expression was normalised to log phase cultured MRC-5 cells ("Negative Control"). Data from Day 5 untreated MRC-5 cells are also included (hatched bars) for comparison. Data represent a single experiment. Samples from day 9 FLASK RGZ treated cells were only available for the 10 μM treatment. Statistical analysis was not performed due to low sample number.

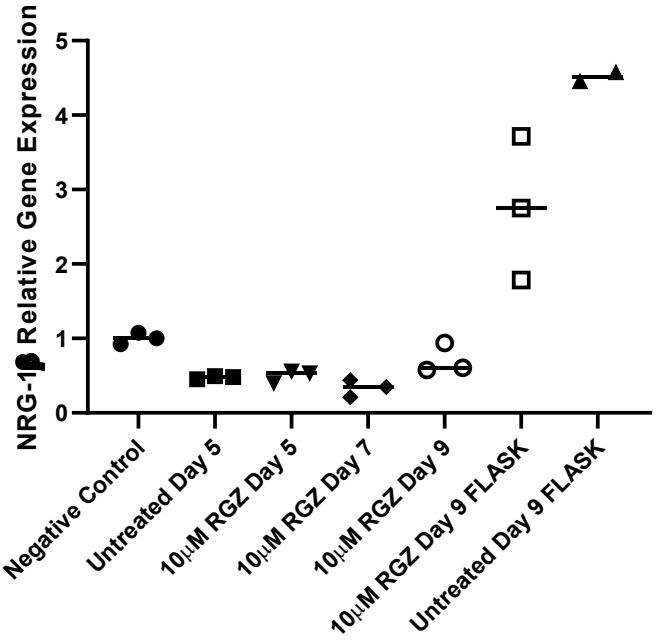

Figure 7.24. The time-course of NRG-1β gene expression in MRC-5 foetal fibroblasts cultured in 10 μM Rosiglitazone (RGZ).
MRC-5 cells were cultured in in six well plates for nine days in F12/10% FBS supplemented 10 μM RGZ with medium exchange according to the schematic (Figure 7.20). The flask cultures (untreated 'Day 9 FLASK' and 10 μM 'RGZ Day 9 FLASK') were left without medium exchange for the final 5 days of culture to allow medium conditioning. On days 5, 7, and 9 RNA was extracted for QRT-PCR analysis with TaqMan™ primer/probe set for *NRG-1β* gene expression. *B2M* was used as a reference gene. Relative expression was normalised to log phase cultured MRC-5 cells ("Negative Control"). Data from Day 5 untreated and untreated "Day 9 FLASK" are included (hatched and chequered bars) for comparison. Data from a single experiment. Samples from day 9 FLASK RGZ treated cells were only available for the 10 μM treatment. Statistical analysis was not performed due to low sample number.

Figure 7.25 summarises the gene expression over the time-course and indicates that in terms of the expression of *PLIN2* and *PTH1R,* 10 μM RGZ was the optimal concentration with no benefits of increased concentration. Previous data (Figure 7.19) alluded that higher concentrations may be toxic and therefore detrimental.

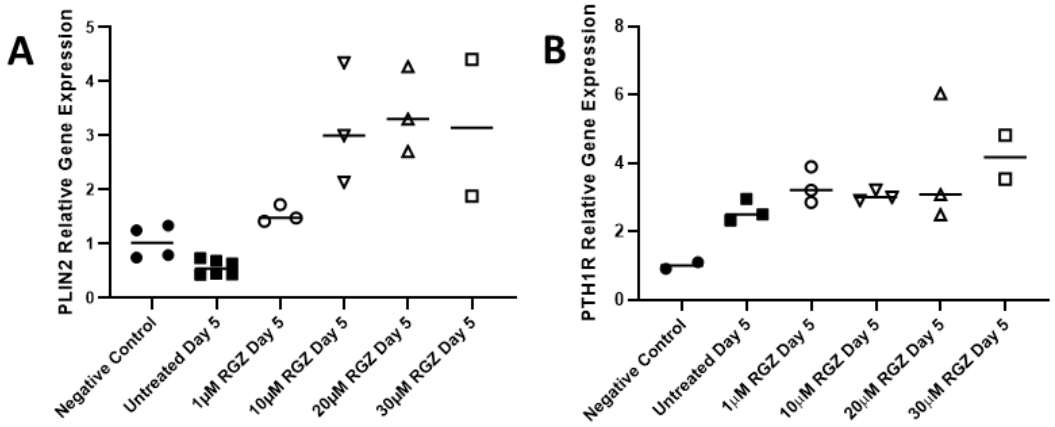

Figure 7.25. Comparison of gene expression of the lipofibroblast markers *PLIN2* and *PTH1R* in increasing concentrations of Rosiglitazone (RGZ) on the fifth day of treatment. MRC-5 were in F12/10% FBS supplemented with 1 μM, 10 μM, 20 μM and 30 μM RGZ with regular medium exchanges according to the schematic (Figure 7.20). On day 5 RNA was extracted for QRT-PCR analysis with TaqMan™ primer/probe set for *PLIN2* (A) and *PTHR1* (B) gene expression with *B2M* as a reference gene. Relative expression was normalised to log phase cultured MRC-5 cells ("Negative Control"). Data from Day 5 non-treated MRC-5 cells are also included (hatched bars) for comparison. Data from a single experiment. Statistical analysis was not performed due to low sample number.

7.3.7 Treatment of A549 Cells with FCM from RGZ Treated MRC-5 Cells

The pattern of SFTP, ATII and epithelial associated gene expression in A549 cells treated with "RGZ-FCM" was similar to that seen with FCM (Figure 7.26, 7.27 and 7.28) and a side by side comparison of the two FCMs showed no significant differences in gene expression of treated A549 cells (Figure 7.29 and Figure 7.30).

No significant advantage was observed with the use of RGZ, however, these were only preliminary experiments. These experiments should be repeated and RGZ treatment may need further optimisation.

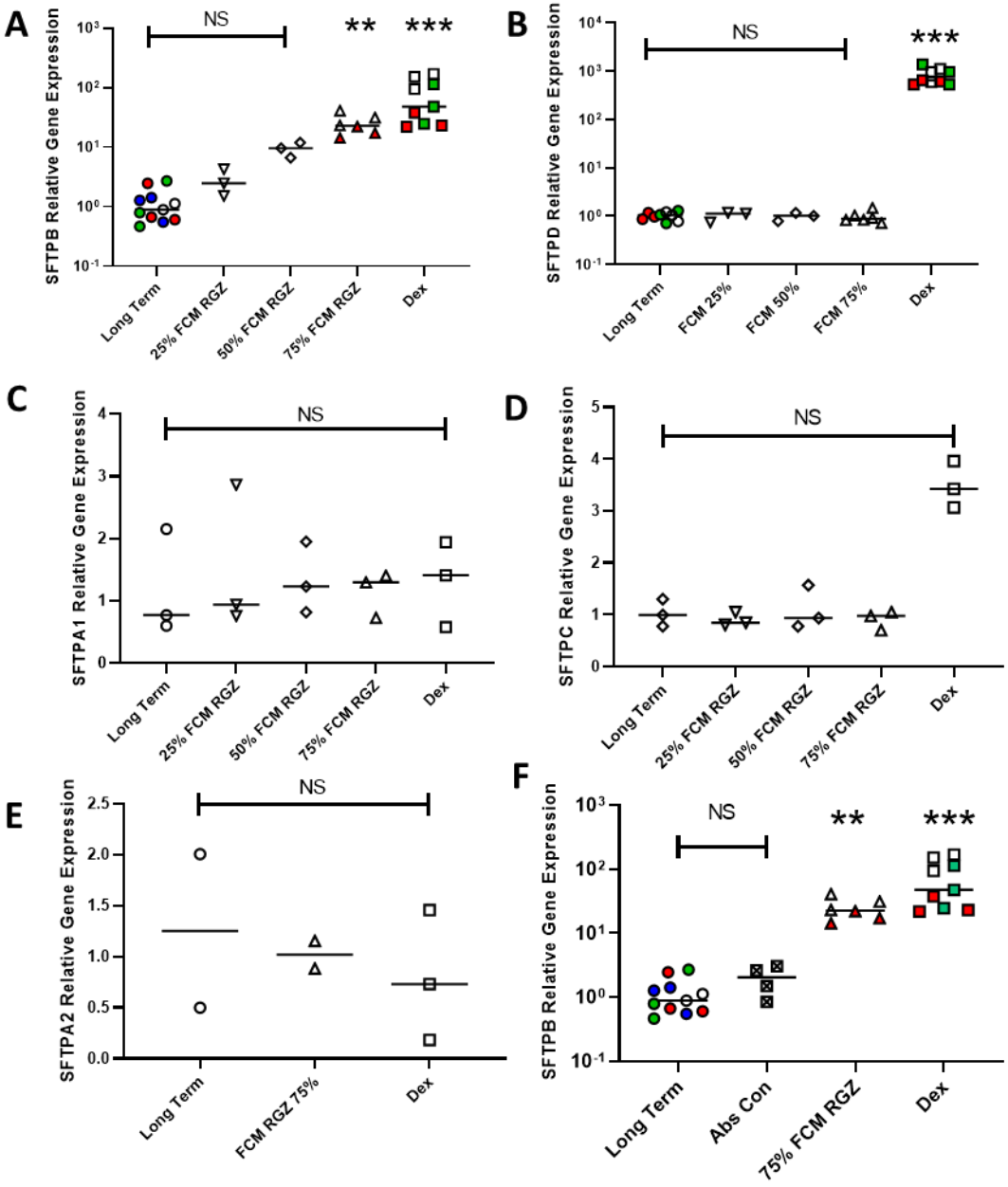

Figure 7.26. Surfactant protein gene expression in long term A549 cultures is influenced by chronic treatment with fibroblast conditioned medium from MRC-5 cells treated with 10 µM Roziglitazone (FCM RGZ).
A549 cells were cultured for three weeks with 0% (Long Term). 25%, 50% and 75% (v/v) RGZ treated fibroblast conditioned medium (FCM RGZ). Cultures were regularly medium exchanged. On day 21 RNA was extracted for QRT-PCR analysis with TaqMan™ primer/probe sets for surfactant protein gene expression. *SFTPB* (A), *SFTPD* (B), *SFTPA1* (C) and *SFTPC* (D) and *SFTPA2* (E). Data from 100 nM Dexamethasone (Dex) treated A549 cells (the previous 'best' treatment for *SFTP* gene induction) are included for comparison. *GAPDH* and *ATP5B* were used as reference genes. Relative expression was normalised to non-treated "Long Term" A549 cells. Non-parametric Kruskal-Wallis test with comparison to Long Term (Control). 25% and 50% FCM RGZ samples were not assessed for SFTPA2 gene expression. Coloured data points represent data from independent experiments. **=p<0.005, ***=P<0.001.
An RGZ 'Absorption' Control (Abs Con) was prepared to evaluate and RGZ carry-over into the FCM and used for all *SFTP*. Example data are included here for *SFTPB* (F). Absorption control data for the other *SFTP* genes is included in Appendix D.

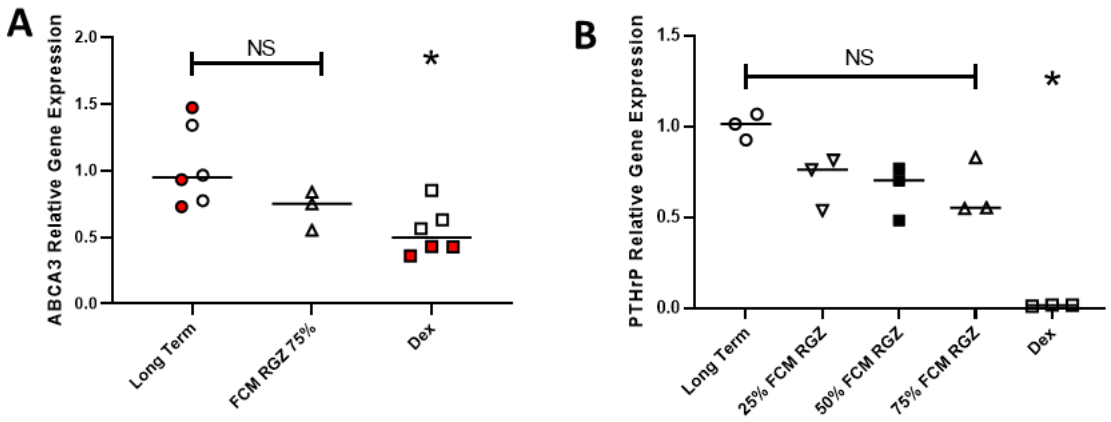

Figure 7.27. The effect of chronic treatment with fibroblast conditioned medium (FCM) on ATII gene expression in long term A549 cultures.
A549 cells were cultured in F12/10% FBS for three weeks with: 0% (Long Term) and 25%, 50% and 75% (v/v) RGZ-fibroblast conditioned medium ('FCM RGZ'). A549 Cultures were regularly medium exchanged. At day 21 RNA was extracted for QRT-PCR analysis with TaqMan™ primer/probe sets for *ABCA3*(A), and *PTHrP* (B). Data from 100 nM Dexamethasone (Dex) treated A549 cells are included for comparison as this treatment has been previously demonstrated effective for ATII specific gene expression but detrimental to *PTHrP* induction in A549. *GAPDH* and A*TP5B* were used as reference genes. Relative expression was normalised to non-treated "Long Term" A549 cells. Non-parametric Kruskal-Wallis test with comparison to Long Term (Control). Coloured data points represent data from independent experiments. 25% and 50% FCM samples were not assessed for ABCA3 expression. . *=$p<0.05$.

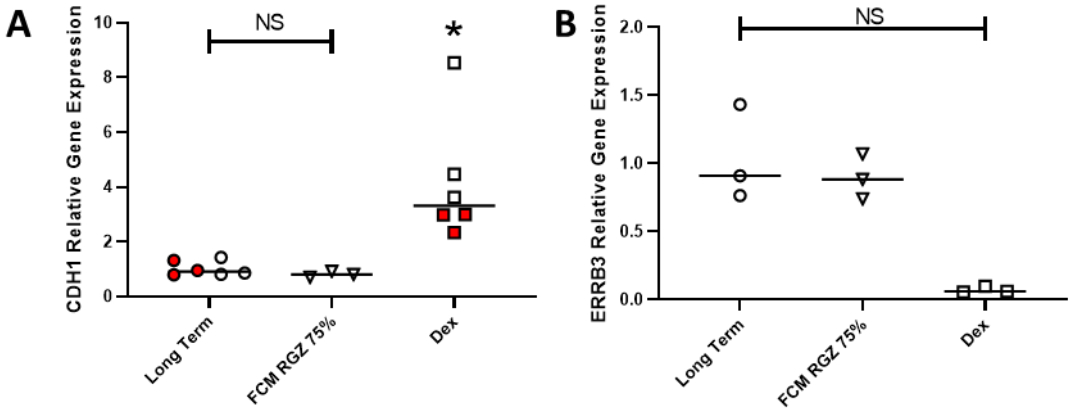

Figure 7.28. The effect of chronic treatment of long term A549 cultures on epithelial gene expression with fibroblast conditioned medium from MRC-5 cells treated with 10 µM Roziglitazone (FCM RGZ).

A549 cells were cultured in F12/10% FBS for three weeks with no treatment ("Long Term") (0%) and with 75% (v/v) RGZ fibroblast conditioned medium (FCM RGZ). Cultures were regularly medium exchanged. On Day 21 RNA was extracted for QRT-PCR analysis with TaqMan™ primer/probe sets for gene expression of *CDH1*(A) and *ERBB3*(B). Data from 100 nM Dexamethasone (Dex) treated A549 cells are included for comparison as this treatment has been previously demonstrated effective for ATII specific gene induction in A549 cells. *GAPDH* and *ATP5B* were used as reference genes. Relative expression was normalised to non-treated "Long Term" A549 cells. Non-parametric Kruskal-Wallis test with comparison to Long Term (Control). Coloured data points represent data from independent experiments. *=$p<0.05$.

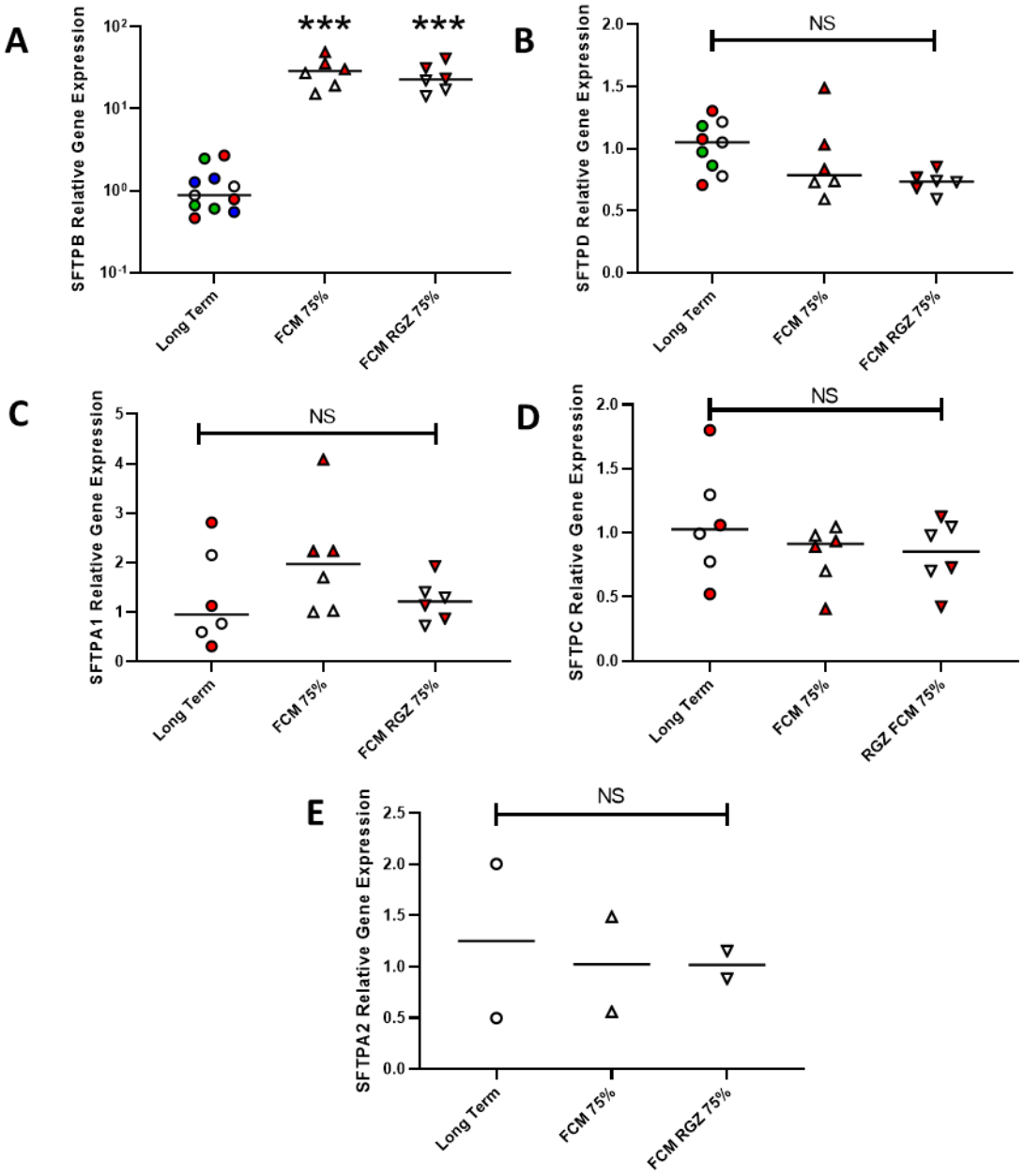

Figure 7.29. Comparison of surfactant protein gene expression in A549 cells treated with fibroblast conditioned medium (FCM) from non-treated MRC-5 fibroblasts and MRC-5 fibroblasts treated with Rosiglitazone (RGZ).
A549 cells were cultured in F12/10% FBS for three weeks with: no treatment ("Long Term") (0%) and 75% (v/v) fibroblast conditioned medium from MRC-5 cells previously treated with 10 μM RGZ (FCM RGZ) and 75% (v/v) fibroblast conditioned medium (FCM) from untreated MRC-5 cells (refer to schematics: Figure 7.5 and Figure 7.20). Cultures were regularly medium exchanged. RNA was extracted for QRT-PCR analysis with TaqMan™ primer/probe sets for surfactant protein gene expression. *SFTPB* (A), *SFTPD* (B), *SFTPA1* (C) and *SFTPC* (D) and *SFTPA2* (E). *GAPDH* and *ATP5B* were used as reference genes. Relative expression was normalised to "Long Term" A549 cells. Non-parametric Kruskal-Wallis test with comparison to Long Term (Control). NS=no significant difference. Coloured data points represent data from independent experiments. *** P<0.001.

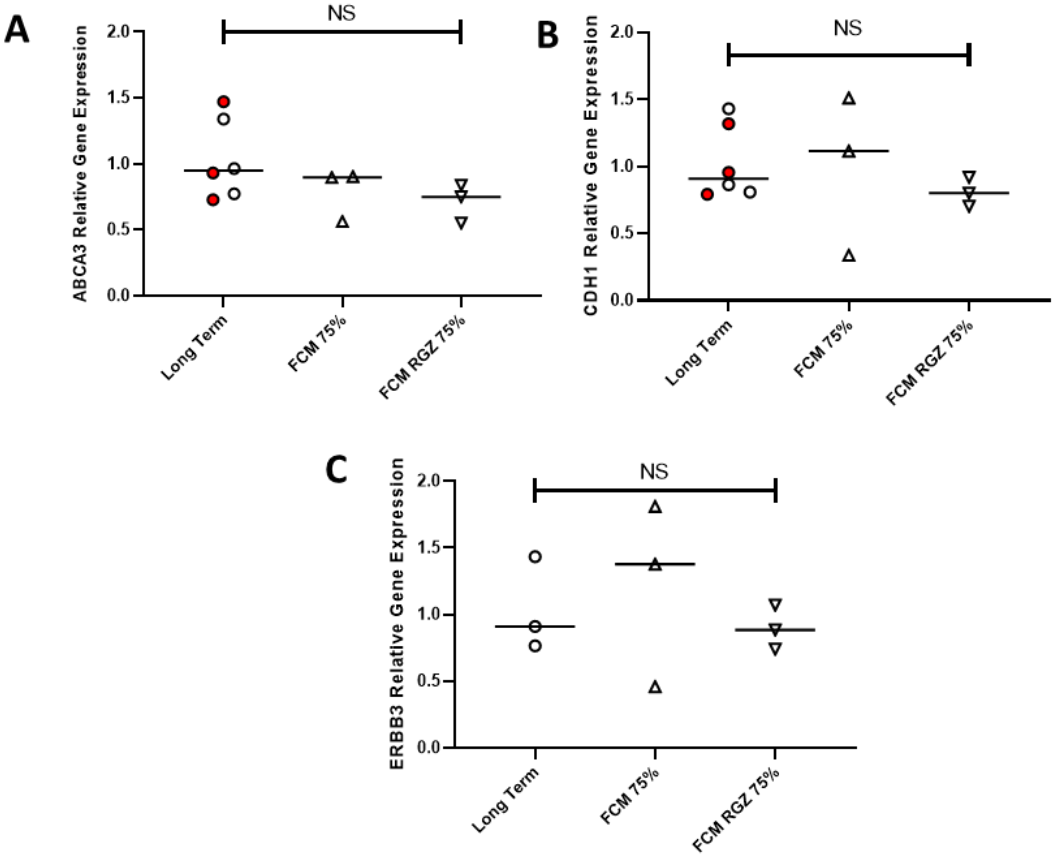

Figure 7.30. Comparison of ATII and epithelial related gene expression in A549 cells treated with fibroblast conditioned medium (FCM) from non-treated MRC-5 fibroblasts and from MRC-5 fibroblasts treated with Rosiglitazone (RGZ).
A549 cells were cultured in F12/10% FBS for three weeks with no treatment ("Long Term") (0%), 75% (v/v) fibroblast conditioned medium from MRC-5 cells previously treated with 10 μM RGZ (FCM RGZ) and 75% (v/v) fibroblast conditioned medium (FCM) from untreated MRC-5 cells (refer to schematics: Figure **7.5** and 7.20). The A549 cultures were regularly medium exchanged. At day 21 RNA was extracted for QRT-PCR analysis with TaqMan™ primer/probe sets for: *ABCA3* (A), *CDH1* (B) and *ERBB3* (C). *GAPDH* and *ATP5B* were used as reference genes. Relative expression was normalised to the average Ct values non-treated "Long Term" A549 cells. (NS) denotes no significant difference was observed between samples using Non-parametric Kruskal-Wallis test with comparison to Long Term control. Coloured data points represent data from independent experiments. NS = not significant

7.3.8 Three-Dimensional (3D) Co-Culture in Alvetex ™ Scaffold

Encouraging results in the form of elevated *SFTPB* gene expression were obtained from the use of MRC-5 conditioned medium on A549 cultures and Transwell™ co-cultures of the two cell lines. Despite the levels of expression remaining far from those seen in primary ATII cells the results imply that further development of a co-culture strategy may be the way forward to drive ATII characteristics in A549 cells in a physiologically relevant *in vitro* model of the alveolar epithelium. Transwell™, plate and flask culture, however, depend on cell culture in two-dimensions for cellular growth and differentiation, whereas *in vivo* cells grown in three-dimensional (3D) relationship with each other allowing the cell to adopt the correct shape and orientation for appropriate physiological function. Although the Transwell™ membrane allowed relatively close contact and molecular cross-talk between the A549 and MRC-5 cells, the cells remained separated from each other by an artificial barrier 10 to 50 μm in thickness (www.corning.com), whereas in *in vivo* tissues the supporting basal lamina that separates the mesenchyme and epithelium is in the order of only a few hundred nanometres in thickness[522]. In addition, *in vivo*, mesenchymal cells tend to establish connective tissue comprised of a combination of cells and extracellular matrix (ECM)[1].

ECM secretion by fibroblasts establishes the cellular environment and provides mechanical and biochemical support for epithelial cells[523]. Fibroblast cells cultured *in vitro* under conventional 2D conditions spread out with elongated morphologies. This Interferes with microtubule formation leading to a high-tension state[524]. Cells in 2D undergo substantial cytoskeletal reorganization to induce actin stress fibres and attachment through focal adhesions (clusters of integrins). This is far from the situation found in normal *in vivo* homeostasis[525]. Indeed 2D culture creates conditions more similar to those found in fibrosis and wound contraction[526].

3D cell culture systems provide completely different physio-typical environments compared to 2D[337 524]. Human Fibroblasts in 3D matrices have a unique morphology that contains microtubule-mediated dendritic formation rather than actin stress fibres. This encourages normal homeostatic gene expression and matrix biosynthesis[527 524].

Previous work (chapter 3) involved the cultivation of A549 cells in mono-culture in 3-D spheroids. This approach led to the cells adopting a mucus secreting phenotype similar to goblet cells of the upper respiratory tract, a tumour -like phenotype or a mixture of both.

To explore the hypothesis that closer proximity between A549 and MRC-5 and 3-D culture may be beneficial, manifested by the establishment of mesenchyme derived ECM, an epithelial barrier and quiescent tissue-like organisation, co-culture in 3-D Alvetex™ Scaffold was explored.

The first step was to determine an appropriate seeding density of MRC-5 cells in "12-well" Alvetex™ Scaffold inserts. (Note although the '12 well' inserts carriers can be trimmed to fit 12-well culture plates, they can be used in 6-well plates). Inserts were seeded with $2.5x10^5$, $5x10^5$ and $1x10^6$ MRC-5 cells and incubated for two weeks before histological examination. It was found that the cells formed a cellular coating on the surface of the scaffold with a small number of cells locating to the inner cavities of the scaffold. No obvious differences were observed between the three seeding densities (Figure 7.31) so it was decided to proceed to co-culture experiments using a $5x10^5$ per 12-well insert inoculum of MRC-5 cells. Note the difference in morphology and distribution of MRC-5 cells in Alvetex™ Scaffold in Figure 7.31 where there were scarce attachment points to the scaffold to the situation in 2D culture from previous sections (e.g. Figure 7.4) where the cells are flattened and attached by their entire ventral surface to the plastic.

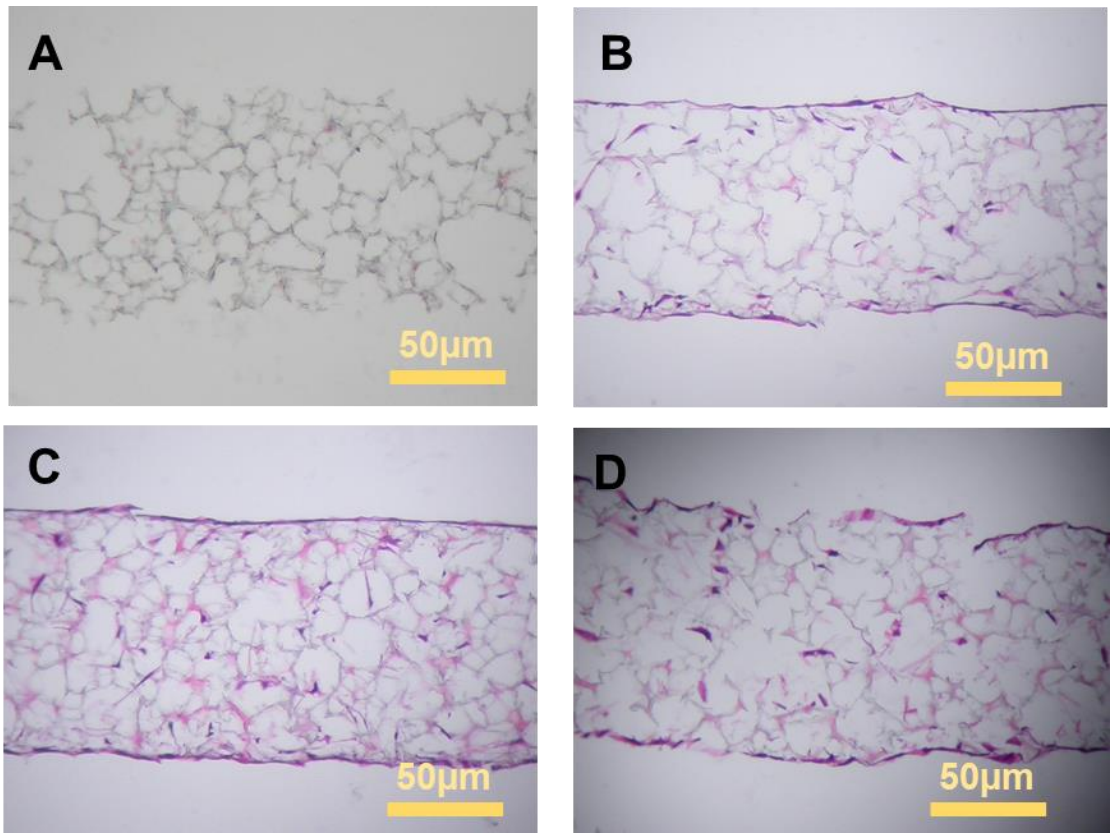

Figure 7.31. The effect of different seeding densities on the establishment of MRC-5 fibroblast culture in Alvetex™ scaffold.
Alvetex™ Scaffold AVP005 12 well inserts were inoculated with MRC-5 fibroblasts at $2.5x10^5$ (B) $5x10^5$ (C) $1x10^6$ cells per insert in F12 medium in 6-well plates. A cell-free control was included (A). Plates were incubated at 37°C for two weeks with a daily medium change before paraformaldehyde fixation, paraffin embedding, sectioning, dewaxing and Haematoxylin-Eosin staining of the Scaffold inserts. Images represent a single experiment.

The next step was to attempt A549 culture in Alvetex™ Scaffold comparing two-week A549 monoculture, two-week MRC-5 monoculture and a co-culture comprising the inoculation of a two-week established MRC-5 scaffold culture with A549 cells followed by a further two-week incubation. The cultures were sectioned and examined by histology. MRC-5 monocultures appeared as expected (Figure 7.32A), however A549 cells in both the mono-culture (Figure 7.32B) and co-culture models (Figure 7.32C) invaded the scaffold with no evidence of epithelial organisation.

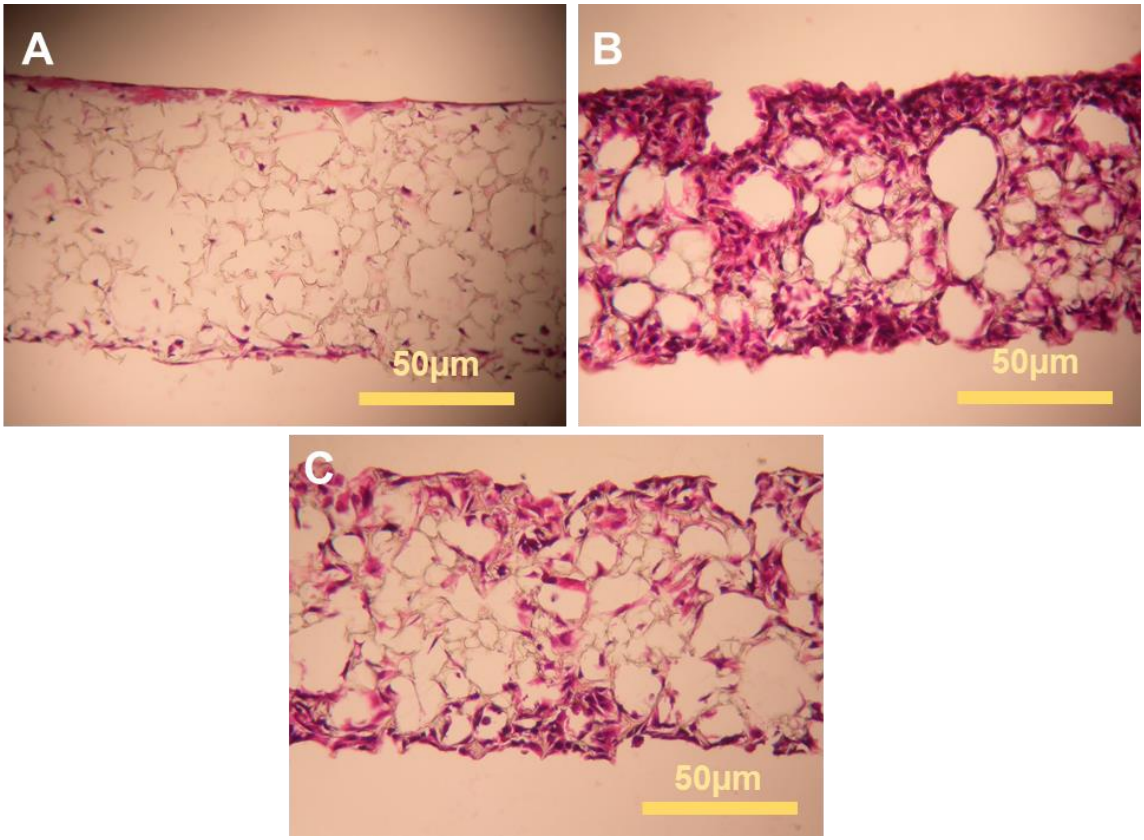

Figure 7.32. Initial attempt at establishing A549/MRC-5 fibroblast co-culture in Alvetex™ scaffold.
Alvetex™ Scaffold AVP005 12 well inserts were inoculated with MRC-5 fibroblasts at $5x10^5$ cells per insert in F12 medium and cultured for two weeks (A), with A549 at $5x10^4$ cells per insert in F12 medium and cultured for two weeks (B) and with a co-culture of MRC-5 and A549 (C). In the co-culture wells, MRC-5 cultures were established from a $5x10^5$ cell inoculum and cultured for two weeks before the addition of $5x10^4$ A549 cells followed by a further two-week incubation. All cultures received a daily medium change before paraformaldehyde fixation, paraffin embedding, sectioning, dewaxing and Haematoxylin-Eosin staining of the Scaffold inserts. Images represent a single experiment.

In vivo, tissues are comprised of epithelia supported on a mesenchymal substrate containing ECM. A major component of the ECM being collagen fibrils. The MRC-5, and A549 scaffold monocultures and scaffold co-cultures were histologically assessed for evidence of collagen secretion using the collagen specific Sirius Red stain (Figure 7.33) and Masson's Trichrome stain for connective tissue (Figure 7.34). No evidence of collagen expression of the development of ECM was seen in these sections.

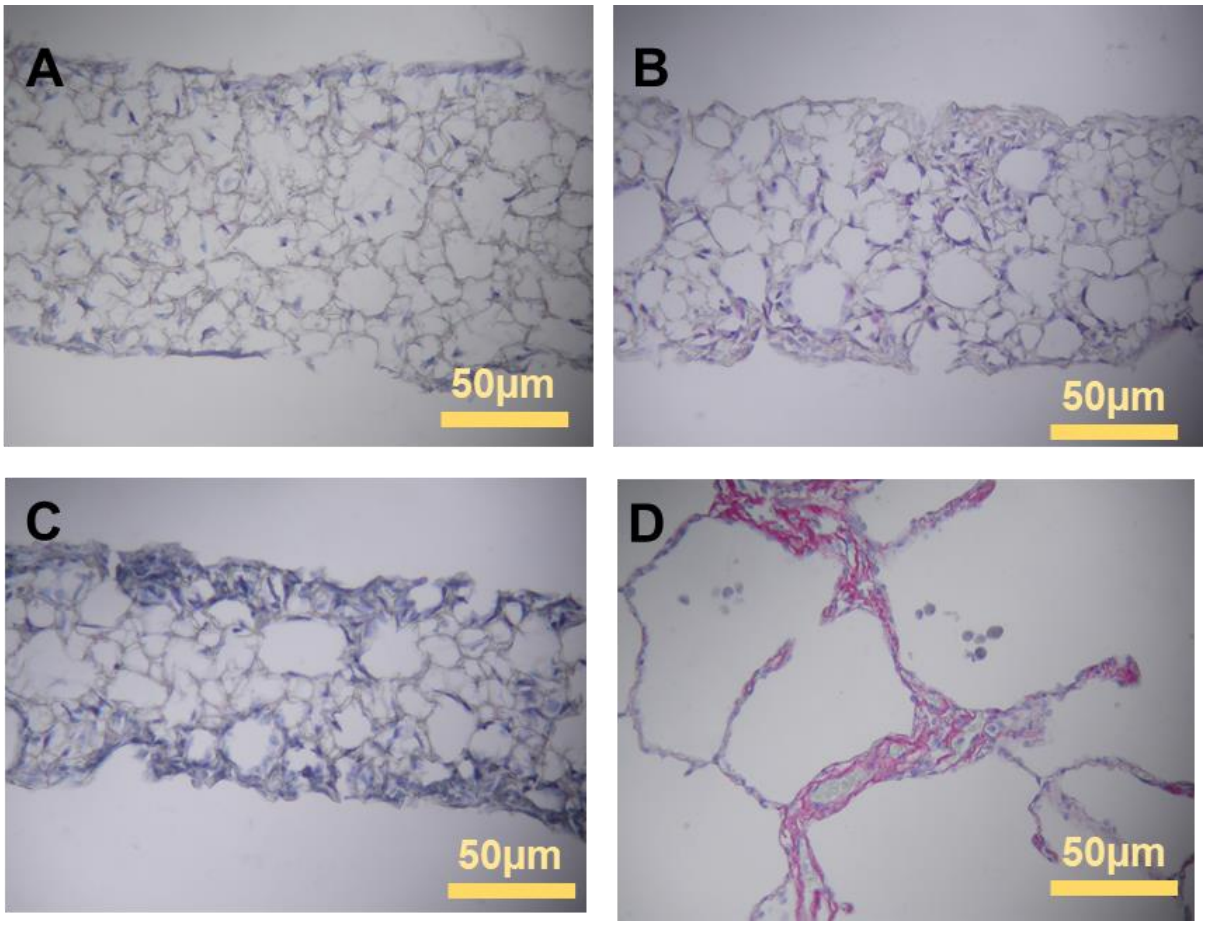

Figure 7.33. Evaluation of collagen expression in the initial attempt at establishing A549/MRC-5 fibroblast co-culture in Alvetex™ scaffold.
Alvetex™ Scaffold AVP005 12 well inserts were inoculated with MRC-5 fibroblasts at $5x10^5$ cells per insert in F12 medium and cultured for two weeks (A), with A549 at $5x10^4$ cells per insert in F12 medium and cultured for two weeks (B) and with a co-culture of MRC-5 and A549 (C). In the co-culture wells, MRC-5 cultures were established from a $5x10^5$ cell inoculum and cultured for two weeks before the addition of $5x10^4$ A549 cells followed by a further two week incubation. All cultures received a daily medium change before paraformaldehyde fixation, paraffin embedding, sectioning, dewaxing and Sirius Red staining for collagen. Collagen should stain red and nuclei blue. A positive control for collagen staining (human lung) was included (D). Images represent a single experiment.

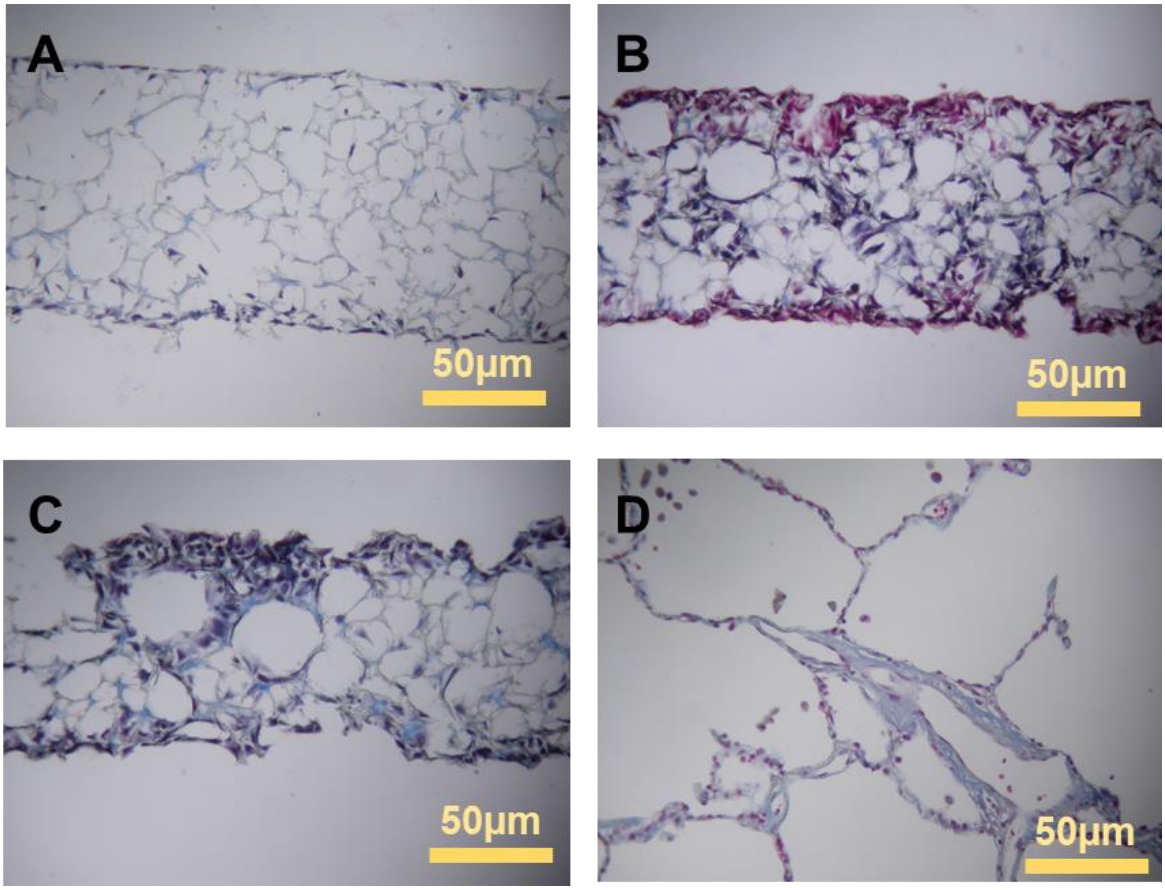

Figure 7.34. Evaluation of collagen expression in the initial attempt at establishing A549/MRC-5 fibroblast co-culture in Alvetex™ scaffold.
Alvetex™ Scaffold AVP005 12 well inserts were inoculated with MRC-5 fibroblasts at $5x10^5$ cells per insert in F12 medium and cultured for two weeks (A), with A549 at $5x10^4$ cells per insert in F12 medium and cultured for two weeks (B) and with a co-culture of MRC-5 and A549 (C). In the co-culture wells, MRC-5 cultures were established from a $5x10^5$ cell inoculum and cultured for two weeks before the addition of $5x10^4$ A549 cells followed by a further two-week incubation. All cultures received a daily medium change before paraformaldehyde fixation, paraffin embedding, sectioning, dewaxing and Masson's Trichrome staining for connective tissue which should stain light blue in contrast to nuclei that should stain blue-black and fibrin which will appear red. A positive control for connective tissue (human lung) was included (D). Images represent a single experiment.

It was observed that the dense infiltration of A549 cells into the scaffold in the co-culture and A549 monoculture bore resemblance to the cellular appearance seen previously in spheroid culture. In spheroids A549 developed a mucus secreting phenotype evident by positive Periodic Acid Schiff (PAS) staining. Evidence of mucus secretion was also seen in PAS stained sections of the A549 populated scaffold (Figure 7.35B and 7.3C) implying that simply adding the two cell types into the scaffold is unlikely to drive and ATII phenotype in the A549 cells.

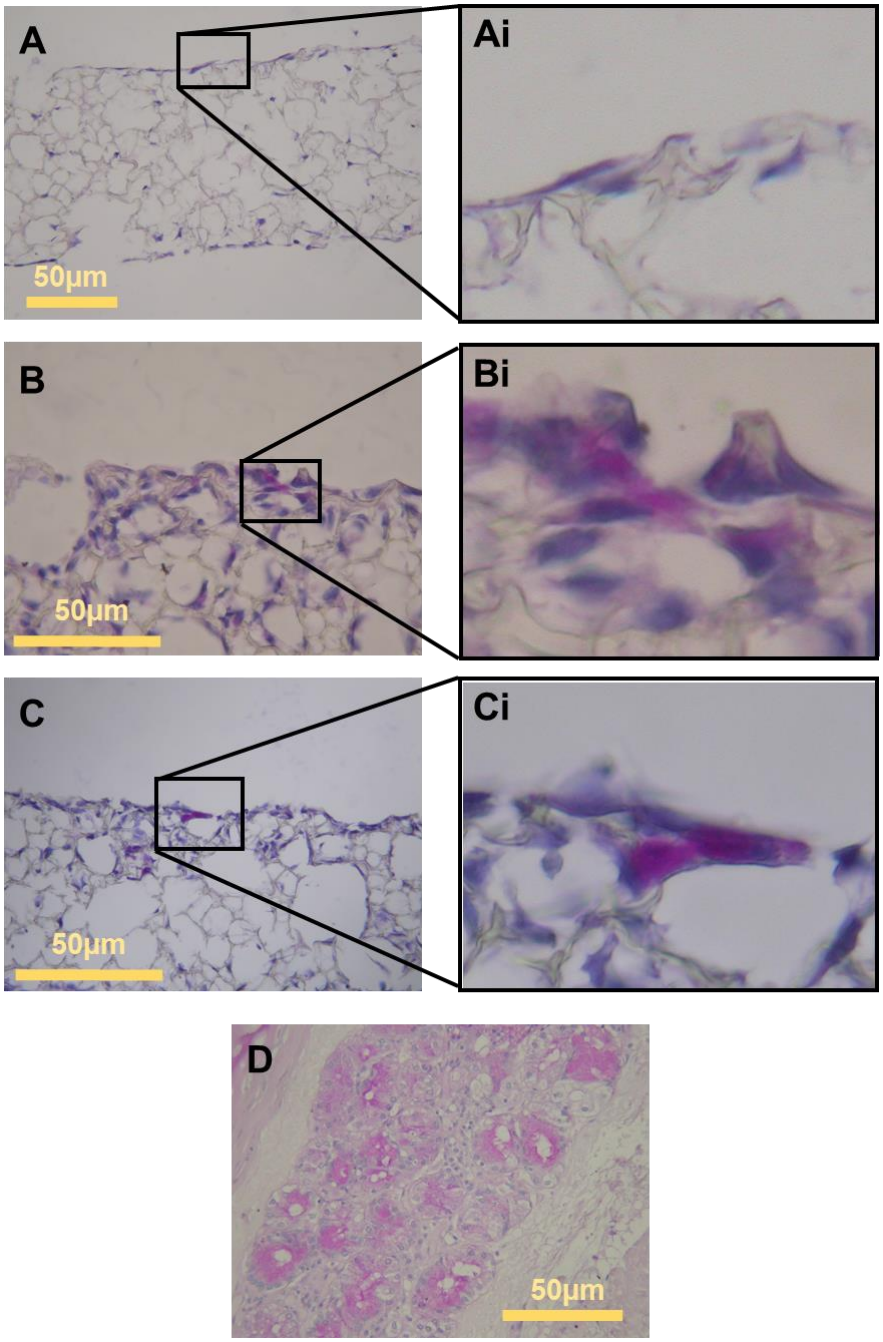

Figure 7.35. Evaluation of mucin expression in the initial attempt at establishing A549/MRC-5 fibroblast co-culture in Alvetex™ scaffold.
Alvetex™ Scaffold AVP005 12 well inserts were inoculated with MRC-5 fibroblasts at $5x10^5$ cells per insert in F12 medium and cultured for two weeks (A), with A549 at $5x10^4$ cells per insert in F12 medium and cultured for two weeks (B) and with a co-culture of MRC-5 and A549 (C). In the co-culture wells, MRC-5 cultures were established from a $5x10^5$ cell inoculum and cultured for two weeks before the addition of $5x10^4$ A549 cells followed by a further two-week incubation. All cultures received a daily medium change before paraformaldehyde fixation, paraffin embedding, sectioning, dewaxing and Periodic Acid Schiff (PAS) staining for mucin tissue which should stain pink in contrast to haematoxylin counterstained nuclei that should stain blue-black. A positive control for mucin (human bronchus) was included (D). Images represent a single experiment.

In order to develop a more physiological mesenchymal support for the A549 cells it was postulated that a longer period of MRC-5 culture in the scaffold together with the supplementation the medium with ascorbic acid in the presence of copper ions in the Ham's F12 medium might encourage LOX mediated fibrillar collagen production in the MRC-5 and production of tissue-like ECM. In a preliminary experiment Alvetex™ Scaffold was seeded with MRC-5 cells and cultured for one month in the presence or absence of 34.5 μM L-ascorbic acid (ascorbic acid 2-phosphate). After a month in culture the scaffolds were inoculated with A549 cells and cultured for a further two weeks before histological investigation using Sirius Read and Masson's Trichrome staining. Surprisingly both the ascorbic acid and non-treated one-month MRC-5 scaffold cultures evolved a layer of ECM on the surface of the scaffold (Figure 7.36). Faint blue staining of this ECM (Figure 7.36C and D) points to the possibility that this ECM might contain collagen however evidence from Sirius Red staining was inconclusive (Figure 7.37A and B). Although it is not possible to be discriminate if the cells observed on and in the ECM are A549 or MRC-5 it seems that the ECM in the ascorbic acid treated cultures may be qualitatively different with cells aligning on the surface of the ECM in the non-ascorbic acid treated cultures (Figure 7.36C) and within the ECM in ascorbic acid treatment (Figure 7.36D).

The addition of TGF-β to skin and intestinal fibroblasts supporting the differentiation of the intestinal cell line CaCo2 has proven to effective in an Alvetex™ based system[528]. Although not employed in the A549 model here it may have some benefit to future work, however there should be attention to the possibility of TGF-β inducing a fibrotic-like response and myoblast differentiation in the MRC-5 fibroblasts[90].

It should be noted that the population of the Alvetex scaffold with MRC-5 cells appeared to be sparse in comparison to previous experiments where the incubation time had been far shorter. Microscopic examination of the wells at the end of the 6-week co-culture revealed that the MRC-5 cells had preferentially populated the well base and formed a thick multi-layer coating of MRC-5 cells at the expense of the Alvetex™. Despite this, the differences between the highly proliferative and invasive phenotype of the cells seen in the initial co culture experiments (Figure 7.32, 7.33, 7.34 and 7.35) and the quiescent, organised appearance of the histological sections from the longer term Alvetex™ cultures (Figure 7.36 and 7.37) are striking.

Scanning electron micrographs of the ascorbic acid treated and non-treated Alvetex™ co-cultures show the presence of two different cell types (Figure 7.38). A uniform covering of the scaffold with what are assumed to be the MRC-5 fibroblasts and ECM with the occasional rounded cell, assumed to be A549. These rounded cells do not appear to be as numerous as

those observed in the histological staining and it may be that they were loosely adherent and their numbers may have been diminished during in sample preparation.

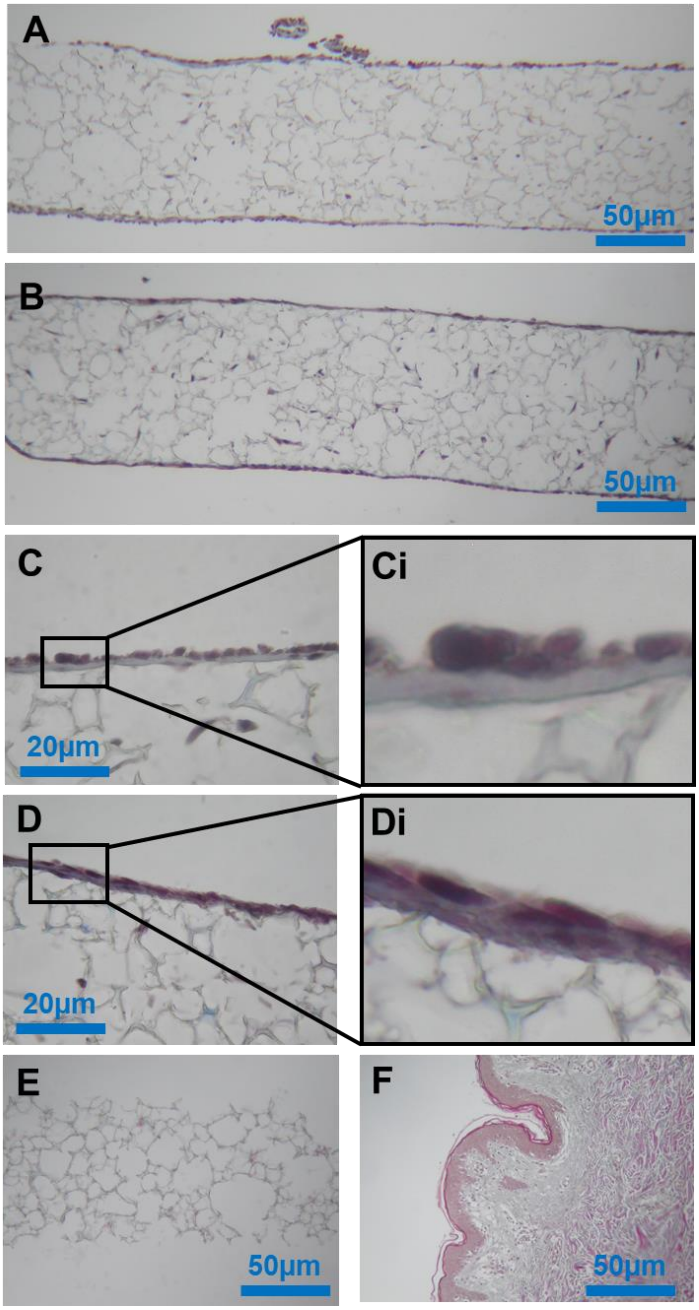

Figure 7.36. Establishment of connective tissue in L-ascorbic acid treated A549/MRC-5 co-cultures in Alvetex™ Scaffold. Masson's Trichrome Stain.
Alvetex™ Scaffold AVP005 12 well inserts were inoculated with MRC-5 fibroblasts at $5x10^5$ cells per insert and incubated for one month in F12/DMEM 10% FBS with and without supplementation with 34.5 µM L-ascorbic acid prior to inoculation with $5x10^4$ A549 cells and a further two-weeks incubation. All cultures received daily medium change before paraformaldehyde fixation, paraffin embedding, sectioning, dewaxing and Masson's Trichrome staining for connective tissue (light blue) in contrast to nuclei (blue-black) and fibrin (red). Ascorbic acid free cultures (A, C and Ci), cultures treated with ascorbic acid (B, D and Di). A cell free Alvetex Scaffold Control is included (E) together with a positive control for the stain (human skin) (F). Images represent a single experiment.

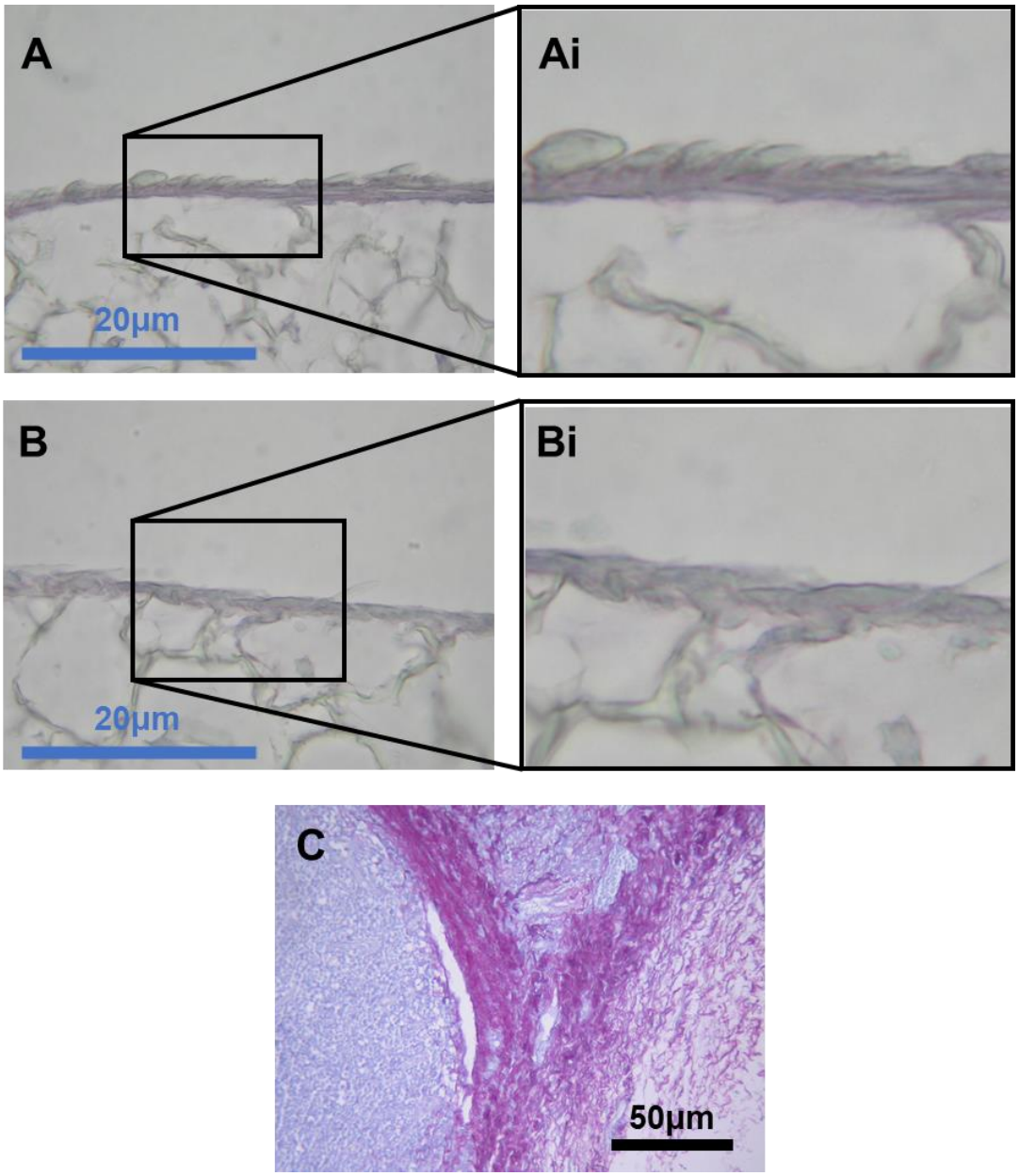

Figure 7.37. Establishment of connective tissue in L-ascorbic acid treated A549/MRC-5 co-cultures in Alvetex™ Scaffold. Sirius Red Stain.
Alvetex™ Scaffold AVP005 12 well inserts were inoculated with MRC-5 fibroblasts at $5x10^5$ cells per insert and incubated for one month in F12/DMEM 10% FBS with and without supplementation with 34.5 µM L-ascorbic acid prior to inoculation with $5x10^4$ A549 cells and a further two-weeks incubation. All cultures received daily medium change before paraformaldehyde fixation, paraffin embedding, sectioning, dewaxing and Sirius Read staining for collagen. Collagen should stain red and nuclei blue. Ascorbic acid free culture (A and Ai); treated with ascorbic acid (B and Bi). A positive control for the stain (human nasal polyp) is included (C). Images represent a single experiment.

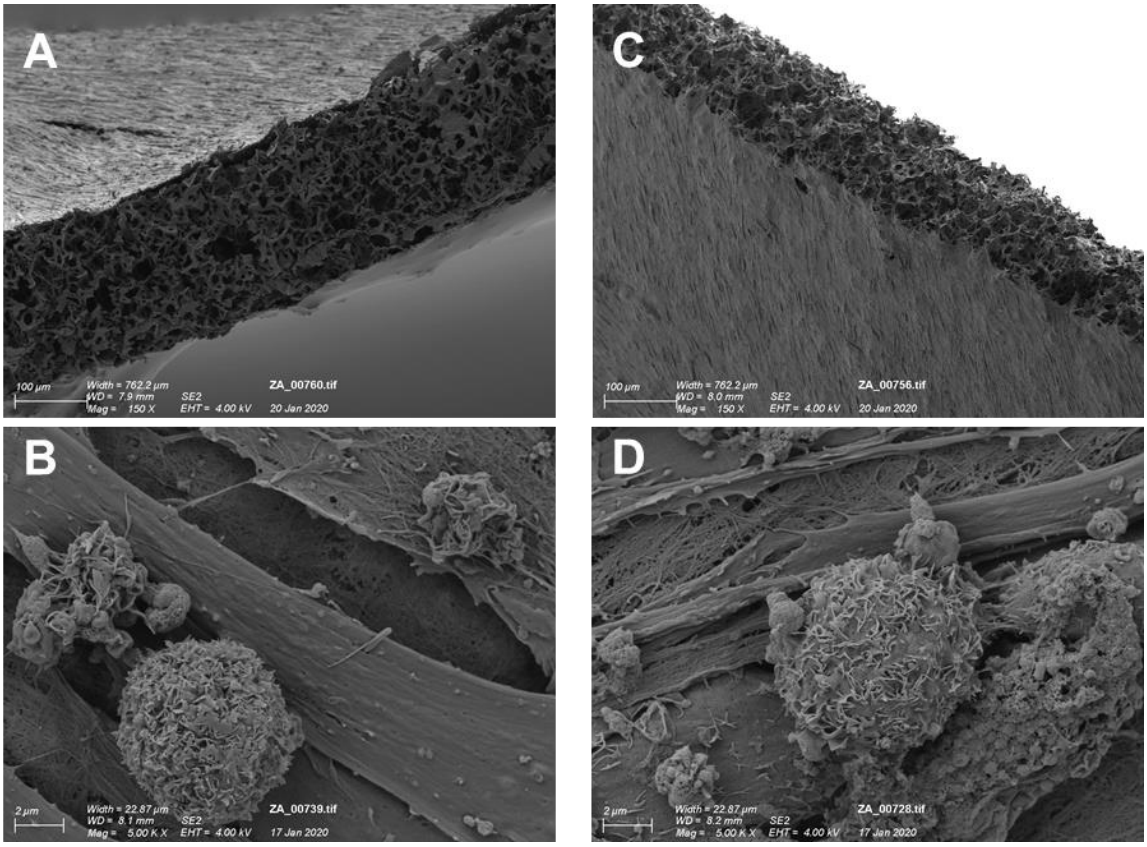

Figure 7.38. SEM micrographs of L-ascorbic acid treated A549/MRC-5 co-cultures in Alvetex™ Scaffold.
Alvetex™ Scaffold AVP005 12 well inserts were inoculated with MRC-5 fibroblasts at $5x10^5$ cells per insert and incubated for one month in F12/DMEM 10% FBS with and without supplementation with 34.5 µM L-ascorbic acid prior to inoculation with $5x10^4$ A549 cells and a further two-weeks incubation. All cultures received daily medium change before glutaraldehyde fixation, dehydration, gold coating and SEM imaging. Non-treated culture (A and B); ascorbic acid treated culture (C and D). Images represent a single experiment.

Finally, the ascorbic acid treated and non-treated scaffold co-cultures were examined by transmission electron microscopy (TEM). Initial results indicated that the ascorbic acid treated co-cultures may be driving A549 cells to produce MLB, however the cells appear flattened and appear to have expressed mucin granules in addition to the MLB (Figure 38B) No evidence of MLB expression was observed in non-ascorbic acid treated cells (Figure 38A) however these were initial results and more work is required to confirm these findings. TEM confirms the presence of ECM (Figure 38D), however the expression of fibrillar collagen was not confirmed, neither was there evidence of the establishment of basement membrane.

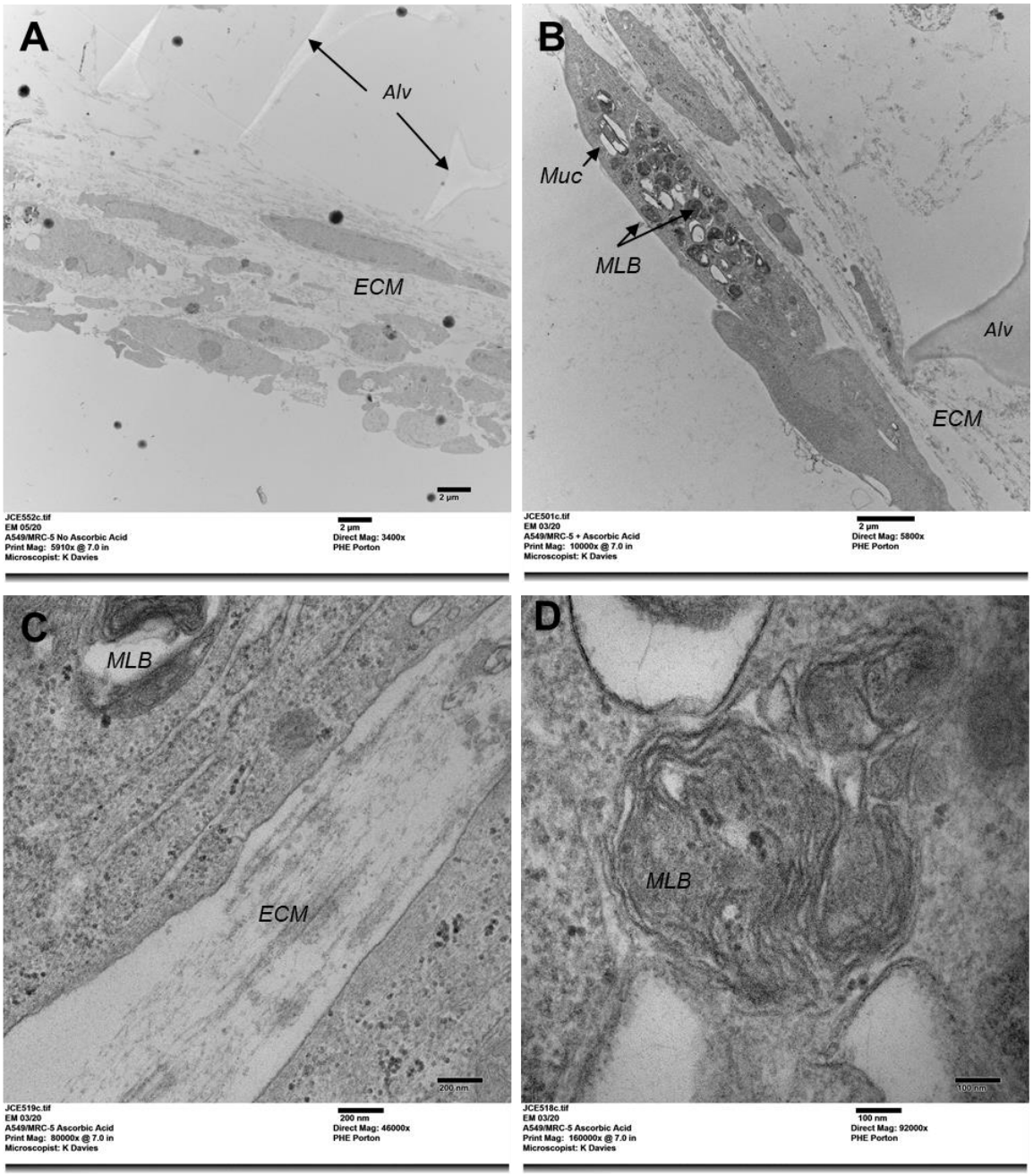

Figure 7.39. TEM micrographs of L-ascorbic acid treated A549/MRC-5 co-cultures in Alvetex™ Scaffold.

Alvetex™ Scaffold AVP005 12 well inserts were inoculated with MRC-5 fibroblasts at $5x10^5$ cells per insert and incubated for one month in F12/DMEM 10% FBS with and without supplementation with 34.5 µM L-ascorbic acid prior to inoculation with $5x10^4$ A549 cells and a further two-weeks incubation. All cultures received daily medium change before glutaraldehyde fixation, resin embedding, sectioning and treatment with osmium tetroxide and uranyl acetate prior to transmission electron microscopy (TEM). Non-treated culture (A); ascorbic acid treated culture (B); extracellular matrix (ECM) from ascorbic acid treated culture (C); multilamellar body (MLB) from ascorbic acid treated culture (D). Images represent a single experiment.

MLB=MLB, *ECM*=ECM, *Muc*=Mucin Granule, *Alv*=Alvetex Scaffold.

7.4 Discussion

The intent of this chapter was to determine if co-culture with MRC-5 fibroblasts might encourage epithelial-mesenchymal cross talk to subsequently enhance the expression of ATII characteristics in A549 cells; allowing refinement and improvement of the models developed in previous chapters. Experiments using conditioned medium and co culture in Transwells™ showed improvement in terms of *SFTPB* expression over the long term A549 culture from Chapter 4[483], evidence of cell-cell communication without the negative effects seen with Dex treatment in chapter 5. Further preliminary experiments using the co-culture approach in Alvetex™ Scaffold led to the generation of two distinct organisational architectures. Firstly: disorganised invasive A549 growth with two week cultured MRC-5 cells, reminiscent of the honeycomb cysts of end stage IPF. Secondly, through longer term culture of the MRC-5 cells in Alvetex™: a more organised, quiescent co-culture with evidence of ECM deposition that might reflect IPF.

Co-culture models involving A549 and MRC-5 have been previously established by others to help understand stromal-tumour metabolic interactions and the tumour microenvironment[529 530 531]or they are developed and utilised on the assumption that they are ready-enabled to recapitulate alveolar function [532]. Work by others using other primary ATII/fibroblast co-cultures have led to the establishment of alveolar epithelial models[533] and as discussed in previous chapters in the elucidation of ATII/mesenchymal cross talk and lung development. The aim of this chapter was to demonstrate some ATII epithelial physiological relevance in a A549/MRC-5 co-culture and to translate the co-culture to an advanced 3D scaffold.

PTHrP is a highly evolutionarily conserved gene and has an important role in the development, repair and homeostasis in the rodent alveolar epithelium[534] and has been show to play a role in response to lung injury in humans[535]. In rodents PTHrP produced by the ATII cell acts on its receptor on fibroblasts and under the influence of Wnt helps to maintain their lipofibroblast phenotype[57]. Dex treatment of A549 cells had a significantly negative impact on the gene expression *PTHrP* in A549 cells, an effect that has been observed in other cell types[536]. Due to this and the previously observed downregulatory effect of Dex on *ERBB* expression in A549 and the likely substantial impact on other glucocorticoid responsive genes[479], it was decided to discontinue investigations using Dex treatment.

During a nine-day time-course, the key markers of *PTH1R* and *NRG1-β* and the lipofibroblastic marker *PLIN2* were upregulated in MRC-5 cells and the cells appeared to express lipid droplets confirmed using Oil Red-O staining. Subsequent treatment of A549 cells with the FCM from MRC-5 augmented the long term A549 culture differentiation protocol from

Chapter 4[483] by significant *SFTPB* gene upregulation whilst retaining the expression of *ERBB3* and *PTHrP* that was ablated in Dex treated cells. In rodents and other mammals[512] lipofibroblasts, appear to support and maintain ATII cells and have been shown to transdifferentiate to a myofibroblast phenotype, typical of the fibrotic cells from fibrotic foci of IPF under the influence of TGF-β signalling. This trans-differentiation process can be experimentally reversed using PPARγ agonists such as Rosiglitazone to restore the lipofibrobastic phenotype[90 89]. The observation of Lipid and *PLIN2* gene expression in MRC-5 cells together with the upregulation of *SFTPB* gene expression seen in A549 cells following FCM treatment suggested the tentative possibility of adoption of a lipofibroblast phenotype in the MRC-5 cells. Attempts to push the cells further to this phenotype by exposing the MRC-5 cells to the PPARγ agonist Rosiglitazone (RGZ) before the generation of FCM had no discernible advantage on the induction of ATII properties in A549, despite earlier upregulation of *PLIN2* in the time-course of MRC-5 growth. However, there was no observed upregulation of *Leptin* which is expressed in the mesenchyme and thought to contribute to the paracrine signalling 'loop' of ATII development[537]. Although it may be tempting to surmise that that these experiments induced a lipofibroblast phenotype in MRC-5 there is a need for caution. The notion of the presence of lipid droplet containing lipofibroblast cells in the human lung is controversial with conflicting evidence[91 92 512]. MRC-5 is a primary diploid cell line with limited proliferative capacity and it is equally likely that the observed lipid expression may have been an early sign of replicative senescence[538], the irreversible growth arrest of human primary diploid cell cultures after serial passage[232]. Senescence is thought to be an age-related tumour control mechanism that guards against unrestricted growth of damaged cells. This hypothesis has become widely supported over following decades and has been causally linked to the cumulative attrition of telomeres during cellular replication of normal cells[539]. Cellular replicative senescence is now recognised as key process whereby cells cease dividing and undergo specific phenotypic alterations which include substantial chromosome, behavioural and secretory changes together with the suppression of tumour activation[540 541]. More recently, additional evidence indicates that cellular senescence extends beyond tumour suppression and ageing and may also be involved with embryonic development, wound healing and tissue remodelling[542 543 544 545]. Lipids are increasingly recognised as central in cell signalling in cell processes that include non-apoptotic cell death[546] and cell division. It has been demonstrated that the lipidome changes throughout the cell cycle resulting in lipid accumulation in senescent human fibroblast cells[547 538].

The positive effect of *SFTPB* gene induction seen with FCM was retained in physical MRC-5/A549 co-culture in Transwells™ strongly supporting evidence of cellular communication possibly through PTHrP secretion from the A549 cells and its interaction with the PTH1R receptor on the MRC-5 cells and subsequent *PLIN2* and *NRG-1β* expression in the fibroblasts,

as shown in the independent culture experiments. These have all been shown to be factors important for the development, maintenance and support of ATII cells and the alveolar epithelium[58]. As well as encouraging direct communication between the two cell types, the Transwell™ system had the added advantage over the FCM approach as it removed the need to independently generate FCM for a protracted period, reducing media volume therefore cost and avoiding the labour-intensive steps of filtering, freezing and logistical issues of storing the FCM. Positive results from Transwell™ culture gave confidence that progression to advanced co-culture in a scaffold might allow closer cell-cell interaction and the possible development of tissue like growth and establishment of epithelial cellular organisation.

Initial attempts at co-culture in Alvetex™ scaffold with two-week culture of MRC-5 cells prior to A549 addition resulted in invasive muco-secretory cultures with little evidence of alveolar organisation. This potentially shows that the A549 cells had reverted to a cancerous phenotype, however the disorganised cellular arrangement, and mucus secretion was reminiscent of the histological appearance of the honeycomb cysts seen in end stage IPF when alveolar architecture becomes destroyed through cellular remodelling[548].

Culture of the MRC-5 cells for an extended (1 month) time-course in Alvetex™ with and without ascorbic acid (AA) followed by addition of A549 cells resulted in a very different picture. Histological and TEM examination demonstrated organised cellular arrangement, with a thin fibroblastic layer each side of the Alvetex™ Scaffold and the deposition of extracellular matrix (ECM). There was little evidence of the previously observed A549 cellular invasion and with these long-term-cultured MRC-5 there were indications of induced growth arrest of the A549 cells. Histochemical staining indicated ECM was present on both sides of the Alvetex™ Scaffold in both AA and non-AA treated cultures, which was not expected. Although MRC-5 cells have been shown to express type 1 collagen[549] the expression cross-linked fibrillar collagen typical of differentiated tissues is dependent on the presence of ascorbic acid[550]together with endogenous Lysyl Oxidase (LOX) enzymes in the cells and copper ions (provided by the FBS Ham's F12 medium) as a co-factor[325]. TEM analysis of the ECM at high magnifications, showed no evidence of the typical banding pattern of fibrillar collagen in either the cultures with or without AA. It would be useful, therefore, in future experiments to consider the addition of exogenous copper to the culture medium to be certain that adequate copper ions were provided.

These findings, however of an apparently quiescent population of MRC-5 fibroblasts within and at the basal an apical surfaced of the scaffold, their apparent secretion of ECM, together with a single cell thick epithelial-like border of A549 cells that appear to be expressing MLB was an extremely positive outcome for the field of research in the field of *in vitro* ATII modelling. These features recapitulate many of those found in the lung parenchyma *in vivo*[3],

however it must be remembered that this was the outcome of a single experiment. The work should be repeated and it is prudent not to over interpret the results of these very interesting findings.

ECM can, however, be comprised of other factors such as polysaccharide chains of glycosaminoglycans (GAGs) (including hyaluronic acid (HA)), which are usually found covalently linked to protein in the form of proteoglycans. ECM can contain other fibrous proteins, such as elastin, fibronectin, and laminin, which have specific structural and adhesive functions[551]. Further work is necessary to determine the true nature of the ECM observed here. Disappointingly, no evidence of the development of basal lamina was observed using TEM which indicates lack of true epithelial differentiation, however these were preliminary experiments and they need to be repeated.

Interestingly, TEM demonstrated the presence of cells that expressed MLB as seen in the long term 2D model from Chapter 4, however, these MLB-expressing ATII-like cells co-expressed mucin granules reminiscent of ATII cells from end stage IPF[383] indicating the possibility that another phenotype has been achieved in the A549 cells in this system, a feature that might be relevant to IPF research.

3D cell culture is known to reduce the proliferative rates of cell lines as compared to their growth in 2D[552 553] and this presents the potential of the cells having adopted differentiated phenotypes[554]. This may be the case with regard to the apparent slowing of the MRC-5 and A549 cells in the Alvetex™ 3D cell culture model, which offers an exciting prospect, however, there could be other reasons for this apparent growth arrest. Quiescence can be caused by necrosis, as has been observed in 3D spheroid cultures[339] or due to cellular senescence[232 555].

It was expected that long term culture of the MRC-5 cells would generate density limited, quiescent growth arrested cultures, as are generally observed in long-term 2D cultured fibroblasts[556]. The "12-well" Alvetex™ Scaffolds used in these experiments were suspended in open capsules submerged in medium in the wells of conventional 6-well cell culture plates. Throughout the time-course it was noted that a thick layer of MRC-5 cells had accumulated on the bottom of the Alvetex wells and after histological examination of the scaffold it was postulated that dividing cells may have migrated out of the scaffold and were preferentially growing on the well base, outnumbering those in the scaffold. This raises the possibility that the MRC-5 cells continued to proliferate in the Alvetex™ wells and that daily medium exchange may have been driving replication, removing dividing cells from the scaffold as well as providing nutrients. The MRC-5 cells were seeded into the scaffold at a population doubling (PD) of 27 which was the lowest PD available. General opinion information provided by suppliers and previous work (data not included) advises that MRC-5 cells

become senescent and growth arrested at PD40-45. Unpublished work and independent assessment[285] has demonstrated that in unrestricted growth, MRC-5 cells have a doubling time in the order of 35 hours. To that end, if the MRC-5 cells had not become density limited and continued to divide throughout the 1 month of AA treatment, they may have accumulated a further fifteen or more population doublings and reached their proliferative limit, reaching senescence at the point the A549 cells were inoculated.

Senescent fibroblasts although growth arrested can develop a Senescence Associated Secretory Phenotype (SASP), as has been shown using X-ray irradiated human fibroblast cells[557]. *In vitro* work, predominantly using human diploid fibroblast cells, has demonstrated that SASP cells secrete inflammatory, growth-promoting and remodelling factors, a list of which was compiled in a 2013 review (Tchkonia *et al*[541]). Factors listed include: TNF-α, IL-1α, IL-6, 7 and 8, MMPs, monocyte chemoattractant protein-1 (MCP-1), Granulocyte-macrophage colony-stimulating factor (GM-CSF), Growth-Related Oncogenes (GROα, GROα,β,γ) and Insulin-like growth factor-7(IGFBP-7)). More recently it has been recognised that TGF-β1, a driver of lung fibrosis[558], is a component of the secretome of SASP[123]. These findings might explain how senescent cells are able to alter tissue microenvironments, attract immune cells, and induce phenotypic change in phenotypes in nearby cells through these multiple autocrine and paracrine factors. On the one hand SASP cells may drive malignancy[559] and on the other the cells may induce the effect of secondary senescence[560] primarily via the action of TGF-β1[123]. It has been demonstrated that the specific tumour suppressive response of oncogene induced senescence (OIS) can be transmitted to neighbouring cells through various secreted factors and may be mediated by Notch signalling in addition to SASP factors. It is further hypothesised that the apparent growth arrest seen in the A549 cells may have been the result of secondary senescence induced by the development of a SASP population in the potentially senescent MRC-5 cells.

Furthermore, these considerations raise a tempting train of thought. Cellular senescence may be an important factor in fibrotic lung disease. As reported in a recent review by Hansel, Jendrossek and Klein (2020) and as discussed in Chapter 1, SASP may arise in the lung, potentially the result of mitochondrial dysfunction[125] and these senescent cells might persist in the lung without clearance, contributing to fibrotic disease by secreting factors such as IL-6, IL8, MMPs and TGFβ[126] and through Nanog mediated fibroblast activation[127]. Senescent fibroblasts have also been implicated in IPF. When lung fibroblasts from IPF patients were compared to age related controls they were found to be growth limited, expressed senescent markers and had reduced mitochondrial function[93].

It has been demonstrated here that MRC-5 cells adopted a *PLIN2* and lipid expressing phenotype which on one hand might indicate the adoption of an adipogenic or lipofibroblast

phenotype or alternatively, as *PLIN2* has been shown to be upregulated in senescent cells[561], a possible sign of early senescence. FCM and co-culture in Transwell™ from these cells had a positive effect on the *SFTPB* gene expression in A549 cells but the effect was not enhanced by the prior treatment of the MRC-5 cells with RGZ suggesting lipofibroblast induction was not a factor, reinforcing the possibility that lipid accumulation in the MRC-5 cells was a symptom of early senescence.

In summary, transfer of the co-culture system to Alvetex™ Scaffold with two-week cultured MRC-5 cells resulted in a disorganised, invasive cultures with observed gel forming mucins that bore similarity to the honeycomb cysts of IPF, whereas longer term culture of the MRC-5 cells in Alvetex™ may have resulted in senescent, secretory SASP fibroblasts and the ascorbic acid independent establishment of ECM with no evidence of fibrillar collagen. It is postulated that these putative SASP MRC-5 may have induced a secondary senescence effect in the A549 cells, arresting cell division and driving an IPF-like ATII phenotype that co-expressed MLB and mucin granules. An emerging but tentative hypothesis is that the second, long term Alvetex™ experiment may have recapitulated a feature of IPF, mimicking *in vitro*, the *PLIN2+* lipofibroblast detected by single cell RNA sequencing of lung cells from IPF patients[95].

Building on the results obtained from the conditioned medium and Transwell™ experiments, by bringing the MRC-5 and A549 cells together in close proximity in a 3D scaffold it was postulated that the 3D environment might help the MRC-5 cells develop a more tissue-like morphology and behaviour to better mimic the gene and protein expression of *in vivo* lung fibroblasts[524]. It was further hypothesised that this, in turn, might encourage tissue-like epithelial to mesenchymal cross talk between the two populations as outlined in Figure 7.1[534]. The positive outcome of quiescent growth, ECM deposition and MLB expression in the A549 goes some way to give some tentative support to these suppositions but much further work is required to confirm these findings.

The next steps are to repeat these experiments, to determine if results can be replicated and further investigate other, senescence related markers (such as confirmation of growth arrest and staining for senescence associated β-galactosidase or gene expression of Cyclin Dependent Kinase Inhibitor 1A (*CDKN1A*)[562]) and IPF related and fibrotic markers in the cells (such as *αSMA*). Further evaluation of the ECM evolved in the Alvetex™ scaffold would be useful to determine its nature. Evidence of hyularonic acid expression, which could be effected using histochemistry with labelled hyaluronan binding protein[563] would be of interest. These data and hypotheses raise the tantalising prospect of an *in vitro* model that expresses some of the features of IPF, however if it transpires that MRC-5 cells do indeed become senescent in long-term Alvetex™ Scaffold culture, an alternative approach with regard to the fibroblast component of a "normal" *in vitro* alveolar epithelial model may be

required, such as human telomerase (hTERT) mediated conditional immortalisation[288] to enable to establishment of a physiologically relevant mesenchyme whilst avoiding senescence.

This might be achieved experimentally by setting up three sets of a three-week time-course of replicate co-cultures in Alvetex™ Scaffold. One set would be harvested at regular points for gene expression analysis by QRT-PCR. RNA extraction of the entire cellular component by flushing the scaffold with RNA homogenisation buffer and then RNA prepared (this would have to be piloted for proof of principle). Genes assessed would include the *SFTP*, epithelial, EMT, mucins and fibroblastic markers used previously but also include analysis of regulation of genes associated with development of senescence such as *CDKN1A*[562]*PVRL4, PRODH, LY6D, DAO, EPN3*, and *GPR172B*[564]. Expression of genes associated with adoption of a myofibroblastic phenotype could also be assessed such as collagen *(COL1A)* and *αSMA (ACTA2)*. Cells from the second set of replicates would be lysed for Western Blot analysis for the immunological confirmation of protein expression from the candidate genes. The final set of samples would be fixed and sectioned for histochemical analysis to further confirm protein expression and distribution, lipid expression, ECM analysis (including staining with labelled hyaluronan binding protein), staining for senescence associated β-galactosidase and TEM for assessment of MLB and mucin granule expression. Further and deeper analyses could be enabled by employing con-focal microscopy to overcome the challenges of imaging thick, light scattering 3D sections and laser capture microdissection[565] of the histological sections and transcriptomic analysis by single cell RNA sequencing[566] to individually characterise cells in the construct.

8. Final Discussion

8.1 Summary

The field of cell and tissue culture was devised at the beginning of the twentieth century as a means of studying the behaviours of animal and human cells isolated from the wider systemic variations that arise *in vivo*. Since inception, cell culture models have delivered a mainstay for life science research and provided researchers with a considerable and increasing understanding of how isolated cells adapt to their *in vitro* conditions[317].

Cells adapt to their environment in response to physical orientation[567], the chemical and physical composition of the substrate[568 337 569] the nature of the biochemical environment and duration in culture[570]. Microfilaments and microtubules extend throughout the cytoplasm and have close association, particularly actin fibres, with the nucleus. This results in cell shape impacting on cellular signal transduction, nuclear shape[571] and gene and protein expression via mechano-transduction[572]. These factors drive cell differentiation and cellular phenotype[573]. On one hand, not only do cells respond to biochemical and temporal cues which drive phenotype and shape, but on the other, shape can also drive cellular behaviour and control differentiation. It is important to note that 3D culture *per se* does not necessarily guarantee physiologically relevant cellular differentiation, it is more important that the cell substrate, cell shape and culture strategy aim to mimic the conditions of the desired cellular niche found *in vivo*[574].

This work aimed to recapitulate the ATII phenotype in A549 lung cancer cells through manipulation of the biochemical environment using defined media formulations, paracrine factors from mesenchymal cells, a range of substrates and 3D spheroid aggregate culture. These biochemical, temporal spatial and paracrine influences resulted in a range of phenotypic outcomes that reflected those of bronchial epithelial cells, ATII cells and aspects of fibrosis. Influences of cell environment and time on phenotype were evident at each stage of this study and could be observed, with significance, within a few days compared to log phase 2D cultured cells. Changes in medium formulation encouraged either proliferation (DMEM) or quiescence (Ham's F12) in A549 cells. Long term spheroid, aggregate culture encouraged 3D non-flattened morphology driving a mucus secreting host defence phenotype, whereas long term 2D culture seemed to better recapitulate the alveolar environment encouraging ATII-like differentiation that could be further modulated by treatment with the synthetic glucocorticoid dexamethasone (Dex) and through paracrine factors from foetal lung fibroblasts. A549 differentiation was further modulated using co-culture with human lung fibroblasts in a 3D cell culture scaffold to generate prolific and invasive cell growth or

quiescent organised structures with evidence of an epithelial-like layer of cells above ECM, seemingly expressed by fibroblasts, depending on their duration in culture (refer to Figure 7.39).

The over-arching aim of this study was to deliver an *in vitro* ATII-like model or models for IPF research. As can be seen in Table 8.1, the methodical approach adopted here seemed to step-wise drive A549 cells closer to the idealistic ATII model as defined by Beers and Moodley[262].

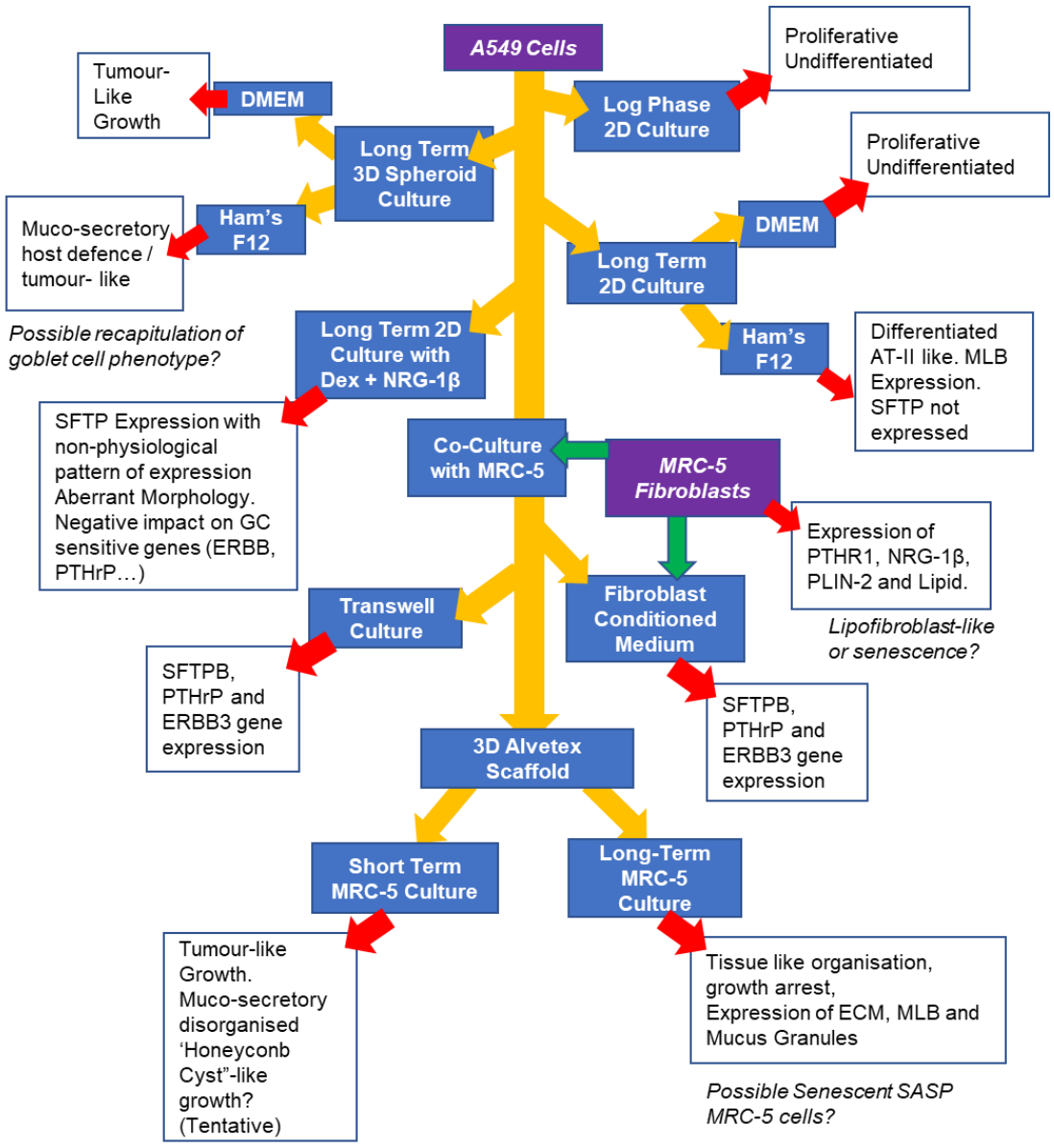

Figure 8.1: Flow diagram describing A549 model development and characterisation.

Feature	Log Phase	3D spheroids	Long term 2D culture	Long term 2D culture + Dex	A549/ MRC-5 Co-culture	Primary ATII Cells
SFTP Gene Expression	-	-	-	SFTPA1+ SFTPA2- SFTPB++ SFTPC+ SFTPD+++	SFTPA1+ SFTPA2+ SFTPB++ SFTPC- SFTPD-	SFTPA1++ SFTPA2+++ SFTPB+++ SFTPC+++ SFTPD+
SFTP Protein Expression	NT	NT	NT	SFTPB+ SFTPC+ Others NT	NT	SFTPB+++ SFTPC NT Others NT
Gene Expression of ABCA3	-	-	+	+	+	+++
MLB Expression	-	-	+++	NT	++	NT
HT-280 ATII Marker	NT	NT	-	-	NT	+++
ATI markers gene expression (Absence expected)	CAV-1+ AQP5-	NT	CAV1- AQP5-	CAV1+++ AQP5-	CAV-1 NT AQP5 NT	CAV1+ AQP5-
HT1-56 ATI Marker	NT	NT	-	+ (with Dex+NRG-1β)	NT	NT
Evidence of epithelial barrier(TEER)	NT	NA	-	-	-	NT
Mucin Gene Expression (absence expected)	-	MUC5AC MUC5B	-	NT	NT	NT
Mucin Protein Expression (absence expected)	-	MUC5AC MUC5B NT	-	NT	Gel Mucin (in Alvetex with short term MRC-5 culture)	NT
Expression of epithelial markers	ERBB3- -	NT	ERBB3+++ CDH1+	ERBB3- CDH1++	ERBB3+++ CDH1+	ERBB3 NT CDH1+++
Presence of ECM	-	-	-	-	++	-
Gene expression of PTHrP	+	NT	+++	-	+++	NT

Table 8.1: Assessment of the A549 models developed in this study against Beers and Moodley guidelines[262] and other physiologically relevant criteria.
(NT=Not tested, NA=Not applicable, - = lack of expression, +++ = strongest expression).
A549/MRC-5 Co-culture would seem to best represent the primary ATII state.

8.2 The Need for *in vitro* Models for IPF research

Since 1972 there have been nearly 7,000 peer reviewed publications devoted to IPF yet only two drugs, Pirfenidone and Nintedanib[575] [576] , have been developed and shown to have some patient benefits. The disease is always fatal, usually within 5 years of diagnosis[577]. Many other potential treatments have been identified but that have all failed at the clinical trials stage. At best they delivered no significant benefits or at worst, they decreased life expectancy; in part due to the previously held belief that the disease was caused by inflammatory processes[70] (see Figure 8.2).

The failure of medical research to deliver safe and effective treatments appears to partly lie within the shortcomings of the IPF drug discovery workflow. In a 2016 review, Froidure[578] *et al* recommended that the search for new IPF therapies requires improved experimental *in vitro* models. To be effective these models need to recreate ATII function and demonstrate epithelial-mesenchymal cross talk. They should be capable of recapitulating abnormalities in biological pathways affecting fibrotic wound repair, including matrix regulation, epithelial reconstitution, defective crosstalk and fibrogenesis[110]. To be effective early in the in the discovery work stream the models should be reproducible, fit for purpose, relatively low cost, accessible and straightforward. They should be suitable for high throughput screening to evaluate candidate treatments for evidence of efficacy and early signs of toxicity or unwanted off-target effects[579].

Despite disappointments of failed treatments, the search for new therapies for IPF continues[110]. Putative drugs include: wound-healing Pentraxin-2 analogues, leukotriene antagonists, anti-integrin antibodies, anti-connective tissue growth factor antibodies, protein kinase inhibitors, autotaxin lysophosphatidic acid (LPA) inhibitors, P13/Akt pathway inhibitors, anti-B-lymphocyte drugs and treatments to target the specific microbiome imbalances found in IPF patients[70].

The range of tools for early discovery in IPF research include the *in vitro* and *in vivo* models introduced in Chapter 1. Although the discussion here primarily concerns *in vitro* models, it is worth considering the fact that animal models are available and much lung fibrosis and IPF research draws on rodent models of fibrosis induced by various means (FITC, radiation, xenotransplantation of human IPF fibroblasts, recombinant animals and recombinant viruses, silica, asbestos amongst others[580]) but by far the most commonly used model is the induction of fibrosis in the rodent lung through intra tracheal administration of bleomycin[180]. The attraction of this model is its recapitulation of TGF-β mediated fibrosis and the induction of collagen synthesising myofibroblasts in the distal lung of a whole living mammal[189], however it is not a true and accurate model of the disease[179]. As was discussed in Chapter 1, (see Table

1.1.1) the bleomycin model has many deficiencies. In short, non-resolvable fibrosis in human IPF develops slowly, has little inflammatory involvement and is restricted to the distal lung whereas bleomycin induced fibrosis develops rapidly, is reversible and more widespread. These shortcomings have contributed to failures in clinical trials[70] A specific example being the failure of Tralokinumab, an anti-IL13 monoclonal antibody that was shown to be effective in the mouse model. Human trials, however, were terminated due to lack of efficacy in patients[204]. The wealth of literature surrounding the bleomycin model[581] and its relative accessibility mean that it its use will continue; the potential future power of its being an iterative analytical approach in conjunction with "omics" and RNA sequencing data from IPF patients[582].

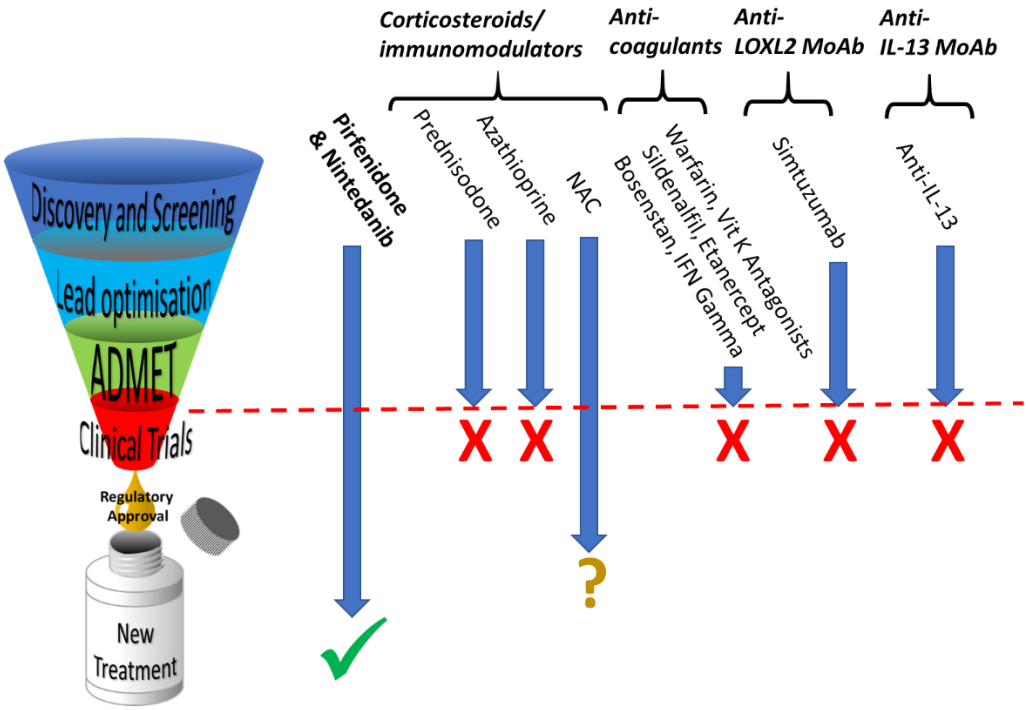

Figure 8.2. IPF drug discovery has failed to deliver new therapies.
Pirfenidone (which inhibits molecules in the fibrotic pathway, principally TGF-β) and Nintedanib (which targets α and β PDGFRs, FGFRs and VEGFRs) are the only approved treatments[575] [576]. The corticosteroids and immunomodulators prednisodone, azathioprine and N-acetylcysteine (NAC) were trialled in the aborted PANTHER clinical study, where treatments were shown to increase mortality[583]. NAC may have limited benefit in a subgroup of IPF patients with specific SNPs[584]. IPF is characterised by a "pro-thrombic state" however anticoagulants including vitamin K antagonists similarly worsened clinical outcomes. Lysyl Oxidases (LOX) family members are involved in collagen cross linking but the anti-LOXL2 monoclonal antibody Simtuzumab failed to show efficacy in the clinic[77]. Upregulation of IL-13 from TH2 cells promotes fibroblast collagen production yet anti IL-13 monoclonal antibodies and inhibitors have shown no clinical effectiveness[204]. (ADMET = Absorption, Distribution, Metabolism, Excretion and Toxicology). Diagram by the author based on a concept by Enzo Life Sciences Inc, New York, USA and numerous references from Chapter 1.

Model	Advantage	Disadvantage
Ex vivo human lung slices	Physiologically relevant – normal and diseased	Short lived, inter-donor variability
Primary Cell Cultures*	Physiologically relevant - normal and diseased	Differentiation, senescence, inter-donor variability
Human ESC and iPSC*	Huge potential	Technically demanding, unproven, specialised techniques
Continuous cell lines e.g. A549*	Accessible, reproducible	Generally cancer derived, cancerous phenotypes
Bleomycin rodent	Accessible, reproducible, whole animal	Does not fully recapitulate human disease, rodent not human.
FITC, radiation, silica, adenovirus vector etc. induced fibrosis in rodents	As above	As above
Other animal models (West Highland Terrier, Horses…)	Similar to human disease	Ethics/husbandry issues
Humanised xenograft rodent models	As with other animal models	
Omics studies	Good for hypothesis generation	Costly, time consuming
**In vitro* fibrosis assays (mono and co-culture of cell lines)	EMT, myofibroblast and collagen readouts. TNFα and CCL18 secretion from monocytes	Might require 3D printing, microfluidics, highly specialised or costly service.

Figure 8.3. A summary of the models available for discovery and screening of novel putative treatments for IPF.
Diagram and table by the author based on a concept by Enzo Life Sciences Inc, New York, USA and numerous references from Chapter 1.

8.3 The range of *in vitro* models for IPF Research

Figure 8.3 includes the range of *in vivo* and *in vitro* models available for early IPF drug screening and discovery.

8.3.1 Primary Cells

The use of *ex vivo* lung slices from cadavers is recognised as a powerful and physiological relevant system for human *in vitro* lung fibrosis research[585]. Although close to the *in vivo* state and having the advantage of being assessed by a range of analytical techniques, including physiologically relevant histology, the slices can only be cultured for one week and are inaccessible by most laboratories through constraints of ethics and availability and are not suitable for high throughput analysis[585].

Primary ATII and Fibroblasts from normal and IPF lungs in monoculture or advanced co-culture techniques[533] (such as "scar in a jar"[586]) with or without immune cell populations[228] are offer the advantage of being physiologically relevant, as they are taken directly from the relevant tissues from unaffected and affected donors, offering great potential for gene and protein expression analysis. Their use, however, is hampered by access to patients, specialised and demanding techniques for cell isolation[587], donor to donor variability, inability to represent tissue architecture and loss of tissue like microenvironment and

resulting in lack of physiological response to stimuli[212], laboratory acquired senescence[212], differentiation and potential contamination[588]. Commercially options are also available, for example Human Type-II Pulmonary Alveolar Epithelial Cells (HPAEpiC-II) (Accegen) Fairfield, New Jersey 07004, USA.

Weigle *et al* developed *in vitro* EMT and 'fibroblast to myofibroblast' assays using primary normal lung fibroblasts and small airway epithelial cells[589] or human primary bronchial epithelial cells. These assays are also offered by contract research organisations. Typically, they demonstrate the protective effect of putative anti-fibrotic agents where inhibition of the TGF-β induced downregulation of E-Cadherin or inhibition of the TGF-β induced up-regulation of fibronectin is measured as an anti-fibrotic readout. For a fibroblastic response, cells are obtained from normal or IPF patients for use in 'fibroblast to myofibroblast assays where down-regulation of collagen and α-SMA expression pre-induced by TGF-β treatment is the read out. Efficacy of such assays has been demonstrated using known ALK5 inhibitors. Other contract fibrosis tests include monocyte assays offered by Charles River, Harlow, Essex, United Kingdom: M1 polarisation of monocytes is measured by TNF-α secretion and M2 polarisation of monocytes measured by CCL18 secretion by IL4/IL10 induced primary human monocytes.

8.3.2 Stem Cell Derived Cultures

More recently the potential of human embryonic (hESC)[590 591] and induced pluripotent stem cells (hiPSC)[592 418 255 593 594] has been proposed as sources for the development of advanced differentiated ATII models. They have immense potential as the undifferentiated stem cells have unlimited proliferative capacity and are accessible from suppliers. Embryonic stem cells however present significant ethical challenge and despite both hiPSC and hESC showing possibility of recapitulating ATII cells *in vitro*, the technology is highly specialised, time consuming, not yet common practice in many laboratories and, as of yet, benefits are largely unproven[212].

(1) Vignette: A Case of Mistaken Identity

It was intended this study would explore the ATII differentiation capacity of a novel lung stem cell line (Chapter 5). The data presented in this chapter serves as a warning to researchers regarding the risks of working with cell lines that have not been fully characterised nor validated, demonstrating the need for rigorous quality control. The problem of cell line misidentification has been known about for many decades[595 596 423] and it is well known that it can arise through common faults such as sharing media and reagents between cell lines, mixing of flasks incubators and simple mislabelling of flasks and cryo-vials in inventory[597]. When misidentified cell lines become circulated the financial and scientific impact can be substantial and devastating[425].

Here, a seemingly original and unique lung progenitor cell line previously described in a peer reviewed publication[420] was assessed according to established guidelines[292]. Results showed that not only were the cells contaminated with mycoplasma but more seriously, forensic short tandem repeat (STR) profiling demonstrated the cells had a profile that matched the commonly used human embryonic kidney cell line '293'. Small differences in the STR profiles of the 'stem cell line' and 293-T were plainly explained through a combination of the known phenomenon of accumulated STR strand slippage[440], the known defective DNA mis-match repair mechanisms[446] and known chromosome instability[457] in 293 cells. These findings resulted in the immediate termination of planned work, significant impact on time and resource and wider, more damaging implications. The originating laboratory must now investigate its stocks of the cell line to determine if non-corrupted cells remain. Any publications using the cells will be reviewed and potentially retracted with subsequent impact on scientific reputations, careers and indirect effects on other researchers who have cited the work. If no genuine stocks of the cells can be located, the cell line will be included in the International Cell Line Authentication Committee ICLAC) database of misidentified cell lines[295]. These outcomes could have been avoided with relative ease if the cells had been tested early and regularly by the originating laboratory with inexpensive simple and accessible testing[333]. This case also highlights the need for journals to be insistent on evidence of cell line validation within submitted manuscripts[426].

8.3.3 Continuous Epithelial Cell Lines as Models for Fibrosis Research

Drawbacks involved with primary cultures and stem cells necessitate widespread use of continuous (immortalized or tumour) cell lines as epithelial models for *in vitro* airway studies. They are less technically demanding than primary cells and their supply is practically unlimited. They do not display inter-donor variability as they are derived from single donors, however this also can be a limitation[212]. Continuous cell lines are either derived from tumours or deliberately transformed using viruses. Free from the homeostatic regulation of the organism, cell lines are subject to selective pressures of the chemical and physical microenvironment of the *in vitro* system, resulting in genotypic and phenotypic adaptation[289]. Cell lines, therefore, may not adequately represent equivalent primary cells nor the tissues they represent as many cellular processes, including cell cycle regulation and differentiation, are deregulated[212]. However, their extended life span, ready availability and requirement for relatively simple, inexpensive culture media make them suitable for high-throughput screening applications in early drug discovery[212].

Epithelial airway cell lines are available to most researchers The SV40 virus immortalized human bronchial epithelial BEAS-2B cell line[598] resembles airway basal epithelial cells, but

does not differentiate nor form a strong epithelial barrier[599]. 16HBE14o- cells, also derived from SV40 transformed human bronchial epithelial cells[600], display a cobblestone morphology and can form polarized cell layers at air-liquid interface (ALI). These two cell lines are most suitable for modelling the bronchial epithelia rather than the alveolus[601]. The Calu-3 cell line was derived from a lung adenocarcinoma from submucosal gland serous cells expresses a muco-secretory phenotype with reasonable barrier function[602 603] but lacks capacity for normal differentiation[212]. The NCI-H441 cell line, derived from a human lung adenocarcinoma provides an effective transport model of distal lung epithelial barrier[604]. It establishes tight junctions and generates high TEER values when cultures on Transwells™ [605] and has a similar expression of the organic cation transporter (OCT) proteins (known to be involved in the transport of bronchodilator drugs in lung epithelia) to ATI cells[604]. NCI-H441 cells appear to be capable of Dex stimulated *SFTPB* gene and SFTPB protein expression in a similar manner to Dex treated A549 cells and there is some evidence of the expression of some ATII characteristics in NCI-H441 cells[606].

To attempt to overcome problems of disruption of cellular processes found in tumour cell lines and caused by viral immortalisation, human telomerase hTERT immortalisation[607] has been employed to obtain immortal bronchial epithelial cell lines[608] and basal cell line (BCi-NS1.1) which has multipotent differentiation capacity to generate goblet, Club and ciliated cells[609]. however as of date it seems only hTERT ATI cells have been generated[283 610] and there seem to be few or no available hTERT immortalised human ATII cells.
The A549 tumour cell line is widely used as a model for alveolar epithelial ATII cells. Developed decades ago it was found to display some ATII characteristics[308]. Despite inability to form tight junctions and its use being controversial[611] it remains a commonly and increasingly utilised cell line in fibrosis research[517 612 613 614 615 616]. A literature search for "A549 and IPF" in the American National Centre for Biotechnology Information 'Pubmed' database, revealed 133 results since 2005 and for "A549 and Alveolar" returned over 1,900 results, with a year on year increasing trend in publications. With a dearth of available ATII *in vitro* models for high throughput drug discovery, the increasing use of A549 and its capacity to differentiate into non-ATII-like phenotypes it is critical that researchers employ appropriate culture conditions for experiments involving A549 cells.

8.3.4 Building an *in vitro* Tool Box

It is unlikely that any *in vitro* model could fully recapitulate the physiological function of a tissue or organ such as the pulmonary alveolus nor wholly reproduce the full clinical presentation of IPF. Hence, rather than thinking of the range of cells and cell lines available for IPF research as competing, individual discrete tools, it is best to consider them as versatile components of a constantly expanding tool box that can be used in monoculture, co-culture or

more advanced and complex state of the art technologies. Additionally, as discussed previously, organoid based approaches may also offer promise[252] with lung organoids being generated from iPSCs to produce differentiated cells with ATI and ATII markers[253].

(1) Advanced Substrates

With the advent of increasingly sophisticated advanced cell culture techniques the range of tools available for *in vitro* research is widening year on year. Biologically derived scaffolds[242], synthetic electrospun, cryogelated or micro-fabricated scaffolds and 3D printing were presented in Chapter 1 together with the concept that hybrid biological and synthetic materials may produce advanced substrates that better recapitulate the *in vivo* state[241]. In addition to 3D systems, synthetic 2D (or planar) surfaces can be made more amenable to the growth of physiologically relevant cell cultures through microscopic physical patterning[617] using techniques such as laser patterning, dry etching and electron beam lithography to create physio-typical surface topographies to produce '2.5D' cell culture systems. These modified and advanced planar substrates can then be further enhanced through the incorporation of biologicals (such as fibronetin), as shown in the physiologically relevant growth or rat liver cells on direct laser written, photo-polymerized substrates[618]. These techniques allow the construction of complex microfluidic arrays that allow the inclusion of electronic biosensors to enable sophisticated, high throughput, high content experimentation with single cells, monoculture and co-cultures of different cell types[619]. These novel approaches increase optimism for the development of physiologically relevant 'organ on a chip' and microfluidic models of fibrosis[620].

(2) Hypoxic Cell Culture

Almost since the inception of cell culture, human and animal cells have been cultured in air supplemented with carbon dioxide[317] which on the one hand allow for experimental reproducibility but on the other does not recapitulate conditions found *in vivo*[621]. In the human body, oxygen concentrations range from 1 to 12%, rather than the 20-21% in the atmosphere[621]. A low oxygen (hypoxic) environment appears to be beneficial to many cell types. For example, primary mouse embryonic fibroblasts (MEFs) cultured in 3% oxygen, avoided senescence. In addition, these hypoxic cultures displayed less DNA damage, and had fewer stress responses[622]. Stem cells are routinely cultured in low oxygen[623], physiologically relevant results were obtained from hypoxic cultures of lymphocytes[624] and there may be advantages associated with the culture A549 cells in low oxygen environments[625]. Many suppliers now offer incubators with hypoxic control (e.g. Thermo Fisher, Waltham,

Massachusetts, USA) and there is also the option of maintain the entire cell culture workflow in hypoxia through the use of hypoxic containment workstations (e.g. 'HypoxyLab™', Oxford Optronix, Abingdon, UK).

(3) Advanced Media

Many cell culture media were developed and formulated decades ago and most rely on the addition of FBS to support cell proliferation. There are a number of reasons this approach may be out-moded. Harvest of serum causes suffering for in the unborn calf. Seasonal and continental variations in the serum composition produce batch-to-batch variations and therefore possible phenotypical differences in the cell cultures and the likelihood of contamination, as much as 20–50% of commercial FBS may be infected with viruses[626]. In addition to these undesirable factors, the physiological response of cells in conventional FBS supplemented media can be far from that seen in the *in vivo* state which has led to the development of novel serum free physiologically relevant media[627].

It is hoped that the combinations of these advanced technologies together with novel cell line developments will provide researchers with a comprehensive *in vitro* ATII and fibrosis and IPF research 'tool box'.

8.4 Normal and Fibrotic Lung Parenchyma Contains a Heterogeneous Mix of Mesenchymal Cells Necessitating the Development of Complex Models

Lung development and wound healing are inextricably linked processes. It is generally accepted that the activation of developmental pathways is a major contributing factor in the pathological progression of fibrosis in IPF[628]. This alludes to the requirement of an understanding of both development and wound healing if effective models of the alveolus and fibrosis are to be developed. In IPF there is an aberrant activation of stromal cells[629]. Mouse lineage tracing and data from single cell RNA Seq in IPF lungs suggest complex heterogeneity in interstitial lung fibroblasts during development, homeostasis and fibrosis and under the finely balanced control of developmental pathways. Lipofibroblasts (in the mouse), pericytes and mesothelial cells may differentiate into myofibroblasts. However, epithelial and bone marrow derived cells may give rise to collagen expressing fibroblasts but not myofibroblasts.. Furthermore, there is evidence for the expansion of pericyte and lipofibroblast derived myofibroblasts with subsequent loss of lipofibroblast-like cells in IPF[629]. These processes are summarised in Figure 8.4.

As discussed in chapter 7, *in vivo* heterogeneity in the fibrotic lung has also been demonstrated through single cell RNA sequencing of cells from the lungs of patients with various fibroses, Phenotypes identified include: myofibroblasts, a PLIN2+ lipofibroblast-like group, and a fibroblast population positive for hyaluronic acid synthetase 'HAS1-hi cells' specific to only IPF patients[95].

These pieces of evidence suggest that to fully recapitulate ATII cells, and to reproduce fibrosis *in vitro*, complex models and sophisticated are analytical techniques, to identify these cell types and the progression of their differentiation, are required.

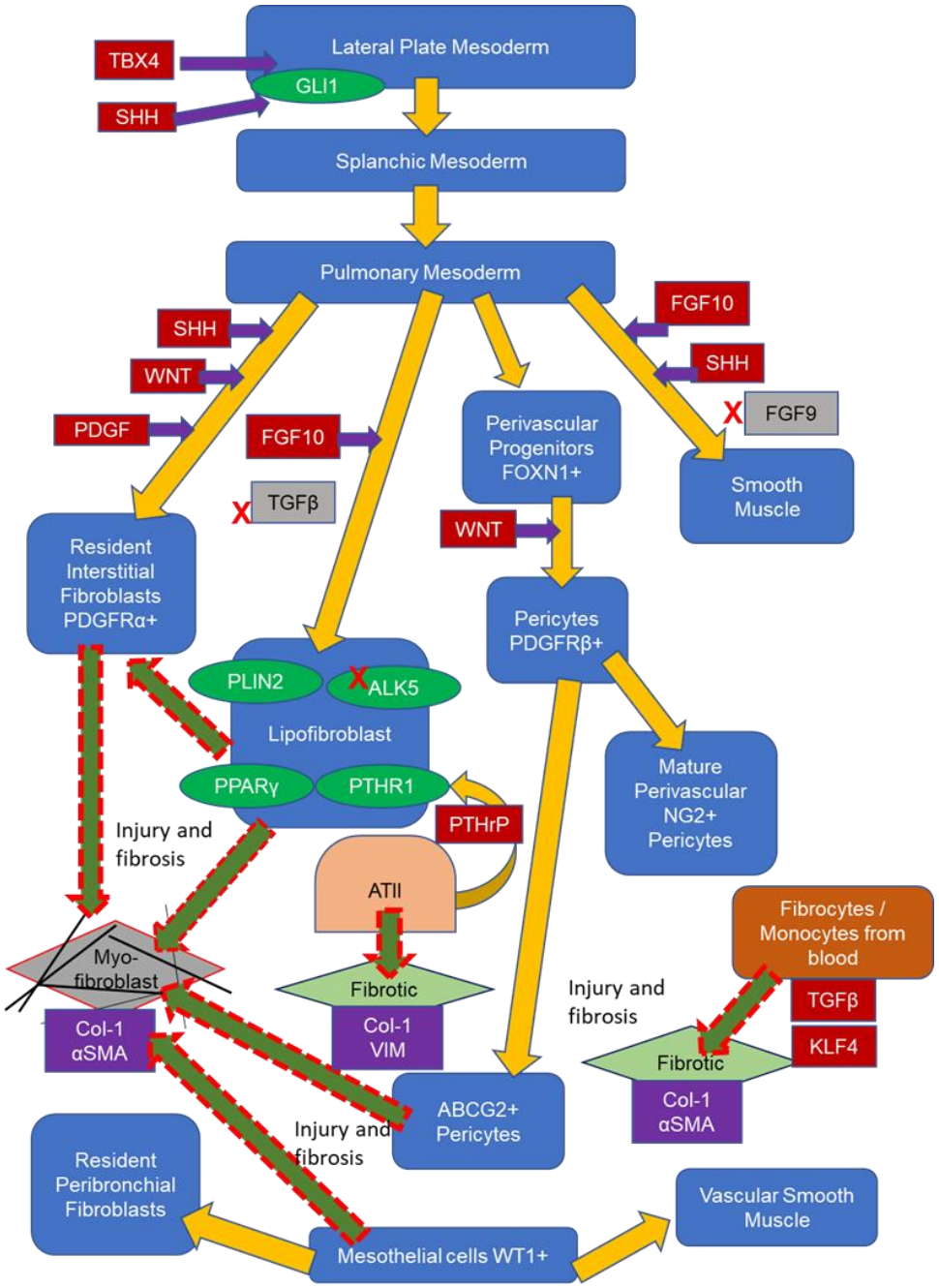

Figure 8.4. Summary of the Role of Mesenchymal Cells in Lung Development and Fibrosis in the Mouse Lung.
Developmental processes are shown by gold arrows and the impact of injury and fibrosis on those populations by green/red-dashed arrows[629 88 89].

TBX4	T-Box Transcription Factor 4	**PDGFR**	Platelet Derived Growth Factor Receptor
SHH	Sonic Hedgehog Transcription Factor	**PDGF**	Platelet Derived Growth Factor
WNT	WNT Transcription Factor	**NG2**	Nueron-Glial Factor 2 (Proteoglycan)
GLI1	Glioma Associated Oncogene	**FGF**	Fibroblast Growth Factor
ALK5	TGFβ Receptor	**ADRP**	Perilipin 2 (
FOXN1	Forkhead Box Protein N1	**KLF4**	Kupfer-Like Factor 4

Diagram constructed by the author from the text of a review by Habiel and Hogaboam (2017)[629].

8.5 Application of the Optimised A549 Models

8.5.1 2D Long Term Culture

As the incidence of A549 use in IPF research is increasing, the published[483] and validated long-term culture technique shown to induce ATII-like differentiation in standard, off the shelf flasks and tissue culture plates is a relatively simple protocol that can readily be adopted. It offers a simple methodology to increase physiological relevance of the cells and is recommended for any researcher intending to use A549 in their ATII related research. The method has advantages in terms of MLB expression and a pattern of gene expression that overlaps with primary ATII cells however it does not express surfactant protein. This disadvantage can be overcome to some extent by Dex treatment increasing the application potential through the induction of SFTP genes, but the benefit comes with limitations brought about through the impact of Dex on GC sensitive genes.

8.5.2 3D Spheroid Culture

Self-assembling 3D spheroid culture in ULA plastic drove a muco-secretory or host defence phenotype with disorganised tissue architecture unlike that of the lung parenchyma but more representative of tumour growth. Indeed, in cancer research, 3D spheroids are considered the foremost cell culture model[630]. They are capable of reproducing structural, physiological and biological features of solid tumours. For example, they display similar growth kinetics; gas, nutrient and waste gradients; a mix of proliferative, senescent and necrotic cells; cellular heterogeneity, tumour like cell–cell signalling; cancer-like ECM deposition and interactions; tumour -like gene expression profiles and cancer stem cell properties[630].

In vivo, the alveolar epithelium is composed sheets of cells with strong intracellular bonds. The epithelial cells anchor to a basal lamina (sometimes also known as the 'basement membrane') comprised of a mixture of collagens, laminin, perlecan and entactin[522]. These proteins bind to each other to make a highly crosslinked extracellular matrix that acts both as a growth support and a selectively permeable layer which is further divided into the three sub layers visible under TEM. From lowermost to uppermost these are: the lamina reticularis, the lamina densa and the lamina lucida, indeed their terminology derives from their relative electron lucent appearance under TEM[522]. As a result of anchorage, ATII epithelial cells become polarised, meaning the apical ends that face the internal lumen of the alveolus, differ from the basolateral ends that attach to the basal lamina[631]. Although the cells in spheroids self-assembled into a tightly packed arrangement, there was no ECM or basal lamina for them to anchor to, hence there was no polarisation. It is postulated that if, in some way, the culture system could be enhanced to incorporate ECM and/or basement membrane analogues, the cells might be encouraged to polarise, which in turn might drive a more physio-typical epithelial phenotype. Building this augmentation into a spheroid model

however presents technical challenges. The most successful source of purified ECM that represents basal lamina is the ECM secreted in excess by the Engelbreth-Holm-Swarm sarcoma of mice[522], commercially available as 'Matrigel™' (Corning®, Glendale, Arizona, USA). Thus, incorporation of Matrigel™ into the spheroid model may have benefits. Possible ways to enable this include the generation of Matrigel™ 'microbeads' that might provide foci on which the spheroids could develop and polarise. This approach has been used to generate prostate glandular acini[632] (clusters of cells that bear some similarity to the developing alveolus). Recent approaches to generate 3D recapitulation of basal lamina for epithelial models use more advanced systems e.g. scaffolds, 'lab-on-chip', 3D bioprinting or hydrogel approaches[633].

Mucus secreting re-modelled pseudostratified alveolar epithelium is a feature of the honeycomb cysts seen in later stage IPF[548] therefore this strategy may have a part to play in IPF research. It will require substantial further work to determine if the cellular phenotype obtained is in any way related to fibrosis. RNA microarray gene expression data suggested the muco-secretory cells may have similar properties to goblet cells of the bronchial epithelium. Chronic obstructive pulmonary fibrosis (COPD) is an increasingly common progressive disease characterized by persistent airflow limitation associated with an enhanced chronic inflammatory response in the airways. Thought to be caused by to noxious particles or gases such as smoke from cigarettes or pollution despite having limited treatments such as β2-agonists or anti-muscarinic bronchodilators[634 635] it is a leading cause of morbidity and mortality. Fibrosis, tissue remodelling and destruction (emphysema) are common in COPD and subset of COPD patients exhibit mucus hypersecretion, resulting in chronic bronchitis due to an increased number of goblet cells in a condition known as 'Goblet Cell Hyperplasia'[636] for which there need for *in vitro* models[637]. Spheroid cultured A549 may have use in the establishment of *in vitro* models of goblet cell hyperplasia[638].

Using spheroids in an epithelial model however presents a technical challenge. Most assays are performed on 2D substrates at air liquid interface (ALI). Resolution of this issue may lie in the field of organoid biology. Organoids grow as aggregate 3D cultures of similar size and shape to the 3D A549 spheroids. Recently protocols have been developed to rapidly adapt cells from differentiated organoids to allow transfer from 3D to 2D culture 'opening them up' without loss of phenotype, permitting them to be used in Transwell™ assays and more convenient analysis[639 640].

8.5.3 Co-Culture and with MRC-5 Human Lung Fibroblasts in Alvetex™ Scaffold; Potential for the Modelling of Lung Parenchyma and Fibrosis

The outcome with most potential from this study was the combination of long term A549 cells co-cultured with MRC-5 lung fibroblasts in Alvetex™ Scaffold. This advanced 3D substrate is a an emulsion-templated porous polymer (PolyHIPE) based on polystyrene[338] and differs from scaffolds produced by particulate leaching[641] in that the pores form a reticulated network of contiguous cavities. Co-culture models of human dermal fibroblasts and keratinocytes have been used to successfully recapitulate *in vitro* models of human skin using Alvetex™ Scaffold[518]. It was postulated that a similar approach might be effective in *in vitro* modelling of the alveolar epithelium. It was expected that the closer proximity of the human foetal MRC-5 fibroblast[516] and tissue-like orientation of MRC-5 and A459 cells would provide appropriate physical cues to increase the efficiency of the epithelial- mesenchymal cross talk[519] previously demonstrated by the use of fibroblast conditioned medium and Transwell™ culture. This cross talk plays a critical part in both normal alveolar development[642 643] and in the progression of fibrosis and wound healing[513 644 645]. In both cases is effected through paracrine factors such as NRG1-β (less relevant in A549 cells due to possible lack of ERBB4 expression), Activin A[646], Wnt3a[647], Hippo and hedgehog[135], Fibroblast Growth Factor(FGF) 10[648] and the related proteins Keratinocyte Growth Factor[649] (also known as FGF7) and Hepatocyte Growth Factor (HGF) leptin[477], PLIN-2 and PTHrP. Close association of the fibroblasts and the A549 cells may be advantageous for development of ATII through direct cell to cell signalling via the Notch pathway (unachievable in Transwell™ systems). Although myofibroblasts are associated with fibrotic disease they are not always linked with pathologic outcomes. Notch signalling between myofibroblasts and ATII cells has been shown to be essential in development for alveogenesis in mice and over-persistent Notch signalling can lead to a similar developmental outcome to the honeycomb cysts of the IPF lung.

The effects of cellular replicative senescence both in ATII cells and in lung fibroblasts are increasingly being thought of as playing a role in the development of IPF. Senescent ATII-like cells can be found in fibroblastic foci[98]. These cells seem to activate aberrant developmental TGF-β, Wnt, hedgehog, Hippo and Notch signalling to drive a senescent secretory phenotype (SASP)[116 96] that may exacerbate fibrosis. Normal ATII function is severely reduced by SASP factors and senescent ATII cells alone may be sufficient to initiate fibrosis[122]. SASP cells can induce a secondary "bystander" senescence in neighbouring populations of cells[123] that, may again, be through direct Notch signalling or via secreted lipid bound extracellular vesicles carrying various senescence inducing cargoes such as DNA and RNA and sequences and peptides[124]. Alvetex™ offers an advantage over conventional substrates by allowing tissue

like orientation of cells, heterotypic cell to cell contact and the potential to investigate either replicative or chemically induced senescence and their effect on fibrotic progression.

The exact processes involved in the ECM deposition and epithelial like organisation of A549 seen in Alvetex™ is not yet known. ECM deposition was observed in both ascorbic and non-ascorbic acid cultures and seemed to be associated with the fibroblasts, however, no evidence of fibrillar collagen was identified in SEM analysis. These experiments will have to be repeated however the observations raise opposing hypotheses for further investigation:

- **Hypothesis (i).** The MRC-5 fibroblasts established a physiologically relevant normal tissue like quiescent mesenchyme and ECM which in turn provided a suitable micro-environment for the A549 cells to adopt an AT-II like epithelial monolayer with homeostatic epithelial-mesenchymal cross talk.
- **Hypothesis (ii).** MRC-5 cells developed replicative senescence through continued proliferation throughout the month of culture in Alvetex™. A significant proportion of the dividing cells migrated out of the scaffold leaving a senescent SASP population of the surface. These senescent cells subsequently induced bystander senescence in the A549 cells through aberrant epithelial-mesenchymal signalling and notch signalling.

There is not yet enough data to make definite conclusions regarding either possibility, however the results raise some interesting ideas. Deposition of ECM by senescent cells is not an expected phenomenon. Disruption of ECM is normally associated with senescence[650] yet in the IPF lung there appears to be a unique population of cells positive for the expression hyaluronic acid (HA) a polysaccharide glycosaminoglycan component of ECM[95]. Hyaluronic acid (HA) has increased abundance in the ECM of the IPF lung and can promote fibroblast invasiveness to mediate progressive lung fibrosis[96]. Analysis of the ECM evolved by cells in Alvetex scaffold by histochemical analysis is required to determine its nature. Furthermore, determination of the phenotypic natures of fibroblasts and any potential trans-differentiation in the co-culture would be useful to shed more light on the processes involved to determine any relevance to clinical IPF. More data needs to be acquired regarding the nature of the A549 cells that were seen to co-express mucin granules and MLB, an observation that indicated adoption of both bronchial and ATII epithelial characteristics in a single cell. It must be remembered that fundamentally A549 is a cancer derived cell line. In the airways bronchioalveolar stem cells (BASCs) are found between the bronchiolar and alveolar regions and are thought to contribute to repair of both bronchiolar and alveolar regions, acting both as stem cells and as cancer progenitors[65]. It is also known that cancers may arise from stem cell populations[651] . Chapter 6 and Appendix C showed expression of the stem cell Oct4, SSEA4 and Tra-1-60 markers in sub populations of Dex and NRG-1β treated A549 cells and a cancer stem cell sub population has been identified by others in A549 cells[506]. Chapters 3 and

4 demonstrated that with appropriate physical and biochemical cues A549 can differentiate into either a muco-secretory (bronchial) or MLB expressing (ATII) phenotype raising the possibility that the tumour from which A549 cells were derived originated in BASC, leading to this bi-potent capability. Alternatively, it is known that ATII in honeycomb cysts can adopt a bronchial mucus (MUC5B) secreting phenotype[383], thus, if the MRC-5 cells had attained senescence then the mucus granule positive A549 cells may be the result of the influence of aberrant, fibrotic epithelial-mesenchymal signalling.

Whatever the biological systems that drove them, there seemed to be two tentatively supported outcomes from the Alvetex™ Scaffold co-culture experiments.

- Short term cultured MRC-5 cells and A549 cells in co-culture generated a proliferative tumour -like culture (stylised in Figure 8.5A) with a cellular phenotype that resembled the cells seen in the spheroid cultures of Chapter 3. The results here represent a single biological replicate, thus there is a need to repeat the experiments to show reproducibility. Further gene expression and protein expression analysis would have to be conducted, however, to better characterise the phenotypes of the cells. As with the spheroid model there was no evidence of basal lamina expression, however, the Alvetex™ Scaffold provides a more practical model into to which Matrigel could be incorporated (as has been demonstrated with the scaffold and prostate cancer cells[553]). There is also tentative conjecture regarding the development of a fibrosis-relevant model. Histological sections of these cultures superficially resembled fibrotic honeycomb cysts of IPF, however it is assumed that most of the apparently proliferative cells in these cultures were A549 (the epithelial component) in origin, not the hyperproliferative mesenchymal cells present in fibrotic tissues. It is not in any way proposed that IPF fibrosis was recapitulated in chapter 7 but it is apparent that the scaffold may have the potential of providing a physical environment suitable for support of *in vitro* fibrosis.
- Secondly the scaffold seems capable of supporting MRC-5 and A549 cells in a tissue like organisation that superficially mimics the lung parenchyma at the very border of the Alvetex™ (rather than the full thickness of the scaffold, see Figure 8.5B), typified by a thin mesenchymal layer expressing ECM, supporting a monolayer of epithelial-like cells (as stylised in Figure 8.5B). It is imperative that the experiments are repeated to confirm reproducibility, however, initial results give cautious confidence that using the correct biochemical cues and optimised culture conditions the scaffold model might be further developed to generate ATII-like cultures (Figure 8.5C) and the possibility model to incorporate AT-1-like cells (either differentiated from the ATII-like A549 or from another cellular source (e.g. hTERT transformed ATI[283] or NCI-

H441) (Figure 8.5D). Ultimately, it is imagined that other components of the alveolus such as endothelial cells and immune cells might be incorporated.

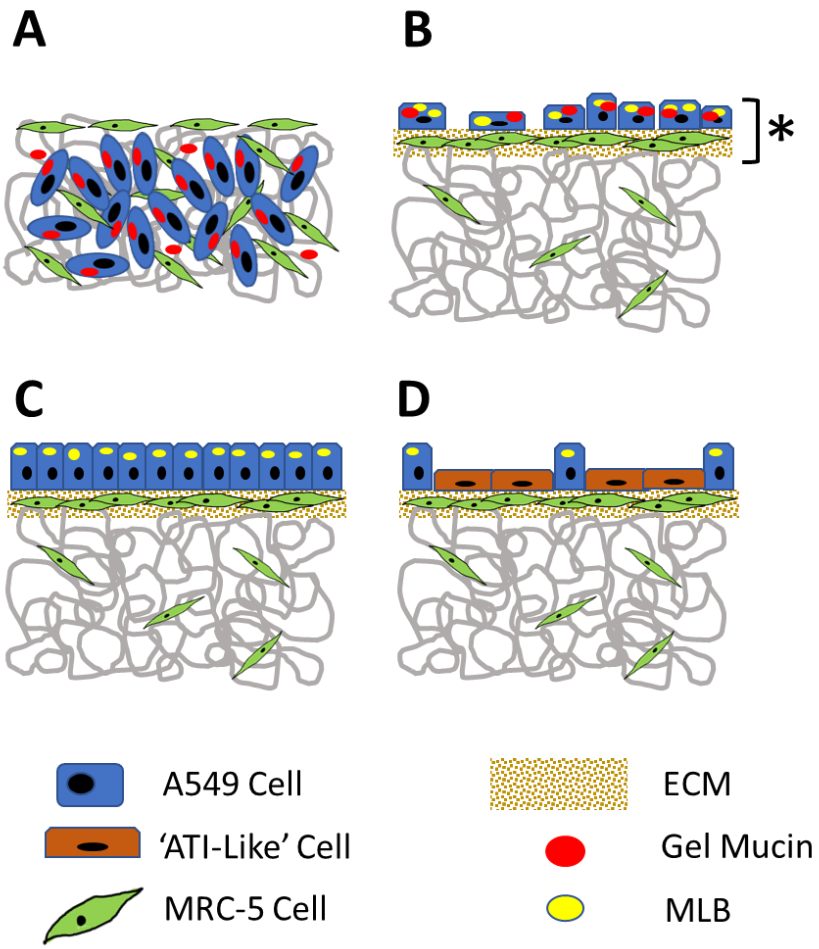

Figure 8.5. Potential development and of the Alvetex™ co-culture model.
A: tumour model, B: a visualisation of the current 'best' model. The bracket and asterisk show the area that most represents alveolar parenchyma. C: aspirational ATII model and D: aspirational ATII and ATI modelling.

8.5.4 Place of the Alvetex™ Model in the IPF Drug Discovery Workflow and Potential Analytical Methodologies

This scaffold is a readily available, relatively low cost off-the-shelf product and cultures can be established and maintained with comparative ease. In this study, the scaffold was used in 6 well plate format, however it is available in a 96 well format suitable for the set-up of high throughput experiments. The main challenges with this approach are predicted in timely and accurate microscopic analysis of the scaffold co-culture and extracting cells from the scaffold for gene and protein analysis. RNA extraction from the scaffold would be relatively simple procedure, scaffold inserts could be removed to ice to slow biochemical processes and inhibit RNA degradation, then standard homogenisation buffer (for example Promega, Madison,

Wisconsin, USA) would be applied and the lysate leeched from the scaffold, total RNA extracted and processed using conventional gene expression techniques using for example QRT-PCR, RNA microarray or single cell RNA sequencing that has the power compare the transcriptomics of single cells[652] enabling deconvolution of the gene expression profiles of the epithelial and mesenchymal components of the co-culture. Similarly, protein expression analysis could be carried out through lysis of the cells on and within the scaffold and subsequent Western Blotting. Such techniques would be beneficial for the analysis of gene and protein expression at the "whole well" scale, however techniques to interrogate specific regions or even single cells would also be required.

3D cell culture systems are becoming increasingly used as cell biology tools in many fields of research, however, conventional microscopy techniques are poorly suited for the imaging of 3D cultures where sections are thick and have high light scattering properties. These issues have driven the development of novel optical methodologies suitable for immunofluorescent and label-free analysis of 3D cell cultures such as confocal microscopy, multiphoton microscopy and optical coherence tomography[653]. Recently these advanced microscopic techniques have been refined and miniaturised to allow high throughput analysis[654] at 96 well scale providing increased numbers of replicates, lower medium volumes, therefore reduced costs and rapid and detailed imaging data to show cell morphologies, distribution of expressed proteins to enable cell characterisation and 3D visualisation of the models in a way not possible with conventional techniques.

An advantage of 3D culture systems is the potential to recapitulate tissue-like states. Techniques used for *ex vivo* single cell analysis from tissues could be employed to perform similar analyses in scaffold developed models. Cells might be enzymatically or chemically liberated and processed by NGS-based technologies such as RNA sequencing enabling genomic, transcriptomic, and epigenomic analysis of individual cells[566].

Alvetex™ Scaffold models can be readily fixed, paraffin embedded, sectioned and analysed by conventional histological techniques. This has been demonstrated here to help understand cellular organisation and protein, lipid and gel mucus expression. Knowledge of the different phenotypic populations of cells within homeostatic, developing, healing and fibrotic lung parenchyma is becoming more deeply understood[629 88 89] and it is envisaged that laser capture mirodissection[565] might be applied to further analyse and characterise individual cells from *in vitro* histological sections at a genomic level.

8.5.5 Drawback: Time Limitation of the Differentiation Protocols

The major disadvantage in the approaches presented here is the requirement for several weeks cell culture and medium exchange to enable a differentiated state. Extended cell culture is not only laborious but it increases the chances of microbial contamination and cross contamination[292]. This time factor might be unattractive to many researchers. However, it needs to be recognised there is a trade-off between convenience and physiological relevance. There may be opportunities for reducing timelines. In chapter 7, although no significant benefit was observed with conditioned medium from fibroblasts treated with Rosiglitazone (RGZ), it was observed that RGZ appeared to increase PLIN-2 gene expression in MRC-5 fibroblasts at an earlier stage, tentatively suggesting that with further optimisation RGZ treatment might speed up development of an ATII supporting fibroblast phenotype.

Perhaps the most attractive strategy to reduce timelines in the hands of the researcher might be for differentiation to be carried out upstream of cryo-preservation and supply. There is already a precedent for this in the supply of frozen, "assay-ready" pre-differentiated cells[655]. Commercial suppliers will provide differentiated frozen assay-ready NIH-3T3, CaCo2, MDCK and THP-1 cells (acCELLerate GMBH, Hamburg, Germany). 2D long term A549 cells could be cultured and differentiated at large scale and then cryo-preserved ready for immediate use from frozen. As mentioned previously, 3D spheroid A549 cultures are similar in dimension to organoid cultures that have been successfully cryopreserved and recovered[656]. Similar advances have been made with 3D cultures grown on scaffolds[657] [658] thus, there is also potential for that 3D Alvetex™ Scaffold cultures to prepared, differentiated and cryopreserved upstream of supply. These "assay-ready" approaches might appeal to end users and provide commercial opportunities but detailed cost-benefit analysis would have to be conducted to ensure incumbent costs were not prohibitive to the end user.

8.6 Future work: Development, ATII Phenotype Characterisation, Optimisation and Onward Characterisation for Fibrosis Research

Although, in Chapter 6, the effect of Dexamethasone on A549 cells was seen to be wide ranging, it is recognised that confirmation of multilamellar body, SFTP expression with a more extensive investigation of EMT and stem cell markers would be of value. However, the heterogeneity of mesenchymal cell populations seen in lung parenchyma *in vivo* together with the importance of epithelial and mesenchymal cross talk in normal and fibrotic states, suggest that future work concentrating on the co-culture models piloted in Chapter 7 might provide the most benefit to IPF research. These future activities can be sequentially broken

down into the short, medium and long term and are diagrammatically represented in Figure 8.6.

8.6.1 Short Term Aims

Much of the work in Chapter 7 is at preliminary stage with tentative conclusions made from single experiments. In the short-term it is proposed that the Transwell™ culture work should be repeated at least twice to increase biological replicate numbers and allow the confident application of statistical analysis to *SFTP, PTHrP, ERBB* and *CDH1* gene expression. These gene expression findings should then be validated with protein expression by Western Blotting, immune histochemistry or con-focal immunofluorescence microscopy.

The hypothesis that benefits seen with gene and presumed protein expression with FCM and Transwell™ culture are translated to the scaffold co-culture should be tested. Application of con-focal immunofluorescence microscopy to evaluate SFTP expression would be of benefit by generating data but also demonstrating the potential of high throughput analysis of the scaffolds. It needs to be determined if the ECM expression was subject to the MRC-5 cells becoming senescent (through assessment such as histological staining for senescence associated β-galactosidase) and the nature of the ECM should be determined by further collagen staining and staining for hyaluronic acid expression[563].
Mucin expression was observed in both A549 spheroid cultures and the "invasive" scaffold cultures seen with shorter term MRC-5 culture. Gene expression analyses indicated the presence of MUC5AC and MUC5B and the former was confirmed by immunohistochemistry. It would be of great benefit to determine if MUC5B was expressed in these systems at the protein level as the gene has a strong association with clinical IPF[383].

8.6.2 Mid Term Aims

In the mid-term, if a homeostatic ATII-like A549 / MRC-5 co-culture model was optimised, refined and established in Alvetex™ scaffold it would require transcriptomic and proteomic validation. ATII-like epithelial protective responses could be obtained through simulated microbiological challenge (with lipopolysaccharide or by particulate challenge, for example) to determine if the cells mount a NF-κB mediated cytokine response to evolve proinflammatory cytokines (as detected by ELISA) such as IL-6, IL-8 or type 1 interferons[659 660]. The model should be assessed for its ability to recapitulate a TGF-β1 induced fibrotic response. With down-regulation of E-Cadherin and upregulation of fibronectin in the A549 cells and expression of α-SMA and collagen in the fibroblast component. The protective properties against these processes by known ALK5 inhibitors should be assessed by QRT-PCR, Western Blotting and con-focal immune fluorescent microscopy or immuno-histochemistry. Once characterised it would be of benefit to translate the protocols to 96 well

format as this would provide the potential for increased numbers of replicates, reduced medium volumes, reduced costs and the increased efficiencies required for high-throughput screening in a drug discovery setting[579].

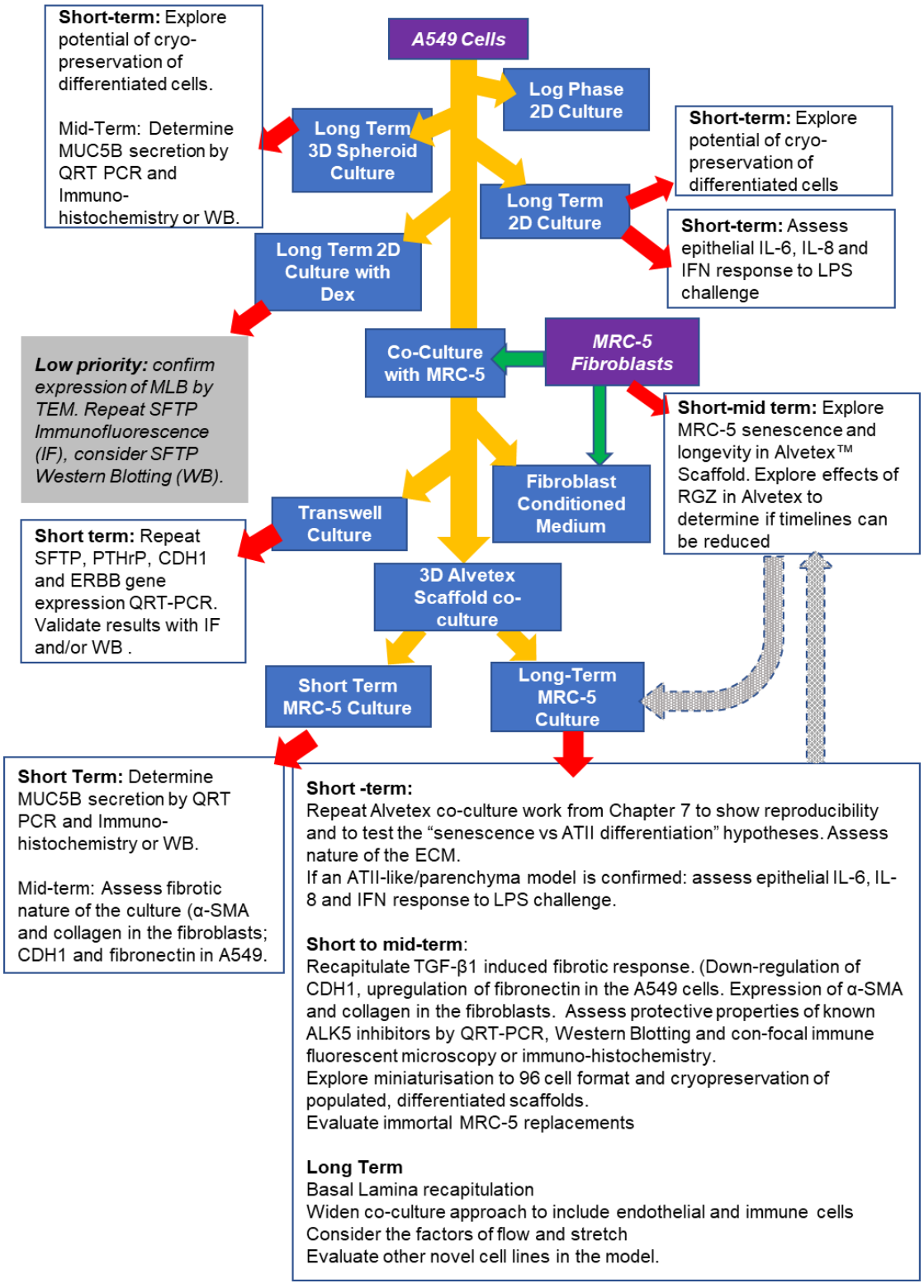

Figure 8.6. Summary of Future Work.

MRC-5 is a well characterised human lung foetal fibroblast[516] and that point of view ideal for incorporation in to this model to provide the mesenchymal component, it is, however, not a continuous cell line and will undergo senescence in long term culture[285], therefore introducing the potential of an unwanted confounding factor. Another mid-term aim therefore would to be determine ways to increase the longevity of the cell either through immortalisation or conditional immortalisation[661] or by exploring the potential of existing immortalised variants of the cell line, for example the SV40 transformed version MRC-5 SV2[662].

The addition of TGF-β together with ascorbic acid to skin and intestinal fibroblasts supporting the differentiation of the intestinal cell line CaCo2 has proven to effective in an Alvetex™ based system in helping drive the deposition of fibrillar collagen in the ECM[528]. This approach may benefit future work, however there should be attention to the possibility of TGF-β inducing a fibrotic-like response and myoblast differentiation in the MRC-5 fibroblasts[90].

8.6.3 Long Term Aims

It should be noted that cells within true alveolar epithelium should anchor to a basal lamina, become polarised and express junctional complexes allowing the cells to form a functional barrier manifested by the establishment of high Trans Membrane Electrical Resistance (TEER)[522]. TEER assessment of the Transwell™ cultures (results not included) did not display any evidence of the establishment of an epithelial barrier in either Transwell™ or Alveletex™ Scaffold and there is scant evidence in the literature to support this a feature of A549 cells[663]. Although ECM expression was observed in the long-term MRC-5/A549 scaffold co-cultures by the TEM there was no evidence of the establishment of a basal lamina. Thus, longer term work should explore ways in which it might be incorporated into the scaffold and subsequently observed by TEM to display its characteristic triple-layer structure (lamina reticularis, lamina densa and lamina lucida[522]). This could be achieved through the use of Matrigel™[238], by optimised growth and *de novo* expression by the mesenchymal/epithelial component[664] or through a combination of both approaches.

Beyond these developments, to fully recapitulate the lung parenchyma and the pulmonary alveolus *in vitro* the developed model would have to include endothelial cells (such as HuVEC cells) to represent the cells of the capillary wall[665], alveolar macrophages (possibly differentiated from the THP-1 cell line[666]) and the ability to operate at air-liquid interface (ALI). *In vivo,* the alveolus is a mechanically dynamic environment, blood flows through the capillaries to enable gaseous exchange, to provide nutrients and to remove waste products of metabolism. The cells of the alveolus are subject to physical stretching from tension and

relaxation in parenchyma due to inhalation and expiration[1]. Flow might be achieved through microfluidic perfusion[667]. Mechanical stretch has been shown to be an important factor in ATII cell differentiation[668], Alvetex™ Scaffold, however, is a rigid structure, therefore long term future developments might have to be translated to a flexible scaffold substrate[669].

Considering these long-term aspirations and ambitions, it is an inescapable fact that A549 is ultimately a cancer derived cell line thus full recapitulation of true ATII function in the cell line may be impossible, however the results of this work show that certain aspects, especially SFTP production can be modulated by optimised culture conditions, therefore potentially improving the cell line's performance, making it more physiologically relevant than log phase cells, if not a perfect model.

It is expected that the outputs of the further work will support the hypothesis that stability and reproducibility in terms of its limited ATII functionality will be demonstrated by repeated experiments with the cell line in co-culture with MRC-5 fibroblasts in Alvetex™ Scaffold. If this reproducibility can be demonstrated it implies that this model may have utility not only as an experimental model but also as a "reference standard" against which other novel models may be measured. There is also an expectation that Alvetex™ Scaffold might provide a "plug-and-play" platform in which A549 and MRC-5 cells might be superseded by other cell lines and cell derived models as they are developed (such as other fibroblast cell lines, fibroblasts from IPF patients and NCI-H441 or iPSC derived ATII-like cells) thereby the scaffold could provide a platform in which other candidate cells might be assessed and explored.

8.7 Final Conclusions

- This work has not fully demonstrated or replicated all aspects of ATII epithelial biology in the commonly used A549 "ATII-like" cancer derived cell line, however, it has defined and validated sets of conditions to optimise and refine the cell line's physiologically relevant use for airways research.
- It has provided a deeper insight into the broncho-alveolar potential and biology of the A549 cancer line particularly into its gene expression under specific 2D and 3D culture conditions.
- The study has provided a strong foundation on which further work can be taken forward, identified key areas to investigate and provided ATII and fibrosis relevant hypotheses to explore.
- It has demonstrated the suitability of a 3D cell culture scaffold system for the modelling of lung parenchyma that provides a platform that may be further developed and using a "plug-and-play" approach with other ATII and fibroblast cellular components for the future development of ATII and fibrotic models.

Appendix A **Appendix to Chapter 4. Comparative Gene Expression from RNA Microarray Analysis for a Selection of Relevant Genes in 2D and 3D A549 Cultures at day 25 of their Time-Courses as Compared to Log Phase A549 Cells.**

Gene	**Gene Regulation. Day 25 2D Culture vs Log Phase A549**		**Gene Regulation. Day 25 3D Culture vs Log Phase A549**	
	Up or Down	**Fold Change**	**Up or Down**	**Fold Change**
CEACAM 6	Up	2.1	Up	1424.1
CECAM 7	Up	9.8	Up	1046.5
Cathelicidin	Up	29.6	Up	24.0
ERBB3	Up	17.3	Up	3.5
SPDEF	Up	8.0	Up	13.3
CDKN1B	Up	3.4	Up	3.7
WNT4	Up	68.0	Up	48.9
NANOG	Up	4.1	Up	2.9
SOX2	Up	3.2	Up	6.5
SOX9	Up	2.8	Up	6.3
MMP7	Up	6.6	Up	6.0
C3	Up	17.4	Up	8.1
C4b	Up	12.0	Up	8.1
C5	Up	6.3	Up	6.3
ABCC11	Up	4.5	N/A	<2
ABCC3	Up	2.8	Up	2.2
Ki67	Down	29.5	Down	7.5
PCNA	Down	2.4	Down	2.7
TCF7L1	Down	5.9	N/A	<2

Appendix A Table 1. Comparative gene expression from RNA microarray analysis for a selection of relevant genes in 2D and 3D A549 cultures at day 25 of their time-courses as compared to log phase A549 cells. Fold change in gene regulation as determined by RNA microarray analysis for a selection of relevant genes in 2D and 3D A549 cultures at day 25 of their time-courses as compared to log phase A549 cells (N/A indicates results were less than a fold change of two).

Appendix B **Appendix to Chapter 5. STR Profiling of TRiP WT Cells. Annotated STR Assay Electropherograms.**

16 Locus STR Electropherograms from Genemapper™ Software

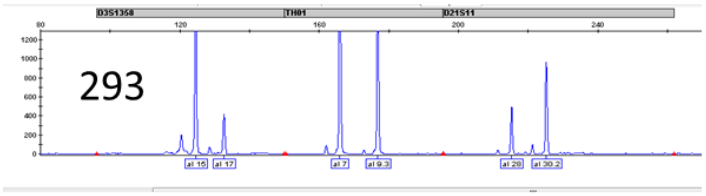

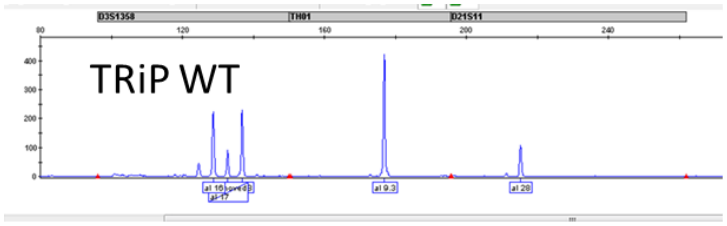

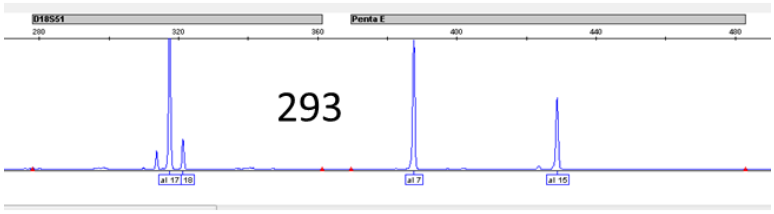

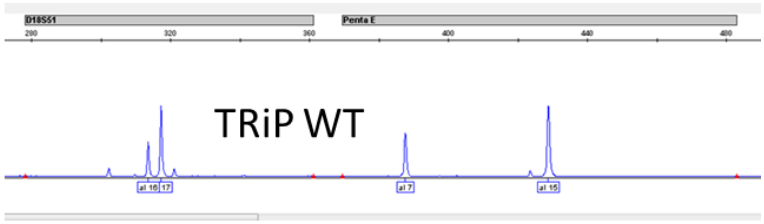

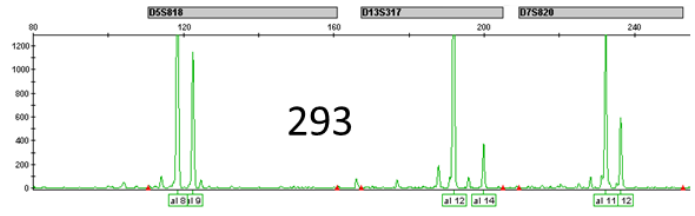

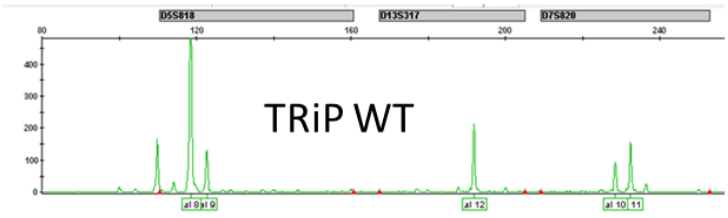

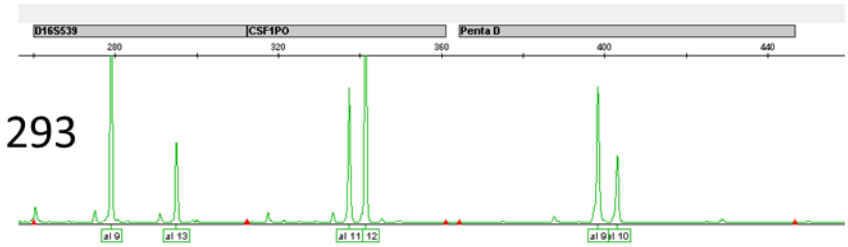
D16S539
CSF1PO
Penta D
293

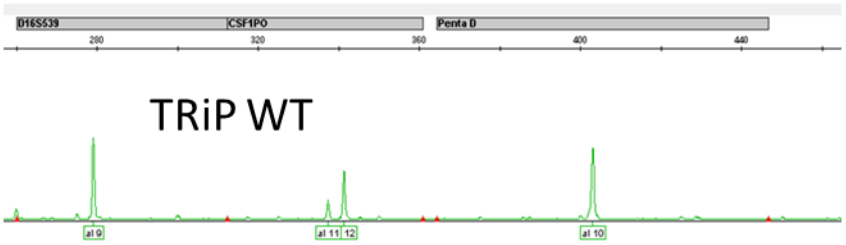
D16S539
CSF1PO
Penta D
TRiP WT

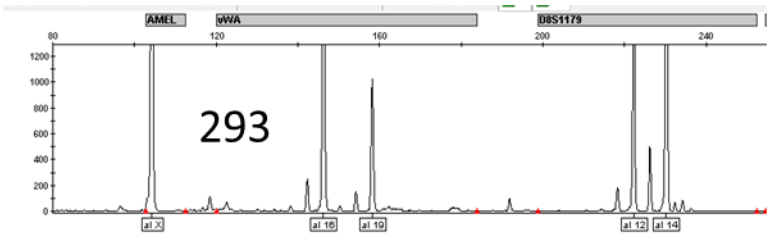
AMEL
vWA
D8S1179
293

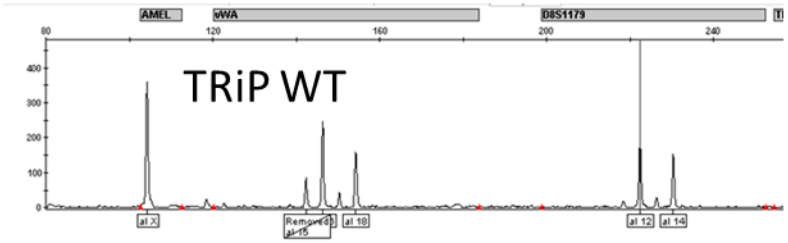
AMEL
vWA
D8S1179
TRiP WT

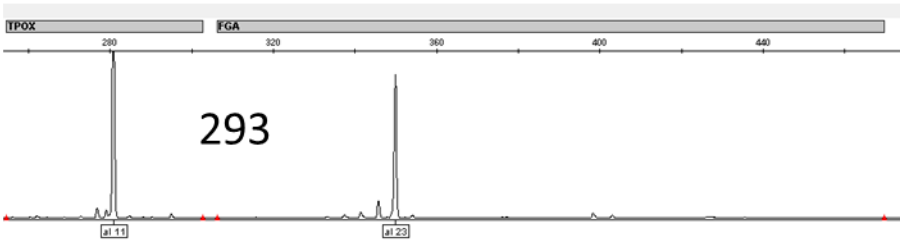
TPOX
FGA
293

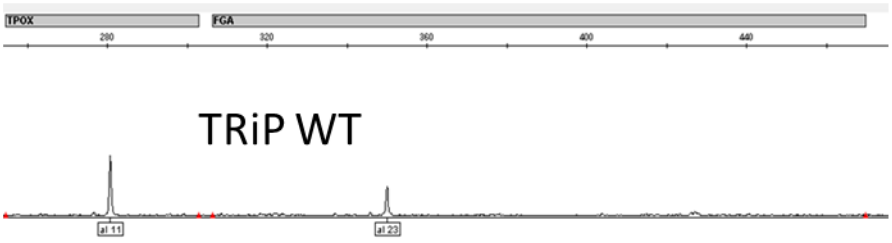
TPOX
FGA
TRiP WT

24 Locus STR Electropherograms from Genemapper™ Software (Annotated)

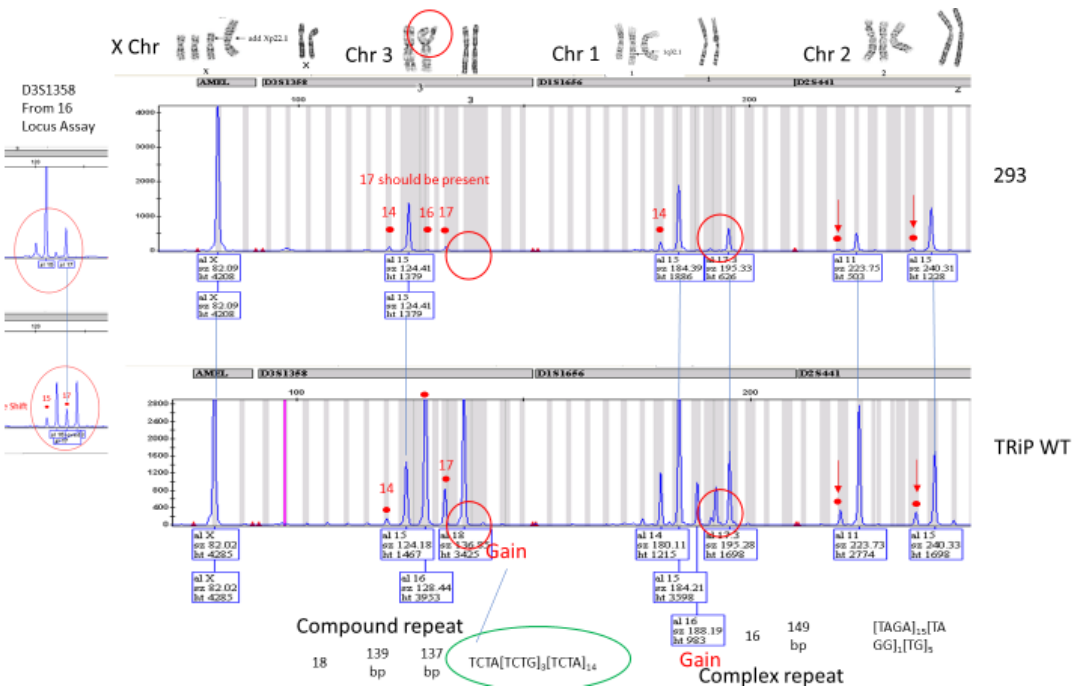

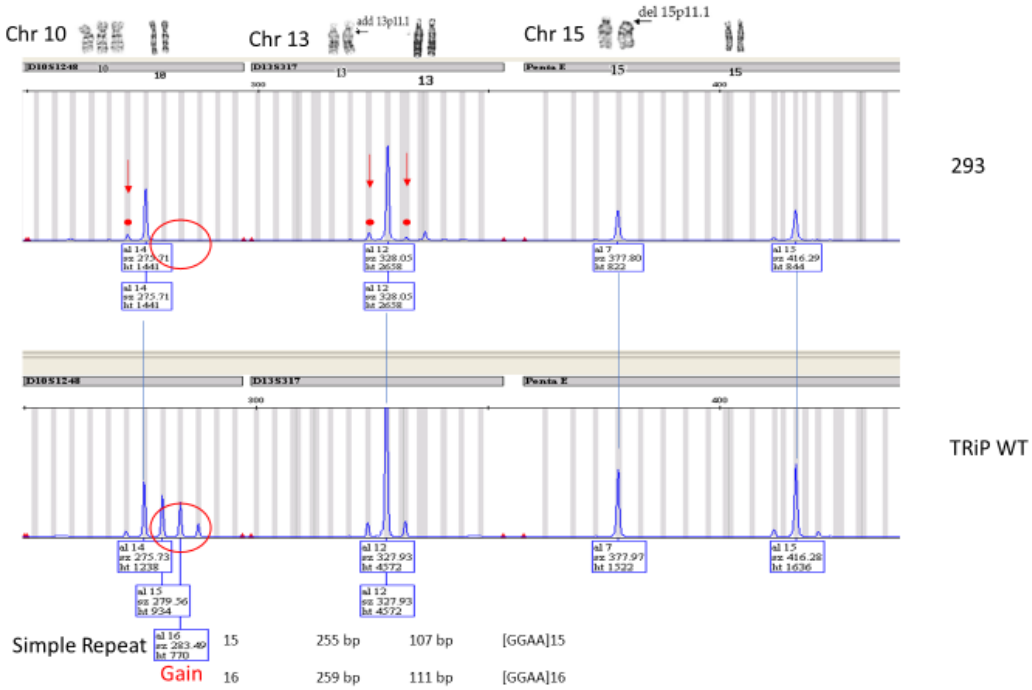

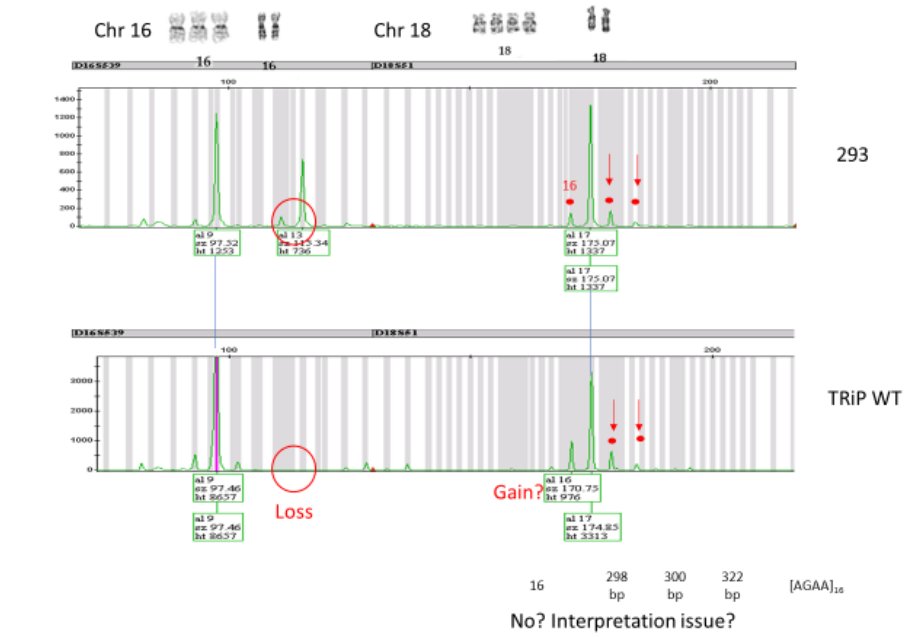
Chr 16
Chr 18
293
16
TRiP WT
Loss
Gain?
16
298 bp
300 bp
322 bp
[AGAA]16
No? Interpretation issue?

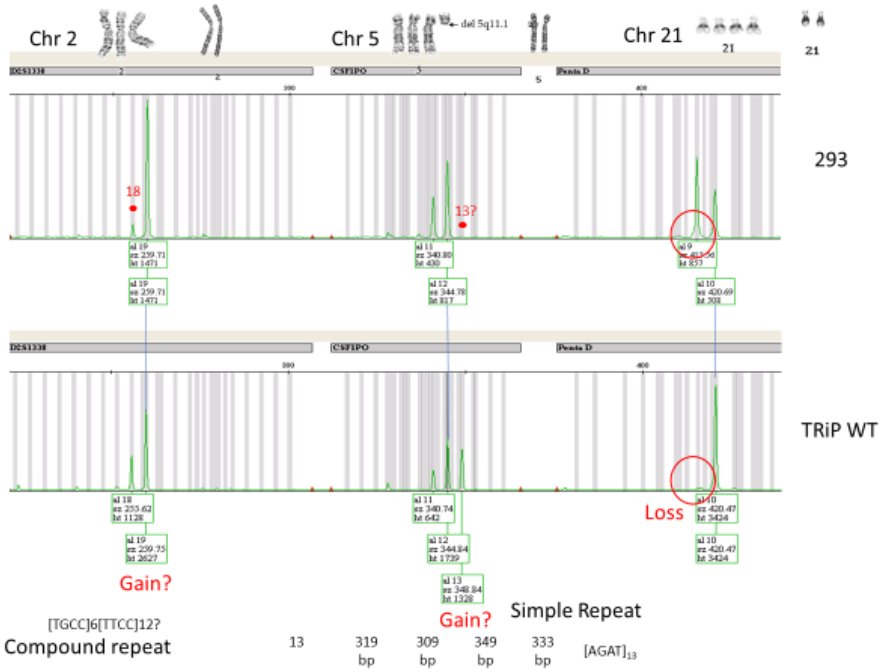
Chr 2
Chr 5
Chr 21
293
18
13?
TRiP WT
Loss
Gain?
Gain?
[TGCC]6[TTCC]12?
Compound repeat
13
319 bp
309 bp
349 bp
333 bp
[AGAT]13
Simple Repeat

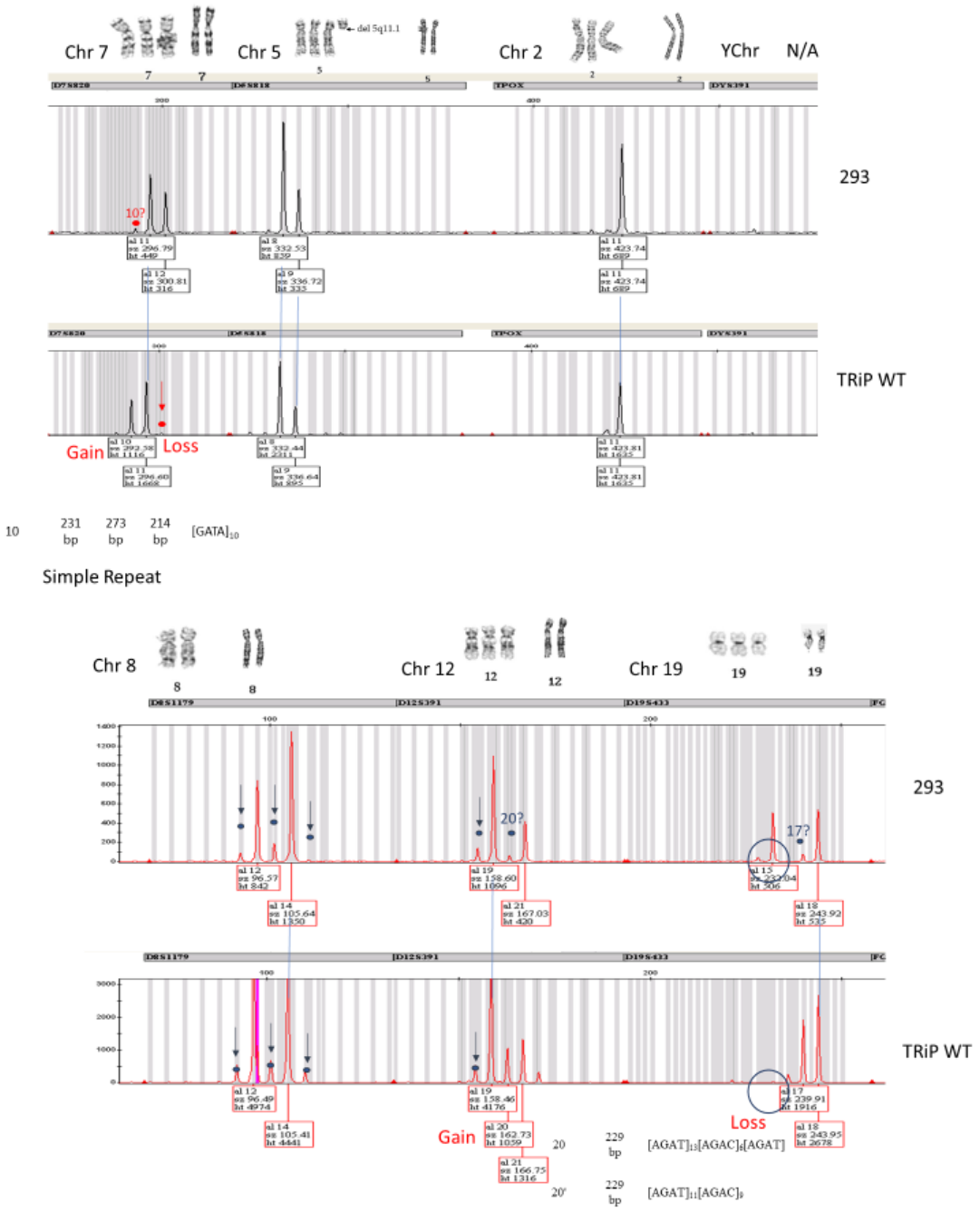
Chr 7
Chr 5
del 5q11.1
Chr 2
YChr
N/A
293
10?
TRiP WT
Gain
Loss
10
231 bp
273 bp
214 bp
[GATA]10
Simple Repeat
Chr 8
Chr 12
Chr 19
293
20?
17?
TRiP WT
Loss
Gain
20
229 bp
[AGAT]13[AGAC]8[AGAT]
20'
229 bp
[AGAT]11[AGAC]8

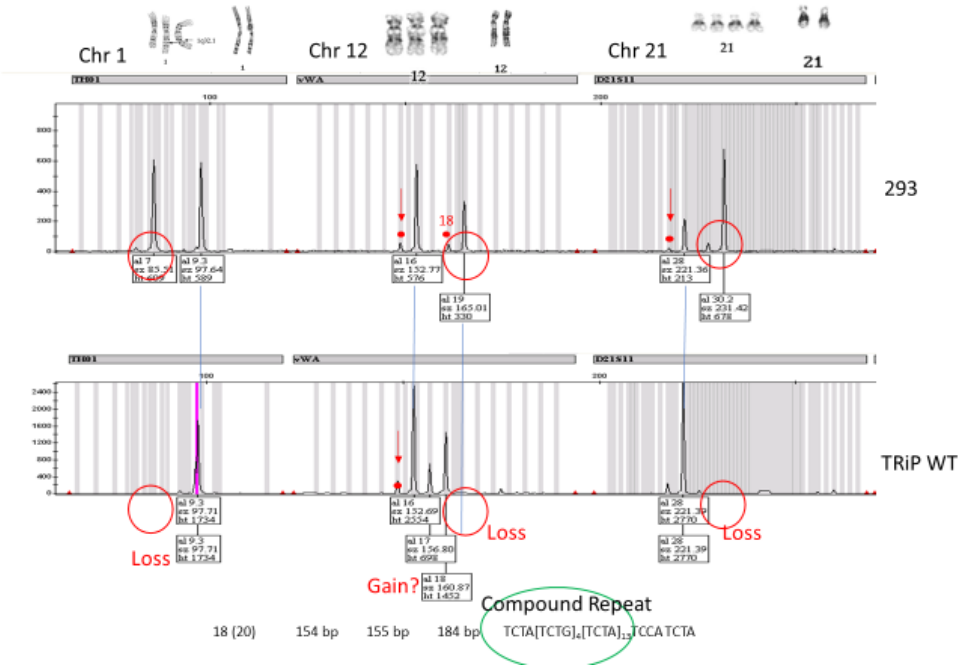
Chr 1
Chr 12
Chr 21
293
18
TRiP WT
Loss
Loss
Loss
Gain?
Compound Repeat
18 (20)
154 bp
155 bp
184 bp
TCTA[TCTG]4[TCTA]11TCCATCTA

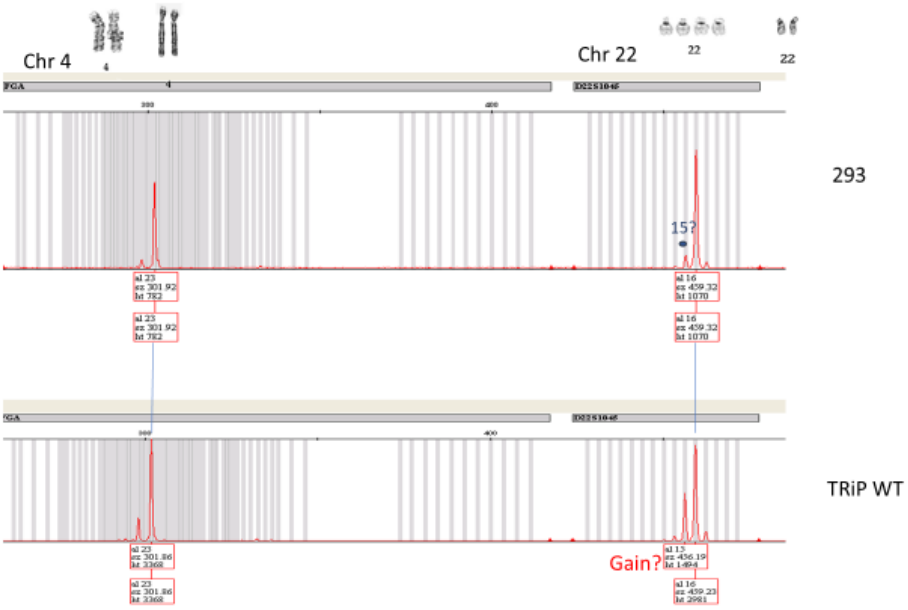
Chr 4
Chr 22
293
15?
TRiP WT
Gain?

Appendix C **Appendix to Chapter 6. Assessment of Epithelial-Mesenchymal Transition and Stem Cell Marker Expression in Dex and Neuregulin-β Treated A549 Cells**

Results

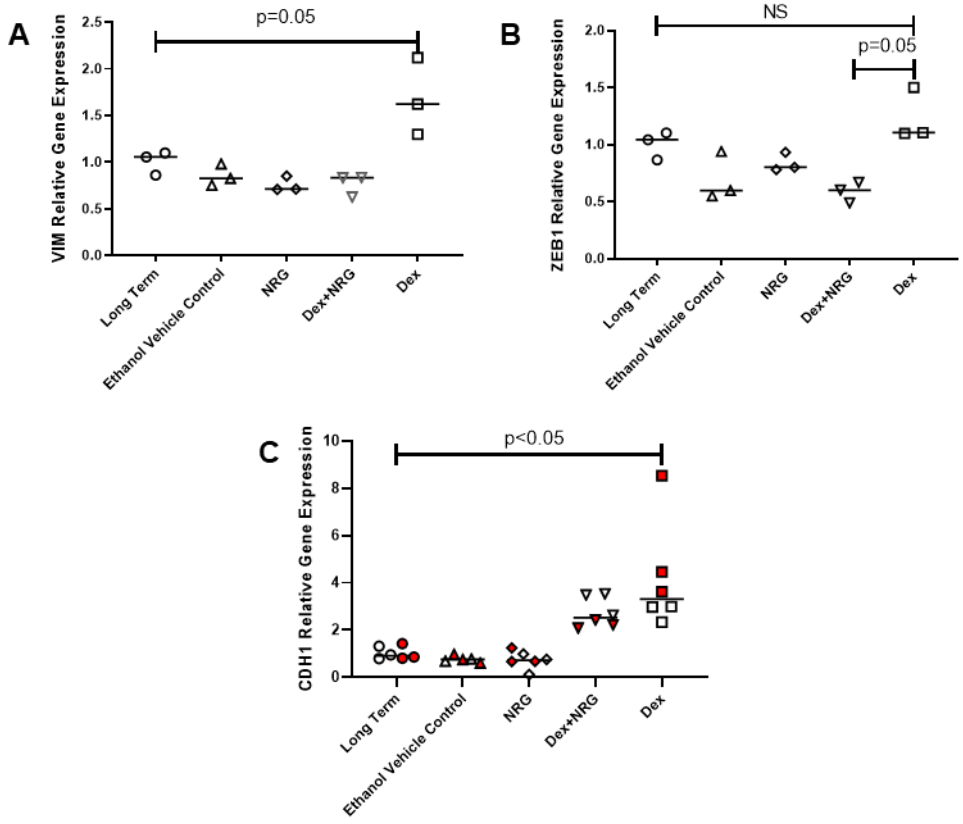

Appendix C Figure 1. Epithelial and EMT marker gene expression in long term A549 cultures is influenced by chronic treatment with Dexamethasone (Dex) and neuregulin-1β (NRG-1β). A549 cells were cultured in six well plates in F12/10% FBS for three weeks with no treatment ("Long Term"), with NRG-1β at 50 ng/mL ("NRG"), Dex at 100 nM ("Dex") and a combination NRG-1β at 50 ng/mL and Dex at 100 nM (Dex+NRG). Dex was solubilised in ethanol hence the inclusion of the "Ethanol Vehicle Control". The cultures were medium exchanged with medium containing their relevant treatments every two to three days for three weeks before RNA was extracted, quantified, normalised and reverse transcribed to cDNA prior to QRT-PCR analysis with TaqMan™ primer/probe sets. Data from the EMT Markers VIM and ZEB1 are shown in Graphs A and B respectively and data from the epithelial marker CDH1 is shown in Graph C. QRT-PCR data were analysed using the Δ-ΔCt method using the geometric means of GAPDH and ATP5B gene Ct values as reference. Relative expression was normalised to the average Ct values non-treated "Long Term" A549 cells. Statistical analyses were performed by Graphpad Prism™ using the Mann-Whitney Non-Parametric Test. A and B from a single experiment, C represents two independent experiments.

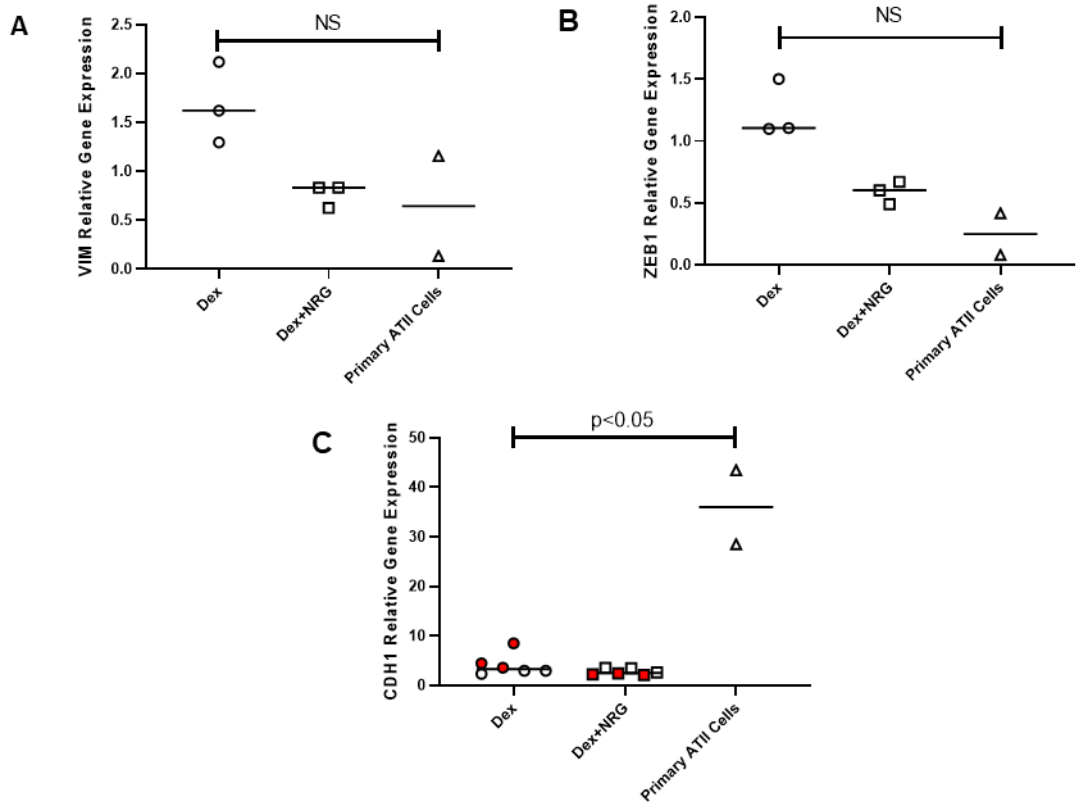

Appendix C Figure 2. Epithelial and EMT marker gene expression in long term A549 cultures treated with Dexamethasone (Dex) and neuregulin-1β (NRG-1β) compared to primary human ATII cells. A549 cells were cultured in six well plates in F12/10% FBS for three weeks with Dex at 100 nM ("Dex") and a combination NRG-1β at 50 ng/mL and Dex at 100 nM (Dex+NRG). The cultures were medium exchanged with medium containing their relevant treatments every two to three days for three weeks before RNA was extracted, quantified, normalised and reverse transcribed to cDNA prior to QRT-PCR analysis with TaqMan™ primer/probe sets. In parallel cDNA was similarly prepared from freshly isolated human primary ATII cells derived from lung biopsies from two different donors and analysed together with the cDNA from Long Term A549 cells. Data from the EMT Markers VIM and ZEB1 are shown in Graphs A and B respectively and data from the epithelial marker CDH1 are shown in Graph C. QRT-PCR data were analysed using the Δ-ΔCt method using the geometric means of GAPDH and ATP5B gene Ct values as reference. Subsequently data were normalised to non-treated "Long Term" A549 cells (data not shown). Statistical analyses were performed by Graphpad Prism using the Mann-Whitney Non-Parametric Test. A and B represent single experiments. In C data from two independent experiments are shown by coloured data points.

(i) Stem cells:

Clusters of Dex+NRG treated A549 cells bore a superficial resemblance to the typical morphology of stem cell colonies (Appendix C Figure 3).

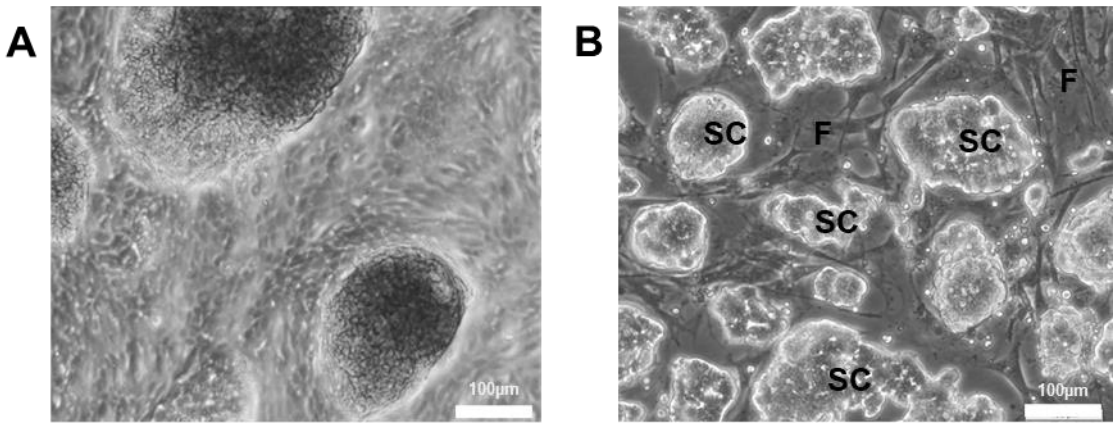

Appendix C Figure 3. Morphology of long term A549 cultures chronically treated with a combination of Dexamethasone (Dex) and neuregulin-1β (NRG-1β) is superficially similar to that of stem cell colonies. A549 cells were cultured in F12/10% FBS for three weeks with a combination NRG-1β at 50 ng/mL and Dex at 100 nM (Dex+NRG). The cultures were medium exchanged with medium containing their relevant treatments every two to three days for three weeks. A representative phase contrast image of the A549 cellular clusters is shown here (A). Image B is of colonies of the mouse embryonic stem cell line H129-1 (ECACC 14040203). Representative stem cell colonies are marked "SC". The background "feeder layer" cells are mouse embryonic fibroblast cells (marked "F").

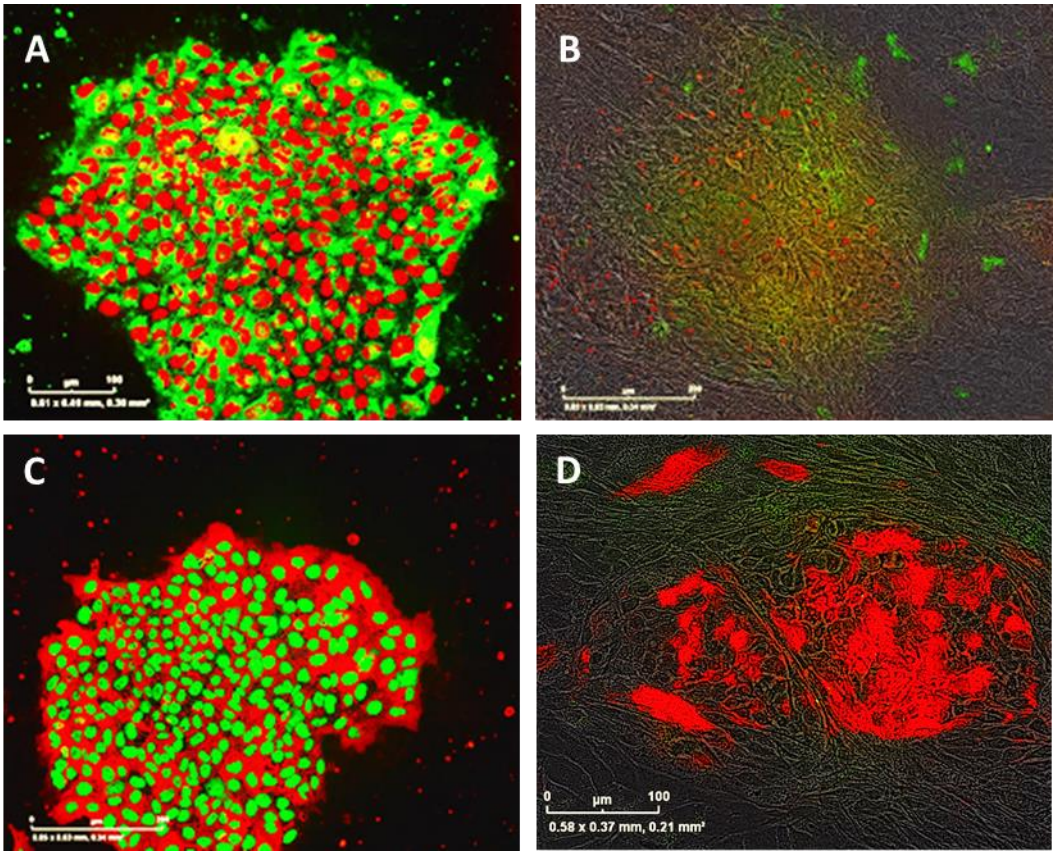

Appendix C Figure 4. Preliminary (single experiment) investigation into potential stem cell marker expression in A549 cultures chronically treated with a combination of Dexamethasone (Dex) and neuregulin-1β (NRG-1β). A549 cells were cultured on coverslips in six well plates in F12/10% FBS for three weeks with NRG-1β at 50 ng/mL and Dex at 100 nM with regular medium changes. In parallel, colonies of the human induced pluripotent stem cell line (hiPSC) UKi2007A were cultivated on coverslips in E8 medium as a positive control. Coverslips of cells were fixed with formaldehyde and stained for pluripotent markers using indirect immunofluorescent staining. The stem cell markers SSEA4 and OCT4 were stained in combination (as shown in A and B) with mouse IgG3 anti-human SSEA4 and rabbit anti-human OCT4 primary antibodies and Alexafluor™ 488 (green) conjugated goat anti-mouse IgG3 and Alexafluor™ 594 (red) conjugated donkey ant-rabbit. Image "A" shows UKi2007A iPSC cells and image "B" shows a Dex+NRG treated A549 colony-like cell cluster. Red OCT4 staining should be associated with cell nuclei and green SSEA4c with the cytoplasm. Stem cell markers SOX2 and TRA-1-60 were similarly stained in combination (C and D) with rat anti human SOX2 and mouse anti human TRA-1-60 primary antibodies and Alexafluor™488 (green) conjugated donkey anti-rat and Alexafluor™ 594 (red) conjugated goat anti mouse secondary antibodies. Green SOX2 staining should be associated with cell nuclei and Red TRA-1-60 with the cytoplasm. Images A and C are of the human induced pluripotent stem cell line (hiPSC) UKi2007A and B and D are of A549 cell clusters following Dex+NRG treatment. No Stem cell marker staining could be observed in any non-clustered areas of A549 the cell culture. A and D scale bar = 100 µm; B and C scale bar = 200 µm. Data from a single experiment.

Appendix D **Appendix to Chapter 7. RGZ Absorption Control Data**

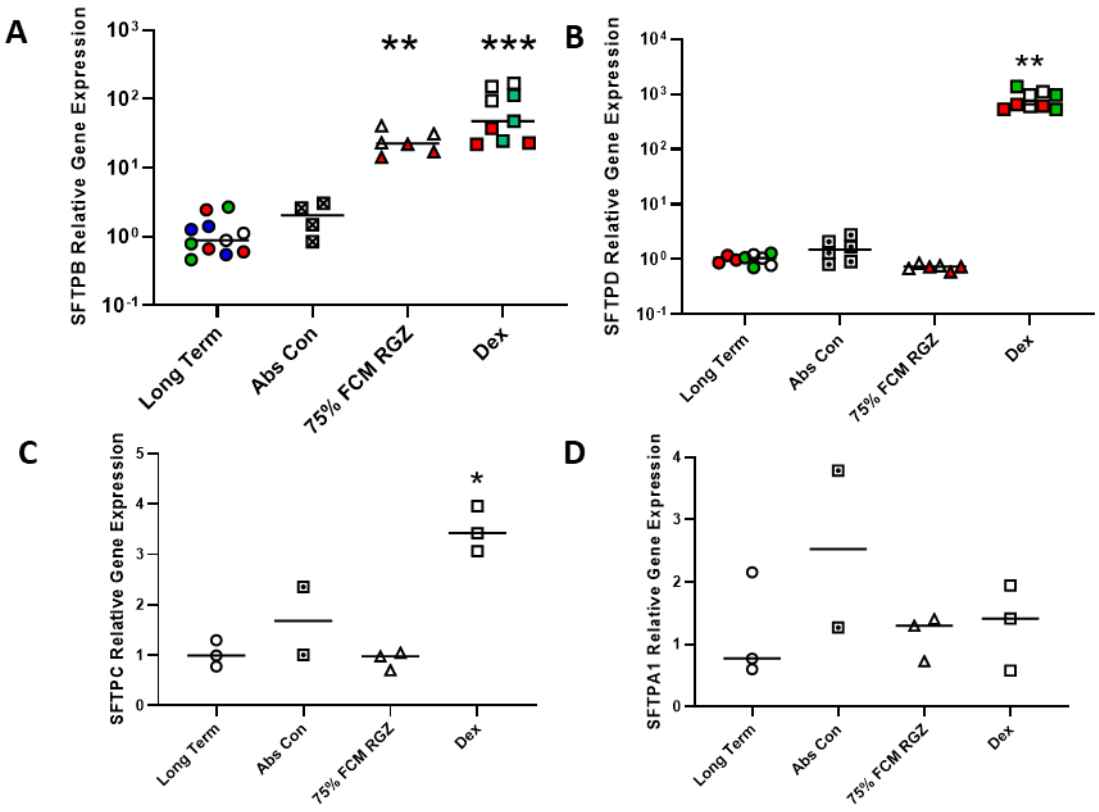

Appendix D Figure 1. An RGZ "Absorption Control" was a prepared by treating and washing a monolayer of cells with 10 μM RGZ for one hour before aspirating to waste and PBS washing the monolayer and subsequently replenishing with RGZ-free F12/10% FBS for a further hour's incubation before harvesting similarly to the FCM. A549 cells were cultured in in six well plates in F12/10% FBS for three weeks with 75 % (v/v) RGZ treated fibroblast conditioned medium (FCM RGZ). A549 Cultures were medium exchanged with medium containing their relevant treatments every two to three days for three weeks before RNA was extracted, quantified, normalised and reverse transcribed to cDNA before QRT-PCR analysis with TaqMan™ primer/probe sets for surfactant protein gene expression. SFTPB, (A) SFTPD (B), SFTPC (C) and SFTPA1 (D). Data from 100 nM Dexamethasone (Dex) treated A549 cells are included for comparison as this treatment has been previously demonstrated as effective for SFTP gene induction in A549 cells. QRT-PCR data were analysed using the Δ-ΔCt method using the geometric means of GAPDH and ATP5B gene Ct values as reference. Relative expression was normalised to the average Ct values non-treated "Long Term" A549 cells. Non-parametric Kruskal-Wallis test with comparison to Long Term (Control). A and B show data from multiple experiments. C and D from a single experiment. Coloured data points indicate data from separate experiments.

Appendix E Genorm Analysis of RNA from A549 Spheroid Cultures

15 RNA triplicate samples were extracted from and 3D spheroids (Chapter 3) and 2D cultures (Chapter 4) representing log phase, day 7 and day 25 of the time-courses. Using QRT-PCR (refer to Chapter 2, Materials and Methods, section 2.12.1) these samples were assessed against 12 reference target genes (*18s, EIF4A2, ACTB, B2M, GAPDH, SHDA, RPL13A, UBC, CYC1, YWHAZ, TOP1* and *ATP5B* using Genorm Kit (Sybr Green), Primer design, Southampton, UK.

Results

- Run layout was 'perfect' as per Hellemans *et al* 2007[670].
- According to the geNorm analysis[670], as carried out by qBase® software (Biogazelle, Zwijnaarde, Belgium), the optimal number of reference targets was two. The optimal normalisation factor for these experiments can be calculated as the geometric mean of the Ct values of the reference targets TOP1 and ATP5B.
- These genes offered high reference target stability.
- qBase software has a limited license duration. Results were printed and the figure below scanned from a laboratory notebook.
- The quality of the figure was not acceptable for inclusion in the main body of the thesis, hence inclusion as an appendix.

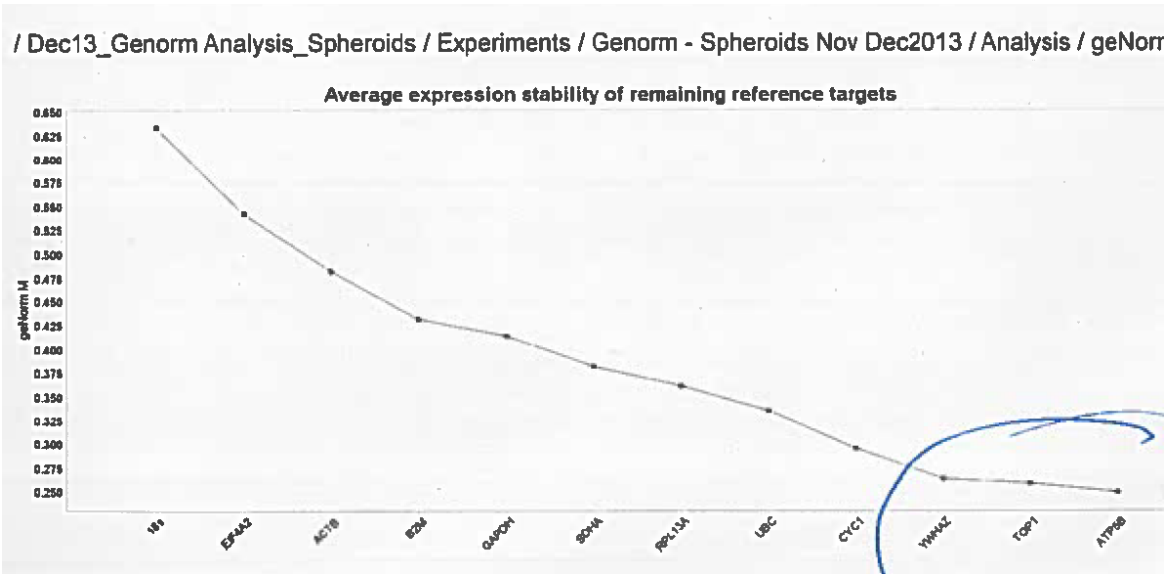

Appendix E Figure 1. Genorm analysis output from qBase® software of 15 RNA triplicate samples from and 3D spheroids (Chapter 3) and 2D cultures (Chapter 4) representing log phase, day 7 and day 25 of the time-courses. X axis shows the reference genes, ranked by stability and Y axis the calculated geNorm M value. Reference gene stability was inversely proportional to the geNorm M value.

Appendix F **Published Work. Cooper, James Ross *et al*. "Long Term Culture of the A549 Cancer Cell Line Promotes Multilamellar Body Formation and Differentiation towards an Alveolar Type II Pneumocyte Phenotype." *PloS one* vol. 11,10 e0164438. 28 Oct. 2016, doi:10.1371/journal.pone.0164438**

PLOS | ONE

RESEARCH ARTICLE

Long Term Culture of the A549 Cancer Cell Line Promotes Multilamellar Body Formation and Differentiation towards an Alveolar Type II Pneumocyte Phenotype

James Ross Cooper[1,2]*, Muhammad Bilal Abdullatif[3], Edward C. Burnett[1], Karen E. Kempsell[3], Franco Conforti[2], Howard Tolley[5], Jane E. Collins[2], Donna E. Davies[2,4]

1 Public Health England, Culture Collections, Porton Down, Salisbury, Wiltshire, United Kingdom, **2** Academic Unit of Clinical and Experimental Sciences, Sir Henry Wellcome Laboratories, University of Southampton Faculty of Medicine, University Hospital Southampton, United Kingdom, **3** Public Health England, Diagnostic Technologies, Porton Down, Salisbury, Wiltshire, United Kingdom, **4** National Institute for Health Research, Respiratory Biomedical Research Unit, University Hospital Southampton, Southampton, United Kingdom, **5** Public Health England, Microbiology Services, Porton Down, Salisbury, Wiltshire, United Kingdom

* jim.cooper@phe.gov.uk

OPEN ACCESS

Citation: Cooper JR, Abdullatif MB, Burnett EC, Kempsell KE, Conforti F, Tolley H, et al. (2016) Long Term Culture of the A549 Cancer Cell Line Promotes Multilamellar Body Formation and Differentiation towards an Alveolar Type II Pneumocyte Phenotype. PLoS ONE 11(10): e0164438. doi:10.1371/journal.pone.0164438

Editor: Francesco Cappello, University of Palermo, ITALY

Received: May 24, 2016

Accepted: September 26, 2016

Published: October 28, 2016

Data Availability Statement: Microarray data files used to generate this publication have now been uploaded, approved and accepted by the NCBI as part of the Gene Expression Omnibus (GEO). The full data series has the GEO accession number GSE88881 and will be available from the following link: http://www.ncbi.nlm.nih.gov/geo/query/acc.cgi?acc=GSE88881. There are also two subsets of data: http://www.ncbi.nlm.nih.gov/geo/query/acc.cgi?acc=GSE88879 and http://www.ncbi.nlm.nih.gov/geo/query/acc.cgi?acc=GSE88880. The

Abstract

Pulmonary research requires models that represent the physiology of alveolar epithelium but concerns with reproducibility, consistency and the technical and ethical challenges of using primary or stem cells has resulted in widespread use of continuous cancer or other immortalized cell lines. The A549 'alveolar' cell line has been available for over four decades but there is an inconsistent view as to its suitability as an appropriate model for primary alveolar type II (ATII) cells. Since most work with A549 cells involves short term culture of proliferating cells, we postulated that culture conditions that reduced proliferation of the cancer cells would promote a more differentiated ATII cell phenotype. We examined A549 cell growth in different media over long term culture and then used microarray analysis to investigate temporal regulation of pathways involved in cell cycle and ATII differentiation; we also made comparisons with gene expression in freshly isolated human ATII cells. Analyses indicated that long term culture in Ham's F12 resulted in substantial modulation of cell cycle genes to result in a quiescent population of cells with significant up-regulation of autophagic, differentiation and lipidogenic pathways. There were also increased numbers of up- and down-regulated genes shared with primary cells suggesting adoption of ATII characteristics and multilamellar body (MLB) development. Subsequent Oil Red-O staining and Transmission Electron Microscopy confirmed MLB expression in the differentiated A549 cells. This work defines a set of conditions for promoting ATII differentiation characteristics in A549 cells that may be advantageous for studies with this cell line.

citation for the GEO database is as follows: Edgar R, Domrachev M, Lash AE. Gene Expression Omnibus: NCBI gene expression and hybridization array data repository Nucleic Acids Res. 2002 Jan 1;30(1):207-10.

Funding: This study was funded by the Pipeline Funding Board of Public Health England (PHE) (at that time the organization was known as the Health Protection Agency (HPA)) as part of its 2012/13 call to fund studies which had the potential to aid life science research. The original bid title was: "Use of microarray analysis in the characterisation of HPACC cell lines for the presence of cell biomarkers". PHE like its predecessor HPA is an executive agency sponsored by the Department of Health (England). The funding was awarded to Dr Edward Burnett of the Culture Collections of PHE; a not for profit Bio-Resource within the PHE National Infections Service (NIS). Five of the authors (James R Cooper, Muhammad Abdullatif, Edward C Burnett, Karen E Kempsell and Howard Tolley) were employed by HPA/PHE during the study but they were not and never have been members of the Pipeline Funding Board. The HPA/PHE Pipeline Funding Board had no role in study design, data collection and analysis, decision to publish, or preparation of the manuscript. Dr Franco Confort's contribution was funded by the British Lung Foundation reference number IPFPG12-2.

Competing Interests: Public Health England, the primary funder of this work and employer of five of the authors is a "not for profit" supplier of the subject of the manuscript: the A549 Cell Line. The authors have declared that no other competing interests exist. This does not alter our adherence to PLOS ONE policies on sharing data and materials.

Introduction

Alveolar Type 1 (ATI) and 2 (ATII) cells are specialised epithelial cells of the distal lung. ATI cells are flattened squamous cells that cover around 95% of the alveolar surface and lie adjacent to capillary endothelial cells to form the pulmonary gas exchange region. ATII cells have a compact morphology and cover the remaining 5% of the alveolar surface. Unlike terminally differentiated and-non replicative ATI cells, ATII cells have multiple roles and have been described as the 'defenders of the alveolus'[1,2]. The ultrastructural hallmark of ATII cells is the expression of multilamellar bodies (MLB)[3] containing dipalmitoylphosphatidyl choline (DPCC), the major lipid component of pulmonary surfactant that reduces surface tension in the alveoli to prevent collapse of the lungs at the end of expiration. ATII cells play an important role in innate immune responses within the lung with evidence that lung surfactant proteins have anti-microbial effects and reduce inflammation caused by the inhalation of irritants. ATII cells also help clear alveolar fluid through active sodium transport and they act as self-renewing progenitors to replace ATI cells that have been damaged[4] to maintain normal lung architecture[5–7].

Research into alveolar physiology and pathologies relevant to acute lung injury[8,9], and diseases such as chronic obstructive pulmonary disease (COPD)[10,11] and interstitial lung diseases such as idiopathic pulmonary fibrosis[12–15] requires *in vitro* models that represent and mimic the alveolar epithelium, in particular the ATII cell. Primary ATII cell cultures are currently considered to be the most useful *in vitro* model for alveolar research, however they are limited by tissue availability which requires ethical approval and patient consent for access to histologically normal regions of resected lung tissue surplus to requirement for diagnosis of lung carcinoma [16,17]. While these cells are useful in short term culture, they spontaneously differentiate to the ATI phenotype over 1–2 weeks[18]. Recent developments have promised the potential of alveolar models from human embryonic stem cells[19], mesenchymal stem cells[20] and induced pluripotent stem cells[21,22], however technical difficulties and issues presented by these systems have limited their widespread uptake and use. As a consequence, there is still considerable reliance and widespread use of authentic[23] continuous cancer or other immortalized cell lines. Sometimes these cell lines are derived by retroviral transduction, as has been demonstrated with mammary and endothelial tissues[24], but more commonly they have been derived from tumours—often many decades previously. These continuous cell lines have the major advantage of ease of cultivation, reproducibility and relatively unlimited supply. However, although they can maintain a stable phenotype through many subcultures if properly maintained[25], this phenotype exhibits differences compared to the original tissue, compromising their ability to fully reproduce *in vivo* physiological state. Often their use is a trade-off of 'ease of use' against suitability, as the cells typically retain features more associated to the original tumour, including uncontrolled proliferative growth and a de-differentiated phenotype. One such commonly used cell model is the lung carcinoma cell line A549. Isolated in 1973 from a pulmonary adenocarcinoma[26] and subsequently characterized as being representative of ATII cells[3,27–29], this cell line has been a mainstay of respiratory research for nearly four decades. However while work with early passage A549 cells provided evidence of their ability to exhibit features of an ATII epithelial cell phenotype[27–29], more recent studies have led to conflicting results[30,31]. Based on early work with A549 cells which reported that extended culture resulted in cellular 'differentiation', as evidenced by high numbers of MLB [3,32], we tested the hypothesis that culture conditions that reduce proliferation of the A549 cell line would promote a more differentiated ATII cell phenotype, as evidenced by mRNA gene expression profiling over time, by comparison with primary cultures of ATII cells and by histological and ultrastructural analysis.

Materials and Methods

Cell Culture

Authentic A549 cells (European Collection of Cell Cultures (ECACC), Salisbury, UK), catalogue number 86012804, were cultured in either Ham's F12 Nutrient Medium (Ham's F12) or Dulbecco's Modified Eagles Medium (DMEM) (both from Sigma Aldrich, Dorset, United Kingdom) supplemented with 2mM L-Glutamine and 10% v/v Foetal Bovine Serum (FBS) (Hyclone SH30071.03 (Hyclone Laboratories, Utah, USA). Proliferative cultures were incubated at 37°C in a humidified 5% CO_2 incubator and subculture carried out by washing the cell monolayers twice with calcium and magnesium-free phosphate buffered saline (PBS) (Severn Biotech (Kidderminster, UK, catalogue number 20–74) followed by addition of 1x Trypsin/EDTA solution (Sigma Aldrich) and incubation at 37°C until the cells detached. Trypsin was inactivated by the addition of growth medium before seeding into fresh flasks at densities of 1.5-2x10^4 cells/cm^2. For the long term 25 day cultures A549 cells were seeded into replicate T25 flasks and medium changed every 2–4 days. Phase contrast images were captured of the monolayers throughout the time course. Cell numbers, viability and size were assessed by Trypan Blue staining and by DAPI dye exclusion using the Nucleocounter™ 3000 viability assay (Chemometec, Allerod, Denmark).

RNA Extraction

Cells were harvested using trypsin/EDTA, counted and washed with PBS by centrifugation at 500g for 5 minutes and snap frozen in pellets of 1.5 x 10^6 cells before storage at -80°C prior to RNA extraction. RNA was extracted using the Promega Maxwell® Low Elution Volume (LEV) Simply RNA Cell kit according to the manufacturer's instructions. In brief 16 samples were processed at a time. Pellets were thawed rapidly and as briefly as possible in a 37°C water-bath, transferred to wet ice where 200μl of homogenisation solution was added to each sample and vortexed to mix before the addition of 200 μl of lysis solution and another vortex mix prior to loading into the Maxwell® cassettes. DNAse was added to remove contaminating genomic DNA. RNA was eluted into 50μl of nuclease free water and supplemented with RNAse inhibitor ("Superase In™", Ambion, Life Technologies, Paisley, UK) before being quantified by spectrophotometry (Nanodrop, Labtech International, Uckfield East Sussex UK) and analyzed by electrophoresis in a 1.4% agarose (Sigma Aldrich) gel and visualised using Ethidium Bromide and UV illumination to ensure there were intact 18S and 28S bands. Extracted RNA was stored at -80°C before RNA microarray analysis prior to which repeat assessment of RNA integrity was carried out using a bio-analyzer (BioAnalyzer 2100, Agilent Technologies, Santa Clara, USA).

Primary ATII Cells

Primary ATII cells were isolated by protease digestion and selective adherence according to published protocols[16] and the commonly adopted strategy of using macroscopically normal tissue from three ex-smokers undergoing lung resection: Donor 1 (female, aged 57), Donor 2 (female, aged 69) and Donor 3 (male, aged 69). Written consent from the donors of the primary lung tissue was given under the governance of the National Health Service (NHS) England Southampton and South West Hampshire 'A' Research Ethics Committee. Local Research Ethics Committee (LREC) Reference Number 08/H0502/32.

The purified ATII cells were re-suspended in DCCM-1 medium (Biological Industries, Israel) supplemented with 1% penicillin, 1%streptomycin and 1% L-glutamine and 10% NCS before plating on collagen I (PureCol 5005-b, Advanced BioMatrix Inc, Carlsbad, USA) coated

24 well plates at 60% confluence. The presence of ATII cells was confirmed by staining for alkaline phosphatase. Replicate RNA samples were isolated from wells of the 24 well plate using Trizol according to the manufacturer's instructions (Life Technologies, Paisley, UK).

QRT-PCR. The extracted RNA was quantified (Denovix, Wilmington, Delaware, USA) and 3ng of each of the RNA samples was then reverse transcribed to cDNA using the Superscript ® II Reverse Transcriptase Kit (Oligo dt) (Life Technologies, Paisley, UK) to the manufacturer's instructions.

QRT PCR was performed on the cDNA using a Quant-Studio 7 thermocycler (Life Technologies, Paisley, UK), and curated Taqman assays (SFTPA1 (Taqman assay ID Hs00831305_m1), SFTPA2 (Taqman assay ID Hs00359837_m1), SFTPB (Taqman assay ID Hs01090667_m1), SFTPC (Taqman assay ID Hs00161628_m1), SFTPD (Taqman assay ID Hs01108490_m1) (Life Technologies, Paisley, UK) using delta-delta Ct analysis to determine relative gene expression [33]. Ct values were normalised to the geometric means of those obtained from the reference genes topoisomerase (TOP1) (Taqman assay ID Hs00243257_m1) and ATP synthase subunit beta, mitochondrial (ATP5B) (Taqman assay ID Hs 00969569_m1) based on the results of a 'genorm' analysis[34] to determine the optimal reference genes. cDNA from log phase A549 cultures was used as the baseline for comparison of relative gene expression for all surfactant proteins except SFTPA2, where cDNA from 25 day differentiated A549 was used.

RNA Microarray Analysis

cRNA labelled with Cyanine 3 was generated from the extracted RNA samples using the Agilent Single Color Low Input Quick Amp Labelling kit and purified prior to hybridisation to Agilent Human Single Color 39494 array slides. Genespring version 13 (Agilent Technologies, Santa Clara, USA). Data was quality controlled by excluding any compromised entities and only entities where all replicates were either detected or not detected. Samples were normalised by shift to the 75th percentile and the baseline transformation on the median of all samples and statistical and comparative analysis at the probe and gene level using parametric statistical analyses including analysis of variance (one way ANOVA) with Benjamini and Hochberg False Discovery Rate (BH FDR) correction. Pathway analyses using Genespring and Wiki Pathways [35–37] were carried out on genes up or down regulated at a fold change of two or more and on the genes shared with differentiated A549 and the ATII cells.

Oil Red O staining

Cell monolayers were rinsed with phosphate buffered saline (PBS), fixed with two applications of 10% formalin before rinsing with purified water followed by addition of 60% isopropanol and air drying. The cells were stained using Oil red-O (Sigma Aldrich, Dorset, UK) (0.21g/ml in isopropanol, filtered), rinsed four times in purified water before imaging by light microscopy.

Transmission Electron Microscopy

Cells were fixed in 2.5% glutaraldehyde solution before staining in osmium tetroxide and embedding in Araldite resin. The resulting blocks were sectioned, placed onto grids before further staining with 2% uranyl acetate and 0.1% lead citrate. Sections were imaged by transmission electron microscopy using Philips CM100 (Philips Electron Optics, Cambridge, UK) and Hitachi H7000 instruments (Hitachi Group, Maidenhead, Berkshire, UK).

To determine the proportion of cells expressing MLBs, 164 cells were assessed by direct counting of TEM micrographs.

Results

It is not clear from the literature which media might induce the most ATII—like phenotype in cultured A549 cells. We compared the effects of two media: Ham's F12 and DMEM on cell proliferation. After 24 hours of plating, the cells cultured in either medium appeared morphologically similar with mitotic cells evident in both conditions. Cells continued to divide as the cultures progressed, however there appeared to be more cell division, crowding and piling up of cells in DMEM (Fig 1A). In contrast, in Ham's F12, the cells displayed a more flattened contact-inhibited quiescent appearance that was maintained until the cultures were terminated at day 25 (B). At this point, cell counts determined using two independent methods demonstrated that culture of cells in DMEM yielded significantly more cells than Ham's F12 (Fig 2A and 2B). Although there was no difference in cell viability between the two culture conditions, cells grown in DMEM had a significantly smaller diameter (Fig 2C and 2D). A series of photomicrographs comparing the growth and morphology over the time course is included in S1 Fig. Closer examination of the cells cultured in Ham's F12 showed the presence of organized vesicles of uniform size within the cells (Fig 1B and S1H Fig (inset)) suggesting the possibility of cellular differentiation.

To obtain deeper insight into the changes occurring in A549 cells during long term culture in Hams F12, we used RNA microarray analysis to evaluate how gene expression changed in comparison with log phase cells. BH FDR corrected ANOVA analysis of microarray data demonstrated that of the 39,013 genes examined, 5,346 were significantly up or down regulated ($p<0.05$) during the 25 day time course and, of these, 3,926 were up or down regulated with a fold change of two or greater (Fig 3). Pathway analysis of the genes regulated at a fold change of two or more highlighted nineteen pathways with significant p values involved with aspects of cell cycle regulation (Table 1). Within these pathways, the markers of proliferation KI-67, PCNA and TCF7L1 were down regulated and the inhibitor of cell cycle progression CDKN1B was upregulated during the 25 day time-course (see S2 Fig). These findings are consistent with reduced proliferation in the cultures over 25 days of culture in Ham's F12.

In addition to a reduction in expression of genes involved in cell proliferation, a small number of pathways involved in cellular autophagy, senescence and apoptosis were modulated during long term culture (Tables 2 and 3). In contrast, there were 28 pathways related to differentiation of epithelial and endodermal tissues (Table 4). For example, WNT4, which has been implicated in lung development and repair, was upregulated as were the pluripotency markers

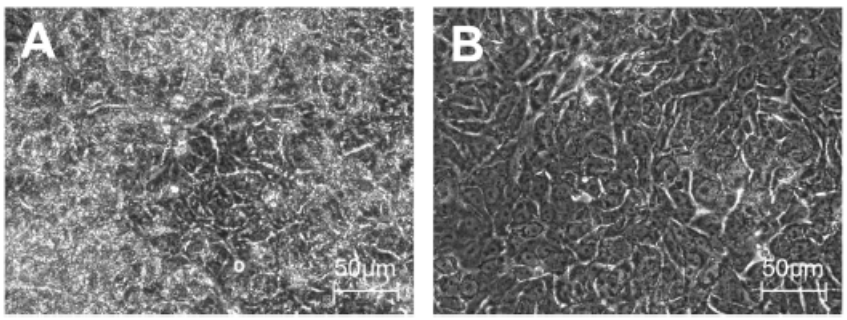

Fig 1. Phase contrast images of A549 monolayers. Images show the differences in morphology of 25 day continuous culture in DMEM (A) or Ham's F12 (B).

doi:10.1371/journal.pone.0164438.g001

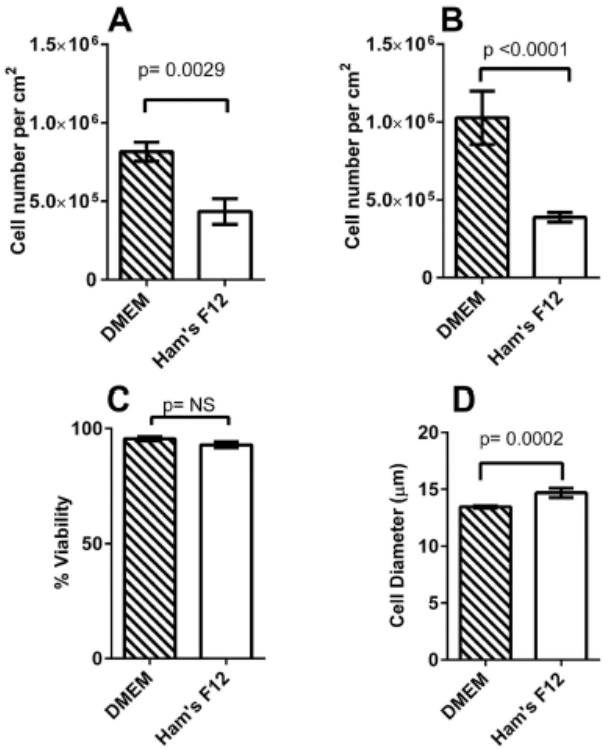

Fig 2. Cell metrics. Cell counts, viability and cell diameters from A549 cell cultures at day 25. A: cell yield per unit area based on cell counting using Trypan blue dye exclusion (n = 3) and B: cell numbers as measured by automated cell counting (n = 5). C: Cell viability based on DAPI dye exclusion (n = 5). D: cell diameter using automated image analysis (n = 5). Data are plotted as mean ± SD; statistical analyses in A, B and D used unpaired Student's T Test. In C statistical testing showed no significant difference (NS).

doi:10.1371/journal.pone.0164438.g002

Nanog and SOX2. Parallel up-regulation of SOX9 was also observed along with the WNT target Metalloproteinase 7 (MMP7) (see S3 Fig). A feature suggestive of ATII cell differentiation was significant expression of complement component pathways with, for example, increased expression of C3, C4b and C5 (S4 Fig). In addition to induction of differentiation pathways, Table 5 shows 10 pathways involved in lipid metabolism that achieved statistical significance over the 25 day time course.

To determine whether modulation of A549 cell growth and differentiation resulted in their transition towards an ATII cell phenotype, we compared gene expression of the long term cultured A549 cells to that of freshly isolated human primary ATII cultures. Comparison of relative gene expression using primary ATII cells from three donors showed a similar pattern of expression of five surfactant proteins (SFTPD, A2, A1, B and C) (S5 Fig); therefore we selected Donor 2 for RNA microarray studies to represent normal ATII cells. In this analysis each of the time-points of A549 differentiation and the primary ATII cells was compared to log phase

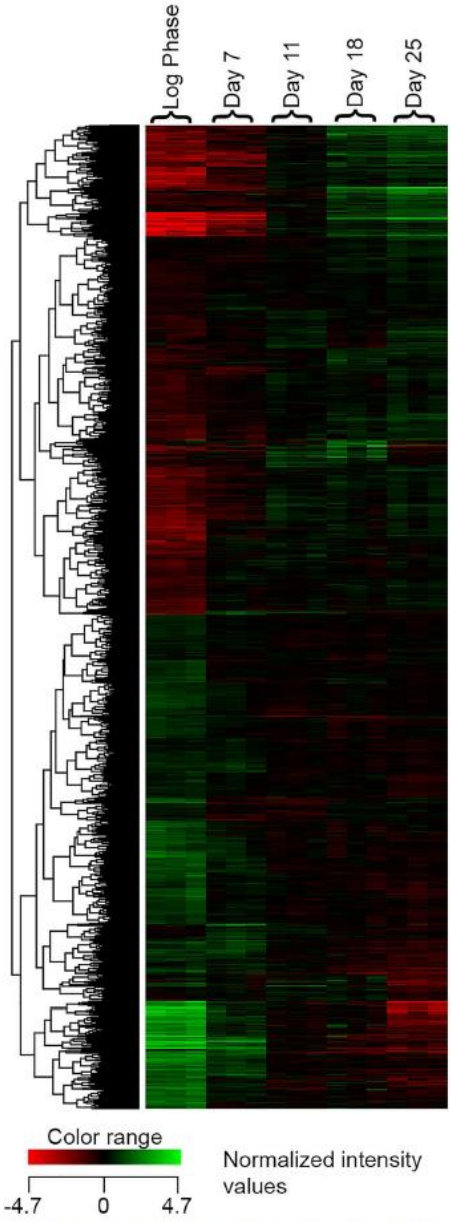

Fig 3. RNA Microarray Heatmap of Gene Expression. Hierarchically clustered (Euclidian similarity measure, clustered using Ward's linkage rule) heat map of gene expression changes in A549 cells cultured in Ham's F12 for up to 25 days; the heat map shows normalised intensity values of significant genes regulated up or down two-fold or more.

doi:10.1371/journal.pone.0164438.g003

Table 1. Pathways Associated with Cell Cycle Control.

Pathway	Wiki-Pathway Reference	P Value	Number of regulated genes	Number of genes in pathway
Cell Cycle	WP179 70629	<0.001	51	103
S Phase	WP2772 77049	<0.001	46	116
Mitotic G1-G1-S phases	WP1858 76928	<0.001	46	120
Mitotic Metaphase and Anaphase	WP2757 77009	<0.001	57	153
Synthesis of DNA	WP1925 76968	<0.001	39	94
Nuclear Receptors Meta-Pathway	WP2882 78569	<0.001	80	318
RB in Cancer	WP2446 78573	<0.001	55	87
Mitotic Prometaphase	WP2652 76819	<0.001	54	98
DNA Replication	WP466 76196	<0.001	31	42
G1 to S cell cycle control	WP45 71377	<0.001	34	68
Telomere Maintenance	WP1928 76893	<0.001	24	37
Cell Cycle Checkpoints	WP1775 76816	<0.001	38	115
Nucleosome assembly	WP1874 76826	<0.001	15	22
miRNA Regulation of DNA Damage Response	WP1530 78503	<0.001	28	98
DNA Damage Response	WP707 78527	<0.001	27	68
Mitotic G2-G2-M phases	WP1859 77022	<0.001	31	89
M-G1 Transition	WP2785 77074	<0.001	27	79
Regulation of DNA replication	WP1898 76824	<0.001	18	70
Mitotic Prophase	WP2654 76823	0.002	12	44

Statistically significant pathways associated with cell cycle contrl for genes expressed over the 25 day time-course of A549 differentation in Ham's F12 medium. Pathways were identified by Genespring pathway analysis after one way ANOVA of all of time points compared to log-phase A549 cells (P cut off = 0.05, Fold change ≥ 2.0).

doi:10.1371/journal.pone.0164438.t001

A549 cells as the point at which it is assumed that most researchers would use their A549 cells in experiments.

The RNA microarray comparison of primary ATII cells with long term cultured A549 showed that for a minimum of fold change of two, the number of shared up regulated genes increased from 280 at day 7 of the differentiation time-course to 591 at day 25. Similarly the number shared down regulated genes increased from 458 at day 7 to 796 at day 25 (Fig 4). Analysis of the shared up regulated genes (Table 6) indicated pathways involved with the Complement System (C3 and C4b), senescence and autophagy, lipid metabolism (including fatty acid biosynthesis, adipogenesis, sphingolipid metabolism, cholesterol and lipid homeostasis, peroxisome proliferator activated receptor alpha), endodermal and cellular differentiation and TGF beta signalling.

Table 2. Pathways Associated with Apoptosis.

Pathway	Wiki-Pathway Reference	P Value	Number of regulated genes	Number of genes in pathway
Apoptosis	WP254 78808	0.021	17	84
FAS pathway and Stress induction of HSP regulation	WP314 71366	0.033	9	38
Apoptotic execution phase	WP1784 76813	0.033	10	46

Statistically significant pathways associated with apoptosis for genes expressed over the 25 day time-course of A549 differentiation in Ham's F12 medium. Pathways were identified using Genespring pathway analysis after one way ANOVA of all of the time points compared to log-phase A549 cells (P cut off = 0.05, Fold change ≥ 2.0).

doi:10.1371/journal.pone.0164438.t002

Table 3. Pathways Associated with Senescence and Autophagy.

Pathway	Wiki-Pathway Reference	P Value	Number of regulated genes	Number of genes in pathway
Senescence and Autophagy	WP615 71375	<0.001	32	106
AMPK Signaling	WP1403 78804	0.006	16	68
Folate Metabolism	WP176 74202	0.020	14	67

Statistically significant pathways associated with senescence and autophagy for genes expressed over the 25 day time-course of A549 differentiation in Ham's F12 medium. Pathways were identified using Genespring pathway analysis after one way ANOVA of all of the time points compared to log-phase A549 cells (P cut off = 0.05, Fold change ≥ 2.0).

doi:10.1371/journal.pone.0164438.t003

Table 4. Pathways Associated with Epithelial and Endodermal Differentiation.

Pathway	Wiki-Pathway Reference	P Value	Number of regulated genes	Number of genes in pathway
miR-targeted genes in epithelium—TarBase	WP2002 78530	<0.001	69	345
Complement and Coagulation Cascades	WP558 67786	<0.001	21	64
TGF Beta Signaling Pathway	WP366 69026	<0.001	21	55
TGF Beta Signaling Pathway	WP560 68944	<0.001	21	55
Cell junction organization	WP1793 77057	<0.001	20	61
Human Complement System	WP2806 78589	<0.001	28	136
Signaling by TGF-beta Receptor Complex	WP2742 76980	<0.001	13	36
Focal Adhesion	WP306 78800	<0.001	41	188
Integrin cell surface interactions	WP1833 77019	<0.001	19	64
Oncostatin M Signaling Pathway	WP2374 73668	<0.001	19	65
Integrin-mediated Cell Adhesion	WP185 71391	<0.001	24	99
Complement cascade	WP1798 77042	<0.001	13	192
Assembly of collagen fibrils and other multimeric structures	WP2798 77089	8.62E-04	11	33
Endoderm Differentiation	WP2853 78496	<0.001	18	146
Differentiation Pathway	WP2848 78558	0.001	14	50
Wnt Signaling Pathway and Pluripotency	WP399 74897	0.003	22	100
Cell Differentiation—meta	WP2023 68892	0.005	7	67
ID signaling pathway	WP53 67360	0.006	6	16
Prostaglandin Synthesis and Regulation	WP98 72088	0.008	9	31
Cell surface interactions at the vascular wall	WP1794 77039	0.008	19	91
Constitutive Androstane Receptor Pathway	WP2875 78537	0.009	8	32
EGF-EGFR Signaling Pathway	WP437 78502	0.010	30	162
Complement Activation, Classical Pathway	WP545 72062	0.011	6	17
Angiogenesis	WP1539 78807	0.015	7	24
Mitotic Telophase-Cytokinesis	WP2765 77030	0.020	5	14
Activation of Matrix Metalloproteinases	WP2769 77041	0.035	5	16
Gap junction trafficking and regulation	WP1820 76886	0.042	3	8
Wnt Signaling Pathway	WP428 78532	0.046	12	61

Statistically significant pathways associated with epithelial and endodermal differentiation for genes expressed over the 25 day time-course of A549 differentiation in Ham's F12 medium. Pathways were identified by Genespring pathway analysis after one way ANOVA of all of the time points compared to log-phase A549 cells (P cut off = 0.05, Fold change ≥2.0).

doi:10.1371/journal.pone.0164438.t004

Table 5. Pathways Associated with Lipid Synthesis and Metabolism.

Pathway	Wiki-Pathway Reference	P Value	Number of regulated genes	Number of genes in pathway
Adipogenesis	WP236 78584	<0.001	38	131
SREBF and miR33 in cholesterol and lipid homeostasis	WP2011 75253	<0.001	9	18
Nuclear Receptors in Lipid Metabolism and Toxicity	WP299 78587	<0.001	12	35
Ganglio Sphingolipid Metabolism	WP1423 76323	0.002	7	18
Signal Transduction of S1P Receptor	WP26 78492	0.005	8	25
Cholesterol biosynthesis	WP1795 77044	0.020	6	21
Regulation of Lipid Metabolism by Peroxisome proliferator-activated receptor alpha (PPARalpha)	WP2797 77088	0.025	21	118
Globo Sphingolipid Metabolism	WP1424 71392	0.026	6	24
Cholesterol Biosynthesis	WP197 78758	0.027	5	15
Fatty Acid Biosynthesis	WP357 70641	0.041	6	22

Statistically significant pathways associated with lipid synthesis and metabolism for genes expressed over the 25 day time-course of A549 differentiation in Ham's F12 medium. Pathways were identified using Genespring pathway analysis after one way ANOVA of all of the time points compared to log-phase A549 cells (P cut off = 0.05, Fold change ≥ 2.0).

doi:10.1371/journal.pone.0164438.t005

Table 7 summarizes the fold changes in gene expression in a selection of key genes and markers involved in ATII differentiation in our experiments by comparing the relative fold change difference of differentiated A549 cells and primary ATII cells compared to log phase A549 cells. ATP lipid transporters have been associated with the organized transport of lipids into developing MLB and are considered a key marker of ATII cells. ABCA3 was expressed in abundance in the primary ATII cells but not significantly upregulated in the differentiated A549 cells. However, other lipid transporters were significantly upregulated in differentiated A549 cells (S6 Fig).

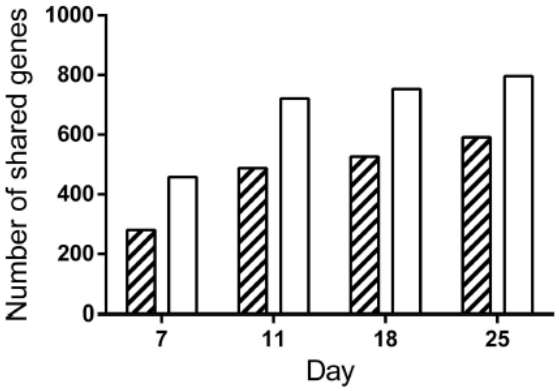

Fig 4. Shared up regulated (≥ 2 fold) gene expression of differentiated A549 with freshly isolated human primary ATII cultures. Gene expression in A549 cells that were cultured for 7, 11, 18 or 25 days or primary ATII cells were compared to log phase A549 cells. The figure shows the number of shared up- (hatched bars) or down- (clear bars) regulated genes between the A549 cells and ATII cells over the A549 time course.

doi:10.1371/journal.pone.0164438.g004

Table 6. Pathways Considered to be Associated with ATII Phenotype.

Pathway	Wiki Pathways Reference	Most significant timepoint (Day)	P Value	Number regulated genes	Number genes in pathway
Complement cascade	WP1798 77042	25	<0.001	9	192
Human Complement System	WP2806 78589	18	<0.001	12	136
Senescence and Autophagy	WP615 71375	25	<0.001	9	106
Complement Activation, Classical Pathway	WP545 72062	25	<0.001	4	17
Complement and Coagulation Cascades	WP558 67786	18	<0.001	6	64
Adipogenesis	WP236 78584	11	<0.001	10	131
Differentiation Pathway	WP2848 78558	11	0.001	5	50
Globo Sphingolipid Metabolism	WP1424 71392	18	0.005	3	24
Sphingolipid Metabolism	WP1422 78591	25	0.006	3	21
Sphingolipid metabolism	WP2788 77079	25	0.010	4	46
SREBF and miR33 in cholesterol and lipid homeostasis	WP2011 75253	11	0.026	2	18
Ganglio Sphingolipid Metabolism	WP1423 76323	7	0.010	2	18
Regulation of Lipid Metabolism by Peroxisome proliferator-activated receptor alpha (PPARalpha)	WP2797 77088	11	0.009	6	118
TGF Beta Signaling Pathway	WP366 69026	7	0.013	3	55
TGF Beta Signaling Pathway	WP560 68944	7	0.013	3	55

Statistically significant pathways considered to be associated with ATII phenotype. Two fold (or greater) upregulated genes shared with primary ATII cells and differentiated A549 cells over the 25 day time-course identified by Genespring pathway analysis of Venn diagram analysis of the two cell populations.

doi:10.1371/journal.pone.0164438.t006

To confirm the presence of lipidogenesis and possible MLB formation, differentiated A549 monolayers were stained with Oil-red-O. This showed that lipid production increased over the time course of differentiation (Fig 5A–5D) and was manifested by an increase in number and size of lipid inclusions, with more than half of the cells in the monolayer at day 18 showing evidence of lipid containing bodies. However from this staining it was not possible to discriminate MLB from oil droplets within the cells. Therefore, TEM microscopy was performed to assess the ultrastructure of the lipid droplets. At day 11, lipid droplets appeared as uniform structures with no evidence of MLB formation (Fig 6A and 6C). However by day 21 of differentiation, the lipid containing structures showed clear evidence of MLB formation (Fig 6B and 6D) with a distribution similar to that identified by the oil red-O staining. A differential count of 164 cells in TEM micrographs of long term differentiated A549 cells showed that 90 (54.9%) of the cells examined contained MLBs.

Discussion

In this study, we report that long term culture of A549 cells in Ham's F12 medium resulted in substantial suppression of genes involved in cell division in association with significant up-regulation of genes involved in autophagic, differentiation and lipidogenic pathways. There were also increased numbers of up- and down-regulated genes shared with primary ATII cells isolated using conventional methodology[31] suggesting adoption of some ATII characteristics including multilamellar body (MLB) development, a feature which was confirmed by electron microscopy. This work defines a set of conditions for promoting ATII differentiation characteristics in A549 cells that may be advantageous for functional studies with these cells. Novel alternative methods for ATII preparation have been defined from which future studies may benefit[38].

The evidence for the A549 cell line's suitability as an *in vitro* ATII model is conflicting and is not fully explored in contemporary literature. The cell line was originally reported to have

Table 7. Genes Related to ATII Differentiation.

Gene Symbol	Up or Down Regulation in A549 Cells throughout time-course	Fold Change at Day 25 in A549 Cells	Up or Down Regulation in ATII primaries compared to log phase A549	Fold Change (ATII vs log Phase A549)
Proliferation Markers				
Ki67	Down	-5.08	Down	-15.83
PCNA	Down	-2.19	Down	-6.17
TCF7L1	Down	-5.85	N/S	
Cell Cycle Inhibitor				
CDKN1B	Up	3.05	N/S	
Lipid Metabolism				
PPAPDC1B	Up	2.45	N/S	
PPAPDC1A	N/S		Up	15.19
PPAP2A	Up	2.62	Up	7.03
PPAP2B	Up	2.90	N/S	
DGAT2	Up	3.21	N/S	
FABP5	Down	-5.96	Down	-3.6
ACSL5	Up	16.00	Up	16.00
Autophagy and Lysosomal				
ULK4	Up	3.64	Down	-3.53
LAMP2	Up	2.08	Up	3.23
LAMP3	Up	2.65	Up	16.00
PLD1	Up	2.0	N/S	
PLD2	N/S		Up	2.83
PLD5	Up	4.97	N/S	
WNT Associated Differentiation				
CASP1	Up	16.00	Up	16.00
CASP4	Up	6.28	Up	16.00
BIRC5	Down	-16.00	Down	-16.00
WNT4	Up	12.10	Up	6.12
Stem Cell Markers and Differentiation				
NANOG	Up	4.06	Up	N/S
SOX2	Up	3.19	Up	4.75
SOX9	Up	2.79	N/S	
Complement Components				
C3	Up	14.92	Up	16.00
C4B	Up	12.00	Up	9.06
C4BPA	Up	16.00	Up	16.00
C5	Up	6.31	Down	-3.25
Cellular Differentiation				
IL1B	Up	16.00	Up	15.56
AGT	Up	16.00	Up	9.92
PPARA	Up	3.71	Up	4.16
FST	Up	8.81	Up	7.75
BMP4	Up	13.65	Up	7.98
TGFBR2	Up	2.93	Up	2.81
ATP Lipid Transporters				
ABCA3	N/S		Up	4.26
ABCC6P1	Up	5.07	Up	16.00
ABCC3	Up	2.7	Down	-8.11

(*Continued*)

Table 7. (*Continued*)

Gene Symbol	Up or Down Regulation in A549 Cells throughout time-course	Fold Change at Day 25 in A549 Cells	Up or Down Regulation in ATII primaries compared to log phase A549	Fold Change (ATII vs log Phase A549)
ABCG1	Up	4.35	Down	-3.44
ABCA1	Up	2.48 (Day 7)	N/S	
ABCA8	Up	4.09	N/S	
ABCA12	Up	3.45	Up	5.06
ABCB4	Up	16.00	N/S	
ABCG2	Up	2.05	Down	-16.00
ABCD3	Down	-3.30	Down	-2.67
ABCC11	Up	4.45	N/S	
Matrix Metalloproteinases				
MMP1	Up	5.76	Up	16.00
MMP15	Down	-3.45	N/S	
MMP7	Up	6.65	Up	2.98
MMP9	Down	2.41	N/S	

Comparison of genes related to ATII differentiation in 25 day differentiated A549 cells grown in F12 compared to ATII Primary Cells compared to ATII Primary Cells using the gene expression of log phase proliferating A549 cells as a baseline.

doi:10.1371/journal.pone.0164438.t007

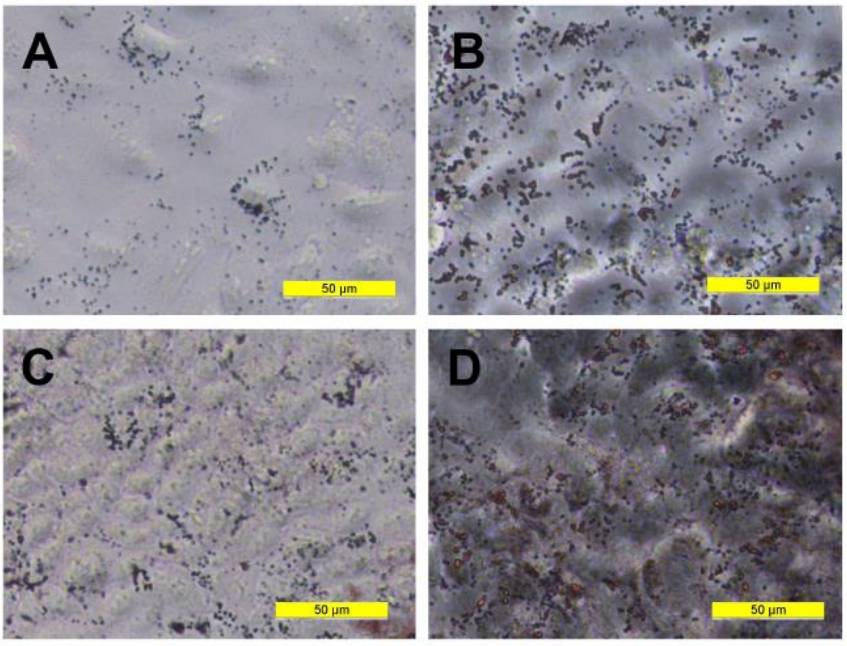

Fig 5. Oil-Red-O Staining of A549 Monolayers. Phase contrast images of Oil-Red-O staining of lipid droplets in log phase A549 monolayers grown in Ham's F12 medium in log phase (A), and cells in the same medium for 7 (B), Day 11 (C) and Day 18 (D) days.

doi:10.1371/journal.pone.0164438.g005

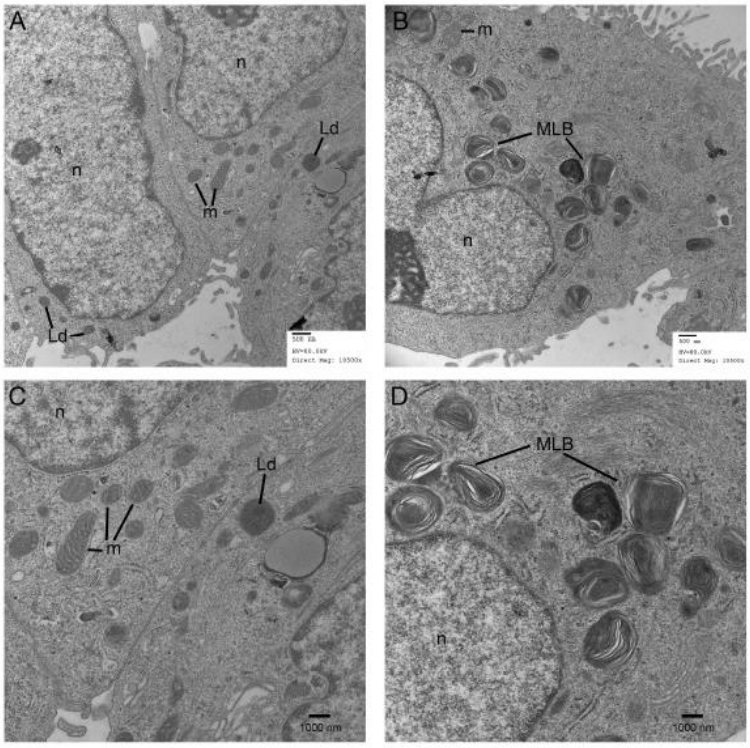

Fig 6. Electron Micrographs Showing Multilamellar Body Expression in A549 Cells. Transmission electron micrographs of sections of A549 cells after 11 (A and C) or 21 (B and B) days of culture in Ham's F12. Lipid bodies (Lb), mitochondria (m), nuclei (n) and multilamellar bodies (MLB) are identified. Scale bars = 500 and 1000 nm.

doi:10.1371/journal.pone.0164438.g006

morphological and ultrastructural similarities to ATII cells. As long ago as 1978[3], Shapiro et al showed that by three weeks in continuous culture, cell division in A549 cells, as measured by DNA content, was low and the authors considered the cells as 'differentiated' as confirmed by the expression of high numbers of MLB similar in phospholipid content to those found in primary lung tissue. These findings were later supported by Nardone et al[29].

It is now well established that environmental factors such as choice of substratum, medium and continuous culture can have a substantial impact on the phenotype and gene expression. For example epithelial differentiation can be induced in continuous cell lines such as CaCo2 [39] and MDCK[40] through the application of well-defined long term cell culture conditions. From the literature, it is evident that pulmonary researchers have not been consistent in the formulation of cell culture medium used in their experiments nor with the phase of growth from which the A549 cells are used. The cell line was originally isolated using RPMI medium [3] yet subsequent researchers have used a number of different media with little or no justification for their choice. By way of example, concerns for the cell line's suitability were raised in 1980[41] with A549 cells cultivated in DMEM and subjected to a 10 day differentiation period.

In this case the MLB content of the cells could be increased with 2 days of serum starvation, however, the lipid content of these A549 cells differed significantly from freshly isolated rat primary ATII cells and the authors advised that the cell line should be considered as a model of ATII dysfunction. More recently, using Raman spectroscopy to investigate the biochemical characteristics of A549 cells, Swain et al[30] cast further doubt on the A549 cell line's performance as an ATII model but used cells grown in DMEM. Heijink et al[42] also reported functional deficiencies of the cell line using cells grown in RPMI 1640 medium. Based on our observations that DMEM supports a proliferative phenotype even in long term culture, it is possible that inconsistency in the choice of medium and/or culture duration used for A549 experiments may contribute to variability in phenotypic properties. This highlights the need for standardization in the use of A549 cells, and speaks to a larger problem that has been identified in life science research[43].

One of the key roles of ATII cells *in vivo* is to secrete surfactant, thus surfactant lipid production and evidence of MLB biogenesis in A549 cells, as originally reported[27] is supportive of their suitability as an ATII model. Lung surfactant has a role in immune protectiveness and the production of complement[44] and our finding of up-regulated gene expression of C3, C4b and C5 suggest the synthesis of components of the classical and alternate complement pathways by the long term A549 cell cultures consistent with their differentiation into a more ATII-like phenotype.

It is generally accepted that MLB biogenesis can be achieved by *de novo* synthesis of DPPC or alternatively through cellular autophagy[45,46]. Since MLB are thought to be lysosomal in origin, the expression of the Lysosomal Associated Membrane Proteins (LAMP) 2, and 3 [46,47] and the lytic phospholipase enzymes PLD1 and 5[45] observed in the present study suggest that the long-term A549 cultures are developing lysosomes. Our data and pathway analyses further support the involvement of autophagy in MLB biogenesis with upregulation of autophagic pathways including the autophagy gene ULK4[48] in the long term A549 cultures. Autophagy seems to be an important process in the early development of the lung in particularly in the intervening period of starvation between birth and nutrient supply from maternal lactation. Autophagy provides a nutritional bridge at this critical stage at which point the lung has to adapt from an environment of amniotic fluid to breathing air and the immediate secretion of surfactant from MLBs[49]. Failure to respond in this manner can lead to infant respiratory distress syndrome[50] and mice with targeted deletions of individual autophagy genes such as ATG16L1[51,52] have high mortality rates in their offspring.

Lipid and fatty acid (FA) precursors for DPPC are not only derived from autophagy in the development of MLB, they can also be synthesized *de novo*. In adults it is thought that FAs are sequestered from the circulation via Fatty Acid Binding Proteins (FABP)[1], however our data show that FAB5 is down regulated throughout the A549 time course and in primary ATII cells, perhaps indicating that there are insufficient FAs provided in the culture medium or that the cells have switched to autophagic and biosynthetic generation of FAs. The significant upregulation of genes involved in lipid biosynthesis and metabolism support this hypothesis.

Membrane bound ATP lipid transporters, for example ABCA3[53], have been associated with the organized transport of lipids into developing MLB and are considered a key marker of ATII cells. Although ABCA3 was not significantly upregulated in the differentiated A549 cells, other ATP lipid transporters are involved MLB formation and surfactant production. For example ABCA1, 2, 3, and 5, have been implicated[54] and ABCA2 has been shown to be associated with the limiting membranes of MLB while other work has demonstrated that ABCA1 is enriched in the lung[55]. Our results with long-term cultures of A549 cells show the upregulation of several candidate ATP Lipid transporters that could play a part in MLB assembly.

Analysis of up-regulated genes that are shared between primary ATII cells and differentiated A549 confirmed that over the 25 day time-course of differentiation the A549 cell line became more similar in terms of gene expression to the ATII cells than log phase A549 cells. However while the 25 day differentiated A549 cultures are more similar to primary ATII cells there are still many differences. This may be because A549 cells retain an abnormal phenotype as a consequence of their malignant background, or because they consist of a phenotypically heterogeneous population possibly due to the presence of cancer stem cells with the potential to differentiate to ATII or non-ciliated bronchial cell types [32]. Increases in expression of the progenitor cell markers SOX2, SOX9 and NANOG in A549 cells seen in the present study could be indicative of the presence of such a cancer stem cell population[56].

As with all models, recapitulation of the *in vivo* state is imperfect but the aim is to reproduce, as faithfully as possible those aspects of the physiology (or pathology) that are being investigated. The gene expression data of the A549 time-course, the upregulated pathways and genes shared with primary ATII cells together with the confirmatory TEM data demonstrates that we have defined a reproducible and standard set of conditions for promoting ATII differentiation characteristics in A549 cells. In conclusion, we suggest that whereas proliferating log-phase A549 cells are most suitable for cancer biology studies, the new long term culture system would be more suitable for *in vitro* studies requiring a more representative and continuous source of ATII-like cells.

Supporting Information

S1 Fig. Images show the differences in morphology over 25 days of continuous culture in DMEM (top row, A-D) or Ham's F12 (bottom row, E-H). Photomicrographs show morphology at day 1 (A and E), days 8 (B and F) and 14 (C and G) and day 25 (D and H). (Inset in H shows higher magnification of cells displaying organized vesicles in F12, inset in D shows a higher magnification of cells grown in DMEM for comparison).
(TIF)

S2 Fig. Box and whisker plots of microarray RNA gene expression in A549 monolayers grown in Ham's F12 (normalized intensity values) of proliferation markers Ki-67 (A), PCNA (B) and TCF7L1 (C) and cell cycle inhibitor CDKN1B (D) over the 25 day time course. 'Day 0' is representative of log phase A549 monolayers.
(TIF)

S3 Fig. Box and whisker plots of microarray RNA gene expression in A549 monolayers grown in Ham's F12 (normalized intensity values) of the expression of WNT4 (A), Nanog (B), SOX2 (C), SOX9 (D) and MMP7 (E). 'Day 0' is representative of log phase A549 monolayers.
(TIF)

S4 Fig. Box and whisker plots of microarray RNA gene expression in A549 monolayers grown in Ham's F12 (normalized intensity values) of the expression of complement components C3 (A), C4b (B) and C5 (C). 'Day 0' is representative of log phase A549 monolayers.
(TIF)

S5 Fig. Relative expression of surfactant protein genes by delta-delta Ct QRT PCR Taqman analysis of human primary ATII isolated from three separate donors. Donor 1 (chequered bars), Donor 2 (hatched bars) and donor 3 (speckled bars). ATII cells from Donor 2 were used for the RNA micro array analysis. ATP5B and TOP1 were used as reference genes. SFTPD, A1, B and C expression was relative to log phase A549 cells. SFTPA2 expression was relative to 25

day differentiated A549 cells.
(TIF)

S6 Fig. Box and whisker plots of microarray gene expression in A549 monolayers grown in Ham's F12 (normalized intensity values) of RNA expression ATP-binding cassette lipid transporters; ABCC11 (A), ABCC3 (B), ABCG1 (C), ABCA1 (D), ABCD4 (E), ABCC8 (F), ABCA12 (G), ABCB4 (H), ABCG2 (I), ABCC6P1 (J), ABCD3 (K) and ABCC6 (L). 'Day 0' is representative of log phase A549 monolayers.
(TIF)

Author Contributions

Conceptualization: ECB DED JEC JRC.

Data curation: MBA KEK JRC DED JEC.

Formal analysis: JRC MBA KEK DED JEC HT.

Funding acquisition: ECB DED.

Investigation: JRC FC MBA HT.

Methodology: FC JRC.

Project administration: ECB DED JEC.

Resources: ECB DED.

Supervision: DED JEC ECB.

Validation: JRC HT MBA DED JEC.

Visualization: JRC DED JEC.

Writing – original draft: JRC DED MBA FC.

Writing – review & editing: JRC DED JEC MBA HT FC KEK.

References

1. Mason RJ. Biology of alveolar type II cells. Respirology. 2006; 11: S12–S15. doi: 10.1111/j.1440-1843.2006.00800.x PMID: 16423262
2. Fehrenbach H. Alveolar epithelial type II cell: defender of the alveolus revisited. Respir Res. 2001; 2: 33–46. doi: 10.1186/rr36 PMID: 11686863
3. Shapiro DL, Nardone LL, Rooney SA, Motoyama EK, Munoz JL. Phospholipid biosynthesis and secretion by a cell line (A549) which resembles type II aleveolar epithelial cells. Biochim Biophys Acta. 1978; 530: 197–207. PMID: 352403
4. Barkauskas CE, Cronce MJ, Rackley CR, Bowie EJ, Keene DR, Stripp BR, et al. Type 2 alveolar cells are stem cells in adult lung. J Clin Invest. 2013; 123: 3025–3036. doi: 10.1172/JCI68782 PMID: 23921127
5. Kotton DN, Fine A. Lung stem cells. Cell Tissue Res. 2007; 331: 145–156. doi: 10.1007/s00441-007-0479-2 PMID: 17805578
6. Rock JR, Hogan BLM. Epithelial Progenitor Cells in Lung Development, Maintenance, Repair, and Disease. Annu Rev Cell Dev Biol. 2011; 27: 493–512. doi: 10.1146/annurev-cellbio-100109-104040 PMID: 21639799
7. Anversa P, Kajstura J, Leri A, Loscalzo J. Tissue-specific adult stem cells in the human lung. Nat Med. 2011; 17: 1038–1039. doi: 10.1038/nm.2463 PMID: 21900912
8. Miyake Y, Kaise H, Isono K, Koseki H, Kohno K, Tanaka M. Protective Role of Macrophages in Noninflammatory Lung Injury Caused by Selective Ablation of Alveolar Epithelial Type II Cells. J Immunol. 2007; 178: 5001–5009. doi: 10.4049/jimmunol.178.8.5001 PMID: 17404282

9. McElroy MC, Kasper M. The use of alveolar epithelial type I cell-selective markers to investigate lung injury and repair. Eur Respir J. 2004; 24: 664–673. doi: 10.1183/09031936.04.00096003 PMID: 15459148
10. Petrache I, Natarajan V, Zhen L, Medler TR, Richter AT, Cho C, et al. Ceramide upregulation causes pulmonary cell apoptosis and emphysema-like disease in mice. Nat Med. 2005; 11: 491–498. doi: 10.1038/nm1238 PMID: 15852018
11. Rennard SI, Wachenfeldt K von. Rationale and Emerging Approaches for Targeting Lung Repair and Regeneration in the Treatment of Chronic Obstructive Pulmonary Disease. Proc Am Thorac Soc. 2011; 8: 368–375. doi: 10.1513/pats.201102-019RM PMID: 21816994
12. Drakopanagiotakis F, Xifteri A, Polychronopoulos V, Bouros D. Apoptosis in lung injury and fibrosis. Eur Respir J. 2008; 32: 1631–1638. doi: 10.1183/09031936.00176807 PMID: 19043009
13. Sisson TH, Mendez M, Choi K, Subbotina N, Courey A, Cunningham A, et al. Targeted Injury of Type II Alveolar Epithelial Cells Induces Pulmonary Fibrosis. Am J Respir Crit Care Med. 2010; 181: 254–263. doi: 10.1164/rccm.200810-1615OC PMID: 19850947
14. du Bois RM. Strategies for treating idiopathic pulmonary fibrosis. Nat Rev Drug Discov. 2010; 9: 129–140. doi: 10.1038/nrd2958 PMID: 20094055
15. King TE, Pardo A, Selman M. Idiopathic pulmonary fibrosis. The Lancet. 2011; 378: 1949–1961. doi: 10.1016/S0140-6736(11)60052-4
16. Rogers DF, Donnelly LE, editors. Human airway inflammation: sampling techniques and analytical protocols. Totowa, N.J: Humana; 2001.
17. Thorley AJ, Ford PA, Giembycz MA, Goldstraw P, Young A, Tetley TD. Differential Regulation of Cytokine Release and Leukocyte Migration by Lipopolysaccharide-Stimulated Primary Human Lung Alveolar Type II Epithelial Cells and Macrophages. J Immunol. 2007; 178: 463–473. doi: 10.4049/jimmunol.178.1.463 PMID: 17182585
18. Fuchs S, Hollins A, Laue M, Schaefer U, Roemer K, Gumbleton M, et al. Differentiation of human alveolar epithelial cells in primary culture: morphological characterization and synthesis of caveolin-1 and surfactant protein-C. Cell Tissue Res. 2003; 311: 31–45. doi: 10.1007/s00441-002-0653-5 PMID: 12483282
19. Fehrenbach H. Alveolar epithelial type II cells from embryonic stem cells: knights in shining armour? Eur Respir J. 2012; 39: 240–241. doi: 10.1183/09031936.00162111 PMID: 22298611
20. Cerrada A, de la Torre P, Grande J, Haller T, Flores AI, Pérez-Gil J. Human Decidua-Derived Mesenchymal Stem Cells Differentiate into Functional Alveolar Type II-Like Cells that Synthesize and Secrete Pulmonary Surfactant Complexes. PLoS ONE. 2014; 9: e110195. doi: 10.1371/journal.pone.0110195 PMID: 25333871
21. Ghaedi M, Calle EA, Mendez JJ, Gard AL, Balestrini J, Booth A, et al. Human iPS cell-derived alveolar epithelium repopulates lung extracellular matrix. J Clin Invest. 2013; 123: 4950–4962. doi: 10.1172/JCI68793 PMID: 24135142
22. Ghaedi M, Mendez JJ, Bove PF, Sivarapatna A, Raredon MSB, Niklason LE. Alveolar epithelial differentiation of human induced pluripotent stem cells in a rotating bioreactor. Biomaterials. 2014; 35: 699–710. doi: 10.1016/j.biomaterials.2013.10.018 PMID: 24144903
23. Marx V. Cell-line authentication demystified. Nat Methods. 2014; 11: 483–488. doi: 10.1038/nmeth.2932
24. O'Hare MJ, Bond J, Clarke C, Takeuchi Y, Atherton AJ, Berry C, et al. Conditional immortalization of freshly isolated human mammary fibroblasts and endothelial cells. Proc Natl Acad Sci U S A. 2001; 98: 646–651. doi: 10.1073/pnas.98.2.646 PMID: 11209060
25. Geraghty RJ, Capes-Davis A, Davis JM, Downward J, Freshney RI, Knezevic I, et al. Guidelines for the use of cell lines in biomedical research. Br J Cancer. 2014; 111: 1021–1046. doi: 10.1038/bjc.2014.166 PMID: 25117809
26. Giard DJ, Aaronson SA, Todaro GJ, Arnstein P, Kersey JH, Dosik H, et al. In vitro cultivation of human tumors: establishment of cell lines derived from a series of solid tumors. J Natl Cancer Inst. 1973; 51: 1417–1423. PMID: 4357758
27. Lieber M, Smith B, Szakal A, Nelson-Rees W, Todaro G. A continuous tumor-cell line from a human lung carcinoma with properties of type II alveolar epithelial cells. Int J Cancer J Int Cancer. 1976; 17: 62–70.
28. Foster KA, Oster CG, Mayer MM, Avery ML, Audus KL. Characterization of the A549 Cell Line as a Type II Pulmonary Epithelial Cell Model for Drug Metabolism. Exp Cell Res. 1998; 243: 359–366. doi: 10.1006/excr.1998.4172 PMID: 9743595
29. Nardone LL, Andrews SB. Cell line A549 as a model of the type II pneumocyte: Phospholipid biosynthesis from native and organometallic precursors. Biochim Biophys Acta BBA—Lipids Lipid Metab. 1979; 573: 276–295. doi: 10.1016/0005-2760(79)90061-4

30. Swain RJ, Kemp SJ, Goldstraw P, Tetley TD, Stevens MM. Assessment of Cell Line Models of Primary Human Cells by Raman Spectral Phenotyping. Biophys J. 2010; 98: 1703–1711. doi: 10.1016/j.bpj.2009.12.4289 PMID: 20409492

31. Corbière V, Dirix V, Norrenberg S, Cappello M, Remmelink M, Mascart F. Phenotypic characteristics of human type II alveolar epithelial cells suitable for antigen presentation to T lymphocytes. Respir Res. 2011; 12: 15. doi: 10.1186/1465-9921-12-15 PMID: 21261956

32. Balis JU, Bumgarner SD, Paciga JE, Paterson JF, Shelley SA. Synthesis of lung surfactant-associated glycoproteins by A549 cells: description of an in vitro model for human type II cell dysfunction. Exp Lung Res. 1984; 6: 197–213. PMID: 6092046

33. Livak KJ, Schmittgen TD. Analysis of Relative Gene Expression Data Using Real-Time Quantitative PCR and the 2−ΔΔCT Method. Methods. 2001; 25: 402–408. doi: 10.1006/meth.2001.1262 PMID: 11846609

34. Vandesompele J, De Preter K, Pattyn F, Poppe B, Van Roy N, De Paepe A, et al. Accurate normalization of real-time quantitative RT-PCR data by geometric averaging of multiple internal control genes. Genome Biol. 2002; 3: research0034.1–research0034.11.

35. Kelder T, Pico AR, Hanspers K, van Iersel MP, Evelo C, Conklin BR. Mining Biological Pathways Using WikiPathways Web Services. PLoS ONE. 2009; 4. doi: 10.1371/journal.pone.0006447 PMID: 19649250

36. Kelder T, van Iersel MP, Hanspers K, Kutmon M, Conklin BR, Evelo CT, et al. WikiPathways: building research communities on biological pathways. Nucleic Acids Res. 2011; gkr1074. doi: 10.1093/nar/gkr1074 PMID: 22096230

37. Pico AR, Kelder T, van Iersel MP, Hanspers K, Conklin BR, Evelo C. WikiPathways: Pathway Editing for the People. PLoS Biol. 2008; 6: e184. doi: 10.1371/journal.pbio.0060184 PMID: 18651794

38. Wang D, Haviland DL, Burns AR, Zsigmond E, Wetsel RA. A pure population of lung alveolar epithelial type II cells derived from human embryonic stem cells. Proc Natl Acad Sci. 2007; 104: 4449–4454. doi: 10.1073/pnas.0700052104 PMID: 17360544

39. Pinto M, Robine-Leon S, Appay M-D, Kedinger M, Triadou N, Dussaulx E, et al. Enterocyte-like differentiation and polarization of the human colon carcinoma cell line Caco-2 in culture. Biol Cell. 1983; 47: 323–330.

40. Cereijido M, Robbins ES, Dolan WJ, Rotunno CA, Sabatini DD. Polarized monolayers formed by epithelial cells on a permeable and translucent support. J Cell Biol. 1978; 77: 853–880. PMID: 567227

41. Mason RJ, Williams MC. Phospholipid composition and ultrastructure of A549 cells and other cultured pulmonary epithelial cells of presumed type II cell origin. Biochim Biophys Acta. 1980; 617: 36–50. PMID: 6243488

42. Heijink IH, Brandenburg SM, Noordhoek JA, Postma DS, Slebos D-J, van Oosterhout AJM. Characterisation of cell adhesion in airway epithelial cell types using electric cell–substrate impedance sensing. Eur Respir J. 2010; 35: 894–903. doi: 10.1183/09031936.00065809 PMID: 19741028

43. Begley CG, Ellis LM. Drug development: Raise standards for preclinical cancer research. Nature. 2012; 483: 531–533. doi: 10.1038/483531a PMID: 22460880

44. Strunk RC, Eidlen DM, Mason RJ. Pulmonary alveolar type II epithelial cells synthesize and secrete proteins of the classical and alternative complement pathways. J Clin Invest. 1988; 81: 1419–1426. doi: 10.1172/JCI113472 PMID: 2966814

45. Schmitz G, Müller G. Structure and function of lamellar bodies, lipid-protein complexes involved in storage and secretion of cellular lipids. J Lipid Res. 1991; 32: 1539–1570. PMID: 1797938

46. Hariri M, Millane G, Guimond M-P, Guay G, Dennis JW, Nabi IR. Biogenesis of Multilamellar Bodies via Autophagy. Mol Biol Cell. 2000; 11: 255–268. PMID: 10637306

47. Lajoie P, Guay G, Dennis JW, Nabi IR. The lipid composition of autophagic vacuoles regulates expression of multilamellar bodies. J Cell Sci. 2005; 118: 1991–2003. doi: 10.1242/jcs.02324 PMID: 15840653

48. Liang C, Jung JU. Autophagy Genes as Tumor Suppressors. Curr Opin Cell Biol. 2010; 22: 226–233. doi: 10.1016/j.ceb.2009.11.003 PMID: 19945837

49. Kuma A, Hatano M, Matsui M, Yamamoto A, Nakaya H, Yoshimori T, et al. The role of autophagy during the early neonatal starvation period. Nature. 2004; 432: 1032–1036. doi: 10.1038/nature03029 PMID: 15525940

50. Copland IB, Post M. Understanding the Mechanisms of Infant Respiratory Distress and Chronic Lung Disease. Am J Respir Cell Mol Biol. 2002; 26: 261–265. doi: 10.1165/ajrcmb.26.3.f231 PMID: 11867331

51. Saitoh T, Fujita N, Jang MH, Uematsu S, Yang B-G, Satoh T, et al. Loss of the autophagy protein Atg16L1 enhances endotoxin-induced IL-1β production. Nature. 2008; 456: 264–268. doi: 10.1038/nature07383 PMID: 18849965

52. Cadwell K, Liu J, Brown SL, Miyoshi H, Loh J, Lennerz J, et al. A unique role for autophagy and Atg16L1 in Paneth cells in murine and human intestine. Nature. 2008; 456: 259–263. doi: 10.1038/nature07416 PMID: 18849966

53. Mulugeta S, Gray JM, Notarfrancesco KL, Gonzales LW, Koval M, Feinstein SI, et al. Identification of LBM180, a Lamellar Body Limiting Membrane Protein of Alveolar Type II Cells, as the ABC Transporter Protein ABCA3. J Biol Chem. 2002; 277: 22147–22155. doi: 10.1074/jbc.M201812200 PMID: 11940594

54. Agassandian M, Mallampalli RK. Surfactant phospholipid metabolism. Biochim Biophys Acta. 2013; 1831: 612–625. doi: 10.1016/j.bbalip.2012.09.010 PMID: 23026158

55. Weaver TE, Na C-L, Stahlman M. Biogenesis of lamellar bodies, lysosome-related organelles involved in storage and secretion of pulmonary surfactant. Semin Cell Dev Biol. 2002; 13: 263–270. doi: 10.1016/S1084952102000551 PMID: 12243725

56. Seo D-C, Sung J-M, Cho H-J, Yi H, Seo K-H, Choi I-S, et al. Gene expression profiling of cancer stem cell in human lung adenocarcinoma A549 cells. Mol Cancer. 2007; 6: 75. doi: 10.1186/1476-4598-6-75 PMID: 18034892

List of References

1. Mason, R. J. *et al. Textbook of Respiratory Medicine*. vol. 1 (Saunders, an imprint of Elsevier Inc., 2010).

2. Stradling, J. R. & Craig, S. E. *The upper respiratory tract* in The Oxford Textbook of Medicine. Ed. Warrell D *et al* 5th edn. Oxford University Press).

3. Wagner, P. D. *Airways and alveoli*. in The Oxford Textbook of Medicine. Ed. Warrell D *et al* 5th edn. (Oxford University Press).

4. Jain, M. & Sznajder, J. I. Bench-to-bedside review: Distal airways in acute respiratory distress syndrome. *Crit. Care* **11**, 1–8 (2007).

5. Davies, D. E. Epithelial Barrier Function and Immunity in Asthma. *Ann. Am. Thorac. Soc.* **11**, S244–S251 (2014).

6. McDowell, E. M., Barrett, L. A., Glavin, F., Harris, C. C. & Trump, B. F. The respiratory epithelium. I. Human bronchus. *J. Natl. Cancer Inst.* **61**, 539–549 (1978).

7. Swindle, E. J., Collins, J. E. & Davies, D. E. Breakdown in epithelial barrier function in patients with asthma: Identification of novel therapeutic approaches. *J. Allergy Clin. Immunol.* **124**, 23–34 (2009).

8. Gordon, S. Non-animal models of epithelial barriers (skin, intestine and lung) in research, industrial applications and regulatory toxicology. *ALTEX* **32**, 327–378 (2015).

9. Reynolds, S. D. & Malkinson, A. M. Clara Cell: Progenitor for the Bronchiolar Epithelium. *Int. J. Biochem. Cell Biol.* **42**, 1–4 (2010).

10. Perl, A.-K. T., Riethmacher, D. & Whitsett, J. A. Conditional Depletion of Airway Progenitor Cells Induces Peribronchiolar Fibrosis. *Am. J. Respir. Crit. Care Med.* **183**, 511–521 (2011).

11. Effros, R. M. Anatomy, development, and physiology of the lungs. *GI Motil. Online* (2006) doi:10.1038/gimo73.

12. Ochs, M. *et al.* The Number of Alveoli in the Human Lung. *Am. J. Respir. Crit. Care Med.* **169**, 120–124 (2004).

13. Hasleton, P. S. The internal surface area of the adult human lung. *J. Anat.* **112**, 391–400 (1972).

14. Fehrenbach, H. Alveolar epithelial type II cell: defender of the alveolus revisited. *Respir. Res.* **2**, 33–46 (2001).

15. Féréol, S., Fodil, R., Pelle, G., Louis, B. & Isabey, D. Cell mechanics of alveolar epithelial cells (AECs) and macrophages (AMs). *Respir. Physiol. Neurobiol.* **163**, 3–16 (2008).

16. Williams, M. C. Alveolar Type I Cells: Molecular Phenotype and Development. *Annu. Rev. Physiol.* **65**, 669–695 (2003).

17. Wang, S. & Hubmayr, R. D. Type I Alveolar Epithelial Phenotype in Primary Culture. *Am. J. Respir. Cell Mol. Biol.* **44**, 692–699 (2011).

18. Sibille, Y. & Reynolds, H. Y. Macrophages and Polymorphonuclear Neutrophils in Lung Defense and Injury. *Am. Rev. Respir. Dis.* **141**, 471–501 (1990).

19. Shapiro, D. L., Nardone, L. L., Rooney, S. A., Motoyama, E. K. & Munoz, J. L. Phospholipid biosynthesis and secretion by a cell line (A549) which resembles type II aleveolar epithelial cells. *Biochim. Biophys. Acta* **530**, 197–207 (1978).

20. Grubor, B., Meyerholz, D. K. & Ackermann, M. R. Collectins and Cationic Antimicrobial Peptides of the Respiratory Epithelia. *Vet. Pathol.* **43**, 595–612 (2006).

21. Marchin J. *English: Conducting passages of the human respiratory system*. (2010) https://courses.lumenlearning.com/boundless-ap/chapter/conducting-zone/.

22. ERS - Respiratory health and disease in Europe. http://www.erswhitebook.org/.

23. Laney, A. S. & Weissman, D. N. Respiratory Diseases Caused by Coal Mine Dust. *J. Occup. Environ. Med. Am. Coll. Occup. Environ. Med.* **56**, S18–S22 (2014).

24. Brown, T. Silica exposure, smoking, silicosis and lung cancer—complex interactions. *Occup. Med.* **59**, 89–95 (2009).

25. Park, R. *et al.* Exposure to crystalline silica, silicosis, and lung disease other than cancer in diatomaceous earth industry workers: a quantitative risk assessment. *Occup. Environ. Med.* **59**, 36–43 (2002).

26. Bourke, S. J. Interstitial lung disease: progress and problems. *Postgrad. Med. J.* **82**, 494–499 (2006).

27. Currie, G. P., Watt, S. J. & Maskell, N. A. An overview of how asbestos exposure affects the lung. *BMJ* **339**, b3209 (2009).

28. Glass, W. I., Taylor, D. R. & Donoghue, A. M. Chronic interstitial lung disease in a welder of galvanized steel. *Occup. Med. Oxf. Engl.* **44**, 158–160 (1994).

29. Sauler, M. & Gulati, M. Newly Recognized Occupational and Environmental Causes of Chronic Terminal Airways and Parenchymal Lung Disease. *Clin. Chest Med.* **33**, 667–680 (2012).

30. Devine, M. S. & Garcia, C. K. Genetic Interstitial Lung Disease. *Clin. Chest Med.* **33**, 95–110 (2012).

31. Margaritopoulos, G. A., Vasarmidi, E., Jacob, J., Wells, A. U. & Antoniou, K. M. Smoking and interstitial lung diseases. *Eur. Respir. Rev.* **24**, 428–435 (2015).

32. Azadeh, N., Limper, A. H., Carmona, E. M. & Ryu, J. H. The Role of Infection in Interstitial Lung Diseases. *Chest* **152**, 842–852 (2017).

33. Fraser, E. Long term respiratory complications of covid-19. *BMJ* **370**, (2020).

34. Rafii, R., Juarez, M. M., Albertson, T. E. & Chan, A. L. A review of current and novel therapies for idiopathic pulmonary fibrosis. *J. Thorac. Dis.* **5**, 48–73 (2013).

35. Verma, S. & Slutsky, A. S. Idiopathic Pulmonary Fibrosis — New Insights. *N. Engl. J. Med.* **356**, 1370–1372 (2007).

36. Bellaye, P.-S. & Kolb, M. Why do patients get idiopathic pulmonary fibrosis? Current concepts in the pathogenesis of pulmonary fibrosis. *BMC Med.* **13**, (2015).

37. Betensley, A., Sharif, R. & Karamichos, D. A Systematic Review of the Role of Dysfunctional Wound Healing in the Pathogenesis and Treatment of Idiopathic Pulmonary Fibrosis. *J. Clin. Med.* **6**, (2016).

38. Daccord, C. & Maher, T. M. Recent advances in understanding idiopathic pulmonary fibrosis. *F1000Research* **5**, (2016).

39. Raghu, G. *et al.* An Official ATS/ERS/JRS/ALAT Statement: Idiopathic Pulmonary Fibrosis: Evidence-based Guidelines for Diagnosis and Management. *Am. J. Respir. Crit. Care Med.* **183**, 788–824 (2011).

40. Wolters, P. J., Collard, H. R. & Jones, K. D. Pathogenesis of Idiopathic Pulmonary Fibrosis. *Annu. Rev. Pathol. Mech. Dis.* **9**, 157–179 (2014).

41. King, T. E., Pardo, A. & Selman, M. Idiopathic pulmonary fibrosis. *The Lancet* **378**, 1949–1961 (2011).

42. Katzenstein, A.-L. A. & Myers, J. L. Idiopathic Pulmonary Fibrosis. *Am. J. Respir. Crit. Care Med.* **157**, 1301–1315 (1998).

43. Cool, C. D. *et al.* Fibroblast Foci Are Not Discrete Sites of Lung Injury or Repair. *Am. J. Respir. Crit. Care Med.* **174**, 654–658 (2006).

44. Jones, M. G. *et al.* Three-dimensional characterization of fibroblast foci in idiopathic pulmonary fibrosis. *JCI Insight* **1**,.

45. Cottin, V. & Richeldi, L. Neglected evidence in idiopathic pulmonary fibrosis and the importance of early diagnosis and treatment. *Eur. Respir. Rev.* **23**, 106–110 (2014).

46. Vašáková, M. *et al.* Does early diagnosis of idiopathic pulmonary fibrosis matter? Real- world´s data from the EMPIRE registry. *Eur. Respir. J.* **48**, (2016).

47. Fastrès, A. *et al.* The Lung Microbiome in Idiopathic Pulmonary Fibrosis: A Promising Approach for Targeted Therapies. *Int. J. Mol. Sci.* **18**, (2017).

48. Maher, T. M. *et al.* Investigating the effects of nintedanib on biomarkers of extracellular matrix turnover in patients with IPF: design of the randomised placebo-controlled INMARK®trial. *BMJ Open Respir. Res.* **5**, e000325 (2018).

49. Cicchitto, G. & Sanguinetti, C. M. Idiopathic pulmonary fibrosis: the need for early diagnosis. *Multidiscip. Respir. Med.* **8**, 53 (2013).

50. Hall, B. K. Epithelial-Mesenchymal Interactions. in *Developmental Biology Protocols* 235–243 (Humana Press, 2000). doi:10.1385/1-59259-066-7:235.

51. Lewis, K. J. R. *et al.* Epithelial-mesenchymal crosstalk influences cellular behavior in a 3D alveolus-fibroblast model system. *Biomaterials* **155**, 124–134 (2018).

52. Chapman, H. A. Epithelial-Mesenchymal Interactions in Pulmonary Fibrosis. *Annu. Rev. Physiol.* **73**, 413–435 (2011).

53. Bhowmick, N. A., Neilson, E. G. & Moses, H. L. Stromal fibroblasts in cancer initiation and progression. *Nature* **432**, 332–337 (2004).

54. Selman, M. & Pardo, A. Role of Epithelial Cells in Idiopathic Pulmonary Fibrosis. *Proc. Am. Thorac. Soc.* **3**, 364–372 (2006).

55. Post, M., Floros, J. & Smith, B. T. Inhibition of lung maturation by monoclonal antibodies against fibroblast–pneumonocyte factor. *Nature* **308**, 284–286 (1984).

56. Demayo, F. *et al.* Mesenchymal-epithelial interactions in lung development and repair: are modeling and remodeling the same process? *Am. J. Physiol.-Lung Cell. Mol. Physiol.* **283**, L510–L517 (2002).

57. Torday, J. S. & Rehan, V. K. Up-Regulation of Fetal Rat Lung Parathyroid Hormone-Related Protein Gene Regulatory Network Down-Regulates the Sonic Hedgehog/Wnt/βcatenin Gene Regulatory Network. *Pediatr. Res.* **60**, 382–388 (2006).

58. Torday, J. S. & Rehan, V. K. The evolutionary continuum from lung development to homeostasis and repair. *Am. J. Physiol.-Lung Cell. Mol. Physiol.* (2007) doi:10.1152/ajplung.00379.2006.

59. King, G., Smith, M. E., Cake, M. H. & Nielsen, H. C. What is the identity of fibroblast-pneumocyte factor? *Pediatr. Res.* (2016) doi:10.1038/pr.2016.161.

60. Thiery, J. P., Acloque, H., Huang, R. Y. J. & Nieto, M. A. Epithelial-Mesenchymal Transitions in Development and Disease. *Cell* **139**, 871–890 (2009).

61. Rock, J. R. *et al.* Basal cells as stem cells of the mouse trachea and human airway epithelium. *Proc. Natl. Acad. Sci.* **106**, 12771–12775 (2009).

62. Kumar, P. A. *et al.* Distal Airway Stem Cells Render Alveoli in Vitro and During Lung Regeneration Following H1N1 Influenza Infection. *Cell* **147**, 525–538 (2011).

63. Giangreco, A., Reynolds, S. D. & Stripp, B. R. Terminal Bronchioles Harbor a Unique Airway Stem Cell Population That Localizes to the Bronchoalveolar Duct Junction. *Am. J. Pathol.* **161**, 173–182 (2002).

64. Song, H. *et al.* Functional characterization of pulmonary neuroendocrine cells in lung development, injury, and tumorigenesis. *Proc. Natl. Acad. Sci. U. S. A.* **109**, 17531–17536 (2012).

65. Kim, C. F. B. *et al.* Identification of Bronchioalveolar Stem Cells in Normal Lung and Lung Cancer. *Cell* **121**, 823–835 (2005).

66. Evans, M. J., Cabral, L. J., Stephens, R. J. & Freeman, G. Renewal of Alveolar Epithelium in the Rat Following Exposure to NO2. *Am. J. Pathol.* **70**, 175–198 (1973).

67. Barkauskas, C. E. *et al.* Type 2 alveolar cells are stem cells in adult lung. *J. Clin. Invest.* **123**, 3025–3036 (2013).

68. Isler, J. A., Skalet, A. H. & Alwine, J. C. Human Cytomegalovirus Infection Activates and Regulates the Unfolded Protein Response. *J. Virol.* **79**, 6890–6899 (2005).

69. Lok, S. S. *et al.* Murine gammaherpes virus as a cofactor in the development of pulmonary fibrosis in bleomycin resistant mice. *Eur. Respir. J.* **20**, 1228–1232 (2002).

70. Torriso, S. E., Khan, N., Vancheri, C. & Kreuter, M. Evolution and treatment of idiopathic pulmonary fibrosis. *Presse Médicale* **49**, 104025 (2020).

71. Boomars, K. A. *et al.* Eosinophil chemotactic activity in bronchoalveolar lavage from idiopathic pulmonary fibrosis is dependent on cytokine priming of eosinophils. *Eur. Respir. J.* **11**, 1009–1014 (1998).

72. Daniil, Z. *et al.* CD8+ T lymphocytes in lung tissue from patients with idiopathic pulmonary fibrosis. *Respir. Res.* **6**, 81 (2005).

73. Samara, K. D., Margaritopoulos, G., Wells, A. U., Siafakas, N. M. & Antoniou, K. M. Smoking and Pulmonary Fibrosis: Novel Insights. *Pulmonary Medicine* https://www.hindawi.com/journals/pm/2011/461439/ (2011) doi:10.1155/2011/461439.

74. Yang, I. V. & Schwartz, D. A. Epigenetics of Idiopathic Pulmonary Fibrosis. *Transl. Res. J. Lab. Clin. Med.* **165**, 48–60 (2015).

75. Sebag, S. C., Bastarache, J. A. & Ware, L. B. Therapeutic Modulation of Coagulation and Fibrinolysis in Acute Lung Injury and the Acute Respiratory Distress Syndrome. *Curr. Pharm. Biotechnol.* **12**, 1481–1496 (2011).

76. Jones, M. G. *et al.* Nanoscale dysregulation of collagen structure-function disrupts mechano-homeostasis and mediates pulmonary fibrosis. *eLife* https://elifesciences.org/articles/36354 (2018) doi:10.7554/eLife.36354.

77. Raghu, G. *et al.* Efficacy of simtuzumab versus placebo in patients with idiopathic pulmonary fibrosis: a randomised, double-blind, controlled, phase 2 trial. *Lancet Respir. Med.* **5**, 22–32 (2017).

78. Rodriguez, H. M. *et al.* Modulation of Lysyl Oxidase-like 2 Enzymatic Activity by an Allosteric Antibody Inhibitor. *J. Biol. Chem.* **285**, 20964–20974 (2010).

79. Wipff, P.-J. & Hinz, B. Integrins and the activation of latent transforming growth factor β1 – An intimate relationship. *Eur. J. Cell Biol.* **87**, 601–615 (2008).

80. Nicholson, A. G. *et al.* The Relationship between Individual Histologic Features and Disease Progression in Idiopathic Pulmonary Fibrosis. *Am. J. Respir. Crit. Care Med.* **166**, 173–177 (2002).

81. Nalysnyk, L., Cid-Ruzafa, J., Rotella, P. & Esser, D. Incidence and prevalence of idiopathic pulmonary fibrosis: review of the literature. *Eur. Respir. Rev.* **21**, 355–361 (2012).

82. Jayachandran, A. *et al.* SNAI transcription factors mediate epithelial–mesenchymal transition in lung fibrosis. *Thorax* **64**, 1053–1061 (2009).

83. Katoh, M. & Katoh, M. Comparative genomics on SNAI1, SNAI2, and SNAI3 orthologs. *Oncol. Rep.* **14**, 1083–1086 (2005).

84. Salton, F., Volpe, M. C. & Confalonieri, M. Epithelial–Mesenchymal Transition in the Pathogenesis of Idiopathic Pulmonary Fibrosis. *Medicina (Mex.)* **55**, (2019).

85. Kretzschmar, K. & Watt, F. M. Lineage Tracing. *Cell* **148**, 33–45 (2012).

86. Borok, Z. Role for α3 integrin in EMT and pulmonary fibrosis. *J. Clin. Invest.* **119**, 7–10 (2009).

87. Epperly, M. W., Guo, H., Gretton, J. E. & Greenberger, J. S. Bone Marrow Origin of Myofibroblasts in Irradiation Pulmonary Fibrosis. *Am. J. Respir. Cell Mol. Biol.* **29**, 213–224 (2003).

88. Marriott, S. *et al.* ABCG2pos lung mesenchymal stem cells are a novel pericyte subpopulation that contributes to fibrotic remodeling. *Am. J. Physiol.-Cell Physiol.* **307**, C684–C698 (2014).

89. Green, J., Endale, M., Auer, H. & Perl, A.-K. T. Diversity of Interstitial Lung Fibroblasts Is Regulated by Platelet-Derived Growth Factor Receptor α Kinase Activity. *Am. J. Respir. Cell Mol. Biol.* **54**, 532–545 (2015).

90. Agha, E. E. *et al.* Two-Way Conversion between Lipogenic and Myogenic Fibroblastic Phenotypes Marks the Progression and Resolution of Lung Fibrosis. *Cell Stem Cell* **20**, 261–273.e3 (2017).

91. Rehan, V. K. *et al.* Evidence for the Presence of Lipofibroblasts in Human Lung. *Exp. Lung Res.* **32**, 379–393 (2006).

92. Tahedl, D., Wirkes, A., Tschanz, S. A., Ochs, M. & Mühlfeld, C. How common is the lipid body-containing interstitial cell in the mammalian lung? *Am. J. Physiol.-Lung Cell. Mol. Physiol.* **307**, L386–L394 (2014).

93. Álvarez, D. *et al.* IPF lung fibroblasts have a senescent phenotype. *Am. J. Physiol.-Lung Cell. Mol. Physiol.* **313**, L1164–L1173 (2017).

94. Caporarello, N. *et al.* PGC1α repression in IPF fibroblasts drives a pathologic metabolic, secretory and fibrogenic state. *Thorax* **74**, 749–760 (2019).

95. Habermann, A. C. *et al.* Single-cell RNA sequencing reveals profibrotic roles of distinct epithelial and mesenchymal lineages in pulmonary fibrosis. *Sci. Adv.* **6**, eaba1972 (2020).

96. Parimon, T., Yao, C., Stripp, B. R., Noble, P. W. & Chen, P. Alveolar Epithelial Type II Cells as Drivers of Lung Fibrosis in Idiopathic Pulmonary Fibrosis. *Int. J. Mol. Sci.* **21**, (2020).

97. Sheppard, D. The role of integrins in pulmonary fibrosis. *Eur. Respir. Rev.* **17**, 157–162 (2008).

98. Kulkarni, T., de Andrade, J., Zhou, Y., Luckhardt, T. & Thannickal, V. J. Alveolar epithelial disintegrity in pulmonary fibrosis. *Am. J. Physiol. - Lung Cell. Mol. Physiol.* **311**, L185–L191 (2016).

99. Liang, J. *et al.* Hyaluronan and TLR4 promote surfactant-protein-C-positive alveolar progenitor cell renewal and prevent severe pulmonary fibrosis in mice. *Nat. Med.* **22**, 1285–1293 (2016).

100. Sack, C. & Raghu, G. Idiopathic pulmonary fibrosis: unmasking cryptogenic environmental factors. *Eur. Respir. J.* **53**, (2019).

101. Garcia, C. K. Insights from human genetic studies of lung and organ fibrosis. *J. Clin. Invest.* **128**, 36–44.

102. Xu, Y. *et al.* Single-cell RNA sequencing identifies diverse roles of epithelial cells in idiopathic pulmonary fibrosis. *JCI Insight* **1**, (2017).

103. Elmore, S. Apoptosis: A Review of Programmed Cell Death. *Toxicol. Pathol.* **35**, 495–516 (2007).

104. Wang, R., Ibarra-Sunga, O., Verlinski, L., Pick, R. & Uhal, B. D. Abrogation of bleomycin-induced epithelial apoptosis and lung fibrosis by captopril or by a caspase inhibitor. *Am. J. Physiol.-Lung Cell. Mol. Physiol.* **279**, L143–L151 (2000).

105. Hagimoto, N. *et al.* Induction of Apoptosis and Pulmonary Fibrosis in Mice in Response to Ligation of Fas Antigen. *Am. J. Respir. Cell Mol. Biol.* **17**, 272–278 (1997).

106. Kropski, J. A. & Blackwell, T. S. Endoplasmic reticulum stress in the pathogenesis of fibrotic disease. *J. Clin. Invest.* **128**, 64–73.

107. Piantadosi, C. A. & Suliman, H. B. Mitochondrial Dysfunction in Lung Pathogenesis. *Annu. Rev. Physiol.* **79**, 495–515 (2017).

108. Rangarajan, S., Bernard, K. & Thannickal, V. J. Mitochondrial Dysfunction in Pulmonary Fibrosis. *Ann. Am. Thorac. Soc.* **14**, S383–S388 (2017).

109. Mora, A. L., Bueno, M. & Rojas, M. Mitochondria in the spotlight of aging and idiopathic pulmonary fibrosis. *J. Clin. Invest.* **127**, 405–414.

110. Datta, A., Scotton, C. J. & Chambers, R. C. Novel therapeutic approaches for pulmonary fibrosis. *Br. J. Pharmacol.* **163**, 141–172 (2011).

111. Selman, M. & Pardo, A. Idiopathic pulmonary fibrosis: an epithelial/fibroblastic cross-talk disorder. *Respir. Res.* **3**, 3 (2002).

112. Broekelmann, T. J., Limper, A. H., Colby, T. V. & McDonald, J. A. Transforming growth factor beta 1 is present at sites of extracellular matrix gene expression in human pulmonary fibrosis. *Proc. Natl. Acad. Sci. U. S. A.* **88**, 6642–6646 (1991).

113. Pierce, E. M. *et al.* Idiopathic pulmonary fibrosis fibroblasts migrate and proliferate to CC chemokine ligand 21. *Eur. Respir. J.* **29**, 1082–1093 (2007).

114. Pan, L.-H. *et al.* Type II alveolar epithelial cells and interstitial fibroblasts express connective tissue growth factor in IPF. *Eur. Respir. J.* **17**, 1220–1227 (2001).

115. Leask, A. & Abraham, D. J. The role of connective tissue growth factor, a multifunctional matricellular protein, in fibroblast biology. *Biochem. Cell Biol.* (2011) doi:10.1139/o03-069.

116. Kovacs, T. *et al.* Alteration in the Wnt microenvironment directly regulates molecular events leading to pulmonary senescence. *Aging Cell* **13**, 838–849 (2014).

117. Königshoff, M. & Eickelberg, O. WNT Signaling in Lung Disease. *Am. J. Respir. Cell Mol. Biol.* (2012) doi:10.1165/rcmb.2008-0485TR.

118. Chilosi, M. *et al.* Aberrant Wnt/β-Catenin Pathway Activation in Idiopathic Pulmonary Fibrosis. *Am. J. Pathol.* **162**, 1495–1502 (2003).

119. Frank, D. B. *et al.* Emergence of a wave of Wnt signaling that regulates lung alveologenesis through controlling epithelial self-renewal and differentiation. *Cell Rep.* **17**, 2312–2325 (2016).

120. Mutze, K., Vierkotten, S., Milosevic, J., Eickelberg, O. & Königshoff, M. Enolase 1 (ENO1) and protein disulfide-isomerase associated 3 (PDIA3) regulate Wnt/β-catenin-driven trans-differentiation of murine alveolar epithelial cells. *Dis. Model. Mech.* **8**, 877–890 (2015).

121. Liu, H. *et al.* Augmented Wnt Signaling in a Mammalian Model of Accelerated Aging. *Science* **317**, 803–806 (2007).

122. Yao, C. *et al.* Senescence of alveolar stem cells drives progressive pulmonary fibrosis. *bioRxiv* 820175 (2019) doi:10.1101/820175.

123. Acosta, J. C. *et al.* A complex secretory program orchestrated by the inflammasome controls paracrine senescence. *Nat. Cell Biol.* **15**, 978–990 (2013).

124. Takasugi, M. Emerging roles of extracellular vesicles in cellular senescence and aging. *Aging Cell* **17**, (2018).

125. Lane, R. K., Hilsabeck, T. & Rea, S. L. The role of mitochondrial dysfunction in age-related diseases. *Biochim. Biophys. Acta BBA - Bioenerg.* **1847**, 1387–1400 (2015).

126. Hansel, C., Jendrossek, V. & Klein, D. Cellular Senescence in the Lung: The Central Role of Senescent Epithelial Cells. *Int. J. Mol. Sci.* **21**, (2020).

127. Chen, X. *et al.* Epithelial cell senescence induces pulmonary fibrosis through Nanog-mediated fibroblast activation. *Aging* **12**, 242–259 (2019).

128. Peng, T. *et al.* Hedgehog actively maintains adult lung quiescence and regulates repair and regeneration. *Nature* **526**, 578–582 (2015).

129. Hu, B. *et al.* Reemergence of Hedgehog Mediates Epithelial–Mesenchymal Crosstalk in Pulmonary Fibrosis. *Am. J. Respir. Cell Mol. Biol.* **52**, 418–428 (2015).

130. Hay, E. D. Collagen and Other Matrix Glycoproteins in Embryogenesis. in *Cell Biology of Extracellular Matrix* 419–462 (Springer, Boston, MA, 1991). doi:10.1007/978-1-4615-3770-0_13.

131. Nieto, M. A. The Ins and Outs of the Epithelial to Mesenchymal Transition in Health and Disease. *Annu. Rev. Cell Dev. Biol.* **27**, 347–376 (2011).

132. Hill, C. & Wang, Y. The importance of epithelial-mesenchymal transition and autophagy in cancer drug resistance. *Cancer Drug Resist.* **3**, 38–47 (2020).

133. Rock, J. R. *et al.* Multiple stromal populations contribute to pulmonary fibrosis without evidence for epithelial to mesenchymal transition. *Proc. Natl. Acad. Sci.* **108**, E1475–E1483 (2011).

134. Tanjore, H. *et al.* Contribution of Epithelial-derived Fibroblasts to Bleomycin-induced Lung Fibrosis. *Am. J. Respir. Crit. Care Med.* **180**, 657–665 (2009).

135. Gokey, J. J. *et al.* Active epithelial Hippo signaling in idiopathic pulmonary fibrosis. *JCI Insight* **3**,.

136. Vaughan, A. E. *et al.* Lineage-negative Progenitors Mobilize to Regenerate Lung Epithelium after Major Injury. *Nature* **517**, 621–625 (2015).

137. Kage, H. & Borok, Z. EMT and Interstitial Lung Disease: A Mysterious Relationship. *Curr. Opin. Pulm. Med.* **18**, 517–523 (2012).

138. Masszi, A. *et al.* Fate-determining mechanisms in epithelial–myofibroblast transition: major inhibitory role for Smad3. *J. Cell Biol.* **188**, 383–399 (2010).

139. Charbonney, E., Speight, P., Masszi, A., Nakano, H. & Kapus, A. β-Catenin and Smad3 regulate the activity and stability of myocardin-related transcription factor during epithelial–myofibroblast transition. *Mol. Biol. Cell* **22**, 4472–4485 (2011).

140. Henderson, W. R. *et al.* Inhibition of Wnt/?-catenin/CREB binding protein (CBP) signaling reverses pulmonary fibrosis. *Proc. Natl. Acad. Sci. U. S. A.* **107**, 14309–14314 (2010).

141. Kim, K. K. *et al.* Epithelial cell α3β1 integrin links β-catenin and Smad signaling to promote myofibroblast formation and pulmonary fibrosis. *J. Clin. Invest.* **119**, 213–224 (2009).

142. Ulsamer, A. *et al.* Axin Pathway Activity Regulates in Vivo pY654-β-catenin Accumulation and Pulmonary Fibrosis. *J. Biol. Chem.* **287**, 5164–5172 (2012).

143. Alcorn, J. F. *et al.* Jun N-terminal kinase 1 regulates epithelial-to-mesenchymal transition induced by TGF-β1. *J. Cell Sci.* **121**, 1036–1045 (2008).

144. Alcorn, J. F. *et al.* c-Jun N-Terminal Kinase 1 Is Required for the Development of Pulmonary Fibrosis. *Am. J. Respir. Cell Mol. Biol.* **40**, 422–432 (2009).

145. Velden, J. L. J. van der, Alcorn, J. F., Guala, A. S., Badura, E. C. H. L. & Janssen-Heininger, Y. M. W. c-Jun N-Terminal Kinase 1 Promotes Transforming Growth Factor–β1–Induced Epithelial-to-Mesenchymal Transition via Control of Linker Phosphorylation and Transcriptional Activity of Smad3. *Am. J. Respir. Cell Mol. Biol.* **44**, 571–581 (2011).

146. Martinelli, M. *et al.* A role for epidermal growth factor receptor in idiopathic pulmonary fibrosis onset. *Mol. Biol. Rep.* **38**, 4613–4617 (2011).

147. Zeisberg, M. & Neilson, E. G. Biomarkers for epithelial-mesenchymal transitions. *J. Clin. Invest.* **119**, 1429–1437 (2009).

148. MacKinnon, A. C. *et al.* Regulation of Transforming Growth Factor-β1–driven Lung Fibrosis by Galectin-3. *Am. J. Respir. Crit. Care Med.* **185**, 537–546 (2012).

149. Mi, S. *et al.* Blocking IL-17A Promotes the Resolution of Pulmonary Inflammation and Fibrosis Via TGF-β1–Dependent and –Independent Mechanisms. *J. Immunol.* **187**, 3003–3014 (2011).

150. Rogliani, P., Calzetta, L., Cavalli, F., Matera, M. G. & Cazzola, M. Pirfenidone, nintedanib and N-acetylcysteine for the treatment of idiopathic pulmonary fibrosis: A systematic review and meta-analysis. *Pulm. Pharmacol. Ther.* **40**, 95–103 (2016).

151. Schaefer, C. J., Ruhrmund, D. W., Pan, L., Seiwert, S. D. & Kossen, K. Antifibrotic activities of pirfenidone in animal models. *Eur. Respir. Rev.* **20**, 85–97 (2011).

152. Di Sario, A. *et al.* Effect of pirfenidone on rat hepatic stellate cell proliferation and collagen production. *J. Hepatol.* **37**, 584–591 (2002).

153. Wollin, L. *et al.* Mode of action of nintedanib in the treatment of idiopathic pulmonary fibrosis. *Eur. Respir. J.* **45**, 1434–1445 (2015).

154. Inomata, M., Nishioka, Y. & Azuma, A. Nintedanib: evidence for its therapeutic potential in idiopathic pulmonary fibrosis. *Core Evid.* **10**, 89–98 (2015).

155. Dimitroulis, I. A. Nintedanib: A Novel Therapeutic Approach for Idiopathic Pulmonary Fibrosis. *Respir. Care* **59**, 1450–1455 (2014).

156. Ahluwalia, N., Shea, B. S. & Tager, A. M. New Therapeutic Targets in Idiopathic Pulmonary Fibrosis. Aiming to Rein in Runaway Wound-Healing Responses. *Am. J. Respir. Crit. Care Med.* **190**, 867–878 (2014).

157. Mazzei, M. E., Richeldi, L. & Collard, H. R. Nintedanib in the treatment of idiopathic pulmonary fibrosis. *Ther. Adv. Respir. Dis.* **9**, 121–129 (2015).

158. Noth, I. *et al.* A Placebo-Controlled Randomized Trial of Warfarin in Idiopathic Pulmonary Fibrosis. *Am. J. Respir. Crit. Care Med.* **186**, 88–95 (2012).

159. Fukihara, J. & Kondoh, Y. Nintedanib (OFEV) in the treatment of idiopathic pulmonary fibrosis. *Expert Rev. Respir. Med.* **10**, 1247–1254 (2016).

160. Margaritopoulos, G. A., Vasarmidi, E. & Antoniou, K. M. Pirfenidone in the treatment of idiopathic pulmonary fibrosis: an evidence-based review of its place in therapy. *Core Evid.* **11**, 11–22 (2016).

161. Gharaee-Kermani, M. & Phan, S. Molecular Mechanisms of and Possible Treatment Strategies for Idiopathic Pulmonary Fibrosis. *Curr. Pharm. Des.* **11**, 3943–3971 (2005).

162. Gharaee-Kermani, M., Hu, B., Phan, S. & Gyetko, M. Recent Advances in Molecular Targets and Treatment of Idiopathic Pulmonary Fibrosis: Focus on TGFβ Signaling and the Myofibroblast. *Curr. Med. Chem.* **16**, 1400–1417 (2009).

163. Macarrón, R. & Hertzberg, R. P. Design and Implementation of High Throughput Screening Assays. *Mol. Biotechnol.* **47**, 270–285 (2011).

164. Tashiro, J. *et al.* Exploring Animal Models That Resemble Idiopathic Pulmonary Fibrosis. *Front. Med.* **4**, (2017).

165. Sime, P. J., Xing, Z., Graham, F. L., Csaky, K. G. & Gauldie, J. Adenovector-mediated gene transfer of active transforming growth factor-beta1 induces prolonged severe fibrosis in rat lung. *J. Clin. Invest.* **100**, 768–776 (1997).

166. Umezawa, H., Maeda, K., Takeuchi, T. & Okami, Y. New antibiotics, bleomycin A and B. *J. Antibiot. (Tokyo)* **19**, 200–209 (1966).

167. Umezawa, H. Bleomycin and other antitumor antibiotics of high molecular weight. *Antimicrob. Agents Chemother.* **5**, 1079–1085 (1965).

168. Umezawa, H., Ishizuka, M., Kimura, K., Iwanaga, J. & Takeuchi, T. BIOLOGICAL STUDIES ON INDIVIDUAL BLEOMYCINS. *J. Antibiot. (Tokyo)* **21**, 592–602 (1968).

169. Povirk, L. F., Han, Y. H. & Steighner, R. J. Structure of bleomycin-induced DNA double-strand breaks: predominance of blunt ends and single-base 5' extensions. *Biochemistry (Mosc.)* **28**, 5808–5814 (1989).

170. Schroeder, B. R. *et al.* The Disaccharide Moiety of Bleomycin Facilitates Uptake by Cancer Cells. *J. Am. Chem. Soc.* **136**, 13641–13656 (2014).

171. Morris, S. M. *et al.* A role for apoptosis in the toxicity and mutagenicity of bleomycin in AHH-1 tk+− human lymphoblastoid cells. *Mutat. Res. Mol. Mech. Mutagen.* **357**, 143–165 (1996).

172. Tounekti, O., Kenani, A., Foray, N., Orlowski, S. & Mir, L. M. The ratio of single- to double-strand DNA breaks and their absolute values determine cell death pathway. *Br. J. Cancer* **84**, 1272–1279 (2001).

173. Tounekti, O., Pron, G., Belehradek, J. & Mir, L. M. Bleomycin, an Apoptosis-mimetic Drug That Induces Two Types of Cell Death Depending on the Number of Molecules Internalized. *Cancer Res.* **53**, 5462–5469 (1993).

174. Lefterov, I. M., Koldamova, R. P., King, J. & Lazo, J. S. The C-terminus of human bleomycin hydrolase is required for protection against bleomycin-induced chromosomal damage. *Mutat. Res. Mol. Mech. Mutagen.* **421**, 1–7 (1998).

175. Ferrando, A. A., Velasco, G., Campo, E. & López-Otín, C. Cloning and Expression Analysis of Human Bleomycin Hydrolase, a Cysteine Proteinase Involved in Chemotherapy Resistance. *Cancer Res.* **56**, 1746–1750 (1996).

176. Brömme, D., Rossi, A. B., Smeekens, S. P., Anderson, D. C. & Payan, D. G. Human Bleomycin Hydrolase: Molecular Cloning, Sequencing, Functional Expression, and Enzymatic Characterization. *Biochemistry (Mosc.)* **35**, 6706–6714 (1996).

177. Snider, G. L., Hayes, J. A. & Korthy, A. L. Chronic Interstitial Pulmonary Fibrosis Produced in Hamsters by Endotracheal Bleomycin. *Am. Rev. Respir. Dis.* **117**, 1099–1108 (1978).

178. Thrall, R. S., McCormick, J. R., Jack, R. M., McReynolds, R. A. & Ward, P. A. Bleomycin-induced pulmonary fibrosis in the rat: inhibition by indomethacin. *Am. J. Pathol.* **95**, 117–130 (1979).

179. Borzone, G. *et al.* Bleomycin-Induced Chronic Lung Damage Does Not Resemble Human Idiopathic Pulmonary Fibrosis. *Am. J. Respir. Crit. Care Med.* **163**, 1648–1653 (2001).

180. Moeller, A., Ask, K., Warburton, D., Gauldie, J. & Kolb, M. The bleomycin animal model: a useful tool to investigate treatment options for idiopathic pulmonary fibrosis? *Int. J. Biochem. Cell Biol.* **40**, 362–382 (2008).

181. Huang, J. *et al.* Nintedanib inhibits fibroblast activation and ameliorates fibrosis in preclinical models of systemic sclerosis. *Ann. Rheum. Dis.* **75**, 883–890 (2016).

182. Vyalov, S. L., Gabbiani, G. & Kapanci, Y. Rat alveolar myofibroblasts acquire alpha-smooth muscle actin expression during bleomycin-induced pulmonary fibrosis. *Am. J. Pathol.* **143**, 1754–1765 (1993).

183. Coker, R. K. *et al.* Transforming growth factors-beta 1, -beta 2, and -beta 3 stimulate fibroblast procollagen production in vitro but are differentially expressed during bleomycin-induced lung fibrosis. *Am. J. Pathol.* **150**, 981–991 (1997).

184. Arribillaga, L. *et al.* Therapeutic effect of a peptide inhibitor of TGF-β on pulmonary fibrosis. *Cytokine* **53**, 327–333 (2011).

185. Pardo, A. & Selman, M. Idiopathic pulmonary fibrosis: new insights in its pathogenesis. *Int. J. Biochem. Cell Biol.* **34**, 1534–1538 (2002).

186. Kapanci, Y., Desmouliere, A., Pache, J. C., Redard, M. & Gabbiani, G. Cytoskeletal protein modulation in pulmonary alveolar myofibroblasts during idiopathic pulmonary fibrosis. Possible role of transforming growth factor beta and tumor necrosis factor alpha. *Am. J. Respir. Crit. Care Med.* **152**, 2163–2169 (1995).

187. Brown, R. F. R., Drawbaugh, R. B. & Marrs, T. C. An investigation of possible models for the production of progressive pulmonary fibrosis in the rat. The effects of repeated intratracheal instillation of bleomycin. *Toxicology* **51**, 101–110 (1988).

188. BRINGARDNER, B. D., BARAN, C. P., EUBANK, T. D. & MARSH, C. B. The Role of Inflammation in the Pathogenesis of Idiopathic Pulmonary Fibrosis. *Antioxid. Redox Signal.* **10**, 287–301 (2008).

189. Williamson, J. D., Sadofsky, L. R. & Hart, S. P. The pathogenesis of bleomycin-induced lung injury in animals and its applicability to human idiopathic pulmonary fibrosis. *Exp. Lung Res.* **41**, 57–73 (2015).

190. Barbas-Filho, J. *et al.* Evidence of type II pneumocyte apoptosis in the pathogenesis of idiopathic pulmonary fibrosis (IFP)/usual interstitial pneumonia (UIP). *J. Clin. Pathol.* **54**, 132–138 (2001).

191. Izbicki, G., Segel, M., Christensen, T., Conner, M. & Breuer, R. Time course of bleomycin-induced lung fibrosis. *Int. J. Exp. Pathol.* **83**, 111–119 (2002).

192. Kawamoto, M. & Fukuda, Y. Cell Proliferation during the Process of Bleomycin-induced Pulmonary Fibrosis in Rats. *Pathol. Int.* **40**, 227–238 (1990).

193. Balestro, E. *et al.* Immune Inflammation and Disease Progression in Idiopathic Pulmonary Fibrosis. *PLoS ONE* **11**, (2016).

194. Homer, R. J., Elias, J. A., Lee, C. G. & Herzog, E. Modern Concepts on the Role of Inflammation in Pulmonary Fibrosis. *Arch. Pathol. Lab. Med.* **135**, 780–788 (2011).

195. Song, M., He, B. & Qiu, Z. [Expressions of TNF alpha, PDGF in alveolar type II epithelial cells of rats with bleomycin-induced pulmonary fibrosis]. *Zhonghua Jie He He Hu Xi Za Zhi Zhonghua Jiehe He Huxi Zazhi Chin. J. Tuberc. Respir. Dis.* **21**, 221–223 (1998).

196. Cavarra, E. *et al.* Early response to bleomycin is characterized by different cytokine and cytokine receptor profiles in lungs. *Am. J. Physiol. - Lung Cell. Mol. Physiol.* **287**, L1186–L1192 (2004).

197. Scotton, C. J. & Chambers, R. C. Molecular targets in pulmonary fibrosis*: The myofibroblast in focus. *CHEST J.* **132**, 1311–1321 (2007).

198. Degryse, A. L. *et al.* Repetitive intratracheal bleomycin models several features of idiopathic pulmonary fibrosis. *Am. J. Physiol. - Lung Cell. Mol. Physiol.* **299**, L442–L452 (2010).

199. Ryerson, C. J., Donesky, D., Pantilat, S. Z. & Collard, H. R. Dyspnea in Idiopathic Pulmonary Fibrosis: A Systematic Review. *J. Pain Symptom Manage.* **43**, 771–782 (2012).

200. Zappala, C. J. *et al.* Marginal decline in forced vital capacity is associated with a poor outcome in idiopathic pulmonary fibrosis. *Eur. Respir. J.* **35**, 830–836 (2010).

201. Irvin, C. G. & Bates, J. H. Measuring the lung function in the mouse: the challenge of size. *Respir. Res.* **4**, 4 (2003).

202. Vanoirbeek, J. *et al.* Lung function measurements in mouse models of lung disease: What to expect from FEV0.1? *Eur. Respir. J.* **48**, PA4131 (2016).

203. Hoymann, H. G. Lung Function Measurements in Rodents in Safety Pharmacology Studies. *Front. Pharmacol.* **3**, (2012).

204. Parker, J. M. *et al.* A Phase 2 Randomized Controlled Study of Tralokinumab in Subjects with Idiopathic Pulmonary Fibrosis. *Am. J. Respir. Crit. Care Med.* (2017) doi:10.1164/rccm.201704-0784OC.

205. Jenkins, R. G. *et al.* An Official American Thoracic Society Workshop Report: Use of Animal Models for the Preclinical Assessment of Potential Therapies for Pulmonary Fibrosis. *Am. J. Respir. Cell Mol. Biol.* **56**, 667–679 (2017).

206. Kass, D. J. & Kaminski, N. Evolving Genomic Approaches to Idiopathic Pulmonary Fibrosis: Moving Beyond Genes. *Clin. Transl. Sci.* **4**, 372–379 (2011).

207. Korfei, M. *et al.* Comparative proteome analysis of lung tissue from patients with idiopathic pulmonary fibrosis (IPF), non-specific interstitial pneumonia (NSIP) and organ donors. *J. Proteomics* **85**, 109–128 (2013).

208. O'Dwyer, D. N. *et al.* The peripheral blood proteome signature of idiopathic pulmonary fibrosis is distinct from normal and is associated with novel immunological processes. *Sci. Rep.* **7**, 46560 (2017).

209. Hu, C. *et al.* Lipidomics Revealed Idiopathic Pulmonary Fibrosis-Induced Hepatic Lipid Disorders Corrected with Treatment of Baicalin in a Murine Model. *AAPS J.* **17**, 711–722 (2015).

210. Yu, G., Ibarra, G. H. & Kaminski, N. Fibrosis: Lessons from OMICS analyses of the human lung. *Matrix Biol. J. Int. Soc. Matrix Biol.* **68–69**, 422–434 (2018).

211. Human lung epithelial cell cultures for analysis of inhaled toxicants: Lessons learned and future directions. *Toxicol. In Vitro* **47**, 137–146 (2018).

212. Hiemstra, P. S., Grootaers, G., van der Does, A. M., Krul, C. A. M. & Kooter, I. M. Human lung epithelial cell cultures for analysis of inhaled toxicants: Lessons learned and future directions. *Toxicol. In Vitro* **47**, 137–146 (2018).

213. Maher, T. M. Idiopathic Pulmonary Fibrosis: Pathobiology of Novel Approaches to Treatment. *Clin. Chest Med.* **33**, 69–83 (2012).

214. Blume, C. & Davies, D. E. In vitro and ex vivo models of human asthma. *Eur. J. Pharm. Biopharm. Off. J. Arbeitsgemeinschaft Für Pharm. Verfahrenstechnik EV* **84**, 394–400 (2013).

215. Hocke, A. C., Suttorp, N. & Hippenstiel, S. Human lung ex vivo infection models. *Cell Tissue Res.* **367**, 511–524 (2017).

216. Crabbé, A., Ledesma, M. A. & Nickerson, C. A. Mimicking the host and its microenvironment in vitro for studying mucosal infections by Pseudomonas-aeruginosa. *Pathog. Dis.* **71**, 1–19 (2014).

217. Rothen-Rutishauser, B., Blank, F., Mühlfeld, C. & Gehr, P. In vitro models of the human epithelial airway barrier to study the toxic potential of particulate matter. *Expert Opin. Drug Metab. Toxicol.* **4**, 1075–1089 (2008).

218. Klein, S. G., Hennen, J., Serchi, T., Blömeke, B. & Gutleb, A. C. Potential of coculture in vitro models to study inflammatory and sensitizing effects of particles on the lung. *Toxicol. In Vitro* **25**, 1516–1534 (2011).

219. Loxham, M. *et al.* The Effects on Bronchial Epithelial Mucociliary Cultures of Coarse, Fine, and Ultrafine Particulate Matter From an Underground Railway Station. *Toxicol. Sci.* **145**, 98–107 (2015).

220. Wohlsen, A. *et al.* The early allergic response in small airways of human precision-cut lung slices. *Eur. Respir. J.* **21**, 1024–1032 (2003).

221. Uhl, F. E. *et al.* Preclinical validation and imaging of Wnt-induced repair in human 3D lung tissue cultures. *Eur. Respir. J.* **46**, 1150–1166 (2015).

222. Liu, G. *et al.* Use of precision cut lung slices as a translational model for the study of lung biology. *Respir. Res.* **20**, 162 (2019).

223. Ruigrok, M. J. R. *et al.* The effects of oxygen concentration on cell death, anti-oxidant transcription, acute inflammation, and cell proliferation in precision-cut lung slices. *Sci. Rep.* **9**, 1–13 (2019).

224. Baker, M. Reproducibility: Respect your cells! *Nature* https://www.nature.com/articles/537433a (2016) doi:10.1038/537433a.

225. Grizzle, W. E., Bell, W. C. & Sexton, K. C. Issues in collecting, processing and storing human tissues and associated information to support biomedical research. *Cancer Biomark. Sect. Dis. Markers* **9**, 531–549 (2010).

226. Hittinger, M. *et al.* Autologous co-culture of primary human alveolar macrophages and epithelial cells for investigating aerosol medicines. Part I: model characterisation. *Altern. Lab. Anim. ATLA* **44**, 337–347 (2016).

227. Greer, R. M., Miller, J. D., Okoh, V. O., Halloran, B. A. & Prince, L. S. Epithelial-mesenchymal co-culture model for studying alveolar morphogenesis. *Organogenesis* **10**, 340–349 (2014).

228. Lehmann, A. D. *et al.* An in vitro triple cell co-culture model with primary cells mimicking the human alveolar epithelial barrier. *Eur. J. Pharm. Biopharm.* **77**, 398–406 (2011).

229. *Human airway inflammation: sampling techniques and analytical protocols*. (Humana, 2001).

230. Thorley, A. J. *et al.* Differential Regulation of Cytokine Release and Leukocyte Migration by Lipopolysaccharide-Stimulated Primary Human Lung Alveolar Type II Epithelial Cells and Macrophages. *J. Immunol.* **178**, 463–473 (2007).

231. Li, S. *et al.* miR-130b-3p Modulates Epithelial-Mesenchymal Crosstalk in Lung Fibrosis by Targeting IGF-1. *PLoS ONE* **11**, (2016).

232. Hayflick, L. & Moorhead, P. S. The serial cultivation of human diploid cell strains. *Exp. Cell Res.* **25**, 585–621 (1961).

233. Fuchs, S. *et al.* Differentiation of human alveolar epithelial cells in primary culture: morphological characterization and synthesis of caveolin-1 and surfactant protein-C. *Cell Tissue Res.* **311**, 31–45 (2003).

234. Bhaskaran, M. *et al.* Trans-differentiation of Alveolar Epithelial Type II Cells to Type I Cells Involves Autocrine Signaling by Transforming Growth Factor β1 through the Smad Pathway. *J. Biol. Chem.* **282**, 3968–3976 (2007).

235. Zhao, L., Yee, M. & O'Reilly, M. A. Transdifferentiation of alveolar epithelial type II to type I cells is controlled by opposing TGF-β and BMP signaling. *Am. J. Physiol. - Lung Cell. Mol. Physiol.* **305**, L409–L418 (2013).

236. Danto, S. I., Shannon, J. M., Borok, Z., Zabski, S. M. & Crandall, E. D. Reversible transdifferentiation of alveolar epithelial cells. *Am. J. Respir. Cell Mol. Biol.* **12**, 497–502 (1995).

237. FOSTER, C. D., VARGHESE, L. S., SKALINA, R. B., GONZALES, L. W. & GUTTENTAG, S. H. In Vitro Transdifferentiation of Human Fetal Type II Cells Toward a Type I–like Cell. *Pediatr. Res.* **61**, 404–409 (2007).

238. Zhang, W.-J. *et al.* The reconstruction of lung alveolus-like structure in collagen-matrigel/microcapsules scaffolds in vitro. *J. Cell. Mol. Med.* **15**, 1878–1886 (2011).

239. Bur, M., Rothen-Rutishauser, B., Huwer, H. & Lehr, C.-M. A novel cell compatible impingement system to study in vitro drug absorption from dry powder aerosol formulations. *Eur. J. Pharm. Biopharm.* **72**, 350–357 (2009).

240. Franks, T. J. *et al.* Resident Cellular Components of the Human Lung. *Proc. Am. Thorac. Soc.* **5**, 763–766 (2008).

241. Santis, M. M. D., Bölükbas, D. A., Lindstedt, S. & Wagner, D. E. How to build a lung: latest advances and emerging themes in lung bioengineering. *Eur. Respir. J.* **52**, (2018).

242. Burgstaller, G. *et al.* The instructive extracellular matrix of the lung: basic composition and alterations in chronic lung disease. *Eur. Respir. J.* **50**, 1601805 (2017).

243. Faffe, D. S. & Zin, W. A. Lung Parenchymal Mechanics in Health and Disease. *Physiol. Rev.* **89**, 759–775 (2009).

244. Chang, J. W. *et al.* Tissue-Engineered Tracheal Reconstruction Using Three-Dimensionally Printed Artificial Tracheal Graft: Preliminary Report. *Artif. Organs* **38**, E95–E105 (2014).

245. Ling, T.-Y., Liu, Y.-L., Huang, Y.-K., Gu, S.-Y. & Lin, F.-H. Differentiation of lung stem/progenitor cells into alveolar pneumocytes and induction of angiogenesis within a 3D gelatin – Microbubble scaffold. *Biomaterials* **35**, 5660–5669 (2014).

246. Singh, D., Zo, S. M., Kumar, A. & Han, S. S. Engineering three-dimensional macroporous hydroxyethyl methacrylate-alginate-gelatin cryogel for growth and proliferation of lung epithelial cells. *J. Biomater. Sci. Polym. Ed.* **24**, 1343–1359 (2013).

247. Lewis, K. J. R. *et al.* In vitro model alveoli from photodegradable microsphere templates. *Biomater. Sci.* **3**, 821–832 (2015).

248. Wilkinson, D. C. *et al.* Development of a Three-Dimensional Bioengineering Technology to Generate Lung Tissue for Personalized Disease Modeling. *Stem Cells Transl. Med.* **6**, 622–633 (2017).

249. Lee, V. K. *et al.* Creating Perfused Functional Vascular Channels Using 3D Bio-Printing Technology. *Biomaterials* **35**, 8092–8102 (2014).

250. Fischer, S. N. *et al.* Organ-derived coatings on electrospun nanofibers as ex vivo microenvironments. *Biomaterials* **32**, 538–546 (2011).

251. Hinton, T. J. *et al.* Three-dimensional printing of complex biological structures by freeform reversible embedding of suspended hydrogels. *Sci. Adv.* **1**, e1500758 (2015).

252. Organoid research. https://www.nature.com/collections/gglyjbyvdq.

253. Miller, A. J. *et al.* Generation of lung organoids from human pluripotent stem cells in vitro. *Nat. Protoc.* **14**, 518–540 (2019).

254. Fehrenbach, H. Alveolar epithelial type II cells from embryonic stem cells: knights in shining armour? *Eur. Respir. J.* **39**, 240–241 (2012).

255. Ghaedi, M. *et al.* Human iPS cell-derived alveolar epithelium repopulates lung extracellular matrix. *J. Clin. Invest.* **123**, 4950–4962 (2013).

256. Ghaedi, M. *et al.* Alveolar epithelial differentiation of human induced pluripotent stem cells in a rotating bioreactor. *Biomaterials* **35**, 699–710 (2014).

257. Huang, S. X. L. *et al.* Efficient generation of lung and airway epithelial cells from human pluripotent stem cells. *Nat. Biotechnol.* **32**, 84–91 (2014).

258. Cerrada, A. *et al.* Human Decidua-Derived Mesenchymal Stem Cells Differentiate into Functional Alveolar Type II-Like Cells that Synthesize and Secrete Pulmonary Surfactant Complexes. *PLoS ONE* **9**, e110195 (2014).

259. Oeztuerk-Winder, F., Guinot, A., Ochalek, A. & Ventura, J.-J. Regulation of human lung alveolar multipotent cells by a novel p38α MAPK/miR-17-92 axis. *EMBO J.* **31**, 3431–3441 (2012).

260. Polak, J. M. & Bishop, A. E. Stem Cells and Tissue Engineering: Past, Present, and Future. *Ann. N. Y. Acad. Sci.* **1068**, 352–366 (2006).

261. Siti-Ismail, N., Samadikuchaksaraei, A., Bishop, A. E., Polak, J. M. & Mantalaris, A. Development of a Novel Three-Dimensional, Automatable and Integrated Bioprocess for the Differentiation of Embryonic Stem Cells into Pulmonary Alveolar Cells in a Rotating Vessel Bioreactor System. *Tissue Eng. Part C Methods* **18**, 263–272 (2012).

262. Beers, M. F. & Moodley, Y. When Is an Alveolar Type 2 Cell an Alveolar Type 2 Cell? A Conundrum for Lung Stem Cell Biology and Regenerative Medicine. *Am. J. Respir. Cell Mol. Biol.* **57**, 18–27 (2017).

263. Mason, R. J. Biology of alveolar type II cells. *Respirology* **11**, S12–S15 (2006).

264. Whitsett, J. A., Wert, S. E. & Weaver, T. E. Alveolar Surfactant Homeostasis and the Pathogenesis of Pulmonary Disease. *Annu. Rev. Med.* **61**, 105–119 (2010).

265. Kalina, M., Mason, R. J. & Shannon, J. M. Surfactant protein C is expressed in alveolar type II cells but not in Clara cells of rat lung. *Am. J. Respir. Cell Mol. Biol.* **6**, 594–600 (1992).

266. Kishore, U. *et al.* Surfactant proteins SP-A and SP-D: Structure, function and receptors. *Mol. Immunol.* **43**, 1293–1315 (2006).

267. Wright, J. R. Immunoregulatory functions of surfactant proteins. *Nat. Rev. Immunol.* **5**, nri1528 (2005).

268. Fitzgerald, M. L. *et al.* ABCA3 inactivation in mice causes respiratory failure, loss of pulmonary surfactant, and depletion of lung phosphatidylglycerol. *J. Lipid Res.* **48**, 621–632 (2007).

269. Mulugeta, S. *et al.* Identification of LBM180, a Lamellar Body Limiting Membrane Protein of Alveolar Type II Cells, as the ABC Transporter Protein ABCA3. *J. Biol. Chem.* **277**, 22147–22155 (2002).

270. Veldhuizen, R., Nag, K., Orgeig, S. & Possmayer, F. The role of lipids in pulmonary surfactant. *Biochim. Biophys. Acta BBA - Mol. Basis Dis.* **1408**, 90–108 (1998).

271. Goss, V., Hunt, A. N. & Postle, A. D. Regulation of lung surfactant phospholipid synthesis and metabolism. *Biochim. Biophys. Acta* **1831**, 448–458 (2013).

272. Hsia, C. C. W., Hyde, D. M., Ochs, M. & Weibel, E. R. An Official Research Policy Statement of the American Thoracic Society/European Respiratory Society:

Standards for Quantitative Assessment of Lung Structure. *Am. J. Respir. Crit. Care Med.* **181**, 394–418 (2010).

273. Dietl, P., Haller, T., Mair, N. & Frick, M. Mechanisms of Surfactant Exocytosis in Alveolar Type II Cells In Vitro and In Vivo. *Physiology* **16**, 239–243 (2001).

274. Hariri, M. *et al.* Biogenesis of Multilamellar Bodies via Autophagy. *Mol. Biol. Cell* **11**, 255–268 (2000).

275. Marconett, C. N. *et al.* Integrated Transcriptomic and Epigenomic Analysis of Primary Human Lung Epithelial Cell Differentiation. *PLoS Genet.* **9**,.

276. Chuman, Y. *et al.* Napsin A, a member of the aspartic protease family, is abundantly expressed in normal lung and kidney tissue and is expressed in lung adenocarcinomas. *FEBS Lett.* **462**, 129–134 (1999).

277. Nielsen, S., King, L. S., Christensen, B. M. & Agre, P. Aquaporins in complex tissues. II. Subcellular distribution in respiratory and glandular tissues of rat. *Am. J. Physiol. - Cell Physiol.* **273**, C1549–C1561 (1997).

278. Williams, M. C., Cao, Y., Hinds, A., Rishi, A. K. & Wetterwald, A. T1 alpha protein is developmentally regulated and expressed by alveolar type I cells, choroid plexus, and ciliary epithelia of adult rats. *Am. J. Respir. Cell Mol. Biol.* **14**, 577–585 (1996).

279. Koval, M. Tight junctions, but not too tight: fine control of lung permeability by claudins. *Am. J. Physiol. - Lung Cell. Mol. Physiol.* **297**, L217–L218 (2009).

280. Canessa, C. M. *et al.* Amiloride-sensitive epithelial Na+ channel is made of three homologous subunits. *Nature* **367**, 463–467 (1994).

281. Kim, K. J. & Suh, D. J. Asymmetric effects of H2O2 on alveolar epithelial barrier properties. *Am. J. Physiol. - Lung Cell. Mol. Physiol.* **264**, L308–L315 (1993).

282. Marmai, C. *et al.* Alveolar epithelial cells express mesenchymal proteins in patients with idiopathic pulmonary fibrosis. *Am. J. Physiol. - Lung Cell. Mol. Physiol.* **301**, L71–L78 (2011).

283. Kemp, S. J. *et al.* Immortalization of Human Alveolar Epithelial Cells to Investigate Nanoparticle Uptake. *Am. J. Respir. Cell Mol. Biol.* **39**, 591–597 (2008).

284. Katsumiti, A., Ruenraroengsak, P., Cajaraville, M. P., Thorley, A. J. & Tetley, T. D. Immortalisation of primary human alveolar epithelial lung cells using a non-viral vector to study respiratory bioreactivity in vitro. *Sci. Rep.* **10**, 1–13 (2020).

285. Bairoch, A. The Cellosaurus, a Cell-Line Knowledge Resource. *J. Biomol. Tech. JBT* **29**, 25–38 (2018).

286. Foster, C. D., Varghese, L. S., Gonzales, L. W., Margulies, S. S. & Guttentag, S. H. The Rho pathway mediates transition to an alveolar type I cell phenotype during static stretch of alveolar type II cells. *Pediatr. Res.* **67**, 585–590 (2010).

287. Marx, V. Cell-line authentication demystified. *Nat. Methods* **11**, 483–488 (2014).

288. O'Hare, M. J. *et al.* Conditional immortalization of freshly isolated human mammary fibroblasts and endothelial cells. *Proc. Natl. Acad. Sci. U. S. A.* **98**, 646–651 (2001).

289. Kaur, G. & Dufour, J. M. Cell lines - Valuable tools or useless artifacts? *Spermatogenesis* **2**, 1–5 (2012).

290. Wendt, H. *et al.* Artificial Skin – Culturing of Different Skin Cell Lines for Generating an Artificial Skin Substitute on Cross-Weaved Spider Silk Fibres. *PLoS ONE* **6**, (2011).

291. Macdonald, C. Development of New Cell Lines for Animal Cell Biotechnology. *Crit. Rev. Biotechnol.* **10**, 155–178 (1990).

292. Geraghty, R. J. *et al.* Guidelines for the use of cell lines in biomedical research. *Br. J. Cancer* **111**, 1021–1046 (2014).

293. Gazdar, A. F., Gao, B. & Minna, J. D. Lung cancer cell lines: Useless artifacts or invaluable tools for medical science? *Lung Cancer Amst. Neth.* **68**, 309–318 (2010).

294. Nelson-Rees, W. A., Daniels, D. W. & Flandermeyer, R. R. Cross-contamination of cells in culture. *Science* **212**, 446–452 (1981).

295. Capes-Davis, A. *et al.* Check your cultures! A list of cross-contaminated or misidentified cell lines. *Int. J. Cancer* **127**, 1–8 (2010).

296. Hay, R. J., Macy, M. L. & Chen, T. R. Mycoplasma infection of cultured cells. *Nature* **339**, 487–488 (1989).

297. Blume, C. & Davies, D. E. In vitro and ex vivo models of human asthma. *Eur. J. Pharm. Biopharm.* **84**, 394–400 (2013).

298. Stokes, C. A. *et al.* Role of Interleukin-1 and MyD88-Dependent Signaling in Rhinovirus Infection ▿ . *J. Virol.* **85**, 7912–7921 (2011).

299. Vinhas, R. *et al.* Pollen proteases compromise the airway epithelial barrier through degradation of transmembrane adhesion proteins and lung bioactive peptides. *Allergy* **66**, 1088–1098 (2011).

300. Banga, A., Witzmann, F. A., Petrache, H. I. & Blazer-Yost, B. L. Functional Effects of Nanoparticle Exposure on Calu-3 Airway Epithelial Cells. *Cell. Physiol. Biochem.* **29**, 197–212 (2012).

301. Heijink, I. H., Brandenburg, S. M., Postma, D. S. & Oosterhout, A. J. M. van. Cigarette smoke impairs airway epithelial barrier function and cell–cell contact recovery. *Eur. Respir. J.* **39**, 419–428 (2012).

302. Harcourt, J. L., Caidi, H., Anderson, L. J. & Haynes, L. M. Evaluation of the Calu-3 cell line as a model of in vitro respiratory syncytial virus infection. *J. Virol. Methods* **174**, 144–149 (2011).

303. MacDonald, C., Shao, D., Oli, A. & Agu, R. U. Characterization of Calu-3 cell monolayers as a model of bronchial epithelial transport: organic cation interaction studies. *J. Drug Target.* **21**, 97–106 (2013).

304. Brower, M., Carney, D. N., Oie, H. K., Gazdar, A. F. & Minna, J. D. Growth of Cell Lines and Clinical Specimens of Human Non-Small Cell Lung Cancer in a Serum-free Defined Medium. *Cancer Res.* **46**, 798–806 (1986).

305. Sporty, J. L., Horálková, L. & Ehrhardt, C. In vitro cell culture models for the assessment of pulmonary drug disposition. *Expert Opin. Drug Metab. Toxicol.* **4**, 333–345 (2008).

306. Tamò, L. *et al.* Generation of an alveolar epithelial type II cell line from induced pluripotent stem cells. *Am. J. Physiol.-Lung Cell. Mol. Physiol.* **315**, L921–L932 (2018).

307. Giard, D. J. *et al.* In Vitro Cultivation of Human Tumors: Establishment of Cell Lines Derived From a Series of Solid Tumors. *J. Natl. Cancer Inst.* **51**, 1417–1423 (1973).

308. Lieber, M., Smith, B., Szakal, A., Nelson-Rees, W. & Todaro, G. A continuous tumor-cell line from a human lung carcinoma with properties of type II alveolar epithelial cells. *Int. J. Cancer J. Int. Cancer* **17**, 62–70 (1976).

309. Foster, K. A., Oster, C. G., Mayer, M. M., Avery, M. L. & Audus, K. L. Characterization of the A549 Cell Line as a Type II Pulmonary Epithelial Cell Model for Drug Metabolism. *Exp. Cell Res.* **243**, 359–366 (1998).

310. Nardone, L. L. & Andrews, S. B. Cell line A549 as a model of the type II pneumocyte: Phospholipid biosynthesis from native and organometallic precursors. *Biochim. Biophys. Acta BBA - Lipids Lipid Metab.* **573**, 276–295 (1979).

311. Swain, R. J., Kemp, S. J., Goldstraw, P., Tetley, T. D. & Stevens, M. M. Assessment of Cell Line Models of Primary Human Cells by Raman Spectral Phenotyping. *Biophys. J.* **98**, 1703–1711 (2010).

312. Corbière, V. *et al.* Phenotypic characteristics of human type II alveolar epithelial cells suitable for antigen presentation to T lymphocytes. *Respir. Res.* **12**, 15 (2011).

313. Ham, R. G. An improved nutrient solution for diploid Chinese hamster and human cell lines. *Exp. Cell Res.* **29**, 515–526 (1963).

314. Ham, R. G. CLONAL GROWTH OF MAMMALIAN CELLS IN A CHEMICALLY DEFINED, SYNTHETIC MEDIUM*. *Proc. Natl. Acad. Sci. U. S. A.* **53**, 288–293 (1965).

315. Dulbecco, R. & Freeman, G. Plaque production by the polyoma virus. *Virology* **8**, 396–397 (1959).

316. Rutzky, L. P. & Pumper, R. W. Supplement to a survey of commercially available tissue culture media (1970). *In Vitro* **9**, 408–409 (1974).

317. R. Ian Freshney. *Culture of Animal Cells: A Manual of Basic Technique and Specialized Applications*. (John Wiley and Sons Inc, 2010).

318. Wong, C., Vosburgh, E., Levine, A. J., Cong, L. & Xu, E. Y. Human Neuroendocrine Tumor Cell Lines as a Three-Dimensional Model for the Study of Human Neuroendocrine Tumor Therapy. *J. Vis. Exp. JoVE* (2012) doi:10.3791/4218.

319. Vinci, M. *et al.* Advances in establishment and analysis of three-dimensional tumor spheroid-based functional assays for target validation and drug evaluation. *BMC Biol.* **10**, 29 (2012).

320. Correa, R. Primary Epithelial Ovarian Cancer Cells form Spheroids when Cultured on Corning (R) Ultra-Low Attachment Surfaces.

321. Tack, L. C., Thomas, M. & Reich, K. Automated forensic DNA purification optimized for FTA card punches and identifiler STR-based PCR analysis. *Clin. Lab. Med.* **27**, 183–191 (2007).

322. King, G. The effects of neuregulin-1β on synthesis and secretion of surfactant phosphatidylcholine by cultured fetal rat type II pneumocytes. (Murdoch University, 2013).

323. Dammann, C. E. L., Nielsen, H. C. & Carraway, K. L. Role of Neuregulin-1β in the Developing Lung. *Am. J. Respir. Crit. Care Med.* **167**, 1711–1716 (2003).

324. King, G., Damas, J. E., Cake, M. H., Berryman, D. & Maker, G. L. Influence of glucocorticoids, neuregulin-1β, and sex on surfactant phospholipid secretion from type II cells. *Am. J. Physiol. - Lung Cell. Mol. Physiol.* **306**, L292–L298 (2014).

325. Kagan, H. M. & Li, W. Lysyl oxidase: Properties, specificity, and biological roles inside and outside of the cell. *J. Cell. Biochem.* **88**, 660–672 (2003).

326. Glassman, A. B., Rydzewski, R. S. & Bennett, C. E. Trace metal levels in commercially prepared tissue culture media. *Tissue Cell* **12**, 613–617 (1980).

327. Eden, E., Navon, R., Steinfeld, I., Lipson, D. & Yakhini, Z. GOrilla: a tool for discovery and visualization of enriched GO terms in ranked gene lists. *BMC Bioinformatics* **10**, 48 (2009).

328. Supek, F., Bošnjak, M., Škunca, N. & Šmuc, T. REVIGO Summarizes and Visualizes Long Lists of Gene Ontology Terms. *PLOS ONE* **6**, e21800 (2011).

329. Livak, K. J. & Schmittgen, T. D. Analysis of Relative Gene Expression Data Using Real-Time Quantitative PCR and the 2−ΔΔCT Method. *Methods* **25**, 402–408 (2001).

330. Vandesompele, J. *et al.* Accurate normalization of real-time quantitative RT-PCR data by geometric averaging of multiple internal control genes. *Genome Biol.* **3**, research0034.1-research0034.11 (2002).

331. Bustin, S. A. *et al.* The MIQE Guidelines: Minimum Information for Publication of Quantitative Real-Time PCR Experiments. *Clin. Chem.* **55**, 611–622 (2009).

332. Masters, J. R. *et al.* Short tandem repeat profiling provides an international reference standard for human cell lines. *Proc. Natl. Acad. Sci. U. S. A.* **98**, 8012–8017 (2001).

333. Masters, J., Reid, Y., Nims, R., Bauer, S. & Furtado, M. ANSI/ATCC ASN-0002-2011 Authentication of Human Cell Lines; Standardisation of STR Profiling. ANSI eStandards Store (2012). (2011).

334. Choppa, P. C., Vojdani, A., Tagle, C., Andrin, R. & Magtoto, L. Multiplex PCR for the detection of Mycoplasma fermentans, M. hominis and M. penetrans in cell cultures and blood samples of patients with chronic fatigue syndrome. *Mol. Cell. Probes* **12**, 301–308 (1998).

335. Pinto, M. *et al.* Enterocyte-like differentiation and polarization of the human colon carcinoma cell line Caco-2 in culture. *Biol Cell* **47**, 323–330 (1983).

336. Cereijido, M., Robbins, E. S., Dolan, W. J., Rotunno, C. A. & Sabatini, D. D. Polarized monolayers formed by epithelial cells on a permeable and translucent support. *J. Cell Biol.* **77**, 853–880 (1978).

337. Cukierman, E. Preparation of Extracellular Matrices Produced by Cultured Fibroblasts. *Curr. Protoc. Cell Biol.* **16**, 10.9.1-10.9.15 (2002).

338. Bokhari, M., Carnachan, R. J., Przyborski, S. A. & Cameron, N. R. Emulsion-templated porous polymers as scaffolds for three dimensional cell culture: effect of synthesis parameters on scaffold formation and homogeneity. *J. Mater. Chem.* **17**, 4088–4094 (2007).

339. Knight, E. & Przyborski, S. Advances in 3D cell culture technologies enabling tissue-like structures to be created in vitro. *J. Anat.* **227**, 746–756 (2015).

340. Tibbitt, M. W. & Anseth, K. S. Hydrogels as Extracellular Matrix Mimics for 3D Cell Culture. *Biotechnol. Bioeng.* **103**, 655–663 (2009).

341. Keller Gordon M. In vitro differentiation of embryonic stem cells. *Curr. Opin. Cell Biol.* **7**, 862–869 (1995).

342. Szczepny, A., Hogarth, C. A., Young, J. & Loveland, K. L. Identification of Hedgehog Signaling Outcomes in Mouse Testis Development Using a Hanging Drop-Culture System. *Biol. Reprod.* **80**, 258–263 (2009).

343. Carterson, A. J. *et al.* A549 Lung Epithelial Cells Grown as Three-Dimensional Aggregates: Alternative Tissue Culture Model for Pseudomonas aeruginosa Pathogenesis. *Infect. Immun.* **73**, 1129–1140 (2005).

344. Barkauskas, C. E. *et al.* Type 2 alveolar cells are stem cells in adult lung. *J. Clin. Invest.* **123**, 3025–3036 (2013).

345. Jain, R. *et al.* Plasticity of Hopx+ Type I alveolar cells to regenerate Type II cells in the lung. *Nat. Commun.* **6**, 6727 (2015).

346. Mason, R. J. & Williams, M. C. Phospholipid composition and ultrastructure of A549 cells and other cultured pulmonary epithelial cells of presumed type II cell origin. *Biochim. Biophys. Acta* **617**, 36–50 (1980).

347. Swain, R. J., Kemp, S. J., Goldstraw, P., Tetley, T. D. & Stevens, M. M. Assessment of Cell Line Models of Primary Human Cells by Raman Spectral Phenotyping. *Biophys. J.* **98**, 1703–1711 (2010).

348. Heijink, I. H. *et al.* Characterisation of cell adhesion in airway epithelial cell types using electric cell–substrate impedance sensing. *Eur. Respir. J.* **35**, 894–903 (2010).

349. Balis, J. U., Bumgarner, S. D., Paciga, J. E., Paterson, J. F. & Shelley, S. A. Synthesis of lung surfactant-associated glycoproteins by A549 cells: description of an in vitro model for human type II cell dysfunction. *Exp. Lung Res.* **6**, 197–213 (1984).

350. Gao, R. *et al.* Retinoic acid promotes primary fetal alveolar epithelial type II cell proliferation and differentiation to alveolar epithelial type I cells. *Vitro Cell. Dev. Biol. - Anim.* **51**, 479–487 (2015).

351. Hanahan, D. & Weinberg, R. A. The Hallmarks of Cancer. *Cell* **100**, 57–70 (2000).

352. Hanahan, D. & Weinberg, R. A. Hallmarks of Cancer: The Next Generation. *Cell* **144**, 646–674 (2011).

353. Polosa, R. *et al.* Expression of c-erbB Receptors and Ligands in Human Bronchial Mucosa. *Am. J. Respir. Cell Mol. Biol.* **20**, 914–923 (1999).

354. Ridley, C. & Thornton, D. J. Mucins: the frontline defence of the lung. *Biochem. Soc. Trans.* **46**, 1099–1106 (2018).

355. Chen, G. *et al.* SPDEF is required for mouse pulmonary goblet cell differentiation and regulates a network of genes associated with mucus production. *J. Clin. Invest.* **119**, 2914–2924 (2009).

356. Antoni, D., Burckel, H., Josset, E. & Noel, G. Three-Dimensional Cell Culture: A Breakthrough in Vivo. *Int. J. Mol. Sci.* **16**, 5517–5527 (2015).

357. Zanoni, M. *et al.* 3D tumor spheroid models for *in vitro* therapeutic screening: a systematic approach to enhance the biological relevance of data obtained. *Sci. Rep.* **6**, srep19103 (2016).

358. MEENACH, S. A. *et al.* Development of three-dimensional lung multicellular spheroids in air- and liquid-interface culture for the evaluation of anticancer therapeutics. *Int. J. Oncol.* **48**, 1701–1709 (2016).

359. Karp, P. *et al.* An In Vitro Model of Differentiated Human Airway Epithelia. in *Epithelial Cell Culture Protocols* (ed. Wise, C.) 115–137 (Humana Press, 2002). doi:10.1385/1-59259-185-X:115.

360. Hidalgo, I. J., Raub, T. J. & Borchardt, R. T. Characterization of the human colon carcinoma cell line (Caco-2) as a model system for intestinal epithelial permeability. *Gastroenterology* **96**, 736–749 (1989).

361. Liu, J. *et al.* Three-dimensional spheroid cultures of A549 and HepG2 cells exhibit different lipopolysaccharide (LPS) receptor expression and LPS-induced cytokine response compared with monolayer cultures. *Innate Immun.* **17**, 245–255 (2011).

362. Mishra, D. K. *et al.* Gene expression profile of A549 cells from tissue of 4D model predicts poor prognosis in lung cancer patients. *Int. J. Cancer* **134**, 789–798 (2014).

363. Wasserman, D. H. Four grams of glucose. *Am. J. Physiol. - Endocrinol. Metab.* **296**, E11–E21 (2009).

364. Marroquin, L. D., Hynes, J., Dykens, J. A., Jamieson, J. D. & Will, Y. Circumventing the Crabtree Effect: Replacing Media Glucose with Galactose Increases Susceptibility of HepG2 Cells to Mitochondrial Toxicants. *Toxicol. Sci.* **97**, 539–547 (2007).

365. Elkalaf, M., Anděl, M. & Trnka, J. Low Glucose but Not Galactose Enhances Oxidative Mitochondrial Metabolism in C2C12 Myoblasts and Myotubes. *PLOS ONE* **8**, e70772 (2013).

366. Young, J. D. Metabolic flux rewiring in mammalian cell cultures. *Curr. Opin. Biotechnol.* **24**, (2013).

367. Mehta, G., Hsiao, A. Y., Ingram, M., Luker, G. D. & Takayama, S. Opportunities and Challenges for use of Tumor Spheroids as Models to Test Drug Delivery and Efficacy. *J. Control. Release Off. J. Control. Release Soc.* **164**, 192–204 (2012).

368. Hirschhaeuser, F. *et al.* Multicellular tumor spheroids: an underestimated tool is catching up again. *J. Biotechnol.* **148**, 3–15 (2010).

369. Loscertales, M. *et al.* Type IV collagen drives alveolar epithelial–endothelial association and the morphogenetic movements of septation. *BMC Biol.* **14**, (2016).

370. Dvorak, H. F. Tumors: wounds that do not heal. Similarities between tumor stroma generation and wound healing. *N. Engl. J. Med.* **315**, 1650–1659 (1986).

371. Johnson, B. & Mahadevan, D. Emerging Role and Targeting of Carcinoembryonic Antigen-related Cell Adhesion Molecule 6 (CEACAM6) in Human Malignancies. *Clin. Cancer Drugs* **2**, 100–111 (2015).

372. Hammarström, S. The carcinoembryonic antigen (CEA) family: structures, suggested functions and expression in normal and malignant tissues. *Semin. Cancer Biol.* **9**, 67–81 (1999).

373. Schölzel, S. *et al.* Carcinoembryonic Antigen Family Members CEACAM6 and CEACAM7 Are Differentially Expressed in Normal Tissues and Oppositely Deregulated in Hyperplastic Colorectal Polyps and Early Adenomas. *Am. J. Pathol.* **156**, 595–605 (2000).

374. Hill, D. J., Edwards, A. M., Rowe, H. A. & Virji, M. Carcinoembryonic antigen-related cell adhesion molecule (CEACAM)-binding recombinant polypeptide confers protection against infection by respiratory and urogenital pathogens. *Mol. Microbiol.* **55**, 1515–1527 (2005).

375. Klaile, E. *et al.* Binding of Candida albicans to Human CEACAM1 and CEACAM6 Modulates the Inflammatory Response of Intestinal Epithelial Cells. *mBio* **8**, e02142-16 (2017).

376. Ou, G., Baranov, V., Lundmark, E., Hammarström, S. & Hammarström, M.-L. Contribution of intestinal epithelial cells to innate immunity of the human gut--studies on polarized monolayers of colon carcinoma cells. *Scand. J. Immunol.* **69**, 150–161 (2009).

377. Zanetti, M., Gennaro, R. & Romeo, D. Cathelicidins: a novel protein family with a common proregion and a variable C-terminal antimicrobial domain. *FEBS Lett.* **374**, 1–5 (1995).

378. Skerlavaj, B. *et al.* Biological characterization of two novel cathelicidin-derived peptides and identification of structural requirements for their antimicrobial and cell lytic activities. *J. Biol. Chem.* **271**, 28375–28381 (1996).

379. Kościuczuk, E. M. *et al.* Cathelicidins: family of antimicrobial peptides. A review. *Mol. Biol. Rep.* **39**, 10957–10970 (2012).

380. Laube, D. M., Yim, S., Ryan, L. K., Kisich, K. O. & Diamond, G. Antimicrobial peptides in the airway. *Curr. Top. Microbiol. Immunol.* **306**, 153–182 (2006).

381. Knowles, M. R. & Boucher, R. C. Mucus clearance as a primary innate defense mechanism for mammalian airways. *J. Clin. Invest.* **109**, 571–577 (2002).

382. Kesimer, M. *et al.* Tracheobronchial air-liquid interface cell culture: a model for innate mucosal defense of the upper airways? *Am. J. Physiol. - Lung Cell. Mol. Physiol.* **296**, L92–L100 (2009).

383. Yang, I. V., Fingerlin, T. E., Evans, C. M., Schwarz, M. I. & Schwartz, D. A. MUC5B and Idiopathic Pulmonary Fibrosis. *Ann. Am. Thorac. Soc.* **12**, S193–S199 (2015).

384. Ballester, B., Milara, J. & Cortijo, J. Mucins as a New Frontier in Pulmonary Fibrosis. *J. Clin. Med.* **8**, (2019).

385. Lin, R.-Z., Lin, R.-Z. & Chang, H.-Y. Recent advances in three-dimensional multicellular spheroid culture for biomedical research. *Biotechnol. J.* **3**, 1172–1184 (2008).

386. Caramori, G. *et al.* MUC5AC expression is increased in bronchial submucosal glands of stable COPD patients. *Histopathology* **55**, 321–331 (2009).

387. Rogers, D. F. Airway goblet cells: responsive and adaptable front-line defenders. *Eur. Respir. J.* **7**, 1690–1706 (1994).

388. Park, K.-S. *et al.* SPDEF regulates goblet cell hyperplasia in the airway epithelium. *J. Clin. Invest.* **117**, 978–988 (2007).

389. Weibel, E. R. On the Tricks Alveolar Epithelial Cells Play to Make a Good Lung. *Am. J. Respir. Crit. Care Med.* **191**, 504–513 (2015).

390. Nicholas A., K. & Jacques P., B. Functions of Basement Membranes. *Curr. Top. Membr.* **56**, 79–111 (2005).

391. Lowe, J. S. & Anderson, P. G. Chapter 3 - Epithelial Cells. in *Stevens & Lowe's Human Histology (Fourth Edition) (Fourth Edition)* 37–54 (Mosby, 2015). doi:10.1016/B978-0-7234-3502-0.00003-6.

392. Lowe, J. S. & Anderson, P. G. Chapter 4 - Support Cells and the Extracellular Matrix. in *Stevens & Lowe's Human Histology (Fourth Edition) (Fourth Edition)* 55–70 (Mosby, 2015). doi:10.1016/B978-0-7234-3502-0.00004-8.

393. Zschenker, O., Streichert, T., Hehlgans, S. & Cordes, N. Genome-Wide Gene Expression Analysis in Cancer Cells Reveals 3D Growth to Affect ECM and Processes Associated with Cell Adhesion but Not DNA Repair. *PLoS ONE* **7**, e34279 (2012).

394. Schmitz, G. & Müller, G. Structure and function of lamellar bodies, lipid-protein complexes involved in storage and secretion of cellular lipids. *J. Lipid Res.* **32**, 1539–1570 (1991).

395. Kumar, V. & Abbas, A. K. Robbins and Cotran Pathologic Basis of Disease, Professional Edition E-Book - Vinay Kumar, Abul K. Abbas, Nelson Fausto, Jon C. Aster - Google Books. https://books.google.co.uk/books?hl=en&lr=&id=jJllBAAAQBAJ&oi=fnd&pg=PP1&ots=AfPVAZ-Y7Z&sig=3hVZxnzMIASAxyw4W6GigoN0o3c&redir_esc=y#v=onepage&q&f=false.

396. Nichols, J. M. *et al.* Cell and molecular transitions during efficient dedifferentiation. *eLife* https://elifesciences.org/articles/55435 (2020) doi:10.7554/eLife.55435.

397. Friedmann-Morvinski, D. & Verma, I. M. Dedifferentiation and reprogramming: origins of cancer stem cells. *EMBO Rep.* **15**, 244–253 (2014).

398. Merrell, A. J. & Stanger, B. Z. Adult cell plasticity in vivo : de-differentiation and transdifferentiation are back in style. *Nat. Rev. Mol. Cell Biol.* **17**, 413–425 (2016).

399. Takahashi, K. & Yamanaka, S. A decade of transcription factor-mediated reprogramming to pluripotency. *Nat. Rev. Mol. Cell Biol.* **17**, 183–193 (2016).

400. Anam, M. B. *et al.* Ribosome induces transdifferentiation of A549 and H-111-TC cancer cell lines. *Biochem. Biophys. Rep.* **26**, (2021).

401. Zemans, R. L. Acute Respiratory Distress Syndrome. in *Lung Epithelial Biology in the Pathogenesis of Pulmonary Disease* 185–209 (Elsevier, 2017). doi:10.1016/B978-0-12-803809-3.00010-5.

402. Wang, D., Haviland, D. L., Burns, A. R., Zsigmond, E. & Wetsel, R. A. A pure population of lung alveolar epithelial type II cells derived from human embryonic stem cells. *Proc. Natl. Acad. Sci.* **104**, 4449–4454 (2007).

403. Begley, C. G. & Ellis, L. M. Drug development: Raise standards for preclinical cancer research. *Nature* **483**, 531–533 (2012).

404. Strunk, R. C., Eidlen, D. M. & Mason, R. J. Pulmonary alveolar type II epithelial cells synthesize and secrete proteins of the classical and alternative complement pathways. *J. Clin. Invest.* **81**, 1419–1426 (1988).

405. Lajoie, P., Guay, G., Dennis, J. W. & Nabi, I. R. The lipid composition of autophagic vacuoles regulates expression of multilamellar bodies. *J. Cell Sci.* **118**, 1991–2003 (2005).

406. Liang, C. & Jung, J. U. Autophagy Genes as Tumor Suppressors. *Curr. Opin. Cell Biol.* **22**, 226–233 (2010).

407. Kuma, A. *et al.* The role of autophagy during the early neonatal starvation period. *Nature* **432**, 1032–1036 (2004).

408. Copland, I. B. & Post, M. Understanding the Mechanisms of Infant Respiratory Distress and Chronic Lung Disease. *Am. J. Respir. Cell Mol. Biol.* **26**, 261–265 (2002).

409. Saitoh, T. *et al.* Loss of the autophagy protein Atg16L1 enhances endotoxin-induced IL-1β production. *Nature* **456**, 264–268 (2008).

410. Cadwell, K. *et al.* A unique role for autophagy and Atg16L1 in Paneth cells in murine and human intestine. *Nature* **456**, 259–263 (2008).

411. Agassandian, M. & Mallampalli, R. K. Surfactant phospholipid metabolism. *Biochim. Biophys. Acta* **1831**, 612–625 (2013).

412. Weaver, T. E., Na, C.-L. & Stahlman, M. Biogenesis of lamellar bodies, lysosome-related organelles involved in storage and secretion of pulmonary surfactant. *Semin. Cell Dev. Biol.* **13**, 263–270 (2002).

413. Seo, D.-C. *et al.* Gene expression profiling of cancer stem cell in human lung adenocarcinoma A549 cells. *Mol. Cancer* **6**, 75 (2007).

414. Gong, X. *et al.* LGR6 Is a High Affinity Receptor of R-Spondins and Potentially Functions as a Tumor Suppressor. *PLOS ONE* **7**, e37137 (2012).

415. Ruiz, E. J., Oeztuerk-Winder, F. & Ventura, J.-J. A paracrine network regulates the cross-talk between human lung stem cells and the stroma. *Nat. Commun.* **5**, ncomms4175 (2014).

416. Snoeck, H.-W. Modeling human lung development and disease using pluripotent stem cells. *Development* **142**, 13–16 (2015).

417. Huang, S. X. L. *et al.* Efficient generation of lung and airway epithelial cells from human pluripotent stem cells. *Nat. Biotechnol.* **32**, nbt.2754 (2013).

418. Ghaedi, M., Niklason, L. E. & Williams, J. Development of Lung Epithelium from Induced Pluripotent Stem Cells. *Curr. Transplant. Rep.* **2**, 81–89 (2015).

419. Leushacke, M. & Barker, N. Lgr5 and Lgr6 as markers to study adult stem cell roles in self-renewal and cancer. *Oncogene* **31**, 3009–3022 (2012).

420. Oeztuerk-Winder, F., Guinot, A., Ochalek, A. & Ventura, J.-J. Regulation of human lung alveolar multipotent cells by a novel p38α MAPK/miR-17-92 axis. *EMBO J.* **31**, 3431–3441 (2012).

421. Buehring, G. C., Eby, E. A. & Eby, M. J. Cell line cross-contamination: how aware are mammalian cell culturists of the problem and how to monitor it? *Vitro Cell. Dev. Biol.-Anim.* **40**, 211–215 (2004).

422. Freshney, R. I., Stacey, G. N. & Auerbach, J. M. *Culture of Human Stem Cells*. (Wiley-Blackwell, 2007).

423. Gartler, S. M. Apparent Hela cell contamination of human heteroploid cell lines. *Nature* **217**, 750–751 (1968).

424. Ye, F., Chen, C., Qin, J., Liu, J. & Zheng, C. Genetic profiling reveals an alarming rate of cross-contamination among human cell lines used in China. *FASEB J.* **29**, 4268–4272 (2015).

425. Vaughan, L., Glänzel, W., Korch, C. & Capes-Davis, A. Widespread Use of Misidentified Cell Line KB (HeLa): Incorrect Attribution and Its Impact Revealed through Mining the Scientific Literature. *Cancer Res.* **77**, 2784–2788 (2017).

426. Masters, J. R. Cell-line authentication: End the scandal of false cell lines. *Nature* **492**, 186 (2012).

427. Lacroix, M. Persistent use of "false" cell lines. *Int. J. Cancer* **122**, 1–4 (2008).

428. Freedman, L. P., Cockburn, I. M. & Simcoe, T. S. The Economics of Reproducibility in Preclinical Research. *PLOS Biol.* **13**, e1002165 (2015).

429. Boonstra, J. J. *et al.* Verification and Unmasking of Widely Used Human Esophageal Adenocarcinoma Cell Lines. *JNCI J. Natl. Cancer Inst.* **102**, 271–274 (2010).

430. Horbach, S. P. J. M. & Halffman, W. The ghosts of HeLa: How cell line misidentification contaminates the scientific literature. *PLOS ONE* **12**, e0186281 (2017).

431. Drexler, H. G. & Uphoff, C. C. Mycoplasma contamination of cell cultures: Incidence, sources, effects, detection, elimination, prevention. *Cytotechnology* **39**, 75–90 (2002).

432. CLASTR. https://web.expasy.org/cellosaurus-str-search/.

433. Reid, Y., Storts, D., Riss, T. & Minor, L. Authentication of Human Cell Lines by STR DNA Profiling Analysis. in *Assay Guidance Manual* (eds. Sittampalam, G. S. et al.) (Eli Lilly & Company and the National Center for Advancing Translational Sciences, 2004).

434. Iuchi, K. *et al.* Different morphologies of human embryonic kidney 293T cells in various types of culture dishes. *Cytotechnology* **72**, 131–140 (2020).

435. Fusenig, N. E., Capes-Davis, A., Bianchini, F., Sundell, S. & Lichter, P. The need for a worldwide consensus for cell line authentication: Experience implementing a mandatory requirement at the International Journal of Cancer. *PLOS Biol.* **15**, e2001438 (2017).

436. Masters, J. R. Cell-line authentication: End the scandal of false cell lines. *Nature* **492**, 186–186 (2012).

437. MacLeod, R. A. *et al.* Widespread intraspecies cross-contamination of human tumor cell lines arising at source. *Int. J. Cancer* **83**, 555–563 (1999).

438. Hebert, P. D. N., Cywinska, A., Ball, S. L. & deWaard, J. R. Biological identifications through DNA barcodes. *Proc. R. Soc. B Biol. Sci.* **270**, 313–321 (2003).

439. Gorphe, P. A comprehensive review of Hep-2 cell line in translational research for laryngeal cancer. *Am. J. Cancer Res.* **9**, 644–649 (2019).

440. Fan, H. & Chu, J.-Y. A Brief Review of Short Tandem Repeat Mutation. *Genomics Proteomics Bioinformatics* **5**, 7–14 (2007).

441. Dutta, P. *et al.* Amelogenin Gene - The Pioneer in Gender Determination from Forensic Dental Samples. *J. Clin. Diagn. Res. JCDR* **11**, ZC56-ZC59 (2017).

442. Li, G.-M. Mechanisms and functions of DNA mismatch repair. *Cell Res.* **18**, 85–98 (2008).

443. Clyde, D. Getting wise about lost Ys. *Nat. Rev. Genet.* **21**, 70–70 (2020).

444. Graham, F. & Smiley, J. Characteristics of a Human Cell Line Transformed by DNA from Human Adenovirus. *J. Gen. Virol.* **36**, 59–74 (1977).

445. Stepanenko, A. A. & Dmitrenko, V. V. HEK293 in cell biology and cancer research: phenotype, karyotype, tumorigenicity, and stress-induced genome-phenotype evolution. *Gene* **569**, 182–190 (2015).

446. Lin, Y.-C. *et al.* Genome dynamics of the human embryonic kidney 293 lineage in response to cell biology manipulations. *Nat. Commun.* **5**, 1–12 (2014).

447. DuBridge, R. B. *et al.* Analysis of mutation in human cells by using an Epstein-Barr virus shuttle system. *Mol. Cell. Biol.* **7**, 379–387 (1987).

448. Debeb, B. G. *et al.* Characterizing cancer cells with cancer stem cell-like features in 293T human embryonic kidney cells. *Mol. Cancer* **9**, 180 (2010).

449. Bojar, D. HEK293: An Essential Human Cell Line with a Unexpected Origin. https://blog.genofab.com/hek293-cell-line.

450. Butler, J. M. *Forensic DNA Typing: Biology, Technology, and Genetics of STR Markers*. (Elsevier, 2005).

451. Cannavo, E. *et al.* Expression of the MutL Homologue hMLH3 in Human Cells and its Role in DNA Mismatch Repair. *Cancer Res.* **65**, 10759–10766 (2005).

452. Lin, Y. & Wilson, J. H. Diverse Effects of Individual Mismatch Repair Components on Transcription-Induced CAG Repeat Instability in Human Cells. *DNA Repair* **8**, 878–885 (2009).

453. Pelletier, R., Farrell, B. T., Miret, J. J. & Lahue, R. S. Mechanistic features of CAG•CTG repeat contractions in cultured cells revealed by a novel genetic assay. *Nucleic Acids Res.* **33**, 5667–5676 (2005).

454. Thomas, R., Marks, D. H., Chin, Y. & Benezra, R. Whole chromosome loss and associated breakage–fusion–bridge cycles transform mouse tetraploid cells. *EMBO J.* **37**, 201–218 (2018).

455. Xu, J. *et al.* Free-living human cells reconfigure their chromosomes in the evolution back to uni-cellularity. *eLife* **6**,.

456. Huang, Y., Liu, Y., Zheng, C. & Shen, C. Investigation of Cross-Contamination and Misidentification of 278 Widely Used Tumor Cell Lines. *PLoS ONE* **12**, (2017).

457. Binz, R. L. *et al.* Identification of novel breakpoints for locus- and region-specific translocations in 293 cells by molecular cytogenetics before and after irradiation. *Sci. Rep.* **9**, (2019).

458. Allele Frequencies. https://www.promega.co.uk/products/pm/genetic-identity/population-statistics/allele-frequencies/.

459. Namiki, K. *et al.* Persistent Exposure to Mycoplasma Induces Malignant Transformation of Human Prostate Cells. *PLoS ONE* **4**, (2009).

460. Nikfarjam, L. & Farzaneh, P. Prevention and Detection of Mycoplasma Contamination in Cell Culture. *Cell J. Yakhteh* **13**, 203–212 (2012).

461. INADA, M., IZAWA, G., KOBAYASHI, W. & OZAWA, M. 293 cells express both epithelial as well as mesenchymal cell adhesion molecules. *Int. J. Mol. Med.* **37**, 1521–1527 (2016).

462. Voronkova, M. A. *et al.* SOX9 Regulates Cancer Stem-Like Properties and Metastatic Potential of Single-Walled Carbon Nanotube-Exposed Cells. *Sci. Rep.* **7**, (2017).

463. Kitchen, P. *et al.* Plasma Membrane Abundance of Human Aquaporin 5 Is Dynamically Regulated by Multiple Pathways. *PLoS ONE* **10**, (2015).

464. Bin, L.-H., Nielson, L. D., Liu, X., Mason, R. J. & Shu, H.-B. Identification of Uteroglobin-Related Protein 1 and Macrophage Scavenger Receptor with Collagenous Structure as a Lung-Specific Ligand-Receptor Pair. *J. Immunol.* **171**, 924–930 (2003).

465. Stewart, G. A. *et al.* 4-Phenylbutyric Acid Treatment Rescues Trafficking and Processing of a Mutant Surfactant Protein–C. *Am. J. Respir. Cell Mol. Biol.* **47**, 324–331 (2012).

466. Kwon, M. S., Park, B., Kim, H. M. & Kim, S. Leucine-Rich Repeat-Containing G-Protein Coupled Receptor 5/GPR49 Activates G12/13-Rho GTPase Pathway. *Mol. Cells* **36**, 267–272 (2013).

467. Chiang, N., Libreros, S., Norris, P. C., Rosa, X. de la & Serhan, C. N. Maresin 1 activates LGR6 receptor promoting phagocyte immunoresolvent functions. *J. Clin. Invest.* **129**, 5294–5311 (2019).

468. Sorensen, G. L. Surfactant Protein D in Respiratory and Non-Respiratory Diseases. *Front. Med.* **5**, (2018).

469. Yevdokimova, N. & Freshney, R. I. Activation of paracrine growth factors by heparan sulphate induced by glucocorticoid in A549 lung carcinoma cells. *Br. J. Cancer* **76**, 281–289 (1997).

470. Rucka, Z. *et al.* Differential effects of insulin and dexamethasone on pulmonary surfactant-associated genes and proteins in A549 and H441 cells and lung tissue. *Int. J. Mol. Med.* **32**, 211–218 (2013).

471. McCormick, C. & Freshney, R. I. Activity of growth factors in the IL-6 group in the differentiation of human lung adenocarcinoma. *Br. J. Cancer* **82**, 881–890 (2000).

472. Smith, B. T. & Sabry, K. Glucocorticoid-thyroid synergism in lung maturation: a mechanism involving epithelial-mesenchymal interaction. *Proc. Natl. Acad. Sci. U. S. A.* **80**, 1951–1954 (1983).

473. Chang, C.-W., Peng, C.-C., Liao, W.-H. & Tung, Y.-C. Polydimethylsiloxane SlipChip for mammalian cell culture applications. *Analyst* **140**, 7355–7365 (2015).

474. Pugin, J. *et al.* Cyclic Stretch of Human Lung Cells Induces an Acidification and Promotes Bacterial Growth. *Am. J. Respir. Cell Mol. Biol.* **38**, 362–370 (2008).

475. Isohama, Y. *et al.* Dexamethasone Increases β2-Adrenoceptor-Regulated Phosphatidylcholine Secretion in Rat Alveolar Type II Cells. *Jpn. J. Pharmacol.* **73**, 163–169 (1997).

476. Jeon, B.-H., Yoo, Y.-M., Jung, E.-M. & Jeung, E.-B. Dexamethasone Treatment Increases the Intracellular Calcium Level Through TRPV6 in A549 Cells. *Int. J. Mol. Sci.* **21**, (2020).

477. King, G., Smith, M. E., Cake, M. H. & Nielsen, H. C. What is the identity of fibroblast pneumocyte factor (FPF)? *Pediatr. Res.* **80**, 768–776 (2016).

478. Menke, A. *et al.* Dexamethasone Stimulated Gene Expression in Peripheral Blood is a Sensitive Marker for Glucocorticoid Receptor Resistance in Depressed Patients. *Neuropsychopharmacology* **37**, 1455–1464 (2012).

479. Wang, J.-C. *et al.* Chromatin immunoprecipitation (ChIP) scanning identifies primary glucocorticoid receptor target genes. *Proc. Natl. Acad. Sci.* **101**, 15603–15608 (2004).

480. Fiaturi, N., Castellot, J. J. & Nielsen, H. C. Neuregulin-ErbB4 signaling in the developing lung alveolus: a brief review. *J. Cell Commun. Signal.* **8**, 105–111 (2014).

481. Dammann, C. Neuregulins and Their Receptors in Lung Development. *Grantome*.

482. King, G., Maker, G. L., Berryman, D., Trengove, R. D. & Cake, M. H. Role of neuregulin-1β in dexamethasone-enhanced surfactant synthesis in fetal type II cells. *FEBS Lett.* **588**, 975–980 (2014).

483. Cooper, J. R. *et al.* Long Term Culture of the A549 Cancer Cell Line Promotes Multilamellar Body Formation and Differentiation towards an Alveolar Type II Pneumocyte Phenotype. *PLOS ONE* **11**, e0164438 (2016).

484. Gonzalez, R. F., Allen, L., Gonzales, L., Ballard, P. L. & Dobbs, L. G. HTII-280, a Biomarker Specific to the Apical Plasma Membrane of Human Lung Alveolar Type II Cells. *J. Histochem. Cytochem.* **58**, 891–901 (2010).

485. Dammann, C. E. L., Nassimi, N., Liu, W. & Nielsen, H. C. ErbB receptor regulation by dexamethasone in mouse type II epithelial cells. *Eur. Respir. J.* **28**, 1117–1123 (2006).

486. Kondo, H., Miyoshi, K., Sakiyama, S., Tangoku, A. & Noma, T. Differential Regulation of Gene Expression of Alveolar Epithelial Cell Markers in Human Lung Adenocarcinoma-Derived A549 Clones. *Stem Cells Int.* **2015**, (2015).

487. Zscheppang, K., Dörk, T., Schmiedl, A., Jones, F. E. & Dammann, C. E. L. Neuregulin Receptor ErbB4 Functions as a Transcriptional Cofactor for the Expression of Surfactant Protein B in the Fetal Lung. *Am. J. Respir. Cell Mol. Biol.* **45**, 761–767 (2011).

488. Okazaki, S. *et al.* Development of an ErbB4 monoclonal antibody that blocks neuregulin-1-induced ErbB4 activation in cancer cells. *Biochem. Biophys. Res. Commun.* **470**, 239–244 (2016).

489. D'Uva, G. & Lauriola, M. Towards the emerging crosstalk: ERBB family and steroid hormones. *Semin. Cell Dev. Biol.* **50**, 143–152 (2016).

490. Lu, N. Z. *et al.* International Union of Pharmacology. LXV. The Pharmacology and Classification of the Nuclear Receptor Superfamily: Glucocorticoid, Mineralocorticoid, Progesterone, and Androgen Receptors. *Pharmacol. Rev.* **58**, 782–797 (2006).

491. Rhen, T. & Cidlowski, J. A. Antiinflammatory Action of Glucocorticoids — New Mechanisms for Old Drugs. *http://dx.doi.org/10.1056/NEJMra050541* https://www.nejm.org/doi/10.1056/NEJMra050541 (2009) doi:10.1056/NEJMra050541.

492. Petta, I. *et al.* The Interactome of the Glucocorticoid Receptor and Its Influence on the Actions of Glucocorticoids in Combatting Inflammatory and Infectious Diseases. *Microbiol. Mol. Biol. Rev.* **80**, 495–522 (2016).

493. Venkatesh, V. C., Iannuzzi, D. M., Ertsey, R. & Ballard, P. L. Differential Glucocorticoid Regulation of the Pulmonary Hydrophobic Surfactant Proteins SP-B and SP-C. *Am. J. Respir. Cell Mol. Biol.* **8**, 222–228 (1993).

494. Huang, H. W., Bi, W., Jenkins, G. N. & Alcorn, J. L. Glucocorticoid Regulation of Human Pulmonary Surfactant Protein-B mRNA Stability Involves the 3′-Untranslated Region. *Am. J. Respir. Cell Mol. Biol.* **38**, 473–482 (2008).

495. Islam, K. N. & Mendelson, C. R. Glucocorticoid/Glucocorticoid Receptor Inhibition of Surfactant Protein-A (SP-A) Gene Expression in Lung Type II Cells Is Mediated by Repressive Changes in Histone Modification at the SP-A Promoter. *Mol. Endocrinol.* **22**, 585–596 (2008).

496. Li, R. *et al.* Chronic IL-1β-induced inflammation regulates epithelial-to-mesenchymal transition memory phenotypes via epigenetic modifications in non-small cell lung cancer. *Sci. Rep.* **10**, 1–15 (2020).

497. Thacker, S. *et al.* Restoration of lung surfactant protein D by IL-6 protects against secondary pneumonia following hemorrhagic shock. *J. Infect.* **68**, 231–241 (2014).

498. Kurt, A. *et al.* Investigation of surfactant protein-D and interleukin-6 levels in patients with blunt chest trauma with multiple rib fractures and pulmonary contusions: a cross-sectional study in Black Sea Region of Turkey. *BMJ Open* **6**, (2016).

499. Kerget, B. *et al.* Are Serum Interleukin 6 and Surfactant Protein D Levels Associated with the Clinical Course of COVID-19? *Lung* 1–8 (2020) doi:10.1007/s00408-020-00393-8.

500. Ladenburger, A. *et al.* Glucocorticoids potentiate IL-6-induced SP-B expression in H441 cells by enhancing the JAK-STAT signaling pathway. *Am. J. Physiol. - Lung Cell. Mol. Physiol.* **299**, L578–L584 (2010).

501. Rawlings, J. S., Rosler, K. M. & Harrison, D. A. The JAK/STAT signaling pathway. *J. Cell Sci.* **117**, 1281–1283 (2004).

502. Polgár, A., Brózik, M., Tóth, S., Holub, M. & Falus, A. A Synthetic Corticosteroid, Dexamethasone Regulates Generation of Soluble Form of Interleukin-6 Receptor of Human Lymphocytes, in vitro. *Acta Biol. Hung.* **53**, 307–315 (2002).

503. Hasegawa, Y. *et al.* Surfactant protein D suppresses lung cancer progression by downregulation of epidermal growth factor signaling. *Oncogene* **34**, 838–845 (2015).

504. Shannon, J. M., Jennings, S. D. & Nielsen, L. D. Modulation of alveolar type II cell differentiated function in vitro. *Am. J. Physiol.-Lung Cell. Mol. Physiol.* **262**, L427–L436 (1992).

505. Shannon, J. M., Pan, T., Edeen, K. E. & Nielsen, L. D. Influence of the cytoskeleton on surfactant protein gene expression in cultured rat alveolar type II cells. *Am. J. Physiol.-Lung Cell. Mol. Physiol.* **274**, L87–L96 (1998).

506. Yang, Y. *et al.* Side population cells separated from A549 lung cancer cell line possess cancer stem cell-like properties and inhibition of autophagy potentiates the cytotoxic effect of cisplatin. *Oncol. Rep.* **34**, 929–935 (2015).

507. Montero, J. C. *et al.* Neuregulins and Cancer. *Clin. Cancer Res.* **14**, 3237–3241 (2008).

508. Liu, H., Seijsing, J., Frejd, F. Y., Tolmachev, V. & Gräslund, T. Target-specific cytotoxic effects on HER2-expressing cells by the tripartite fusion toxin ZHER2:2891-ABD-PE38X8, including a targeting affibody molecule and a half-life extension domain. *Int. J. Oncol.* **47**, 601–609 (2015).

509. Mujoo, K., Choi, B.-K., Huang, Z., Zhang, N. & An, Z. Regulation of ERBB3/HER3 signaling in cancer. *Oncotarget* **5**, 10222 (2014).

510. Rehan, V. K. & Torday, J. S. PPARγ Signaling Mediates the Evolution, Development, Homeostasis, and Repair of the Lung. *PPAR Res.* **2012**, (2012).

511. McGowan, S. E., Harvey, C. S. & Jackson, S. K. Retinoids, retinoic acid receptors, and cytoplasmic retinoid binding proteins in perinatal rat lung fibroblasts. *Am. J. Physiol.-Lung Cell. Mol. Physiol.* **269**, L463–L472 (1995).

512. Ahlbrecht, K. & McGowan, S. E. In search of the elusive lipofibroblast in human lungs. *Am. J. Physiol.-Lung Cell. Mol. Physiol.* **307**, L605–L608 (2014).

513. Herriges, M. & Morrisey, E. E. Lung development: orchestrating the generation and regeneration of a complex organ. *Development* **141**, 502–513 (2014).

514. Nabhan, A. N., Brownfield, D. G., Harbury, P. B., Krasnow, M. A. & Desai, T. J. Single-cell Wnt signaling niches maintain stemness of alveolar type 2 cells. *Science* **359**, 1118–1123 (2018).

515. Zacharias, W. J. *et al.* Regeneration of the lung alveolus by an evolutionarily conserved epithelial progenitor. *Nature* **555**, 251–255 (2018).

516. Jacobs, J. P., Jones, C. M. & Baille, J. P. Characteristics of a Human Diploid Cell Designated MRC-5. *Nature* **227**, 168–170 (1970).

517. Prasad, S., Hogaboam, C. M. & Jarai, G. Deficient repair response of IPF fibroblasts in a co-culture model of epithelial injury and repair. *Fibrogenesis Tissue Repair* **7**, 7 (2014).

518. Hill, D. S. *et al.* A novel fully-humanised 3D skin equivalent to model early melanoma invasion. *Mol. Cancer Ther.* **14**, 2665–2673 (2015).

519. Baarsma, H. A. & Königshoff, M. 'WNT-er is coming': WNT signalling in chronic lung diseases. *Thorax* **72**, 746–759 (2017).

520. Kirabo, A. *et al.* Neuregulin-1β induces proliferation, survival and paracrine signaling in normal human cardiac ventricular fibroblasts. *J. Mol. Cell. Cardiol.* **105**, 59–69 (2017).

521. Ahlbrecht, K. & McGowan, S. E. In search of the elusive lipofibroblast in human lungs. *Am. J. Physiol.-Lung Cell. Mol. Physiol.* **307**, L605–L608 (2014).

522. Arends, F. & Lieleg, O. Biophysical Properties of the Basal Lamina: A Highly Selective Extracellular Matrix. (2016) doi:10.5772/62519.

523. Holmbeck, K. & Szabova, L. Aspects of extracellular matrix remodeling in development and disease. *Birth Defects Res. Part C Embryo Today Rev.* **78**, 11–23 (2006).

524. Rhee, S. Fibroblasts in three dimensional matrices: cell migration and matrix remodeling. *Exp. Mol. Med.* **41**, 858–865 (2009).

525. Petroll, W. M. & Ma, L. Direct, dynamic assessment of cell-matrix interactions inside fibrillar collagen lattices. *Cell Motil.* **55**, 254–264 (2003).

526. Kessler, D. *et al.* Fibroblasts in Mechanically Stressed Collagen Lattices Assume a "Synthetic" Phenotype *. *J. Biol. Chem.* **276**, 36575–36585 (2001).

527. Schaefer, A. W. *et al.* Cytoskeletal Dynamics Underlying Neurite Outgrowth. *Dev. Cell* **15**, 146–162 (2008).

528. Darling, N. J., Mobbs, C. L., González-Hau, A. L., Freer, M. & Przyborski, S. Bioengineering Novel in vitro Co-culture Models That Represent the Human Intestinal Mucosa With Improved Caco-2 Structure and Barrier Function. *Front. Bioeng. Biotechnol.* **8**, (2020).

529. Koukourakis, M. I. *et al.* Metabolic cooperation between co-cultured lung cancer cells and lung fibroblasts. *Lab. Investig. J. Tech. Methods Pathol.* **97**, 1321–1331 (2017).

530. Mahale, J., Smagurauskaite, G., Brown, K., Thomas, A. & Howells, L. M. The role of stromal fibroblasts in lung carcinogenesis: A target for chemoprevention? *Int. J. Cancer* **138**, 30–44 (2016).

531. Movia, D., Bazou, D. & Prina-Mello, A. ALI multilayered co-cultures mimic biochemical mechanisms of the cancer cell-fibroblast cross-talk involved in NSCLC MultiDrug Resistance. *BMC Cancer* **19**, (2019).

532. Harrington, H. *et al.* Immunocompetent 3D Model of Human Upper Airway for Disease Modeling and In Vitro Drug Evaluation. *Mol. Pharm.* **11**, 2082–2091 (2014).

533. Sucre, J. M. S. *et al.* Successful Establishment of Primary Type II Alveolar Epithelium with 3D Organotypic Coculture. *Am. J. Respir. Cell Mol. Biol.* **59**, 158–166 (2018).

534. Torday, J. S. & Rehan, V. K. The evolutionary continuum from lung development to homeostasis and repair. *Am. J. Physiol.-Lung Cell. Mol. Physiol.* **292**, L608–L611 (2007).

535. Stern, J.-B. *et al.* Parathyroid Hormone-Related Protein in Epithelial Lining Fluid in Humans Negatively Correlates With the Severity of Lung Injury. *CHEST* **121**, 852–857 (2002).

536. Abe, M. & Horiuchi, N. Dexamethasone Suppresses Parathyroid Hormone-related Protein Expression by Human Oral Squamous Carcinoma Cells (HSC-3). *J. Oral Biosci.* **52**, 51–59 (2010).

537. Torday, J. S., Sun, H., Wang, L. & Torres, E. Leptin mediates the parathyroid hormone-related protein paracrine stimulation of fetal lung maturation. *Am. J. Physiol.-Lung Cell. Mol. Physiol.* **282**, L405–L410 (2002).

538. Lizardo, D. Y., Lin, Y.-L., Gokcumen, O. & Atilla-Gokcumen, G. E. Regulation of lipids is central to replicative senescence. *Mol. Biosyst.* **13**, 498–509 (2017).

539. Bodnar, A. G. *et al.* Extension of Life-Span by Introduction of Telomerase into Normal Human Cells. *Science* **279**, 349–352 (1998).

540. López-Otín, C., Blasco, M. A., Partridge, L., Serrano, M. & Kroemer, G. The Hallmarks of Aging. *Cell* **153**, 1194–1217 (2013).

541. Tchkonia, T., Zhu, Y., van Deursen, J., Campisi, J. & Kirkland, J. L. Cellular senescence and the senescent secretory phenotype: therapeutic opportunities. *J. Clin. Invest.* **123**, 966–972 (2013).

542. Muñoz-Espín, D. *et al.* Programmed Cell Senescence during Mammalian Embryonic Development. *Cell* **155**, 1104–1118 (2013).

543. Rajagopalan, S. & Long, E. O. Cellular senescence induced by CD158d reprograms natural killer cells to promote vascular remodeling. *Proc. Natl. Acad. Sci.* **109**, 20596–20601 (2012).

544. Jun, J.-I. & Lau, L. F. The matricellular protein CCN1 induces fibroblast senescence and restricts fibrosis in cutaneous wound healing. *Nat. Cell Biol.* **12**, 676–685 (2010).

545. Krizhanovsky, V. *et al.* Senescence of activated stellate cells limits liver fibrosis. *Cell* **134**, 657–667 (2008).

546. Magtanong, L., Ko, P. J. & Dixon, S. J. Emerging roles for lipids in non-apoptotic cell death. *Cell Death Differ.* **23**, 1099–1109 (2016).

547. Atilla-Gokcumen, G. E. *et al.* Dividing Cells Regulate Their Lipid Composition and Localization. *Cell* **156**, 428–439 (2014).

548. Seibold, M. A. *et al.* The Idiopathic Pulmonary Fibrosis Honeycomb Cyst Contains A Mucocilary Pseudostratified Epithelium. *PLoS ONE* **8**, e58658 (2013).

549. Rieske, P., Krynska, B. & Azizi, S. A. Human fibroblast-derived cell lines have characteristics of embryonic stem cells and cells of neuro-ectodermal origin. *Differentiation* **73**, 474–483 (2005).

550. Schafer, I. A., Silverman, L., Sullivan, J. C. & Robertson, W. V. B. ASCORBIC ACID DEFICIENCY IN CULTURED HUMAN FIBROBLASTS. *J. Cell Biol.* **34**, 83–95 (1967).

551. Alberts, B. *et al.* The Extracellular Matrix of Animals. (2002).

552. Lagies, S. *et al.* Cells grown in three-dimensional spheroids mirror in vivo metabolic response of epithelial cells. *Commun. Biol.* **3**, 1–10 (2020).

553. Edmondson, R., Broglie, J. J., Adcock, A. F. & Yang, L. Three-Dimensional Cell Culture Systems and Their Applications in Drug Discovery and Cell-Based Biosensors. *Assay Drug Dev. Technol.* **12**, 207–218 (2014).

554. Estefanía, M. M. *et al.* DNA Replication Fading As Proliferating Cells Advance in Their Commitment to Terminal Differentiation. *Sci. Rep.* **2**, 1–8 (2012).

555. Campisi, J. & Fagagna, F. d'Adda di. Cellular senescence: when bad things happen to good cells. *Nat. Rev. Mol. Cell Biol.* **8**, 729–740 (2007).

556. Pallen, C. J. & Tong, P. H. Elevation of membrane tyrosine phosphatase activity in density-dependent growth-arrested fibroblasts. *Proc. Natl. Acad. Sci. U. S. A.* **88**, 6996–7000 (1991).

557. Rodier, F. *et al.* Persistent DNA damage signaling triggers senescence-associated inflammatory cytokine secretion. *Nat. Cell Biol.* **11**, 973–979 (2009).

558. Fernandez, I. E. & Eickelberg, O. The Impact of TGF-β on Lung Fibrosis. *Proc. Am. Thorac. Soc.* **9**, 111–116 (2012).

559. Coppé, J.-P., Desprez, P.-Y., Krtolica, A. & Campisi, J. The Senescence-Associated Secretory Phenotype: The Dark Side of Tumor Suppression. *Annu. Rev. Pathol.* **5**, 99–118 (2010).

560. Lee, S. & Schmitt, C. A. The dynamic nature of senescence in cancer. *Nat. Cell Biol.* **21**, 94–101 (2019).

561. Flor, A. C., Wolfgeher, D., Wu, D. & Kron, S. J. A signature of enhanced lipid metabolism, lipid peroxidation and aldehyde stress in therapy-induced senescence. *Cell Death Discov.* **3**, 1–12 (2017).

562. Muñoz-Espín, D. & Serrano, M. Cellular senescence: from physiology to pathology. *Nat. Rev. Mol. Cell Biol.* **15**, 482–496 (2014).

563. de la Motte, C. A. & Drazba, J. A. Viewing Hyaluronan. *J. Histochem. Cytochem.* **59**, 252–257 (2011).

564. Nagano, T. *et al.* Identification of cellular senescence-specific genes by comparative transcriptomics. *Sci. Rep.* **6**, 1–13 (2016).

565. Espina, V. *et al.* Laser-capture microdissection. *Nat. Protoc.* **1**, 586–603 (2006).

566. Hwang, B., Lee, J. H. & Bang, D. Single-cell RNA sequencing technologies and bioinformatics pipelines. *Exp. Mol. Med.* **50**, 1–14 (2018).

567. Baker, B. M. & Chen, C. S. Deconstructing the third dimension – how 3D culture microenvironments alter cellular cues. *J. Cell Sci.* **125**, 3015–3024 (2012).

568. Vergani, L., Gratteaola, M. & Nicolini, C. Modifications of chromatin structure and gene expression following induced alterations of cellular shape. *Int. J. Biochem. Cell Biol.* **36**, 1447–1461 (2004).

569. Bissell, M. J. & Barcellos-Hoff, M. H. The influence of extracellular matrix on gene expression: is structure the message? *J. Cell Sci. Suppl.* **8**, 327–343 (1987).

570. Bissell, M. J. Goodbye flat biology – time for the 3rd and the 4th dimensions. *J. Cell Sci.* **130**, 3–5 (2017).

571. Thomas, C. H., Collier, J. H., Sfeir, C. S. & Healy, K. E. Engineering gene expression and protein synthesis by modulation of nuclear shape. *Proc. Natl. Acad. Sci. U. S. A.* **99**, 1972–1977 (2002).

572. Schwarz, U. S. & Gardel, M. L. United we stand – integrating the actin cytoskeleton and cell–matrix adhesions in cellular mechanotransduction. *J. Cell Sci.* **125**, 3051–3060 (2012).

573. Xie, X., Mahmood, S. R., Gjorgjieva, T. & Percipalle, P. Emerging roles of cytoskeletal proteins in regulating gene expression and genome organization during differentiation. *Nucleus* **11**, 53–65 (2020).

574. Przyborski, S. *Technology Platforms for 3D Cell Culture: A User's Guide*. (John Wiley & Sons, Inc., 2017).

575. Azuma, A. *et al.* Double-blind, Placebo-controlled Trial of Pirfenidone in Patients with Idiopathic Pulmonary Fibrosis. *Am. J. Respir. Crit. Care Med.* **171**, 1040–1047 (2005).

576. Richeldi, L. *et al.* Efficacy of a Tyrosine Kinase Inhibitor in Idiopathic Pulmonary Fibrosis. *N. Engl. J. Med.* **365**, 1079–1087 (2011).

577. Ley, B., Collard, H. R. & King, T. E. Clinical Course and Prediction of Survival in Idiopathic Pulmonary Fibrosis. *Am. J. Respir. Crit. Care Med.* **183**, 431–440 (2011).

578. Froidure, A., Joannes, A., Mailleux, A. A. & Crestani, B. New targets in idiopathic pulmonary fibrosis: from inflammation and immunity to remodeling and repair. *Expert Opin. Orphan Drugs* **4**, 511–520 (2016).

579. *Assay Guidance Manual*. (Eli Lilly & Company and the National Center for Advancing Translational Sciences, 2004).

580. B. Moore, B. *et al.* Animal Models of Fibrotic Lung Disease. *Am. J. Respir. Cell Mol. Biol.* **49**, 167–179 (2013).

581. Liu, T., Santos, F. G. D. L. & Phan, S. H. The Bleomycin Model of Pulmonary Fibrosis. in *Fibrosis* 27–42 (Humana Press, New York, NY, 2017). doi:10.1007/978-1-4939-7113-8_2.

582. Ammar, R., Sivakumar, P., Jarai, G. & Thompson, J. R. A robust data-driven genomic signature for idiopathic pulmonary fibrosis with applications for translational model selection. *PLOS ONE* **14**, e0215565 (2019).

583. Network, T. I. P. F. C. R. Prednisone, Azathioprine, and N-Acetylcysteine for Pulmonary Fibrosis. *N. Engl. J. Med.* **366**, 1968–1977 (2012).

584. Oldham, J. M. *et al.* TOLLIP, MUC5B, and the Response to N-Acetylcysteine among Individuals with Idiopathic Pulmonary Fibrosis. *Am. J. Respir. Crit. Care Med.* **192**, 1475–1482 (2015).

585. Liu, G. *et al.* Use of precision cut lung slices as a translational model for the study of lung biology. *Respir. Res.* **20**, 162 (2019).

586. Rønnow, S. R. *et al.* Prolonged Scar-in-a-Jar: an in vitro screening tool for anti-fibrotic therapies using biomarkers of extracellular matrix synthesis. *Respir. Res.* **21**, 108 (2020).

587. Mao, P. *et al.* Human alveolar epithelial type II cells in primary culture. *Physiol. Rep.* **3**, e12288 (2015).

588. Vierck, J. L., Byrne, K., Mir, P. S. & Dodson, M. V. Ten commandments for preventing contamination of primary cell cultures. *Methods Cell Sci.* **22**, 33–41 (2000).

589. Weigle, S., Martin, E., Voegtle, A., Wahl, B. & Schuler, M. Primary cell-based phenotypic assays to pharmacologically and genetically study fibrotic diseases in vitro. *J. Biol. Methods* **6**, (2019).

590. Wang, D., Haviland, D. L., Burns, A. R., Zsigmond, E. & Wetsel, R. A. A pure population of lung alveolar epithelial type II cells derived from human embryonic stem cells. *Proc. Natl. Acad. Sci.* **104**, 4449–4454 (2007).

591. Coraux, C. *et al.* Embryonic Stem Cells Generate Airway Epithelial Tissue. *Am. J. Respir. Cell Mol. Biol.* **32**, 87–92 (2005).

592. Zhou, Q. *et al.* Differentiation of Mouse Induced Pluripotent Stem Cells Into Alveolar Epithelial Cells In Vitro for Use In Vivo. *Stem Cells Transl. Med.* **3**, 675–685 (2014).

593. Ghaedi, M. *et al.* Alveolar epithelial differentiation of human induced pluripotent stem cells in a rotating bioreactor. *Biomaterials* **35**, 699–710 (2014).

594. Wang, C. *et al.* Differentiation of Urine-Derived Human Induced Pluripotent Stem Cells to Alveolar Type II Epithelial Cells. *Cell. Reprogramming* **18**, 30–36 (2015).

595. Nelson-Rees, W. A. & Flandermeyer, R. R. Inter- and intraspecies contamination of human breast tumor cell lines HBC and BrCa5 and other cell cultures. *Science* **195**, 1343–1344 (1977).

596. Nelson-Rees, W. A. & Flandermeyer, R. R. HeLa cultures defined. *Science* **191**, 96–98 (1976).

597. Capes-Davis, A., Dirks, W. G., MacLeod, R. A. F. & Uphoff, C. Quality Matters Cell Lines and their Use in Research. *GIT Lab. J. Eur.* **17**, 12–13 (2014).

598. Reddel, R. R. *et al.* Transformation of Human Bronchial Epithelial Cells by Infection with SV40 or Adenovirus-12 SV40 Hybrid Virus, or Transfection via Strontium Phosphate Coprecipitation with a Plasmid Containing SV40 Early Region Genes. *Cancer Res.* **48**, 1904–1909 (1988).

599. Stewart, C. E. *et al.* Evaluation of Differentiated Human Bronchial Epithelial Cell Culture Systems for Asthma Research. *Journal of Allergy* https://www.hindawi.com/journals/ja/2012/943982/ (2012) doi:https://doi.org/10.1155/2012/943982.

600. Cozens, A. L. *et al.* CFTR expression and chloride secretion in polarized immortal human bronchial epithelial cells. *Am. J. Respir. Cell Mol. Biol.* **10**, 38–47 (1994).

601. Zhu, J., Rogers, A. V., Burke-Gaffney, A., Hellewell, P. G. & Jeffery, P. K. Cytokine-induced airway epithelial ICAM-1 upregulation: quantification by high-resolution scanning and transmission electron microscopy. *Eur. Respir. J.* **13**, 1318–1328 (1999).

602. Kreft, M. E. *et al.* The characterization of the human cell line Calu-3 under different culture conditions and its use as an optimized in vitro model to investigate bronchial epithelial function. *Eur. J. Pharm. Sci.* **69**, 1–9 (2015).

603. BéruBé, K., Balharry, D., Sexton, K., Koshy, L. & Jones, T. Combustion-derived nanoparticles: mechanisms of pulmonary toxicity. *Clin. Exp. Pharmacol. Physiol.* **34**, 1044–1050 (2007).

604. Salomon, J. J. *et al.* The Cell Line NCl-H441 Is a Useful in Vitro Model for Transport Studies of Human Distal Lung Epithelial Barrier. *Mol. Pharm.* **11**, 995–1006 (2014).

605. Ren, H., Birch, N. P. & Suresh, V. An Optimised Human Cell Culture Model for Alveolar Epithelial Transport. *PLoS ONE* **11**, (2016).

606. Gazdar, A. F. *et al.* Peripheral Airway Cell Differentiation in Human Lung Cancer Cell Lines. *Cancer Res.* **50**, 5481–5487 (1990).

607. Meyerson, M. Telomerase enzyme activation and human cell immortalization. *Toxicol. Lett.* **102–103**, 41–45 (1998).

608. Vaughan, M. B., Ramirez, R. D., Wright, W. E., Minna, J. D. & Shay, J. W. A three-dimensional model of differentiation of immortalized human bronchial epithelial cells. *Differentiation* **74**, 141–148 (2006).

609. Walters, M. S. *et al.* Generation of a human airway epithelium derived basal cell line with multipotent differentiation capacity. *Respir. Res.* **14**, 135 (2013).

610. Sweeney, S. *et al.* Pulmonary surfactant mitigates silver nanoparticle toxicity in human alveolar type-I-like epithelial cells. *Colloids Surf. B Biointerfaces* **145**, 167–175 (2016).

611. Cooney, D. J. & Hickey, A. J. Cellular response to the deposition of diesel exhaust particle aerosols onto human lung cells grown at the air–liquid interface by inertial impaction. *Toxicol. In Vitro* **25**, 1953–1965 (2011).

612. Gabasa, M. *et al.* Epithelial contribution to the profibrotic stiff microenvironment and myofibroblast population in lung fibrosis. *Mol. Biol. Cell* **28**, 3741 (2017).

613. Song, P. *et al.* β-catenin induces A549 alveolar epithelial cell mesenchymal transition during pulmonary fibrosis. *Mol. Med. Rep.* **11**, 2703–2710 (2015).

614. Ihara, H. *et al.* Nintedanib inhibits epithelial-mesenchymal transition in A549 alveolar epithelial cells through regulation of the TGF-β/Smad pathway. *Respir. Investig.* **58**, 275–284 (2020).

615. Molina-Molina, M. *et al.* Anti-fibrotic effects of pirfenidone and rapamycin in primary IPF fibroblasts and human alveolar epithelial cells. *BMC Pulm. Med.* **18**, (2018).

616. Sugizaki, T. *et al.* Idebenone has preventative and therapeutic effects on pulmonary fibrosis via preferential suppression of fibroblast activity. *Cell Death Discov.* **5**, 1–15 (2019).

617. Schulte, V. A., Díez, M., Möller, M. & Lensen, M. C. Surface Topography Induces Fibroblast Adhesion on Intrinsically Nonadhesive Poly(ethylene glycol) Substrates. *Biomacromolecules* **10**, 2795–2801 (2009).

618. Greiner, A. M. *et al.* Cell type-specific adaptation of cellular and nuclear volume in micro-engineered 3D environments. *Biomaterials* **69**, 121–132 (2015).

619. Mirbagheri, M. *et al.* Advanced cell culture platforms: a growing quest for emulating natural tissues. *Mater. Horiz.* **6**, 45–71 (2019).

620. Sacchi, M., Bansal, R. & Rouwkema, J. Bioengineered 3D Models to Recapitulate Tissue Fibrosis. *Trends Biotechnol.* **38**, 623–636 (2020).

621. Carreau, A., Hafny-Rahbi, B. E., Matejuk, A., Grillon, C. & Kieda, C. Why is the partial oxygen pressure of human tissues a crucial parameter? Small molecules and hypoxia. *J. Cell. Mol. Med.* **15**, 1239–1253 (2011).

622. Parrinello, S. *et al.* Oxygen sensitivity severely limits the replicative lifespan of murine fibroblasts. *Nat. Cell Biol.* **5**, 741–747 (2003).

623. Abdollahi, H. *et al.* The Role of Hypoxia in Stem Cell Differentiation and Therapeutics. *J. Surg. Res.* **165**, 112–117 (2011).

624. Atkuri, K. R., Herzenberg, L. A., Niemi, A.-K., Cowan, T. & Herzenberg, L. A. Importance of culturing primary lymphocytes at physiological oxygen levels. *Proc. Natl. Acad. Sci. U. S. A.* **104**, 4547–4552 (2007).

625. Simiantonaki, N. *et al.* Hypoxia-induced epithelial VEGF-C/VEGFR-3 upregulation in carcinoma cell lines. *Int. J. Oncol.* **32**, 585–592 (2008).

626. van der Valk, J. *et al.* Optimization of chemically defined cell culture media--replacing fetal bovine serum in mammalian in vitro methods. *Toxicol. Vitro Int. J. Publ. Assoc. BIBRA* **24**, 1053–1063 (2010).

627. Adams, J. C. A new initiative for AJP-Cell Physiology: "Making Cell Culture More Physiological". *Am. J. Physiol.-Cell Physiol.* **316**, C828–C829 (2019).

628. Chanda, D. *et al.* Developmental pathways in the pathogenesis of lung fibrosis. *Mol. Aspects Med.* **65**, 56–69 (2019).

629. Habiel, D. M. & Hogaboam, C. M. Heterogeneity of Fibroblasts and Myofibroblasts in Pulmonary Fibrosis. *Curr. Pathobiol. Rep.* **5**, 101–110 (2017).

630. Nunes, A. S., Barros, A. S., Costa, E. C., Moreira, A. F. & Correia, I. J. 3D tumor spheroids as in vitro models to mimic in vivo human solid tumors resistance to therapeutic drugs. *Biotechnol. Bioeng.* **116**, 206–226 (2019).

631. Rohrbach, D. H. & Timpl, R. *Molecular and Cellular Aspects of Basement Membrane*. (Elsevier, 1993). doi:10.1016/C2012-0-01643-2.

632. Dolega, M. E., Abeille, F., Picollet-D'hahan, N. & Gidrol, X. Controlled 3D culture in Matrigel microbeads to analyze clonal acinar development. *Biomaterials* **52**, 347–357 (2015).

633. Torras, N., García-Díaz, M., Fernández-Majada, V. & Martínez, E. Mimicking Epithelial Tissues in Three-Dimensional Cell Culture Models. *Front. Bioeng. Biotechnol.* **6**, (2018).

634. Decramer, M. & Cooper, C. B. Treatment of COPD: the sooner the better? *Thorax* **65**, 837–841 (2010).

635. Cazzola, M. & Page, C. Long-acting bronchodilators in COPD: where are we now and where are we going? *Breathe* **10**, 110–120 (2014).

636. Vestbo, J. *et al.* Global Strategy for the Diagnosis, Management, and Prevention of Chronic Obstructive Pulmonary Disease. *Am. J. Respir. Crit. Care Med.* **187**, 347–365 (2013).

637. Vinken, M. 3Rs toxicity testing and disease modeling projects in the European Horizon 2020 research and innovation program. *EXCLI J.* **19**, 775–784 (2020).

638. Haswell, L. E., Hewitt, K., Thorne, D., Richter, A. & Gaça, M. D. Cigarette smoke total particulate matter increases mucous secreting cell numbers in vitro: A potential model of goblet cell hyperplasia. *Toxicol. In Vitro* **24**, 981–987 (2010).

639. Roodsant, T. *et al.* A Human 2D Primary Organoid-Derived Epithelial Monolayer Model to Study Host-Pathogen Interaction in the Small Intestine. *Front. Cell. Infect. Microbiol.* **10**, (2020).

640. van der Hee, B. *et al.* Optimized procedures for generating an enhanced, near physiological 2D culture system from porcine intestinal organoids. *Stem Cell Res.* **28**, 165–171 (2018).

641. Levenberg, S. *et al.* Differentiation of human embryonic stem cells on three-dimensional polymer scaffolds. *Proc. Natl. Acad. Sci. U. S. A.* **100**, 12741–12746 (2003).

642. Fiske, B. Wnt signals lead cells down the caudal path. *Nat. Neurosci.* **5**, 510–510 (2002).

643. Martyn, I., Kanno, T. Y., Ruzo, A., Siggia, E. D. & Brivanlou, A. H. Self-organization of a human organizer by combined Wnt and Nodal signalling. *Nature* **558**, 132–135 (2018).

644. Wong, A. Y. & Whited, J. L. Parallels between wound healing, epimorphic regeneration and solid tumors. *Development* **147**, (2020).

645. Lee, Y.-S., Wysocki, A., Warburton, D. & Tuan, T.-L. Wound Healing in Development. *Birth Defects Res. Part C Embryo Today Rev.* **96**, 213–222 (2012).

646. Jones, R. L., Salamonsen, L. A. & Findlay, J. K. Activin A Promotes Human Endometrial Stromal Cell Decidualization *in Vitro*. *J. Clin. Endocrinol. Metab.* **87**, 4001–4004 (2002).

647. Coudreuse, D. & Korswagen, H. C. The making of Wnt: new insights into Wnt maturation, sorting and secretion. *Development* **134**, 3–12 (2007).

648. Igarashi, M., Finch, P. W. & Aaronson, S. A. Characterization of Recombinant Human Fibroblast Growth Factor (FGF)-10 Reveals Functional Similarities with Keratinocyte Growth Factor (FGF-7). *J. Biol. Chem.* **273**, 13230–13235 (1998).

649. Borok, Z. *et al.* Keratinocyte Growth Factor Modulates Alveolar Epithelial Cell Phenotype In Vitro: Expression of Aquaporin 5. *Am. J. Respir. Cell Mol. Biol.* **18**, 554–561 (1998).

650. Mavroganatou, E., Pratsinis, H., Papadadopolou, A., Karamanos, N. K. & Kletsas, D. Extracellular matrix alterations in senescent cells and their significance in tissue homeostasis. *Matrix Biol.* **75–76**, 27–42 (2019).

651. Bonnet, D. & Dick, J. E. Human acute myeloid leukemia is organized as a hierarchy that originates from a primitive hematopoietic cell. *Nat. Med.* **3**, 730–737 (1997).

652. Haque, A., Engel, J., Teichmann, S. A. & Lönnberg, T. A practical guide to single-cell RNA-sequencing for biomedical research and clinical applications. *Genome Med.* **9**, 75 (2017).

653. Graf, B. W. & Boppart, S. A. Imaging and Analysis of Three-Dimensional Cell Culture Models. *Methods Mol. Biol. Clifton NJ* **591**, 211–227 (2010).

654. Cutrona, M. B. & Simpson, J. C. A High-Throughput Automated Confocal Microscopy Platform for Quantitative Phenotyping of Nanoparticle Uptake and Transport in Spheroids. *Small* **15**, 1902033 (2019).

655. Cawkhill, D. & Eaglestone, S. S. Evolution of cell-based reagent provision. *Drug Discov. Today* **12**, 820–825 (2007).

656. Clinton, J. & McWilliams-Koeppen, P. Initiation, Expansion, and Cryopreservation of Human Primary Tissue-Derived Normal and Diseased Organoids in Embedded Three-Dimensional Culture. *Curr. Protoc. Cell Biol.* **82**, e66 (2019).

657. Costa, P. F., Dias, A. F., Reis, R. L. & Gomes, M. E. Cryopreservation of Cell/Scaffold Tissue-Engineered Constructs. *Tissue Eng. Part C Methods* **18**, 852–858 (2012).

658. Rupf, T., Ebert, S., Lorenz, K., Salvetter, J. & Bader, A. Cryopreservation of Organotypical Cultures based on 3D Scaffolds. *CryoLetters* **31**, 157–168 (2010).

659. Nova, Z., Skovierova, H. & Calkovska, A. Alveolar-Capillary Membrane-Related Pulmonary Cells as a Target in Endotoxin-Induced Acute Lung Injury. *Int. J. Mol. Sci.* **20**, (2019).

660. Kido, T. *et al.* Particulate Matter Induces Translocation of IL-6 from the Lung to the Systemic Circulation. *Am. J. Respir. Cell Mol. Biol.* **44**, 197–204 (2011).

661. Wu, X. *et al.* Conditional reprogramming: next generation cell culture. *Acta Pharm. Sin. B* **10**, 1360–1381 (2020).

662. Huschtscha, L. I. & Holliday, R. Limited and unlimited growth of SV40-transformed cells from human diploid MRC-5 fibroblasts. *J. Cell Sci.* **63**, 77–99 (1983).

663. Srinivasan, B. *et al.* TEER measurement techniques for in vitro barrier model systems. *J. Lab. Autom.* **20**, 107–126 (2015).

664. Ghalbzouri, A. E., Jonkman, M. F., Dijkman, R. & Ponec, M. Basement Membrane Reconstruction in Human Skin Equivalents Is Regulated by Fibroblasts and/or Exogenously Activated Keratinocytes. *J. Invest. Dermatol.* **124**, 79–86 (2005).

665. Zhang, W., Choi, J. K. & He, X. Engineering Microvascularized 3D Tissue Using Alginate-Chitosan Microcapsules. *J. Biomater. Tissue Eng.* **7**, 170–173 (2017).

666. Sadofsky, L. R. *et al.* Characterisation of a New Human Alveolar Macrophage-Like Cell Line (Daisy). *Lung* **197**, 687–698 (2019).

667. Park, D. H. *et al.* Development of a microfluidic perfusion 3D cell culture system. *J. Micromechanics Microengineering* **28**, 045001 (2018).

668. Sanchez-Esteban, J. *et al.* Mechanical stretch promotes alveolar epithelial type II cell differentiation. *J. Appl. Physiol.* **91**, 589–595 (2001).

669. Nikolova, M. P. & Chavali, M. S. Recent advances in biomaterials for 3D scaffolds: A review. *Bioact. Mater.* **4**, 271–292 (2019).

670. Hellemans, J., Mortier, G., De Paepe, A., Speleman, F. & Vandesompele, J. qBase relative quantification framework and software for management and automated analysis of real-time quantitative PCR data. *Genome Biol.* **8**, R19 (2007).